

Impact of water deficit on degradability, cell wall biochemistry and lignified tissue distribution in the maize internode, and genetic determinism of these traits

Fadi El Hage

▶ **To cite this version:**

Fadi El Hage. Impact of water deficit on degradability, cell wall biochemistry and lignified tissue distribution in the maize internode, and genetic determinism of these traits. Plant breeding. Université Paris Saclay (COmUE), 2018. English. ⟨NNT : 2018SACLS609⟩. ⟨tel-03512644⟩

HAL Id: tel-03512644

https://theses.hal.science/tel-03512644v1

Submitted on 5 Jan 2022

HAL is a multi-disciplinary open access archive for the deposit and dissemination of scientific research documents, whether they are published or not. The documents may come from teaching and research institutions in France or abroad, or from public or private research centers.

L'archive ouverte pluridisciplinaire **HAL**, est destinée au dépôt et à la diffusion de documents scientifiques de niveau recherche, publiés ou non, émanant des établissements d'enseignement et de recherche français ou étrangers, des laboratoires publics ou privés.



HAL Authorization

NNT : 2018SACLS609

Thèse de doctorat

Impact du déficit hydrique sur la dégradabilité, la biochimie pariétale et la répartition des tissus lignifiés chez l'entrenœud de maïs et déterminisme génétique de ces caractères.

Thèse de doctorat de l'Université Paris-Saclay
préparée à l'Université Paris-Sud
et l'Institut Jean-Pierre Bourgin
INRA de Versailles

École doctorale n°567 : sciences du végétal :
Du gène à l'écosystème (SDV)
Spécialité de doctorat: Biologie

Thèse présentée et soutenue à Versailles, le 20/12/2018, par

Fadi EL HAGE

Composition du Jury :

Mme Christine Dillmann Professeure, INRA du Moulon	Présidente
Mme Fabienne Guillon Directrice de recherche, INRA Nantes	Rapporteure
M. Simon Hawkins Professeur, Université de Lille 1	Rapporteur
Mme Sylvie Jaffuel Chargée de recherche, CIRAD Montpellier	Examinatrice
Mme Eliette Combes Breeding technology program manager, Syngenta	Examinatrice
M. Matthieu Reymond Chargé de recherche, INRA Versailles	Directeur de thèse
Mme Valérie Méchin Directrice de recherche, INRA Versailles	Directrice de thèse (invitée)



Merci !

Presque quatre années depuis mon Master 2. Quatre années riches tant sur le plan professionnel que personnel. Beaucoup de choses apprises, tentées, ratées, réussies et aussi beaucoup de rencontres et d'échanges. Et tout ce travail n'aurait pas été possible sans vous tous. C'est pourquoi je vous remercie tous.

J'aimerais tout d'abord remercier Valérie et Matthieu de m'avoir encadré, supporté et d'avoir travaillé avec moi pendant presque quatre ans. J'ai beaucoup appris et ce fut un réel plaisir de travailler et d'échanger des idées avec vous.

Je remercie aussi toute l'équipe Qualibiosec de m'avoir accompagné tout au long de la thèse en commençant par Marie-Pierre, Yves, Christine, Sylvie, Lucie et Sébastien ; ainsi que tous ceux qui sont partis depuis ; Aurélie, Wahid, Camille, Sandrine et Clément sans oublier tous les stagiaires.

J'aimerais aussi remercier tout particulièrement Laëtitia avec qui les heures passées à coder sur R et à échanger autour des QTLs ont été géniales. Merci aussi pour toute l'aide et le temps que tu m'as consacré Laëtitia, ils ont été très précieux ! Merci pour tout.

Un grand merci aussi à Florian qui a récupéré les données de ma thèse, pas une, mais deux fois ! Un véritable sauveur, merci beaucoup.

Merci aux membres de mon comité de thèse qui m'ont accompagné scientifiquement et avec bienveillance au cours de ce projet.

Merci beaucoup aux membres de mon Jury d'avoir accepté de relire mon travail et de le corriger.

Merci aux plateformes de biochimie et de l'observatoire du végétal et aux gens qui y travaillent pour m'avoir aidé et formé, notamment Émilie, Nero et Bertrand.

Merci à David de la plateforme BIA de l'INRA de Nantes pour tous ces échanges autour des plug-ins ImageJ, ce fut un véritable plaisir de travailler avec toi.

Merci à l'unité Diascope et particulièrement à Serge pour avoir conduit les expérimentations aux champs.

Merci à tous les non-permanents de l'institut avec qui j'ai pu échanger et passer de bons moments pendant une pause ou une soirée.

Merci bien évidemment à tous les doctorants, déjà partis ou encore là pour quelques temps. Les soirées à l'IJPB ont été riches en rebondissements et en aventures !



Merci au ♪♫ Green Band ♪♫ et son esprit détendu et barré. Les rendez-vous du lundi ont toujours été top !

Merci au Club BD et au club Api de m'avoir fait passer de bons moments de lecture et de bzz-bzz même si je n'ai pas été toujours très présent.

Un ?!?!UrhuuuurhuuuuuUruuuuru?!?! merci à Olivier de m'avoir supporté pendant toutes ces années tant à l'appartement, qu'en rando ou à l'INRA. Ce fut pas banal !

Merci à Carole, Charlotte et Yoann pour ces supers rando itinérantes organisées au pied levé en France et ailleurs. Much fun ! Au plaisir de remettre ça un de ces jours !

Merci à toute la team de l'X and Co pour ces supers randos itinérantes dans les Alpes. Des paysages de fous, de chouettes ambiances, des chansons à ripouner ♪♫, de la haute gastronomie, bref, une recette tip, top !

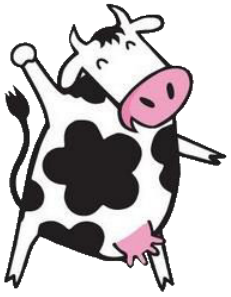
Merci à tous mes amis d'école, merci à tous ceux qui ont suivi de près ou de loin ce que je faisais et qui m'ont soutenu durant cette épopée.

Merci à toute la team du voyage au Népal, Auriane, Cécile, Yoann et Rémi qui m'auront permis de réaliser un rêve, tel la horde du contrevent ! ♪♫ Om mani padme Huuuuum ♪♫

Un grand merci à toute ma famille de m'avoir soutenu et apporté du réconfort tout au long de cette aventure, dans tous les moments. Je n'ai probablement pas été toujours très calme avec vous, mais votre soutien a été précieux. J'ai une tendre pensée pour ma Mamie. Sa force et sa volonté sont une source inépuisable d'inspiration. Elle est probablement l'une des femmes les plus admirables qu'il m'ait été donné de côtoyer et de passer tant de bons moments avec. Merci pour tout Mamie.

Enfin, et surtout, merci, merci, mille merci, une infinité de merci du fond du cœur pour ma sœur Sophie. Tes mots et ton réconfort ont toujours su trouver leur chemin et viser juste pour me faire aller mieux dans les moments les plus difficiles comme dans les meilleurs. J'aurais envie d'ajouter plein de choses, tellement la liste des bonnes choses est longue te concernant. ☺ Je terminerai juste sur : « Lèves les braaaas Maurice, c'est plus rigolo quand tu lèves les braaaas ! ». :D

Merci !



List of abbreviations

4CL : hydroxycinnamate CoA Ligase
5OHG : 5-hydroxy-Guaiacyl
ADF : Acid Detergent Fiber
ADL : Acid Detergent Lignin
AT : Arabidopsis thaliana
bm : brown midrib
C3H : *p* -Coumarate 3-Hydroxylase
C4H : Cinnamate-4-Hydroxylase
CAD : Cinnamyl Alcohol Dehydrogenase
CCoAOMT : Caffeoyl CoA O-Methyl Transferase
CCR : Cinnamoyl CoA Reductase
CoA : Coenzyme A
CP : Crude Protein
DM : Dry Matter
F5H : Ferulate-5-Hydroxylase
FA : Ferulic Acid
FAest: esterified ferulic acid
FAeth : etherified ferulic acid
G or BO4.G : Guaiacyl subunit
GC : Gaz Chrommatography
GWAS : Genome-Wide Association Mapping
H or BO4.H : Hydroxyguaiacyl subunit
HPLC : High Pressure Liquid Chromatography
IN : Internode
IN n : Internode carying the main ear
IR : Infra Red
IVCWRD : In Vitro Cell Wall Residue Degradability
IVDMD: In Vitro Dry Matter Degradability
IVNDFD : In Vitro NDF Degradability
KL.CWR : Klason Lignin of the CWR
MAS : Marker-Assisted Selection
MS : Mass-Spectrometry
NDF : Neutral Detergent Fiber
NIRS : Near Infra-Red Spectrometry
NWM : New washing-machine
OMT : O-Methyl Transferase
PAL : Phenylalanin Ammonia Lyase
PCA : *p* -coumaric acid
PCAest : esterified *p* -coumaric acid
PWE : Plant Without Ear
QTL : Quantitative Trait Locus
RFLP : Restricted Fragment Length Polymorphism
RILs : Recombinant Inbred Lines
S or BO4.S : Syringyl subunit
TAL : Tyrosine Ammonia Lyase
UFL : Unité Fourragère et Laitière
UFO : Unidentified flying object
UV : Ultra Violet

Table of contents

INTRODUCTION ..... - 1 -

General introduction ..... - 2 -

I. The maize plant ..... - 3 -

a) Back to origins ..... - 3 -

b) Anatomy of the maize plant ..... - 5 -

c) Maize crop production and valorization ..... - 7 -

1. The digestibility of corn silage, degradability of the walls seen from the side of the cow - 9 -

i. In vivo or in vitro estimation of digestibility. ..... - 9 -

ii. Criteria for registration in the French official catalog and impact on varietal selection - 10

2. Bioethanol production from maize crop residues, degradability seen from the EZ process side ..... - 12 -

i. Biomass and 2nd generation biorefineries ..... - 12 -

ii. Pretreatment of lignocellulosic biomass for bioethanol production ..... - 13 -

1- Chemical pretreatments ..... - 13 -

2- Physicochemical pretreatments ..... - 14 -

II. Cell wall in grasses ..... - 15 -

a) Structure ..... - 16 -

b) Polysaccharidic compounds ..... - 18 -

1. Cellulose ..... - 18 -

2. Hemicelluloses ..... - 20 -

3. Pectins ..... - 21 -

c) Phenolic compounds ..... - 23 -

1. Lignins ..... - 23 -

i. Composition of the lignins ..... - 23 -

ii. Impacts of the modifications of the lignin biosynthesis pathway ..... - 26 -

2. *p*-hydroxycinnamic acids ..... - 28 -

i. Ferulic acids ..... - 28 -

ii. *p*-coumaric acids ..... - 29 -

III. Distribution of the lignification within the maize stem tissues ..... - 31 -

a) Tissue anatomy in maize ..... - 31 -

b) Methods to investigate the tissue specificities ..... - 33 -

1. Imaging techniques ..... - 34 -

i. Darkfield microscopy ..... - 34 -

ii. Brightfield microscopy ..... - 35 -

2. Conclusion ..... - 38 -

IV. Cell wall establishment during maize stem development. ..... - 38 -

a) Genetic variation for internode elongation, cross section surface and cell size within the three genotypes throughout internode development ..... - 39 -

b) The main differences for internode elongation and cell wall phenolic composition were positioned at young stages, before silking ..... - 41 -

c) Different developmental patterns were observed for lignin content, composition, structure and distribution ..... - 43 -

1. Evolution of lignin content all along the internode development ..... - 43 -

2. Evolution of lignin structure and composition all along development ..... - 43 -

3. Evolution of lignin distribution at tissue level all along the internode development ..... - 45 -

d) Throughout internode growth different developmental patterns were observed for p-hydroxycinnamic acids accumulation ..... - 47 -

1. Evolution of esterified p-coumaric acid content all along internode development ..... - 47 -

e) Esterified ferulic acids were deposed all along plant development but used to anchor lignification only at early stages ..... - 49 -

f) Combination of the biochemical and histological findings to propose a model of spatiotemporal cell wall development ..... - 50 -

V. Relationships between cell wall degradability and 1- biochemical cell wall components and 2- the distribution of lignification. ..... - 52 -

a) Impact of the cell wall biochemistry on the cell wall degradability ..... - 52 -

b) Impact of the distribution of the lignification on cell wall degradability ..... - 55 -

VI. Impact of water stress on cell wall composition and on lignification distribution ..... - 58 -

VII. Genetic determinism of the cell wall traits under different watering conditions. ..... - 62 -

a) QTLs of cell wall components ..... - 63 -

b) QTLs of tissue distribution ..... - 65 -

c) QTLs under different watering conditions ..... - 65 -

VIII. Objectives of my PhD ..... - 67 -

Chapter 1 ..... - 70 -

Introduction ..... - 71 -

Material and Methods ..... - 74 -

Histological analyses ..... - 75 -

(Accepted Article) Histological quantification of maize stem sections from FASGA-stained images. ..... - 79 -

Dedicated NIRS predictive equations establishment and NIRS predictions of cell wall related traits in maize internodes ..... - 91 -

I. (Accepted article) Impact of the water deficit on the biochemical composition of the cell wall, the lignification distribution with the tissues and the degradability of the cell wall of maize stems..... ..... - 97 -

II. F2bm3 does not respond histologically or biochemically to water deficit. ..... - 107 -

a) Cell wall composition of F2bm3 internode and response to water deficit ..... - 108 -

1. F2bm3 and the NIRS predictions ..... - 108 -

2. Estimations of the F2bm3 cell wall components values ..... - 109 -

3. Biochemical relationships and response to water deficit. ..... - 110 -

b) Histological profiles of F2bm3 and response to water deficit ..... - 113 -

Conclusion ..... - 117 -

Chapter 2 ..... - 118 -

Introduction ..... - 119 -

Material and Methods ..... - 123 -

Plant materials and field experiments ..... - 123 -

NIRS predictive equations construction and NIRS predictions ..... - 123 -

I. Results ..... - 127 -

a) 2 years of field experiments declined in 4 irrigation conditions due to different environmental context. ..... - 127 -

b) Phenotypic variations ..... - 131 -

1. The parental inbred lines and their characteristics under different irrigation conditions ..... - 131 -

2. Variations of biochemical and histological traits among the recombinant inbred lines showed transgression and allowed to obtain expected correlations between traits ..... - 133 -

c) Genetic determinism of histological traits under different irrigation conditions. ..... - 137 -

d) QTLs involved in the variation of biochemical traits and co-localizations with QTLs involved in the variation of histological traits ..... - 139 -

e) Genetic determinism for biochemical cell wall traits of the whole plant without ears matches with the genetic determinism for biochemical cell wall traits of the internode in maize and with ..... - 142 -

II. (Submitted article) Water deficit responsive QTLs for cell wall degradability and composition traits in maize at silage stage ..... - 144 -

Conclusion ..... - 174 -

Chapter 3 ..... - 175 -

Introduction ..... - 176 -

I. Variation of cell wall biochemistry of the internode carrying the main ear reflects the variations of cell wall biochemistry of the whole plant without ear. ..... - 178 -

Material and Methods ..... - 178 -

Results and discussion ..... - 179 -

II. The histology of the internode carrying the main ear reflects the mean all the internodes of the stem. ..... - 183 -

Material and Methods ..... - 183 -

a) Histological pattern of the internode carrying the main ear reflects the average histological pattern of all the internodes of a maize stem. ..... - 185 -

b) Histological variations of the internode carrying the main ear partially reflect variation of the biochemistry of the whole plant without ears ..... - 196 -

Conclusion ..... - 200 -

Chapter 4 ..... - 201 -

I. What bricks do we bring to the cell wall degradability understanding? ..... - 203 -

a) Development and probation of high-throughput tools ..... - 203 -

b) The understanding of cell wall degradability ..... - 204 -

c) Impact of water deficit on the biomass quality ..... - 205 -

d) From the internode to the whole plant ..... - 206 -

II. All these results may be discussed further ..... - 208 -

a) Going further in the improvement of the high-throughput tools ..... - 208 -

b) Choice of the plant material and and monitoring of the water deficit conditions to address the PhD questions ..... - 208 -

c) Relationships between cell wall degradability and lignification at different scales ..... - 209 -

1. Targeting the general cell wall composition within the plant ..... - 209 -

2. Targeting tissues specificities within the plant ..... - 211 -

d) Impact of the water deficit on the lignification at different scales ..... - 212 -

III. Perspectives ..... - 215 -

References ..... - 218 -

French abstract ..... - 237 -

ANNEXES ..... - 239 -



INTRODUCTION

General introduction

Nowadays, maize is one of the most important cereals in the world both for human and animal consumption. Grain and forage are valorized depending of the region of cultivation. The diversity of uses of maize and its high potential of valorization puts it at a central position to answer to many issues such as the food security and its quality, the environmental durability of crops and the production of green energies. In the case of lignocellulosic biomass in maize, the valorizations concern mainly the animal feeding for the silage production and the production of biofuels from the agricultural co-products. In both cases the environmental sustainability of the crops is at stake and the potential of valorization of maize consist in good yields and a good quality. This quality goes through good conversion of fermentable sugars from the cell wall into energy and their accessibility remains an issue. Thus a good evaluation of this quality goes through the quantification of the degradability of the biomass. The soluble compounds of the biomass are fully degradable and cell wall degradability is thus the limiting factor. The degradability of the cell wall has been studied for years and it was shown that it is influenced by many factors, from the biochemical composition and the structure of the cell wall to the spatial distribution of the lignification at the tissues level.

Furthermore, as the effects of the global warming are more and more visible, drought periods will occur more frequently, even in the less pessimistic scenarios. Along with the actual agro-environmental policies which encourage decreasing inputs in fields and particularly the water supply, field irrigation will be constrained. It is then a real issue to understand how plants respond to these non-optimal growing conditions. Consequently, the modified and sometimes drastic growth conditions may have a potential effect on biomass production and quality. It is therefore necessary to better understand the effect of a reduced water supply on the biomass quality in maize, through the investigation of the biochemical cell wall and the distribution of the lignification responses.

The objective of the present work was to better understand the involvement of both the spatial lignification and the biochemical components of the lignocellulosic biomass in the variations of the cell wall degradability in response to a water deficit in maize. The results were particularly centered on the impact of the water deficit on the spatial lignification and the cell wall biochemistry of the internode carrying the main ear with however many comparison with the cell wall biochemistry and degradability of the whole plant both for the genetic determinism and at the biochemical level. Finally we evaluated the part that can play the spatial lignification within the biomass quality traits of the whole plant. The results will lead to a better understanding of the role of the spatial lignification in the variation of cell wall

degradability and the proposition of the combination of original targets of selection to improve the quality of the biomass in maize in response to a water deficit.

I. The maize plant

a) Back to origins

Maize was domesticated around 8700 years ago in the highlands of Mexico from the subspecies *Zea Mays ssp. Parviglumis* (Matsuoka et al., 2002). Thanks to a large-scale molecular analysis of maize from both Europe and the Americas, it is established that for thousands of years maize spread in South America and in North America, and about 8200 years after its domestication maize was introduced in Europe by colonization (Fig. 1). These studies confirmed that the diversity of European maize derives from the American maize for at least 75 % (Tenaillon et al., 2011).

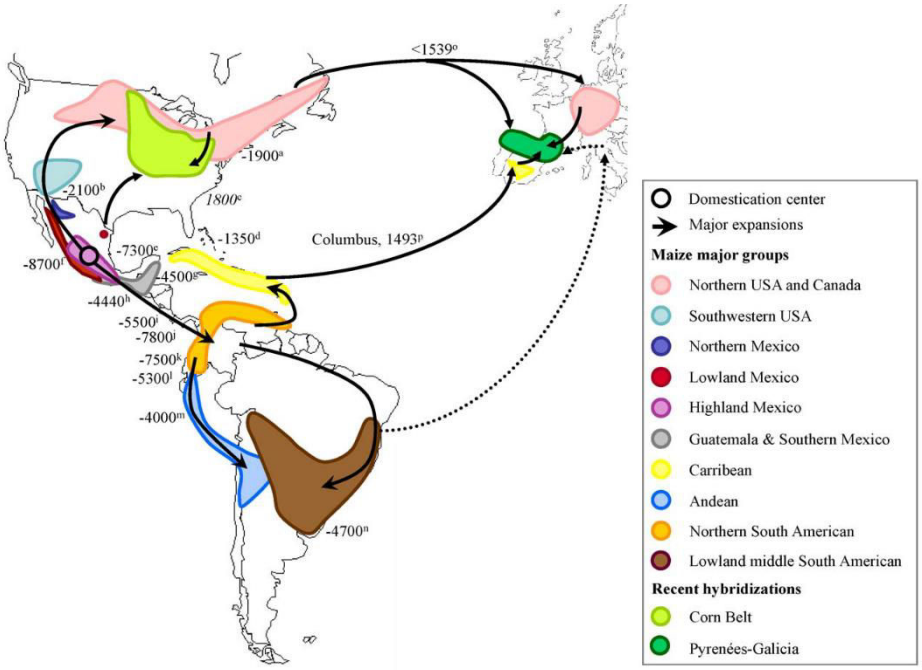


Figure 1. Domestication and hypothetical diffusion of maize through the Americas and Europe (adapted from Tenaillon et al., 2011).

But the modern maize we currently cultivate is not similar as the one first found by men in Mexico. Cultivated maize, *Zea mays,* presents profound morphological differentiations with its wild ancestor called Balsas teosinte, *Zea mays supsp. parviglumis*, which includes (Fig. 2): modifications in vegetative architecture with the reduction in branching; also modification of the ear morphology in term of number, position along vegetative axes, size, shape and number of rows per ear; modifications in the kernel morphology for its shape, size, and hardness; and modification of kernel characteristics like dormancy, shattering, starch and protein content.



Figure 2. Modern maize (right), Zea mays, and its wild ancestor Balsas teosinte (left), Zea mays subsp. Parviglumis (adapted from Nicole Rager Fuller, National Science Foundation).

So far, two domestication genes have been identified as specific of the domesticated maize and they have been cloned: tb1, *teosinte branched 1*, a transcription factor whose overexpression represses the growth of axillary meristems and results in the unbranched plant architecture typical of maize (Doebley et al., 1997; Wang et al., 1999); and tga1, teosinte glume architecture 1, a transcription factor responsible for the 'naked' grain phenotype of maize and contributing to the organization of an ear cob being able to bear several hundreds of kernels (Wang et al., 2005). Recently, another gene, znc8, involved in flowering time, presents allelic variation that shows evidence of domestication. (Guo et al., 2018).

b) Anatomy of the maize plant

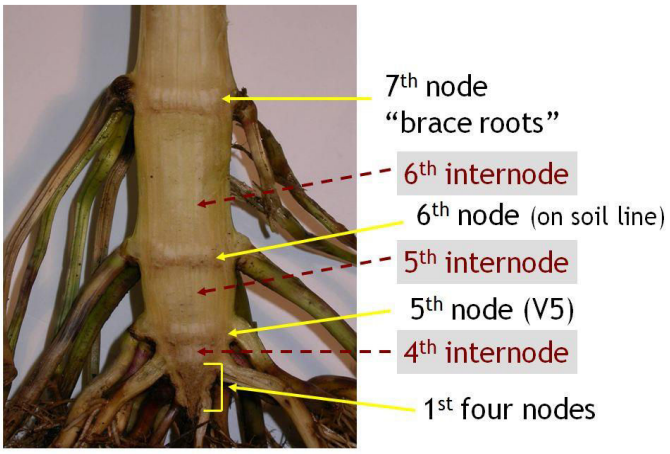


Figure 3a. Transition between the root system and the stem in maize (from Corn Agronomy, University of Wisconsin).

More often, the modern maize plant is 3 meters high. It is composed of (Figure 3a and 3b):

- a root system which is a fibrous adventitious type. Primary root abort after germination and are then replaced by fibrous adventitious ones developing in successive crowns (also called brace roots) around the first nodes of the stalk. They form then a dense root system which can reach a depth of a meter (Gay, 1984);

- between the root system and the stem 5 to 7 internodes may be found before the ground level (Figure 3a);

- a main stem which can be accompanied with a few tillers, and which can comprise until 20 internodes of about 18 cm each (Wellhausen, 1952; Stevenson and Goodman, 1972);

- from each node of the stem, a leaf is growing and is composed of three parts, the leaf sheath, the ligule and in the continuity of it, the leaf blade . The leaf blade can reach 9 cm in width and 120 cm in length;

- in the midsection of the plant stem, ears are developing between the stem and the leaf sheath. They have an elongating rate of 3 mm

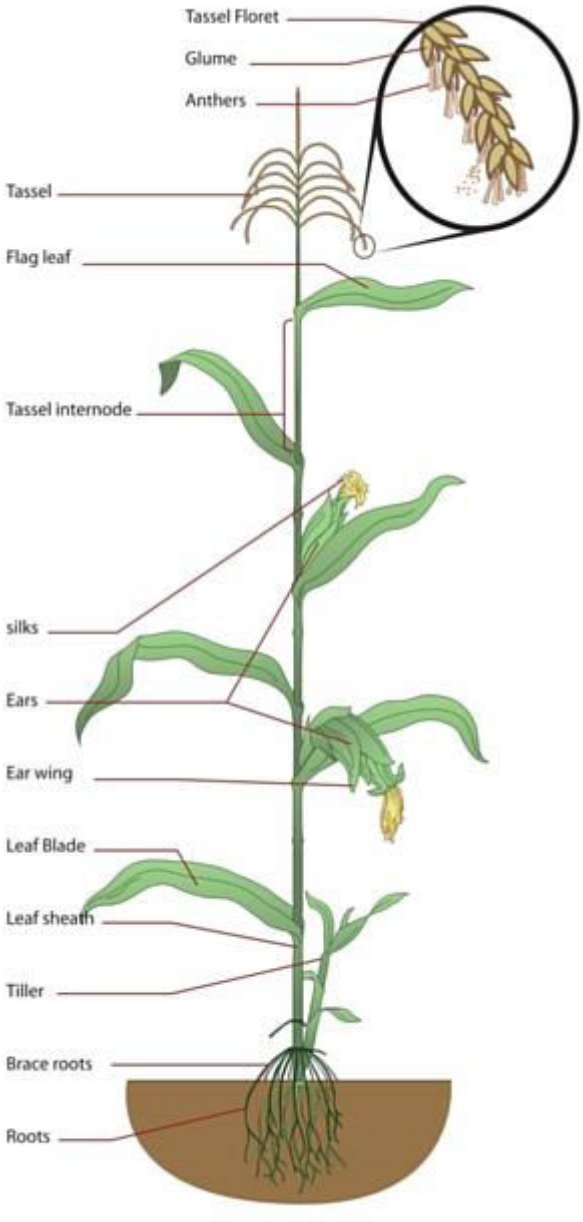


Figure 3b. Maize plant anatomy.

per day and can reach an average of 18 cm (even 60 cm in some tropical subspecies). Ears are female inflorescences, tightly enveloped by several layers of ear leaves which can be called ear wing or husks. Certain varieties of maize present a greater amount of ears than others which is a result of the breeding at the service of the food industry;

- elongated stigmas, called silks, are emerging from the top of the ears. Each silk can reach 18 cm and is connected to a carpel which may develop into a “kernel” if fertilized by a pollen grain.
- the apex of the stem is called the tassel and is the male inflorescence of the plant. When they are mature, they release pollen which is anemophilous and is therefore dispersed by wind.
- The entire kernel is often referred to as “seed” but is in reality the typical fruit of the Poacee called “caryopsis”. It means that the pericarp of the fruit is fused with the seed coat. The size of the kernel can reach 2.5 cm (Grobman, 1961) and an ear can contain an average of 600 kernels.

The maize plant possess both male and female organ and may perform both autogamy (i.e. self-reproduction) and allogamy (i.e. reproduction with other members of the specie), and is therefore capable of auto-allogamy.

As the two sexes are separated on the plant, at the flowering time, they do not get mature at the same time. This is called the Anthesis to Silking Interval (or ASI), which measure the time in days between pollen shed and silk emergence. Originally, the pollen was shedding before the silk emergence. Pollen shed occurs over a 5 to 8 days period and silks are viable and receptive to pollen up to 7 to 10 days. Smaller ASI values means a greater chance of successful seed set, increased kernel numbers and increased yield. That is why, over the last 5 to 6 decades, maize breeders worked toward developing hybrids that shed pollen and silk at nearly the same time.

During flowering, maize plants need more water than at any other time (Elmore, 2012). This is in part because silks have the highest water content among all parts of the maize plant. A water stress during this period will increase the ASI and is associated to a yield potential reduction. This makes ASI a good indicator of stress and its reduction by the breeders help to stabilize maze corn yields in stressed environments (Elmore, 2012).

Maize is considered to be a day-neutral or a short-day plant. The radiation is positively affecting growth. Therefore, for optimum light interception, the density index (number of plants per ha/row spacing) may reach until 100 000 plants per ha.

c) Maize crop production and valorization

I chose to present the state of the art of the production and the valorization of maize through the first part of an accepted chapter in Chimie Verte et IAA (Ed. Stéphanie Baumberger – Lavoisier) : « L'imagerie, un outil puissant pour étudier les variabilités de répartition et de composition des tissus de la biomasse lignocellulosique - Perspectives dans l'amélioration de la dégradabilité des parois chez le maïs » by Valérie Méchin, Matthieu Reymond, David Legland, Mathieu Fanuel, Fadi El Hage, Aurélie Baldy, Yves Griveau, Marie-Pierre Jacquemot, Sylvie Coursol, Marie-Françoise Devaux, Hélène Rogniaux, and Fabienne Guillon.

In 2015, in France, cereals covered 11 million hectares (ha), while oilseeds occupied 2.2 million ha. Cereals are therefore very important crops in our territory. Among these cereals, common wheat ranked first with 5.2 million ha under cultivation, followed by corn that covered 3.1 million ha (1.7 ha for grain corn and 1.4 ha for forage corn).

Fodder maize is a European specificity and, in particular, German and French, with 60% of maize forage crops found in Germany and France. In France, fodder maize growing areas overlap perfectly with areas of high dairy farming (Figure 4.1) (Battegay, 2016). Corn silage is actually the basis of feeding dairy herds in France.

Corn silage cultivation developed in France from the 1970s through the creation and marketing of early varieties adapted to the rainy climate of large dairy farming areas. Since 1970, plants have changed completely; they are now much higher and have a very different port. Farmland dedicated to silage maize grew from about 350,000 ha in the 1970s to stabilize at 1.4 million ha today (Arvalis, 2011).

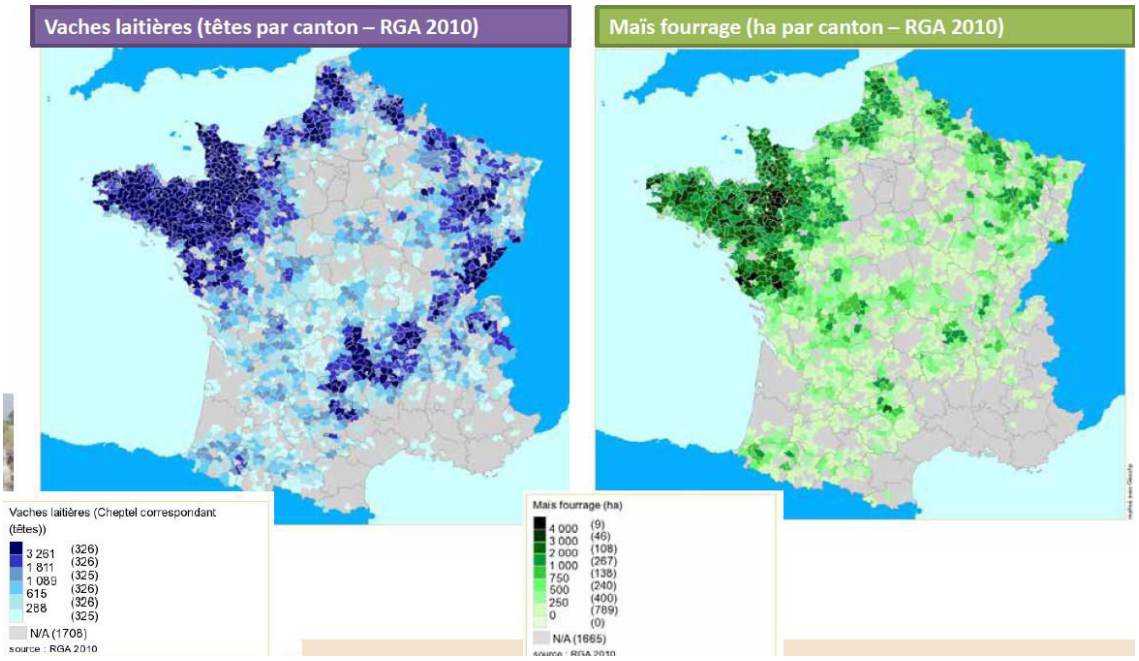


Figure 4.1. Map of France illustrating co-locations between dairy farming (in blue, on the left) and corn silage growing areas (in green, on the right) (Battegay, 2016).

Currently, the biomass yields of hybrids marketed and grown in France reach up to 20 tonnes of dry matter (DM) per hectare (t MS.ha-1) while they amounted to just 2 t DM. ha-1 in the 1970s, representing genetic progress estimated between 0.12 and 0.22 t MS.ha-1.year-1, depending on the precocity group. In 2017, Baldy et al. (2017) cultivated on 47 maize hybrids marketed in France between 1958 and 2015 and showed that under absolutely comparable culture conditions the genetic progress on yield was 0.2 t.ha-1.year-1. A hybrid marketed in 1960 shows a yield of 11 t MS.ha-1, while modern hybrids reach 22 t MS.ha-1. This increase in yields was accompanied by a subsequent decrease / stagnation of the energy value and digestibility of hybrids created during breeding. Although since 1998, the UFL content (for Dairy Fodder Unit, (Andrieu and Aufrère, 1996)) is the criterion related to the energy value retained for the listing of corn silage varieties in the French official catalog, the weight given to the productivity at registration remained well above the weight given to the energy value. It is generally accepted that this has led to the stagnation of the energy values of fodder maize in France since the 2000s, without improving them.

In the world, 60% of grain corn is American or Chinese. In Europe, France is the leader in terms of production volume (source : http://www.agpm.com/mais_grain.php).

The industrial sector transforms every year 3 million t of corn on the territory (1.5 million t exported). The starch industry is the majority industrial sector (2 million t) followed by semolina. Corn stover (stems, leaves and husks) left over after grain harvest is an important co-product and accounts for about 70% of the amount of dry matter harvested as grain. It is thus possible to harvest 5-6 t MS ha-1 of canes with a harvest cost of 90 € / ha. The average UFL of these ensiled canes is 0.6 kg-1 DM (far from the 0.95 of corn silage but close to the UFL of conventional hays) and can therefore possibly be used to feed animals. not demanding or to complement a diet rich in concentrates in long fibers. Another valuation of this co-product can be its use as lignocellulosic biomass input biorefineries for the production of bioethanol second generation. A potential deposit of 10 million tonnes per year is thus available by simply adding a co-product from the grain corn crop.

At present, therefore, we can consider two uses of corn biomass: a historical and conventional silage use where the whole plant is used in animal feed, and a use of crop co-products from grain corn where the biomass would then be oriented. at the entrance of the biorefinery. In both cases, the objective is to optimize the sugars constituting biomass (in addition to starch for silage) and thus to digest or degrade most effectively the parietal polysaccharides: cellulose and hemicelluloses.

1. The digestibility of corn silage, degradability of the walls seen from the side of the cow.

i. In vivo or in vitro estimation of digestibility.

Fodder is normally characterized by its dietary value, which is expressed by the potential for milk production in dairy cows or weight gain in bull calves. However, this type of measurement on animals with high potential and on their performance zootechniques is not feasible routinely due to the heaviness of experiments. They can only be used to estimate the dietary value of some genotypes and validate the evaluation criteria that can be used routinely. In vivo, the most widely used tool used as a reference for estimating the energy value of corn is the standard sheep in a cage. In routine, it is mainly used in vitro in vitro digestibility estimation techniques where enzymatic cocktails (amylases, pepsins and a mixture of cellulases and hemicellulases) mimic digestion by ruminants (Aufrère and Michalet-Doreau, 1983, Lila et al., 1986, De Boever et al., 1988, Ronsin, 1990). The so-called Aufrère method is the one that refers in the world of maize silage selection to estimate the in vitro

digestibility of the dry matter. Work developed over the past 60 years has also highlighted the strong relationship between the energy value of forage and the degradability of the walls (Aufrère et al., 2007). These in vitro estimates account for about 60% of the genetic variability observed in vivo (Argillier et al., 1998).

Degradability is the main target for improving energy value at the moment, and Near InfraRed Spectroscopy (NIRS) prediction equations are being developed to predict this character in broadband. The degradability of plants is very much limited by the degradability of the walls surrounding each cell. The walls consist of polysaccharides (highly degradable: cellulose and hemicelluloses) and phenolic compounds (non-degradable and limiting the degradability of polysaccharides in the parietal assembly: lignin and ferulic and p-coumaric acids). These walls are therefore at the center of targets for improving degradability.

ii. Criteria for registration in the French official catalog and impact on varietal selection

In the 1950s, the goal of the official French catalog was to facilitate responses to post-war challenges to ensure food security. Improving productivity has therefore been the major objective of this era. Before the 1980s, the corn market was a grain market divided into six precocity groups corresponding to the agro-climatic zones. The "fodder" market appeared with the creation of varieties with high dry matter production of the whole plant and in 1985 the creation of a specific section of the official catalog amplified this segmentation. In fifty years forage maize has seen an incredible rise. Since 1986, entries in the official French catalog are made in "corn grain" or "corn fodder" (Surault et al., 2005). The varieties listed in "fodder" are evaluated for their traditional agronomic values (yield, precocity, and stem behavior) but also, since 1998, for their qualitative value via the consideration of their energy value (UFL). The goal was clearly to promote the UFL / kg MS energy concentration of the whole plant in the breeding objectives. Indeed, from 1985 to 2000, genetic progress was remarkable in productivity. Nevertheless, the value of food has made little progress because of the priority given to improving grain yield and agronomic qualities. Improving the energy value remains an important point to consider in breeding programs. For illustration, an improvement of 0.05 point of UFL allows the production of 1.8 kg of supplementary milk per day and per cow consuming a ration of 16 kg of MS (Barrière and Emile, 2000) or 600 kg per cow and per year, which represents about € 160 extra cash per cow for farmers. In a recent study of a cohort of representative corn hybrids from the last 50 years of breeding, Baldy et al. (2017) showed that, up to 2012, the UFL value fell before stabilizing and starting to recover in the last 5 years (Figure 4.2). It was therefore necessary to wait 15 years for selection efforts on silage quality to be visible on the silage market. Strong differences exist between marketed hybrids and a

further increase in UFL values is always possible by targeting the right traits to improve this quality without penalizing agronomic qualities.

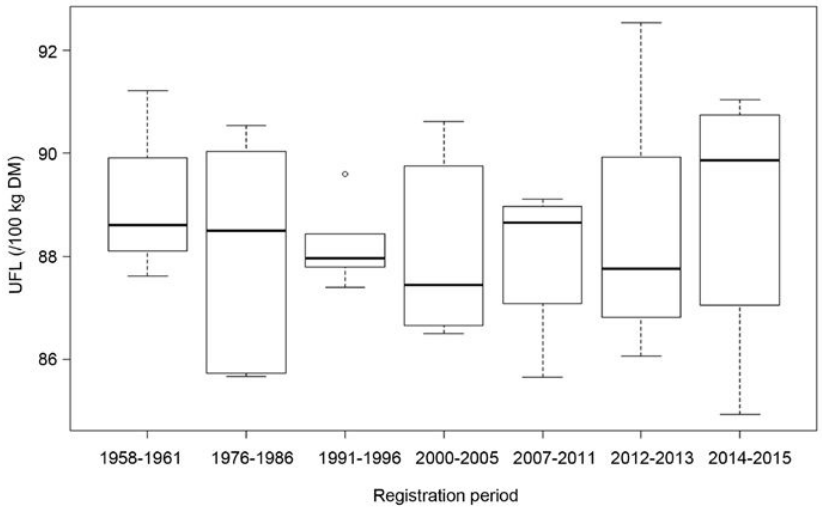


Figure 4.2. Evolution over time of the UFL values of a cohort of corn hybrids representative of the last 50 years of selection.

Equations for forecasting the energy value of forage maize were established during the 1990s (Andrieu, 1995) and have just been confirmed and very slightly updated in 2016 (Peyrat, 2016). Equation M4.2 (Model 4 equation update) predicts the UFL value using two variables: the total nitrogen content (MAT = protein) and the in vitro digestibility of dry matter by the Aufrère method (DCS)

UFL (for 100 kg MO) = 18,77 + 0,1389 x MAT (g/kg MO) + 0,9491 x DCS (%)

(N=290; R^2=0,53; ETR=0,032)

This equation is the reference used nowadays for the official catalog entry French maize fodder.

The energy provided to ruminants by silage comes on the one hand from the starch fraction and on the other hand from the walls of the "stems + leaves" part. The starch is almost completely digested on the entire digestive tract, while the degradation of the walls remains partial. This parietal degradability therefore remains the preferred target for improving forage degradability and the UFL values of modern hybrids.

2. Bioethanol production from maize crop residues, degradability seen from the EZ process side

i. Biomass and 2nd generation biorefineries

Biomass is expected to play an important role in achieving the objectives of the Energy Transition for Green Growth Bill (Report of the Parliamentary Office for the Assessment of Science and Technology Choices, 2015). The use of biomass will thus contribute to:

- reduce greenhouse gas emissions by 40% between 1990 and 2030 and divide by 4 by 2050,
- reduce the share of nuclear energy to 50% in the production of electricity by 2025,
- reduce overall energy consumption by 50% in 2050 compared to 2012,
- reduce fossil energy consumption by 30% in 2030 compared to 2012 with the joint objectives of achieving this: 38% of heat from renewable resources, 15% of biofuels as a substitute for fossil fuels and 10% biogas injected into the gas network..

Without denigrating the role played by first-generation biofuels, France has a ceiling of 7% on the rate of incorporation into fuels in order not to risk using the land available for food crops and to compete with them. The increase in the rate of incorporation of biofuels will have to go through the production of second generation biofuels (2G) (see part 2 - chapter 3).

The actual 2G biorefineries and species used worldwide are shown in Figure 4.3. The industrial takeoff of 2G ethanol production is underway. The first step of this production is the implementation of pretreatments which aim to facilitate the access of enzymes to the parietal polysaccharides and thus optimize their recovery.

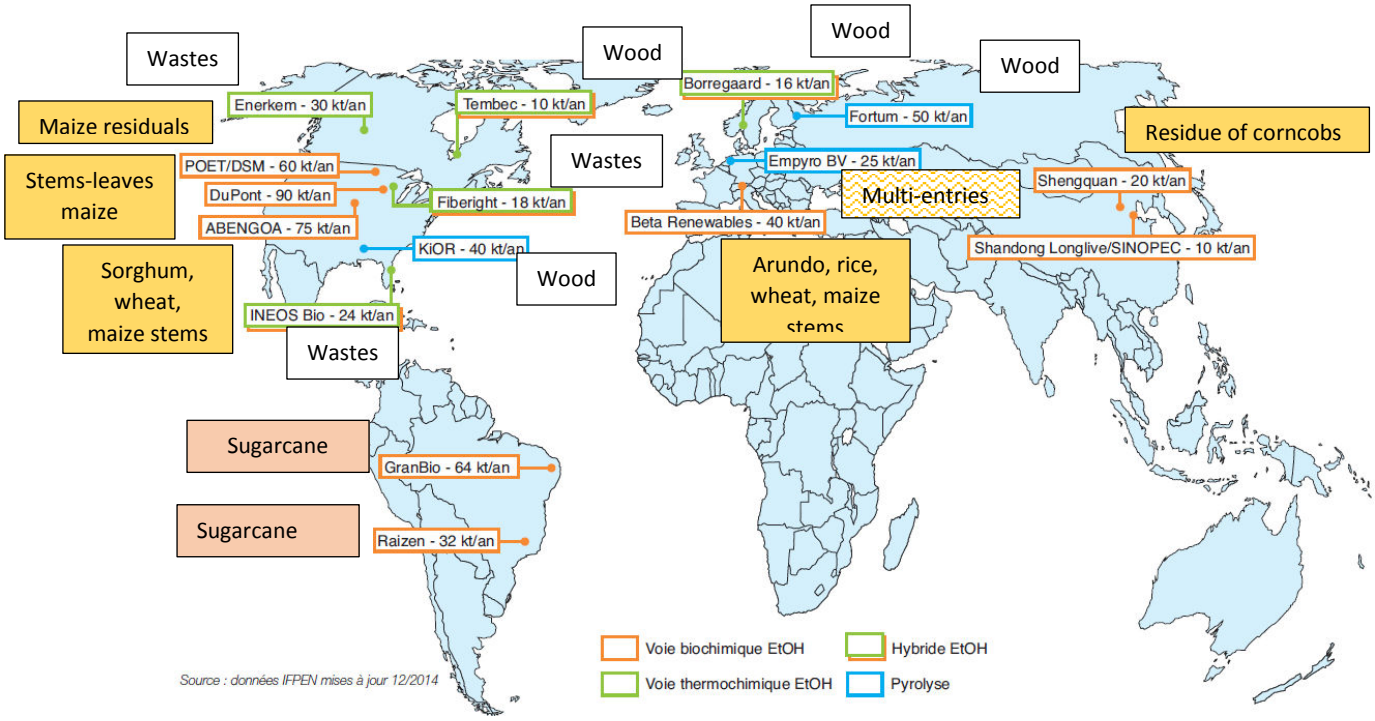


Figure 4.3. 2G commercial biofuel units under construction or production based on IFPEN data updated in December 2014. This map has been modified to indicate the main biomasses used at the factory gate.

ii. Pretreatment of lignocellulosic biomass for bioethanol production

1- Chemical pretreatments

There are different types of chemical pretreatments, distinguished by the reagent or solvent used and their effect on lignocellulosic biomass:

- **alkaline,** the most used (mainly NaOH and Ca (OH) 2) to remove lignins and hemicelluloses and destructure the biomass into lignocellulosic fibers by breaking the ester bonds (and ethers depending on the hardness of the pretreatment) and / or swelling of the cellulose,
- **acids,** which target the glycosidic bonds of hemicelluloses and cellulose. Diluted acid pretreatments are preferred to those with concentrated acid that severely degrade cellulose, create high concentrations of inhibitors and cause corrosion of equipment (Alvira et al., 2010**)**,
- **by oxidative delignification,** using an oxidizing agent (O3, O2, H2O2, ClO2, etc.) which performs a fragmentation of the lignins resulting in the release of free radicals and the fragmentation of the lignin network, while the hemicelluloses and the cellulose have little impact. The cost of this pretreatment is higher than that of alkaline or acidic pretreatments

and its use is generally limited to supplementing alkaline pretreatment to remove residual lignins (Qi et al., 2009),

- **organosolves**, where an aqueous or organic solvent (often in the presence of a catalyst to improve fractionation) is used to extract lignins and thereby reduce the lignin content of the biomass and also increase the accessible surface of lignocellulosic material. Ethanol is the most commonly used solvent due to its low toxicity and ease of recycling. The low environmental impact of these pretreatments, as well as the good quality of the lignins recovered as co-products, encourage the use of these organosolve processes,
- **by ionic liquids,** effectively dissolving cellulose or biomass. They allow a large increase in the specific surface area of the biomass accessible to enzymes. However, the enzymes are difficult to operate in ionic liquids and it is therefore necessary to regenerate the lignocellulosic biomass in an anti-solvent of the ionic liquid. The cost of most ionic liquids, however, remains high and their recycling is still to be improved.

2- Physicochemical pretreatments

Physicochemical pretreatments combine the action of temperature, pressure and possibly chemical agents:

- **by steam explosion,** the most commonly used and with low environmental impact. When the pressure is instantly reduced to atmospheric pressure, biomass explodes into fibers where hemicelluloses and lignins are variably removed. Gentle explosion conditions are favored to limit the production of enzyme inhibitors and an impregnating agent such as H2SO4 is used. H2SO4 accelerates the hydrolysis of polysaccharides, catalyzes enzymatic hydrolysis and the concentration of inhibitors remains correct,
- **hydrothermal,** to get rid of hemicelluloses and some lignins without degrading cellulose below 240 ° C. They also make it possible to increase the accessible surface allowing an increase in the enzymatic digestibility. Hydrothermal fluid rich in hemicelluloses or sugars derived from hemicelluloses can also be used for the production of furfural,
- **AFEX** (explosion and exposure to liquid ammonia), allowing the swelling of lignocelluloses and a change in the crystalline structure of the cellulose under the effect of the ammonia solution and the explosion, resulting in physical breaks and a decrease of crystallinity. This pretreatment makes it possible to remove few lignins and hemicelluloses but can improve the enzymatic conversion for low enzyme loads. The benefits of this pretreatment are many: environmental, energy efficiency, moderate temperature, ammonia recycling and low inhibitor formation,
- **to supercritical CO2,** with many advantages, such as low cost, non-toxicity, non-flammability, are recyclable and respectful of the environment,

- **using micro-organisms or enzymes,** white rot fungi being the most used and producing enzymes (laccases and peroxidases) to degrade lignins. These biological pretreatments consume little energy and no chemicals but must extend for long enough to reach a sufficient level of enzymatic hydrolysis, which often limits their industrial use.

Due to the recalcitrance of lignocellulosic biomass new pretreatments are always tested and very often several are combined to arrive at an optimal result.

From the point of view of the cow or from the point of view of the biorefinery and whatever the type of biomass used, the complexity of the lignocellulosic biomass limits its valuation. To allow an optimal use of this biomass, it is crucial to identify which are the locks that limit the access and the use of the polysaccharides present within the walls.

II. Cell wall in grasses

Investigating the relationships between the lignocellulosic biomass and its degradability does not go without a good understanding of its biochemical components and structure. All plant cells present a wall, called “cell wall”, which is playing many key roles: it strengthens the plant structure, but also takes part in plant growth, cell differentiation, intercellular communication, water movement and defence against biotic or abiotic stress.

However some plant orders show specificities in the biochemical composition of the cell wall and its structure. Thus significant compositional differences between grass (which are monocots) and dicots cell walls have been known for now more than 50 years (Higuchi et al., 1967). Whereas the overall architectures of grass and dicot cell walls are similar in that they both consist of a network of cellulose fibers surrounded by a matrix of non-cellulosic polysaccharides, they differ considerably in the types and relative abundance of non-cellulosic polysaccharides, cross-linking of the polysaccharides, and abundance of proteins and phenolic compounds (Vogel et al., 2008).

a) Structure

The type of cell wall present in grasses (family Poaceae) is common to other monocots (like sedges, rushes, and gingers) and is called a type II cell wall. It is composed of cellulose fibers encased in glucuronoarabinoxylans (GAX), high level of hydroxycinnamates and very low levels of pectin and structural proteins (Table 1) they may also contain significant quantities of mixed linkage glucans (MLG).

Table 1: Approximate composition [a] (% dry weight) of typical dicot and grass primary and secondary cell walls (Adapted from Vogel, 2008)

	Primary wall		Secondary wall	
	Grass	**Dicot**	**Grass**	**Dicot**
Cellulose	20–30[b, c]	15–30[c, d, e]	35–45[c, f]	45–50[c]
Hemicelluloses				
Xylans	20–40[d]	5[c]	40–50[c, g]	20–30[c, g]
MLG	10–30[d]	Absent	Minor	Absent
XyG	1–5[c, d, g]	20–25[g]	Minor	Minor
Mannans and glucomannans	Minor	5–10[d]	Minor	3–5[g]
Pectins	5[c]	20–35[d]	0.1[c]	0.1[c]
Structural proteins	1[d]	10[d,e]	Minor	Minor
Phenolics				
Ferulic acid and ρ-coumaric acid	1–5[c, d]	Minor (except order Caryophyllales)	0.5–1.5[c]	Minor (except order Caryophyllales)
Lignin	Minor	Minor	20[c]	7–10[c]
Silica			5–15[c]	Variable

[a] Numbers in this table were taken from several sources to provide rough approximations of generalized cell wall composition from typical dicots and grasses. Some of the numbers are averages or ranges based on multiple sources.

[b](Mitchell et al., 2007) [c](Ishii, 1997) [d](O'Neill and York, 2003) [e](Zblackis et al., 1995)

[f](Hatfield et al., 1999) [g](Ebringerova et al., 2005)

MLG : Mixed linkage glucans - XyG : Xyloglucans

Plant cells grow by expanding their cell walls through a process of controlled polymer creep. Several layers are built by the cell wall along its development.

The cell wall is organizing in 3 main layers (Figure 5):

- the middle lamella which is rich in pectins. It is the first layer synthetized and it plays a role of matrix between the cells.
- the primary cell wall, mainly composed of cellulose, hemicelluloses and pectins (30 % of the cell wall in dicots and only 10% in Poales (Carpita, 1996)). It is a very smooth layer compared to the secondary cell wall.
- the secondary cell wall which is set in the same time than the cell stops to grow. The building is made by successive deposits of crystalline cellulose and phenolic compounds. This is these elements which make the cell wall strong and rigid.

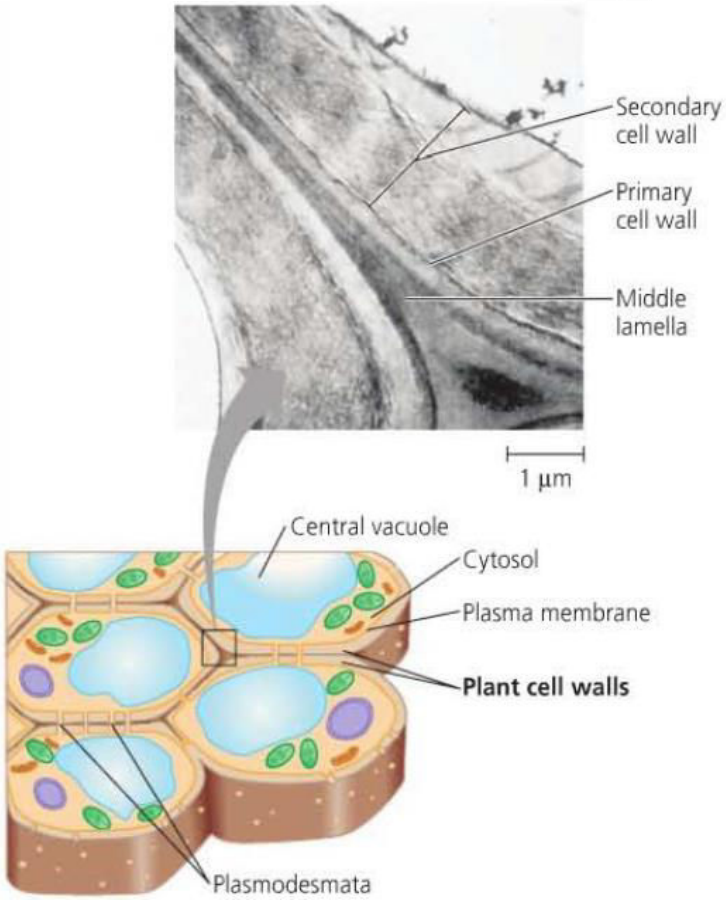


Figure 5. Electronography of the different layers composing the plant cell wall. (adapted from ©Pearson Education.)

The Figure 6 sums up the composition and proposes an organization of the different polymers within the secondary cell wall in grasses.

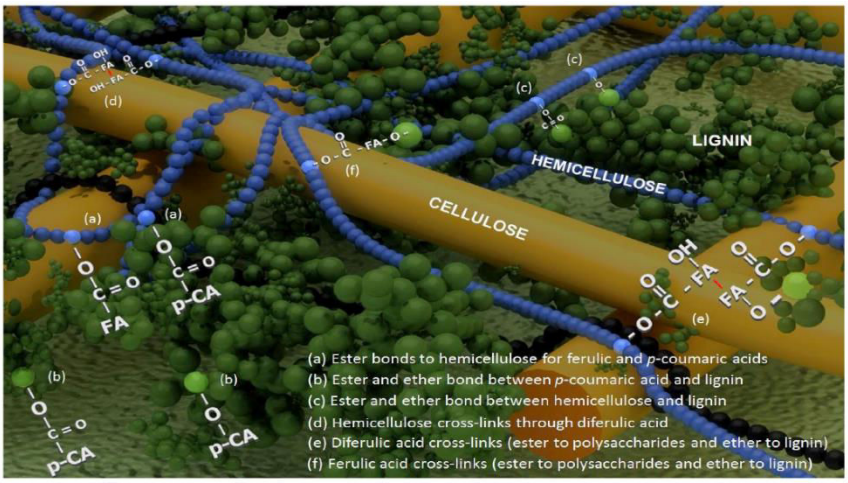


Figure 6. Model of organisation of a secondary cell wall in grasses (adapted from Barros-Rios et al., 2011)

The typical grass secondary cell wall is largely composed of 2 main catergories of components:

- polysaccharidic compounds : cellulose, hemicellulloses (specifically glucurono-arabino-xylans or GAX) and few pectins
- phenolic compounds : lignins and *p*-hydroxycinnamic acids.

The secondary cell wall of grasses comprise more than 50 % of the cell wall mass in both leaves and stem (MacAdam and Grabber, 2002; Jung, 2003). In the rest of this introduction, it is mainly the specificity of composition of the secondary cell walls which will be presented as it is the most abundant part of the cell wall at the silage stage (mature) in maize. The understanding of their composition and structure leads to more accurate hypotheses when considering their relationships with cell wall degradability.

b) Polysaccharidic compounds

1. Cellulose

Cellulose is the only polymer of the cell wall which is fully synthetized directly at the membrane of the cell. Its synthesis is made at the plasma membrane by enzymes called cellulose synthases (CESAs) (McFarlane et al., 2014). Each CESA is hypothesized to synthetize a single glucan chain by polymerizing b-D-glucose derived from cytosolic UDP-glucose (uridine-diphosphate-glucose) (Morgan et al., 2013). The number of CESA genes in the genome varies among plant species, with different sets of CESAs required for cellulose synthesis in primary and secondary cell walls (Caroll and Specht, 2011). The CESAs involved in the secondary cell wall synthesis were first identified by the characteristic phenotype of irregular xylem (*irx*) in Arabidopsis stem sections (Turner and Somerville, 1997).

Although each CESA is believed to be capable of glucan synthesis independently, in plants cellulose is synthetized at the plasma membrane by a multi protein complex called the cellulose synthase complex (CSC) (Figure 7). The structure of this complex was hypothetized a long time ago thanks to fracture/transmission electron microscopy (TEM) of various moss and vascular plants plasma membranes. They showed on the extracellular surface hexameric rosette structures approximately 25 nm in diameter (Mueller and Brown 1980; Giddings et al., 1980). It was since believed that 36 or more CESAs made up a complete CSC, based on the number of chains that could account for the observed microfibril width, and the six-fold symmetry of rosettes (McFarlane et al., 2014). However, recent work have shown that CSCs are more likely composed of either 18 CESAs (Newman et al. 2013, Oehme et al. 2015, Nixon et al., 2016) or 24 CESAs (Thomas et al. 2013, Oehme et al., 2015). With each CESA weighing

about 120 kDa, the emerging model of the CSC is a hexamer of CESA trimers or tetramers producing 18 to 24 b-(1-4)-D-glucan chains that assemble into a microfibril.

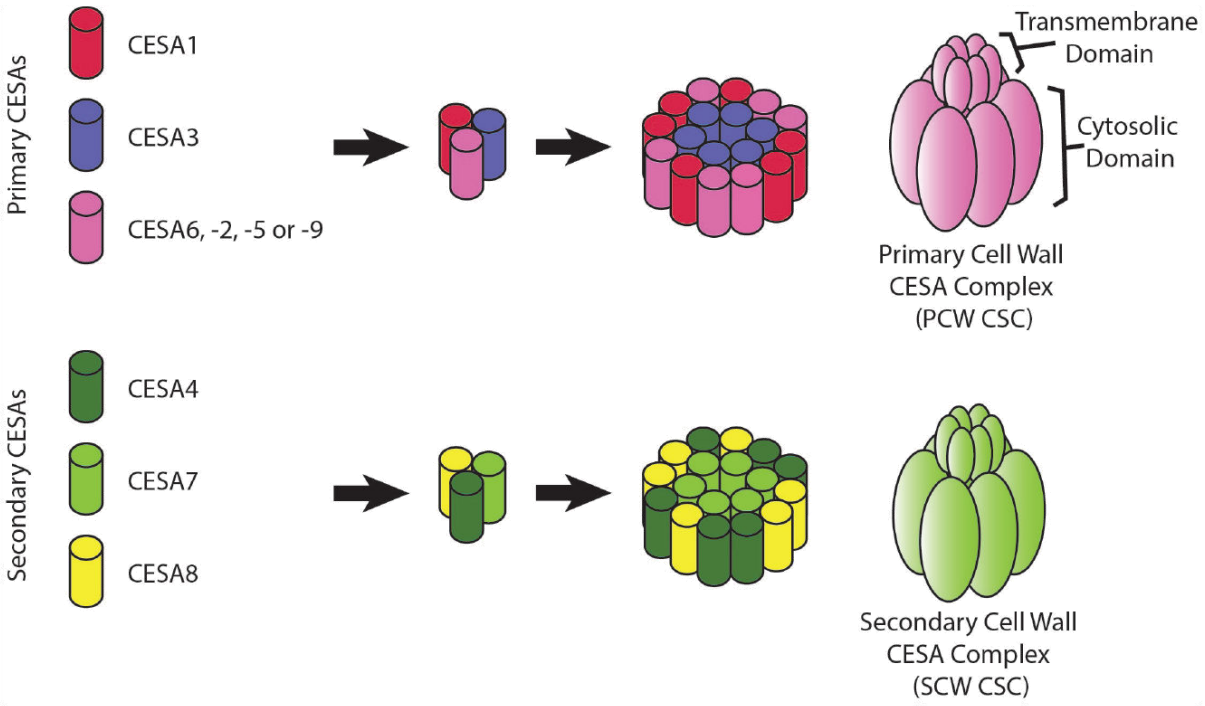


Figure 7. Cellulose synthase (CESA) in cellulose synthases complex (CSCs) organization (from Watanabe, 2018).

The structure of cellulose microfibrills may vary and can differ between the primary and the secondary cell wall (McNeil et al., 1984). The crystalline state and therefore the degree of crystallinity, of these microfibrils is one of the features that can differ and is determined by the arrangement of the individual chains within the array (Brown and Saxena, 2007). In nature, cellulose never occurs as a single chain but as a paracrystalline microfibril of many glucan chains. The free hydroxyl groups present in the cellulose macromolecule are involved in a number of intra and inter-molecular hydrogen bonds that form various ordered crystalline arrangements (Nobles et al., 2001). The most common crystalline state (allomorph) of cellulose produced is called cellulose I (Figure 8). It can be further divided into two sub-allomorphs, cellulose I-alpha and cellulose I-beta, which differ in the arrangement of their hydrogen bondings. Each microfibrill contains both types and how this ratio and so the degree of crystallinity is controlled during synthesis is still not understood. Cellulose of type II is a “man-made” from of cellulose (Figure 8) which can be obtained by dissolving cellulose and then swelling it in concentrated alkali solution (e.g. > 10 % NaOH) (Aalto University).

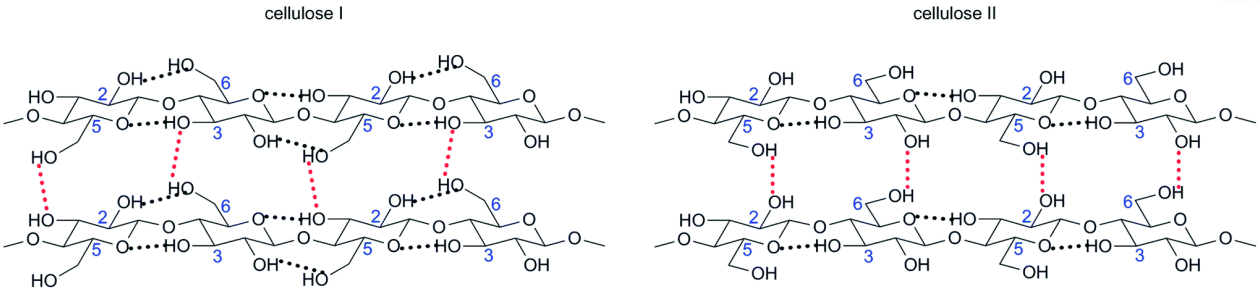


Figure 8. Distinction between cellulose I and cellulose II inter- and intra-molecular hydrogen bonds (from Credou and Berthelot., 2014).

2. Hemicelluloses

When cellulose microfibrils are extruded from the cellulose synthase complexe CSC at the plasma membrane forming the secondary cell wall, they interact with hemicelluloses and altogether they form a stable network (Simmons et al., 2016). The hemicelluloses make up 10 - 40% (of dry weight) of the secondary cell wall. They are mentioned to be essential for normal growth and development (Scheller and Ulvskov, 2010; Rennie and Scheller, 2014; Kumar et al., 2016). They are synthetized in the Golgi and then transported at the membrane to be excreted into the cell wall by exocytose (Meyer et al., 1991; Myton and Fry, 1994).

Hemicelluloses are polysaccharidic chains which are more various than cellulose in their composition and present therefore a higher diversity of structure. Basically, they are composed of a main chain of either glucans, mannans, or xylans, and they are then decorated by many simple or complex side chains. This typical structural characteristic allows hemicelluloses to make a dense network and hydrogen bonds within the hemicelluloses or even with the cellulose (Carpita and Gibeaut, 1993; Willats et al., 2001; Cosgrove, 2005). Recent studies explain that during secondary cell wall production, the Golgi is remobilized from primary cell wall production to begin assembly of xylans and manans and to modify and traffic the large number of proteins required for proper cellulose and lignin deposition such as CESA proteins, laccases or peroxydases. Synthesis of xylan alone is thought to require over a dozen proteins including glycosyl transferases, acetyltranferases, methyltransferases and many other proteins involved in transporters synthesis (Rennie and Scheller, 2014; Kumar et al., 2016).

Hemicelluloses make one of the specificity of the grasses cell wall as the main chain is composed of xylans and the decoration is composed of arabinose and glucuronic acid (Figure 9). Therefore Hemicelluloses of the grasses are mainly called glucuronoarabinoxylans or GAX.

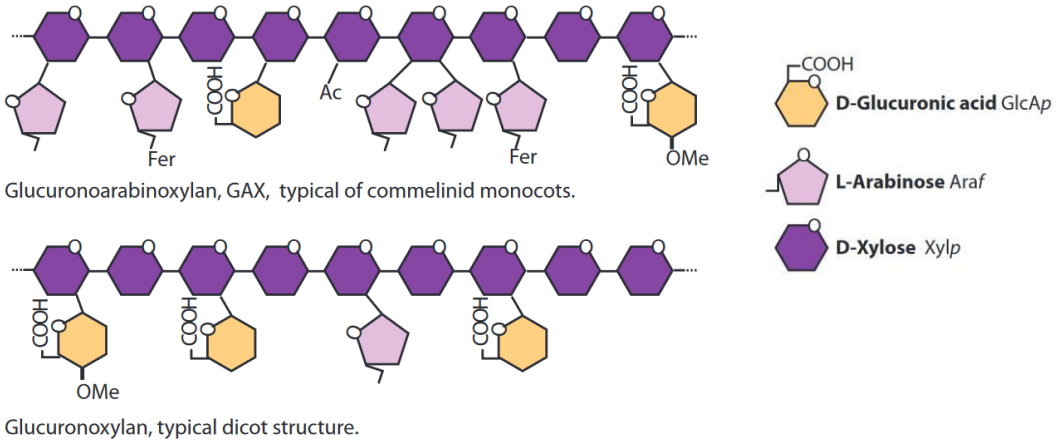


Figure 9. Structure and composition of hemicelluloses in grasses vs the composition in dicots (adapted from Scheller and Ulvskov, 2010).

As it presents a high diversity of composition and structure the way hemicellulose is inserted with the other components in the cell wall vary from one specie to another. In grasses secondary cell walls, GAX has a fewer side-chains than the GAX of primary cell walls. This results in a stronger GAX-lignins interaction (Vogel, 2008). More particularly in grasses, GAX can be connected to lignin via hydrogen bonds but also via some molecules which are also one of the particularity of this family: the *p*-hydroxycinnamic acids. It has been shown that ferulic acid esters could bind GAX on the arabinan (Lam et al., 1992). These ferulic esters would be already bond in the Golgi by a feruloyl transferase from a feruloyl-glucan precursor (Obel et al., 2003). Several studies point out the importance of this binding as the ferulic esters may polymerize in dimers which can form bridges within hemicellulose (Ralph et al., 1994) but also between hemicelluloses and lignin (Grabber, 2005).

3. Pectins

Although not particularly abundant in secondary cell walls of grasses Pectin is one of the most complex family of polysaccharides in nature. It composes about 35 % of primary cell walls in dicots and 2 to 10 % of the grasses primary cell wall (O'Neill et al., 1990; Ridley et al., 2001). Pectin is therefore abundant in cell walls that surround growing and dividing cells but also in the junction zone between cells with secondary walls including xylem and fiber cells in woody tissue (Mohnen, 2008).

Chemically, pectin can be extracted from cell wall using hot acid, mild alkaline treatment and chelating compounds (Scheller et al., 2007). The composition of the pectin obtained is generally approximatively of 70 % of galacturonic acid. The different polymers composing this galacturonic acid part is divided into homogalacturonan (HGA) which represents up to 65%, rhamnogalacturonan I (RGI), rhamnogalacturonan II (RGII) and xylogalacturonan (XGA) (Willats et al., 2001). It has been suggested that these polymers would

covalently linked altogether suggesting a strong network of polysaccharides (Ishii and Matsunaga 2001, Nakamura et al., 2002)

Globally, the most abundant pectic polysaccharide is homoglacturonan (HG), a linear polymer of alpha-(1-4)-galacturonic acid. Then different polysaccharides can be then acetylated, or esterified to decorate the polymer (Figure 10).

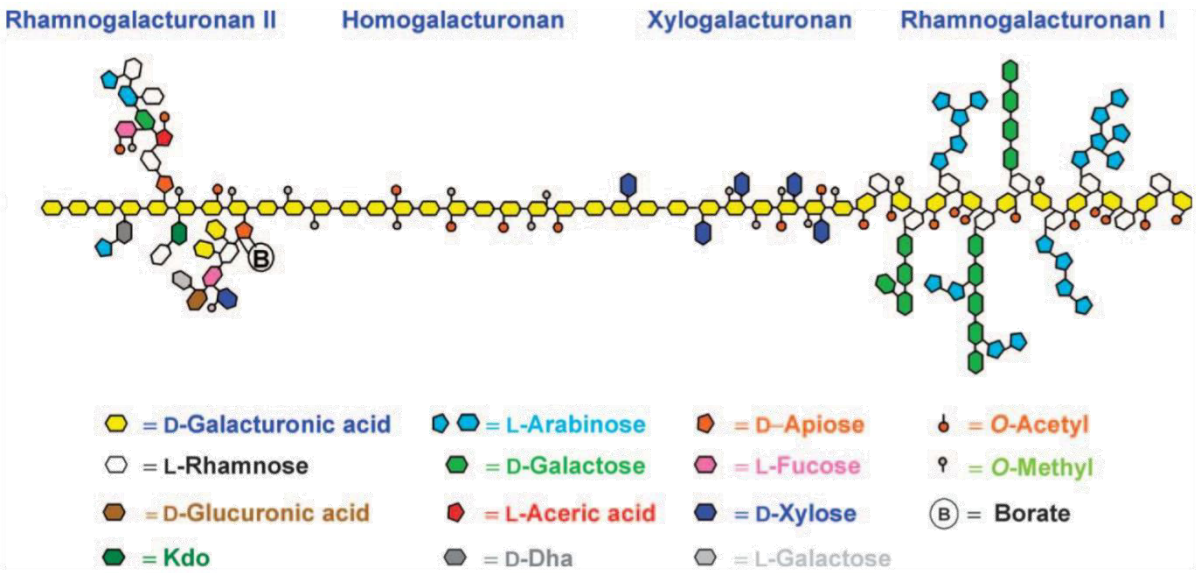


Figure 10. Schematic structure of pectin (from Scheller et al. 2007). The figure illustrates the four different domains of pectin that are generally found. The relative abundance of the different types of pectin varies but rhamnogalacturonan I (RGI) and homogalacturonan are the major components, whereas xylogalacturonan and rhamnogalacturonan II (RGII) are minor components. Many different variations exist especially on the side chains of RGI.

The other pectic polysaccharides are more complex in structure than HG. The most structurally complex pectin is the substituted HG: rhamnogalacturonan II (RG-II) which makes up to 10 % of pectin. Its structure is largely conserved across plants species and consists in a linear chain of alpha-(1-4)-galacturonic acid decorated with side branches of polysaccharides in over 20 different linkages (Mohnen, 2008). RG-II dimerization is possible and form cross-links with HG domains which from a macromolecular pectin network (Matsunaga et al., 2004).

The correlation of increased amounts of pectin RG-II in vascular plants and its appearance as plants adapted to growth on land and developed lignified secondary walls (Matsunaga et al., 2004) suggests that pectin has fundamental roles in both primary and secondary cell wall structure and function. In 2005, Zykwinska et al., thanks to a surface complementarity study, showed on sugar beet and potatoe some interactions between pectins and cellulose microfibrils.

c) Phenolic compounds

Plant cell wall phenolic compounds consist of two main groups of components: 1- lignin, a complex polymer of pcoumarylic (H), coniferylic (G) and sinapylic (S) alcohols, and traces of potential atypical subunits (acids, aldehydes, etc…) and 2- para-hydroxycinnamic acids (ferulic and pcoumaric acids mainly in grasses) which have a much lower molecular weight than lignin. These two main groups may bind to various cell wall components and the last one is also involved in cross linkages (Wallace and Fry, 1994). Cell wall phenolic compounds are thought to have several important roles in providing mechanical strength, regulation of growth and morphogenesis, and responses to stresses and pathogens.

1. Lignins

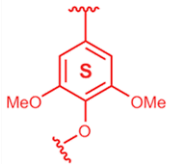
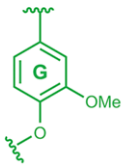
As it is the major component of the wood in the wood species, lignins are the second most abundant biopolymers on earth after cellulose. The lignification process is a major innovation in the adaptation of plant on earth. Over the course of the adaptation of the bryophytes (mosses phylogenetic group), the lignification of the vascular system through tracheid structure in Monilophytes and Licopodiophytes (ferns phylogenetic groups) allowed plants to colonize much more efficiently the aerial environment. It is now remarkable through the amount of forest and the height that wood species can reach (Koch et al., 2004). Lignins make the cell wall rigid, their hydrophobicity allow a good conductivity of the ions and the water in the xylem tubes.

Lignification is a process which starts in the middle lamella at the particular moment where the secondary cell wall develops and get thicker. Then it spreads to the primary cell wall and progressively reaches the secondary cell wall (Chesson et al., 1997). If the lignin concentration is the highest in the middle lamella and in the primary cell wall (Wilson and Hatfield, 1997), it is the secondary cell wall which present the highest amount of lignin in the plant because of its consequent thickness (1-5 µm vs <1µm in the primary cell wall and the middle lamella).

i. Composition of the lignins

Lignins comprise a substantial portion (20% to 30%) of the grass secondary cell wall and essentially fill the pores between the polysaccharides (Campbell and Sederoff, 1996). Unlike these ones, lignin is a heteropolymer of 4-hydroxyphenylpropanoids derived from the phenylalanine amino acid but also the tyrosine amino acid in maize (Baucher et al., 1998). It is the presence of the three phenyl propane units: sinapyl alcohol, coniferyl alcohol and p-coumaryl alcohol at the oxidized state which allow the coupling into S-, G-, H-lignin, respectively (Table 2).

Table 2. Structure and nomenclature of the lignin monolignols (adapted from Ralph, 2010)

Structure & Symbol			
Unit	Syringyl	Guaiacyl	*p*-Hydroxyphenyl
Alcohol	Sinapylic	Coniferylic	*p*-Coumarylic

Grass lignin is primarily composed of guaiacyl (~35–49%) and syringyl (~40–61%) units. It also contains a small but significant percentage (~4–15%) of *p*-hydroxyphenyl units that are only found in trace levels in dicot lignin (Grabber et al., 2004). The monolignols units are synthetized in cytosol via the general phenylpropanoid and monolignol biosynthetis pathways (Figure 11). This has been demonstrated by many studies with loss of function mutants and knoch-downs genes of the key enzymes participating to this biosynthesis and in several species like Arabidopsis, poplar and alfalfa (Bonawitz and Chapple, 2010).

Monolignol are first oxidized, presumably by laccases and/or peroxydases, to form a radical monomer (Achyutan et al., 2010). After their synthesis, the monolignols are thought to be transported under a glycosylated form to the cell wall where oxidative polymerization takes place (Steeves et al., 2001). This last step in lignin synthesis is still not completely described but many studies admit the involvement of peroxidases (among others enzymes) to catalyse the production of monolignol radicals (Onnerud et al., 2002; Boerjan et al., 2003; Barcelo et al., 2004). Then the formation of the polymer result from radical couplings between two dehydrogenated compounds, the oxidized monomer and the growing polymer phenoxy radical (endwise polymerization) or two oligomer phenoxy radicals (bulk polymerization) (Brunow, 1998).

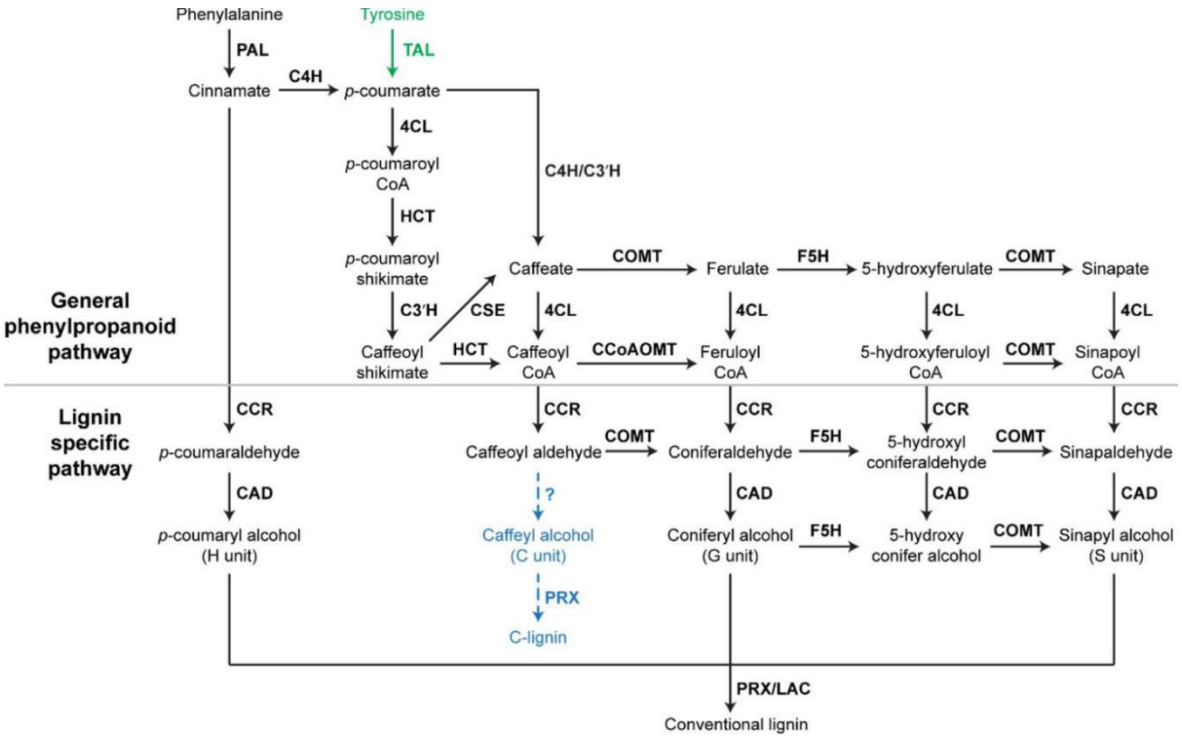


Figure 11. A scheme of lignin biosynthesis in plants. Black arrow indicates the canonical lignin biosynthesis in plants. Green arrow indicates the tyrosine shortcut pathway found in *Brachypodium distachyon*. Blue dashed arrow indicates the putative C-lignin biosynthesis pathway found in seed coats of vanilla orchid and most Cactoidae genera. Bold font indicates enzymes. PAL, phenylalanine ammonia-lyase; C4H, cinnamate 4-hydroxylase; 4CL, 4-coumarate: CoA ligase; HCT, quinateshikimate p-hydroxycinnamoyltransferase; C3'H, p-coumaroylshikimate 3'-hydroxylase; CCoAOMT, caffeoyl-CoA O-methyltransferase; CCR, cinnamoyl-CoAreductase; F5H, ferulate 5-hydroxylase; CAD, cinnamyl alcohol dehydrogenase; COMT, caffeic acid O-methyltransferase; CSE, caffeoyl shikimate esterase; PRX, peroxidase; LAC, laccase (adapted from Xie et al., 2018).

Within the polymer, the three main lignin subunits can connect between each other through different type of linkages. The type of linkage called "condensed" is named so because these linkages are chemically strong and difficult to degrade chemically or enzymatically. The "condensed" linkages comprise carbon-carbon linkages such as 5-5, beta-1, beta-5 and beta-beta and diaryl ether linkages such as 4-O-5. Another type of linkage is called "non-condensed" or "labile" and qualify ether linkages like alpha-O-4 and beta-O-4. The beta-O-4 linkage is the most frequent in the natural lignins and is generally the target of the chemical degradation by thioacidolysis or oxidation (Lapierre et al., 1995). The ratio of each of these linkages depend especially on the supply speed in monolignols. When monolignols are brought to the cell wall quickly, as it is the case in the middle lamella and the primary cell wall, 2 radicals monomers may spontaneously bind, establishing a covalent linkage between the 2 sub-units (Vanholme et al., 2010). The formed dimer is then dehydrogenated and is bound to the growing polymer. This process conducts at a polymer formation called "bulk" (Syrjanen and Brunow, 2000). In

this case, Mechin et al 2007 showed that the C-C linkages (beta-beta, beta-5) were favored. In the secondary cell wall, the monolignols are provided much slower and this would be an explanation for a higher amount of ether linkage between the monomers: beta-O-4 linkages (Jurasek, 1998; Mechin et al., 2007). In the secondary cell wall, the lignin polymer is therefore less condensed and rather linear.

The proportions of the different type of monolignol composing lignin polymer differ a lot between species. In Gymnosperms, Coniferophytes lignins are composed of 5 % of H, 95 % of G and traces of S. In dicots, only traces of H are found, 14 to 66% of G and 34-86% of S. In Monocots, and particularly in Poaceae, the lignin found in the straw of wheat presents 5 % of H, 49% of G and 46% of S; in the straw of rice, lignins are composed of 15% of H, 45 % of G and 40% of S. In maize stem, the proportion are 5% of H, 49% of G and 46% of S (Pouzet, 2011). This shows a natural diversity of the lignin composition between groups, families and even species of the same family. But in addition to this structural and chemical variability, it is possible to observe a spatial diversity of the lignification within the plant, and particularly during the development of the stem of the plant, which goes along with the secondary cell wall deposition.

ii. Impacts of the modifications of the lignin biosynthesis pathway

Modification of monolignol metabolism has a strong impact on plant growth. It has been shown in arabidopsis mutants for *c3'h, hct* and *cse* (genes encoding for key enzymes in the monolignol biosynthesis pathway) which present a dwarf phenotype (Bonawitz and Chapple, 2010; Vanholme et al., 2012). These phenotypes were mainly explain by a great reduction in the lignin content. However, in 2015 Anderson et al., showed in Arabidopsis disrupted for genes encoding cinnamyl alcohol dehydrogenases that the dwarf phenotype was not associated to a reduction of the lignin content. Indeed, in these mutants, the lignin content did not differ from the wild type but the amounts of hydroxycinnamaldehyde monomer incorporated did differ. This demonstrates that the composition and structure of lignin is also very important for the mechanical properties of the cell wall, not only the lignin content.

More recently, mutants for cinnamoyl CoA reductase which leads to cell wall deficient in lignin content was shown to be associated to a decrease of the proportion of oriented cellulose fibrils in Arabidopsis (Liu et al., 2016). The modification of the orientation and the order of cellulose fibrils was observed in all tissues of the stem and it suggests that the impacts on the lignin biosynthesis pathway have direct consequences on the structure of other cell walls components.

It exists some natural mutation in Poaceae which impact directly the biosynthesis of monolignols and the structure of the lignins in the plant. More particularly, in maize, brown-midrib mutants have been reported for now 90 years. Maize brown-midrib mutants exhibit a reddish-brown pigmentation of the leaf midrib and stalk pith, associated with lignified tissues (Figure 12). They were first described and investigated successively by Kiesselbach (1922), Eyster (1926), and Jorgenson (1931). The latter established that these three brown-midrib mutations were «due to identical factors» and that the corresponding «brown-midrib character» segregated as «a simple Mendelian recessive » trait. This gene was then named *bm1*. A second non-allelic mutant was described by Burnham and Brinks (1932) which was named *bm2*. A little later, two other genes inducing the brown-midrib phenotype were described as *bm3* (Emerson, 1935) and *bm4* (Burnham, 1947). Since its identification in maize, the brown midrib mutants have been isolated in two other C4 grasses, sorghum (Sorghum bicolor) (Porter et al., 1978) and pearl millet (Pennisetum glaucum) (Chemey et al., 1990). The *bm1* gene, the *bm2*, *bm3*, and *bm4* genes originated from natural mutations and segregated as simple Mendelian recessive traits. No new maize brown-midrib mutations were characterized for nearly 60 years after the Burnham's paper (1947), despite the mention of additional natural brown-midrib mutants in the MaizeGDB database. Recent allelic tests of these latter mutants allowed to discover 3 new *bm5*, *bm6* and *bm7* mutations (Haney et al., 2008; Ali et al., 2010). However, the *bm7* mutant was shown to be allelic to bm1 afterwards (Barrière et al., 2013).



Figure 12. Brown-midrib line F7803bm1 (from Barrière, 2017)

As all the *bm* mutations are associated with reduced lignin contents and altered lignin composition compared to wild type (Chemey et al., 1990) two-brown midrib mutations have been shown to alter genes of the monolignol pathway : the *bm1* and the *bm3* mutations. More particularly the *bm3* mutation provokes a significant decrease in the lignin content, but also in the *p*-coumaric acid content which is twice lower than for normal plants. This is due to the COMT which is completely inactivated and depleted therefore a lot the lignin composition in S subunits (Barrière et al., 2004). And as the COMT is depleted, 5-Hydroxy-coniferyl alcohol (or 5-OH-G) is accumulating from the substrate of the COMT, the 5-hydroxy-coniferaldehyde.

Thus lignin in plants, and therefore in grasses, show a great complexity as well as a major role into the development, the resistance to biotic and abiotic-stresses, and are a key component of the lignocellulosic biomass recalcitrance.

2. *p*-hydroxycinnamic acids

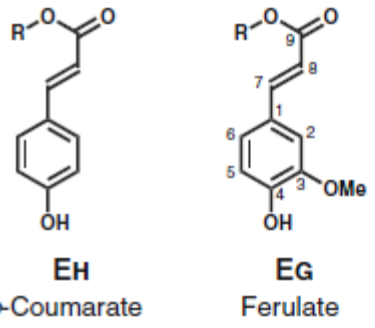


Figure 12. *p*-coumaric acid and ferulic acid structure (adapted from Ralph et al. 2010)

One of the specificity of the grasses cell wall is the rather elevated amount of *p*-hydroxycinnamic acids and particularly the *p*-coumaric and the ferulic acids (Figure 12). As lignins, these acids also come from the phenylpropanoid biosynthesis pathway, while the synthesis of the ferulic acid stays poorly understood, and are able to form ester and/or ether linkages to cell wall polymers.

i. Ferulic acids

Ferulic acid (FA) was first isolated in 1866 from Ferula foetid (Fazary and Ju, 2007). It is found in the two types of cell walls, either in the primary or in the secondary cell wall (Harris and Hartley, 1976). It is the most abundant in the epidermis, the xylem vessels, the bundle sheaths and sclerenchyma (Faulds and Williamson, 1999).

In monocotyledons, and more particularly in grasses, the ferulic acid plays an important role of structuration of the cell wall. It is ester-linked on side chains of arabinose within hemicelluloses (Ralph and Helm, 1993; Wende and Fry, 1997). It may also realize cross-linking between cell wall polysaccharides thanks to different conformations (Figure 13). Ralph and al. showed in 1994 and 1995 that ferulic acids were able to form dimers (Figure 13-b) altogether and thus cross-link arabinoxylans chains to each other. Bunzel et al reported in 2005 and 2008 that ferulic acids could even form higher order oligomers like trimmers and tetramers in maize bran. It may also links to the lignins (Figure 13-c) via ether bounds (Ralph et al., 1994, 1995; Ishi et al., 1997) and preferentially on the G subunit of the lignins (Kondo et al., 1990, Jacquet et al., 1997). As the G and H subunits would be deposited first in the lignin polymer it suggests that this linkage happen in the early stage of the lignification. MacAdam et al proposed in 2002 that the cross-linking between arabinoxylan and lignins would be the mechanism indicating that grass cells end their elongation process and shift from primary to secondary wall development.

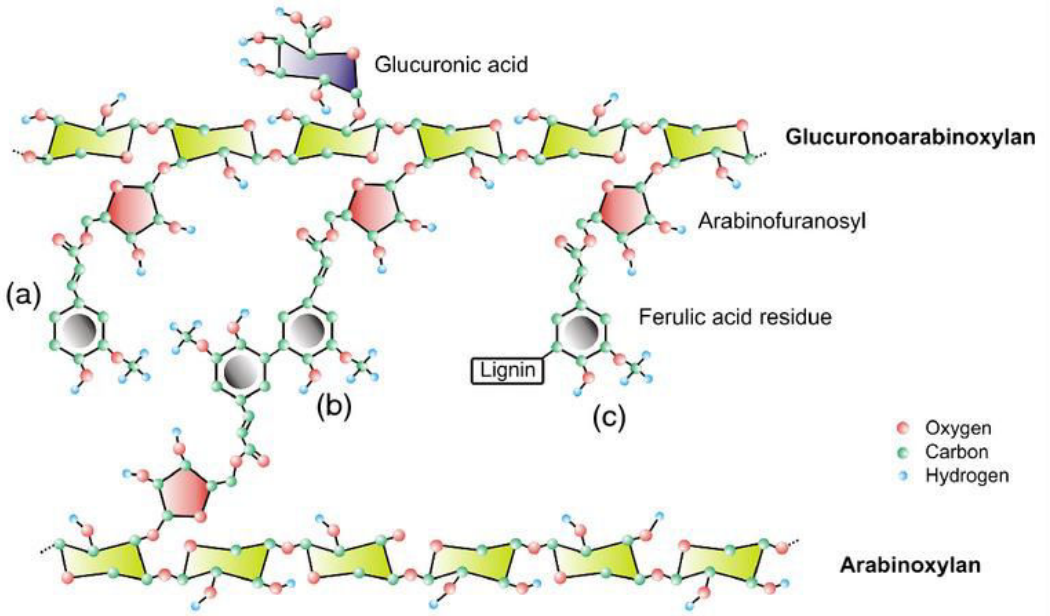


Figure 13. Different way of ferulic acid to bond hemicelluloses and/or lignins. a. ferulic acid residue esterified to the hemicelluloses arabinoxylan chains. b. diferulic acid cross-linking two FA-GAX. c. ferullic acid residue ponting lignin to hemicelluloses (from De Oliveira, 2015).

Candidate genes involved in feruloylation of arabinoxylans were first identified by differential expression between grasses and dicots (Mitchell et al., 2007) as residing within a clade of genes in the BAHD acyl-coenzyme A (CoA) transferase superfamily. The most likely candidate within this clade for involvement in arabinoxylan feruloylation based on absolute expression level and co-expression was identified as the rice gene LOC_Os01g09010. Suppression of this gene by RNA interference (RNAi) in rice was correlated with decreased cell-wall FA (Piston et al., 2010).

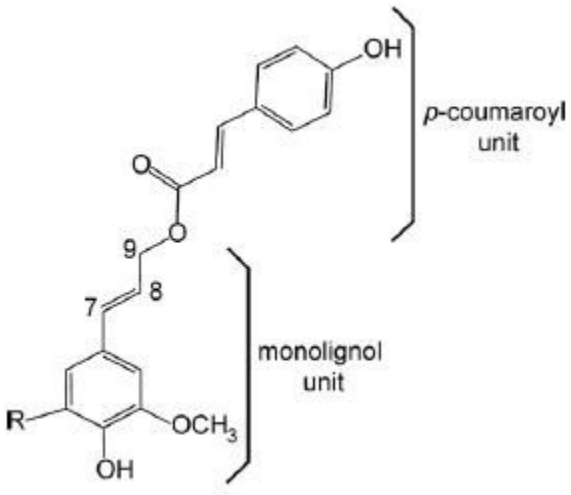


Figure 14. Molecular diagram of the *p*-coumaroylation of the monolignols in grasses. R= H for coniferylic alcohol; R = OCH3 for sinapylic alcohol (Lu and Ralph, 1999; Hatfield et al., 2009) (From Zhang, 2012).

ii. *p*-coumaric acids

In grasses, the esterified *p*-coumaric acid (PCAest) is found mainly acylated to S subunits of the lignins with an ester bound (Grabber et al., 1996a; Lu and Ralph, 1999). Until 40 % of the lignins may be acylated (Whiters et al., 2012). More particularly, it was demonstrated by structural analyses of lignin in maize that PCAest is exclusively attached to the C-9 (or γ) position (Figure 14) of the monolignols.

After the acylation of PCAest on a monolignol unit by an enzymatic process, the conjugated form is transfered at the cell wall and incorporated into the lignin polymer by polymerisation. In 2008, Hatfield et al even proposed that the acylation of the monolignols by *p*-coumaric acid would help to initiate the monolignol deposition.

With *p*-coumaric acid levels reaching until 18% of the maize cell wall lignins, the acylated monolignols represent a very high fraction of the monomer pool of the lignins. Still, Ralph reported in 2010 that if *p*-coumaric acid could have radicals polymerized on it *in vitro*, no evidences were leading to think that the same was happening into grass cell walls. In 2009 Hatfield et al proposed that the *p*-coumaroylation of the S subunits could be a good way to incorporate radicals into the lignin polymer. Indeed, a transfer of the radical on the *p*-coumaric acid onto the S subunit would be enhanced and would therefore allow their incorporation into the lignin polymer (Figure 15). The function of this acylation still needs to be understood completely.

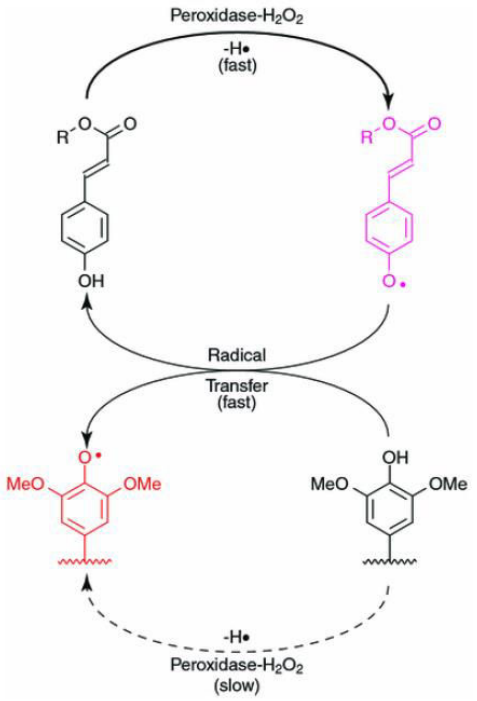


Figure 15. Hypothetical model of radical transfer from *p*-coumaric acid to S subunit of lignins (Hatfield et al, 2009).

As reviewed by Wang et al., (2013) several studies on transgenics plants with higher or lower feruloylation levels have suggested that some members of the BAHD acyl-CoA transferase protein family may be responsible for catalysing the addition of ester-linked coumarate to cell wall arabinoxylans (Piston et al., 2010; Withers et al., 2012; Bartley et al., 2013; Molinari et al., 2013). A member of the BAHD acyl transferase family was also identified in rice genome (Withers et al., 2012). Analyses of the recombinant protein produced in E. coli showed that it had a specific coumaroyl transferase activity. This enzyme OsPMT (O. sativa p-coumaric acid monolignol transferase) catalyzes the acylation of a monolignol with p-coumaric acid via p-coumaroyl CoA.

Karlen et al., (2018) confirmed in a recent study within nine families belonging to the same monophyletic group than Poaceae that, as in the Poaceae, lignin-linked p-coumarate occurs exclusively on the hydroxyl group on the γ-carbon side chains of lignin units, mostly on syringyl units. Although they did not study the mechanism of acylation directly in these species, they hypothesized that this acylation would occur similarly as in the Poaceae, acylated by BAHD acyl-CoA monolignol transferases.

So far, we have seen many characteristics of the cell wall structure and composition, which is why we may now wonder if this lignification presents spatial particularities according to the tissue within the maize stem.

III. Distribution of the lignification within the maize stem tissues

a) Tissue anatomy in maize

One of the main differences between dicotyledon and monocotyledon stems is that dicot stems have a circular arrangement of vascular tissues, whereas the stems of monocotyledon have vascular tissue bundles scattered within the whole stem (Figure 16).

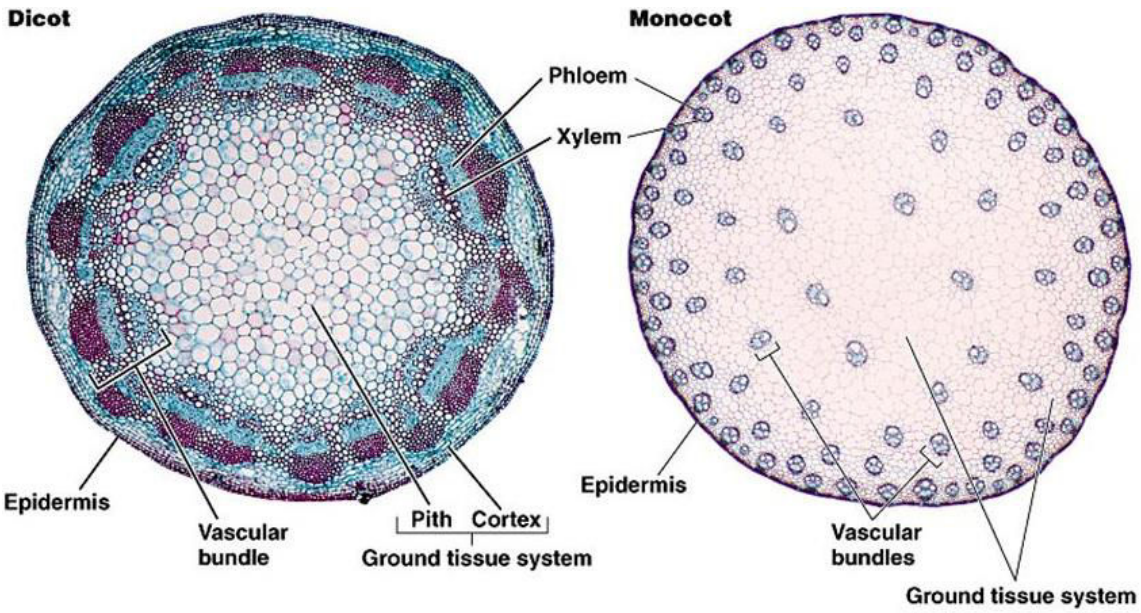


Figure 16. Comparison between the anatomy of a dicotyledon stem and a monocotyledon stem (Benjamin Cummings, Pearson Education, 2003)

As a monocotyledon, Maize has a stem of the second type (Figure 16). Particularly, the parenchyma, colored in pink/magenta in the figure 17, is usually composed of cells with a thin cell wall and a large vacuole (Bowes and Mauseth, 2012). These cells form a continuous tissue in the pith of the stem. If the cell wall is thin, in the pith, the parenchyma cells present generally a thick secondary cell wall.

In the Gramineae, there are two types of arrangement of vascular bundles: in the first one they are arranged in two circles, the outer circle consisting of thin bundles and the inner of thick bundles, for example in: *Triticum, Hordeum, Avena,* and *Oryza*; and in the second type the bundles are scattered throughout the entire cross-section of the stem, for example in: *Sorghum, Saccharum*, and *Zea*. However in this second type, the vascular bundles within the pith are much bigger than peripheral ones. As these latter are enclosed by a bundle sheath of

parenchyma cells, the type of vascular bundles is called “closed”. Xylem and Phloem are disposed in opposition to each other. The phloem cells, colored in teal in figure 17, are all concentrated in one spot and present low lignified cell walls. On the other side of the vascular bundle, xylem cells are sorted in different type, the smallest ones at the edge are constituting the protoxylem and the two bigger ones are called the metaxylem. The cell walls of the xylem are strongly lignified (Bowes and Mauseth, 2012).

More particularly in the cortex of a maize internode, vascular bundles present a tissue particularity: they are surrounded by a sclerenchyma sheath (Metcafe, 1960; Figure 17). Sclerenchyma is characterized by thick and much lignified secondary cell walls (Bowes and Mauseth, 2012). Cells in sclerenchyma are dead and the protoplasts which were constituting them died during the maturation of the tissue. It constitutes the main supporting tissue of the mature stem and forms in monocot lignified fibers.

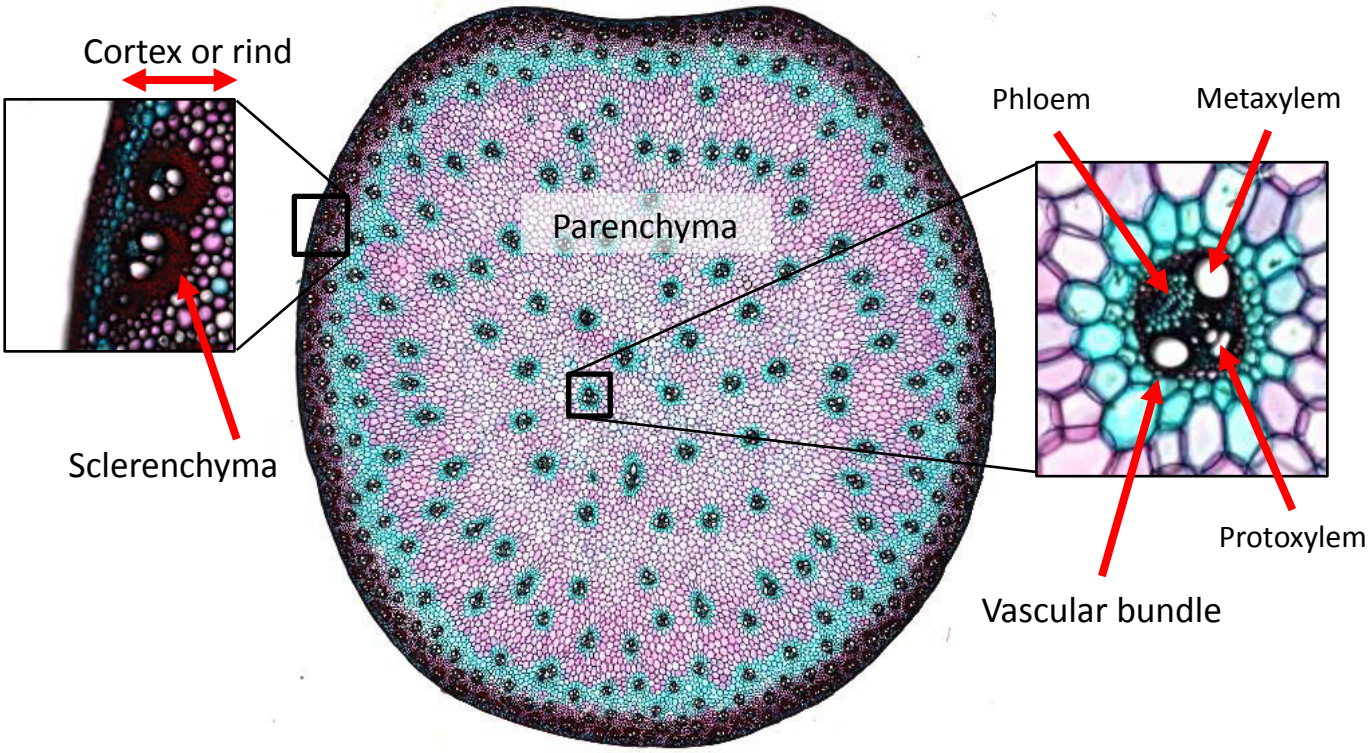


Figure 17. Tissue anatomy of the maize stem. (Cross-section of the internode carrying the main ear, harvested at silage stage)

As presented by the Figure 17, all the diversity of tissues are stained with FASGA (for Fuschina Alcian blue Safranina Glycerina Agua; Tolivia and Tolivia, 1987) to be further analysed. Many techniques and methods exist to investigate the lignification within the tissues, and part of them will be exposed hereinafter.

b) Methods to investigate the tissue specificities

I chose to present actual methods of staining and imaging to quantify and investigate further the distribution of the lignification in tissues through the second part of the accepted chapter in Chimie Verte et IAA (Ed. Stéphanie Baumberger – Lavoisier) : « L'imagerie, un outil puissant pour étudier les variabilités de répartition et de composition des tissus de la biomasse lignocellulosique - Perspectives dans l'amélioration de la dégradabilité des parois chez le maïs » by Valérie Méchin, Matthieu Reymond, David Legland, Mathieu Fanuel, Fadi El Hage, Aurélie Baldy, Yves Griveau, Marie-Pierre Jacquemot, Sylvie Coursol, Marie-Françoise Devaux, Hélène Rogniaux, and Fabienne Guillon.

As far as phenolic constituents are concerned, all studies show that lignin content is the first factor that is negatively correlated with the degradability of the walls (Jung and Deetz 1993, Méchin et al., 2000 and Méchin et al., 2005). Lignins limit the degradability of the walls both by their bonds with the polysaccharides within the wall but also by their hydrophobic properties, absorbing and preventing the progression of cellulolytic enzymes. However, a drastic reduction in lignin levels can not be considered since this decrease also leads to a significant loss of agronomic performance of plants such as height, resistance to lodging and pest attacks. For this reason, several groups have focused their research on other factors besides the lignin content to improve the degradability of plants. Our work has repeatedly emphasized the strong impact of lignin structure and the amount of p-coumaric acid on the limitation of wall degradability (Méchin et al., 2000, Mechin et al., 2005; et al., 2011, Mechin et al., 2014, El Hage et al., 2018). The ferulic acid content is also a factor that can limit the degradability of the walls. As regards polysaccharides, the presence of acetyl groups or side chains on hemicelluloses negatively affect the release of sugars. It is the same with the level of crystallinity of cellulose.

In this chapter, we have chosen not to detail the impact of biochemical factors on degradability variations. The literature is already very rich in this respect and we decided to focus on the impact of the distribution of lignified tissues within the stems on the degradability of the biomass. This distribution varies according to the genotype, the development stage of the plant and the hydric conditions of culture, and it is an important lever to modulate the degradability of the walls. It is therefore crucial to develop powerful analytical tools to characterize biomass and update the parameters to be selected to improve degradability or to allow significant resilience to plants in the current context of global warming.

1. Imaging techniques

According to the representative scale of the structures of interest, various image acquisition devices can be used to study their morphology, their spatial organization or their chemical composition (Rousseau et al., 2015). Historically, microscopy was the technique used to study plant anatomy at the cellular or tissue level. Macroscopic image acquisition systems have also been developed. They allow to quickly observe surfaces of the order of the cm2 with a minimum sample preparation, which allows to observe large series. Confocal microscopy has emerged as a means of volumetric investigation of samples with a gain in axial resolution and minimal preparation.

For imaging at the cell wall or organelle level within cells, electron microscopy has often been the method of choice, reaching nanoscale resolutions. The 3D structure can also be explored, either by combining scanning electron microscopy with the serial section of the sample (Bhawana et al., 2014), or by adapting the tomography algorithms to transmission electron microscopy. Magnetic resonance imaging (MRI) and X-ray tomography are popular methods for the non-destructive study of the 3D architecture of biological samples, without requiring staining, sectioning or inclusion. The high resolution obtained by tomodensitometry (below the micron) is often the best method for the study of plant organs (Stuppy et al., 2003, Cloetens et al., 2006, Dhondt et al., 2010). We present briefly some techniques commonly used in our laboratories.

i. Darkfield microscopy

Darkfield microscopy is a simple method that makes non-colored and transparent objects visible. It is used to visualize small objects such as bacteria or in the case of plant tissues, cell structures. In this mode, the central light rays along the optical axis of the microscope, which usually pass through and around the sample are blocked. Only oblique rays from large angles strike the sample. They are diffracted, reflected and / or refracted by optical discontinuities, such as the cell membrane, nucleus and internal organelles, allowing these rays to reach the objective. A macrovision device based on this principle was developed at INRA in Nantes to observe plant tissues (Devaux et al., 2009) (Figure 18.1). The speed of sample preparation and acquisition makes it possible to image large series on which image analysis processes can then be applied to extract morphological parameters such as cell size, beam size and density. at the scale of the observed section and compare different genotypes on morphological criteria (Legland et al., 2012; Legland et al., 2014).

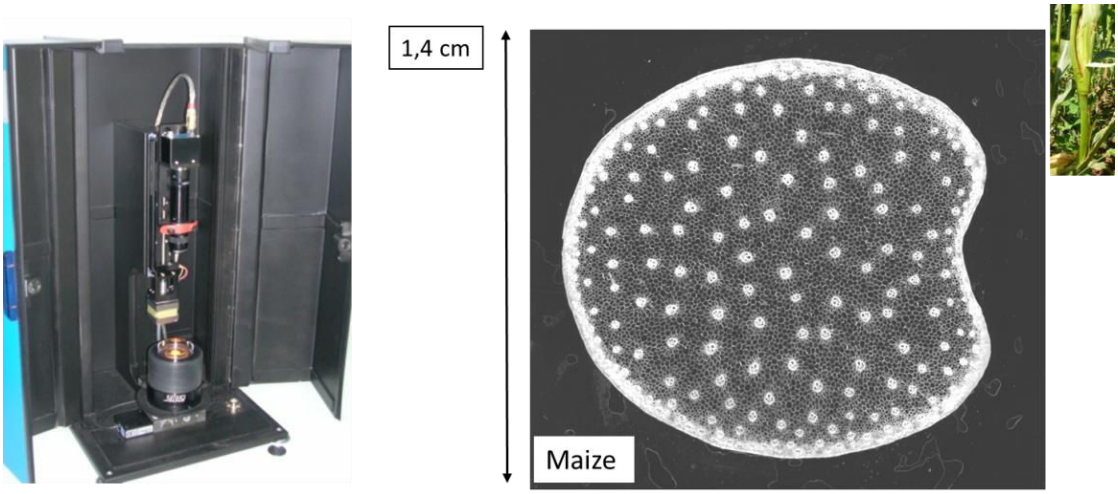


Figure 18.1. Macrovision apparatus and image of a cross-section of maize interlock. The device consists of a CDD camera, a lens, a ring of optical fibers placed on a black background to backlight the cuts at an angle of 35 °, a lighting system, motorized plates for position the camera and the sample. A fresh tissue section (75 to 300 µm) is deposited in a petri dish on the motorized stage. Adjacent images are acquired and assembled as mosaic images to observe a representative region of the sample.

ii. Brightfield microscopy

Brightfield microscopy is very often the first technique used for histological studies. The sample is illuminated by transmission. The structures are made visible by their local differences in light transmission factors. The biological structures are naturally little contrasted. Contrast is obtained with the use of dyes that selectively interact with chemical functions of the molecules (Spence, 2001). In Table 3.1, some staining techniques used on lignocellulosic substrates are indicated.

Table 3.1 Examples of dyes- fluorochrome for visualization of parietal polymers.

Dyes-fluorochrome	**Excitation λ**	**Applications**	**References**
Toluidin blue	Brightfield	Metachromatic dye Cellulose, cytoplasm, and nuclei stained blue, and lignins, blue-green	(Locquin et Langeron, 1978; Grimault *et al.*, 1997)
Ruthenium red	Brightfield	Pectins stained in pink	(Locquin et Langeron, 1978)
Alcian Blue	Brightfield	Polymers with sulphate or carboxylic groups. Pectins	(Scott, 1985)
Schiff periodic acid (or acriflavine)	Brightfield	Polysaccharides having vicinal hydroxyl functions stained in violet-pink (fluorescence, yellow)	(Kasten *et al.*, 1959)
FASGA staining (Safranin O' + Alcian Blue)	Brightfield	Lignified tissues colored in pink and non-lignified tissues in blue	(Tolivia et Tolivia, 1987 ; Méchin *et al.* 2005)
Safranin O'- Astra Blue	Brightfield	Non-lignified cell walls in blue and lignified cell wall in red	(Srebotnik et Messner, 1994)
Phloroglucinol or Weisner staining	Brightfield	Reacts with terminal p-hydroxycinnamaldehyde functions present in native lignins. Lignins colored in red	(Nakano et Meshitsuka, 1992; Vallet *et al.*, 1996)
Maüle reagent	Brightfield	Lignines rich in S units colored in purple red and G units colored in brown	(Meshitsuka et Nakano, 1979; Nakano et Meshitsuka, 1992)
Red sudan	Brightfield	Cutins colored in red	(Waduwara *et al.*, 2008)
Blue Nile	Brightfield	Acid lipids colored in blue and neutral lipids in red	(Spence, 2001)

Acridine orange	Fluo, Blue excitation	Metachromatic dye. Xylem vessels: yellow, phloem region: orange, rich orange-red pectin walls	(Guillemin *et al.*, 2004)
Calcofluor white	Fluo, UV excitation	Fluorescence of the beta-glucans	(Wood *et al.*, 1983; Spence, 2001)
Direct Red 23	Fluo, Excitation at 488 nm	Fluorescence of the cellulose	(Liesche *et al.*, 2013)
Aniline blue	Fluo, UV Excitation	Fluorescence of the callose	(Wood *et al.*, 1983; Spence, 2001)

Figure 18.2 presents examples of stainings applied on maize internodes tranversal cross-sections. The automatisation des acquisitions d'images avec le développement des passeurs de lames permet d'envisager cette approche aussi pour l'analyse de grandes collections d'échantillons avec une bonne résolution spatiale de quelques µm (Zhang *et al.*, 2013; Legland *et al.*, 2017).

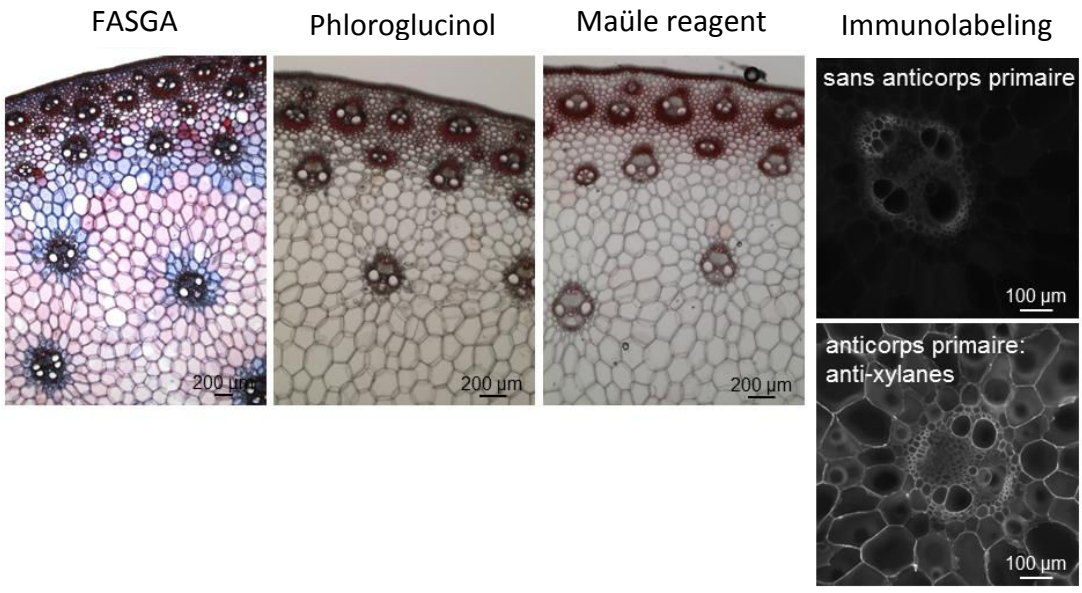


Figure 18.2. Exemples de coloration et d'immunomarquage des polymères pariétaux dans une coupe transversale d'entrenœud de tige de maïs.

2. Conclusion

The development of imaging and information extraction tools opens new horizons for analyzing biological systems. Until recently, microscopy accompanied by staining or labeling was the method of choice to observe, at limited rates, the spatial or temporal distribution of molecules in tissues. Advances in these areas, as well as the development of mass spectrometry imaging, now make it possible to perform mapping of spatial distribution of molecules at the plant or specific tissue level. Therefore, the study of the quality of lignocellulosic biomass can be considered from a tissue point of view. Until recently, this scale was rather difficult to access and only microdissection approaches, coupled with delicate biochemical analyzes (because of the small quantity of dissected material) or labeling with specific antibodies, allowed to approach him. The analytical flows to which we have access today make it possible to envisage in a realistic way the study of the variability (genetic, environmental, developmental, etc.) of distributions of the molecules within different tissues constituting the biomass and to propose new ways of selecting and/or improving the quality of this biomass.

IV. Cell wall establishment during maize stem development.

In this part, a better understanding and deciphering of the establishment of the cell wall in the maize stem all along its development is presented. This establishment is deciphered in the cell wall biochemical composition as well as in the distribution of the lignification at several developmental stages of the stem. This work has been initiated during the PhD of Yu Zhang in 2012, the integration of the data and reflections relating to their analysis and meaning continued and it is now a recent submitted article I attended: “Cell wall lignification and p-coumaroylation evolved differently in pith and rind of maize internodes”. The complete version of it is added in the Annexe part.

Three public early/medium-early maize inbred lines were selected on the bases of results obtained from experiments performed in 2006 and 2008 at INRA Lusignan. F324, F66 and F7037 lines were chosen to display fairly comparable lignin contents (5.2, 4.8 and 5.1 % of ADL in the cell wall respectively) for very different cell wall degradability (38.8, 34.8 and 27.6 % of the cell wall respectively) at silage stage. Cell wall deposition was studied all along plant development for these three inbred lines to decipher on the existence of one or more cell wall developmental models both biochemically and in terms of lignin distribution within the different stem tissues. Most of the scientists currently working on lignification rely on the models of cell wall polymers deposition presented in Terashima et al.. Briefly, in this model,

the authors presented the successive formation of cell layers in the order of middle lamella, primary wall, outer, middle and inner layers of secondary wall. They described both the deposition of carbohydrates and phenolic compounds. Concerning lignification they argued that monolignols were provided in the order of H, G and S lignin subunits and that lignins formed at an early stage were always more condensed than those formed at a late stage. They also stated that ferulic acids were incorporated earlier than p-coumaric acids in cell wall. The results obtained in this study will be discussed with regard to this model.

a) Genetic variation for internode elongation, cross section surface and cell size within the three genotypes throughout internode development

The length of the principal ear's internode was measured at each developmental stage for each genotype. The three inbred lines presented different elongation patterns along development (Figure 18.3a). F66 and F324 were two early genotypes and presented a rapid growth compared to F7037 which was medium-early and displayed a slower elongation. The 10cm length was reached in about 10 days for F66 and F324 against more than 20 days for F7037. However, it should be noted that the 3 genotypes completed their elongation at or just before silking, regardless the silking date. This physiological stage marked the end of the internode elongation whatever the considered genotype. At silage maturity, the length of F7037 internode was greater than the two others. Scobbie et al. (1993) showed that, when elongation ceased in maize internodes cells near the upper part of the internode had already shifted to extensive secondary wall deposition, whereas at the bottom of the internode cell walls appeared to still be more primary in nature. Similarly, Jung indicated that cell wall development shifted from a mixture of primary and secondary wall deposition to only secondary wall development after the end of elongation of the internode. Thus, in our three inbred lines the shift in the developmental pattern for internode elongation should be associated with different process of cell wall development/deposition over time. These differences should be visible in our in depth biochemical and histological characterizations.

Evolution of internode diameter was less important than length and was also complete when elongation ended for the three inbred lines. At silage stage, F7037 showed a larger internode diameter (1.33 ± 0.01 cm) than F324 (1.20 ± 0.05 cm) and F66 (1.13 ± 0.02 cm). The stem cross section surface did not evolve considerably after the second stage (V10, Figure 18.3b). The cell size (Figure 18.3c) was stable within each line over time but was contrasted between lines. Indeed, a twofold variation was observed between lines with F7037 which displayed 45 µm cell size and F324 which presented 75µm cell size. Thus F7037 while it has the largest internode diameter displayed the smallest cell size which implied an increased cell wall density compared to the two others genotypes and

potentially associated with its lower degradability.

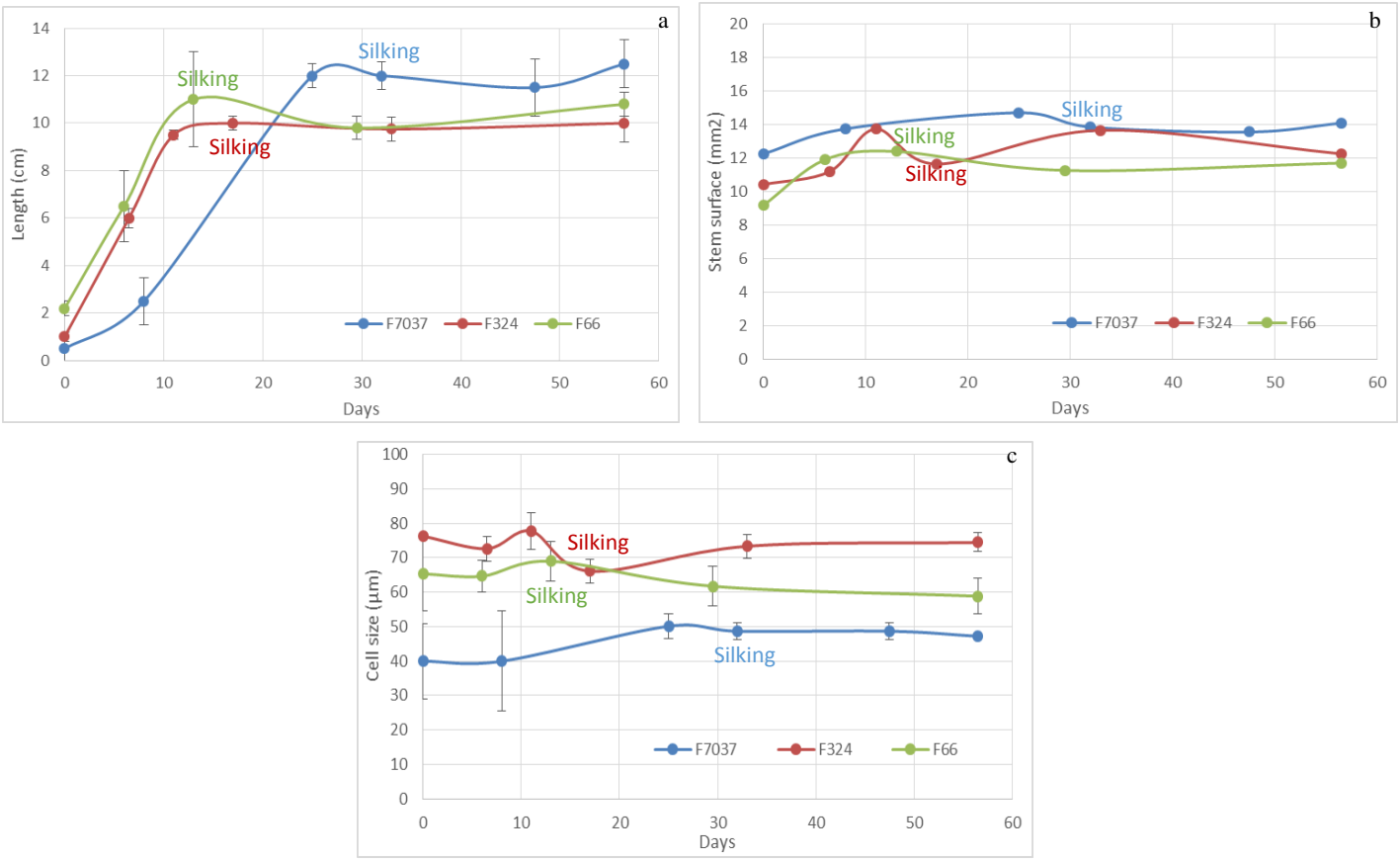


Figure 18.3. Evolution of morphological parameters during internode development for the three genotypes. a: length of the principal ear's internode, b: cross section surface and c: cell size of the parenchyma cells. Data were averaged across the three blocks collected in 2011. «Silking » indicated the time of female flowering for each genotype. Smooth curves were used only for graphical purposes.

b) The main differences for internode elongation and cell wall phenolic composition were positioned at young stages, before silking

The variance analysis for cell wall biochemical composition indicated that throughout internode development, the three inbred lines differed for most biochemical parameters. Indeed, the genotype effect was very significant ($P < 0.001$) for Klason lignin content, G, β- O-4 yield, *p*-coumarate esters and ferulate esters (Table 3.2). In previous studies, no differences in pattern of development have been pointed out according to species. The inbred lines used in our study have been chosen to limit the variation in lignin content in the cell wall at silage stage. They showed significant difference in phenolic composition during internode development suggesting that the cell wall pattern of lignification differed. This is the first time that genetic variation for cell wall phenolic composition during internode development is reported.

As observed in previous studies, the stage effect was very significant ($P < 0.001$) for all cell wall phenolic parameters. To further investigate the stage effect variance analyses was applied to two distinct periods, from V8 to silking and from silking to silage (Table 3.2). The variance analysis carried out for each period indicated no significant genotype*stage interaction over the late stages (Table 3.2). Thus at late stages, accumulation of cell wall components among the three inbred lines followed similar pattern. The main differences for all phenolic parameters were thus concentrated at young stages, before silking.

Table 3.2. ANOVA results for fixed effects for cell wall biochemical composition of the principal ear's internode for the three maize lines (F324, F66, and F7037) grown in 2009 and 2010 and sampled at 6 developmental stages.

		Variance effects					
		Y_i	G_j	S_k	YG_{ij}	YS_{ik}	GS_{jk}
All stages	L Internode	ns	*	***	ns	ns	**
	KL	***	***	***	ns	***	***
	G	***	***	***	**	***	ns
	S	***	**	***	ns	***	***
	β-O-4 yield	***	***	***	ns	***	**
	S/G	ns	ns	***	***	ns	***
	PC est	***	***	***	ns	***	***
	SPC	ns	**	***	ns	*	***
	FA est	***	***	***	*	***	***
	FA eth	***	ns	***	ns	*	***
V8 to silking stages	L Internode	ns	ns	***	ns	ns	**
	KL	***	***	***	ns	**	***
	G	***	***	***	ns	***	ns
	S	***	*	***	ns	***	**
	β-O-4 yield	***	***	***	ns	***	*
	S/G	ns	ns	***	*	*	***
	PC est	***	***	***	**	***	***
	SPC	ns	ns	***	ns	*	**
	FA est	***	***	***	ns	***	***
	FA eth	ns	**	***	ns	ns	***
Silking to silage stages	L Internode	ns	***	ns	ns	ns	ns
	KL	*	***	*	*	ns	ns
	G	***	**	**	**	ns	ns
	S	***	***	***	ns	ns	ns
	β-O-4 yield	***	***	***	*	ns	ns
	S/G	ns	ns	***	**	ns	ns
	PC est	ns	***	***	ns	ns	ns
	SPC	ns	***	**	ns	*	*
	FA est	***	***	***	ns	ns	**
	FA eth	***	ns	*	ns	ns	ns

*: $P < 0.05$; **: $P < 0.01$; ***: $P < 0.001$; ns: $P > 0.05$.

L internode: length of the internode supporting the ear, KL: klason lignin content in the cell wall, G and S: molar yield in β-O-4 linked G and S lignin-derived monomers calculated on the basis of the Klason lignin content in the cell wall, β-O-4 yield: sum of the H, G and S β-O- 4 linked lignin-derived monomers, S/G: S/G ratio, PC est: esterified *p*-coumaric acid content in the cell wall, SPC: percentage of S lignin units acylated by p-coumaric acid, FA est: esterified ferulic acid content in the cell wall, FA eth: etherified ferulic acid content in the cell wall.

c) Different developmental patterns were observed for lignin content, composition, structure and distribution

1. Evolution of lignin content all along the internode development

The three genotypes were initially retained to display quite similar lignin content on the basis of their ADL lignin content at silage stage (from 4.8 to 5.2%). The Klason lignin content for these three genotypes at silage stage were ultimately quite comparable (from 14% for F66 and F324 to 16% for F7037, Figure 18.4a). As exposed in Hatfield and Fukushima when applied to grasses, the acid detergent solution used in the Van Soest procedure dissolves more than 50% of the lignin, which explains the drastically lower values encountered for the ADL lignin content compared to the values obtained with the Klason procedure. As detailed in Zhang et al. lignin content estimated by the Van Soest (ADL) or the Klason methods do not represent the same lignin part. The Klason lignin is a better estimation of the whole lignin content in the cell wall whereas the ADL lignin content represents mainly the condensed (C-C linkages) lignin part.

Among the three genotypes, quite similar low lignin contents were observed at first stages of development (4.5 ± 0.5 %, 5.6 ± 1.0% and 5.2 ± 1.0% for F324, F66 and F7037 respectively, Figure 18.4a). A rapid increase in Klason lignin content was observed for the three genotypes in a first developmental period between V8 and Silking stages (Figure 18.4a). At silking stage all the three genotypes nearly reached their final Klason lignin content (Figure 2a). F66 and F324 thus accumulated about 10% of lignin in their cell walls in only 2 weeks while F7037 accumulated about 10% of lignin in more than 4 weeks (Figure 2a). After silking, in a comparable way for the three genotypes, lignin content increased negligibly (Table 1 and Figure 2a).

2. Evolution of lignin structure and composition all along development

The proportion of H, G and S lignin subunits was evaluated by thioacidolysis and thus reflects the lignin units only involved in β-O-4 bonds. The total β-O-4 yield provides an estimate of the proportion of lignin units only involved in β-O-4 bonds (β-O-4 yield), the so-called “uncondensed” part of the lignin polymer. An important effect of stage ($P < 0.001$, Table 3.2) was observed for β-O-4 yield which corresponded to a consistent increase of the uncondensed part of the lignin polymer in the principal ear’s internode during internode development (Figure 18.4b).

At earlier stages, the three studied genotypes presented poor β-O-4 linkages in their lignins. In accordance with Terashima et al., lignin formed at an early stage were always more

condensed than those formed at a late stage. The three genotypes did not differ drastically in their developmental pattern for β-O-4 yield accumulation, but differed for their developmental pattern for Klason lignin content. Between Silking and Silage stages about 150 µmol.g-1 Klason lignin of β-O-4 lignin units were deposited while the total lignin content only increased in a very few extent. Therefore, β-O-4 was probably the main linkage formed during this late and slow lignification period. Rapid polymerization favors C-C coupling of monolignols; in contrast, gradual polymerization favors β-O-4 coupling between monolignols into lignin polymer. This is in accordance with our results which showed that rapid lignin accumulation was certainly the place for mixed bonding pattern within the lignin polymer, with an important place for C-C bonds whereas the slow and late lignin accumulation period was the place of β-O-4 bonding pattern within the lignin polymer. We can wonder if the establishment of β-O-4 bonds is only constrained by chemical features (oxidative coupling, reactivity, quinone stability and so one) or if genetic determinism involved in spatio-temporal regulation of this pattern also occurred, but the objective of this paper is not to debate this point.

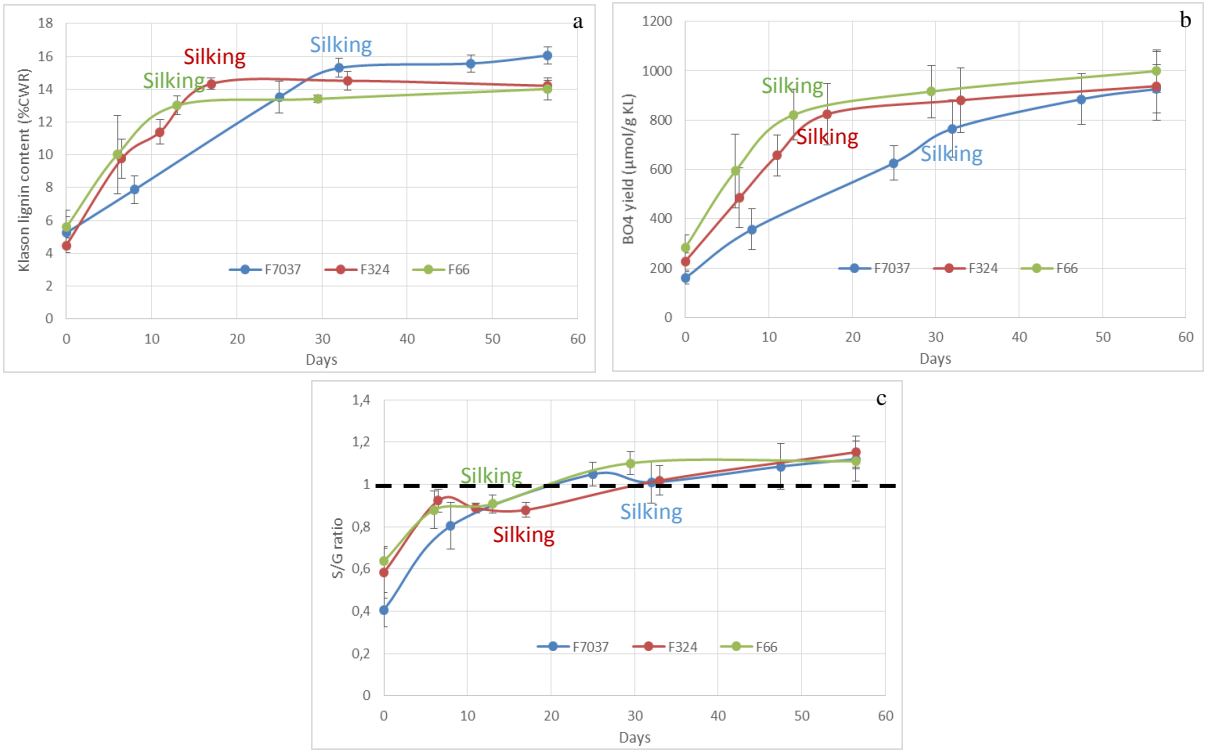


Figure 18.4. Evolution of lignin content, composition and structure during internode development for the three genotypes. a: Klason lignin content, b: lignin units only involved in β-O-4 bonds (uncondensed lignin part) and c: S/G thioacidolysis ratio. Data were averaged across the blocks collected in 2009 and 2010. «Silking » indicated the time of female flowering for each genotype. Smooth curves were used only for graphical purposes.

At the first stage of development, the relatively low syringyl to guaiacyl ratio (S/G ratio) was consistent with the well-known shift in H, G and S lignin subunit deposition during lignification as highlighted by Terashima et al. (1993). We actually observed that G accumulation ceased before S accumulation which continued until the last stage (S/G > 1, Figure 18.4c). Surprisingly, the S/G ratio evolution for F7037 was quite synchronous with that of F66 and F324 despite the important delay in their lignin deposition. Thus, during more than half of the accumulation phase of its lignins F7037 accumulated more S than G units contrary to the other two genotypes (Figure 18.4c). Therefore, in addition to the Gramineae lignification model proposed by Terashima et al. we believed that many lignification models are possible. A strong genetic variability is present in maize (and more generally in grass) in the timing of lignin composition evolution even if indeed the S/G ratio increases all along development. Jung and Casler (2006) stated that the shift from guaiacyl rich lignin to syringyl rich lignin is a general phenomenon of secondary cell wall development in grass tissues and Terashima et al. (1993) proposed that when lignification reached the secondary cell wall, syringyl rich lignin content and S/G ratio increased. That would mean that for F7037 either the deposition of the secondary wall started earlier, or the primary wall was richer in S units.

3. Evolution of lignin distribution at tissue level all along the internode development

Tissue lignification on internode development was followed by fasga staining. Lignified tissues are stained in red, whereas non lignified or poorly lignified tissues are colored in cyan/blue. For each fasga stained cross section of the three genotypes at the 6 developmental stages (Figure 18.5a) we evaluated the red/blue intensity ratio relative to the distance to the outer epidermis using the plugin developed and presented in Zhang et al. (2013). We defined three main regions from the color profiles: pith, blue layer in the pith and rind. We assessed the evolution of the lignification rate for each region, at each stage for each genotype (Figure 18.5c). The blue ring appeared at the third stage (tasseling) for the 3 genotypes. The lignification of this poorly-lignified parenchyma region was low and did not change along internode development after tasseling stage.

As presented in details for F324 in Zhang et al. (2013) a great increase in the red/blue intensity ratio of the rind and pith regions for the 3 genotypes between V10 (stage 2) and tasseling (stage 3) was related to the lignification of these two regions. In the rind region, relatively high values of the red/blue intensity ratio indicated that cells from this region were much more lignified than those of other regions. After tasseling the red/blue intensity ratio in the pith remained steady whereas in the rind this ratio continued to increase (Figure 18.5c). Thus both blue ring and pith regions stopped their lignification after tasseling. Therefore the lignins which accumulated after this stage were deposited

predominantly in the rind region. This was perfectly illustrated by figure 18.5a and even more by figure 18.5b on which we could observe the intense lignification of the rind region for all the 3 genotypes after tasseling.

If we compared the 3 genotypes, the three main points to keep in mind are i) the highest blue intensity of the F324 blue ring, ii) the highest red/blue rind ratio for F7037 compared to F66 and F324 and at least iii) the quite comparable profiles of pith region lignification for the 3 genotypes. F7037 was thus globally a more intensely lignified genotype with in particular a highly lignified rind.

In conclusion, lignification takes place largely before flowering stage both in the pith and in the rind. After flowering and until maturity, the deposited lignins are very rich in BO4 bonds and mainly localized in the rind.

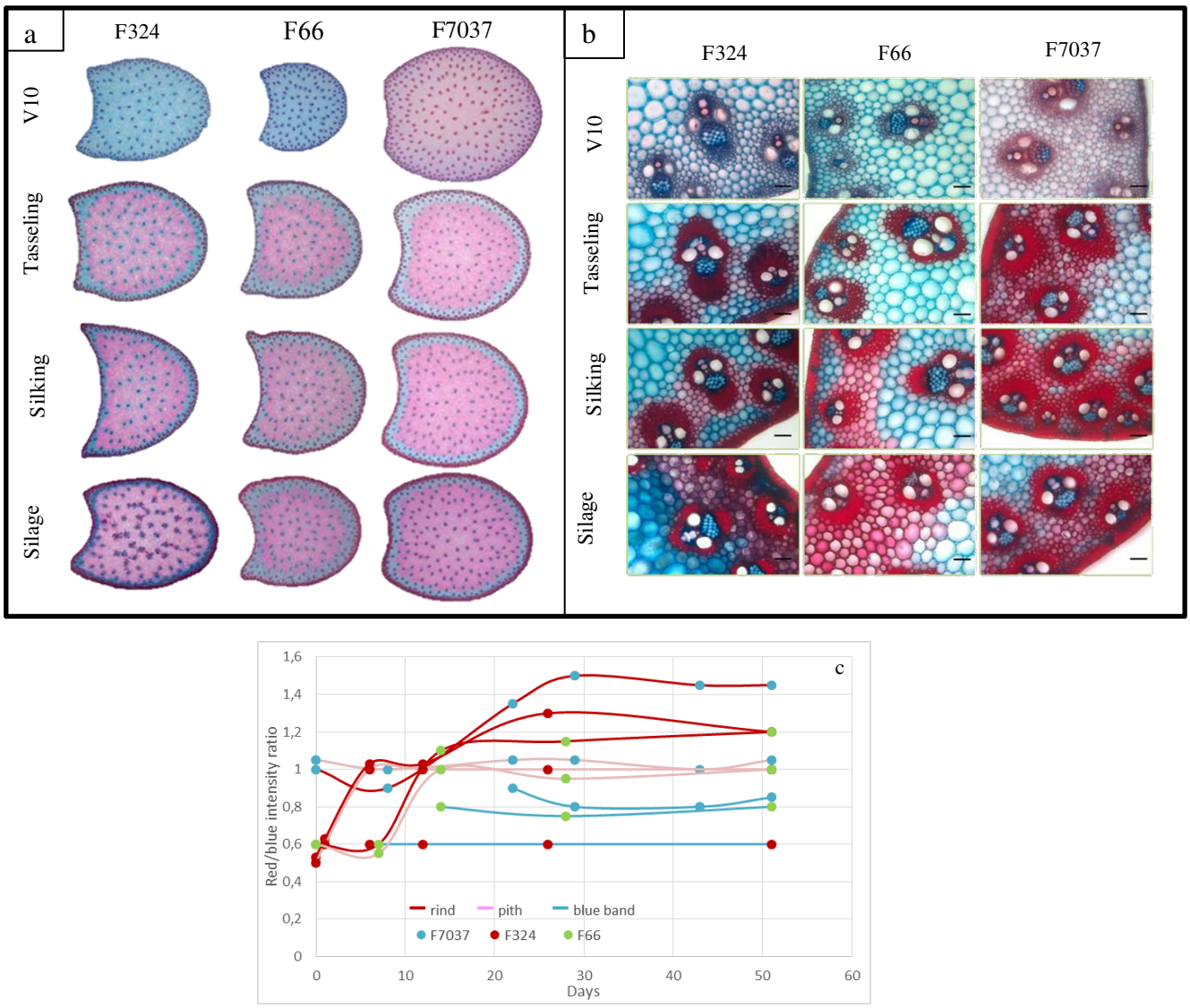


Figure 18.5. Evolution of tissues lignification during internode development for the three genotypes.a: whole internode FASGA stained cross section, b: rind region of the FASGA stained cross section (bar = 100µm) and c: Red/blue intensity ratio. Smooth curves were used only for graphical purposes.

d) Throughout internode growth different developmental patterns were observed for p- hydroxycinnamic acids accumulation

1. Evolution of esterified p-coumaric acid content all along internode development

Deposition of *p*-coumaric acid followed the same pattern as observed for the Klason lignin content (Figure 18.6a). Strong correlation was observed between esterified *p*-coumaric acid content and Klason lignin content over both the earlier and maturity stage intervals (Data not shown).

The %S-PC increased amazingly over earlier stages nearly reaching its maximum at V10 (stage 2) for F66 and F324 by going from 12-15% to 25% in just a few days. However, for F7037 the %S-PC increased from 7% to 30% in 3 weeks. Analysis of variance showed a significant genotype effect for *p*-coumaric acid content and %S-PC over the maturity stages. At the silage stage, large genotypic variations were observed for *p*-coumaric acid content and %S-PC. F7037 which had the highest Klason lignin content had also the highest *p*-coumaric acid content and %S-PC. F324 and F66 had similar Klason lignin content and also presented similar *p*-coumaric acid content and %S-PC.

In grass, *p*-coumaric acid is mainly esterified to the γ-position of the side chains of S lignin units, making *p*-coumaric acid accumulation an indicator of lignin deposition. Several studies have shown a positive relationship between *p*-coumaric acid content in the cell wall and level of lignin. The current study reinforces this observation. During maize cell wall development esterified *p*-coumaric acid content increased following the same trajectory as Klason lignin content.

It is well established that *p*-coumaric acid content in the cell wall dramatically increased during maize secondary cell wall deposition and that *p*-coumaric acid is mainly associated to the syringyl-rich lignin. Recent work has demonstrated that S units were enzymatically preacylated by *p*-coumaric acid in the cytosol, these acylated monolignols are then incorporated into the lignin polymer by polymerization and co-polymerization with the traditional monolignols, resulting in acylated lignin. The role of lignin acylated by *p*- coumaric acid is not yet very clear. It is pretty sure that *p*-coumaroylated S unit is crucial for radical transfer mechanisms in order to improve S unit incorporation into lignin polymer. From stage three, the %S-PC leveled off. This plateau was higher for F7037 compared to F324 and F66. Thus, about 31% of the S units appeared to be acylated by *p*-coumaric acid in F7037 to about 25% in the two other genotypes. We have shown that at late stages, mainly uncondensed β-O-4 lignin was formed; these lignins are thus also strongly p-coumaroylated. The enzymatic

step of S unit acylation by *p*-coumaric acid could thus be a key step to control lignin final structure and composition. Especially when considering the results obtained by Zhang et al. (2011) which demonstrated that *p*-coumaroylated S lignin units were a major limiting factor for cell wall degradability when lignin content variations were small. Works presented by Withers et al. (2012) on an acyltransferase that catalyzes the acylation of monolignols in grass open up the possibility to modify gene expression and thus to modulate and regulate acylation in plants. In a recent study, Sibout et al. introduced such a brachypodium *p*-coumaroyl-coenzyme A monolignol transferase in arabidopsis and succeeded in altering both the arabidopsis lignin content/structure/composition and consequently in impacting cell wall degradability.

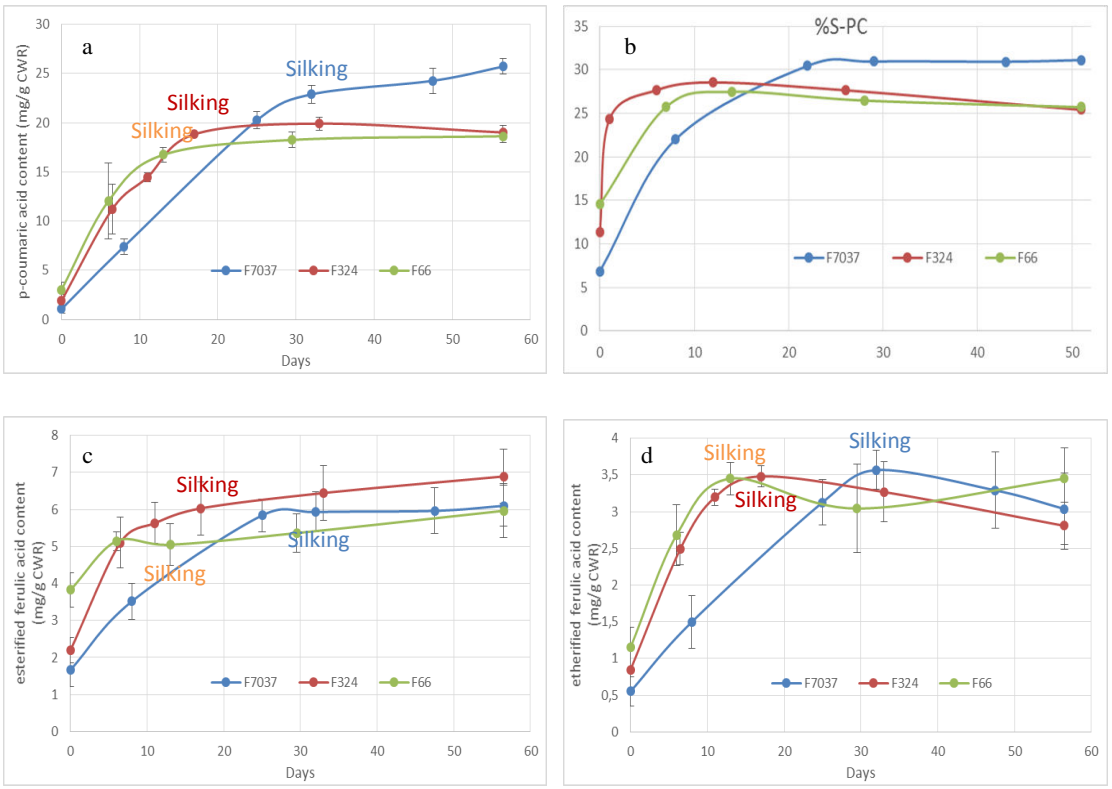


Figure 18.6. Evolution of *p*-coumaroylation and feruloylation during internode development for the three genotypes. a: esterified *p*-coumaric acid content, b: percentage of S lignin subunit acylated by *p*- coumaric acid, c: esterified ferulic acid content and d: etherified ferulic acid content. Data were averaged across the blocks collected in 2009 and 2010. «Silking » indicated the time of female flowering for each genotype. Smooth curves were used only for graphical purposes.

e) Esterified ferulic acids were deposed all along plant development but used to anchor lignification only at early stages

Variance analysis indicated that the three genotypes differed for esterified ferulic acid content (FAest) over developmental stages ($P < 0.01$) (Table 3.2). In grass ferulic acid firstly ester linked to arabinoxylans are deposited in the primary cell wall. Once incorporated into the wall peroxidases oxidize the ferulic acid to form several possible ferulic acid dimers but also couple ferulic acid to monolignols. Ralph et al. suggested that esterified ferulic acid probably serve as initialization site for lignification. In the present study, esterified ferulic acid was relatively high from the first stage, especially for F66 (Figure 18.6c). This early deposition of esterified ferulic acid should play a crucial role for the development of lignification in primary wall. Esterified ferulic acid accumulation was high during the three first stages and slowed down once secondary wall deposition begun. Esterified ferulic acid accumulation continued during the late stages for F66 and F324 but surprisingly not for F7037 (Figure 18.6c). Our results are consistent with those presented by Jung (2003) indicating that esterified ferulic acid deposition is not limited to primary walls but that approximately 60% of esterified ferulic acid are presents when the secondary wall formation begins in maize. In 2008, Hatfield et al. reported the constant level of ester linked ferulic acid across internodes tissues of developing maize stems thus demonstrating that ferulic acid was continually incorporated in secondary cell walls as well as primary walls. The highest amount of etherified ferulic acid was quantified at the third stage. Etherified ferulic acids are supposed to bridge together hemicelluloses and lignins. Beyond stage three, the etherified ferulic acid content did not further increased suggesting that no supplementary bridge between these two polymers were thus set up (Figure 18.6d). The possibility remained that feruloyl arabinoxylan polymers continued to be laid down in the secondary wall, but no more ferulic acid radically couple to monolignol. This is extremely consistent with the fact that lignin synthesized during the last stages were mainly constituted of β-O-4 bond subunits. This predominance of β-O-4 bonds was the sign of an endwise mechanism as debate in Demont-Caulet et al. (2010). Thus, at the end of the plant development few lignins were synthesized but the new ones were not fixed to new ferulic acid primers but were an elongation via β-O-4 bonding of the existent lignins. Ferulic acid primers were thus recruited before stage 4 to install lignification.

f) Combination of the biochemical and histological findings to propose a model of spatiotemporal cell wall development

In the present study, we combined biochemical and histological approaches to characterize cell wall deposition and lignification during maize stem development. Maize internode cell wall development followed three different steps (1) a fast deposition of primary cell wall in the whole cross section; (2) a fast deposition of secondary wall and (3) a slow deposition of secondary wall in the cortical region (Figure 18.7). Spatial and temporal deposition of cell wall components and development of cell wall structure varied among these three cell wall developmental steps and was also clearly genotype dependent. In primary cell wall, esterified ferulic acid was predominantly deposed, and the large genetic variation for esterified ferulic acid content was likely to be critical for the variation of lignification in the primary cell wall. In the second step, deposition of both fast C-C and β-O-4 bonds lignins lead to the fast deposition and lignification of secondary cell wall. Once the fast C-C bonds lignin deposition ended, β-O-4 bonds lignins were likely the major ones formed during the late lignification and were predominantly deposited in the cortical region. This cortical region thus appeared to be very specific regarding its composition. Our results suggested that cortical region was in fact highly lignified with lignin rich in β-O-4 bonds and highly p-coumaroylated. Barros-Rios et al. (2012) compared cell wall composition in separated maize pith and rind tissues. They demonstrated that rind tissues were less degradable than pith tissues and richer in etherified ferulic acids, in esterified p-coumaric acids and also more lignified. In the same way, Hatfield and Chapman (2009) have demonstrated that pith tissues had lower levels of lignin and *p*- coumaric acid. As established in Zhang et al. (2011) lignin rich in bO4 bonds and highly *p*- coumaroylated were the more inhibitory ones for cell wall degradability. Thus the spatial and temporal developmental scheme for cortical region made it a highly undegradable and resistant tissue. This reinforced our recent results suggesting that in drought context rind region was preferentially lignified and *p*-coumaroylated in order to assure plant posture and resistance with a decreased global lignification at internode level. In agreement with Hatfield and Chapman (2009) in particular, we think that *p*-coumaric acid have an active role in the formation of lignin in grass cell walls and results presented in this publication underline also the fact that its distribution at the tissue level is important to take into account to better understand genetic variation of overall cell wall composition and degradability of internode. In our opinion, the impact of lignified tissue distribution on cell wall degradability is preponderant and has long been underestimated.

Selection of lines with improvement of cell wall degradability should include these considerations of lignin and *p*-hydroxycinnamic acids tissue distribution both in quantity and composition.

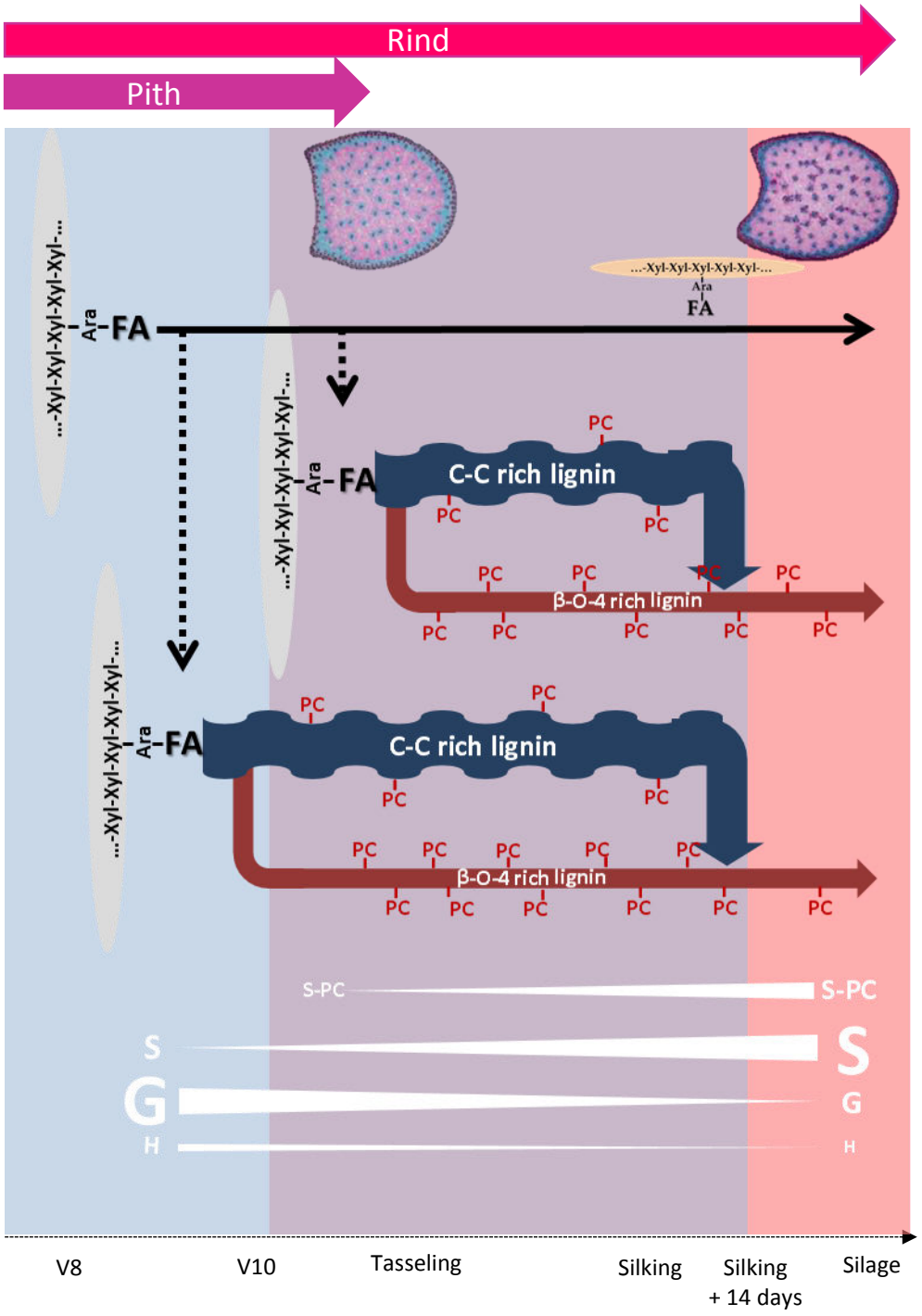


Figure 18.7. Schematic illustration of the spatio-temporal evolution of the maize internode cell wall.

V. Relationships between cell wall degradability and 1- biochemical cell wall components and 2- the distribution of lignification

Fodder degradability may be directly quantified *in situ*, with the model of reference: sheep. However, this method is tedious and requires a good mastering of the composition of the ration. Moreover, strong racial or individual variations were observed among the animals, results are obtained after a very long time and it is very expansive.

As presented in the part I-c) of this introduction, degradability may also be estimated by *in vitro* methods (Jung and Engels, 2002) with the aim to simulate the digestion process in the animal with rumen juice or with enzymes. Enzymatic methods allows to quickly quantify the *in vitro* dry matter degradability (IVDMD) and the *in vitro* cell wall residue degradability (IVCWRD) but it gives results less accurate with the *in vivo* methods than the microbiological methods (Schubiger et al., 2001).

a) Impact of the cell wall biochemistry on the cell wall degradability

In fodder plants, enzymatic degradability have been reported to decrease with plant maturity (Morrison et al., 1998), and this is linked among other things with a progressive lignification of the cell wall (Jung and Deetz, 1993; Kondo et al., 1998). The lignin content has been therefore pinpointed as the major recalcitrant factor to cell wall degradability a long time ago. However in brown-midribs mutants the increase of the cell wall degradability is often associated to the reduced lignin content whereas, considering all the structural and lignin composition impacted by the mutation, the factors impacting cell wall degradability could be multiples.

If it has many adaptative advantages for the plant point of view, lignin presence is not always an advantage considering industrial processes or animal nutrition. Indeed, lignins are extremely resistant to any degradation, chemical or enzymatic. By forming hydrogen bonds with cellulose and direct or indirect linkages via ferulic acids to hemicelulloses, lignin form a glue polymer making a hydrophobic barrier for any chemical solvant or enzymes. It impacts negatively the possibility to degrade the polysaccharides of the cell wall which are the main targets of the biomass valorisation.

The monomeric composition of the lignins is also influencing the cell wall degradability. This has been shown in numerous species. The specie of the plant determines strongly the type of lignins which are found in the cell wall. Thus, in the gymnosperms, lignins are mainly

composed with G subunits and have therefore a very condensed structure (Achyutan et al., 2010). Whetten and Sederoff showed in 1991 that this leads to the fact that the gymnosperm wood was less suitable to produce paper paste with all the treatments. In angiosperms, Boerjan et al., 2003 mentioned that transgenic poplar downregulated for the 4CL enzyme presented a lower lignin content and this was associated to a better yield of paper pulp. Santos et al., in 2012 showed that a higher S/G ratio combined with a lower lignin content would be associated to a better saccharification rate and concluded that if lignin content was the same, a higher S/G ratio by removal of guaiacyl units promoted a more accessible substrate which increased enzyme adsorption and resulted in higher enzymatic hydrolysis efficiency. These observations about the S/G ratio have been supported by other studies on biofuels made from wood material which showed that lignin composed mainly of Syringyl subunits are easier to solubilize during pretreatments (Li et al., 2010 & Santos et al., 2010). But S/G ratio has a controversial role in other studies. In some studies, the digestibility was found to be positively associated with this S/G ratio in switchgrass (Jung and Vogel, 1992) and in maize (Mechin et al., 2000). In contrast, at a constant lignin level, results obtained on tobacco (Bernard-Vailhé et al. 1996), on alfafa (Baucher et al., 1999), and on Arabidopsis (Goujon et al., 2003) suggest that a better digestibility is associated with a decrease of the S/G ratio. However it was shown on a selection of maize lines for a constant lignin levels that the BO4 yied and the PCAest were the main cell wall traits involved in the variations of the cell wall degradability (Zhang et al., 2011). In this last study, S/G ratio was not identified as the main factor explicating the variations of cell wall degradability.

The investigation of the G and S lignin subunits synthesis led Anderson et al., (2015) to down-express or over express ferulate 5-hydroxylase (F5H) which resulted in an increase of the G units or the S units respectively. They showed between these mutants that hydroxycinamaldehyde content was more determinant for the degradability than the lignin content.

The cross-linking of FA between hemicelluloses and lignins (Ishii, 1997; Ralph et al., 1998, 2004; Ralph, 2010) was also reported as impacting negatively the cell wall degradability and was therefore a lot investigated as a target to improve biomass degradability in grasses (de Oliveira et al., 2015). These cross-links inhibit degradability by preventing enzyme access and by tightly binding the polysaccharide substrate to non-degradable lignin. This hypothesis is supported by many works. *In vitro* studies showed inhibition by FA of polysaccharide saccharification to sugars (Grabber et al., 1998a, b); natural variation in FA content was associated to negative correlation with degradability (Lam et al., 2003; Casler & Jung, 2006); biomass degradability was increased by heterologous expression in festuca of feruloyl

esterase (Buanafina et al., 2008); and screens for increased degradability in mutant populations frequently identified low ferulate lines (Hirano et al., 2017). Recently, De Souza et al., (2018) showed in grass widely spread in fields, *Setaria viridis*, and an emerging model for molecular and genetic studies that the suppression of BAHD gene lead to a decrease of the cell wall feruloylation and this was associated to an increase of the biomass degradability. This year too, Li et al., (2018) overexpressed a BAHD acyltransferase gene from rice (OsAT10) in switchgrass. They observed a significant decrease of cell wall bound FA in green leaves and an increase of *p*-coumaric acid content in green leaves associated to a 40 % increase of saccharification efficiency of the biomass with no or minimal effects on plant growth. BAHD gene family appear to be a promising target for selecting plants with an increased degradability along without depleting the agronomical performances.

In 2012 Barros-Rios et al., showed in 2 populations of maize hybrids that FA dimers, i.e. diferulates, which binds two chains of arabinoxylans grasses, were involved in the variations of the cell wall degradability. Indeed an increase of ester linked diferulates was associated to a decrease of the glucose content in the cell wall and a decrease of the cell wall residue. On the opposite, a decrease of the content of these dimers induced an increase of cell wall degradability. In some others studies, Barros Rios et al., also showed that the presence of a high total concentration of diferulic acids in the cell wall in a maize population was significantly decreasing from 29 % the tunnelling by corn borer species, meaning literally that the borer could not well degrade the stem tissues of this maize population (Barros Rios et al., 2012, 2015).

Among the relationships between *p*-hydroxycinnamic acids and the cell wall degradability PCAest has been reported by many studies to present a positive relationship with the lignin content. Therefore PCAest content increases with the lignifications of the cell wall (Scobbie et al., 1993; Morrison et al., 1998; Hatfield and Chaptman, 2009, Zhang et al., submitted). However its role is not indirect because of this positive correlation with the lignin content. Zhang et al., (2011) have shown on a selection of maize lines with similar lignin content in the cell wall, that the BO4 yied and the PCAest were the main cell wall traits involved in the observed variations of the cell wall degradbility. The radical transfert concept of the PCAest presented previously also support the crucial role of PCAest in the polymerisation of lignins in grasses. If Jung et al., (2012) associated the *p*-coumarate as a factor increasing the degradability of the cell wall, several studies reported the negative role of PCAest on the degradability of the cell wall (Mechin et al., 2000, 2005; Taboada et al., 2010).

In 2016, Costa et al., investigated in 6 sugarcane hybrids the specific hemicelluloses distribution and they showed that pith regions of hybrids with a high level of mixed-linked glucans (MLG) reached up to 85 % of the glucan conversion. They showed also a rind more lignified than the pith with cellulose microfibrills more crystalline associated to a decreased glucan conversion. However, if the percentage of crystallinity in cellulose, which may be measured by x-ray diffraction, is hypothetized to have a role in the rigidity of the cell wall, some studies showed that alone, it may not explain the result in saccharification (Puri et al., 1984).

The cell wall biochemistry is therefore very complex and the relationships between its components and the cell wall degradability still remain to be deciphered further as some studies show controversial thesis. However, promising targets are emerging along with the BAHD gene family characterization and the *p*-coumaroylation of the lignins.

b) Impact of the distribution of the lignification on cell wall degradability

If the link between the lignification distribution and the degradability is more and more studied, it is possible to find a few studies before 2000 on this topic.

Indeed in 1992 Grabber et al., carried out dissections of pith and sclerenchyma tissues in switchgrass and in orchardgrass. After a digestion of these tissues with rumen fluid at different stages, the indigestible residue (IR) of sclerenchyma was poorly correlated to neutral sugars, esterified phenolics, and lignin concentrations whereas the IR of parenchyma was positively correlated to several components: suggesting composition of this tissue could be targeted to improve IVCWRD. More specifically, rate of digestion of sclerenchyma was more important than what we could see in literature. So they hypothesized that the anatomical configuration of the sclerenchyma was maybe the major factor limiting its digestion.

In 1993 Lopez et al., showed on the 2 highest, and therefore youngest, internodes of maize plants harvested 5 days after anthesis, that the sclerenchyma fraction, isolated from the rind, was presenting thicker cell walls than the parenchyma fraction cell walls and were therefore more lignified. This was associated with a greater degradability of the parenchyma fraction compared to the sclerenchyma fraction.

Five years later, in 1998, Morrison et al., evaluated by liquid chromatography the neutral sugar residues before and after fermentation of 2 separated fractions: the pith and the rind. They showed that degradability of cell wall polysaccharides decreased with internode development. For the younger internodes pith was degraded more quickly and more intensively than the rind. They also showed that the potentially degradable polysaccharides (calculated after 96h incubation) were of 90 % in both the pith and the rind tissues. In older

internodes, these potentially degradable polysaccharides remained above 75 % in the pith but were lowered at only 67 % in the rind.

In 2005, Mechin et al., analysed 22 maize inbred lines and quantified histological traits such as the blue area on the FASGA-stained section (equivalent to the surface of non-lignified tissues), the red area on the FASGA stained section (equivalent to the surface of lignified tissues, the cortical area, the thickness of cell layers of the cortical sclerenchyma and the number of cell layers in the cortical sclerenchyma. By coupling these histological quantifications to cell wall biochemical analyses they showed that they could explain degradability with the lignified region coloured by the FASGA and the S/G ratio impacting negatively and positively the cell wall degradability respectively. Based on all their biochemical and histological analyses they even proposed a maize ideotype which would have lignins richer in S than G subunits, p-coumaroylated and deposited preferentially in the cortical region rather than in the pith. These results meet the hypotheses suggested by Zhang et al., submitted and presented in part IV of this chapter. Indeed, at a late stage of maturity, lignins are preferentially deposited in the rind and therefore more p-coumaroylated, and with more BO4 linkages. This hypothesis could be investigated further thanks to a study of the cell wall degradability along with the quantification of the *p*-coumaric acid content in the rind during several late stages of maturity.

Digestion of cross sections has been carried out by Jung and Calser (2006). Indeed, they did a kinetic of degradation of maize stem cross sections by rumen microbes. They observed that pith parenchyma under the cortex was almost completely degraded within 24h. They also showed that after 96h of degradation, all the tissues within the cross sections were not degraded equally. Indeed, all the parenchyma tissue surrounding the bundles and under the cortex were degraded while the cortex, the sclerenchyma and the bundles were weakly degraded (Figure 19).

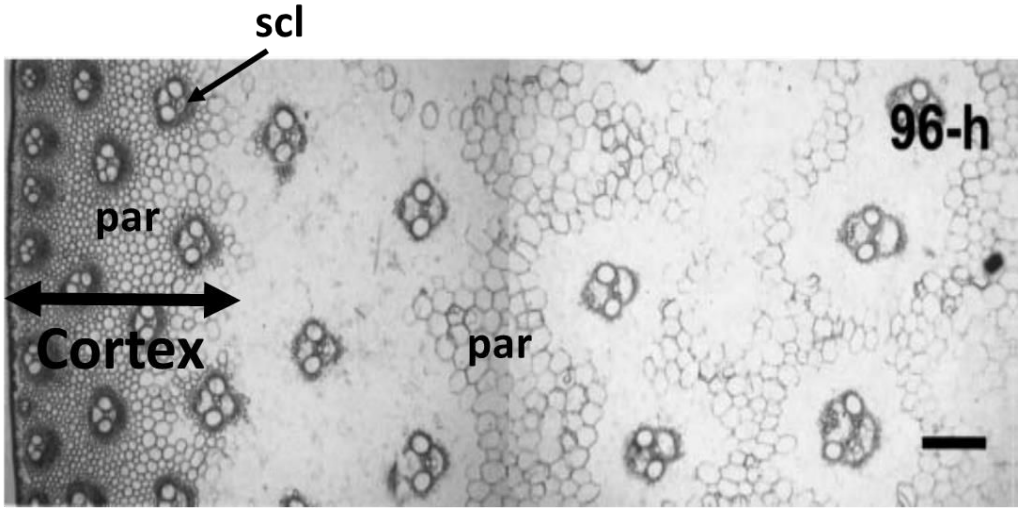


Figure 19. In vitro degradability on a maize stem cross-section by rumen microbes during 96h (adapted from Jung and Casler, 2006a). par = parenchyma; scl = sclerenchyma; Bar = 500 µm.

Investigating the characteristic of the rind region in stems, Boon et al., (2012) showed on two different lines of maize that the lower degradability of the line 2 was associated to a greater area of sclerenchyma and thicker xylem cell walls (Figure 20). A similar study on the xylem cell walls in the rind region was previously made on alfalfa (ref). They showed with image analysis on FASGA stained cross-sections that the thickness of the cortex and the thickness of the cell walls of the xylem vessels were negatively correlated to the digestibility (Guines et al., 2001; 2003). In 2013 Bottcher et al., investigated the differential lignification of the rind and the pith from young to mature internodes of 2 sugarcane lines contrasting for lignin content. In the rind of both sugarcane lines they observed a marked decrease in the S/G ratio in intermediate and mature tissues compared to the young tissues, caused by an increase in the G-unit content. Conversely, the S/G ratio in the pith regions increased during the stem maturation. Similarly, Siqueira et al. (2011) observed that sugarcane pith samples were promptly hydrolyzed by cellulases, while the conversion of cellulose in rind samples was dependent on chlorite pre-treatments. The significantly higher cell wall recalcitrance of sugarcane rind samples was mainly attributed to

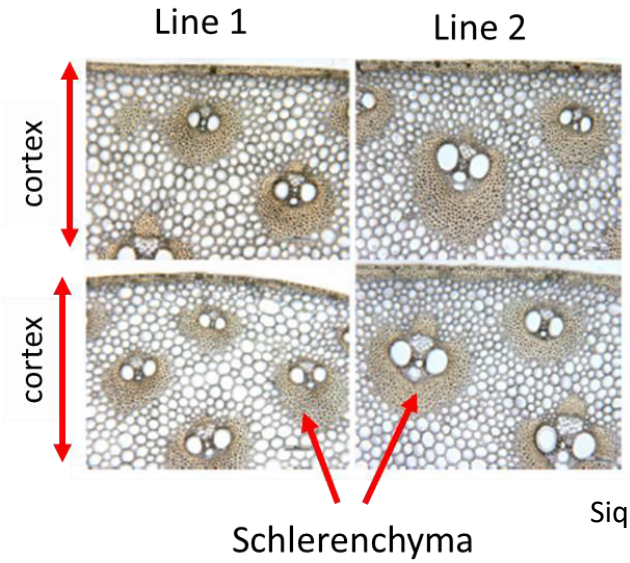


Figure 20. Histological cross-sections of 2 maize lines different for their amount of sclerenchyma around the vascular bundles. Line 2 presents more sclerenchyma than line 1. (adapted from Boon et al., 2012).

the massive presence of lignin-rich fibers and vessels. The presence of a more condensed G-rich lignin in the rind of the stem in Bottcher et al., (2013) might also be implicated.

Very recently, more and more studies investigated the distribution of lignification and its relationship with cell wall degradability, particularly in grasses. In 2015, Guzzo de Carli Poelking et al., associated the low sugar release efficiency of an ancient sugarcane genotype to a higher lignin content and a rind more lignified with greater sclerenchyma sheath around the bundles. Costa et al., went further in 2016 by quantifying tissue specific xylans. They showed that the rind was more lignified than the pith for 6 sugarcane hybrids with more crystalline cellulose within. Investigating this tissue specificity, Smith et al., (2017) used tissue specific promoters (specifically for xylary parenchyma and ficher cells) in Arabidopsis stem and they showed that lignification was specific according to a tissue.

Thus the distribution of lignification has a key role to play in the explanation of the variations of cell wall degradability. More and more results are being reported, revealing the interest to investigate these relationships. However, the mechanisms of the distribution of the lignification are still poorly understood and need to be further investigated.

VI. Impact of water stress on cell wall composition and on lignification distribution

As the reports on the climate change are worse and worse, and all the agro-environmental policies are encouraging the reduction of the water use in crops, more and more studies are investigating the potential effects that a water loss could have on the biomass quality, and therefore its composition.

Reduction in leaf expansion with water deficit is an adaptive process that reduces transpiration rate via a decreased leaf area. It saves water during vegetative stages in favor of reproductive stages and avoids deleteriously low leaf water potentials at a given soil water status (Tardieu and Tuberosa, 2010). Stress affects growth and development because plants need to re-allocate energy to adapt to the limiting conditions (Skirycz & Inze, 2010).

The induction of lignin in plants has been correlated to stresses such as cold, drought or light as well as mechanical injuries in a number of plant species such as poplar, rice, pine, Arabidopsis and soybean (Moura et al., 2010). Moura-Sobczak et al., (2011) reported that *Eucalyptus urograndis* subjected to drought decreased the amount of lignin in the stem apical regions and increased lignin in the basal region while *E. globulus* showed an opposite behavior in apical regions and showed no significant changes in the basal regions. A hybrid between both species (*E. uroglobulus*) showed a pattern similar to *E. urograndis* in apical regions and similar to *E. globulus* in the basal regions. Therefore, drought may not induce the same

responses between 2 different genotypes of the same species. Thus Wildhagen et al., (2018) showed it on poplar that a cultivar from Spain with the same lignin content than a cultivar from Italy showed a much higher saccharification than the italian one under drought condition. Suggesting that, even between cultivars of the same species, the lignin content under drought condition do not explains the observed variation of degradability.

A recent study on spruces showed that drought induces stem cracks along the trunk and that it was associated to the production of extremely thin cell walls in earlywood which lead to the collapse of tracheid walls (Rosner et al., 2018). This depletion in lignin content in tracheids in response to drought was recently reviewed by Pereira et al., (2018) who pinpointed that understanding embolism resistance is a key factor to elucidate plant responses to drought and adaptive strategies in both dry and wet environments (Choat et al., 2012; Lens et al., 2013; Anderegg et al., 2016). Thus a greater lignin content in the xylem could improve resistance to embolism induced by drought. A study of 2016, compared grasses and angiosperms trees for drought-induced embolism and they confirmed that grasses with a stem more lignified, particularly in the xylem was more resistant to embolism (Lens et al., 2016).

Several studies have also reported an impact of the water deficit on the biomass composition and quality. Thus, in 2014, Sanaullah et al. showed that high temperatures mimicking drought had an effect on the composition of the cell wall in fescue and orchardgrass. Indeed, in response to the high temperatures they applied to mimic drought, both species presented a reduction in their lignin content and this was associated to an increase of non-cellulosic sugars. In another study on crops in fields in the United (Figure 21), Emerson et al. (2015) analysed the biomass quality of several grasses after a normal year of culture in 2010 and a drought event which occurred 2012, causing lots yield redutcion in the cultures in the United States. They showed that miscanthus, mixed grass and maize had their cell wall composition heavily impacted. Along with the yield, xylans, lignins and cellulose content were decreasing significantly with drought in two different Pioneer maize hybrids, miscanthus and mixed fodder grasses.

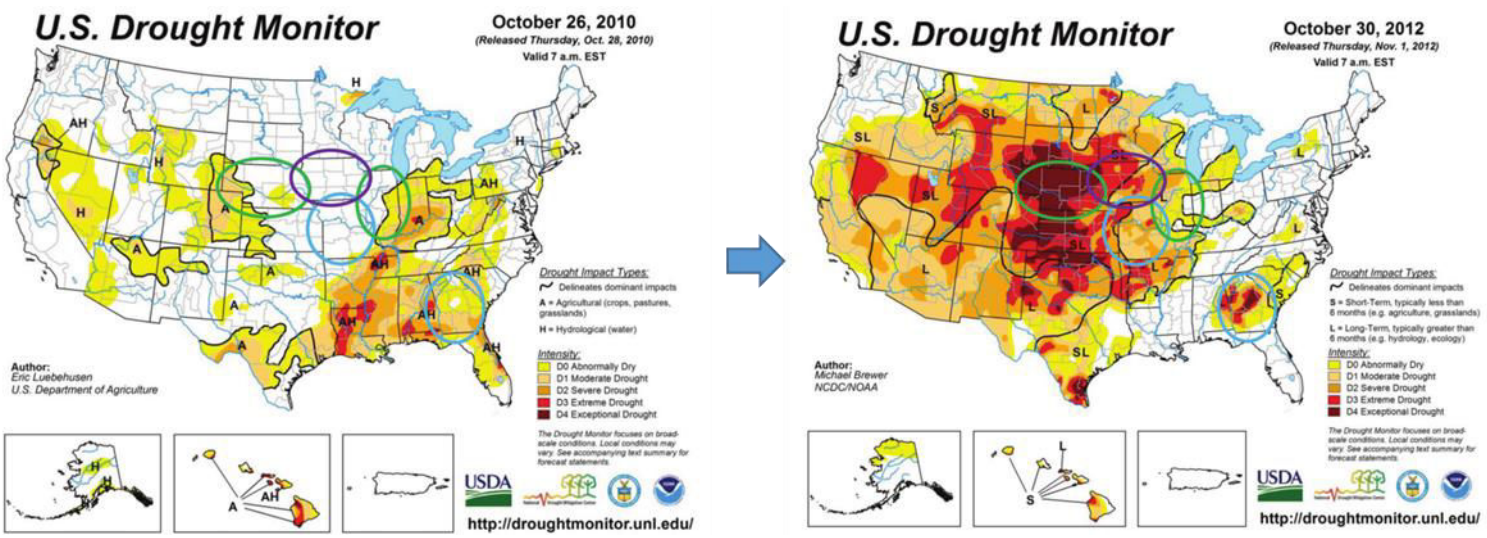


Figure 21. U.S. drought monitor for October 26th of 2010 (left) and U.S. drought monitor for October 30th of 2012 (right) (from Emerson et al., 2015).

More recently, in 2017 Naz et al. studied the effect of drought on 179 barley genotypes and particularly the effect on the straw. They applied drought under a foil tunnel in order to reduce water supply until reaching 5% of the volumetric moisture content within 2 weeks. They showed strong effect on the C/N ratio which was increasing significantly under the drought condition. This was associated with a significant decrease of the lignin content, total phenolic compounds and crude proteins concentrations. The lignin content was the most impacting trait for the energy conversion. It was not significant but the digestibility of the organic matter seemed to increase with drought. A recent characterization of new varieties drought tolerant, *Cenchrus purpureus*, a grass plant from Africa used as fodder, showed an impact of drought on the regrowth of the plant (Ledea-rodriquez et al., 2018). Indeed the interaction of the regrowth of the plant with the climatic conditions in leaves was a significant reduction for cellulose, hemicelluloses and cell wall residue. This interaction of the regrowth of the plant with the climatic conditions in stem was a significant reduction only for ADF (Acid Detergent Fiber: Lignin + Cellulose content extracted via Van Soest Method).

Investigating the impact of drought on biomass for bioethanol valorization, Van der Weijde et al., (2017) performed a drought experiment in greenhouse on 50 miscanthus by applying 28 days without watering. They analysed the biomass quality in both the leaves and the stems. They observed a great decrease both in the leaves and in the stem of the biomass fraction along with the cell wall residue and cellulose. Surprisingly, the ADL (Acid Detergent Lignin: lignin content extracted via VanSoest Method) decreased very little and still, drought improved the saccharification significantly among the 50 individuals. We can hypothesize that drought induced spatial and/or structural/compositional modifications other than reducing

simply the lignin content. Moreover, with the observations of genotypes which did present a response on the biomass yield side but not on the saccharification yield, the author proposed the possibility to identify genotypes resilient to the water deficit for the saccharification.

More recently Yan et al., (2018) engineered Arabidopsis plants to be more drought tolerance. To do so, they expressed different genes which induced a low degree of xylan acetylation, low lignin content (expression of the gene Qsub, a dehydroshikimate dehydratase) and low xylan content. They demonstrated that plants engineered to accumulate low levels of these components were more tolerant to drought and activated drought responses faster than control plants. This suggest that modifications of the cell wall components, and particularly the lignin content do not necessarily lead to negative performances of the plants.

As the histology is being investigated for about 10 years only, the impact of a drought stress on the different tissues of the stem have not been much investigated. However a few studies have come up lately.

In 2015 Dos Santos et al., showed on 2 sugarcane genotypes that drought was impacting the composition but also that it was associated with tissue specificity. Thus they demonstrated that drought significantly impacted the cortical region (Figure 21-A) and evaluated that in the cortex of young internodes there were a 60% increase in lignin content induced by water stress (Figure 21-B). Nevertheless, soluble sugars seemed not to be impacted.

Last year, in 2017, Perrier et al. showed in 2 sorghum hybrids cultivated 2 years in Mauguio (Hérault, South of France) under a control and a water-deficit condition that the distribution of the lignification was impacted. On FASGA-stained cross sections of the stem, they showed that the percentage of sclerenchyma of the cortex region was decreasing under drought condition. This was associated with a decrease of ADL and cellulose under the water deficit condition. Hemicelluloses however, did not respond to drought.

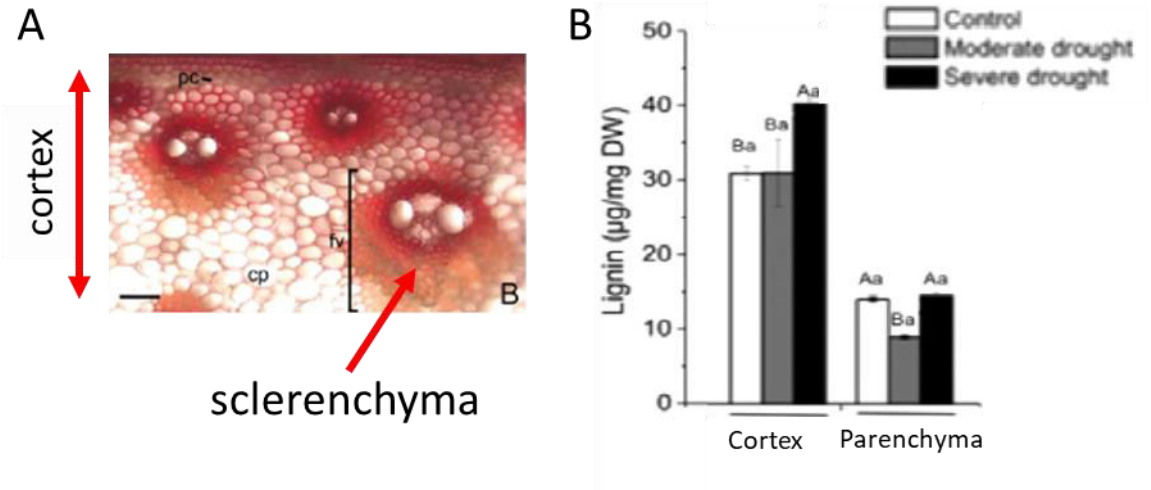


Figure 21: Effect of the drought on the tissue type in sugarcane (adapted from Dos Santos et al., 2015). A. Maüle stained cross section of sugarcane stem, epidermis is at the top, and pith is at the bottom. B. Lignin content measured in the cortex or in the parenchyma of the sugarcane stem in 3 conditions: control, moderate drought and severe drought.

More recently, Wildhagen et al., 2018 showed on poplar cultivated in well-watered and drought treatments for 5 weeks in 3 different countries (Spain, Italy and France) that the drought condition induced a significant increase in the cell wall area of vessels and fibers.

Thus, water deficit impacts the stem of the plants and its cell wall degradability at several levels; on the gene expressions, the biochemical cell wall component contents/structure and on the distribution of the lignification. Investigating further the responses of plants to water deficit will lead to a better understanding of the mechanisms of the cell wall lignification and will allow the selection of plant resilient to water deficit.

VII. Genetic determinism of the cell wall traits under different watering conditions

With the emerging of the molecular biology during the second part of the 20th century, genomic studies yielded a lot of results. Molecular markers allows a precise investigation of heredity of complex traits. The study of the genetic determinism of quantitative traits consists in identifying the genetic factors or regions of the genome involved in the variation of complex (or quantitative) traits. A quantitative trait results in the segregation of numerous genes which for the most present a weak individual effect. So the question is to know how many genes or loci explain significantly a quantified proportion of the phenotypic variability. The study of the quantitative traits heredity implicate at least 3 steps: 1) the establishment of a genetic map thanks to a genotyping of markers, 2) identify on this map the locus significantly correlated to the observed variation of the investigated trait, 3) the constitution of a population of

cartography. These loci are then called QTL or quantitative trait loci. QTL detection or QTL mapping is the processes to identify QTL through an experimental cross (QTL mapping) or through a population of genetic diversity (GWAS).

In such an analysis, the quantified traits are required to vary among the population analysed in order to ensure the find of loci. Variations in such quantitative traits are often due to the effects of multiple genetic loci as well as environmental factors (Broman and Sen, 2009). It is then the knowledge of the number, the locations and the effects of QTL that are under investigation in these kind of studies. Furthermore, the co-localisation studies allow to postulate genetic hypothesis on the links between the variations of different traits. It rises the questions of linked genes and/or pleiotropic effects between genes. Concerning the breeding, the use of markers to select genotypes with performant aptitudes is a method largely performed.

The fundamental idea of QTL mapping is therefore to associate genotype and phenotype in a population exhibiting genetic variations. Numerous QTLs have been detected in many model species, concerning biomass quality mainly, but it is also possible to find a few studies about QTLs under drought conditions and very few on histological traits.

a) QTLs of cell wall components

For now more than 20 years, several quantitative trait locus (QTL) analysis on the cell wall components of maize have been performed on different recombinant inbred lines populations, generating (or issued) from the cross of lines. In these studies the quantifications and the evaluation of the cell wall composition is widely estimated using NIRS predictive equations according to the Goering and Van Soest procedure (1970) where the neutral detergent fiber (NDF = cell wall residue), acid detergent fiber (ADF= Lignin + cellulose), acid detergent lignin (ADL = lignin content), cellulose (CL.NDF = ADF-ADL) and hemicelluloses (HC.NDF = NDF-ADF) contents.

QTL analyses which have been performed to determine the genetic factors involved in the variation of cell wall degradability and composition in maize using mainly biparental populations are numerous (Lübberstedt et al., 1997a,b; Bohn et al., 2000; Barrière et al., 2001, 2008, 2012; Méchin et al., 2001; Papst et al., 2001; Roussel et al., 2002; Cardinal et al., 2003, 2005; Fontaine et al., 2003; Krakowsky et al., 2005, 2006; Riboulet et al., 2008; Wei et al., 2009; Lorenzana et al., 2010, Torres et al., 2015, Leng et al., 2018). Over 400 QTLs related to cell wall degradability and composition have been mapped all over the maize genome (Barrière et al., 2008). A meta-analysis of QTLs carried out by Truntzler et al. (2010) resulted in the identification of 26 meta-QTLs for cell wall degradability and 42 meta-QTLs for cell wall composition, suggesting that the genetic determinism of these traits are complex but might

be reduced to a smaller number of genomic regions. Interestingly, only less than half of the meta-QTLs for cell wall degradability co-localized with meta-QTLs for cell wall composition. Moreover, only few major QTLs (which explained more than 20% of the observed variation) have been reported for cell wall-related traits (Roussel et al., 2002, Courtial et al., 2013), underlying the fact that cell wall composition and degradability are under a complex genetic determinism.

Cardinal et al., 2003 performed a QTL detection in a recombinant inbred lines (RILs) population from the cross of B73 (which is the maize reference genome) with B52. They detected QTLs for NDF, ADF and ADL, and more particular in different fraction of the maize plant. Thus, they found 12 QTLs for ADL in stalks and 8 QTLs for the leaf sheath tissues. 2 years later, Krakowsky et al., (2005) performed also a QTL detection in a recombinant inbred lines population from B73 x De811. Particularly they performed the detection on the cell wall traits of the stalk (2005) and then on the leaf sheath tissues (2006). They found co-localisation between the two studies, particularly at bin 1.02 and 7.02 for the ADL. They also pinpointed potential genes candidates for cellulose and starch biosynthesis under NDF and ADF QTLs.

In 2017 Li et al. 2017 analysed the genetic determinism of cell wall traits at anthesis stage of the 2nd to 5th internodes of a RIL population of 220 lines from the cross between lines Zheng58 and HD568. They predicted the Cellulose, lignin content, ADF, and NDF thanks to NIRS predictive equations. They detected a total of 47 QTLs and 29.7 % of them explained more than 10 % of the phenotypic variation in the RIL population. It shows the complexity of the genetic behind these cell wall traits. Their variations are not driven by 2 main regions but by many little regions, which make difficult the full-understanding of the genetic determinism of these traits. However, some regions are often cited between studies on the cell wall traits in maize even between different RILs populations and it suggests some important regions for the variations of these traits (Barrière et al., 2005).

The literature is rich of QTLs studies for the cell wall traits and the biomass quality, because it represents a good base of research and selection for breeders. However, QTL studies for the variations of histological traits are less abundant because these traits are still little known.

b) QTLs of tissue distribution

Using the strategy of QTL mapping, a number of QTLs related to vascular bundle system (morphology, number, density, composition) have been mapped in plants of agronomical interest such as in tomato, where they mapped QTL for the size of primary vascular bundles, morphology of the stem, and the thickness of the secondary vascular tissue (Coaker et al., 2002), in wheat (Sang et al., 2010) and rice (Sasahara et al., 1999; Zhang et al., 2002; Cui et al., 2003; Bai et al., 2012). In contrast, the genetic determinism of such histological traits in maize were much less investigated. To my knowledge, only one study in 2015 from Huang et al., report the identifications of QTLs involved in the number of vascular bundles within a population of maize-teosinte back-cross recombinant inbred lines to assess or not if the domestication of maize selected or not the number of bundles. They found that the number of vascular bundles is driven by a large number of small effects QTLs in which 16 QTLs which explained altogether 52.2% of the observed phenotypic variation. In these ones, a single QTL was explaining more than 6 % of variation. They concluded that this trait was not under domestication. They fine-mapped a QTL of 1.8 Mb on chromosome 9 thanks to the development of Near Isogenic Lines (NILs) for this locus.

The main reason of the low amount of studies for the genetic determinism of these traits is the long and tedious phenotyping work it represents. As an example, Huang et al., (2015) did quantify by hand the number of vascular bundles for 3 plants multiplied by 866 recombinant inbred lines. However, more and more automated tools are developed to quantify such traits. Heckwolf et al., proposed in 2015 an image analysis tool to quantify the parenchyma area within the pith and the number of bundles within parenchyma in sorghum stem.

c) QTLs under different watering conditions

In maize, QTLs for drought tolerance in grain yield have been largely studied and reported in literature (Ribault et al., 2007; Collins et al., 2008) and a more recent study investigated the early vigor and stay-green conferring tolerance to drought in grain in maize in 2 backcross populations in tropical maize (Trachsel et al., 2016). So far, in maize, no QTL for cell wall degradability or composition or any histological traits under water deficit conditions has been reported yet, although several reports recently showed that water deficit impacts cell wall degradability, composition and spatial lignification (in this introduction part VI). Interestingly, in 2015, Torres et al., studied the genotypic variation for maize cell wall traits across environments. They cultivated 34 lines coming from a doubled-haploid maize family and also the cross of these 34 lines with a commercial tester in 4 environments which differed

according to the daily mean temperature and the relative humidity over the growing season. They showed that the cell wall traits presented generally a high heritability, suggesting that the differences between genotypes remained constant across different environmental conditions.

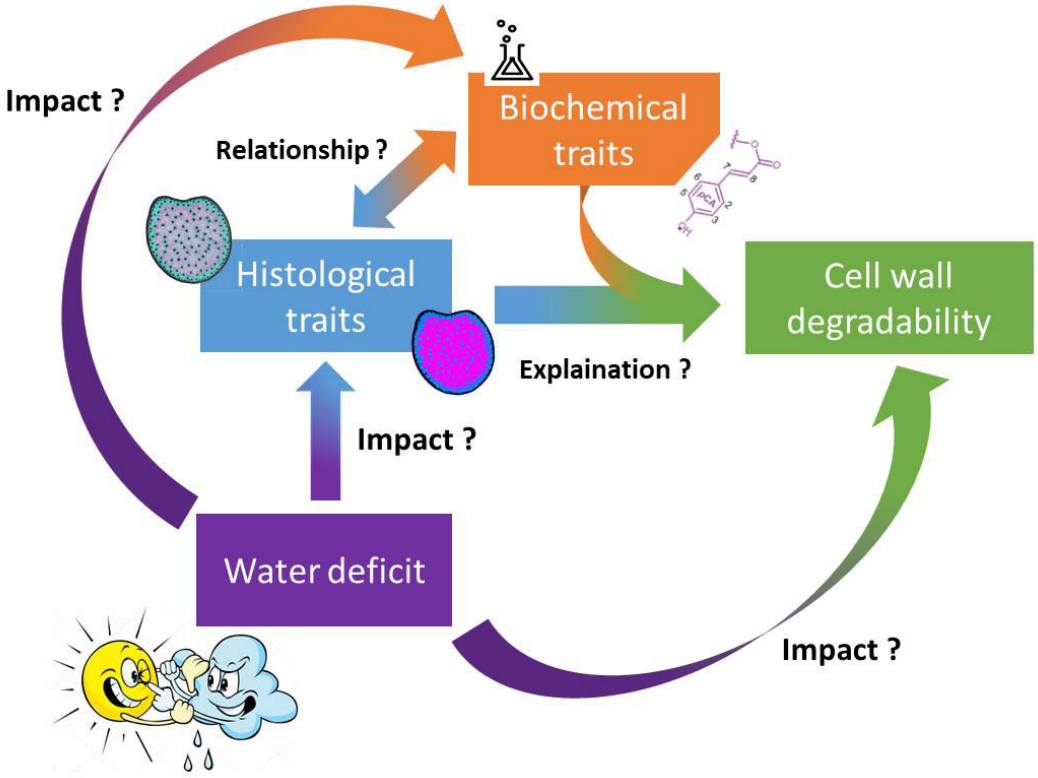
Recently, Naz et al., (2017) investigated cell wall composition traits such as the lignin content and total phenolics (TP) contents within the straw of a population of 179 barley accessions grown under control and drought conditions (water supply reduced until reaching a volumetric moisture content of 5% within two weeks and maintained this level for another 2 weeks). They detected 4 loci significantly associated with the lignin content non-dependant of the water status which explained between 22.5 and 38.7 % of the phenotypic variation.

The genetic determinism of cell wall composition or distribution of lignification under water deficit has still to be investigated in maize to be able to conclude whether or not some particular genomic regions are involved in the response to water deficit of these traits.

If Van der Weijde et al., (2017) and Yan et al., (2018) showed that it was possible to dissociate biomass yield and response to drought of the traits of interest, then it becomes interesting to investigate the regions of the genome which are responsible of the variations of these traits in order to select plants resilient to water deficit. It would allow the selection of plant producing a biomass with a good quality in an environment of water deficit.

VIII. Objectives of my PhD

It is in a context of reduction of the water supply in the crops to face to the climate change consequences and the agro-environmental policies that my phD subject inserts. The main objectives are to further investigate biochemical and histological variations and modifications under contrasted water deficit in maize internodes and to decipher the respective role of these modifications on cell wall degradability.



The rest of my manuscript will be organized around three main chapters which will be followed by a general discussion:

Chapter 1 : Histological and biochemical traits involved in cell wall degradability variations in response to water deficit within maize internode using a set of 12 inbred lines

In this first chapter, we decided to investigate the response to water deficit of the cell wall biochemistry, the histological lignification, the degradability and the impact on their relationships within a panel of genotypes chosen to maximise the range of variations for cell wall degradability and to have a greater diversity of FASGA-stained histological profiles. We cultivated these genotypes during 3 years and under 2 irrigation conditions every years. Facing

a great amount of sample, we developed therefore two accurate and high-throughput tools to be able to characterize and phenotype the cell wall biochemical traits and the histological traits of all the genotypes. Then we decided to investigate a bit further a natural mutant impacted in its lignin biosynthesis pathway in these environments.

This chapter will therefore be structured in 3 parts: firstly, the published manuscript presenting the high-throughput image analysis tool developed for FASGA-stained cross section analyses (Legland et al., 2017) will be presented. Then, another published manuscript dealing with the study on the impact of water deficit on cell wall degradability, histological traits and biochemical traits in a panel of 11 inbred lines (El Hage et al., 2018) will be included in this chapter. Finally, the behaviour of the mutant F2bm3 will be presented and discussed along with the other inbred lines previously studied.

This chapter allowed us to draw general trends on the impact of water deficit on cell wall degradability, biochemical composition/structure and histological pattern. In addition the respective roles of histological and biochemical features on cell wall degradability are reported.

Chapter 2: Genetic determinism of histological and biochemical traits according to the water status

In this second chapter, we decipher the genetic determinism of histological and biochemical traits of maize internode under irrigated and non-irrigated conditions. There are only very few studies on the genetic determinism of histological traits and as far as we know, this is the first time that genetic determinism of such traits has been investigated under contrasted irrigation conditions. One of the reason of this scarcity resides in the tedious phenotyping of these traits. The high-throughput tools we developed in the team paved us the way to access to the histological and biochemical phenotyping of a large amount of samples. Here we present a QTL analysis of about 200 recombinant inbred lines cultivated in 2014 and 2015 in 2 contrasted irrigation scenarios.

The objectives of this chapter were triple; first to investigate the loci involved in variations of histological and/or biochemical traits of maize internodes in different irrigations conditions, and secondly to investigate co-localisation between QTL for histological traits and QTL for biochemical traits at the internode and/or at the whole plant levels mapped on the same RILs population, and finally to present the loci involved in the variation of the cell wall traits in the whole plant without ears.

Chapter 3: Does histology of the internode carrying the main ear represent all the internodes of the stem and even reflect the biochemistry of whole plant without ears?

After presenting 2 chapter mainly dedicated on the internode carrying the main ear, the question of whether or not its biochemistry or its lignification distribution reflects the biochemistry of the whole plants is addressed in this third chapter. This is why I decided to investigate further the relationships between this internode and the biochemistry of whole plant without ears. Furthermore, the stems of 8 genotypes where further investigated to test if the internode bellow the main ear is representative of all the internodes of the stem at the histological level and if genotypic differences highlighted for this internode revaled genotypic differences of the stems.

Chapter 4: General conclusion and discussion.



Chapter 1

Chapter 1 : Histological and biochemical traits involved in cell wall degradability variations and responses to water deficit of maize internode using a set of 12 inbred lines

Introduction

For more than 60 years now, parameters influencing the cell wall degradability of the maize stem has been investigated (Nordfeldt, 1959 ; Gondos et al., 1960 ; Hartley et al., 1978 ; Albrecht et al., 1986 ; Deinum and Struik, 1989, Barriere et al., 1991; Wolf et al., 1993; Jung and Buxton, 1994; Argillier et al., 1995; Méchin et al., 2000; Casler and Jung, 2006; Baumont et al., 2009; El Hage et al., 2018). Among all these studies, lignin content in the cell wall remains the trait influencing the most strongly and negatively cell wall degradability. It appears then that reducing lignin content in the cell wall would be a seducing lever to select maize plants with an improved cell wall degradability but the side effects of such a selection are too risky. Indeed, a low lignin content level in the cell wall has negative impacts on the mechanical resistance of the plant to the environmental aggressions such as wind or insects bites. Moreover, it affects negatively other agronomical performances, the height and the yield are decreased (Barrière et al., 1988; Barrière et Argillier, 1993). It also decreases the resistance of the cell wall to fungus or pathogens attacks (Ride, 1975; Barros-Rios et al., 2012, Miedes et al., 2014). Even more, some studies show plant would not survive without a minimal lignification particularly to conduct the xylem and the phloem to the different organs of the plant (Goujon et al., 2003; Reddy et al., 2005; Vignau-Loustau and Huyghe, 2008).

Facing this reality, additional lever than the lignin content have been investigated in order to improve cell wall degradability with the smaller possible impact on plant's overall agronomical performances. With this purpose, and despite the strong influence of lignin content on cell wall degradability, some studies investigated the cell wall components and showed that the lignin composition could play a significant role in the variations of cell wall degradability. It was demonstrated in gymnosperm by measuring the paper paste potential of the wood (Whetten and Sefderoff, 1991; Achyutan et al., 2010), in raygrass and wheat straw (Taboada et al., 2010) but also in maize (Jung et al., 1999; Mechin et al., 2000; Grabber et al., 2009, He et al., 2018). Others studies showed that the lignin structure, i.e. the yield of BO4 linkages within the polymer, was also influencing the degradability of the cell wall (Grabber et al., 1998a ; Baucher et al., 1999, Grabber, 2005; Mechin et al., 2005; Casler et al., 2008; Zhang et al., 2011). At last and specifically in grasses, the *p*-hydroxycinnamic acid contents were shown to play a negative role in the variations of cell wall degradability (Jung et al., 1983 ; Eraso and Hartley, 1990 ; Jung and Engels, 2002, Taboada et al., 2010 ; Piston et al., 2010 ;

Ralph, 2010 ; Siqueira et al., 2011 ; Chong et al., 2016). More particularly, in 2011, Zhang et al. showed on a set of selected lines having a similar lignin content in the cell wall, that the cell wall traits explaining the best the cell wall degradability were the BO4 linkages yield, ie the general structure of the lignins, and the *p*-coumaric acid content.

On the other hand, looking for the distribution of the lignification within the tissues, some studies have shown that all the tissues in maize stem were not degraded with the same efficiency (Jung and Casler, 2006; Devaux et al., 2018), some others have shown that lignification in particular tissues such as the sclerenchyma around the bundles and the rind of the stem significantly impacted cell wall degradbaility (Lopez et al., 1993 ; Hatfield et al., 1999 ; Guines et al., 2001 ; Boon et al., 2011; Siqueira et al., 2011 ; Boon et al., 2012 ; Sanaullah et al., 2013 ; Perrier et al., 2017). Some studies even looked closer into the links between cell wall composition and the lignification distribution within the stem. More precisely, in 2005, Mechin et al. proposed a maize ideotype with several histological and biochemical traits, based on the study of twenty-two maize inbred lines. Among these inbred lines, they deciphered the link between the cell wall degradability, the cell wall composition and the distribution of the lignification. Then they proposed a silage maize ideotype which would present a reduced lignin content with lignin enriched in syringyl subunit, but also with lignin preferentially localized in the cortical region of the stem rather than in the pith.

Finally, with the will to produce crops with a greater sustainability and a low impact on the environment, the agro-environmental policies are more and more encouraging the reductions of inputs and especially the irrigation of the crops. The global warming also brings questions about the impact of a lack of water on the crops and the quality of their biomass. More and more studies are showing results about the impact of a drought stress on plant cell wall composition, and the main results tend to show a systematic reduction of the lignin content and a greater degradability in response to water deficit but accompanied with a significant decrease of biomass yield. It has been shown on maize (Sanaullah et al., 2014; Emerson et al., 2014), on sugarcane (Benjamin et al., 2014; Dos Santos et al., 2015) on sorghum (Perrier et al., 2017), on miscanthus (Emerson et al., 2014 ; van der Weijde et al., 2017), on barley (Naz et al., 2017). If drought was associated to a decrease in lignin biosynthesis in maize roots and leaves (Alvarez et al., 2008; Vincent et al., 2005), however certain studies on maize leaves and on flax show the opposite tendency. The leaf of the plant responds to water deficit with an upregulation of the lignin biosynthesis pathway, suggesting a strategy to face and reduce the water loss and increase mechanical stress and/or water impermeability (Hu et al., 2009; Le Roy et al., 2017).

Among these issues, my PhD project is addressing two questions; the different kind of biochemical or histological lever, along with the lignin content, which could impact the cell

wall degradability of the maize stem; and more specifically the impact of the irrigation scenario on these traits.

In this first chapter, a set of 11 maize inbred lines selected for showing a large range of degradability and lignin content variation, but also for presenting diversity of histological profiles has been studied. The plants were cultivated during three years (from 2012 to 2014) under 2 different irrigation scenarios in two blocs per scenario at Mauguio (Hérault, France).

In the first part of this chapter, we present how we first phenotyped 124 harvested internode samples for all the cell wall biochemical related traits using dedicated Near Infra-Red Spectrometry (NIRS) prediction equations. Secondly, for every genotypes, internode carrying the main ear was also harvested to quantify histological traits on FASGA stained cross-sections thanks to the development of a high-throughput image analysis pipeline which was published in Plant Methods (Legland et al., 2017). We then analyzed the relationships between these biochemical and histological traits and the cell wall degradability of the internodes. More particularly, we investigated the response to the irrigation scenario of the cell wall composition and on the distribution of the lignification. These results were published and discussed in the Journal of Agricultural and Food Chemistry in 2018 (El Hage et al., 2018).

In the second part of this chapter, we completed our reflection with a discussion focused on the mutant F2bm3 in these approaches The brown-midrid mutation *bm3* is a historical model which has been investigated to better understand the lignin biosynthesis pathway together with its plasticity, but also, in the particular case of the fodder selection, to decipher its relationships with cell wall degradability (Weller and Phipps, 1985; Marita et al., 2003; Sattler et al., 2010). F2bm3 was previously studied and cultivated in Lusignan France, 86, (Mechin et al., 2000; Barrière et al., 2004; Mechin et al., 2005) and also in Estrées-Mons France, 80 (Machinet et al., 2011). As far as we know, the response to water deficit of this mutant has never been reported in literature. We discussed here the particularities of this genotype and the several phenotypes we could observe in different environments, at the biochemical and histological level.

Material and Methods

Plant material. Twelve public maize inbred lines (Table 3) were selected from previous experiments performed at INRA Lusignan between 1997 and 2008 (Méchin et al., 2000; Méchin et al., 2005; Barrière et al., 2009).

Table 3. Pedigree of the studied inbred lines

Line	Pedigree
F4	Northern Flint
F7082	M13 Dent x BSSS
F66	Soest Flint
F7019	M13 Dent x BSSS
F7025	Iodent x M13 Dent
F2	Lacaune Flint
F2bm3	Lacaune Flint
F271	Canadian dent
F874	Complex Dent
Cm484	Canada-Morden – 1989
F7092	Lacaune Flint
F98902	CRANaMOF 7-2-1-2-5-4

Field experiments were carried out at Mauguio (Hérault, France) during three successive years: 2012, 2013 and 2014. Each inbred line was cultivated each year (except F4 absent in 2012 and F7082 absent in 2014) under 2 contrasted irrigation scenarios. Under the non-irrigated scenario watering was no more provided from the emergence of the 5th ligulated leaf on F2 inbred until 14 days after flowering of all the lines (i.e. from June to August without irrigation). The trials were randomized block designs with 2 replicates. Length of the rows was 4.20 m, the inter-row spacing was 0.80 m and the density was of 80,000 plants per hectare. F2bm3 was also cultivated in 2012 and 2014 in Le Moulon (Essonne, France) and in 2017 in Versailles (Yvelines, France) without any irrigation supplied, the climate of the region, the soil depth and the summer rains are supposed to provide a sufficient natural water supply.

For each year, each condition and each block, the whole internode located under the main ear was collected for thirteen plants at silage stage for each line. Ten of these internodes were oven-dried at 55 °C during 72h and then grinded with a hammer mill (1 mm grid) before biochemical analyses and NIRS predictions. The remaining three internodes were stored in 70 % ethanol in order to perform histological analyses.

Histological analyses

Two cross-sections of 150 µm thickness were cut from two internodes of each line in each block, each condition and each year. A total of 528 cross-sections were obtained using an HM 650V Vibratome from MicroMicrotech France and stored in 70 % ethanol. They were then stained with FASGA solution (derived from Tolivia and Tolivia, 1987). The FASGA staining presents lignified tissues in red, whereas non lignified or poorly lignified tissues are colored in cyan/blue. The FASGA solution was prepared with a previous preparations of the staining solutions: Safranin and Alcian blue. They were prepared according to these proportions (Table 4):

Table 4. Compositions of the solutions composition the FASGA solutions.

1)

Safranin solution (1%) (1 month conservation)			
Reference	**Solution**	**Volume**	**Weight**
SIGMA S8884	Safranin O.		1 g
SIGMA S2889	Sodium Acetate		1 g
	Absolute ethanol	75 mL	
	mQ H_2O	25 mL	
SIGMA F8775	Formaldehyde	2 mL	

2)

Reference	**Alcian blue solution 0,5% (3 month conservation)**		
SIGMA S2889	Bleu alcian 8GX		500 mg
	Absolute ethanol	100 mL	

3)

Reference	**FASGA solution (1 month conserved)**	
	Safranin solution 1%	3 mL
	Alcian blue solution 0,5%	11 mL
SIGMA G7893	Glycerin 99%	30 mL
	mQ H_2O	20 mL
SIGMA 1005706	Pure acetic acid	1 mL

Then 65 ml of FASGA solution was prepared. Before being diluted in 1/8 in mQ water, the FASGA solution was filtrated with filter-syringe (filters with 0.45 µm pores). The cross-sections were put in a 12 wells plate with always a control stained cross-section coming from successive cross sections obtained from a F273 internode cultivated under irrigated scenario at Mauguio in 2013 (Figure 22-A). Then they were stained during 24h in 3 ml of the 1/8 diluted FASGA solution while stirring continuously (Figure 22-B-C). They were washed in mQ water during 24h hours while stirring continuously again (Figure 22-D). After 2 others successive washing during 5 mn in mQ water, all the cross-sections were mounted in distilled water on slides with a barcode identifying univocally each cross-section (Figure 22-E).

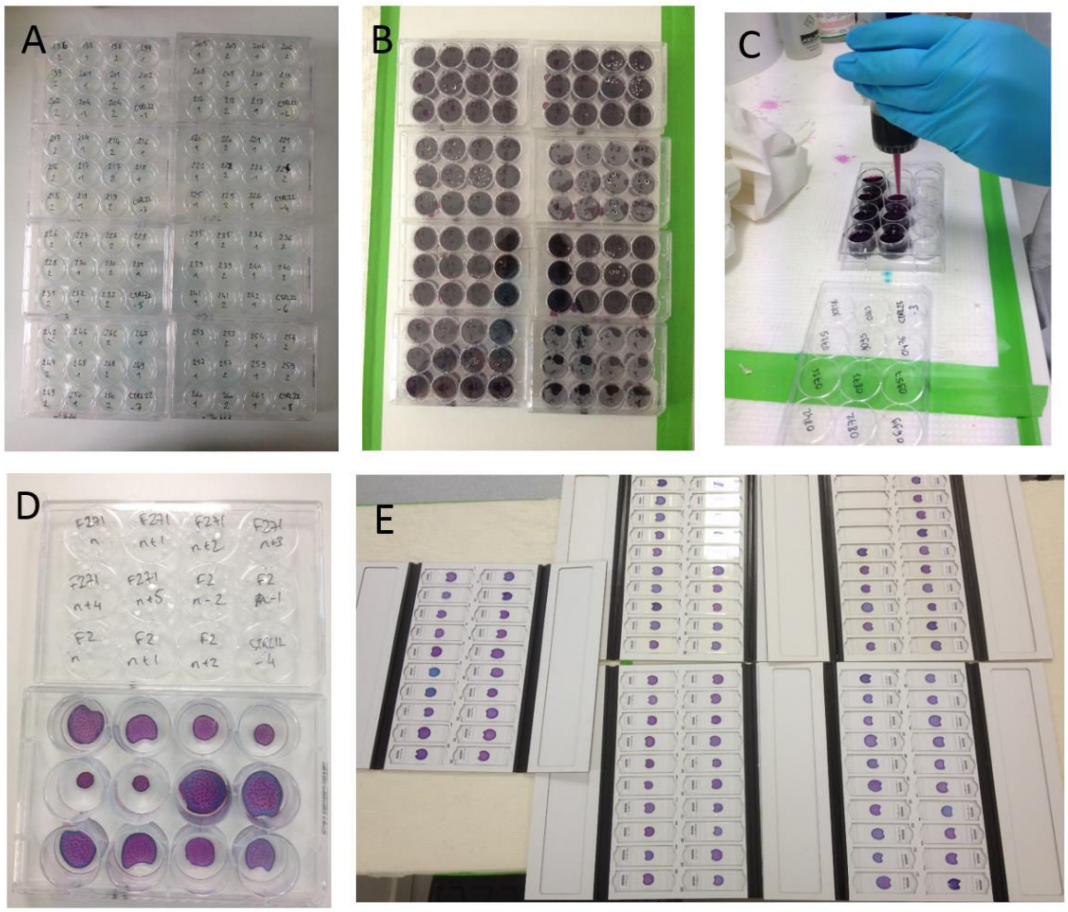


Figure 22. FASGA staining and slide set-up of the cross-sections. A. Preparation of the 12 wells plates. B. 12 wells plates filled in with 3mL of FASGA solution diluted 1/8e. C. Filling in of the wells with the FASGA solution. D. 12 wells plate after staining and washing in water. E. Cross-sections set-up in slides.

An image of every cross-section was acquired with the objective x5 of an AxioImager Z2 Zeiss and a CoolCube 1 camera with a 1360 x 1024 pixels resolution piloted by the software Metafer from MetaSystems (Figure 23). 30 focus points were made per slides and 300 pictures were taken per slides and then assembled with the software VSide from MetaSystems (Figure

23-C). Then the image were viewed and extracted in .tif format thanks to the software Metaviewer from MetaSystems (Figure 23-D).

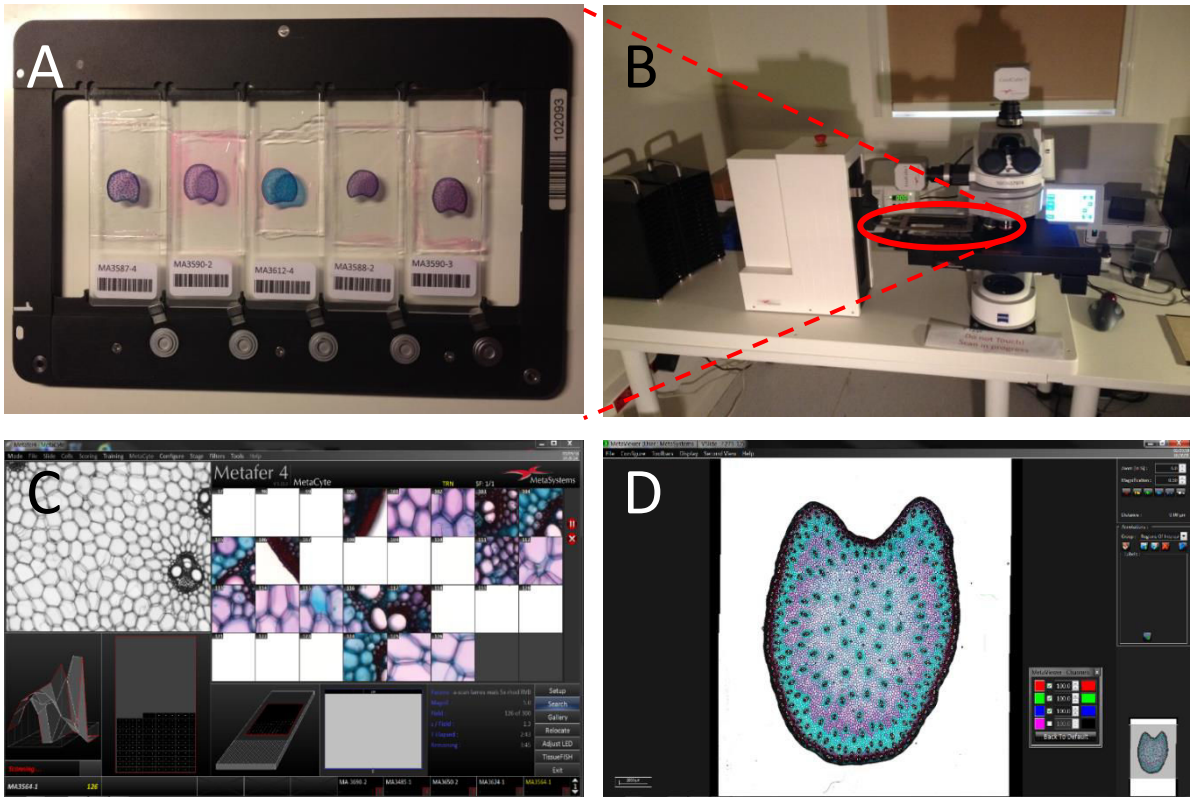


Figure 23. Image acquiring of the cross-sections. A. Disposal of the slides before the microscope acquisition in racks. B. Rack brought automatically under the microscope objective. C. Acquisition of the 300 pictures per slides. D. Viewing of the reconstructed image.

During my phD, the improvement of all this pipeline was an important part, from the cutting of the cross-sections until the acquisition in the most repeatable and high-throughput way. It is currently possible in 10 days to obtain the cross-sections and the pictures of 196 samples.

Then, each image was numerically analyzed on the ImageJ software with the plugin presented in Legland et al. (2017) to segment and quantify the following histological traits:

- Stem_Area, which is the area in cm^2 of the cross-section (Figure 24-A);
- Bundle_area (Figure 24-E), which is the area occupied by the bundles in percentage of the total area;
- Bundle_number (Figure 24-E), which is the number of bundles of the cross-section;
- Lignified_area (Figure 24-B in pink), which represents the surface of parenchyma stained by the Safranin;
- Non-lignified_area (Figure 24-B in blue), which represents the surface of parenchyma stained by the Alcian blue;
- Rind_area (Figure 24-B in black), which represents the rind of the stem;
- All the numerical, each encoded between 0 and 255, Red, Green and Blue intensities of the areas cited above (Figure 24-G, H, I).

From all these traits quantified by the plugin we calculated composite variables to synthetize the informations:

- Blue_parenchyma (Figure 24-D), which refers to the amount of blue intensity in the blue parenchyma;
- Red_parenchyma (Figure 24-C), which refers to the amount of red intensity in the red parenchyma;
- Red_rind (Figure 24-F), which refers to the amount of red intensity in the rind.

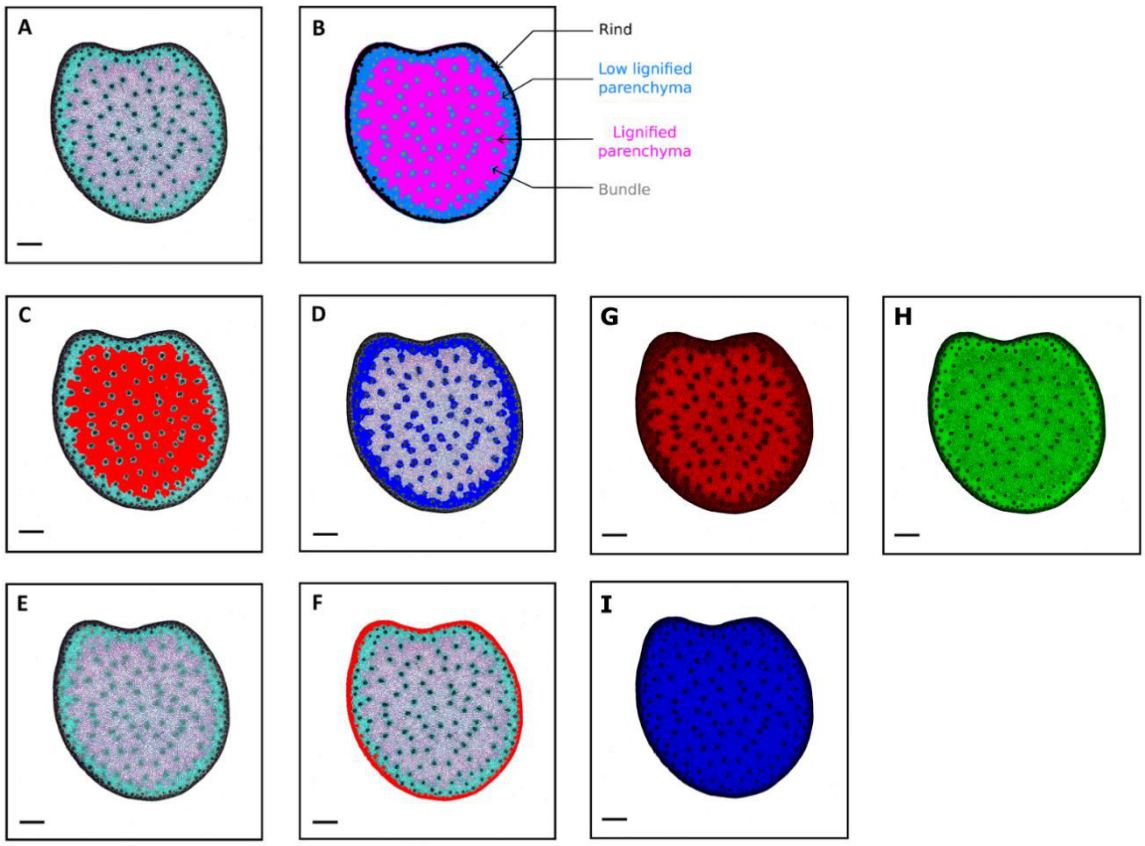


Figure 24. Histological traits quantified by the plugin (Legland et al. 2017) and additional composite traits.

A. FASGA stained cross-section of F2 genotype. B. Output of the image analysis with the different histological fractions segmented. C. Red_parenchyma trait in red color overlaid on the FASGA cross-section. D. Blue_parenchyma trait in blue overlaid on the FASGA cross-section. E. Bundle_area trait in grey overlaid on the FASGA cross-section. F. Red_rind trait in red overlaid on the FASGA cross-section. G. Red field of the cross-section where the intensity is calculated for each area quantified by the plugin. H. Green field of the cross-section where the intensity is calculated for each areas quantified by the plugin. I. Blue field of the cross-section where the intensity is calculated for each areas quantified by the plugin. Bar = 2 mm.

Presentation of the article Legland et al., 2017 published in Plant Methods:

Histological quantification of maize stem sections from FASGA-stained images.

D. Legland[1], F. El Hage[2], V. Méchin[2], M. Reymond[2]

Legland *et al. Plant Methods (2017) 13:84*
DOI 10.1186/s13007-017-0225-z

Plant Methods

METHODOLOGY

Open Access

Histological quantification of maize stem sections from FASGA-stained images

David Legland[1*], Fadi El-Hage[2], Valérie Méchin[2] and Matthieu Reymond[2]

Abstract

Background: Crop species are of increasing interest both for cattle feeding and for bioethanol production. The degradability of the plant material largely depends on the lignification of the tissues, but it also depends on histological features such as the cellular morphology or the relative amount of each tissue fraction. There is therefore a need for high-throughput phenotyping systems that quantify the histology of plant sections.

Results: We developed custom image processing and an analysis procedure for quantifying the histology of maize stem sections coloured with FASGA staining and digitalised with whole microscopy slide scanners. The procedure results in an automated segmentation of the input images into distinct tissue regions. The size and the fraction area of each tissue region can be quantified, as well as the average coloration within each region. The measured features can discriminate contrasted genotypes and identify changes in histology induced by environmental factors such as water deficit.

Conclusions: The simplicity and the availability of the software will facilitate the elucidation of the relationships between the chemical composition of the tissues and changes in plant histology. The tool is expected to be useful for the study of large genetic populations, and to better understand the impact of environmental factors on plant histology.

Background

Crop species like maize (*Zea mays* L.) are of increasing interest both for cattle feeding [1] and for bioethanol production [2–5]. The polysaccharidic fraction, mainly composed of the stem and the leaf cell walls, is digested or transformed into energy or fuel after several mechanical, biochemical and/or enzymatic processes. Many studies have been devoted to the elucidation of relationships between cell wall chemical composition and degradability [3, 6–9]. The lignin content is a key factor for explaining degradability. Several authors have reported that the variations of lignification according to the tissue may explain differences in the digestibility of plants at similar maturity stages [4, 10–12]. There is therefore a need to better understand variations in tissue lignification within stems and their relationships with external factors such as water availability or genotype.

Differences in the biochemical composition of tissues may be assessed by several methods. Manual dissection of tissues makes it possible to compare their biochemical composition and degradability [12]. However, these micro dissections entail very tedious work [3, 12] and are limited to an a priori choice of specific tissues.

The continuous development of imaging techniques has led to promising ways for investigating the chemical composition of plant tissues. Fluorescence imaging techniques allow for the localisation of specific proteins, polysaccharides and phenolic compounds [13, 14]. Vibrational microspectroscopies such as infra-red or Raman spectroscopies provide complementary information about the molecular composition of the observed materials [15]. However, the imaging of plant tissues is usually performed within a small field of view, making it difficult to quantify the variations of compositions within an organ such as a stem. X-ray computed (micro-) tomography is a powerful tool that enables the acquisition of 3D

*Correspondence: david.legland@inra.fr
[1] UR1268 Biopolymères, Interactions et Assemblages, INRA, Nantes, France
Full list of author information is available at the end of the article

BioMed Central

© The Author(s) 2017. This article is distributed under the terms of the Creative Commons Attribution 4.0 International License (http://creativecommons.org/licenses/by/4.0/), which permits unrestricted use, distribution, and reproduction in any medium, provided you give appropriate credit to the original author(s) and the source, provide a link to the Creative Commons license, and indicate if changes were made. The Creative Commons Public Domain Dedication waiver (http://creativecommons.org/publicdomain/zero/1.0/) applies to the data made available in this article, unless otherwise stated.

images of a whole sample, and several studies have been performed on plant materials [16–18]. However, the lack of information about chemical composition of cell walls limits the differentiation of lignified and non-lignified tissues. Mass spectrometry imaging has shown promising results for the visualisation of the distribution of specific chemical structures within a whole slice [19, 20]. The spatial resolution is larger than that of microscopy.

Plant cross-section staining is an alternative that can reveal components on a thin stem cross-section [9, 21–27]. In a previous study, Méchin et al. [5] compared the use of Maüle [28], phloroglucinol [29] and FASGA stainings [30] to assess the global lignification of maize stem cross-sections. FASGA staining coupled with image analysis was shown to be the best-adapted method. FASGA stains lignified tissues in red, whereas non-lignified or poorly lignified tissues are stained in blue. In a recent study, Zhang et al. [31] proposed an automated image analysis method for quantifying the histology of FASGA-stained sections of maize stems. However, the resolution of the images did not allow an accurate estimation of the proportion of the various tissue types, and it was not possible to quantify the histology of the different tissues.

In order to increase the resolution of acquired images, microscopy slide scanners provide promising features. They allow the scanning of an entire whole mounted histology sample, with a resolution of a few microns [32], making it possible to observe cellular morphology and organisation at the scale of the whole organ, with a resolution comparable to that of microscopy. It consequently appears to be a method of choice for the quantitative analysis of lignification within a whole stem section. The recording of the colorimetric information provided by the staining makes it possible to develop an automated image analysis procedure [33]. However, the huge amount of data generated increases the difficulty of processing and analysis [34].

The aim of this work is to present an automated method for the analysis of stained images of stem sections observed with a microscopy slide scanner. The method combines the identification of the different tissue regions that constitute the section based on colorimetric and morphological information, the quantification of the morphometry and the colorimetry of each tissue region. The method is illustrated on a collection of stem sections from several genotypes obtained with contrasted growing conditions.

Methods

Sample preparation

Four maize inbred lines (Cm484, F4, F271 and F7025) were selected from preliminary experiments performed at INRA Lusignan between 2006 and 2008 [2]. Plants were cultivated in Mauguio (southern France) during the years 2013 and 2014. Two different irrigation scenarios were used: one with irrigation, and the other one without irrigation where the watering was stopped after appearance of the 5th "liguled" leaf on the plant of a reference genotype and then restarted 14 days after flowering (i.e., from June to August without artificial watering). For each condition (with or without irrigation) the trials were randomised block designs with two replicates. The length of the rows was 4.20 m, the inter-row spacing was 0.80 cm and the density was 80,000 plants per hectare. The whole internode located under the main ear was collected for three plants at the silage stage (~ 30% of dry matter content) for each condition, block and genotype. Internodes were stored in 70% ethanol before quantitative histological analysis.

Image acquisition and preparation

A 1-cm-long segment was sampled in the upper part of each internode. For each segment, 15 cross-sections with a thickness of 150 µm were prepared using an HM 650 V Vibratome from MicroMicrotech France. Sections were stained for 24 h using a FASGA solution diluted in distilled water (1:8, v/v). The FASGA solution was composed of 0.05% safranin O, 0.2% Alcian blue, 1.5% acetic acid and 46% glycerine in distilled water. Safranin is a red, basic, cationic dye, and Alcian blue is an acidic anionic dye. Because lignin is acidic (due to its phenolic hydroxyl groups), lignified tissues are stained in red even if this stain is not completely specific for only lignin. FASGA thus stains lignified tissues in red, whereas non-lignified or poorly lignified tissues appear as blue. After staining, sections were rinsed for 24 h with distilled water while stirring continuously.

An image of each cross-section was acquired using a slide scanner piloted by the Metafer scanning and imaging platform (MetaSystems GmbH, Altlussheim, Germany). The complete system is composed of an AxioImager Z2 Zeiss microscope equipped with a CoolCube 1 camera, a robotic system consisting of a rotating feeder module that delivers samples to the microscope stage, and a computer piloted by Metafer software. Each image was acquired with the 5× objective lens. To reduce computation time and memory space, each picture was converted into a plain TIFF image by choosing the 6× zoom with MetaViewer software. Resulting images had a size of 4000 × 4000 pixels approximately and a resolution of 5.17 µm per pixel. Sample images for each genotype and each water treatment are presented in Fig. 1.

Image processing

A fully automated image processing workflow was designed for identifying the different tissue regions that compose the internode sections. The workflow is summarised in Fig. 2.

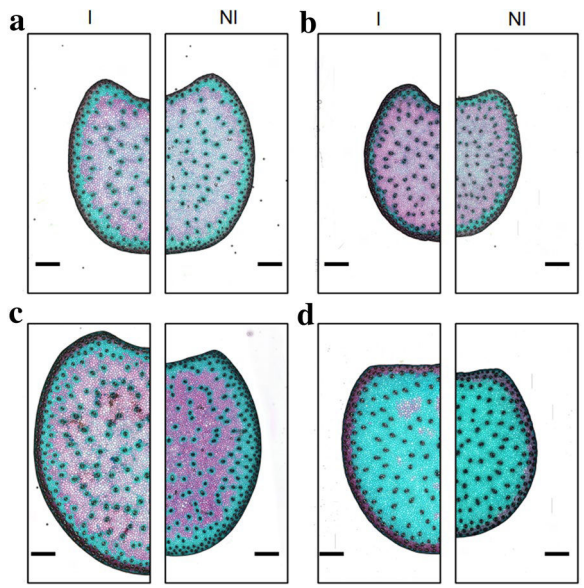


Fig. 1 Sample images of FASGA-stained cross sections of maize stems showing the heterogeneity of coloration for four genotypes and two irrigation conditions. **a**: Cm484; **b**: F271; **c**: F7025; **d**: F4. Left-hand panels correspond to the irrigated condition, right-hand panels to the non-irrigated condition

Filtering was first applied to the image to enhance the colour contrast and reduce acquisition noise. A combination of morphological opening and closing was applied [35], followed by a Gaussian smoothing (Fig. 2b).

The processing of colour images often takes advantage of transforming the RGB colours into a colour space that better discriminates the colours, such as HSV or Lab colour spaces [36–38]. The segmentation of the different tissue regions was based on the hue and luminance images. The hue represents the pure colour of a pixel, and the luminance quantifies the brightness.

The luminance image was used to identify the stem section (Fig. 2c). A hysteresis thresholding was applied to identify the regions of the stem occupied by tissues, while removing the regions corresponding to holes. Air bubbles could be observed on some images, resulting in thin dark artefacts outside of the stem. An additional morphological closing was added to remove eventual bubble boundaries. The result was a binary mask, used for restricting further processing of the valid regions (Fig. 2d).

The highly lignified tissues corresponding to vascular bundles and to the rind were identified by thresholding low values in the luminance image (Fig. 2e). Area opening was applied to remove segmentation noise [35]. A connected component labelling was used to identify the largest region that corresponded to the rind (Fig. 2f). Since some bundles could be connected to the region corresponding to the rind, a morphological opening was applied to separate them from the rind. From the luminance image it was then possible to identify the rind (containing outer vascular bundles) and the vascular bundles of the pith (Fig. 2g).

The hue component of the filtered colour image was used to discriminate between highly and lowly lignified

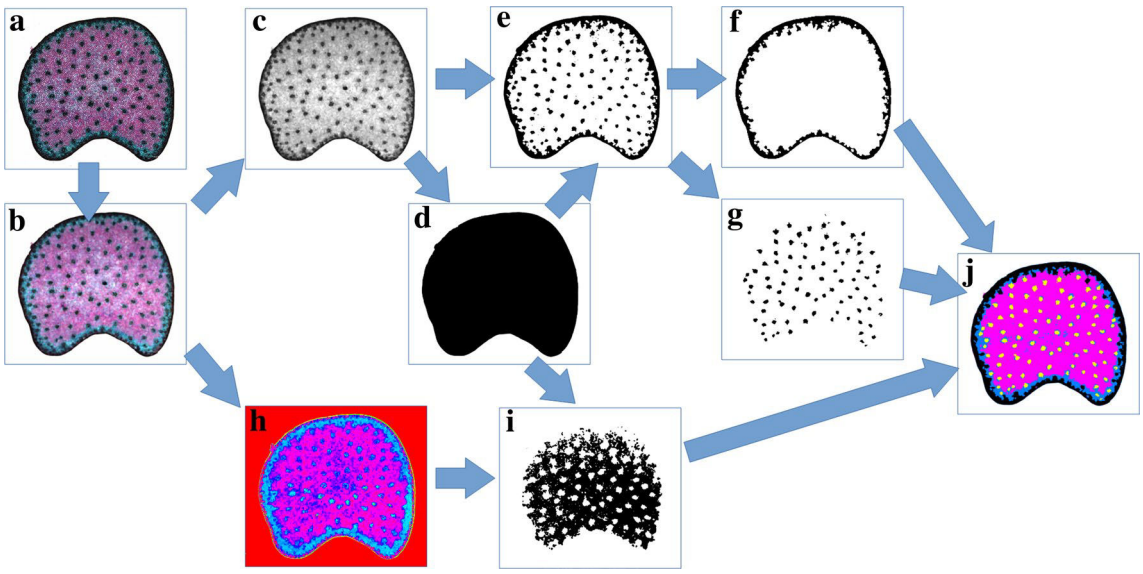


Fig. 2 Image segmentation workflow. **a** Original image. **b** Result of morphological filtering and Gaussian smoothing. **c** Luminance image. **d** Stem mask computation. **e** Dark structures identification. **f** Rind identification. **g** Bundles identification. **h** Colour representation of the hue image. **i** Identification of the lignified regions. **j** Result of composite image

Table 1 List and description of the 19 descriptors obtained by automated image analysis and used for statistical analysis

Feature name	Description	Type
Stem area	The area occupied by the stem section, in cm^2	Morphometry
Bundle number	The number of vascular bundles in the pith	
Bundle intensity	The numerical intensity of bundles, in cm^{-2}	
Lignified fraction	The tissue fraction corresponding to lignified pith	
Non lignified fraction	The tissue fraction corresponding to non-lignified pith	
Rind fraction	The tissue fraction corresponding to the rind	
Bundle fraction	The tissue fraction corresponding to vascular bundles in pith	
Lignified mean red	The mean red intensity in the lignified fraction	Colorimetry
Lignified mean green	The mean green intensity in the lignified fraction	
Lignified mean blue	The mean blue intensity in the lignified fraction	
Non-lignified mean red	The mean red intensity in the non-lignified fraction	
Non-lignified mean green	The mean green intensity in the non-lignified fraction	
Non-lignified mean blue	The mean blue intensity in the non-lignified fraction	
Rind mean red	The mean red intensity in the rind	
Rind mean green	The mean green intensity in the rind	
Rind mean blue	The mean blue intensity in the rind	
Bundles mean red	The mean red intensity in the vascular bundles	
Bundles mean green	The mean green intensity in the vascular bundles	
Bundles mean blue	The mean blue intensity in the vascular bundles	

regions of the pith parenchyma (Fig. 2h). The application of a threshold image could discriminate between lignified tissues (red-magenta colour) and non-lignified tissues (light cyan colour) (Fig. 2i).

Finally, the elementary binary images corresponding to the different tissue regions (rind, pith vascular bundles, lignified pith parenchyma, non-lignified pith parenchyma) were combined to create a label image used for histology quantification. A colour image showing each tissue with a specific colour was eventually used for final validation (Fig. 2j).

Image analysis

Several morphometric descriptors were computed from the label images corresponding to segmented tissue regions. The total area and the area fraction of each tissue region were computed on each image. The average values of the red, green and blue channels were also computed for each tissue region. The number of pith vascular bundles was counted automatically on each section. The ratio of the number of vascular bundles over the area of the section led to a measurement of vascular bundle intensity. In total, 19 descriptors were obtained (Table 1). Seven of them corresponded to morphometric features (area, area fractions of tissue regions, or bundle number). The remaining 12 descriptors corresponded to the measure of colorimetry in a specific tissue region.

Software implementation

The whole image processing workflow was developed within the ImageJ/Fiji plateform [39], using the MorphoLibJ library [40]. The whole workflow was implemented as an ImageJ/Fiji plugin, freely available on the Internet [41]. The plugin provides the possibility to finely tune the different parameters used at each step of the workflow. A macro is also provided, making it possible to process a whole batch of images using the same parameters.

Statistical analyses

Statistical analyses were performed within the Matlab software (The Mathworks, Natick, MA, USA), using the statistics toolbox and the MatStats library, a collection of functions developed in-house to facilitate the exploration and the analysis of statistical data sets [42].

Analyses of variance were performed by applying a general linear model to each of the 19 descriptors. Each model took the fixed effects of the genotype, the water treatment and the year, their interactions, the random effect of the sampling block nested to fixed effects, and the random effect of the stem nested to the block into account. The model for a descriptor f is given by the following equation:

$$f_{ijklm} = \mu + G_i + T_j + Y_k + (GT)_{ij} + (GY)_{ik} + (TY)_{jk} + (GTY)_{ijk} + B_l\left(GTY_{ijk}\right) + S_m\left(GTYB_{ijkl}\right) + \varepsilon_{ijklm}$$

where μ is the constant, G_i, T_j and Y_k are the fixed effects of the genotype, the water treatment and the year, respectively, $(GT)_{ij}$, $(GY)_{ik}$, $(TY)_{jk}$ and $(GTY)_{ijk}$ are the fixed effects of the interactions up to the third order, $B_l(GTK_{ijk})$ is the random effect of the block nested to the genotype, the treatment and the year, $S_m(GTYB_{ijkl})$ is the random effect of the stem nested to all other effects, and ε_{ijklm} is the residual error term. The "anovan" function of the statistics toolbox of Matlab was used for each of the 19 models. The resulting p values of all the models were concatenated in a data table using the descriptors as rows and the effects as columns.

Results and discussion

Acquisition of digital images

Figure 1 shows images of sample sections from each genotype and each irrigation condition. The size of sections depends largely on the genotype. After FASGA staining, lignified tissues appear in red, whereas non-lignified tissues appear in light blue. The vascular bundles and the rind usually appear in dark red or brown. Except for one genotype that generally appears to be non-lignified, a peripheral blue ring located below the rind was observed. On some sections, a blue ring around vascular bundles corresponding to non-lignified tissues can be clearly recognised.

The genotypes present clearly distinct responses to the coloration. For instance, the F4 genotype shows a small amount of lignified parenchyma. Variations in section size and in proportion of the tissue regions may also be observed. For each genotype, some variations in histology may be distinguished between irrigated and non-irrigated conditions. For example, section size seems to be smaller as does rind thickness in the case of water deficit. However, a large variability in the size and shape of the sections may be observed.

Segmentation of FASGA images

Figure 3 shows sample results of the automated labelling of tissues from FASGA stained sections. The segmented images correspond to the images presented in Fig. 1. The lignified and the non-lignified tissues can be clearly discriminated. The peripheral rind can also be identified, as well as the inner ring of lowly lignified parenchyma. The variations of rind thickness can be better distinguished after automated labelling of tissues. The vascular bundles are nearly all identified. The vascular bundles located within or close to the rind are difficult to separate from the rind.

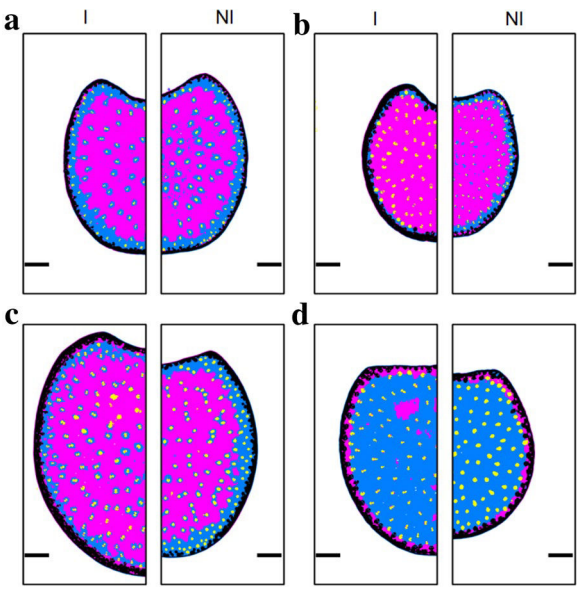


Fig. 3 Result of automated labelling of tissue regions from FASGA-stained sections. Each tissue region is represented with a different colour. Black: rind; yellow: vascular bundles; magenta: lignified tissues; blue: non-lignified tissues. **a**: Cm484; **b**: F271; **c**: F7025; **d**: F4. Left-hand panels correspond to the irrigated condition, right-hand panels to the non-irrigated condition

Quantification of histology

The main results of the linear models applied to each descriptor are presented in Table 2.

For most features, the genotype effect is highly significant (p values lower than 0.01 for 12 features). This validates the methodology for discriminating contrasted genotypes based on quantitative histology.

The effect of the water treatment is significant for several descriptors as well. In particular, the area of the section and the area fraction occupied by the bundles vary with the water treatment. The water treatment also has a significant effect on the coloration of the tissue fraction. The interaction of the genotype and water treatment effect is significant on the fraction of lignified tissue (p value ≈ 0.036), on the mean red value of lignified regions (p value ≈ 0.013), and on the mean green value of the rind tissue (p value ≈ 0.024). This can be interpreted as differentiated responses of each genotype to the water treatment.

The average value for each morphometric descriptor is given in Table 3. In addition to the global average value, the average value by combination of genotype and water treatment is also provided.

Table 2 Results of the analysis of variance performed on each descriptor

Name	G	T	Y	B (G x T x Y)	S (G x T x Y x B)	G x T	G x Y	T x Y	G x T x Y
Morphometry									
Stem area (cm^2)	*0.000****	*0.005***	0.196	0.958	*0.000****	0.464	*0.002***	0.189	0.156
Bundle number	*0.000****	0.578	0.219	0.013*	*0.000****	0.661	0.188	0.606	0.565
Bundle intensity	*0.000****	*0.001***	0.472	0.748	*0.000****	0.432	0.043*	0.172	0.268
Tissue fractions									
Lignified fraction	*0.000****	0.024*	0.826	0.090	*0.000****	0.036*	0.406	0.901	0.592
Non lignified fraction	*0.000****	0.079	0.154	0.773	*0.000****	0.062	0.386	0.838	0.019*
Rind fraction	*0.007***	0.542	0.290	0.011*	*0.000****	0.394	0.022*	0.198	0.318
Bundle fraction	*0.000****	*0.009***	0.400	0.050	*0.000****	0.402	0.221	0.073	0.904
Lignified fraction									
Mean red	*0.000****	*0.003***	*0.008***	0.143	*0.000****	0.195	*0.009***	0.484	0.281
Mean green	*0.000****	0.328	0.411	0.473	*0.000****	0.462	0.058	0.088	0.032*
Mean blue	*0.000****	0.125	0.841	0.567	*0.000****	0.201	0.037	0.087	0.031*
Non-lignified fraction									
Mean red	*0.004***	0.040*	0.134	0.234	*0.000****	0.013*	0.027*	0.395	0.685
Mean green	*0.000****	0.160	*0.002***	0.535	*0.000****	0.836	0.061	0.175	*0.005***
Mean blue	*0.000****	*0.009***	0.034	0.334	*0.000****	0.530	0.039*	0.241	*0.006***
Rind fraction									
Mean red	0.021*	*0.001***	0.040*	0.174	*0.000****	0.228	*0.006***	0.727	0.031*
Mean green	*0.000****	*0.004***	*0.001***	0.331	*0.000****	0.024*	*0.002***	*0.008***	0.272
Mean blue	*0.001***	0.256	*0.006***	0.167	*0.000****	0.099	*0.002***	0.032*	0.289
Bundle fraction									
Mean red	*0.002***	*0.000****	0.250	0.032*	0.132	0.213	0.004**	0.685	0.104
Mean green	0.023*	*0.001***	0.032*	0.021*	0.171	0.492	0.791	0.722	0.288
Mean blue	0.716	*0.000****	0.146	0.027*	0.492	0.082	0.059	0.335	0.342

The table provides the *p* values for each fixed effect of the main factors (genotype, water treatment, year), their interactions, and for the random effects of the block and of the stem. *p* values lower than 0.05, 0.01 and 0.001 are indicated with *, ** and ***, respectively. *p* values lower than 0.01 are in italic type

Comparison of genotypes

Several histological parameters are useful for discriminating the genotypes. In the following section, the genotypes are compared based on the irrigated condition. The area of the section is approximately 1.81 cm^2 (SD 0.75), with a significant effect of the genotype (p value < 1e−3). It is larger for the F7025 line (3.02 cm^2, SD 0.79) and smaller for the F271 genotype (1.29 cm^2, SD 0.18).

F7025 has the largest number of vascular bundles (214.1, SD 38.9), whereas the average value is 153.2 (SD 46.2). However, F7025 is also the genotype with the largest sections. When considering the numerical density of vascular bundles per unit area, the F7025 genotype is comparable to the genotypes Cm484 and F4 (74.5, 66.6 and 85.3 cm^{-2}, respectively, with SD ranging from 10.1 to 18.7). In that case, the increase in the number of bundles seems to be a direct consequence of the increase in the size of the section. On the contrary, the genotype F271 presents larger bundle intensity (111.2 cm^{-2}, SD 17.2 cm^{-2}).

The fraction of lignified tissue is around 60–75% for most genotypes except for the F4 genotype whose lignified fraction is 15.6% (SD 9.1%). This corresponds to the large proportion of blue area that can be observed on the segmented images for this genotype (Fig. 3). F271 presents the largest fraction of lignified tissue (72.8%, SD 4.0%). It is also the one with the largest rind fraction (15.9%, SD 3.1%), whereas the average rind fraction is around 12.9% (SD 3.9%) among the studied genotypes in both conditions. The lignified fraction of the F4 genotype appears to be darker than the other genotypes. The mean red value for F4 is 124.3 (SD 25.8), compared to that of the global average of 157.8 (SD 29.0). Similar variations occur for the green and blue mean values. On the contrary, the non-lignified fraction of the F4 genotype appears to be lighter. The mean green or blue values are 195 (SD 7.7) and 200.1 (SD 4.8), whereas they are 149.8 (SD 31.3) and 156.6 (SD 28.6) on average for the studied genotypes in both irrigation conditions. These two observations may indicate a differentiation in the lignification of the tissues for the F4 genotype.

Table 3 Average value of each parameter measured on cross-section images

	Global	Genotypes							
		Cm484		F271		F4		F7025	
		I	NI	I	NI	I	NI	I	NI
Count	125	16	16	14	15	16	16	16	16
Morphometry									
Stem area (cm^2)	1.81 *(0.75)*	1.75 *(0.22)*	1.64 *(0.21)*	1.29 *(0.18)*	1.02 *(0.19)*	1.55 *(0.41)*	1.44 *(0.21)*	3.02 *(0.79)*	2.66 *(0.42)*
Bundle number	153.2 *(46.2)*	114.7 *(9.4)*	128.8 *(20.0)*	143.1 *(27.9)*	134.6 *(33.0)*	129 *(23.9)*	147.9 *(32.3)*	214.1 *(38.9)*	211.3 *(38.7)*
Bundle intensity	91.2 *(26.9)*	66.6 *(10.1)*	79.8 *(14.2)*	111.2 *(17.2)*	133.8 *(28.6)*	85.3 *(10.7)*	103.3 *(17.1)*	74.5 *(18.7)*	80.5 *(17.5)*
Tissue fractions									
Lignified fraction	51.9 *(24.5)*	61.1 *(2.7)*	65.3 *(3.5)*	72.8 *(4.0)*	68.9 *(2.4)*	15.6 *(9.1)*	8.2 *(2.3)*	68.1 *(4.5)*	58.6 *(9.1)*
Non lignified fraction	30.1 *(25.3)*	23.8 *(3.7)*	20.9 *(4.0)*	6.8 *(3.3)*	8.9 *(3.8)*	68.3 *(9.6)*	73.4 *(5.9)*	14.2 *(3.8)*	19.8 *(7.2)*
Rind fraction	12.9 *(3.9)*	12 *(0.9)*	10.3 *(1.4)*	15.9 *(3.1)*	16.8 *(4.5)*	11.6 *(3.0)*	11.5 *(4.1)*	11.7 *(2.2)*	14.2 *(5.3)*
Bundle fraction	5.2 *(2.0)*	3.1 *(0.8)*	3.5 *(0.7)*	4.5 *(1.0)*	5.5 *(1.4)*	4.5 *(1.1)*	6.9 *(2.0)*	6.1 *(1.6)*	7.3 *(2.2)*
Lignified fraction									
Mean red	157.8 *(29.0)*	182.1 *(7.3)*	182.6 *(6.7)*	173.3 *(5.9)*	159.3 *(4.1)*	124.3 *(25.8)*	107.3 *(19.2)*	172.5 *(6.7)*	162.8 *(5.3)*
Mean green	145.6 *(25.6)*	174.2 *(13.5)*	177.7 *(8.8)*	147.1 *(10.0)*	146.3 *(9.2)*	127.4 *(27.8)*	114.7 *(23.5)*	140 *(13.3)*	137.6 *(8.1)*
Mean blue	180 *(24.7)*	204.9 *(8.6)*	207.1 *(4.2)*	184.8 *(6.7)*	178.2 *(6.5)*	158.1 *(27.4)*	143 *(23.0)*	181.6 *(9.0)*	182.4 *(6.2)*
Non-lignified fraction									
Mean red	70 *(13.3)*	76.7 *(9.0)*	78.7 *(9.0)*	66 *(11.4)*	74.3 *(9.1)*	78.6 *(11.7)*	61.3 *(12.4)*	68.9 *(12.7)*	55.2 *(9.8)*
Mean green	149.8 *(31.3)*	155.5 *(15.3)*	153.3 *(11.6)*	113.2 *(14.9)*	115.4 *(17.6)*	195 *(7.7)*	186.5 *(19.6)*	138.3 *(10.3)*	134.5 *(14.4)*
Mean blue	156.6 *(28.6)*	157.8 *(12.8)*	156.4 *(8.8)*	126.9 *(13.1)*	119.1 *(20.7)*	200.1 *(4.8)*	188.6 *(15.6)*	153.3 *(7.2)*	145 *(12.0)*
Rind fraction									
Mean red	40.2 *(7.6)*	43.3 *(6.4)*	42 *(6.0)*	45.2 *(5.3)*	39.1 *(12.0)*	43.7 *(4.4)*	37 *(6.6)*	41 *(3.1)*	30.9 *(4.4)*
Mean green	42.9 *(7.0)*	43.8 *(3.3)*	48.3 *(5.6)*	42 *(3.3)*	43.5 *(9.3)*	45.8 *(6.5)*	45.5 *(5.0)*	32.5 *(3.5)*	41.8 *(4.6)*
Mean blue	50.4 *(6.7)*	47.7 *(2.6)*	52.1 *(4.9)*	50.3 *(4.3)*	48.6 *(11.0)*	56.2 *(6.5)*	54.4 *(4.8)*	44.1 *(4.1)*	49.3 *(4.5)*
Bundle fraction									
Mean red	43.4 *(7.4)*	42.7 *(3.7)*	39.4 *(3.8)*	53.2 *(4.3)*	44.3 *(5.9)*	45.4 *(3.7)*	36.9 *(6.3)*	48.4 *(8.4)*	38 *(5.8)*
Mean green	59.2 *(6.8)*	65.4 *(4.5)*	60.5 *(4.6)*	62.2 *(5.3)*	52.9 *(7.7)*	62.2 *(6.4)*	57.3 *(4.4)*	58.1 *(6.1)*	54.9 *(6.0)*
Mean blue	65.4 *(7.0)*	67.3 *(3.5)*	62.7 *(4.6)*	73.7 *(6.2)*	59.5 *(9.3)*	66.7 *(5.7)*	61.7 *(5.3)*	68.7 *(4.9)*	63.3 *(5.4)*

For each parameter, the table presents the global average as well as the average for each combination of genotype and water treatment. The standard deviations are given in brackets

Depending on the genotypes, some tissues may present specific colour variations. The rind of F7025 is slightly darker than the rind of the other genotypes. For instance the mean green value is 32.5 (SD 3.5) for F7025, whereas the average values for other genotypes are around 42–45.8 (global SD 7.0). This can be interpreted as an increase in the lignification of the rind of F7025. The vascular bundles of the F271 genotype appear to have a greater value in the red component. The mean red value is 53.2 (SD 4.3), and ranges between 42.7 and 48.4 (global SD 7.4) for other genotypes. This suggests an increase of lignification in the bundles of the F271 genotype.

The discriminative power of morphometry parameters obtained from quantitative histology is summarized on Fig. 4. The F4 genotype is characterised by a large fraction of non-lignified tissue. The size of the stem section helps to discriminate the three other genotypes.

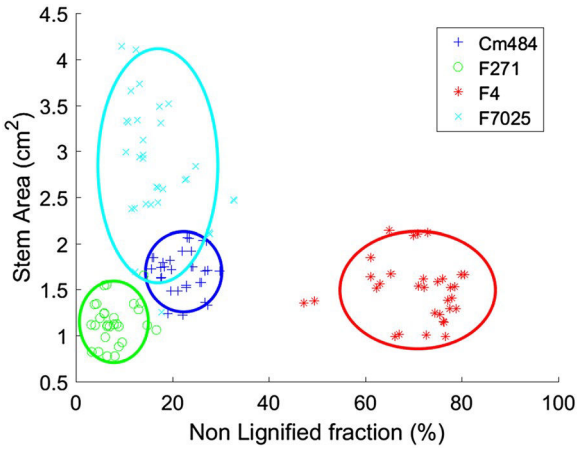


Fig. 4 Scatter plots of the whole slide microscopy images according to the stem area and the fraction of non-lignified tissue region, grouped by genotype

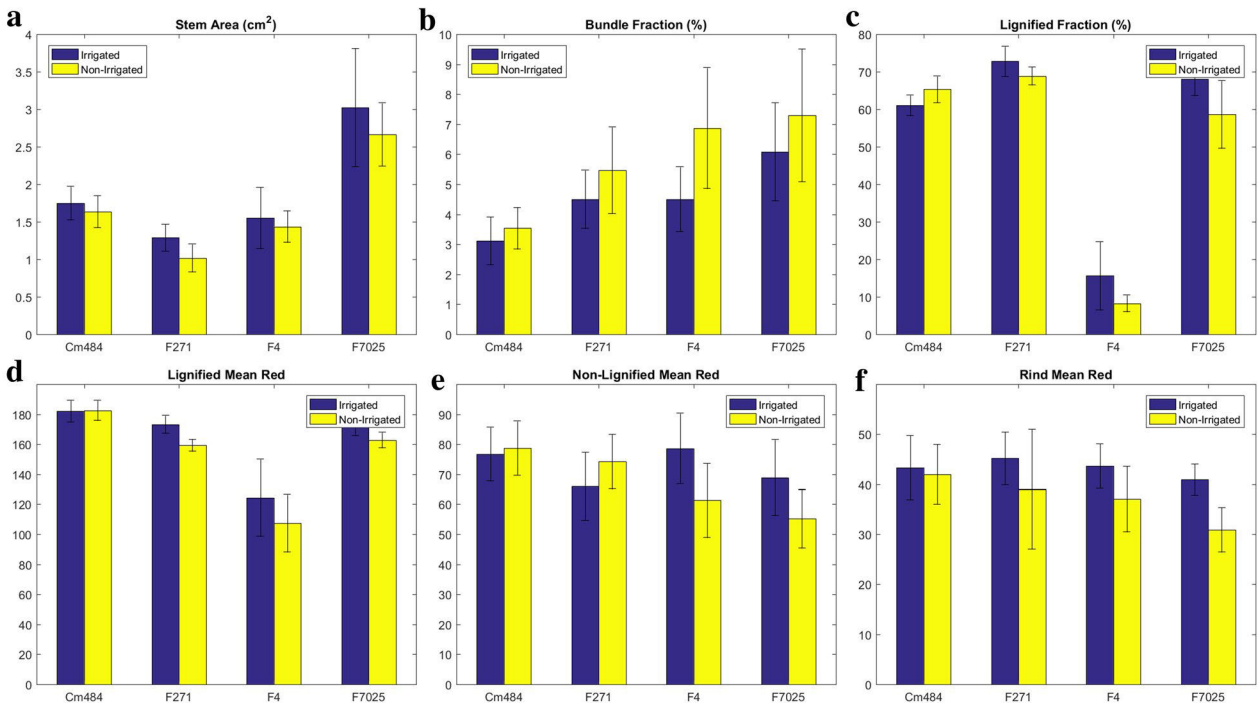


Fig. 5 Variations of several descriptive parameters depending on both the genotype and the water treatment. **a** stem area, in cm^2, **b** bundle fraction, **c** lignified fraction, **d** mean red value in lignified fraction, **e** mean red value in non-lignified fraction, **f** mean red value in the rind tissue region

Comparison of water treatments

The effect of water treatment can be observed on several parameters (Table 1 and Additional file 1). Some of them are represented in Fig. 5.

For all genotypes, the stem area of the section is smaller in the case of water deficit (p value of the water treatment effect ≈ 0.005) (Fig. 5a). The area fraction occupied by vascular bundles increases for all genotypes (p value of the water treatment effect ≈ 0.009) (Fig. 5b). Since the number of vascular bundles remains the same, it seems that water deficit favours the production of larger vascular bundles.

Several (genotype $\times$ water treatment) interactions are significant, showing a specific response of the genotypes to the water treatment (Table 1). The proportion of lignified tissue regions changes with water treatment (p value of the water treatment effect ≈ 0.024), but the change depends on the genotype (p value of the genotype-water treatment interaction ≈ 0.036). For F4 and F7025 genotypes, the fraction of lignified tissues decreases with water deficit (Fig. 5c). The effect is less visible for the F271 genotype and the opposite for the Cm484 genotype.

The coloration of the tissue regions changes with water deficit. The mean red value of the lignified fraction is globally smaller in the case of water deficit (p value of water treatment effect ≈ 0.003). Specific response of the genotypes can be observed (p value of water treatment effect ≈ 0.008), revealing that the diminution occurs for all genotypes except for Cm484 (Fig. 5d). The change in coloration with water deficit of the non-lignified tissue fraction depends on the genotype (p value of the interaction ≈ 0.013). The mean red value of the non-lignified tissues is smaller for F4 and F7025 genotypes, larger for the F271 genotype, and does not change for the Cm484 genotype (Fig. 5e). For all genotypes except Cm484, the mean red value of the rind tissues is smaller in the case of water deficit (p value of water treatment effect ≈ 0.001) (Fig. 5f).

For all genotypes, the water deficit is related to a diminution of the mean value of each colour component of the bundle fraction that can be observed as a darkening of the vascular bundles. Such darkening may be interpreted either as an increase in lignification of the cell walls or as a densification of the cell walls in the tissue region, making the coloration more difficult to quantify.

Summary

Both genotypes and water treatments can be discriminated based on parameters obtained from quantitative histology. For all genotypes, water deficit results in smaller sections and larger bundles. The bundle fraction and the mean red colour in the bundle fraction represents

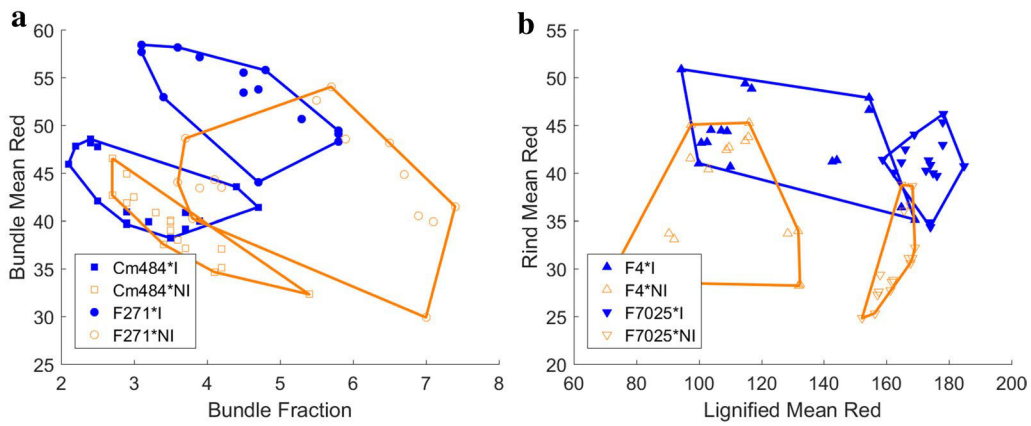


Fig. 6 Scatter plots of the stem sections depending on specific histological parameters. **a** Effect of the water treatment on F271 and Cm484 genotypes. **b** Effect of the water treatment on F4 and F7025 genotypes

the differences in histology occurring in the bundle fraction for the F271 and the Cm484 genotypes (Fig. 6a). The mean red values in the lignified fraction and in the rind fraction are better suited for the representation of histological changes due to water treatments for genotypes F4 and F7025 (Fig. 6b).

Conclusions

We have presented a complete image processing workflow for the automated analysis of images of FASGA-stained sections of maize internodes. The FASGA staining enhances the contrast of the tissues observed within the sections, and makes it possible to discriminate between lignified and non-lignified tissues. The automated segmentation procedure can identify the different regions within the section, and determine whether they are lignified or non-lignified. The quantitative characterisation results in morphometric parameters that describe the size, the proportion and the colorimetric information of each tissue.

The set of parameters can successfully discriminate contrasted genotypes, validating the proposed approach. The key parameters for discriminating genotypes are the size of the section, the relative area fractions of the tissues, the number of bundles and the colour of the different tissue fractions. Moreover, contrasted effects of the water treatment can be observed on some genotypes. Water stress seems to increase the bundle fraction in some genotypes and to decrease the lignification of the rind fraction in other genotypes. These first results are promising for studying the effects of environmental factors on the variations in chemical composition and histology of large collections of genotypes [43]. In particular, it would be of interest to verify if the effects observed on the four genotypes are observed in a wider genetic population.

The obtained results validate the use of whole slide scanners for quantitative histology of stained plant tissues. Since the images were not processed with the maximum resolution, it is expected that more precise tissue segmentation could be obtained. In particular, it may be possible to quantify the cell morphology or the cell wall thickness. The quantification of the heterogeneity of cellular morphology within the section could provide new insights into previous results [16, 31, 43, 44]. However, the large size of images obtained at full resolution (typically, several gigabytes) also complicates the development of high-throughput image analysis algorithms.

The quantitative features obtained from histological staining can also be related to the chemical composition of the tissues, such as the lignin content [31]. Acquisition devices such as confocal microscopy or microspectroscopy can provide more detailed information about the chemical content of plant tissues [13–15]. The field of view is however limited to several dozen cells. Future work may therefore focus on the fusion of information obtained from different modalities in order to calibrate high-throughput methods with acquisition methods that are more informative, but that may require more time to analyse large quantities of samples.

Additional file

Additional file 1. Sample image showing the result of segmentation of tissue regions superimposed on the original image. Some vascular bundles that could not be discriminated from the rind are manually highlighted in magenta.

Authors' contributions
DL wrote the manuscript, developed the methodology and implemented the software. MR and VM piloted the study and supervised the plant sampling. MR, VM and FEH sampled the maize internodes. FEH prepared the samples for image acquisition and performed the quantification of histology. DL performed the statistical analyses. All authors read and approved the final manuscript.

Author details
[1] UR1268 Biopolymères, Interactions et Assemblages, INRA, Nantes, France. [2] UMR 1318, Institut Jean-Pierre Bourgin, INRA-AgroParisTech, CNRS, Universite Paris-Saclay, Versailles, France.

Acknowledgements
We sincerely acknowledge N. Borrega (Observatoire du Végétal, IJPB, Versailles, France) for its participation in sample preparation and image acquisition, and S. Malavieille and P. Sartre (UE Diascope, Mauguio, France), for their precious contribution to field experiments.

Competing interests
The authors declare they have no competing interests.

Availability of data and materials
The code for the segmentation of tissue regions and the quantification of histology is freely available on the Internet through the GitHub platform at http://github.com/ijpb/fasga-quantif/releases (last accessed: August 8, 2017). The data are available from the authors upon request.

Consent for publication
The authors consent to the publication of the manuscript.

Ethics approval and consent to participate
Field studies were conducted in accordance with local legislation.

Funding
This work has benefited from French Government Grants (LabEx Saclay Plant Sciences-SPS, ref. ANR-10-LABX-0040-SPS, and ANR-11-BTBR-0006 BIOMASS FOR THE FUTURE), managed by the French National Research Agency under an "Investments for the Future" programme (ref. ANR-11-IDEX-0003-02).

Publisher's Note

Springer Nature remains neutral with regard to jurisdictional claims in published maps and institutional affiliations.

Received: 31 May 2017 Accepted: 11 September 2017
Published online: 01 November 2017

References

1. Baldy A, Jacquemot MP, Griveau Y, Bauland C, Reymond M, Méchin V. Energy values of registered corn forage hybrids in France over the last 20 years rose in a context of maintained yield increase. Am J Plant Sci. 2017;8(6):1449–61.
2. Barrière Y, Méchin V, Riboulet C, Guillaumie S, Thomas J, Bosio M, Fabre F, Goffner D, Pichon M, Lapierre C, Martinant JP. Genetic and genomic approaches for improving biofuel production from maize. Euphytica. 2009;170:183–202.
3. Barros-Rios J, Santiago R, Malvar RA, Jung HG. Chemical composition and cell wall polysaccharide degradability of pith and rind tissues from mature maize internodes. Anim Feed Sci Technol. 2012;2012(172):226–36.
4. Jung HG, Samac DA, Sarath G. Modifying crops to increase cell wall digestibility. Plant Sci. 2012;185:65–77.
5. Méchin V, Argillier O, Rocher F, Hebert Y, Mila I, Pollet B, Barrière Y, Lapierre C. In search of a maize ideotype for cell wall enzymatic degradability using histological and biochemical lignin characterization. J Agric Food Chem. 2005;53:5872–81.
6. Casler MD, Jung HG. Relationships of fibre, lignin, and phenolics to in vitro fibre digestibility in three perennial grasses. Anim Feed Sci Technol. 2006;125:151–61.
7. Méchin V, Laluc A, Legée F, Cézard L, Denoue D, Barrière Y, Lapierre C. Impact of the brown-midrib bm5 mutation on maize lignins. J Agric Food Chem. 2014;62(22):5102–7.
8. Sarath G, Dien B, Saathoff AJ, Vogel KP, Mitchell RB, Chen H. Ethanol yields and cell wall properties in divergently bred switchgrass genotypes. Biores Technol. 2011;102:9579–85.
9. Zhang Y, Culhaoglu T, Pollet B, Melin C, Denoue D, Barrière Y, Baumberger S, Méchin V. Impact of lignin structure and cell wall reticulation on maize cell wall degradability. J Agric Food Chem. 2011;59:10129–35.
10. El Hage F, Jaquemot MP, Griveau Y, Borrega N, Dubreucq B, Legland D, Baldy A, Méchin A, Reymond M. What does the histology and the biochemistry of the maize stem bring to the understanding of the degradability under contrasted watering conditions in a panel of 11 genotypes? In preparation.
11. Jung HG, Casler MD. Maize stem tissues: impact of development on cell wall degradability. Crop Sci. 2006;46:1801–9.
12. Wilson JR, Mertens DR, Hatfield RD. Isolates of cell types from sorghum stems: digestion, cell wall and anatomical characteristics. J Sci Food Agric. 1993;63:407–17.
13. Corcel M, Devaux MF, Guillon F, Barron C. Comparison of UV and visible autofluorescence of wheat grain tissues in macroscopic images of cross-sections and particles. Comput Electron Agric. 2016;127:281–8.
14. Jamme F, Kascakova S, Villette S, Allouche F, Pallu S, Rouam V, Réfrégiers M. Deep UV autofluorescence microscopy for cell biology and tissue histology. Biol Cell. 2013;105:277–88.
15. Chylińska M, Szymańska-Chargot M, Zdunek A. Imaging of polysaccharides in the tomato cell wall with Raman microspectroscopy. Plant Methods. 2014;10:14.
16. Du J, Zhang Y, Guo X, Ma L, Shao M, Pan X, Zhao C. Micron-scale phenotyping quantification and three-dimensional microstructure reconstruction of vascular bundles within maize stalks based on micro-CT scanning. Funct Plant Biol. 2016;44:10–22.
17. Milien M, Renault-Spilmont AS, Cookson SJ, Sarrazin A, Verdeil JL. Visualization of the 3D structure of the graft union of grapevine using X-ray tomography. Sci Hortic. 2012;144:130–40.
18. Stuppy WH, Maisano JA, Colbert MW, Rudall PJ, Rowe TB. Three-dimensional analysis of plant structure using high-resolution X-ray computed tomography. Trends Plant Sci. 2003;8:2–6.
19. Boughton BA, Thinagaran D, Sarabia D, Bacic A, Roessner U. Mass spectrometry imaging for plant biology: a review. Phytochem Rev. 2016;15:445–88.
20. Kaspar S, Peukert M, Svatos A, Matros A, Mock HP. MALDI-imaging mass spectrometry—an emerging technique in plant biology. Proteomics. 2011;11:1840–50.
21. Ding L, Hofius D, Hajirezaei M-R, Fernie AR, Boernke F, Sonnewald U. Functional analysis of the essential bifunctional tobacco enzyme 3-dehydroquinate dehydratase/shikimate dehydrogenase in transgenic tobacco plants. J Exp Bot. 2007;58:2053–67.
22. Piquemal J, Chamayou S, Nadaud I, Beckert M, Barrière Y, Mila I, Lapierre C, Rigau J, Puigdomenech P, Jauneau A, Digonnet C, Boudet AM, Goffner D, Pichon M. Down-regulation of caffeic acid *O*-methyltransferase in maize revisited using a transgenic approach. Plant Physiol. 2002;130:1675–85.
23. Roth R, Boudet AM, PontLezica R. Lignification and cinnamyl alcohol dehydrogenase activity in developing stems of tomato and poplar: a spatial and kinetic study through tissue printing. J Exp Bot. 1997;48:247–54.
24. Sibout R, Eudes A, Mouille G, Pollet B, Lapierre C, Jouanin L, Seguin A. Cinnamyl alcohol dehydrogenase-C and -D are the primary genes involved in lignin biosynthesis in the floral stem of Arabidopsis. Plant Cell. 2005;17:2059–76.
25. Tamasloukht B, Lam MS-JWQ, Martinez Y, Tozo K, Barbier O, Jourda O, Jauneau A, Borderies G, Balzergue S, Renou J-P, Huguet S, Martinant JP, Tatout C, Lapierre C, Barrière Y, Goffner D, Pichon M. Characterization of a cinnamoyl-CoA reductase 1 (CCR1) mutant in maize: effects on lignification, fibre development, and global gene expression. J Exp Bot. 2011;62:3837–48.
26. Vermerris W, Sherman DM, McIntyre LM. Phenotypic plasticity in cell walls of maize brown midrib mutants is limited by lignin composition. J Exp Bot. 2010;61:2479–90.
27. Zhong RQ, Ripperger A, Ye ZH. Ectopic deposition of lignin in the pith of stems of two Arabidopsis mutants. Plant Physiol. 2000;123:59–69.

28. Browning B. Methods of wood chemistry, vol. I and II. New York: Wiley; 1967.
29. Brauns F. The chemistry of lignin. New York: Academic Press; 1952.
30. Tolivia D, Tolivia J. Fasga: a new polychromatic method for simultaneous and differential staining of plant tissues. J Microsc. 1987;148:113–7.
31. Zhang Y, Legay S, Barrière Y, Méchin V, Legland D. Color quantification of stained maize stem section describes lignin spatial distribution within the whole stem. J Agric Food Chem. 2013;61:3186–92.
32. Diamond J, McCleary D. Virtual microscopy. In: Hannon-Fletcher M, Maxwell P, editors. Advanced techniques in diagnostic cellular pathology. Chichester: Wiley; 2009.
33. Gürcan MN, Boucheron LE, Can A, Madabhushi A, Rajpoot NM, Yener B. Histopathological image analysis: a review. IEEE Rev Biomed Eng. 2009;2009(2):147–71.
34. Deroulers C, Ameisen D, Badoual M, Gerin C, Granier A, Lartaud M. Analyzing huge pathology images with open source software. Diagn Pathol. 2013;8:92.
35. Soille P. Morphological image analysis. Berlin: Springer; 2003.
36. Hamuda E, Ginley BM, Glavin M, Jones E. Automatic crop detection under field conditions using the HSV colour space and morphological operations. Comput Electron Agric. 2017;133:97–107.
37. Lootens P, Ruttink T, Rohde A, Combes D, Barre P, Roldán-Ruiz I. High-throughput phenotyping of lateral expansion and regrowth of spaced *Lolium perenne* plants using on-field image analysis. Plant Methods. 2016;12:32.
38. Philipp I, Rath T. Improving plant discrimination in image processing by use of different colour space transformations. Comput Electron Agric. 2002;35:1–15.
39. Schindelin J, Arganda-Carreras I, Frise E, Kaynig V, Longair M, Pietzsch T, Preibisch S, Rueden C, Saalfeld S, Schmid B, Tinevez JY, White DJ, Hartenstein V, Eliceiri K, Tomancak P, Cardona A. Fiji: an open-source platform for biological-image analysis. Nat Methods. 2012;9:676–82.
40. Legland D, Arganda-Carreras I, Andrey P. MorphoLibJ: integrated library and plugins for mathematical morphology with ImageJ. Bioinformatics. 2016;32:3532–4.
41. Legland D. QuantifFasga: an ImageJ plugin for quantifying the histology of fasga-stained maize sections. 2015. http://github.com/ijpb/fasga-quantif/releases. Accessed 8 Aug 2017.
42. Legland D. MatStats: a matlab toolbox for statistical data analysis. 2017. https://github.com/mattools/matStats. Accessed 8 Aug 2017.
43. Heckwolf S, Heckwolf M, Kaeppler SM, de Leon N, Spalding EP. Image analysis of anatomical traits in stalk transections of maize and other grasses. Plant Methods. 2015;11:1–10.
44. Legland D, Devaux MF, Guillon F. Statistical mapping of maize bundle intensity at the stem scale using spatial normalisation of replicated images. PLoS ONE. 2014;9:e90673.

Submit your next manuscript to BioMed Central and we will help you at every step:

- We accept pre-submission inquiries
- Our selector tool helps you to find the most relevant journal
- We provide round the clock customer support
- Convenient online submission
- Thorough peer review
- Inclusion in PubMed and all major indexing services
- Maximum visibility for your research

Submit your manuscript at
www.biomedcentral.com/submit



Dedicated NIRS predictive equations establishment and NIRS predictions of cell wall related traits in maize internodes

For this first study, we harvested a total of 124 internodes samples to characterize for the cell wall biochemical components. As it is too much work to realize in a short amount of time, Near Infra-Red Spectrometry predictive equations were developed to predict cell wall composition and structure of all these samples. But to do so, for five years the team has been building predictive equations for every biochemical components based on biochemical values of the genotypes we are studying in the team. In the literature, only a few predictive equations have been reported for the cell wall components of the maize stem. One set of equations has been developed for now more than 20 years in Lusignan (France, 86) on the whole plant without the ear and based on the values of 500 to 1000 maize samples (Riboulet et al., 2008). More precisely at the internode level, there was only one set of equations which was developed on the internode of the bottom of the stem (starting from the ground). This set was never published and was specific of a very lignified and mature part of the stem and not adapted to maize cultivated under non-irrigated condition in the south of France. In 2017, Li et al. used NIRS equations to predict the cell wall biochemical components of internodes of the bottom of the stem (2nd to the 5th, starting from the ground) but they did not publish them either.

It was therefore decided to build a set of NIRS predictive equations on all the cell wall components of the maize internode. This work was initiated 5 years ago and a long and tedious work of biochemistry and NIRS was made by the team to build dedicated NIRS predictive equations for the internode carrying the main ear at silage stage.

Building of the dedicated NIRS predictive equations for the cell wall components of maize internodes

As described by Manley, (2014) : “The shorter NIR wavelengths (800–2500 nm), compared to those in the midinfrared (MIR) range (2500–15000 nm) enable increased penetration depth and subsequent nondestructive, non-invasive, chemical-free, rapid analysis possibilities for a wide range of biological materials. A disadvantage of NIR spectroscopy is its reliance on reference methods and model development using chemometrics. NIR measurements and predictions are, however, considered more reproducible than the usually more accurate and precise reference methods. The advantages of NIR spectroscopy contribute to it now often being favoured over other spectroscopic (colourimetry and MIR) and analytical methods, using chemicals and producing chemical waste, such as gas chromatography (GC) and high performance liquid chromatography (HPLC).” The

mathematical principle of the building of a NIRS equation consists in a partial least square regression (PLSR) of the biochemical trait measured on the near infra-red absorption of calibration samples. These calibration samples have all been quantified by wet chemistry for every single cell wall biochemical trait. All the NIRS predictive equations were built using 53 calibration samples of the panel of genotypes we are studying, 22 calibration samples coming from genotypes cultivated in Lusignan and 35 calibration sample from other projects. In total 55 to 123 (according to the considered biochemical trait, cf. Table 5) calibration samples were selected among hundreds of internode samples to be representative of the spectrum variation obtained over 5 years in field trials. These samples were chosen to represent the best the spectral variability of all the samples, thanks to a principal component analysis (PCA) of all the spectrums (Figure 25).

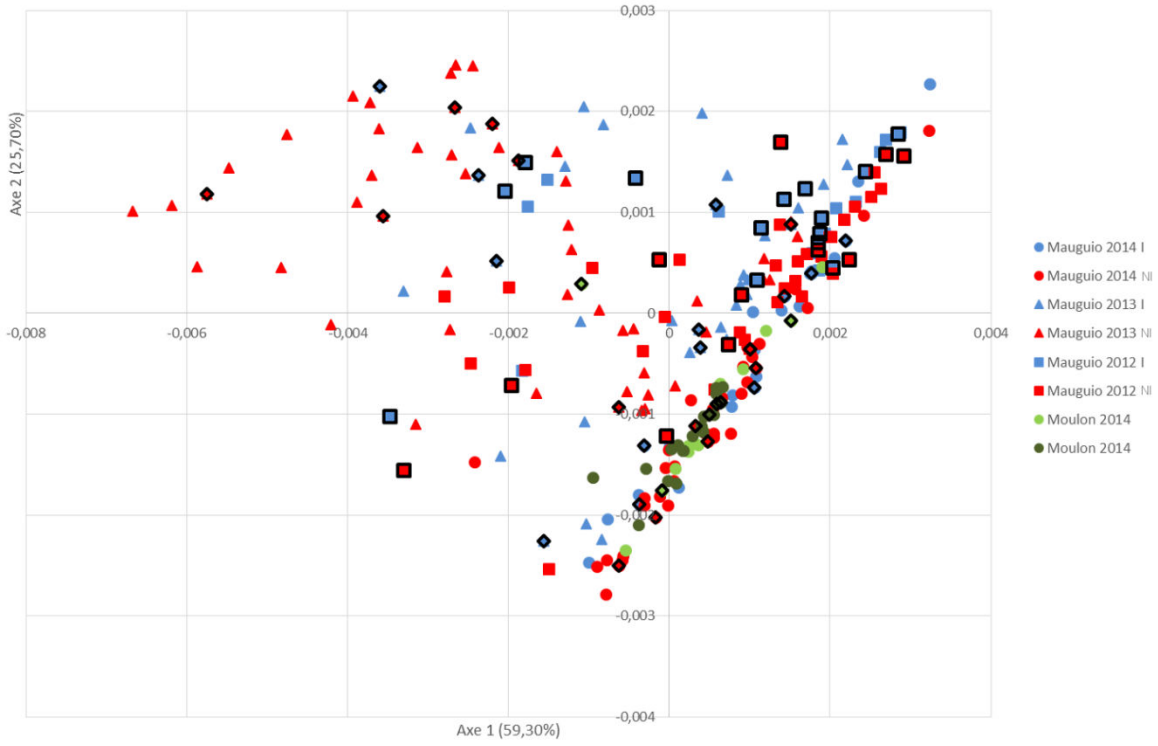


Figure 25. Principal component analysis (PCA) of the near infra-red spectrums of the individuals for the choice of the calibration samples. Each point represents the near infra-red spectrum of a sample. The two first axes of the PCA represent 85 % of the total variability of all the samples. The points surrounded were the one chosen for the calibration of the equations.

Once the calibration samples were selected and used to build NIRS predictive equations, a step of validation is performed to test the sturdiness of established predictive equations. Generally, it is necessary to have a pool of samples which have been quantified by wet chemistry but which were not used in the calibration samples. Thus one can compare and

calculate the R^2 between the biochemical values obtained by wet chemistry and the values predicted by the equations. In our case, as the number of calibration samples was relatively low, a test of cross-validation was performed. The principle of the cross-validation is the building of the equation by taking one sample out of the calibration pool, then by predicting it and comparing the predicted value to the one obtained in wet biochemistry. These steps are repeated for every calibration samples. If the predictions and the values of the wet biochemistry are close, the NIRS predictive equations are precise.

Biochemical quantifications of the cell wall components

Biochemical quantifications performed on the calibration samples set were the following (Table 5): Cell wall content (CWR), obtained with a water/ethanol extraction (Soxhlet). Lignin content in the cell wall (KL.CWR) was estimated using the Klason method (Dence et al., 1992), the composition and structure of lignins were obtained by thioacydolysis (Lapierre et al., 1986). Esterified and etherified *p*-hydroxycinnamic acids contents (PCAest, FAest and FAeth) were obtained by alkaline hydrolysis (Morrison et al., 1993; Culhaoglu et al., 2011). Glucose, Xylose and Arabinose contents were quantified by acidic hydrolysis (Updegraff et al., 1969 ; Harholt et al., 2006). Acidic pretreatment of the dry matter followed by an enzymatic hydrolysis (Onozuka cellulase R10) bring the *in vitro* dry matter degradability or IVDMD (Ronsin et al., 1990). Onozuka cellulose R10 is a A multi-component enzyme system. Although the preparation has high cellulase activity, it still contains hemicellulases, and it degrades mannans, xylans, galactomannans, pectins and other polysaccharides. It is widely used for the isolation of protoplasts, for its ability to degrade cell walls, often in combination with Macerozyme R-10 (cat. no. 28302). Its Temperature optimum is 40 - 50 °C and its pH-optimum is 4 – 5. Its unit definition : 1 U catalyzes the liberation of 1 µmole of glucose from sodium carboxymethyl cellulose per minute at 40 °C, pH 4.5 (glucose determined with alkaline copper reagent). Its extraneous activities: α-amylase ca. 0.8 U, pectinase ca. 0.4 U, protease ca. 0.01 DMC-U, hemicellulase ca. 1 U/mg (1 U catalyzes the liberation of 1 µmole reducing groups from xylan per hour at 37 °C, pH 5.5, calculated as xylose).

Finally the *in vitro* cell wall residue degradability or IVCWRD (Méchin et al., 1998) was calculated as follow: $\mathrm{IVCWRD} = \frac{100 \text{ x } (\mathrm{IVDMD} - 100 + \mathrm{CWR})}{\mathrm{CWR}}$ assuming that the non-CWR part was completely degradable.

Biochemical values were afterwards predicted with accurate NIRS predictive equations for the 124 harvested internode samples.

Table 5. Cell wall biochemical related traits quantified, associated reference methods and NIRS prediction equation characteristics.

Trait	Designation	Reference Method	Units	Min	Max	N[a]	R[b]	SEC[c]
Cell wall residue	CWR	Soxhlet Extraction	% DM	32.87	58.95	76	0.95	1.65
Lignin content	KL.CWR	Klason	% CWR	11.59	21.11	123	0.84	0.88
βO4 yield	βO4_yield	Thioacidolysis	µmol/ g KL	497.76	1174	123	0.77	80
H lignin subunit yield	βO4_H			4.66	48			
S lignin subunit yield	βO4_S			263.62	614.1	123	0.72	52
G lignin subunit yield	βO4 _G			203	569.3	123	0.78	54
Etherified ferulic acids	FAeth	Alkaline hydrolysis	mg/g CWR	1.92	5.16	102	0.76	0.52
Esterified ferulic acids	FAest			3.72	8.14	101	0.76	0.52
Esterified p-coumaric acids	PCAest			14.55	30.02	101	0.66	2.30
Glucose content	Cellulose	Acidic hydrolysis	% CWR	31.5	49.89	55	0.89	1.84
Hemicelluloses content	Hemicelluloses			20.11	45.47	55	0.85	2.44
In vitro dry mater digestibility	IVDMD	Acid pretreatment + cellulolyse	% DM	49.96	81.2	55	0.98	1.5
In vitro cell wall digestibility	IVCWRD		% CWR	6.16	49.44	55	0.94	4.71

[a]: number of samples used to calibrate NIRS predictive equations. b: correlation coefficient between biochemical values and predicted values. c: standard error of calibration calculated on the prediction of the calibration samples.

When we look at the correlations between the predicted data and the samples evaluated by wet chemistry, we obtained quite good correlations, especially for the major cell wall traits such as the Klason lignin content (R^2=0.601) and the IVCWRD (R^2=0.906) (Figure 26-A, B).

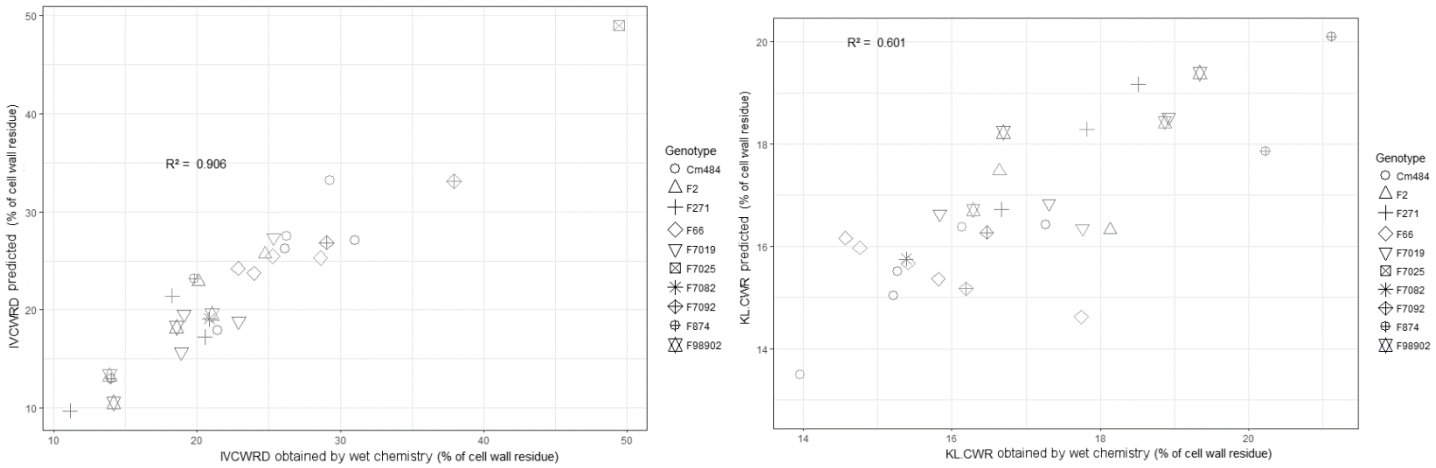


Figure 26. Relationships between the biochemical traits predicted and their biochemical values obtained by wet chemistry. A. IVCWRD predicted vs IVCWRD obtained by wet chemistry, R^2=0.906. B. KLCWR predicted vs KLCWR obtained by wet chemistry, R^2= 0.601.

Statistical Analyses

All the statistical analyses have been performed on R. Following standard procedures, an analysis of variance was performed according to the following model:

Yijkl = μ + Aj + Gi + Tk + Bl + Aj x Gi + Gi x Tk + Aj x Tk + Aj x Gi x Tk + Rijkl

where Yijkl is the value of the genotype I , in year j, under condition k and in block l; μ = overall mean; Aj = the main effect of year j; Tk = the main effect of the condition k; Gi = the effect of genotype i; Bl = the main effect of the block l; Aj x Gi = the interaction effect between genotype i and year j; Aj x Tk = the interaction effect between the condition k and the year j; Gi x Tk = the interaction effect between the genotype I and the condition k; Aj x Gi x Tk = the interaction effect between genotype i under the condition k in year j; and Rijkl = the random residual term.

As the interactions with the year or the block were much less significant than the other effects (not showed), we corrected the data set for block and year effects.

For the correction of the block effect, we calculated the block effect with an analysis of variance (ANOVA), extracting the coefficient of this effect from the ANOVA summary and doing a subtraction it to each value of the data set according to the block in which the sample was.

The correction of the year effect was the evaluated by performing the same ANOVA without the testing of the block effect. As the year effect was much less significant than the effect of the genotype and the treatment, we calculated for each genotype in every treatment adjusted means over the 3 years.

On the corrected data set, another analysis of variance has been performed with the following linear model for each trait:

$$Yij = \mu + Gi + Tj + Gi \times Tj + Rij$$

where Yij is the value of the genotype i, under condition j; μ = overall mean; Tj = the main effect of the condition k; Gi = the effect of genotype i; Gi x Tj = the interaction effect between the genotype i and the condition j and Rij = the random residual term.

Pearson correlations have been estimated on the corrected data set.

I. Impact of the water deficit on the biochemical composition of the cell wall, the lignification distribution with the tissues and the degradability of the cell wall of maize stems

Here, we present the study published in April 2018 in the Journal of Agricultural and Food Chemistry.

JOURNAL OF AGRICULTURAL AND FOOD CHEMISTRY

Article

Cite This: J. Agric. Food Chem. 2018, 66, 4800−4808

pubs.acs.org/JAFC

Tissue Lignification, Cell Wall *p*-Coumaroylation and Degradability of Maize Stems Depend on Water Status

F. El Hage,[†,‡] D. Legland,[§] N. Borrega,[†] M.-P. Jacquemot,[†] Y. Griveau,[†] S. Coursol,[†] V. Méchin,*[,†] and M. Reymond[†]

[†]UMR 1318, Institut Jean-Pierre Bourgin, INRA-AgroParisTech, CNRS, Universite Paris-Saclay, 78026 Versailles Cedex, France

[‡]École Doctorale 567 Sciences du Vegetal, University Paris-Sud, University of Paris-Saclay, bat 360, Orsay Cedex 91405, France

[§]UR1268 Biopolymères, Interactions et Assemblages, INRA, 44 316 Nantes Cedex 3, France

Supporting Information

ABSTRACT: Water supply and valorization are two urgent issues in the utilization of maize biomass in the context of climate change and replacement of fossil resources. Maximizing maize biomass valorization is of interest to make biofuel conversion competitive, and to increase forage energetic value for animal fodder. One way to estimate biomass valorization is to quantify cell wall degradability. In this study, we evaluated the impact of water supply on cell wall degradability, cell wall contents and structure, and distribution of lignified cell types in maize internodes using dedicated high-throughput tools to effectively phenotype maize internodes from 11 inbred lines under two contrasting irrigation scenarios in field trials over three years. Overall, our results clearly showed that water deficit induced significant changes in lignin content and distribution along with a reduction in lignin *p*-coumaroylation, thereby impacting cell wall degradability. Additionally, we also observed that responses to a water deficit varied between the lines examined, underscoring biochemical and histological target traits for plant breeding.

KEYWORDS: *maize, water stress, degradability, tissue distribution, lignification, p-coumaroylation*

INTRODUCTION

Currently, the use of fossil energy is primarily responsible for greenhouse gas production. Additionally, as fossil resources become more limited,[1] it is necessary to investigate the use of renewable carbon sources such as lignocellulosic biomass. With regards to the maize biomass, it is used traditionally as silage for dairy cows, as well as an emerging source of valorization for bioethanol production. In both cases, the goal is to convert fermentable sugars from the cell wall into energy, although their accessibility remains the main issue. One way to evaluate this conversion is to quantify cell wall degradability using enzymatic cocktails in vitro.[2] Many studies have been carried out on maize to better understand the relationship between lignification and cell wall degradability.[3−9]

Cell wall degradability is strongly influenced by cell wall structure and composition. In grasses, *p*-hydroxycinnamic acids, mainly ferulic (FA) and *p*-coumaric (pCA) acids, are responsible for creating cross-links between cell wall polymers. pCA is ester-linked with S-lignins units[10−12] whereas FA appears to be associated with hemicelluloses and lignin through ester linkages and ether linkages, respectively.[13] Cell wall degradability was shown to be strongly influenced by the presence of phenolic compounds[3,14−18] and lignin content is the main recalcitrant factor of cell wall degradability. Several studies also showed that monomeric lignin composition affects cell wall degradability, but the results are still controversial. The lignin polymeric structure estimated by the amount of βO4 linkage is another feature whose role in degradability remains controversial. Zhang et al.[18] showed, using maize lines with a similar lignin content, that the amount of βO4 linkage was negatively correlated with cell wall degradability. However, it is important to note that variations in cell wall degradability cannot be simply attributed to lignin content and severe reductions in lignin content is likely to negatively impact plant physiology. As such, it is necessary to identify targets for enhancing cell wall degradability that can be fed into breeding programmes.

Cell wall degradability of stems can be affected not only by variations in the proportions of cell walls components, but also by relative proportions of different cell types.[7,19] In 1991, Grabber and co-workers showed that sclerenchyma and the parenchyma of switchgrass stem cross sections were degraded with rumen fluid after several hours.[20] Jung and Casler[17] conducted a similar study on maize stem cross sections and showed interestingly that degradability differed between cell types. Méchin et al.[21] investigated the link between lignin distribution in maize stem, cell wall biochemical traits and cell wall degradability. They showed that highly digestible maize silage was poorly lignified. Notably, its lignins were enriched in S units than in G units and preferentially localized in the cortical region rather than in the pith. In alfalfa, variations in cell wall degradability can be attributed to differences in the proportion of different cell types.[22,23] An anatomical comparison of switchgrass stems selected for differences in cell wall degradability showed striking differences in the distribution of lignified cell types.[24] Overall, these studies clearly showed that differences between tissue lignification can influence cell wall degradability at the organ level.[25,26]

Received: December 8, 2017
Revised: April 20, 2018
Accepted: April 24, 2018
Published: April 24, 2018

Downloaded via FRENCH NATL INST AGRICULTURAL RSRCH on October 30, 2018 at 23:29:27 (UTC).
See https://pubs.acs.org/sharingguidelines for options on how to legitimately share published articles.

© 2018 American Chemical Society

DOI: 10.1021/acs.jafc.7b05755
J. Agric. Food Chem. 2018, 66, 4800−4808

Recently, studies have shown that water deficit arising from global climate change can also affect biomass quality, and hence cell wall degradability in grasses. Sanaullah et al.[27] investigated the effect of water deficit on festuca and dactylis and showed an increase of noncellulosic sugars in the cell wall and concomitant reduction in lignin content. In contrast, a study on two sugar cane genotypes reported an increase in lignin content of about 60% of in the rind of young internodes.[28] Emerson et al.[29] showed that the xylan, cellulose, and lignin contents were reduced under water deficit in maize, miscanthus and mixed grasses.

In the present study, 11 maize inbred lines were selected for their wide range of degradability and lignin content and were cultivated under different irrigation scenarios in field trials and harvested at silage stage over 3 consecutive years. Dedicated biochemical and histological high-throughput tools were developed in order to quantify a large number of parameters on a large number of internodes samples. We observed significant negative correlations between pCA content and cell wall degradability in maize. Our results clearly showed that a water deficit induced significant changes in lignin content and distribution along with a reduction in lignin *p*-coumaroylation, thereby impacting cell wall degradability. Our results open up the possibility of selecting maize genotypes tolerant to water deficit that can be used in breeding programs for enhancing biomass utilization.

MATERIALS AND METHODS

Plant Material. Eleven public maize inbred lines (Table 1) were selected from previous experiments performed at INRA Lusignan between 1997 and 2008.[3,5,18]

Table 1. Pedigree of the Studied Inbred Lines

line	pedigree	precocity
F4	Northern Flint	early
F7082	M13 Dent x BSSS	midearly
F66	Soest Flint	early
F7019	M13 Dent x BSSS	midearly
F7025	Iodent x M13 Dent	midearly
F2	Lacaune Flint	early
F271	Canadian dent	early
F874	Complex Dent	early
Cm484	Canada-Morden-1989	early
F7092	Lacaune Flint	midearly
F98902	CRANaMOF 7-2-1-2-5-4	early

Field experiments were carried out at Mauguio (France) over three consecutive years: 2012, 2013, and 2014. All inbred lines were cultivated each year with the exception of F4 in 2012 and F7082 in 2014 under two contrasting irrigation scenarios. Under the nonirrigated scenario, watering was stopped from the emergence of the fifth ligulated leaf on F2 inbred until 14 days after flowering (no irrigation from June to August). The trials were conducted in randomized block designs with two replicates. Length of the rows was 4.20 m, the inter-row spacing was 0.80 m, and the density was 80 000 plants per hectare.

In all years, conditions and blocks, the whole internode located under the main ear was collected for 13 plants at silage stage (about 30% dry matter content of the whole plant) for every line. Ten of these internodes were dried in an oven at 55 °C and then ground with a hammer mill (1 mm grid) before biochemical analyses and NIRS predictions. The remaining three internodes were stored in 70% ethanol in order to perform histological analyses.

Histological Analyses. Two cross sections of 150 μm thickness were cut from two internodes. A total of 528 cross sections were obtained using an HM 650 V Vibratome from MicroMicrotech France and stored in 70% ethanol. They were then stained with FASGA solution (derived from Tolivia and Tolivia, 1987).[30] The FASGA solution stains lignified tissues in red, whereas nonlignified or poorly lignified tissues are stained cyan/blue. 65 mL of FASGA solution was prepared adding 3 mL of Safranin red (SIGMA S8884) solution at 1%, 11 mL of alcian blue (SIGMA S2889) solution at 0.5%, 30 mL of glycerin (SIGMA G7893), 20 mL of ultrapure water, and 1 mL of pure acetic acid. This solution was 1/8 diluted in ultrapure water. The cross sections were stained for 24 h in 3 mL of the 1/8 diluted FASGA solution under constant agitation. They were washed in ultrapure water for 24 h under constant agitation. All the cross sections were mounted in distilled water on slides after two more washes for 5 min in ultrapure water.

Cross-section images were acquired with the 5× objective of an AxioImager Z2 Zeiss and a CoolCube 1 camera with a 1360 × 1024 pixels resolution piloted by the software Metafer (Figure 1A). Each image was numerically analyzed on the ImageJ software with the plugin as described in Legland et al.[31] to segment and calculate the histological traits (Figure 1B). In order to synthesize all the variations given by all these 18 traits, we chose to retain three original variables: Stem_Area; Bundle_area and Bundle_number and to calculate three additional variables: Blue_parenchyma (Figure 1D), which refers to the amount of blue intensity in the blue parenchyma; Red_parenchyma (Figure 1C), which refers to the amount of red intensity in the red parenchyma; Red_rind (Figure 1F), which refers to the amount of red intensity in the rind. These six variables were kept for further statistical analyses.

NIRS Predictive Equations Construction and NIRS Predictions. According to the considered biochemical parameter, 51 to 123 calibration samples were chosen among hundreds of internode samples to be representative of the spectrum variation obtained over five years of field trials, including samples from this study. Biochemical quantifications were performed on the calibration sample set (Table 2). Cell wall residue content (CWR), obtained with a water/ethanol extraction (Soxhlet). Lignin content in the cell wall (KL.CWR) was estimated using the Klason method,[32] the composition and structure of lignins were obtained by thioacydolysis.[33] Esterified and etherified *p*-hydroxycinnamic acids content (PCAest, FAest and FAeth) were obtained by alkaline hydrolysis.[34] Glucose, xylose, and arabinose content were quantified by acidic hydrolysis.[35,36] Acid pretreatment of the dry matter followed by a cellulolysis (Onozuka cellulase) for *in vitro* dry matter degradability or IVDMD,[37] and the *in vitro* cell wall residue degradability or IVCWRD[38] was calculated. Biochemical values were afterward predicted with accurate NIRS predictive equations for the 124 harvested internode samples.

Statistical Analyses. All the statistical analyses were performed on R. Following standard procedures, an analysis of variance was performed according to the following model:

$$Y_{ijkl} = \mu + A_j + G_i + T_k + B_l + A_j \times G_i + G_i \times T_k + A_j \times T_k + A_j \times G_i \times T_k + R_{ijkl}$$

where Y_{ijkl} is the value of the genotype I, in year j, under condition k and in block l; μ = overall mean; A_j = the main effect of year j; T_k = the main effect of the condition k; G_i = the effect of genotype i; B_l = the main effect of the block l; $A_j \times G_i$ = the interaction effect between genotype i and year j; $A_j \times T_k$ = the interaction effect between the condition k and the year j; $G_i \times T_k$ = the interaction effect between the genotype I and the condition k; $A_j \times G_i \times T_k$ = the interaction effect between genotype i under the condition k in year j; and R_{ijkl} = the random residual term.

As the interactions with the year or the block were much less significant than the other effects (not shown), we corrected the data set for block and year effects. On the corrected data set, another analysis of variance has been performed with the following linear model for each trait:

$$Y_{ij} = \mu + G_i + T_j + G_i \times T_j + R_{ij}$$

where Y_{ij} is the value of the genotype i, under condition j; μ = overall mean; T_j = the main effect of the condition j; G_i = the effect of

DOI: 10.1021/acs.jafc.7b05755
J. Agric. Food Chem. 2018, 66, 4800−4808

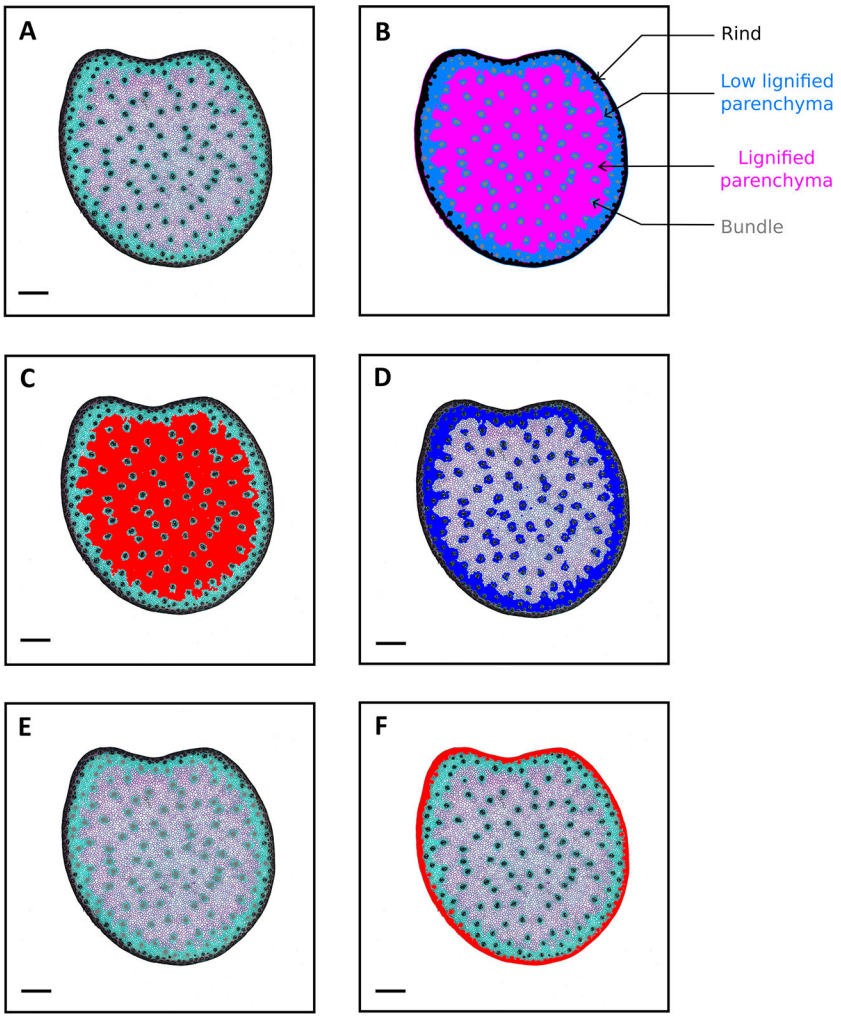


Figure 1. Automatic image analysis of FASGA stained maize stem cross sections. (A) FASGA stained cross-section of F2 genotype. (B) Output of the image analysis with the different histological fractions segmented. (C) Red_parenchyma trait in red color overlaid on the FASGA cross-section. (D) Blue_parenchyma trait in blue overlaid on the FASGA cross-section. (E) Bundle_area trait in gray overlaid on the FASGA cross-section. (F) Red_rind trait in red overlaid on the FASGA cross-section. Bar = 2 mm.

Table 2. Cell Wall Biochemical Related Traits Quantified, Associated Reference Methods, and NIRS Prediction Equation Characteristics

trait	designation	reference method	units	N^a	R^b	SEC^c
cell wall residue	CWR	Soxhlet extraction	% DM	76	0.95	1.65
lignin content	KL.CWR	Klason	% CWR	123	0.84	0.88
βO4 yield	βO4_yield	thioacidolysis	μmol/g KL	123	0.77	80
S lignin subunit yield	βO4_S		μmol/g KL	123	0.72	52
G lignin subunit yield	βO4 _G		μmol/g KL	123	0.78	54
etherified ferulic acids	FAeth	alkaline hydrolysis	mg/g CWR	102	0.76	0.52
esterified ferulic acids	FAest		mg/g CWR	101	0.76	0.52
esterified *p*-coumaric acids	PCAest		mg/g CWR	101	0.66	2.30
glucose content	cellulose	acidic hydrolyses	% CWR	55	0.89	1.84
hemicelluloses content	hemicelluloses		% CWR	55	0.85	2.44
in vitro dry mater digestibility	IVDMD	acid pretreatment + cellulolyse	% DM	51	0.98	1.5
in vitro cell wall digestibility	IVCWRD		% CWR	51	0.94	4.71

[a]Number of samples used to calibrate NIRS predictive equations. [b]Correlation coefficient between biochemical values and predicted values. [c]Standard error of calibration calculated on the prediction of the calibration samples.

genotype i; $G_i \times T_j$ = the interaction effect between the genotype i and the condition j; and R_{ij} = the random residual term. Pearson correlations were estimated on means over the years, the blocks per genotype and irrigation condition.

DOI: 10.1021/acs.jafc.7b05755
J. Agric. Food Chem. 2018, 66, 4800−4808

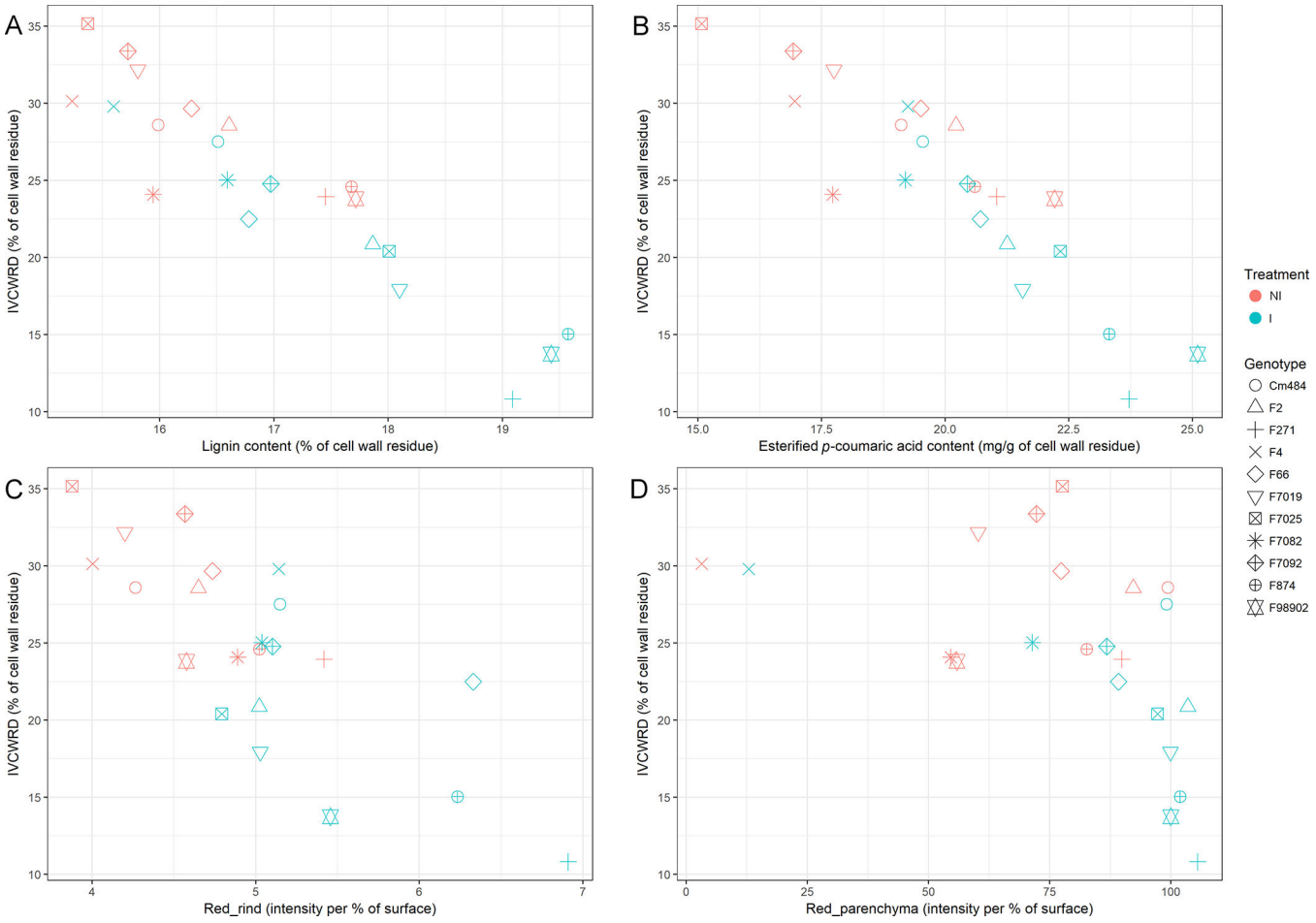


Figure 2. Relationships between the in vitro cell wall residue degradability (IVCWRD) and 4 others traits: the lignin content (KL.CWR, A), esterified *p*-coumaric acid content (PCAest, B), the amount of red in the rind (Red_rind, C) and the amount of red in the red parenchyma (Red_parenchyma, D). Inbred lines are represented with a different shape and the treatment with a different color: Pink for the nonirrigated condition and blue for the irrigated conditions.

RESULTS

Genotypic Variation and Responses to Irrigation Scenario. *Biochemical, Histological, and Cell Wall Degradability Variations.* For the experiments carried out under two different irrigation scenarios, IVCWRD as well as KL.CWR varied on average 3.5- and 1.3-fold, respectively, among the cultivated inbred lines (Figure 2A). More importantly, the F7025 inbred line cultivated under the nonirrigated condition showed the highest IVCWRD (35% of CWR) while exhibiting medium cell wall degradability under the irrigated condition (Figure 2A). On the other hand, the F271 inbred line exhibited one of the lowest IVCWRD in both conditions (10.8% and 23.9% of CWR under irrigated and nonirrigated conditions, respectively; Figure 2A).

Histological traits quantified by automatic image analysis consistently showed a variation rate above 65%. Significant differences were observed for the blue staining in the parenchyma (Figure 3). The F4 inbred line showed a strong blue intensity in the parenchyma (about 0.50) while F271 had a lower blue intensity (about 0.04) and a high red intensity (about 0.37) in the parenchyma. The number of bundles identified within the parenchyma varied from 76 for F7019 under the nonirrigated scenario to 203 for F7025 under the nonirrigated scenario.

Responses of Degradability, Biochemical, and Histological Traits to the Irrigation Scenario. Overall, inbred lines grown under the nonirrigated scenario have a higher degradability (above 24% of CWR) and a lower lignin content (below 18% of KL.CWR) compared to those grown under the irrigated scenario (Figure 2A, Table 3). Under the irrigated scenario, the same lines showed a wider range of both IVCWRD and KL.CWR with 80% of the genotypes showing cell wall degradability below 25% of CWR, and a lignin content above 16.7% of CWR (Figure 2A, Table 3). The combination of the two irrigation scenarios increased the range of variation of these traits. PCAest also showed important variations which depended on the irrigation status (Figure 2B, Table 3). Thus, the PCAest levels varied from 19.2 mg/g of CWR to 25.1 mg/g of CWR under the irrigated condition, while it varied from 15.1 mg/g of CWR to 22.2 mg/g of CWR under the nonirrigated condition.

Responses of the biochemical traits to irrigation scenarios varied among the studied inbred lines. F4 with a high IVCWRD under the irrigated condition did not show a remarkable increase of IVCWRD under the nonirrigated condition (29.8 and 30.1% of CWR under irrigated and nonirrigated scenarios, respectively). Similarly, IVCWRD of Cm484 and F7082 did not vary between the irrigation scenarios (27.5% and 28.6% of CWR for Cm484 and 25% and 24.1% of CWR for F7082 under irrigated and nonirrigated scenario, respectively) while having more lignin in the cell wall when grown under water deficit. Other lines such as F7025 responded significantly to irrigation.

DOI: 10.1021/acs.jafc.7b05755
J. Agric. Food Chem. 2018, 66, 4800−4808

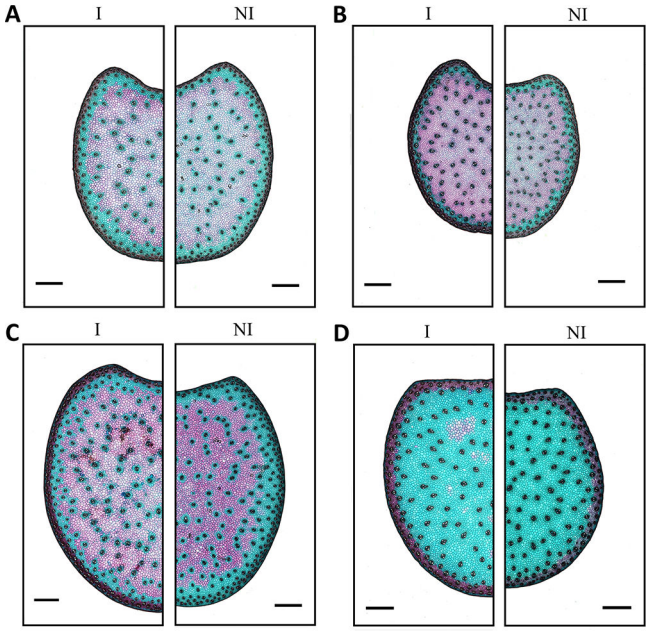


Figure 3. Genotypic diversity and response to water deficit of the histological profiles. Image acquisition of Fasga stained cross sections of 4 genotypes internode (Cm484, F271, F7025, and F4 in parts A, B, C, and D, respectively) cultivated in 2014. Lignified tissues are stained from red to magenta while tissues with a low lignin content are stained from blue to cyan. On the left of each panel, fasga-stained cross section harvested in irrigated scenario (I) is presented whereas fasga-stained cross section harvested in nonirrigated scenario (NI) is presented on the right. Scale bar: 2 mm.

The IVCWRD of F7025 increased by 15% under the nonirrigated condition. Consistently, KL.CWR of F7025 decreased by 4% when cultivated under the nonirrigated condition (Figure 2A). This result highlighted overall responses of IVCWRD and KL.CWR to irrigation and the presence of important genetic diversity for these responses.

Significant differences in histological traits (except Bundle_number and Blue_parenchyma) among irrigated and nonirrigated conditions were observed (Table 3 and Figure 4). Among the set of studied lines, different responses of histological traits to irrigation regimes were observed. Cm484 kept approximatively the same histological profile under the contrasted water regimes (Figure 3A). F7082 is another genotype which is did not respond at the histological level as shown for Red_rind (Figure 2C). In contrast, F7025 had a red intensity in the rind which decreased (0.38 vs 0.30 under irrigated and nonirrigated conditions, respectively) and this is consistent with an extended blue zone around the bundles both in the parenchyma in the rind regions (Figure 3C).

We used variance analyses to determine the impact of genetic and irrigation scenarios on the variation of each quantified biochemical and histological trait. The effects of irrigated scenario (Treatment) and of the genotype (Genotype) were always highly significant except for the treatment effect on Bundle number (Figure 4 and Table S1). It is worth noting that even if the interaction between Genotype and Treatment were significant for most of the traits, its level of significance was always lower than that observed for the treatment or the Genotype, except for FAeth where the interaction between Genotype and Treatment was higher than Genotype effect (Figure 4 and Table S1).

Table 3. Variation Ranges for Evaluated Biochemical and Histological Traits under Irrigated Condition (I) and Nonirrigated Condition (NI)

		IVCWRD	Stem_area	Bundle Area	Bundle Number	Blue Parenchyma	Red Parenchyma	Red_rind	KL. CWR	BO4 yield	S/G	PCAest	FAeth	FAest	cellulose	hemicelluloses
	t test *p*-value[a]	2×10^{-10}	9×10^{-4}	8×10^{-7}	7×10^{-1}	7×10^{-1}	4×10^{-4}	1×10^{-8}	2×10^{-7}	3×10^{-6}	9×10^{-8}	9×10^{-7}	9×10^{-8}	2×10^{-1}	2×10^{-5}	4×10^{-4}
	significance[b]	***	***	***			***	***	***	***	***	***	***		***	***
I	Mean	20.76	1.79	131	6.96	30.34	87.94	5.47	17.68	697.1	1.16	21.49	3.17	4.81	43.76	35.79
	Min	10.81	1.25	99	4.75	7.91	12.91	4.79	15.60	630.9	1.09	19.19	2.71	4.30	41.29	33.91
	Max	29.80	2.99	206	9.23	123.67	105.49	6.91	19.57	754.1	1.25	25.10	3.73	5.59	46.25	38.27
NI	Mean	28.55	1.45	130	8.49	35.28	69.56	4.56	16.34	630.0	1.26	18.83	2.80	4.96	41.69	37.70
	Min	23.80	1.00	77	5.91	11.41	3.19	3.88	15.23	527.9	1.14	15.07	2.31	4.47	38.10	34.13
	Max	35.16	2.63	203	9.52	130.92	99.35	5.42	17.72	686.9	1.40	22.21	3.15	5.67	44.31	40.61

[a] *t* test performed between the average of every traits in the two watering conditions. [b] Significance: no symbol, $p \leq 0.1$; *, $p \leq 0.05$; **, $p \leq 0.01$; ***, $p \leq 0.001$.

DOI: 10.1021/acs.jafc.7b05755
J. Agric. Food Chem. 2018, 66, 4800−4808

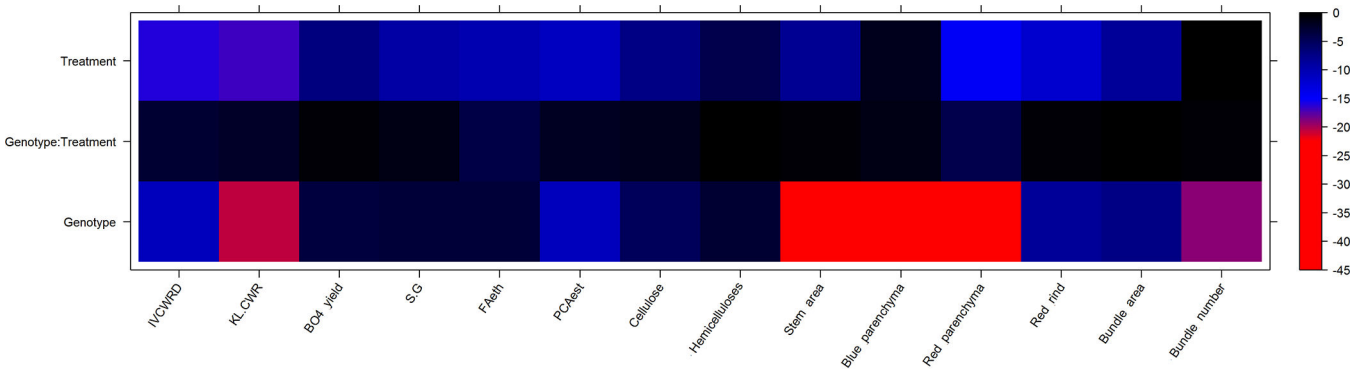


Figure 4. Heat map of the significance (decimal log of the *p*-value) of the genotype, the treatment, and their interaction effects for biochemical and histological traits (see Table 2 for the meaning of each trait).

Table 4. Relationship between Biochemical and Histological Traits under Irrigated Condition (in Blue) and Nonirrigated Condition (in Red)

	IVCWRD	Stem_area	Bundle_number	Bundle_area	Red_parenchyma	Blue_parenchyma	Red_rind	KL.CWR	BO4_yield	S/G	PCAest	FAeth	FAest	Cellulose	Hemicelluloses
IVCWRD	1	-0.01	-0.25	-0.03	-0.66 *	0.62 *	-0.59 .	-0.95 ***	-0.64 *	0.72 *	-0.93 ***	-0.92 ***	-0.09	-0.72 *	-0.06
Stem_area	0.40	1	0.87 ***	0.37	0.12	-0.16	-0.56 .	0.15	0.14	-0.14	0.20	-0.19	0.32	-0.10	-0.02
Bundle_number	-0.02	0.77 **	1	0.27	0.15	-0.15	-0.25	0.32	0.45	-0.32	0.40	0.05	0.20	0.18	-0.21
Bundle_area	0.11	0.20	0.26	1	-0.17	-0.18	-0.02	-0.02	0.02	0.35	-0.04	-0.09	0.56 .	-0.42	0.52 .
Red_parenchyma	-0.07	0.03	-0.21	-0.47	1	-0.92 ***	0.25	0.70 *	-0.01	-0.59 .	0.57 .	0.68 *	-0.13	0.63 *	0.16
Blue_parenchyma	0.07	0.01	0.27	0.12	-0.89 ***	1	-0.26	-0.60 .	0.11	0.42	-0.46	-0.64 *	-0.10	-0.44	-0.40
Red_rind	-0.75 **	-0.60 .	-0.26	-0.09	0.39	-0.44	1	0.44	0.39	-0.23	0.46	0.61 *	-0.25	0.40	-0.21
KL.CWR	-0.78 **	-0.22	-0.08	-0.08	0.38	-0.39	0.74 **	1	0.58 .	-0.73 *	0.94 ***	0.81 **	-0.03	0.75 **	0.07
BO4_yield	-0.72 *	0.02	0.31	-0.13	0.20	-0.17	0.35	0.50	1	-0.52	0.72 *	0.52	0.23	0.35	-0.42
S.G	0.56 .	0.03	-0.32	0.49	-0.29	0.09	-0.52	-0.48	-0.47	1	-0.77 **	-0.79 **	-0.12	-0.83 **	0.29
PCAest	-0.79 **	-0.42	-0.27	-0.30	0.32	-0.27	0.67 *	0.92 ***	0.53 .	-0.41	1	0.80 **	0.05	0.72 *	-0.16
FAeth	-0.46	-0.31	0.11	-0.50	-0.09	0.30	0.43	0.27	0.06	-0.72 *	0.32	1	0.19	0.75 **	0.03
FAest	0.01	0.27	0.13	0.54 .	-0.09	-0.26	-0.18	-0.04	0.32	0.26	-0.14	-0.63 .	1	-0.31	0.25
Cellulose	-0.69 *	-0.49	-0.17	-0.55 .	0.36	-0.15	0.78 **	0.66 *	0.26	-0.73 *	0.71 *	0.77 **	-0.60 .	1	-0.13
Hemicelluloses	-0.12	0.02	-0.17	0.67 *	0.10	-0.46	0.17	0.21	0.07	0.50	0.08	-0.65 *	0.67 *	-0.34	1

Among the histological traits, except for the Red_rind and the Bundle_area, the most significant effect remained the genotypic effect (Figure 4 and Table S1).

Concerning the biochemical traits, the Treatment effect was significantly higher than the genotypic effect for the 3 following biochemical traits: IVCWRD, PCAest, and FAeth (Figure 4 and Table S1). The genotypic effect was stronger only for KL.CWR (decimal log (p-value = 3.09×10^{-21}) = −20.5) than the treatment effect (decimal log (p-value = 2.11×10^{-17}) = −16.7).

Relationships between Biochemical and Histological Traits and Cell Wall Degradability. *Relationships between Histological and Biochemical Parameters.* Pearson correlations between histological and biochemical traits are shown in Table 4. The pattern of correlations was modified between the two irrigated scenarios. Under the irrigated scenario, Red_parenchyma was positively and significantly correlated to KL.CWR (r = 0.70), FAeth (r = 0.68), Cellulose (r = 0.63), and PCAest (r = 0.57). Red_rind was also positively and significantly correlated to FAeth (r = 0.61). Blue_parenchyma was negatively correlated to KL.CWR (r = −0.60) and FAeth (r = −0.64). Under the nonirrigated scenario, Red_rind was significantly and positively correlated to KL.CWR (r = 0.74), PCAest (r = 0.67), and Cellulose (r = 0.78) (Table 4). Bundle_area was correlated with both the hemicellulose (r = 0.67) and the cellulose (r = −0.55) contents (Table 4).

Relationships between Cell Wall Degradability and Biochemical and Histological Traits. Coefficient of determination between IVCWRD and biochemical and histological traits was estimated in each irrigation scenario separately (Table 4). Biochemical traits were highly correlated to IVCWRD under the irrigated conditions (Table 4), especially the lignin content (KL.CWR, r = −0.95), the esterified p-coumaric acid content (PCAest, r = −0.93), and the etherified ferulic acid content (FAeth, r = −0.92). KL.CWR and PCAest were also highly correlated to IVCWRD (r = −0.78 and r = −0.79, respectively) under the nonirrigated scenario.

Under the irrigated conditions, Red_parenchyma (r = −0.66) and Blue_parenchyma (r = 0.62) were significantly correlated to IVCWRD, whereas Red_rind was the only histological trait where significant correlations to IVCWRD under the nonirrigated condition were observed (r = −0.75) (Table 4).

DISCUSSION

Robust and Accurate High-Throughput Biochemical and Histological Tools Development. NIRS predictive equations have been developed to evaluate the quality of agricultural products such as forage[39] and are available for maize harvested at the silage stage to evaluate digestibility and compositions.[40,41] They were then developed and applied in plant breeding and for studying traits such as digestibility and cell wall related traits.[42,43] To our knowledge, the only specific NIRS equations for a corn organ were those developed by the Yves Barrière team on maize internodes/lower stem (INRA Nouvelle-Aquitaine-Poitiers UR3PF, unpublished data).

NIRS predictive equations for p-hydroxycinnamic acids are rarely available. It is noteworthy that the r^2 of these predictive equations are often good for PCAest, ranging from 0.87

DOI: 10.1021/acs.jafc.7b05755
J. Agric. Food Chem. 2018, 66, 4800−4808

(Riboulet et al., 2008) to 0.95 (Lorenzana et al., 2010[41,44]). However, the r^2 of predictive equations for ferulic acid content is lower, ranging from 0.66[41] to 0.04.[44] In the established NIRS predictive equations used in this study, similar values were observed for both traits, with a r^2 of 0.44 and 0.58 for PCAest and FAtot, respectively. To the best of our knowledge, this is the first example of a NIRS predictive equation for lignin structure and composition as determined by thioacidolysis, and thus representative of lignin (unlike nitrobenzene determination). The robust statistical parameters of established equations enabled us to predict lignin structure and composition with confidence. In addition, internode samples used to calibrate the NIRS predictive equations have been selected from different field trials carried out in France, including internodes from the field trials set up in Mauguio with different irrigation scenarios.

Variations in the distribution of lignified tissues of maize stem cross sections, and its link to biochemical traits, have been well-studied in maize[17,21,31,41,45] and more recently in sorghum.[46] Jung and Casler[17] reported variations between two maize hybrids and provided relationships between histological patterns and cell wall biochemistry over the development of internodes. On the other hand, Méchin et al.[21] showed, using a semiautomated image analysis tool on FASGA stained cross sections, that a highly digestible maize may possess only a small surface of lignified material, a low number of cell layers in the cortical sclerenchyma, a low cortex and vessel surfaces, and thin cortical cell walls. Perrier et al.[46] studied the morphological, biochemical, and histological traits underlying biomass accumulation in sorghum stems and their plasticity in response to water deficit using a dedicated tool on ImageJ Freeware, but with manual interventions to delimited cortical and pith areas. In the present study, a fully automated image analysis tool[31] was used to quantify the histological pattern of hundreds of internodes. Together, these NIRS equations and high-throughput tools for histological quantitation pave the way for detailed analyses of biochemical and histological patterns of maize internodes and their responses to drought.

Water Deficit Strongly Amplified the Range of Variation for Cell Wall Degradability, Biochemical, and Histological Traits. Our knowledge to date on cell wall degradability, biochemical, and histological traits have been based on studies involving a limited number of genotypes. Dos Santos et al.[28] investigated the response to drought of two sugar cane genotypes and, more recently, Perrier et al.[46] performed a similar study on two sorghum genotypes. Van der Weije et al.[47] was the only study to consider a large number of genotypes by studying the water deficit response of predicted biochemical parameters of 50 *Miscanthus* genotypes.

Under the irrigated conditions, lignin content in the cell wall and cell wall degradability showed a large range of variations (4% and 19%, respectively). Under the nonirrigated conditions, the range of the lignin content was shifted and shortened, and the range of cell wall degradability increased to about 25% of the cell wall residue. As such, the irrigation scenario increased the range of variation for these traits. This range of variation is not common even in studies including brown-midrib three maize mutants which exhibited a very high degradability. Marita et al.[48] showed a variation of only 3.4% of lignin content in the cell wall residue and 16% of degradability studying five maize brown-midrib mutant lines and one normal line. Méchin et al.[21] characterized 22 maize lines, including four brown-midrib 3 (bm3) mutants and reported 8% of variation for lignin content in the cell wall and 18% for cell wall degradability. This study in which F4 was also included showed that this inbred line has a cell wall degradability comparable to bm3 mutants. The enlarged range of the IVCWRD and of other biochemical and especially for histological parameters can therefore be attributed to the inclusion of F4 in the corresponding study.

Similar trends in the variations and the responses to irrigation scenario to lignin content were observed for esterified *p*-coumaric acid content, βO4 yield and etherified ferulic acid. These reinforce the link between all these parameters in the building of the cell wall.[7,10,11,49]

The histological traits showed noticeable responses to irrigation scenarios. The bundle number presented a range tightly related to the Stem_area, suggesting that under both conditions, the bigger the stem, the more bundles were present. F4 presented a very particular histological profile with a parenchyma almost completely stained in blue and therefore poor in lignin and phenolic compounds in agreement with Méchin et al.[21] The Red_rind trait varied considerably between the irrigation scenarios and showed a wider range of variation under the nonirrigated conditions.

Different Patterns of Lignification Depending on the Water Status. *Water Deficit Induces an Upheaval of Lignin Content and Distribution along with a Reduced Lignin p-Coumaroylation.* Lignin and *p*-coumaric acid contents decreased when plants were cultivated under the nonirrigated scenario. As proposed by Perrier et al.,[46] this response could be related to a reduction of C allocation to these compounds to favor the synthesis of soluble compounds associated with osmoregulation and storage to ensure recovery after rewatering.[50] Three genotypes (F4, Cm484, and F7082) were surprisingly able to maintain their lignin content under drought conditions. F7082 remained the only genotype to exhibit similar lignin and *p*-coumaric acid contents and distribution patterns of Red_rind and Red_parenchyma under both irrigation scenarios. All the other genotypes showed a reduction in the overall quantity of lignin deposited in the rind.

Different Strategies of Tissues Lignification According to the Water Status. The relationships between biochemical and histological traits have enabled us to better understand the mode of distribution of lignin under two contrasting irrigation scenarios. When irrigated, plants synthesized more lignins that preferentially accumulate in the parenchyma rather than in the rind (r = 0.70 between KL.CWR and Red_parenchyma vs r = 0.44 between KL.CWR and Red_rind). In contrast, under water deficit conditions, plants synthesized less lignin and accumulated them preferentially in the rind rather than in the parenchyma (r = 0.74 between KL.CWR and Red_rind vs r = 0.38 between KL.CWR and Red_parenchyma). This is in agreement with the observations of Dos Santos et al.[28] who showed that sugar cane stems from genotype IACSP95-500 subjected to severe drought accumulated 30% more lignin in mature rind compared to irrigated plants. Our results and those of others showed clearly that the distribution of lignin is dependent on the water status.

Under irrigated conditions, as demonstrated by Zhang,[45] lignification was limited to the parenchyma when silks appeared while it continued up to the mature silage stage in the rind. Additionally, lignin in the rind was also richer in βO4 bonds than in parenchyma. In our study, under water deficit, the parenchyma was as rich as the rind in βO4 bonds, suggesting that lignification was maintained in both tissues for the same duration. Plants therefore synthesize fewer lignin when they are

DOI: 10.1021/acs.jafc.7b05755
J. Agric. Food Chem. 2018, 66, 4800−4808

under water limiting conditions. In the same way, the relationships between biochemical and histological characteristics strongly suggest that under water-deficit conditions, the rind was also richer in PCAest than the parenchyma. The rind of nonirrigated plants compared to the irrigated plants appeared to be enriched in with more linear and *p*-coumaroylated lignins. These tissue characteristics is likely to result in a stronger barrier in the rind of water stressed plant stems. More precise determination of differential tissue distribution will depend on the development of mass spectrometry imaging approaches that will enable us to reconstruct *p*-coumaroylation maps of internode cross sections. Additionally, microdissection approaches followed by biochemical analyzes could also be considered.

Impact of These Different Strategies of Tissues Lignification on Cell Wall Degradability. In both hydric scenarios, lignin and *p*-coumaric acid contents were the two major recalcitrant factors for cell wall degradability. Under the irrigated conditions, the impact of lignification in pith and in rind on cell wall degradability was quite similar and both significantly negative. In contrast, under the nonirrigated conditions, the quantity of lignin and *p*-coumaric acids in the rind limited overall cell wall degradability of the internode, while the quantity of lignin in the pith did not. As hypothesized by Dos Santos et al.[28] in sugar cane, we succeeded in demonstrating that lignin deposition affects recalcitrance and hydrolysis efficiency. In 2005, Méchin et al. established that an ideotype of maize silage for cell wall digestibility may contain a reduced quantity of lignin that is preferentially localized in the cortical region rather than in the pith.[21] In the same way, the increase in cell wall degradability induced by water deficit was found to be associated with a reduced lignin content and a preferential rind lignification compared to parenchyma lignification.

This study enabled us to shed light on the crucial role of lignin repartitioning in both rind and pith to ensure high cell wall degradability when plants were subjected to water deficit. The other striking observation among the studied genotypes was the diversity of responses to water deficit. Our results suggest a crucial role for preferential tissue distribution of lignin and *p*-coumaroylation in the context of cell wall degradability. This opens up interesting prospects in terms of plant breeding in the current context of climate change.

■ ASSOCIATED CONTENT

Supporting Information

The Supporting Information is available free of charge on the ACS Publications website at DOI: 10.1021/acs.jafc.7b05755.

Table of means squares and *p*-value of the genotype, the treatment, and their interaction effect on every biochemical and histological trait (PDF)

■ AUTHOR INFORMATION

Corresponding Author

*E-mail: valerie.mechin@inra.fr.

ORCID

V. Méchin: 0000-0003-3743-7225

Funding

This work has benefited from French Government Grants (LabEx Saclay Plant Sciences-SPS, Grants ANR-10-LABX-0040-SPS and ANR-11-BTBR-0006 BIOMASS FOR THE FUTURE), managed by the French National Research Agency under an "Investments for the Future" program (Grant ANR-11-IDEX-0003-02). This work has also benefited from CEPIA INRA Division grants (AIC HistoChem and Intégrale). The École Doctorale Sciences du Végétal provided funding for Fadi El Hage's salary.

Notes

The authors declare no competing financial interest.

■ ACKNOWLEDGMENTS

We sincerely acknowledge S. Malavieille and P. Sartre (UE Diascope, Mauguio, France) for their precious contribution to field experiments. We also acknowledge Carl Ng for revising our manuscript.

■ REFERENCES

(1) Sabine, C.; Bala, G.; Bopp, L.; Brovkin, V.; Canadell, J.; Chhabra, A.; DeFries, R.; Galloway, J.; Heimann, M.; Jones, C.; et al. Contribution of working group I to the fifth assessment report of the intergovernmental panel on climate change coordinating. *GIEC Rep.* **2013**, 514−545.

(2) Aufrere, J. Etude de la prévision de la digestibilité des fourrages par une méthode enzymatique. *Ann. Zootech.* **1982**, *31*, 111−130.

(3) Méchin, V.; Argillier, O.; Menanteau, V.; Barrière, Y.; Mila, I.; Pollet, B.; Lapierre, C. Relationship of cell wall composition toin vitro cell wall digestibility of maize inbred line stems. *J. Sci. Food Agric.* **2000**, *80*, 574−580.

(4) Grabber, J. H.; Ralph, J.; Lapierre, C.; Barrière, Y. Genetic and molecular basis of grass cell-wall degradability. I. Lignin-cell wall matrix interactions. *C. R. Biol.* **2004**, *327*, 455−465.

(5) Barrière, Y.; Méchin, V.; Lafarguette, F.; Manicacci, D.; Guillon, F.; Wang, H.; Lauressergues, D.; Pichon, M.; Bosio, M.; Tatout, C. Toward the discovery of maize cell wall genes involved in silage quality and capacity to biofuel production. *Maydica* **2009**, *54*, 161−198.

(6) Somerville, C.; Youngs, H.; Taylor, C.; Davis, S. C.; Long, S. P. Feedstocks for lignocellulosic biofuels. *Science* **2010**, *329*, 790−792.

(7) Barros-Rios, J.; Santiago, R.; Malvar, R. A.; Jung, H. J. G. Chemical composition and cell wall polysaccharide degradability of pith and rind tissues from mature maize internodes. *Anim. Feed Sci. Technol.* **2012**, *172*, 226−236.

(8) Loqué, D.; Scheller, H. V.; Pauly, M. Engineering of plant cell walls for enhanced biofuel production. *Curr. Opin. Plant Biol.* **2015**, *25*, 151−161.

(9) Hatfield, R. D.; Marita, J. M.; Hatfield, R. D.; Marita, J. M. Maize development: cell wall changes in leaves and sheaths. *Am. J. Plant Sci.* **2017**, *8*, 1248−1263.

(10) Ralph, J.; Hatfield, R. D.; Quideau, S.; Helm, R. F.; Grabber, J. H.; Jung, H.-J. G. Pathway of p-Coumaric acid incorporation into maize lignin as revealed by NMR. *J. Am. Chem. Soc.* **1994**, *116*, 9448−9456.

(11) Lu, F.; Ralph, J. Detection and determination of p-coumaroylated units in lignins. *J. Agric. Food Chem.* **1999**, *47*, 1988−1999.

(12) Grabber, J. H.; Quideau, S.; Ralph, J. p-Coumaroylated syringyl units in maize lignin: implications for beta-ether cleavage by thioacidolysis. *Phytochemistry* **1996**, *43*, 1189−1194.

(13) Hatfield, R. D.; Rancour, D. M.; Marita, J. M. Grass cell walls: a story of cross-linking. *Front. Plant Sci.* **2017**, *7*, 2056.

(14) Hartley, R. D. p-Coumaric and ferulic acid components of cell walls of ryegrass and their relationships with lignin and digestibility. *J. Sci. Food Agric.* **1972**, *23*, 1347−1354.

(15) Grabber, J. H.; Hatfield, R. D.; Ralph, J. Diferulate cross-links impede the enzymatic degradation of non-lignified maize walls. *J. Sci. Food Agric.* **1998**, *77*, 193−200.

(16) Casler, M. D.; Jung, H.-J. G. Selection and evaluation of smooth bromegrass clones with divergent lignin or etherified Ferulic acid concentration. *Crop Sci.* **1999**, *39*, 1866−1873.

(17) Jung, H. G.; Casler, M. D. Maize stem tissues: Impact of development on cell wall degradability. *Crop Sci.* **2006**, *46*, 1801−1809.

(18) Zhang, Y.; Culhaoglu, T.; Pollet, B.; Melin, C.; Denoue, D.; Barrière, Y.; Baumberger, S.; Méchin, V. Impact of lignin structure and cell wall reticulation on maize cell wall degradability. *J. Agric. Food Chem.* **2011**, *59*, 10129−10135.
(19) Hatfield, R. D.; Wilson, J. R.; Mertens, D. R. Composition of cell walls isolated from cell types of grain sorghum stems. *J. Sci. Food Agric.* **1999**, *79*, 891−899.
(20) Grabber, J. H.; Jung, G. A.; Hill, R. R. Chemical composition of parenchyma and sclerenchyma cell walls isolated from orchardgrass and switchgrass. *Crop Sci.* **1991**, *31*, 1058−1065.
(21) Méchin, V.; Argillier, O.; Rocher, F.; Hébert, Y.; Mila, I.; Pollet, B.; Barriére, Y.; Lapierre, C. In search of a maize ideotype for cell wall enzymatic degradability using histological and biochemical lignin characterization. *J. Agric. Food Chem.* **2005**, *53*, 5872−5881.
(22) Jung, H. G.; Engels, F. M. Alfalfa stem tissues: cell wall deposition, composition, and degradability. *Crop Sci.* **2002**, *42*, 524−534.
(23) Guines, F.; Julier, B.; Ecalle, C.; Huyghe, C. Among and within-cultivar variability for histological traits of lucerne (Medicago sativa L.) stem. *Euphytica* **2003**, *130*, 293−301.
(24) Sarath, G.; Baird, L. M.; Vogel, K. P.; Mitchell, R. B. Internode structure and cell wall composition in maturing tillers of switchgrass (Panicum virgatum. L). *Bioresour. Technol.* **2007**, *98*, 2985−2992.
(25) Sarath, G.; Akin, D. E.; Mitchell, R. B.; Vogel, K. P.; Sarath, G.; Mitchell, R. B.; Vogel, K. P.; Akin, D. E. Cell-wall composition and accessibility to hydrolytic enzymes is differentially altered in divergently bred switchgrass (Panicum virgatum L.) genotypes. *Appl. Biochem. Biotechnol.* **2008**, *150*, 1−14.
(26) Lopez, S.; Murison, S. D.; Travis, A. J.; Chesson, A. Degradability of parenchyma and sclerenchyma cell walls isolated at different developmental stages from a newly extended maize internode. *Acta Bot. Neerl.* **1993**, *42*, 165−174.
(27) Sanaullah, M.; Chabbi, A.; Girardin, C.; Durand, J. L.; Poirier, M.; Rumpel, C. Effects of drought and elevated temperature on biochemical composition of forage plants and their impact on carbon storage in grassland soil. *Plant Soil* **2014**, *374*, 767−778.
(28) Dos Santos, A. B.; Bottcher, A.; Kiyota, E.; Mayer, J. L. S.; Vicentini, R.; Dos Santos Brito, M.; Creste, S.; Landell, M. G. A.; Mazzafera, P. Water stress alters lignin content and related gene expression in two sugarcane genotypes. *J. Agric. Food Chem.* **2015**, *63*, 4708−4720.
(29) Emerson, R.; Hoover, A.; Ray, A.; Lacey, J.; Cortez, M.; Payne, C.; Karlen, D.; Birrell, S.; Laird, D.; Kallenbach, R.; et al. Drought effects on composition and yield for corn stover, mixed grasses, and Miscanthus as bioenergy feedstocks. *Biofuels* **2014**, *5*, 275−291.
(30) Tolivia, D.; Tolivia, J. Fasga: A new polychromatic method for simultaneous and differential staining of plant tissues. *J. Microsc.* **1987**, *148*, 113−117.
(31) Legland, D.; El Hage, F.; Méchin, V.; Reymond, M. Histological quantification of maize stem sections from FASGA-stained images. *Plant Methods* **2017**, *13*, 84.
(32) Dence, C. The Determination of Lignin. In *Methods in Lignin Chemistry*; Lin, S. Y., Dence, C. W., Eds.; Springer: Berlin, Germany, 1992; pp 33−61.
(33) Lapierre, C.; Monties, B.; Rolando, C. Preparative thioacidolysis of spruce lignin: isolation and identification of main monomeric products. *Holzforschung* **1986**, *40*, 47−50.
(34) Culhaoglu, T.; Zheng, D.; Méchin, V.; Baumberger, S. Adaptation of the Carrez procedure for the purification of ferulic and p-coumaric acids released from lignocellulosic biomass prior to LC/MS analysis. *J. Chromatogr. B: Anal. Technol. Biomed. Life Sci.* **2011**, *879*, 3017−3022.
(35) Updegraff, D. M. Semimicro Determination of Cellulose in Biological Materials. *Anal. Biochem.* **1969**, *32*, 420−424.
(36) Harholt, J.; Krü Ger Jensen, J.; Sørensen, S. O.; Orfila, C.; Pauly, M.; Scheller, H. V. Arabinan deficient 1 is a putative arabinosyltransferase involved in biosynthesis of pectic arabinan in arabidopsis. *Plant Physiol.* **2006**, *140*, 49−58.
(37) Ronsin, T. Use of NIR prediction of digestibility in a breeding program for silage maize. In *Proceeding of the 15th Congress of Maize and Sorghum Section of Eucarpia*, Baden, Austria, 1990; pp 277−288.
(38) Mechin, V.; Argillier, O.; Barrière, Y.; Menanteau, V. Genetic variation in stems of normal and brown-midrib 3 maize inbred lines. Towards similarity for in vitro digestibility and cell wall composition. *Maydica* **1998**, *43*, 205−210.
(39) Norris, K. H.; Barnes, R. F.; Moore, J. E.; Shenk, J. S. Predicting Forage Quality by Infrared Replectance Spectroscopy. *J. Anim. Sci.* **1976**, *43*, 889−897.
(40) Dardenne, P.; Andrieu, J.; Barrière, Y.; Biston, R.; Demarquilly, C.; Femenias, N.; Lila, M.; Maupetit, P.; Rivière, F.; Ronsin, T. Composition and nutritive value of whole maize plants fed fresh to sheep. II. Prediction of the in vivo organic matter digestibility. *Ann. Zootech.* **1993**, *42*, 251−270.
(41) Riboulet, C.; Lefèvre, B.; Dénoue, D.; Barrière, Y. Genetic variation in maize cell wall for lignin content, lignin structure, p-hydroxycinnamic acid content, and digestibility in set of 19 lines at silage harvest maturity. *Maydica* **2008**, *53*, 11−19.
(42) Truntzler, M.; Barrière, Y.; Sawkins, M. C.; Lespinasse, D.; Betran, J.; Charcosset, A.; Moreau, L. Meta-analysis of QTL involved in silage quality of maize and comparison with the position of candidate genes. *Theor. Appl. Genet.* **2010**, *121*, 1465−1482.
(43) Torres, A. F.; Slegers, P. M.; Noordam-Boot, C. M. M.; Dolstra, O.; Vlaswinkel, L.; van Boxtel, A. J. B.; Visser, R. G. F.; Trindade, L. M. Maize feedstocks with improved digestibility reduce the costs and environmental impacts of biomass pretreatment and saccharification. *Biotechnol. Biofuels* **2016**, *9*, 63.
(44) Lorenzana, R. E.; Lewis, M. F.; Jung, H.-J. G.; Bernardo, R. Quantitative Trait Loci and trait correlations for maize stover cell wall composition and glucose release for cellulosic ethanol. *Crop Sci.* **2010**, *50*, 541−555.
(45) Zhang, Y. *Mise en place de la réticulation des parois de maïs au cours du développement et impact sur la variabilité de la dégradabilité des polysaccharides pariétaux*; AgroParisTech: Paris, France, 2012; pp206.
(46) Perrier, L.; Rouan, L.; Jaffuel, S.; Clément-Vidal, A.; Roques, S.; Soutiras, A.; Baptiste, C.; Bastianelli, D.; Fabre, D.; Dubois, C.; et al. Plasticity of Sorghum Stem Biomass Accumulation in Response to Water Deficit: A Multiscale Analysis from Internode Tissue to Plant Level. *Front. Plant Sci.* **2017**, *8*, 1−14.
(47) Van Der Weijde, T.; Huxley, L. M.; Hawkins, S.; Sembiring, E. H.; Farrar, K.; Dolstra, O.; Visser, R. G. F.; Trindade, L. M. Impact of drought stress on growth and quality of miscanthus for biofuel production. *GCB Bioenergy* **2017**, *9*, 770−782.
(48) Marita, J. M.; Vermerris, W.; Ralph, J.; Hatfield, R. D. Variations in the Cell Wall Composition of Maize brown midrib Mutants. *J. Agric. Food Chem.* **2003**, *51*, 1313−1321.
(49) Hatfield, R. D.; Chaptman, A. K. Comparing corn types for differences in cell wall characteristics and p-coumaroylation of lignin. *J. Agric. Food Chem.* **2009**, *57*, 4243−4249.
(50) Luquet, D.; Clément-Vidal, A.; Fabre, D.; This, D.; Sonderegger, N.; Dingkuhn, M. Orchestration of transpiration, growth and carbohydrate dynamics in rice during a dry-down cycle. *Funct. Plant Biol.* **2008**, *35*, 689−704.

DOI: 10.1021/acs.jafc.7b05755
J. Agric. Food Chem. 2018, 66, 4800−4808

II. F2bm3 does not respond histologically or biochemically to water deficit

Brown-midrib mutants are spontaneus mutants and we found them in different species: in sorghum (*Sorghum bicolor),* in pearl millet (*Pennisetum glaucum*) and in maize (*Zea mays*) (Sattler et al., 2010). The characteristic phenotype of the brown midrid mutants is the brown coloration of the leaf mid-veins. These mutations are associated with a reduced lignin content, an altered lignin composition and in maize with an increased cell wall degradability despite a decrease in forage and grain yield (Barrière et Argillier, 1993). A study reported that on 15 *bm3* lines and their 15 normal isogenic lines, the average stover yield was reduced by 17% (Lee et al., 1984). Another one showed a 15 to 20% reduction of the dry matter yield (Inoue et al., 1989). However, the maize *bm3* mutation has been incorporated into commercial hybrids and would represent 5% of the silage market in Canada (Zandbergen, 2006).

The maize gene *Bm3* has been cloned and it encodes caffeic O-methyltransferase (COMT) (Collazo et al., 1992; Vignols et al., 1995; Bout et al., 2003). In penultimate step of monolignol biosynthesis, COMT transfers a methyl group from S-adenosyl-methionine (SAM) to the 5-hydroxyl group of 5-hydroxyl-coniferyl to form synapyl products (Figure 27).

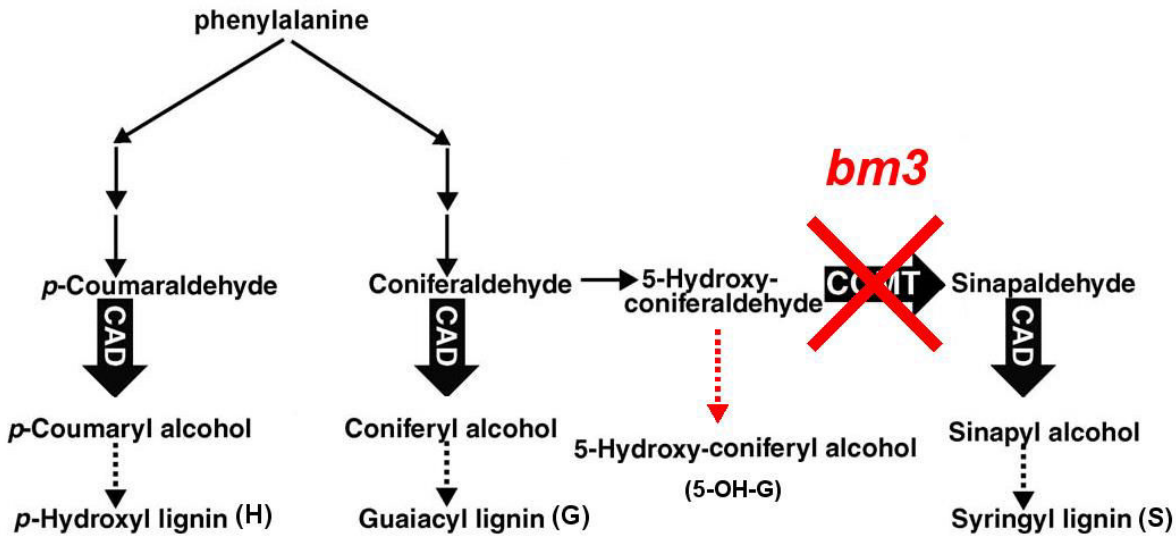


Figure 27. Simplified model of the depleted COMT action in *bm3* monolignol synthesis (adapted from Sattler et al., 2010).

The monomeric composition of the lignins has been studied in *bm3* and it has been shown that syringyl-lignins were greatly reduced while *p*-hydroxyphenil and guaiacyl-lignin were slightly reduced. In the meantime, the absence of the COMT induces an accumulation of 5-hydroxy-coniferyl alcohol (5-OH-G) (Marita et al., 2003; Mechin et al., 2000; Barrière et al., 2004; Palmer et al., 2008).

a) Cell wall composition of F2bm3 internode and response to water deficit

1. F2bm3 and the NIRS predictions

F2bm3 was cultivated in the field trails (Mauguio) from 2012 to 2014. 3 bm samples (2014 – Irrigated; 2012- Irrigated, 2012 Non-irrigated) were characterized by wet biochemistry for the cell wall components. When we predict them and look at the relationships between wet biochemistry and the predictions, we observed for many traits that F2bm3 values are included within the variation range of the other studied genotypes (exemple with the IVCWRD and the Klason lignin content, R^2 = 0.9 & R^2 = 0.6, respectively, Figure 28-A, B) without decreasing much the correlation values observed without F2bm3 (Figure 28-A, B). However it was surprising to observe that F2bm3 presented a higher amount of Klason lignin content evaluated by wet biochemistry than predicted.

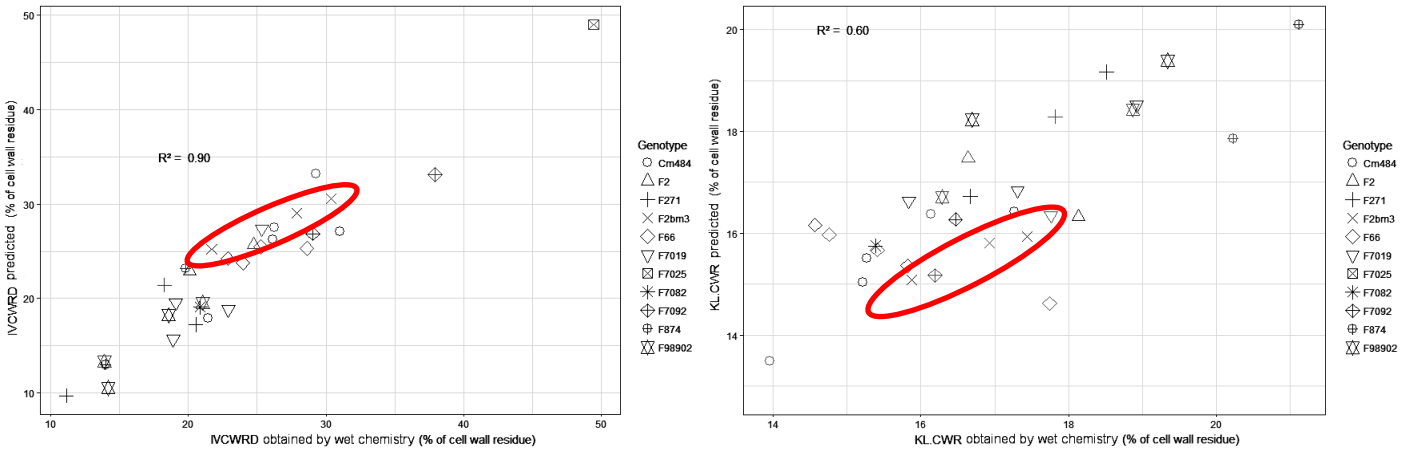


Figure 28. Relationships between two biochemical traits predicted and the wet biochemical values associated. A. Relationship between predicted and biochemical values of the *in vitro* the cell wall residue degradability (IVCWRD) R^2=0.9. B. Relationship between predicted and biochemical values Klason lignin content (KL.CWR) R^2=0.6. The red circles surround the F2bm3 individuals.

Apart for the lignin content, the predictions over-evaluated the real values of F2bm3 for the esterified *p*-coumaric acid content (Figure 29-A) and for the S/G lignin subunits ratio compared to the wet biochemistry (Figure 29-B).

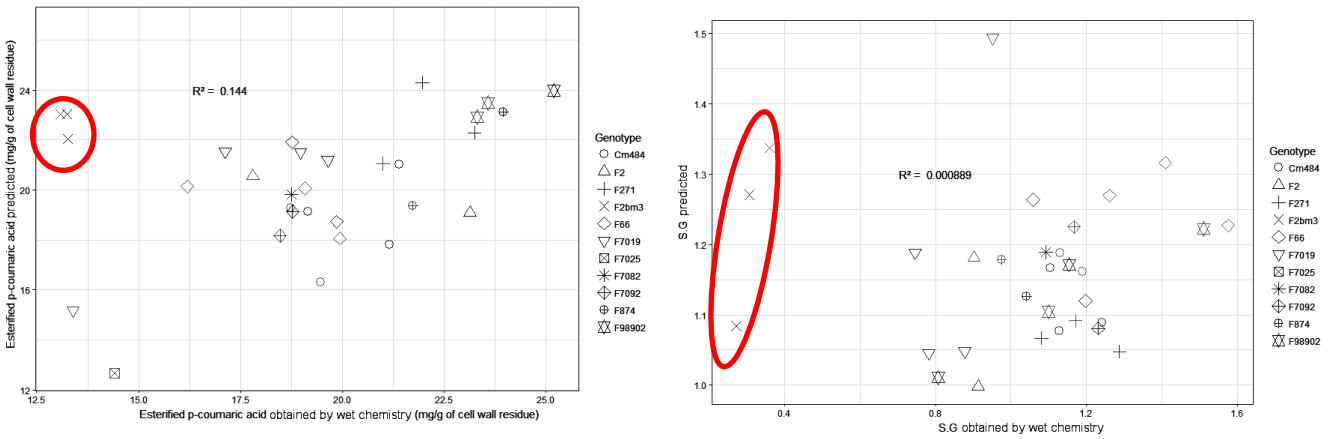


Figure 29. Relationships between two biochemical traits predicted and the wet biochemical values associated. A. Relationship between predicted and biochemical values of Esterified *p*-coumaric acid content in the cell wall. B. S/G lignin subunits ratio predicted values vs wet biochemical values. The red circles surround the F2bm3 individuals.

The main reason of the predictions errors is that these equations cover a range of value in which F2bm3 is not. The minimum of the range of the esterified p-coumaric acid content predictive equation is 14.55 mg/g CWR (Table 5) and the wet biochemistry values of F2bm3 are under 13.30 mg/g CWR (Table 6). It is the same for the S/G ratio which can only be predicted with a minimum of 1.29 (Table 5) while the F2bm3 values evaluated by wet biochemistry are under 0.4. So we can suppose that if the equations of the esterified p-coumaric acid content and S/G ratio had a larger range of predictions, they could be able to predict F2bm3 correctly for all the cell wall components.

2. Estimations of the F2bm3 cell wall components values

To be able to analyze F2bm3 cell wall component quantifications for this experiment of 3 years in Mauguio, we decided to consider the biochemical values estimated by wet biochemistry for a few individuals in the different irrigating conditions (Table 6).

Table 6. Cell wall biochemical components of F2bm3 quantified by wet biochemistry. In red, the values which are sensibly different than the predicted values.

Year	Treatment	IVCWRD	KL/CWR	PCAest	Faeth	BO4 yield	S/G	Cellulose	Hemicellulose
2014	I	21.70	15.88	13.25	3.80	766.50	0.27	40.42	27.58
2012	I	27.87	17.44	13.26	4.45	490.22	0.31	44.86	39.07
2012	NI	30.37	16.93	13.07	3.40	461.57	0.36	42.26	39.84

We calculated a coefficient for each scenario/year between the wet chemistry and the predicted value (for each trait : $\text{coef} = \frac{\text{Value Wet biochemistry}}{\text{Value predicted}}$) and we re-calculated the values

of F2bm3 by multiplicating this coefficient to the predicted values of the scenario/years corresponding. The coefficient applied on the predicted values of the 2013 irrigated scenario was the mean of the coefficient calculated for 2012 and 2014 irrigated scenarios. The coefficient applied on the NIRS values of the 2013 and 2014 non-irrigated scenarios was the one calculated for the 2012 non-irrigated scenario (Table 6).

F2bm3 was originally chosen along with all the other genotypes to enlarge and maximize the range of prediction of the biochemical cell wall components. But the amount of esterified *p*-coumaric acid content and S/G ratio is so low that they are hardly predictable even among all the diversity that the other genotypes represent.

3. Biochemical relationships and response to water deficit

The new estimations of the F2bm3 individuals values for the biochemistry of the cell wall lead to results more expected and more accurate with the literature (Table 7 and Figure 30). Especially for the *p*-coumaric acid content and the S/G ratio.

Table 7. Mean, minimum and maximum values for the biochemical cell wall component of F2 and F2bm3 with estimated values.

			IVCWRD	KL.CWR	BO4 yield	S/G	PCAest	FAeth	Cellulose	Hemicelluloses
F2	I	**mean**	**20,9**	**17,9**	**680**	**1,18**	**21,3**	**3,1**	**44,7**	**36,7**
		min	14,4	17,5	598	1,11	18,8	2,9	43,8	32,4
		max	27,6	18,5	744	1,38	25,2	3,4	46,3	43,5
	NI	**mean**	**28,6**	**16,6**	**674**	**1,23**	**20,2**	**2,6**	**42,5**	**36,7**
		min	25,7	16,0	603	1,14	19,5	2,4	40,6	35,9
		max	33,8	17,3	783	1,30	20,6	2,9	43,9	38,8
F2bm3	I	**mean**	**26,5**	**17,7**	**526**	**0,31**	**13,3**	**4,1**	**46,3**	**39,0**
		min	21,4	17,3	445	0,28	12,7	3,7	43,5	32,0
		max	30,3	18,0	638	0,32	13,7	4,5	50,3	44,7
	NI	**mean**	**32,6**	**18,1**	**388**	**0,38**	**13,1**	**3,4**	**45,9**	**46,8**
		min	27,1	16,8	320	0,36	12,5	3,2	42,2	39,2
		max	36,7	19,8	472	0,41	13,5	3,8	49,6	51,8

The relationship between IVCWRD and the Klason lignin content on the corrected values showed a greater value in IVCWRD under the non-irrigated condition (from 25.7 to 36.7 % of the CWR, table 7) than under the irrigated condition (21.4 to 30.3 % of the CWR, table 7). Surprisingly, F2bm3 plants show a relatively similar amount of Klason lignin content compared to its normal isogenic line F2 (Figure 30-A). Indeed under irrigated condition F2bm3 presents 17.3 to 18 % of CWR of Klason lignin content (Table 6) while F2 goes from 17.5 to 18.5 % of CWR and under non-irrigated condition F2bm3 has a lignin content going from 16.8 to 19.8 %

of CWR (Table 6) while F2 has from 16 to 17.3 % of CWR (Table 6). It is generally expected that the *bm3* lines presents a reduction of about 40 to 50% of the lignin content. Mechin et al., (2000) showed it in 4 genetic backgrounds and Barrière et al., (2004) showed it in 2. Oba and Allen (2000) and Marita et al., (2003) showed it also on the wild type A619. Several other studies also showed a reduction about 40 to 50 % of the lignin content in F2bm3 compared to its normal isogenic line F2 cultivated in Lusignan (France, 86) (Mechin, 2000 ; Mechin et al., 2005, Barrière et al., 2013). In 2012, Cabané et al., reported that the lignin deposition was impacted by abiotic stress such as drought. As in Mauguio the plants were cultivated in a place with a warmer climate, we could hypothetize that depending on the environment, the bm3 mutation is not impacting the lignin content in the same way. In 2011 Machinet et al., did a study not on the maize stem but on the roots of F2, F2bm3, F292 and F292bm3, and they found a similar or higher amount of Klason and Van Soest lignin content for the bm3 mutants in the F2 and F292 genetic backgrounds in roots. Which let suppose that in addition to the environment, depending also on the organ the bm3 mutation impacts the lignin content differently.

On the other hand, as expected, the S/G ratio was very low for the F2bm3 compared to all the other genotypes (between 0.2 and 0.4 for F2bm3 vs from 1.0 to 1.7 for all the other genotypes). But once again, the response to water deficit was practically null (Figure 30).

And finally, as expected by previous studies on the *bm3* *p*-hydroxycinnamic acid contents quantifications, the esterified *p*-coumaric acid content was almost twice lower for F2bm3 than for F2 and the other genotypes. As for the S/G ratio, the effect of the irrigation scenario was practically null.

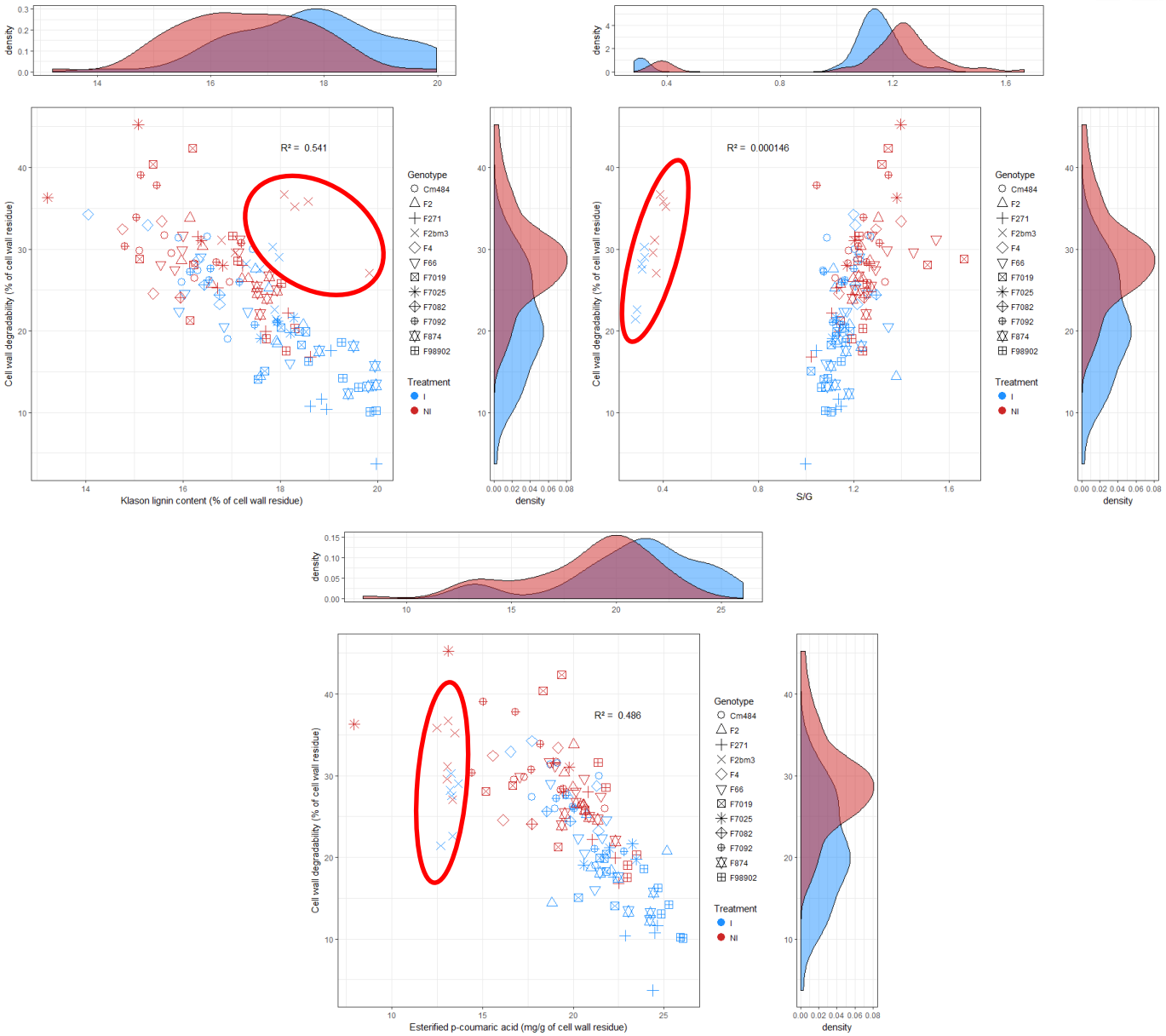


Figure 30. Relationships between the *in vitro* cell wall residue degradability and 3 other cell wall components for the 3 years 2012, 2013 and 2014 with recalculated values for F2bm3 : A. vs the Klason lignin content. B. vs the S lignin subunit on G lignin subunit ratio. C. vs the esterified *p*-coumaric acid content. For each trait its density is associated either at the top or at the right of each plot and according to each treatment: irrigated (I) in blue and non-irrigated (NI) in red. The red circles surround F2bm3 individuals.

Considering these results the irrigation scenario and the particularly warm environment of Mauguio would impact mainly the lignin content but not the other typical aspects of the *bm3* mutants which are the low amount of syringyl units and esterified *p*-coumaric acid content. As far as we know, no study reported brown-midrib plants cultivated under a water stress condition.

b) Histological profiles of F2bm3 and response to water deficit

So far, the *bm3* mutants have been histologically studied only by Mechin et al. in 2005. In this study, the *bm3* mutation was systematically leading to a FASGA profile with a parenchyma largely colored in blue compared to the normal isogenic lines, whatever the genetic background where bm3 mutation was introduced (F271, F7025, W117 and also F2). All the observations reported in Mechin et al. (2005) were carried out on internodes from plants cultivated in Lusignan (Figure 31).

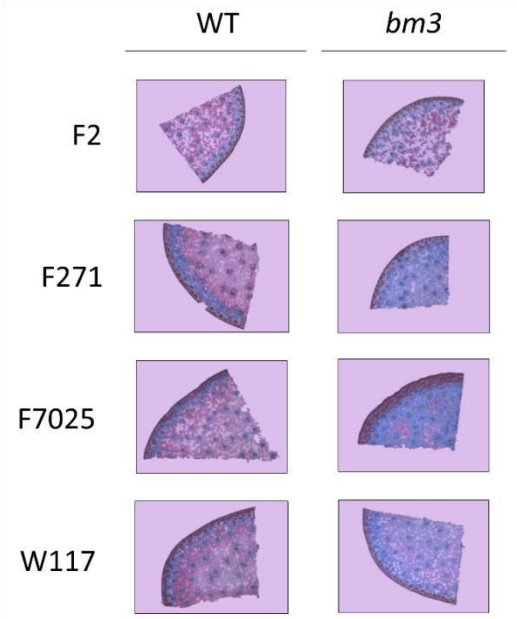


Figure 31. Histological profile of a FASGA stained cross-section of F2, F271, F7025 and W117 and their mutant counterparts cultivated in 2000 in Lusignan (France, 86)(adapted from Mechin, 2000).

As we observed, the *bm3* mutation had a greater histological effect, presenting a parenchyma much bluer compared to the normal isogenic lines. This suggests that cell wall of parenchyma cells is poorly lignified in F2bm3, W117bm3, F7026bm3 and F271bm3. We can hypothesized that, in Lusignan culture conditions, the *bm3* mutation seems to induce a parenchyma bluer than in the normal line F2, suggesting that the bm3 mutation impact the composition of the lignins but also its distribution. We may also note that the mutation impacted less the specificity of distribution of the lignins in the genotype F2 than in the 3 others genotypes.

We cultivated F2 and F2bm3 in Mauguio (2012, 2013, 2014 – in irrigated and non-irrigated condition) but also in Le Moulon (2012, 2014) and in Versailles (2017). As we can see, when it was cultivated in Lusignan F2 had a classical FASGA profile, a large red parenchyma surrounded by a band of blue parenchyma and then a rind mainly stained in red (Figure 32).



Figure 32. Histological profile of FASGA stained cross-section of F2 and F2bm3 between 2012 and 2014 in 3 different places and under different irrigation scenarios in Mauguio : irrigated (I) and non-irrigated (NI) and without any artificial water supply in Le Moulon and in Versailles.

We observed the same histological profile for F2 cultivated between 2012 and 2014 in Mauguio in 2 different irrigation scenarios. The rind seems to be bigger in irrigated condition than in the non-irrigated one. However the non-lignified parenchyma and the lignified parenchyma did not respond much to the irrigation scenario. It was also cultivated in 2012 and 2014 in Le Moulon and the histological profile stood about the same except a reduction of the stem area.

As for F2bm3, when cultivated in Lusignan showed a much greater amount of blue parenchyma within the red parenchyma (Figure 32). Surprisingly, when cultivated in Mauguio during 3 years or in Le Moulon or in Versailles, F2bm3 did not present a great blue FASGA stained parenchyma and was on the contrary showing a FASGA histological profile more classical, with a developed red parenchyma, and a band of blue parenchyma. (Figure 32).

Table 8. Mean, minimum and maximum of the histological traits quantified for F2 and F2bm3 cultivated in 2012, 2013 and 2014 under Irrigated (I) and Non-irrigated (NI) condition.

			Stem area	Lignified fraction	Non-lignified fraction	Rind fraction	Bundle fraction	Bundle number	Blue parenchyma	Red parenchyma	Red Rind
F2	I	**mean**	**1.58**	**0.63**	**0.19**	**0.13**	**0.05**	**125**	**15.90**	**103.48**	**5.02**
		min	1.33	0.60	0.13	0.10	0.04	102	10.50	98.11	4.53
		max	1.81	0.68	0.23	0.15	0.07	150	21.56	114.89	5.97
	NI	**mean**	**1.31**	**0.61**	**0.17**	**0.14**	**0.08**	**122**	**13.55**	**92.22**	**4.65**
		min	1.12	0.54	0.10	0.09	0.06	83	7.44	83.86	4.13
		max	1.46	0.62	0.25	0.19	0.10	162	20.08	100.72	5.30
F2bm3	I	**mean**	**1.31**	**0.69**	**0.11**	**0.13**	**0.07**	**123**	**8.31**	**101.80**	**4.76**
		min	1.04	0.63	0.08	0.11	0.06	105	6.39	89.93	4.43
		max	1.56	0.73	0.15	0.15	0.08	151	12.07	112.34	5.11
	NI	**mean**	**1.15**	**0.65**	**0.13**	**0.13**	**0.08**	**125**	**9.19**	**86.82**	**4.25**
		min	1.03	0.64	0.11	0.13	0.07	114	7.44	81.16	3.77
		max	1.31	0.67	0.15	0.14	0.09	135	10.61	91.65	4.82

More precisely, none of the histological parameters seemed to differ between F2 and F2bm3 except for the blue parenchyma and the non-lignified fraction which are much lower for F2bm3 in every conditions (Table 9). This is consistent with what we observed on the cross-sections (Figure 32). However, the blue parenchyma represents the less lignified parenchyma (with the fewer amount of components stained in red) and is often associated to a higher cell wall degradability (cf. F4 in part I). Here F2bm3 presented a lower blue parenchyma along with a higher cell wall degradability (Table 9). This suggests that in the case of F2bm3 the tissue type increasing degradability is different than for the other genotypes.

In order to investigate if F2bm3 is responding according to the model proposed in the part 1 of this chapter, we analyzed the relationships between the lignin content, the esterified *p*-coumaric acid content, the Red parenchyma and the Red rind according to the irrigation condition (Table 9). F2 suits well the model by responding to the water deficit with a Red_rind a bit more lignified and *p*-coumaroylated, but however with a red parenchyma presenting no apparent relations with the lignin content. In the case of F2bm3 these relationships between the Red rind, Red parenchyma and the lignin content and the *p*-coumaric acid content are completely changed and does not follow the model proposed (Table 9).

Table 9. Correlation of KL.CWR, PCAest, Red_parenchyma and Red_rind under irrigated condition (in blue) and under non irrigated condition (in pink) for F2 and F2bm3 overall the 3 years 2012, 2013 and 2014.

F2	KL.CWR	PCAest	Red parenchyma	Red Rind
KL.CWR		0.97	0.04	0.52
PCAest	0.66		0.20	0.40
Red_parenchyma	0.03	-0.31		-0.41
Red_Rind	0.65	0.54	-0.70	

F2bm3	KL.CWR	PCAest	Red parenchyma	Red Rind
KL.CWR		0.09	0.07	-0.10
PCAest	0.17		0.70	-0.46
Red_parenchyma	0.61	-0.39		-0.55
Red_Rind	0.23	-0.69	0.53	

On the other hand, as the lack of response of the lignin content in F2 and F2bm3 suggested, the environment is not influencing the lignification distribution within the stem (Table 8 and 9). Another hypothesis is the fact that the normal line F2 is not responding much to the irrigation scenario biochemically and histologically either. So a potential tolerance to the water deficit brought by the genetic background could also be a reason of the lack of response. Indeed, in Mechin et al., 2005, all the *bm3* mutants in other genetic backgrounds W117, F7025, F271 presented a FASGA blue stained parenchyma more largely developed than in F2. Moreover, others studies of *bm3* in different genetic background (Chabbert et al., 1993b; Marita et al., 2003) showed a stronger impact of the mutation, reducing significantly the lignin content. More recently in 2018, Barrière et al., showed that the *bm3* mutation inserted in the F4 genotype was not improving the cell wall degradability. To sum up, biochemically, histologically and in the case of the response of these traits to the water deficit, the genetic background in which the *bm3* mutation is inserted seems to play a very important role. In such a case, a good check of these hypotheses would be to cultivate in non-irrigated conditions the other *bm3* mutants cultivated in Lusignan in 2000: F271, F7025 and W117 to check if they show the same histological profile and furthermore if they present any responses to the water deficit.

Conclusion

In this chapter, we presented the establishment of 2 high-throughput tools with a good accuracy to phenotype biochemically and histologically hundreds of samples of maize internodes. Moreover, these tools are able to pinpoint the effect of contrasted irrigation scenario carried out. This allowed us to suggest a general trend of lignification modifications in response to water deficit at the histological and biochemical levels. Under well irrigated condition Red_parenchyma is more correlated to esterified *p*-coumaric acid and lignin contents in the cell wall than Red_rind. This is not the case under non-irrigated condition, were lignin and esterified *p*-coumaric acid contents were more related to Red_rind than to Red_parenchyma (Figure 33). This suggests that the plant would preferentially deposit more *p*-coumaroylated lignins in the rind region of the internode in response to a water deficit.

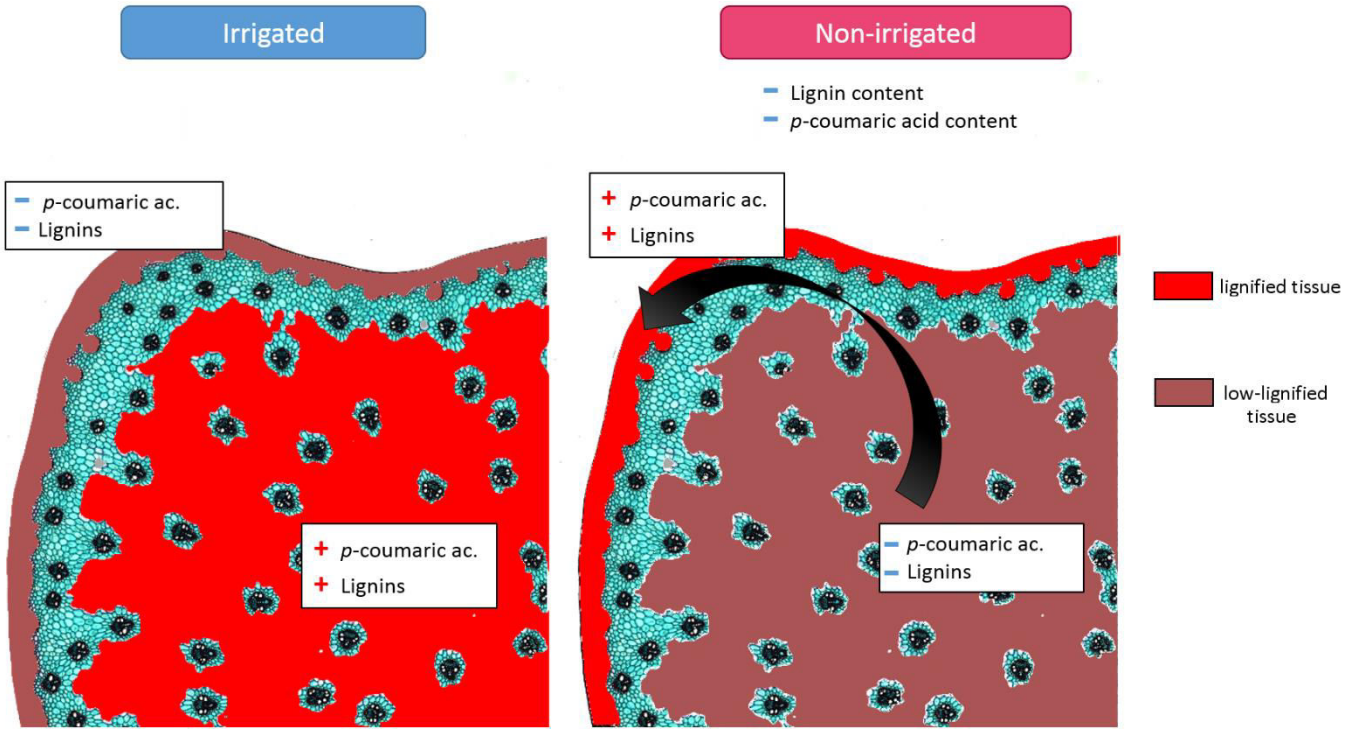


Figure 33. Model of biochemical and histological responses of the maize internode depending on the water status.

Finally we show that F2bm3 is a mutant which needs to be analysed separately from the other genotypes but only for the biochemical traits which are particularly different in this line (S/G ratio and esterified *p*-coumaric acid content). Its histological profiles depending on the places where it was cultivated rises several questions about the influences of the environment and in which genetic background is inserted the *bm3* mutation.

All these developed tools proved their worth on these studies and pave the way for further analyses requiring a large amount of samples such as the phenotyping of recombinant inbred lines.



Chapter 2

Chapter 2: Genetic determinism of histological and biochemical traits according to the water status

This chapter will be divided into two main parts; the first one, written as close as possible to be submitted will present the results of the QTL detection for the biochemical cell wall traits and histological cell wall traits within the maize internode and the second part will be the article of Virlouvet et al., where I am co-author and where we present the results of the QTL detection for the biochemical cell wall traits within the whole plant of the same RILs population.

Introduction

Plant biomass represents 90 % of the total biomass on earth (Bar-on et al., 2018). It is therefore a formidable resource. Whether providing fodder to ruminants or a biological substrate to bioethanol production, it is plant biomass which is valorised. In regard to maize, the plant biomass may be valorised either into silage, produced to feed ruminants (Barrière et al. 2004a), or into a fermentable substrate for the conversion into bioethanol (Bhalla et al., 2013). In both cases, the goal is to convert structural sugars from the cell wall into energy and their accessibility remains the main issue. One way to evaluate this conversion is to quantify *in vitro* cell wall degradability using enzymatic cocktails (Aufrere, 1982). Many studies have been carried out on maize to better understand the relationship between lignification and cell wall degradability (Mechin et al., 2000; Grabber et al., 2004; Barrière et al., 2009; Somerville et al., 2010; Barros-Rios et al., 2012; Loqué et al., 2015; Hatfield et al; 2017).

Cell wall degradability is strongly influenced by cell wall structure and composition. In grasses *p*-hydroxycinnamic acids, mainly ferulic (FA) and *p*-coumaric (pCA) acids, are able to create cross-links between cell wall polymers. pCA is ester-linked with S-lignins units (Ralph et al., 1994; Grabber et al., 1996; Lu and Ralph, 1999) and FA appears to be associated with hemicelluloses through ester linkages and with lignins through ether linkages (Hatfield et al., 2017). Cell wall degradability was shown to be strongly influenced by phenolic compounds (Méchin et al., 2000; Hartley et al., 1972; Grabber et al., 1998; Casler and Jung, 1999; Jung and Casler, 2006; Zhang et al., 2011, El Hage et al., 2018). Over the last two decades, quantitative trait locus (QTL) analyses have been performed to determine the genetic factors involved in the variation of cell wall degradability and composition in maize using mainly biparental populations (Lübberstedt et al., 1997a,b; Bohn et al., 2000; Barrière et al., 2001, 2008, 2012; Méchin et al., 2001; Papst et al., 2001; Roussel et al., 2002; Cardinal et al., 2003, 2005; Fontaine et al., 2003; Krakowsky et al., 2005, 2006; Riboulet et al., 2008; Wei et al., 2009; Lorenzana et al., 2010, Torres et al., 2015, Leng et al., 2018). Over 400 QTLs related to cell wall

degradability and composition have been mapped all over the maize genome (Barrière et al., 2008). In 2010, Truntzler et al., presented a meta-analysis of QTLs and they identified 26 meta-QTLs for cell wall degradability and 42 meta-QTLs for cell wall composition, suggesting that the genetic determinisms of these traits are distinct and complex and related to many regions of the genome. Moreover, they identified only few major QTLs (which explained more than 20% of the observed variation) for cell wall-related traits (Roussel et al. 2002, Courtial et al. 2013), reinforcing the fact that cell wall composition and degradability are under a complex genetic determinism.

Overall, lignin content is the main recalcitrant factor of cell wall degradability. Several studies also showed the role of monomeric lignin composition but the results are still controversial. The lignin polymeric structure estimated by the amount of βO4 linkage is another feature whose role on degradability remains controversial. Zhang et al. (2011) showed, on maize lines with a similar lignin content, that the amount of βO4 linkage was actually significantly and negatively correlated to cell wall degradability. In Zhang et al., (2011), the pCA content was also strongly negatively correlated to cell wall degradability. Some stand controversial but in any case, all these traits, along with the lignin content, do not pretend to explain the total observed variation of cell wall degradability. Moreover even if lignin content can explain a large part of this variation it is not conceivable to reduce it severely without impacting plant's integrity and agronomical performances. Consequently it is necessary to find other targets combinations to enhance cell wall degradability.

The last years, considerable progress has been made in understanding the development of the tissue and its lignification. Several studies pinpoint the links between the tissue-specific lignification and the cell wall composition and degradability. It has been shown in maize that cell wall degradability was different between the sclerenchyma regions of the rind and the parenchyma of the pith (Lopez et al., 1993) then that lignins deposited in sclerenchyma of maize internodes were composed differently than in the parenchyma of the pith (Chabbert et al., 1997). More recently, several studies on maize internodes highlighted the link between the distribution of the ignification and cell wall degradability (Jung and Casler, 2006; Boon et al., 2008, 2012; El Hage et al., 2018), in sugarcane internodes (Dos Santos et al., 2015) and in sorghum internodes (Perrier et al., 2017). Using the strategy of QTL mapping, a number of QTLs for vascular bundle system have been mapped in plants of agronomical interest such as in tomato (Coaker et al., 2002), wheat (Sang et al., 2010) and rice (Sasahara et al., 1999; Zhang et al., 2002; Cui et al., 2003; Bai et al., 2012). In contrast, the genetic determinism of such histological traits in maize were much less investigated. To our knowledge, only one study in 2015 from Huang et al., report the identifications of QTLs involved in the number of vascular bundles within a population of maize-teosinte back-cross

recombinant inbred lines. The main reason of the low amount of studies for the genetic determinism of these traits is the long and tedious phenotyping work it represents. As an example, Huang et al., (2015) did quantify by hand the number of vascular bundles for 3 plants multiplied by 866 recombinant inbred lines. However, more and more automated tools are developed to quantify such traits. Heckwolf et al., showed in 2015 an image analysis tool to quantify the parenchyma area within the pith and the number of bundles. More recently, in Legland et al., (2017), we proposed a high-throughput image analysis tool for histological traits on FASGA stained cross-sections of maize (cf. chapter 1 of this PhD manuscript). These tools pave the way to the possibility of quantifying a high number of samples and then investigating the genetic determinism of histological traits.

Cell wall also plays important roles in plant responses to various abiotic stresses, such as drought, flooding, heat or cold, and is essential in stress sensing and signal transduction. As the effects of the global warming are more and more visible, some study warn about the arrival and the increase of drought periods frequency, even in the less pessimistic scenarios (Samaniego et al., 2018). Along with the actual agro-environmental policies which encourage to decrease inputs in the field and especially the water supply, filed irrigation will be constrained. It is then a real issue to understand how plants respond to these non-optimal growing conditions. Consequently, the modified and sometimes drastic growth conditions may have a potential effect on biomass production and quality (this was reviewed in Reynolds and Langridge, 2016; Tardieu et al., 2018). Water deficit also impacts underlying physiological processes including cell division, hydraulics, cell wall mechanics and primary and secondary metabolism. As a consequence, crop plants under water deficit often contain excess carbon, and roots and reproductive organs show signs of experiencing sink limitation. Furthermore, the dysregulation of the silk-anthesis interval, ie the time interval between male and female flowering, is often reported to be impacted under water deficit, leading to grain abortion and massive yield loss (Denmead and Shaw, 1960; Elmore, 2012, Reynolds and Lanridge, 2016). The genetic determinism of drought tolerance in maize grain yield has been largely studied and reported (Ribault et al. 2007; 2010; Collins et al. 2008). Several studies also showed a large variability in the drought responses and sensitivity to soil water deficit of leaf elongation rate in maize (Reymond et al., 2003, 2004; Welcker et al., 2007; Chenu et al., 2009). However, no QTL for cell wall degradability or composition or any histological traits under water deficit conditions has been reported yet, although several reports recently showed that although several reports recently showed that water deficit impacts cell wall degradability, composition and spatial lignification in maize (El Hage et al., 2018) in sorghum (Perrier et al., 2017) and in sugarcane (Dos Santos et al., 2015) but also in miscanthus for the cell wall composition

(Emerson et al; 2014, Van der Weijde et al. 2017) and in poplar for the tissue specific lignification (Wildhagen et al., 2018).

In the present study, for the first time, the genetic determinism for histological traits under different irrigation conditions was investigated in maize internode along with biochemical cell wall traits. To do so, QTL mapping was performed using a maize recombinant inbred lines (RILs) population derived from the cross of two parental inbred lines, F271 and Cm484, cultivated in field trials over two consecutive years under both irrigated and non-irrigated scenarios. Using 2 high-throughput tools developed for the histological phenotyping (Legland et al., 2017) and the cell wall biochemical traits characterization with dedicated NIRS predictive equations, the objectives of this study were: (1) to decipher the genetic determinism of these traits under irrigated and non-irrigated conditions and (2) to better understand the genetic links between cell wall degradability, histological traits and cell wall biochemical traits by analysing the potential co-localisations in genome regions implied in the variations of both histological and biochemical cell wall traits. Our results present here the first QTLs for a large number of histological traits in maize internode which co-localize or not with QTLs involved in the variations of cell wall biochemical traits and this, in different irrigation conditions. It highlights the complex links between spatial lignification, cell wall composition and degradability and present new regions of interest for breeding in maize.

Material and Methods.

Plant materials and field experiments

A RIL population consisting of 267 lines was developed at INRA by single seed descent (SSD) up until 6 generations in a cross between maize inbred lines F271 (Canadian dent; Roussel et al., 2002, Barrière et al., 2001) and Cm484 (Canada-Morden – 1989; Méchin et al., 2000; Barrière et al., 2007). All the RILs were sown in a randomized augmented bloc design with one replicate of both parents in each bloc at Mauguio (34, France) over two years (2014, 2015). Plants were cultivated in open field under an irrigated (I) scenario, the water being supplied with a mobile ramp of sprinklers, and a non-Irrigated (NI) scenario, which consisted of a dry-down period that began when controlled line F2 plants had, on average, 5 ligulated leaves and finished 14 days after flowering of all the lines. Each line was grown in a single 4.20 m row with 0.80 m between rows and a planting density of 80,000 plants/ha. At the silage stage, per RIL, the internode carrying the main ear of the plants was harvested in two groups: 2 internodes were harvested and stored in 70% ethanol for further histological analyses; and 10 internodes were harvested for the biochemical analyses and NIRS predictions and then were dried in an oven at 55 °C for 72 hours and ground with a hammer mill (1 mm grid).

NIRS predictive equations construction and NIRS predictions

Biochemical quantifications performed on the calibration samples set were the following (Table 10): Cell wall content (CWR), obtained with a water/ethanol extraction (Soxhlet). Lignin content in the cell wall (KL.CWR) was estimated using the Klason method (Dence et al., 1992), the composition and structure of lignins were obtained by thioacydolysis (Lapierre et al., 1986). Esterified and etherified p-hydroxycinnamic acids contents (PCAest, FAest and FAeth) were obtained by alkaline hydrolysis (Morrison et al., 1993; Culhaoglu et al., 2011). Cellulose and Hemicelluloses contents were quantified by acidic hydrolysis (Updegraff et al., 1969; Harholt et al., 2006). Acid pre-treatment of the dry matter followed by a cellulolysis (Onozuka cellulase) brought the *in vitro* dry matter degradability or IVDMD (Ronsin et al., 1990) and the *in vitro* cell wall residue degradability was measured directly by performing an acid pre-treatment followed by a cellulolysis on the cell wall content (CWR).

Dry samples were scanned through a near-infrared reflectance spectrometer (Antaris II, thermos Fischer scientific). For this study, the establishment of the NIRS predictive equations for the internode presented in El Hage et al., 2018 was enriched with the results from wet biochemistry analyses of 56 samples from the RIL population harvested in Mauguio 2014 and 2015. The biochemical traits were then estimated using the updated NIRS predictive equations for 683 harvested internodes samples.

Table 10. Characteristics of NIRS calibrations developed for cell wall traits in maize internodes, at silage stage harvest updated with 56 samples from the RIL population cultivated in 2014 and 2015. Cell wall biochemical related traits quantified, associated reference methods and NIRS prediction equation characteristics.

Trait	Designation	Reference Method	Units	Min	Max	N[a]	R[b]	SEC[c]
Cell wall residue	CWR	Soxhlet Extraction	% DM	32.87	77.32	95	0.972	2.16
Lignin content	KL.CWR	Klason	% CWR	11.59	21.11	129	0.799	0.93
βO4 yield	βO4_yield	Thioacidolysis	µmol/g KL	497.76	1155.4	129	0.6465	98.11
H lignin subunit yield	βO4_H			4.66	58.1	129	0.814	5.83
S lignin subunit yield	βO4_S			261.7	614.1	129	0.384	65.28
G lignin subunit yield	βO4 _G			203.05	580.12	129	0.694	60.12
Etherified ferulic acids	FAeth	Alkaline hydrolysis	mg/g CWR	1.92	7.61	112	0.4995	1.16
Esterified ferulic acids	FAest			2.15	8.14	113	0.804	0.69
Esterified p-coumaric acids	PCAest			13.39	30.02	112	0.84	1.6
Glucose content	Cellulose	Acidic hydrolysis	% CWR	31.5	49.89	99	0.878	2.08
Hemicelluloses content	Hemicelluloses			20.11	31.16	99	0.915	1.85
In vitro dry mater degradability	IVDMD	Acid pretreatment + cellulolyse	% DM	34.5	81.32	99	0.987	1.69
In vitro cell wall degradability	IVCWRD		% CWR	21.94	50.65	98	0.934	2.24

[a]: number of samples used to calibrate NIRS predictive equations. [b]: correlation coefficient between biochemical values and predicted values. [c]: standard error of calibration calculated on the prediction of the calibration samples.

Histological analyses

Two cross-sections of 150 µm thickness were cut from two internodes of each line in each block, each condition and each year. A total of 1367 cross-sections were obtained using a sledge-microtome GSL1 (Gärtner et al., 2015) and stored in 70 % ethanol. They were then stained with FASGA solution (derived from Tolivia and Tolivia, 1987). The FASGA solution, the staining protocol and the image analysis were performed according to Legland et al., (2017) and the protocols presented in the Material and methods of the Chapter 1.

Statistical analyses of the cell wall dataset

All statistical analyses were performed using R software (R CRAN Project, 2014). To eliminate the field effects, single-plot values were corrected by a subtraction of the best linear unbiased prediction (BLUP) value of the bloc effect for each line, using the following mixed linear model (1):

$$Y_{ijkl} = \mu + g_i \, x(1-t_i) + C_i \, x \, t_i + y_j + e_k + B_{jkl} + g_i \, x \, y_j + g_i \, x \, e_k + y_j \, x \, e_k + E_{ijkl} \quad (1)$$

where Y_{ijkl} is the phenotypic value of the "*i*"th inbred line in the "*j*"th year, in the "*k*"th irrigation scenario and located in the "*l*"th bloc in field. In this model, µ is the intercept. Effect of line i is considered as fixed and note C_i if it was one of the two parental lines used as checks and as random and noted g_i if i was one of the RIL. The parameter t_i was set to one for checks and zero otherwise. The B_{jkl} bloc was considered as random effects, as well as the interaction between the g_i genetic and the y_j year or the e_k irrigation scenario effects. The interaction between the e_k irrigation scenario and the y_j year effects was considered as fixed effect. By using the parental replicates in each bloc, the parameter t_i was used to distinguish the RILs lines from the F271 and CM484 lines.

On the corrected data set, another analysis of variance (ANOVA) was performed with the following linear model for each trait:

$$Yij = \mu + A_i + T_j + A_i \, x \, T_j + R_{ij}$$

where Y_{ij} is the value of the year I under the condition j; µ = overall mean; A_i = the main effect of the year I; T_j = the main effect of the condition j; i; A_i x T_j = the interaction effect between the year i and the condition j and R_{ij} = the random residual term.

"Two-samples" T-tests were performed for each year to evaluate the significance of the differences between the two irrigation conditions. Pearson correlations have been estimated on the corrected data set.

Genotyping and genetic map construction

Leaf tissues were collected from all 261 RILs and parental inbred lines F271 and Cm484 and freeze-dried at -70°C. Genomic DNA was extracted using a procedure derived from Tai and Tanksley (1990), Dellaporta et al. (1983) and Michaels et al. (1993). The genomic DNA was used for genotyping with the genotyping by sequencing (GBS) approach (Elshire et al., 2011). Briefly, the genomic DNA was digested with the restriction enzyme ApeK1 and used to construct GBS libraries in 96-plex. The GBS libraries were sequenced on Illumina HiSeq2000 and SNP calling were performed using TASSEL GBS pipeline with B73 as the reference genome (Glaubitz et al., 2014).

Initially, 955,720 markers were identified well distributed on maize chromosomes 1 to 10. 2,806 markers were selected because of being polymorphic between parental lines and with a proportion of missing data lower than 15% among the RILs. These markers were then used to construct the linkage map using R scripts interacting with the CarthaGene software (De Givry et al., 2004, bioinformatics 21:1703), as described in Ganal et al. (2011). Specifically, a scaffold map of 1,775 cM containing 20 to 39 markers per chromosome was first built with very stringent criteria for order robustness (minimum spacing of 5cM between adjacent markers), and then densified with additional markers to produce a framework map containing 62 to 161 markers per chromosome while keeping a LOD threshold for order robustness greater or equal to 3.0. Finally, 1,000 markers were retained following this procedure. The total length of that framework map was 2,355 cM with an average of spacing around 2.4 cM. By looking posteriori at singletons in the data, we checked that the increase of genetic map length when saturating the scaffold with additional markers was not attributable to genotyping errors, but probably to the rather high level of missing data which introduces a bias in the imputation procedure (EM algorithm) of CarthaGene because of genetic interference. This bias in map length is not expected to significantly affect QTL detection.

QTL detection

QTL detection was performed using the multi-QTL mapping (mqm) method in the R/qtl package (Broman et al., 2003; Arends et al., 2010). The function mqmscan was used, setting the maximum cofactor marker number (number of individual minus 12, depending on the year and the condition), with a further processing by backward elimination. To quantify the explained variance, QTLs above a LOD score at 3 (corresponding to approximatively the 5 % significance threshold using 1000 permutations) were selected and then fitted into a multiple QTL model using the function fitQTL based on the Haley–Knott regression method. The QTL detection by the MQM method was performed on the data corrected for the bloc effect *per* year and *per* irrigation scenario data.

I. Results

a) 2 years of field experiments declined in 4 irrigation conditions due to different environmental context

All the recombinant inbred lines along with the parental lines were cultivated during two successive years in 2014 and 2015 in the same location in the South of France. The non-irrigated condition was conducted as presented in the bottom of Figure 34, with, for the non-irrigated condition, a stop of the watering at the appearing of the 5th ligulated leaf and a restart of the watering 14 days after flowering. When considering the rainfall during this period, in 2015 particularly, a storm occurred on the 10th of June, providing up to 80 mm of water to both irrigated and non-irrigated conditions during the elongation of the internode carrying the main ear (Figure 34).

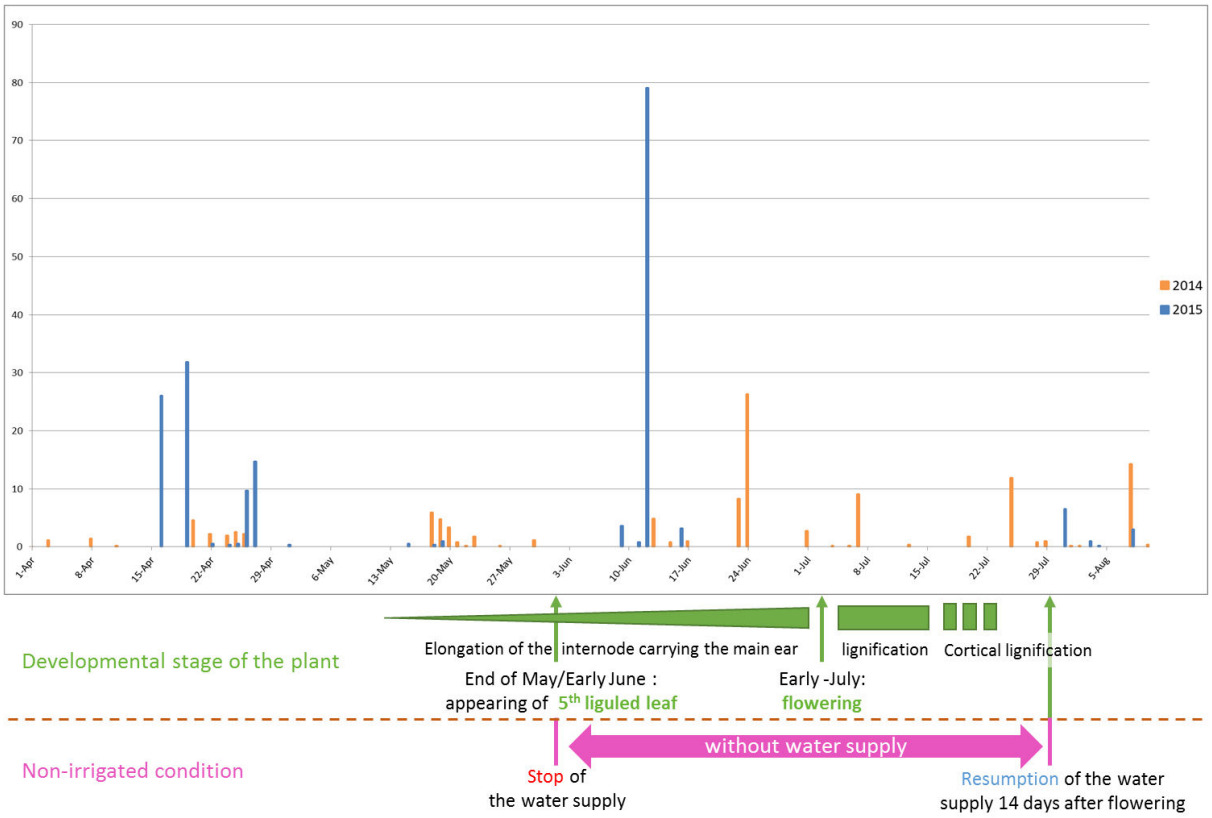


Figure 34. Rainfall (in mm) in fields and watering protocol of the non-irrigated condition for 2014 and 2015 between April and August.

Thus all the plants under the non-irrigated condition in 2015 did beneficiated from a great water supply right at the beginning of the water stress set up. Consequently the non-irrigated conditions from 2014 and 2015 could not be considered as the same conditions. The stress applied was definitely not the same and this was confirmed with the results of capacitive sensors in fields on a trial conducted in 2018 at the same location (Figure 35). Capacitive sensors give the water pressure in the soil (here at 60 cm deep) meaning that the higher is the

pressure, the less available is the water and therefore the less the plant will be able to access to it. In this 2018 trial, the plants were separated in 4 conditions, one irrigated condition, one non-irrigated conditions, one irrigated conditions with 2 flooding events simulated by an addition of 75 mm of water in two times and one non-irrigated condition with 2 flooding events. These flooding events mimic potentially well the storm which occurred in 2015. The capacitive sensors showed that the non-irrigated condition with 2 flooding events, figured with the red curve (Figure 35) present a pressure profile close to the pressure profile of the irrigated condition (black curve), which suggests that the water for the plants under this condition is as available as when plants are under the irrigated condition are as good as the for the plant when irrigated, even 1 month after the flooding. The rainfall at the 10th of June 2015 was approximately as high as the water supply by the flooding of these conditions which suggests that the recombinant inbred lines in 2015 under non-irrigated condition did not sensed the water stress as the ones under the non-irrigated condition in 2014.

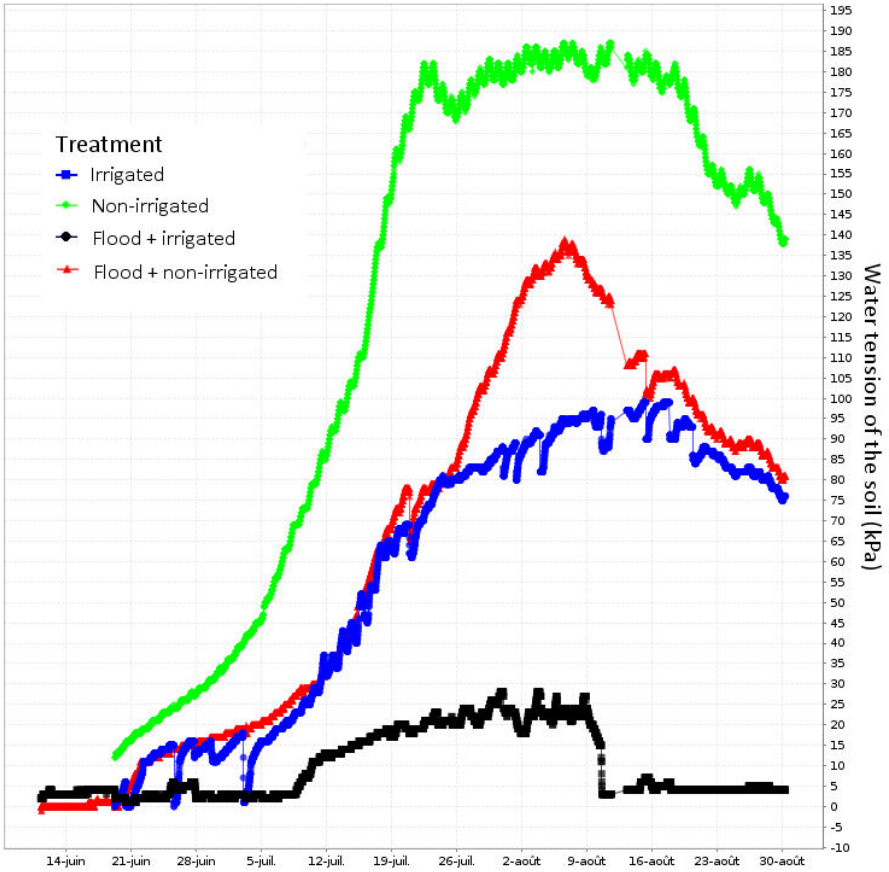


Figure 35. Water tension of the soil (in kPa) for 4 trials in field conducted June and August 2018. Capacitive sensors were set 60 cm deep. In black was the irrigated condition, in green the non-irrigated condition, in blue the irrigated-condition with 2 flood events (75 mm in total) and in red the non-irrigated condition with 2 flooding events (75 mm in total).

As expected by these environmental conditions, the agronomical traits were impacted accordingly. When considering the yield of the whole plant without ears for both years and both irrigation conditions, the difference between the 2 non-irrigated conditions is noticeable (Figure 36). All the recombinant inbred lines (RILs) cultivated under non-irrigated condition in 2014 (red rounds) are more impacted for the yield compared to irrigated conditions than the ones cultivated under non-irrigated condition in 2015 (dark red diamonds). Furthermore, yield of the RILs under non-irrigated condition in 2014 was 40 % lower than the yield under the non-irrigated condition in 2015 (Table S1).

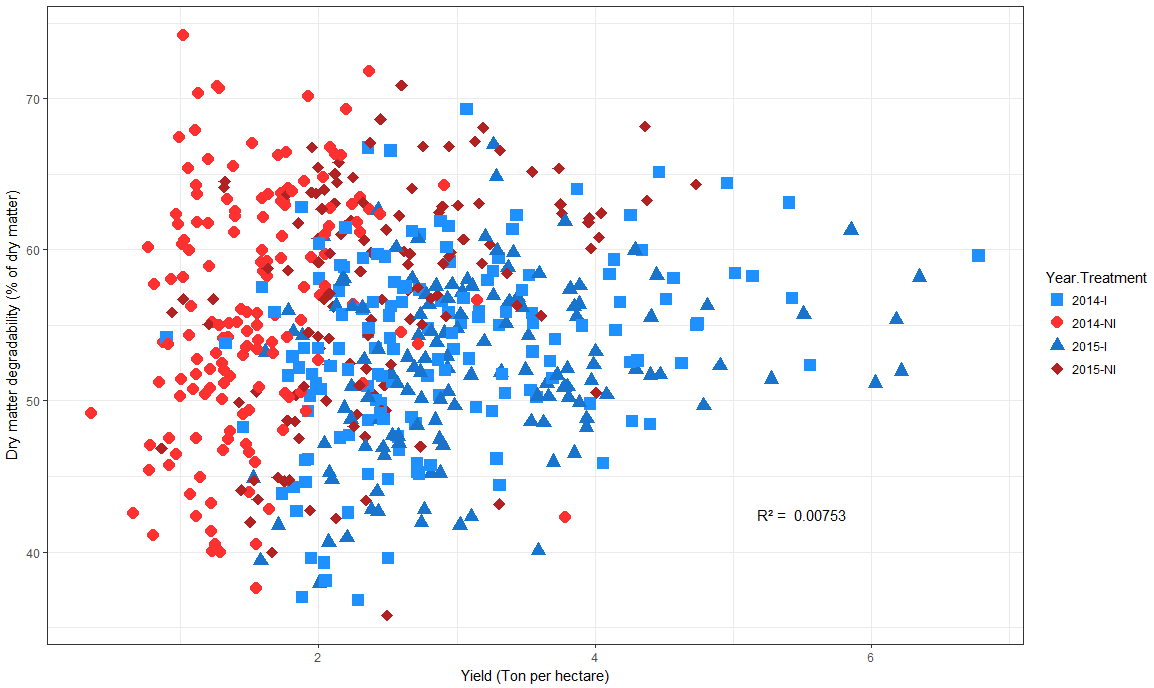


Figure 36. Relationship between dry matter degradability and yield for 2014 and 2015 under irrigated and non-irrigated condition.

Another result which may help to understand the differences between the 2 years is the relationship for one trait between the year 2014 and 2015. More particularly, for the lignin content, which is a trait that we know to be impacted by the watering condition, it was noteworthy that in 2015 the global range of variations of the lignin content was reduced of 2 % of CWR compared to the year 2014 (from 12.86 % of CWR under 2015-NI to 18.54 % of CWR under 2015-I; from 12.03 under 2014-NI to 19.55% under 2014-I; Table S1, Figure 37)

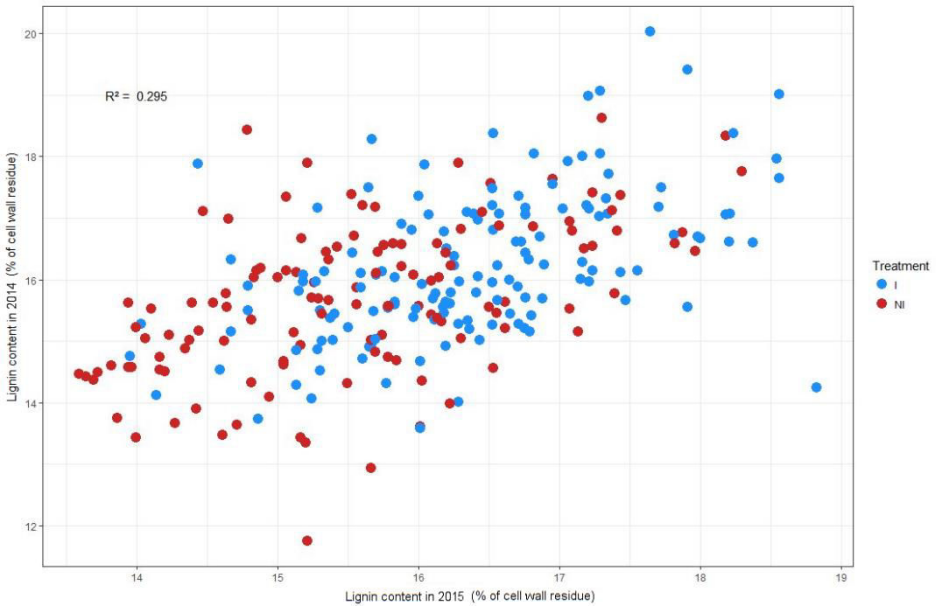


Figure 37. Relationship between the lignin content in 2014 and the lignin content in 2015 in the RILs population. Coefficient of determination $R^2 = 0.295$.

The effects of the year, the condition and more particularly the interaction between the year and the condition which represents the fact that the condition may have been different one year from another, were evaluated in an analysis of variance (Figure 38). As expected, the interaction between the year and the treatment was very significant for a large majority of the quantified traits (the red color was applied for p-values under 0.001). These results illustrate partly how the interactions with the environment for the same inbred lines may occur.

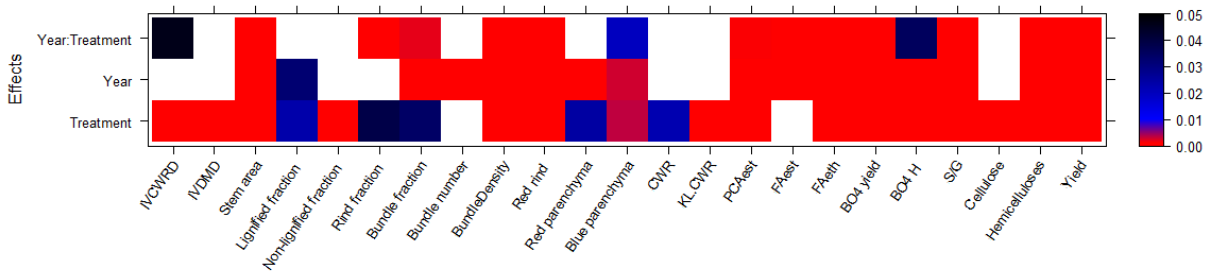


Figure 38. ANOVA for all the biochemical and histological traits of the RILs. The linear model was: $y = \mu + Year + Treatment + Year \times Treatment + e$. Where de the Treatment was the irrigation condition. P-value under 0.001 is in red, above 0.01 in blue and then dark until 0.05. In white, p-value are above 0.05.

As a consequence of all these results, the following study will consider the 2 non-irrigated conditions of 2014 and 2015 differently with the one in 2015 considered as a less strong water deficit than in 2014, because more water was available in depth in 2015 but there was still less humidity and high temperature for the vegetative parts of the plants, and the results will be presented for the four following conditions: 2014-irrigated (2014-I); 2014-non-irrigated (2014-NI); 2015-irrigated (2015-I); 2015-non-irrigated (2015-NI) separately.

b) Phenotypic variations

1. The parental inbred lines and their characteristics under different irrigation conditions

Concerning the cell wall biochemical traits, the 2 inbred lines F271 and Cm484 were previously characterized in Lusignan between 1997 and 2008 (Mechin et al., 2000; Barrière et al., 2009; Zhang et al., 2011). They were then selected for having different cell wall degradabilities. As presented in the Figure 39, this was confirmed by EL Hage et al., 2018 when cultivated during 3 years under different irrigation scenarios (chapter 1). F271 is less degradable than Cm484. Plants of F271 were taller than Cm484 and stover yield of F271 was higher than the one of Cm484. In addition, cell wall lignin content of F271 was more important in F271 (Figure 39). The *p*-hydroxycinnamic acid contents were also higher in F271 for the esterified *p*-coumaric and etherified ferulic acid contents, and the structure of the lignins in F271 presented a higher yield of BO4 linkages than in Cm484 (El Hage et al., 2018). The same tendencies were observed when both these parental lines were cultivated in 2014 and 2015 as check. F271 presented higher values for all these cell wall components associated with a decreased cell wall degradability compared to Cm484 (Table S1). It was therefore expected to observe variations for these traits in the RIL population derived from a cross between these two inbred parental lines.

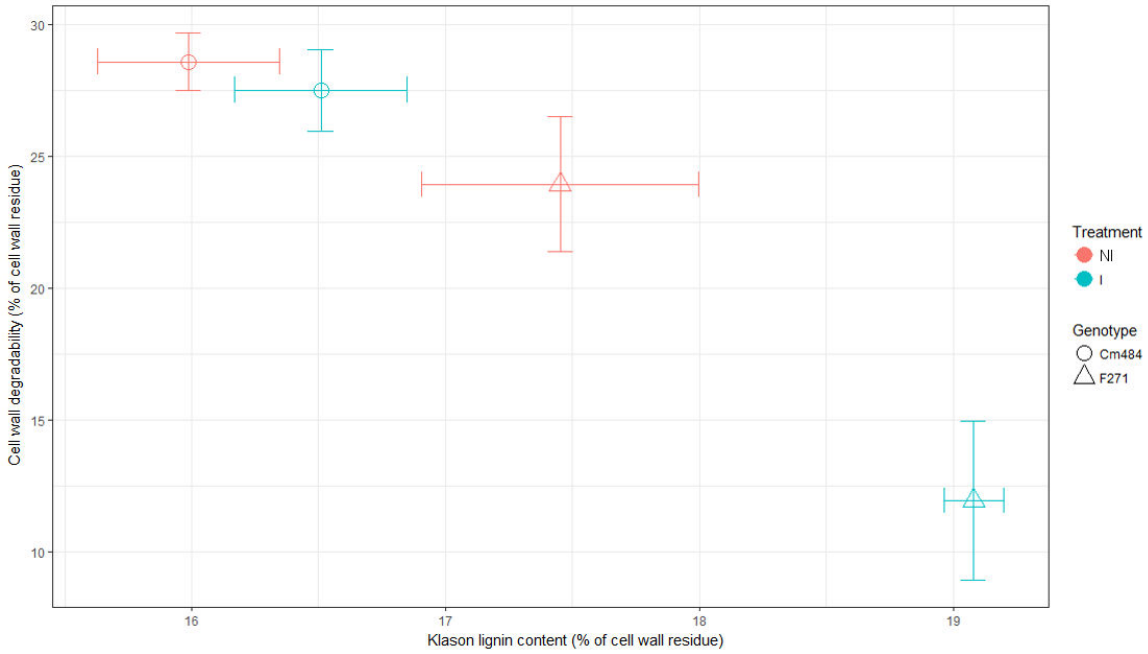


Figure 39. Relationship between cell wall degradability and Klason lignin content for parental lines of the RIL population characterized in EL Hage et al., (2018). Plants have been cultivated during 3 years under two irrigated conditions. In cyan and in pink are values obtained under irrigated and non-irrigated conditions, respectively.

Concerning the histological traits, from the first characterization of these inbred lines in Lusignan (Mechin, 2000; Mechin et al., 2005, Barrière et al., 2009), Cm484 was reported to have a FASGA stained profile with a large amount of blue-stained parenchyma in the pith while F271 presented a much more magenta-FASGA-stained parenchyma. They were therefore presenting 2 contrasted histological profiles. Once cultivated in an environment much sunnier and dry during the growing season (between May and August) they presented histological profiles less contrasted (Figure 40). Indeed, Cm484 presented a histological profile with a greater amount of lignified parenchyma in the pith than expected (Figure 40).

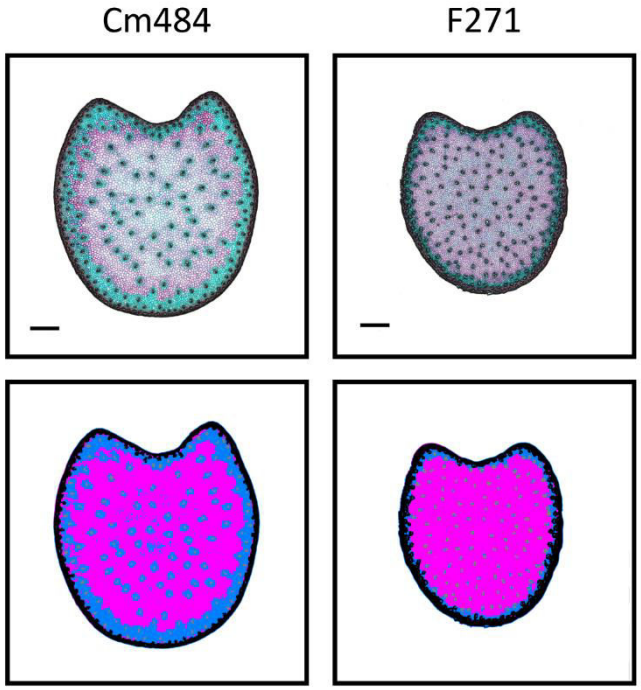


Figure 40. Histological profiles of Cm484 and F271 cultivated under irrigated condition in 2014 and their segmented analysed FASGA profile under. Bar = 2mm

Nevertheless, in 2014 and 2015 Cm484 showed in average a greater non-lignified parenchyma 18 and 19 % respectively under irrigated condition than F271 with 10 and 7% of the total stem area respectively (Table S1-2, 3). While producing more biomass than Cm484, area of the stem of F271 was smaller than Cm484 (1.42 cm² and 1.73 cm² for F271 *versus* 1.79 cm² and 1.79 cm² for Cm484 in 2014 and 2015, respectively Table S1-2, 3). This was associated to a much greater bundle density from F271 with 81.54 bundles/cm² in 2014 and 74.06 bundles/cm² in 2015 vs 64.03 bundles/cm² in 2014 and 68.70 bundles/cm² in 2015 for Cm484 under irrigated condition. This is particularly visible on their histological profile (Figure 40). Despite the surprising histological profile of Cm484, variations within the RIL population were still expected.

The impact of the irrigation scenario was different whether we consider the biochemical cell wall composition or the histological traits. Overall, this impact was more significant on the biochemical cell wall composition than on the histological traits for both inbred lines and for both years.

The non-irrigated condition induced a significant increase of 2.5 % of cell wall residue degradability of Cm484 in 2014 and 3.8 % of CWR in 2015 associated to a decrease of 0.27 % of CWR in the lignin content (KL.CWR) in 2014 and 0.64 % of CWR in 2015. Whereas in F271 cell wall degradability increased not significantly in 2014 and very significantly in 2015, despite a non-irrigated condition less strong (1.8 % of CWR and 7 % of CWR respectively, Table S1-2, 3). In El Hage et al., (2018 – results presented in Chapter 1) F271 was also responding greatly to the irrigation scenario compared to Cm484, particularly by presenting a great decrease in Klason lignin content (up to 3% of cell wall residue) associated to an increase of cell wall degradability (up to 11% of cell wall degradability) under non-irrigated condition (Figure 39). So these responses of irrigation condition on cell wall traits of Cm484 and F271 were expected to be greater but they are still in the same tendency. On the other hand, only a few histological traits appeared to present significant differences between the irrigations conditions for both inbred lines. Particularly, the Stem area, the bundle fraction and the bundle density presented significant differences between the irrigations conditions.

Overall, considering both parental lines, predicted biochemical traits were affected between both irrigation conditions carried out whereas histological quantified traits were less impacted.

2. Variations of biochemical and histological traits among the recombinant inbred lines showed transgression and allowed to obtain expected correlations between traits

For all the biochemical, histological and agronomical traits quantified within the RILs population (Table S1-1) the range of variations were greater than the difference between Cm484 and F271 parental lines. It illustrates a transgression effect in the progeny for every measured traits. It was noticeable that the histological traits of the RILs population were impacted significantly by the irrigation condition only in 2014 while only the Bundle density seemed impacted in 2015. This suggest that at the internode scale, the difference between the 2 non-irrigated conditions were much more striking for the histology than for the cell wall biochemistry. Consequently histology may be considered here as a different sensor for the environmental conditions changings than cell wall biochemistry. According to the variations of the environmental conditions, plants dispose of several strategies from modifying the

spatial distribution of the lignified tissues to modifying the contents and the composition/structure of the cell wall. This was reported on one sugarcane mature stem, where under moderate drought the lignin content in the pith and in the rind do not vary whereas under severe drought, the lignin content increased significantly in the rind but not in the pith (Dos Santos et al., 2015).

As each condition were considered separately, no heritability was possibly determined, but an analysis of the relationships between all the biochemical and histological traits gave a good overview and estimation of the conserved relationships between traits from a condition to another and from a year to another. Thus relationships between all the biochemical cell wall traits and 4 histological traits; the Blue parenchyma, the Red parenchyma, the Red rind and the Bundle density were analysed through Pearson correlation network within each condition and year among the RILs population (Figure 41).

Concerning the biochemical cell wall traits, the relationship between the cell wall degradability (IVCWRD) and the Klason lignin content (KL.CWR) was strong and very significant within each condition (Figure 41) with pearson correlation factor R=-0.85, R=-0.84, R=-0.85, R=-0.77 for 2014-I, 2014-NI, 2015-I, 2015-NI respectively (Table S2). This tightly relationship between lignin content and cell wall degradability has been often reported on many species (Jung and Buxton, 1994; Argillier et al., 1996; Casler, 2005; Grabber et al., 2010; Canbolat, 2012; Wang et al., 2012, Emerson et al., 2014, Dos Santos et al., 2015; Perrier et al., 2017, Van der Weijde et al., 2017, El Hage et al., 2018) and it was then expected in the RILs population. As the esterified *p*-coumaric acid content (PCAest) was previously described to be a good sensor of the lignin deposition and to present therefore a positive relationship with the lignin content (Hatfield et al., 1999; Grabber et al., 2004; Zhang et al., 2011; El Hage et al., 2018), it also presented here a very significant and positive relationship with KL.CWR as well in each condition (Pearson correlation factor R=0.53, R=-0.44, R=0.48, R=0.49 for 2014-I, 2014-NI, 2015-I, 2015-NI respectively; Table S2). However, this relationship was weaker than what was previously observed in a panel of genetic diversity cultivated at the same place in 2012, 2013 and 2014 (El Hage et al., 2018) where Pearson correlation factors were R=0.94 and R=0.92 under irrigated and non-irrigated condition respectively. Furthermore, in the conclusions of this previous study, a model of response was proposed following the analysis of the relationships between the biochemical and histological traits under irrigated and non-irrigated condition. In this panel of genetic diversity, under non-irrigated condition lignins deposited in the rind were more *p*-coumaroylated than in the pith while under irrigated condition the pith presented better relationships than the rind for the lignin content and the *p*-coumaric acid content. Here, the relationships showed that the RILs population did not follow the same pattern of correlations; either in 2014 or in 2015, the Red rind did not

presented significant relationships with the lignin content nor with the esterified *p*-coumaric acid content under non-irrigated condition. The other biochemical traits presented also general relationships overall the conditions; the S/G ratio was positively and strongly correlated to the cell wall degradability, BO4 yield presented significant and positive relationships with PCAest and KL.CWR, the cellulose content was negatively correlated to the IVCWRD while the hemicelluloses content was positively correlated to it.

The histological traits correlated as "satellites" around the biochemical traits relationships (Figure 41). Theirs positions in the correlation networks indicated that they explain other types of variations than the biochemical cell wall traits. As the biochemical traits depicted mainly the overall composition and structure of the cell wall, the histological traits reflected a spatial variability (lignified parenchyma or rinds…) and morphological characteristics (stem area, bundle density...). However, they did present noteworthy relationships with biochemical traits, according to the condition. Thus the Red parenchyma presented each year a stronger relationship with the IVCWRD under non-irrigated condition than under irrigated condition (R=-0.10 in 2014-I; R=-0.21 in 2014 NI; R=-0.22 in 2015-I; R=-0.32 in 2015-NI; Table S2). More particularly, in 2014, the Red parenchyma presented also stronger and more significant relationships with PCAest and KL.CWR under non-irrigated condition (R=0.19 and R=0.26 respectively; Table S2) than under irrigated condition (R=-0.06 and R=0.10, respectively; Table S2). This suggests that water deficit may have induced a greater deposition of lignins more *p*-coumaroylated within the parenchyma under non-irrigated condition. On the other hand, the bundle density positioned aside of the biochemical traits but also aside from the other histological traits. It presented significant relationships under each condition with the etherified ferulic acid content (R=0.26 in 2014-I; R=0.27 in 2014-NI; R= 0.19 in 2015-I; R= 0.19 in 2015-NI; Table S2) and the cell wall residue (R=0.27 in 2014-I; R=0.28 in 2014-NI; R= 0.19 in 2015-I; R= 0.19 in 2015-NI; Table S2). This may suggests that, in this RILs population the bundle density influences positively the cell wall residue content and that bundles would present a lignification more feruloylated, no matter the condition. It was previously shown and mentioned that vascular bundles, which are made of a diversity of types of tissues, are hardly degradable (Wilson, 1993; Jung and Casler, 2006). Here the negative correlation between the bundle density and the IVCWRD (Figure 41) goes along with a greater CWR and higher deposition of etherified ferulic acid content on lignins.

Altogether, the results under the 4 conditions, 2014-I, 2014-NI, 2015-I and 2015-NI, suggest a repeatability of the correlation between the traits.

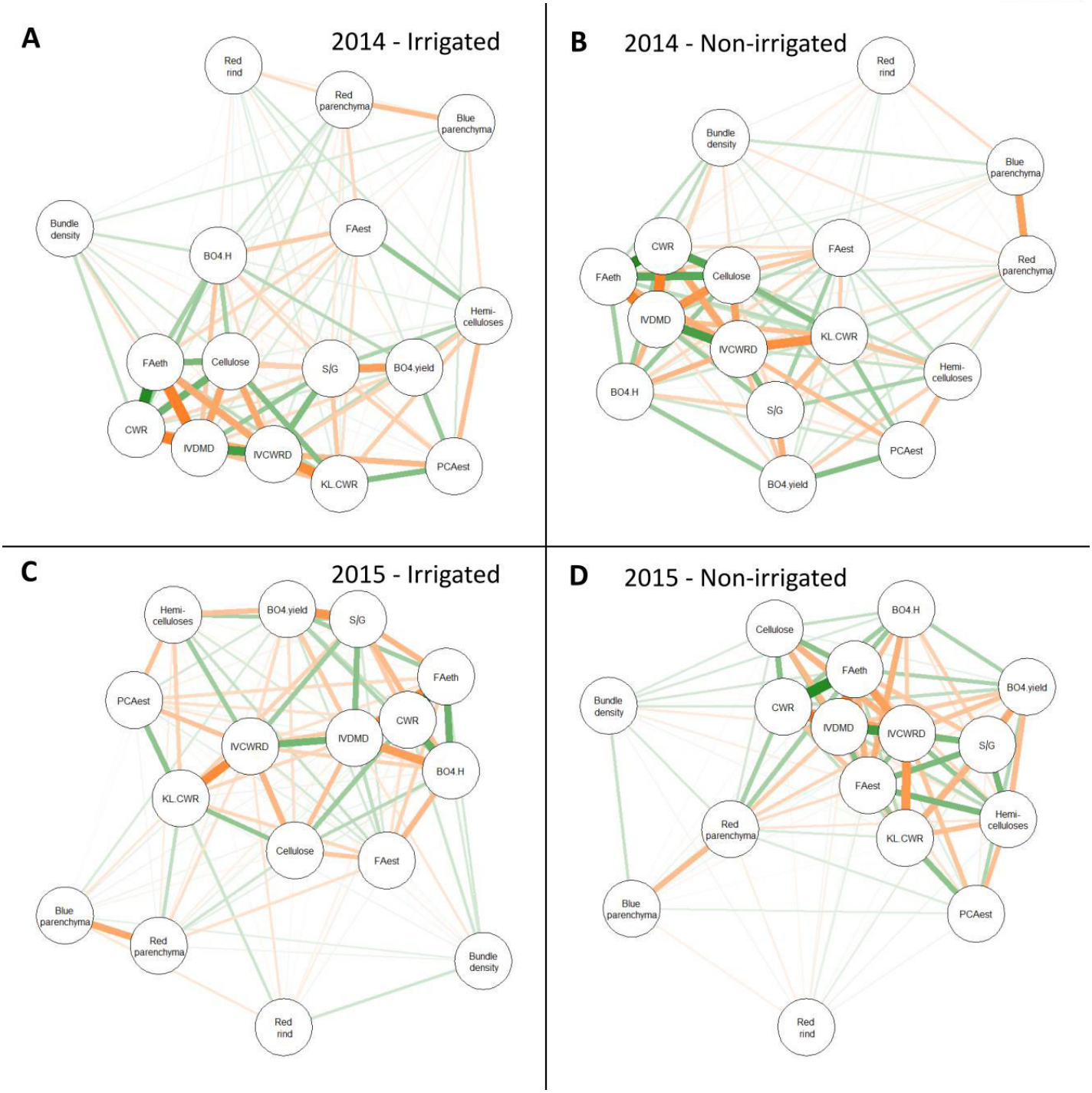


Figure 41. Relationships between all the biochemical cell wall traits and 4 histological traits for the RILs population under the 4 conditions. The 4 histological traits chosen were the Blue parenchyma, the Red parenchyma, the Red rind and the Bundle density. Every lines represents the Pearson correlation value between the two linked traits. In green are the positive correlation values, in orange the negative correlation values. The closer the traits are, the more significant is their correlation. The thicker is the line, the closer to 1 or -1 is the correlation value. A. In 2014 under irrigated condition. B. In 2014 under non-irrigated condition. C. In 2015 under irrigated condition. D. In 2015 under non-irrigated condition.

c) Genetic determinism of histological traits under different irrigation conditions

Overall the 4 conditions, 90 QTLs for the histological traits were mapped, with a threshold of 3 (Figure 42 and Table S3). Per condition the number of QTLs detected varied from 20 in 2014-NI, 21 in 2015-I, 21 in 2015-NI to28 in 2014-I.

The first striking result was to notice a large region on the down of chromosome 1, where many QTLs were detected for being involved in the variation of numerous histological traits. The region spreads between 223.5 cM and 324.0 cM (corresponding to bin 1.07 to 1.11) (Figure 42 & Table S3). The main traits which co-localized on this region were the Bundle number and the Stem area common to all the irrigated conditions, Rind fraction was also detected in both irrigated conditions, Non-lignified fraction was common to 2014-I and 2015-NI, and Blue parenchyma and Red rind were detected in this regions only in 2014-I. This region seems to be undoubtedly involved in the spatial distribution and development of the vascular bundles and the lateral size of the internode. All the 16 QTLs that Huang et al., (2015) mapped for the number of vascular bundles within a population of maize-teosinte back-cross recombinant inbred lines were presented with cM positions so the comparison cannot be strictly precise; however they detected QTL involved in vascular bundle number on all the maize chromosomes. Here QTLs for the variations of the bundle number were detected mainly on the chromosome 1 in all conditions, 1 at the bottom of the chromosome 2 in 2014-I, 1 at the bottom of the chromosome 6 in 2014-I and 2014-NI one on the chromosome 9 in 2015-I apparently at a different locus than the one Huang et al., (2015) cloned from a NIL in their study.

Another region seemed to be, over all the conditions, specific to a type of trait; at the middle of the chromosome 10, between 68.70 cM to 119.30 cM (corresponding to bin 10.03 to 10.06) where systematically a trait related to the vascular bundles was detected no matter the condition. Thus the Bundle density was detected in 2014-I, 2015-I and 2014-NI, the Bundle fraction in 2015-I and 2014-NI and finally the bundle number in 2015-NI.

The watering condition did not reveal specific regions, except maybe the 2015-NI condition, despite being a non-irrigated condition with a flooding event. This condition revealed indeed more QTL for the non-lignified fraction on the chromosome 1 and 6.

Despite the impossibility to evaluate the heritability of the traits properly, overall, major regions of many QTLs were detected in all years and conditions between bin 1.07 and bin 1.11 and between bin 10.03 and 10.06 suggesting that these positions are genetically important in the variations of these traits independently of the environmental condition.

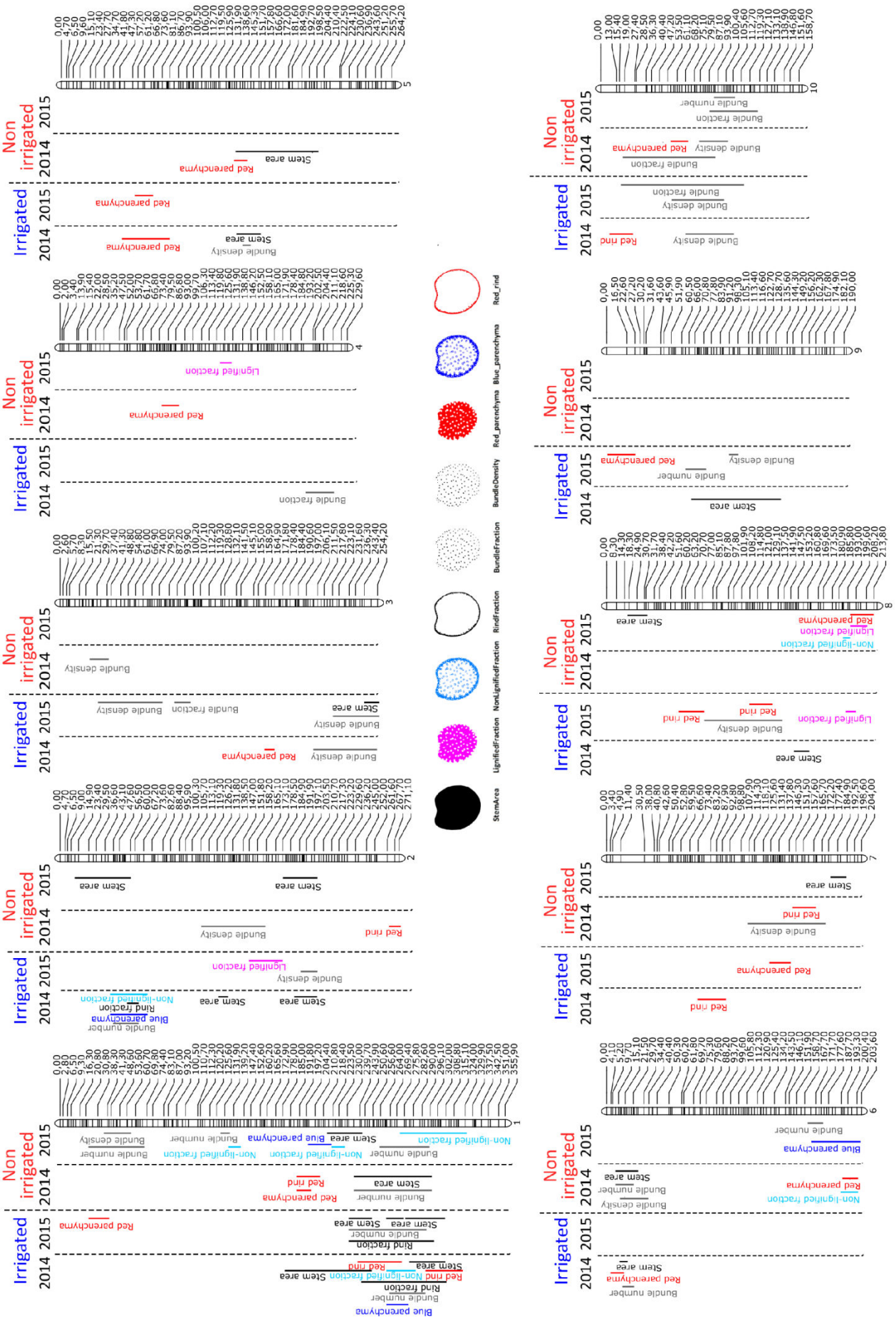


Figure 42. Mapping of QTLs involved in the variations of histological traits for the 4 conditions : 2014 I, 2015-I, 2014-NI, 2015-NI.

d) QTLs involved in the variation of biochemical traits and co-localizations with QTLs involved in the variation of histological traits

If already a few studies published QTLs analyses for quality traits of the biomass within maize stalk (Cardinal et al., 2003, Krakowsky et al., 2005; Li et al., 2017), it is the first time that QTL for biochemical cell wall traits as fine and precise are investigated. The biochemical components usualy quantified are coming from the Van Soest chain: NDF, ADF and ADL. Here the biochemistry of major components as the *p*-hydroxycinnamic acids and the lignin structure are presented.

As mentioned by Barrière et al., (2005) and Truntzler et al., (2010) several bins have been often reported to be involved in biochemical cell wall traits and cell wall degradability, more particularly at bin 1.02/03, 4.05, 4.08 and 6.05. As they are present in different RILs populations they are suggested as being major regions involved in the variations of many cell wall traits and degradability. Thus here, on the internode of maize, many QTLs were detected at these same major regions. At bin 1.02, in 2015-NI, a QTL for the cell wall degradability variations has been detected. At bin 4.05, many QTLs of mainly phenolics compounds have been detected over several conditions (for KL.CWR in 2015-I, 2014-NI and 2015-NI; for PCAest in 2014-I, 2015-I, and 2014 NI; FAeth in 2015-I, Figure 43). And finally at bin 6.05 there was QTLs detected mainly for Hemicelluloses in all years and conditions but also for FAest in 2015-I and 2014-NI. All these major regions present QTLs of cell wall components present in the stalk and also in the whole plant according to the previous studies suggest probably the presence of master genes in these regions which would be involved in the variation of these traits within the whole plant but also at the scale of the internode.

Several co-localizations have been noticed between histological and biochemical traits QTLs. Thus in the major region of QTL for the histological traits from bin 1.07 to bin 1.11, in 2014-NI QTLs for PCAest, KL.CWR, BO4 yield, Hemicelluloses and the agronomical trait Plant height. In the same region in 2014-I QTLs for Hemicelluloses, PCAest, S/G ratio and plant height were also detected (Figure 43). Along with the relationships mentioned in literature between these traits and the spatial distribution of the lignification (Dos Santos et al., 2015; Perrier et al., 2017; El Hage et al., 2018), it suggests that this region could to be involved either in the lignification, the *p*-coumaroylation and the set-up of the bundle number, the stem area and the rind lignification.

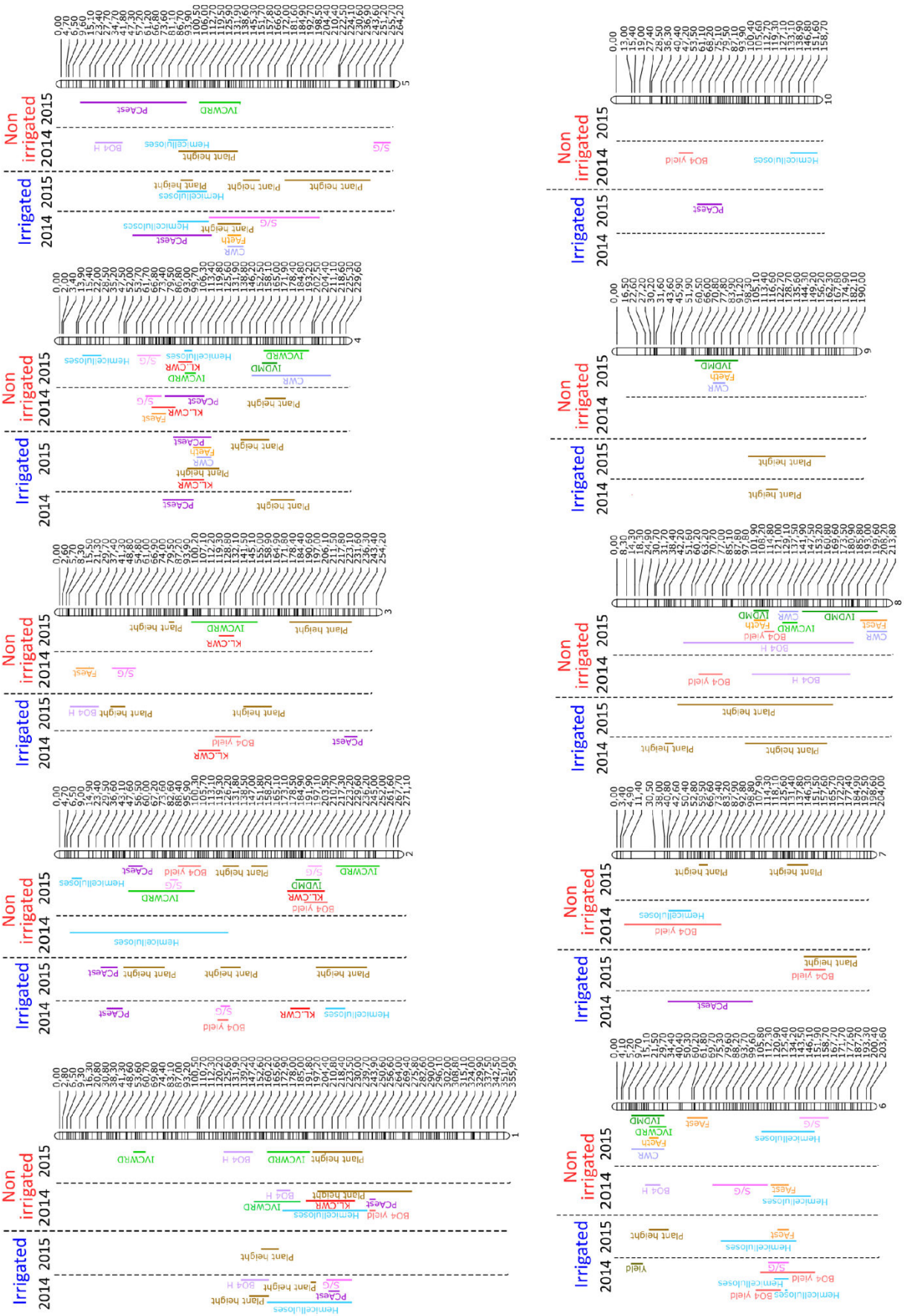


Figure 43. Mapping of QTLs involved in the variations of biochemical traits for the 4 conditions : 2014 I, 2015-I, 2014-NI, 2015-NI.

It was surprising to note that no QTL for the cellulose content was detected. Another surprising was to detect QTL of IVDMD and IVCWRD exclusively in 2015-NI except for 1 QTL of IVCWRD at bin 1.07 in 2014-NI. This may suggest that the QTL detection was not powerful enough to detect them the other years. However, when a QTL of degradability was detected, it did not systematically colocalize with lignin content as it was often reported (Riboulet et al., 2008, Lorenzana et al., 2010; Torres et al., 2015). Thus, as in these studies, at bin 3.05 a colocalization with QTL for IVCWRD and KL.CWR was observed in the internode in 2015-I. Nevertheless, in 2014-I, at bin 1.07 and 1.08 QTL for IVCWRD and KL.CWR respectively did not colocalize. As commented in previous studies, it witnesses, at the internode scale too, that genetic determinism of the cell wall traits are complex (Barrière et al., 2008; Truntzler et al., 2010; Penning et al., 2014).

Comparing with other studies which detected QTL on the maize stalk, it was possible to find QTLs which were previously published in common with this detection. Thus Li et al., in 2017 harvested the 2^{nd}-5^{th} internodes above the ground in a RIL population of 220 lines developed by SSD until the F10 generation in a cross between line Zheng58 and HD568 which are the parental lines of the elite commercial hybrid Zhongdan909 in China. Despite the fact they harvested at anthesis stage, a younger developmental stage than the silage stage, 2 co-localizations of QTLs for the IVDMD were observed at bin 8.05 and bin 9.02. These co-localisations may suggest that these genetic regions drive the variation of the IVDMD at different developmental stages and in different genetic background, so potentially some conserved regions between maize cultivars.

Under irrigated condition in 2014 a few colocalizations were interesting between QTLs of PCAest and Red parenchyma at bin 4.05 and between PCAest and Red_rind at bin 7.02 with in each case, an absence of QTL for the lignin content. This pinpoints loci where allelic variation induced variation of PCAest along with variation of the spatial distribution of lignification without the systematic affecting variation of cell wall lignin content. These regions may be of interest in selection of plants for a good degradability and to influence cell wall properties and lignification distribution without selecting on the lignin content.

Finally, under non-irrigated condition in 2014, several co-localizations were noteworthy: at bin 1.06 QTLs for Red parenchyma, Red rind, IVCWRD, BO4 H were detected; and at bin 4.05 where QTL for Red parenchyma, KL.CWR, FAest content and S/G ratio were mapped. As presented in previous studies and as suggests this QTL mapping these biochemical traits could be altogether relevant in the lignification of the maize stem and the explanation of the variations of cell wall degradability (Mechin et al., 2005; Zhang et al., 2011; El Hage et al., 2018).

e) Genetic determinism for biochemical cell wall traits of the whole plant without ears matches with the genetic determinism for biochemical cell wall traits of the internode in maize

The genetic determinism of the cell wall biochemical traits were also studied in the same RILs population issued from CM484 x F271 but within the whole plant without ears (Virlouvet et al., in prep). In this study, plants were harvested also in 2013 in addition of 2014 and 2015. The results over the 3 years allowed performing an analysis over the years thanks to a better uniformity of the statistical effect of the water deficit from one year to another.

It was worthy to notice that at bin 1.07 and 1.08, QTLs for KL.CWR, PCAest and Hemicelluloses at the internode level were co-localizing with QTLS for IVCWRD KL.CWR, PCAest, and Hemicelluloses at the whole plant level. This suggests that the variations of these traits at the internode level reflected the variations at the whole plant level and a potential genetic link could partly explain it. It may either be a pleiotropic gene which would be involved in the variations of several traits or clusters of linked genes which are individually involved in the variation of a different trait.

Another locus where the QTL detection of both studies joins at the internode level and at the whole plant without ears level was the bin 4.05. Here QTLs for IVCWRD, PCAest, KL.CWR and Hemicelluloses were mapped (at the internode level and at the whole plant level).

At bin 6.05, a QTL region already identified in several genetic studies on the biochemical cell wall traits in a RIL population coming from the F271xF288 cross (Roussel et al., 2002; Courtial et al., 2013, 2014), the QTL analysis on the whole plant revealed a strong QTL region. The QTL mapping for biochemical cell wall traits in the internode showed at the same bin in every conditions QTL for the Hemicelluloses content, for the FAest in 2015-I and 2014-NI and S/G in all condition except 2015-I. Virlouvet et al., (in prep) suggested that alleles from F271, the common parent, might have a particularity, which confers some cell wall properties relative to those from the parental inbred lines F288 and Cm484.

It was also striking to realize that the QTL detection on the whole plant without ear detected much more QTLs involved in the variations for cell wall degradability than the detection performed on the internode. We could hypothesize that under cell wall degradability QTLs detected for the whole plant without ears are present genes involved in the regulations of this trait at the whole plant scale.

To go further in the co-localization study, it was tempting to compare the QTLs detected for histological traits and QTLs for cell wall traits in the whole plant. Thus it was worthy to note that 2 QTLs for IVCWRD of the whole plant co-localized with the major QTL of

histological traits for Stem Area and Bundle number at bin 1.08 and 1.10/11 along with other QTLs for lignin content, structure and *p*-hydroxycinnamic acids (Figure 42 and Figure 2 of Virlouvet et al., in prep). In an original way, at bin 10.03/04, a co-localization between cell wall degradability in the whole plant and the second major region of histological trait (mainly for the Bundle Density and the Bundle number) was observed (Figure 42 and Figure 2 of Virlouvet et al., in prep) without QTL for the lignin content/structure or for hydroxycinnamic acids. This last co-localization opens perspectives and hypotheses about the genetic relationships whichcould exist between histological traits and cell wall degradability of the whole plant.

In this second part, the paper of Virlouvet et al., very close to be submitted, will be presented. The QTL detection was performed on the same RILs population for biochemical cell wall traits and degradability at the scale of the whole plant without ears and cultivated 3 years (2013-2014-2015) under contrasted irrigation conditions.

II. Water deficit responsive QTLs for cell wall degradability and composition traits in maize at silage stage

Laëtitia Virlouvet[1], Fadi El Hage[1], Yves Griveau[1], Marie-Pierre Jacquemot[1], Emilie Gineau[1], Aurélie Baldy[1], Sylvain Legay[1], Christine Horlow[1], Valérie Combes[2], Cyril Bauland[2], Carine Palafre[3], Matthieu Falque[2], Laurence Moreau[2], Sylvie Coursol[1], Valérie Méchin[1], Matthieu Reymond[1]*.

[1]Institut Jean-Pierre Bourgin, INRA, AgroParisTech, CNRS, Université Paris-Saclay, 78000, Versailles, France.
[2]Génétique Quantitative et Evolution - Le Moulon, INRA, Université Paris-Sud, CNRS, AgroPArisTech, Université Paris-Saclay, 91190, Gif-Sur-Yvette, France.
[3]Unité Expérimentale du Maïs, INRA, 40390, Saint Martin de Hinx, France

***Corresponding author:** Matthieu Reymond Tel: +33 1 30 83 32 14. Email: matthieu.reymond@inra.fr

Author email addresses: laetitia.virlouvet@inra.fr, fadi.el-hage@inra.fr, yves.griveau@inra.fr, marie-pierre.jacquemot@inra.fr, emilie.gineau@inra.fr, aurelie.baldy@gmail.com, legainsy@gmail.com, Christine.horlow@inra.fr, valerie.combes@inra.fr, cyril.bauland@inra.fr, carine.palaffre@inra.fr, matthieu.falque@inra.fr, laurence.moreau@inra.fr, sylvie.coursol@inra.fr, Valerie.mechin@inra.fr

Key words: Cell-wall composition, degradability, drought response, Quantitative Trait Locus, maize

INTRODUCTION

Lignocellulosic plant biomass is commonly valorized to produce energy for animal feeding or for biofuel production (Bichot et al., 2018; Torres et al., 2015; Vermerris and Abril, 2015). The biomass degradability is measured as the percentage of lignocellulosic biomass that is assimilated by the animal or by the amount of sugars released from a biorefinery process. The polysaccharidic fraction of the biomass is thus degraded more or less totally. The recalcitrant nature of lignocellulose to digestion, mainly related to its phenolic fraction, limits its valorization. Therefore, limiting biomass recalcitrance without affecting agronomical performances of plant such as yield, resistance to pest and resilience for water deficit for instance, is an important breeding target for increasing biomass valorization for feed and biorefinery applications (van der Weijde et al., 2013).

Lignocellulosic biomass corresponds to cell wall that surrounds each plant cell. Available studies have shown that grass cell walls are composed of celluloses (nearly 45%), hemicelluloses (nearly 45%) and phenolics (nearly 10%). These values vary depending on the plant developmental stage, the considered tissue and the studied genotype. Cell wall degradability was shown to be strongly influenced by phenolic compounds such as lignin and *p*-hydroxycinnamic acids content (Casler and Jung, 1999; El Hage et al., 2018; Grabber et al., 1998; Hartley, 1972; Jung and Casler, 2006; Méchin et al., 2001; Zhang et al., 2011). Lignin content in cell wall affects strongly and negatively cell wall degradability. Linkage feature between lignin subunits can also affect degradability (El Hage et al., 2018; Méchin et al., 2000). To avoid the strong negative correlation between the lignin content and the cell wall degradability, Zhang et al. (2011) fixed the lignin content and reported that amount of □O4 link in the lignin polymer was negatively correlated to cell wall degradability. The influence of lignin composition, in guiacyl (G), syringil (S) and *p*-hydroxyphenyl (H) subunits, on cell wall degradability is still controversial, and results can be very different when studying monocotyledons (El Hage et al., 2018; Méchin et al., 2000; Zhang et al., 2011), dicotyledons (Baucher et al., 1999; Casler and Jung, 1999; Goujon et al., 2003) or artificially lignified cell walls (Grabber et al., 2003).

In grasses, *p*-hydroxycinnamic acids are more abundant that in other plant clades. Among them, *p*-coumaric acids are mainly esterified (PCAest) to S lignin units (Grabber et al., 1996; Lu and Ralph, 1999; Ralph et al., 1994), while ferulic acids (FA) are associated with hemicelluloses through ester (FAest) linkages or/and with lignin through ether (FAeth) linkages (Hatfield et al., 2017). It has been shown that the PCAest content was negatively correlated to cell wall degradability on maize lines (El Hage et al., 2018; Gabrielsen et al., 1990;

Méchin et al., 2000; Taboada et al., 2010; Zhang et al., 2011) and the FA might also have a role in cell wall degradability (Barrière et al., 2005).

Biosynthesis and regulatory pathways for cell wall components have been proposed (Boerjan et al., 2003; Gray et al., 2012; Riboulet et al., 2009; Vanholme et al., 2008), with numerous genes encoding enzymes and transcription factors involved in the establishment of plant cell wall all along plant development. In addition, over the last two decades, quantitative trait locus (QTL) analyses have been performed to determine the genetic factors involved in the variation of cell wall degradability and composition in maize using mainly biparental populations (Barrière et al., 2001, 2008, 2012; Bohn et al., 2000; Cardinal et al., 2003; Cardinal and Lee, 2005b; Fontaine et al., 2003; Krakowsky et al., 2005, 2006; Leng et al., 2018; Lorenzana et al., 2010; Lübberstedt et al., 1997c, 1997b; Méchin et al., 2001; Papst et al., 2004; Riboulet et al., 2008a; Roussel et al., 2002; Torres et al., 2015; Wei et al., 2009). Over 400 QTLs related to cell wall degradability and composition have been mapped all over the maize genome (Barrière et al., 2008). A meta-analysis of QTLs carried out by Truntzler et al. (2010) resulted in the identification of 26 meta-QTLs for cell wall degradability and 42 meta-QTLs for cell wall composition, suggesting that the genetic determinism of these traits was complex but might be reduced to a smaller number of genomic regions. Interestingly, only less than half of the meta-QTLs for cell wall degradability co-localized with meta-QTLs for cell wall composition. Moreover, only few major QTLs (which explained more than 20% of the observed variation) have been reported for cell wall-related traits (Courtial et al., 2013; Roussel et al., 2002), underlying the fact that cell wall composition and degradability are under a complex genetic determinism. Even if a negative correlation between yield and degradability has been reported (Barrière et al., 2004), breeding forage maize hybrids with increased cell wall degradability has been carried out, without impacting plant yield progress (Baldy et al., 2017).

In the context of climate changes, several predictive scenarios have been suggested (Samaniego et al., 2018). Most of these studies predict that occurrence of drought periods will arise more often and may impact yields (Webber et al., 2018). In a context of sustainable production, inputs in the field including water, will be provided with parsimony in rainfed crops and plants will not always be irrigated. In fact, water deficit affects leaf and root growth within minutes which are likely to affect whole-plant transpiration and water uptake over days to months, and consequently having a potential effect on biomass production and/or quality (for reviews see Reynolds and Langridge, 2016; Tardieu et al., 2018). Water deficit also impacts underlying physiological processes including cell division, hydraulics, cell wall mechanics and primary and secondary metabolism. As a consequence, crop plants under water deficit often contain excess carbon, and roots and reproductive organs show signs of experiencing sink

limitation. Furthermore, under agronomical conditions, dysregulation of synchronization of male and female flowering time are often reported under water deficit, leading to grain abortion and massive yield loss (Denmead and Shaw, 1960; Reynolds and Langridge, 2016; Turc and Tardieu, 2018). The genetic determinism of drought tolerance in maize grain yield has been largely studied and reported (Collins et al., 2008; Ribaut et al., 2010; Ribaut and Ragot, 2007). However, no QTL for cell wall degradability or composition in response to water deficit has been reported yet, although several reports recently showed that water deficit impacts both cell wall degradability and composition in maize (El Hage et al., 2018; Emerson et al., 2014), sorghum (Perrier et al., 2017), miscanthus (Emerson et al., 2014; van der Weijde et al., 2017) and sugarcane (dos Santos et al., 2015).

In the present study, to explore the genetic architecture for cell wall-related traits response to water deficit in maize plant, QTL mapping was conducted using a maize recombinant inbred lines (RIL) population derived from the cross of two parental inbred lines, F271 and Cm484, and evaluated in field trials over three consecutive years under both irrigated and non-irrigated scenarios. The objectives of this study were: (1) to determine the impact of non-irrigated scenario on cell wall-related traits using maize stover and dedicated near infrared spectroscopy (NIRS) predictive equations; (2) to identify 'constitutive' QTLs (Collins et al., 2008) across contrasted irrigation conditions for cell-wall related traits and 'responsive' QTLs to water deficit. Our results highlight again the strong complexity of the genetic determinism of traits related to the cell wall composition and degradability (Torres et al., 2005, Barrière et al., 2008) and chromosomic regions usable in breeding programs especially in response to water deficit condition.

Materials and Methods

Plant materials and field experiments

A RIL population consisting of 267 lines was developed at INRA by single seed descent (SSD) up until 6 generations in a cross between maize inbred early lines F271 (INRA private line bred from Canadian dent; Barrière et al., 2001; Roussel et al., 2002) and Cm484 (Canada-Morden – 1989; Barrière et al., 2007; Méchin et al., 2000). All the RILs were planted in a randomized augmented bloc design with one replicate of both parents in each bloc at Mauguio (France, Mediterranean climate) over three years (2013, 2014, 2015). Plants were grown in open field under an Irrigated (I) scenario, the water being supplied with a mobile ramp of sprinklers, and a Non-Irrigated (NI) scenario, which consisted of a dry-down period that began when INRA check early line F2 showed the 5th leave ligulated and finished 14 days after all the RILs flowered. Each line was grown in a single 4.20 m row with 0.80 m between rows and a planting density of 80,000 plants/ha. At the silage stage, ears with husks and peduncle were removed manually from the plants just before the stover plots were machine-harvested with a forage chopper. In the field, plant height and biomass yield were quantified. A representative sample of nearly 350 g fresh chopped stover per plot was collected for dry-matter (DM) content estimation and biochemical and NIRS analyses. All samples were dried in a forced-air oven at 55 °C and ground with a hammer mill (1 mm grid).

NIRS predictive equations establishment and biochemical analyses

Cell wall biochemical related traits of all the harvested dried samples have estimated using NIRS predictive equations. To do so, NIRS predictive equation were developed at INRA Versailles for maize plants without ears harvested at silage stage (Table 1). Depending on the trait, 60 to 200 samples were biochemically analyzed to calibrate and to validate the established equations. Out of these 200 samples, 49 were selected from the F271 × Cm484 RIL progeny evaluated in the I (23 samples) and NI (26 samples) scenarios over three years (6 and 9 samples from the I and NI scenarios, respectively, in 2013; 14 and 11 samples from the I and NI scenarios, respectively, in 2014; 3 and 6 samples from the I and NI scenarios, respectively, in 2015). This selection was carried out to make the predictive equations accurate to the samples harvested in the present study. Calibration equations were validated by using a set of 20 to 40 calibration samples for all traits, excepted neutral detergent fiber (NDF), acid detergent lignin (ADL.NDF), and polysaccharides (CL.NDF and HC.NDF) obtained by the Goering and Van Soest method where cross validation approach was applied (Table 1).

Table 1. Characteristics of NIRS calibrations developed for cell wall traits in stover maize plants without ears.

Categories	Traits[a]	Units	Range	Calibration		Validation		
				n	r	n	r	SECV
Cell Wall residues	NDF	%DM	43.34 - 69.2	57	0,983	0	0,95	1,77
Degradability	IVDMD	%DM	32.3 - 66.9	160	0,963	38	0,93	2,22
	IVCWRD	%CWR	25.67 - 51.02	161	0,805	38	0,81	3,28
Lignin content	KL.CWR	%CWR	11.06 - 18.67	167	0,852	40	0,83	0,77
	ADL.NDF	%NDF	3.21 - 6.91	57	0,925	0	0,83	0,48
Lignin structure	βO4	µmole g^{-1} KL	255 - 1023	168	0,893	40	0,90	86,00
	βO4.H	µmole g^{-1} KL	3 - 28.5	166	0,636	40	0,71	4,08
	βO4.G	µmole g^{-1} KL	132.15 - 564.24	166	0,869	40	0,88	50,80
	βO4.S	µmole g^{-1} KL	119.06 - 540.39	166	0,855	40	0,86	52,40
	S/G		0.46 - 1.68	166	0,709	40	0,62	0,19
Hydroxycinamic acids	PCAest	mg g^{-1} CWR	4.66 - 17.94	164	0,864	39	0,78	1,71
	FAest	mg g^{-1} CWR	2.05 - 6.92	164	0,802	39	0,83	0,54
	Faeth	mg g^{-1} CWR	1.59 - 3.88	164	0,451	39	0,45	0,31
Structural sugars	CL.NDF	%NDF	43.42 - 54.48	57	0,903	0	0,78	1,52
	GLU	%CWR	28.73 - 43.35	81	0,835	19	0,76	3,22
	HC.NDF	%NDF	39.67 - 51.89	57	0,905	0	0,77	1,81
	ARA	%CWR	3 - 4.84	81	0,843	19	0,77	0,26
	GAL	%CWR	0.6 - 2.06	81	0,945	19	0,93	0,15
	XYL	%CWR	16.64 - 23.39	81	0,623	19	0,70	1,08

[a]NDF, neutral detergent fiber; IVDMD, *in vitro* dry matter degradability; IVCWRD, *in vitro* cell wall residus degradability; ADL, acid detergent lignin; KL, Klason lignin; PCAest, esterified *para*-coumaric acid; FAeth, etherified ferulic acid; FAest, esterified ferulic acid; CL, cellulose; HC, hemicellulose; GLU, glucose; ARA, arabinose; GAL, galactose; XYL, xylose.

Concerning the biochemical analyses performed on the calibration and validation sets, cell wall residues (CWR) was obtained with a water/ethanol extraction (Soxhlet). NDF, acid detergent fiber (ADF), ADL, cellulose (CL.NDF = 100*(ADF-ADL)/NDF) and hemicellulose (HC.NDF = 100*(NDF-ADF)/NDF) contents were estimated according to Goering and Van Soest (1970). Lignin content in the cell wall (KL.CWR) was estimated using the Klason method according to Dence (1992). Contents in esterified and etherified *p*-hydoxycinamic acids (PCAest, FAest, FAeth) were estimated after alkaline hydrolysis of the cell wall residues (Culhaoglu et al., 2011; Méchin et al., 2000). In order to investigate the monomeric structure and composition of lignin (units BO4.H, BO4.S and BO4.G), oxidation of cell wall residues was performed by thioacydolysis (Lapierre et al., 1986). Glucose (GLU), Xylose (XYL) and Arabinose (ARA) contents were quantified by acidic hydrolysis (Harholt et al., 2006; Updegraff, 1969). The *in vitro* dry matter degradability (IVDMD) and cell wall residues degradability (IVCWRD) were estimated according to Aufrère and Michalet-Doreau (1983). Briefly, 30 mg of dry matter were pretreated in an acid solution (HCL 0.1N) at 40°C during 24 h and stopped with NaOH 2 M. The sample was then incubated in a cellulase solution (Cellulase Onozuka R10 8 $mg.ml^{-1}$,

NaAc 0.1M pH 4.95, Na_2CO_3 0.4 %) at 50 °C during 72 h. After centrifugation, the pellet was washed wither water and freeze before lyophilization and the loss of weight was calculated in percentage. Dry samples were scanned through a near-infrared reflectance spectrometer (Antaris II, thermos fischer scientifc) and biochemical traits were estimated using NIRS equations.

Statistical analyses of the cell wall dataset

All statistical analyses were performed using R software (R Core Team, 2014). To eliminate the environmental effects, single-plot values were corrected by a subtraction of the best linear unbiased prediction (BLUP) value of the bloc effect for each line, using the following mixed linear model (1):

$$Y_{ijkl} = \mu + g_i \text{ x}(1\text{-}t_i) + C_i x\, t_i + y_j + e_k + B_{jkl} + g_i \text{ x } y_j + g_i \text{ x } e_k + y_j \text{ x } e_k + \varepsilon_{ijkl} \quad (1)$$

where Y_{ijkl} is the phenotypic value of the *i*th line in the *j*th year, in the *k*th irrigation scenario and located in the *l*th bloc in field. In this model, μ is the intercept. The genetic effect of line i is considered as fixed and note C_i if *i* was one of the two parental lines used as checks and as random and noted g_i if *i* was one of the RIL. The parameter t_i was set to one for checks and zero otherwise. The genetic effects were assumed to be independent and identically distributed. The B_{jkl} bloc effects were considered as random, as weel as the interactions between the g_i genetic and the y_j year or the e_k irrigation scenario effects. The interaction between the e_k irrigation scenario and the y_j year effects was considered as fixed effect.

A principal component analysis (PCA) was carried out on the corrected data to better understand the relationship between the traits. The R package FactoMineR was used for the PCA (Lê et al., 2008).

Corrected data for each trait were then used to estimate variance components and trait heritabilities, using the following model (2):

$$Y'_{ijk} = \mu + g_i + g \text{ x } y_{ij} + g \text{ x } e_{ik} + y_j + e_k + y \text{ x } e_{jk} + \varepsilon_{ijk} \quad (2)$$

where Y'_{ijk} is the corrected phenotypic value of the "i"th line in the "j"th year, in the "k"th irrigation scenario. In this equation, the g_i represents the genetic effect, the y_j and the e_k the year and irrigation scenario effects, and the ε_{ijk} the residual error effect.

Broad sense heritability was calculated using the variance components estimated with the linear model (2) where the g_i genetic effects and the interactions between the g_i genetic and the y_j year or the e_k irrigation scenario effects were considered as random effects, as follow:

$$h^2 = \sigma^2_g / (\sigma^2_g + \sigma^2_{ge} / k + \sigma^2_{gy} / j + \sigma^2_E / (obs / i))$$

where σ^2_g represents the genetic variance, σ^2_{ge} is the variance of interaction between the genotype and the irrigation scenario, σ^2_{gy} is the variance of interaction between the genotype and the year, σ^2_E is the residual error variance item, and k, j, obs, i are the number of irrigation scenarios, years, observations and lines.

The corrected data obtained with the model (1) were also used to compute least-square means (ls-means) of each recombinant inbred line using specific models. To obtained ls-means by lines using both irrigation condition jointly ("all"), we used a linear model including genotype, year, irrigation scenario and interaction between year and irrigation scenarios effects, all considered as fixed. For the ls-means of the irrigation conditions separately ("I" and "NI" for irrigated and non-irrigated, respectively), we used the linear model including only the genotype and year effects on the corrected data for irrigated or non-irrigated condition.

Genotyping and genetic map construction

Leaf tissues were collected from all 261 RILs and parental inbred lines F271 and Cm484 and freeze-dried at -70°C. Genomic DNA was extracted using a procedure derived from Tai and Tanksley (1990), Dellaporta et al. (1983) and Michaels et al. (1993). The genomic DNA was used for genotyping with the genotyping by sequencing (GBS) approach (Elshire et al., 2011). Briefly, the genomic DNA was digested with the restriction enzyme ApeK1 and used to construct GBS libraries in 96-plex. The GBS libraries were sequenced on Illumina HiSeq2000 and SNP calling were performed using TASSEL GBS pipeline with B73 as the reference genome (Glaubitz et al., 2014).

Initially, 955,720 markers were identified well distributed on maize chromosomes 1 to 10. 2,806 markers were selected because of being polymorphic between parental lines and with a proportion of missing data lower than 15% among the RILs. These markers were then used to construct the linkage map using R scripts interacting with the CarthaGene software (De Givry et al., 2004, bioinformatics 21:1703), as described in Ganal et al. (2011). Specifically, a scaffold map of 1,775 cM containing 20 to 39 markers per chromosome was first built with very stringent criteria for order robustness (minimum spacing of 5cM between adjacent markers), and then densified with additional markers to produce a framework map containing 62 to 161 markers per chromosome while keeping a LOD threshold for order robustness greater or equal to 3.0. Finally, 1,000 markers were retained following this procedure. The total length of that framework map was 2,355 cM with an average of spacing around 2.4 cM. By looking posteriori at singletons in the data, we checked that the increase of genetic map length when saturating the scaffold with additional markers was not attributable to genotyping errors, but probably to the rather high level of missing data which introduces a

bias in the imputation procedure (EM algorithm) of CarthaGene because of genetic interference. This bias in map length is not expected to significantly affect QTL detection.

QTL detection

To integrate the response to the water treatments, single-marker analysis was also performed on the corrected data for each trait and the coordinates of the PCA components. The genome was scanned with the following model (3):

$$Y'_{ijk} = \mu + g_i + y_j + e_k + y_j \times e_k + m_p x_{ip} + m_p \times e_{kp} x_{ip} + \varepsilon_{ijkp} \quad (3)$$

where Y'_{ijkl} is the corrected phenotypic value of the "i"th line in the "j"th year, in the "k"th irrigation scenario and for the "p"th allele at the tested marker. In this model, μ is the intercept and g_i which is the residual genetic effect, not accounted for by the marker effect, was considered as random. The 1,000 markers identified on the genetic map were analyzed one by one using their "p" allele genotype for all the lines. The markers with a p-value inferior to 0.005% were selected for the marker effect (named constitutive QTL) and for the interaction between the marker and the irrigation scenario (named responsive QTL). The interval around the peak was delimited by the most distant markers with a p-value inferior to 0.005% on each side of the peak. To estimate the percentage of variance (r^2) explained by each detected QTLs, we used the linear model (4) including the irrigation scenario, the marker and the interaction between the marker and the irrigation scenario effects on the ls-mean data *per* irrigation scenario.

$$Y'_{ki} = \mu + e_k + m_p + m_p \times e_k + \varepsilon_{ki} \quad (4)$$

where Y'_{ik} is the corrected phenotypic value of the "i"th line in the "k"th irrigation scenario.

To calculate the r^2 explained by the QTL, we calculated the difference between the total r^2 from the full model (4) and the r2 from the model (4) without the maker effect for the constitutive QTL or the interaction between the marker effect and the irrigation scenarios for the responsive QTL.

To calculate the effect of the QTL, we used the ls-mean data of both irrigation conditions jointly ("all") and separately ("I" and "NI" for irrigated and non-irrigated, respectively). For the constitutive QTL, the QTL effect was estimated at the marker position as the difference between the two parental allele effects divided by the range of variation of the trait on the recombinant inbred lines population. For the responsive QTL, obtained with the "$m_p \times e_k$" factor, the QTL effect was calculated at the marker position by dividing the difference of the irrigation scenario response between the two parental allele with the range of variation of the response of the trait on the recombinant inbred progeny.

Results

Dedicated and robust NIRS predictive equations for cell wall composition and degradability

NIRS spectrum have been acquired for every samples harvested under both irrigation scenarios and every year. NIRS predictive equation have been set up to estimate 19 traits related to cell wall composition and degradability for stover samples harvested at silage stage (material and methods and Table 1). The range of variation obtained among the calibration samples set for most of the traits was considerable and allowed us to develop robust calibrations (Table 1). The *r* values for the validation of the established equations were good (ranging from 0.70 to 0.95) for all the traits except for the S/G ratio (*r* = 0.62) and the Faeth (*r* = 0.45) traits. These predictive equations established permitted to predict cell wall composition and structure of all the harvested samples from the RIL population with high confidence.

Parental inbred lines contrasted for cell wall composition and degradability and responded to the irrigation scenario

Agronomical and cell wall-related traits were then evaluated in the two parental inbred lines F271 and Cm484 under the I scenarios (Table 2). At the agronomical level, F271 was higher and produced more biomass than Cm484. All the 19 traits related to cell wall composition and degradability were found distinct between the two parental inbred lines, except the FAest trait. The biomass produced by F271 was less degradable (IVDMD) than that produced by Cm484. This was corroborated by a higher NDF content in F271 than in Cm484. At the cell wall level, F271 had more lignin in its cell wall (LK.CWR and ADL.NDF) than Cm484Lignin structure was also different between the two parental lines, F271 having more ßO4-linked lignin than Cm484. Moreover, PCAest and FAeth contents were higher in F271 than in Cm484. Consequently, IVCWRD was lower in F271 than in Cm484. Finally, the structural sugars GLU and XYL were higher in F271 than Cm484, while HC.NDF, ARA and GAL were lower in F271 that in Cm84.

When the two parental inbred lines were cultivated under the NI scenario, most of the investigated traits were significantly impacted, except the structural sugars (Table 2). Plant height and produced biomass yield were much lower under the NI scenario compared to the I scenario. NDF increased while lignin contents in cell wall decreased, leading to an increase of both IVDMD and IVCWRD. The overall ßO4 yield decreased under the NI scenario compared to the I scenario. The S units content decreased while the G units content remained unchanged, leading to a decrease of the S/G ratio. In contrast, the H units increased under the NI scenario relative to the I scenario. The PCAest content decreased under the NI scenario compared to the I scenario. It is noteworthy that the scenario explained 49.45% of the observed variation for this trait over both studied irrigation scenarios (Table 2). In contrast, there had been a less reduction in FAest and FAeth. As such, the effect of the irrigation

scenarios explained only 8.0 and 6.6 % of the observed variation in FAest and FAeth, respectively (Table 2).

Table 2. Agronomical, cell wall composition and degradability traits for the two parental inbred lines F271 and Cm484.

Categories	Traits[e]	Units	Irrigated		Non-Irrigated		% of response		Genetic[g]	Irrigation scenario[g]	Genetic x Irrigation scenario[g]
			F271[f]	Cm484[f]	F271[f]	Cm484[f]	F271	Cm484			
Agronomic	Plant height	cm	172.08 ^{d} ± 9.73	134.06 ^{b} ± 8.78	143.52 ^{c} ± 11.22	122.91 ^{a} ± 7.94	16,6	8,3	50.2 ***	24.3 ***	4.91 ***
	Yield	t ha^{-1}	3.83 ^{c} ± 0.36	2.48 ^{b} ± 0.39	2.43 ^{ab} ± 0.75	2.09 ^{c} ± 0.45	36,6	15,7	23.69 ***	29.43 ***	9.23 ***
Cell Wall residue	NDF	%DM	52.82 ^{b} ± 2.01	47.83 ^{a} ± 1.75	54.58 ^{c} ± 2.2	52.45 ^{b} ± 2.14	3,3	9,7	30.99 ***	24.02 ***	4.99 ***
Degradability	IVDMD	%DM	46.78 ^{a} ± 2.38	55.68 ^{c} ± 1.88	50.95 ^{b} ± 2.39	56.28 ^{c} ± 2.35	8,9	1,1	63.2 ***	7.81 ***	4.13 ***
	IVCWRD	%CWR	30.11 ^{a} ± 2.25	36.49 ^{b} ± 1.42	38.16 ^{c} ± 2.43	43.19 ^{d} ± 2.31	26,7	18,4	30.27 ***	53.06 ***	0.47 *
Lignin content	KL.CWR	%CWR	16.41 ^{c} ± 0.56	14.61 ^{b} ± 0.37	14.67 ^{b} ± 0.4	13.3 ^{a} ± 0.27	10,6	9,0	44.68 ***	42.49 ***	0.89 **
	ADL.NDF	%NDF	5.74 ^{c} ± 0.36	4.75 ^{b} ± 0.21	4.66 ^{b} ± 0.26	3.85 ^{a} ± 0.18	18,8	18,9	38.42 ***	48.73 ***	0.44 *
Lignin structure	βO4	µmole g^{-1} KL	587.81 ^{c} ± 56.17	492.34 ^{ab} ± 51.9	529.41 ^{b} ± 64.09	475.02 ^{a} ± 71.58	9,9	3,5	24.94 ***	6.96 ***	2.07 *
	βO4.H	µmole g^{-1} KL	15.24 ^{b} ± 1.27	13.94 ^{a} ± 0.98	17.8 ^{c} ± 1.75	17.18 ^{c} ± 1.15	16,6	23,2	5.82 ***	52.22 ***	0,68
	βO4.G	µmole g^{-1} KL	288.42 ^{b} ± 34.71	240.24 ^{a} ± 26.35	271.06 ^{b} ± 34.45	245.21 ^{a} ± 36.39	6,0	2,1	23.23 ***	0,87	2.34 *
	βO4.S	µmole g^{-1} KL	280.66 ^{c} ± 27.1	247.34 ^{b} ± 29.32	242.86 ^{ab} ± 30.01	224.33 ^{a} ± 38.35	13,5	9,3	11.88 ***	17.21 ***	1,08
	S/G		0.95 ^{b} ± 0.08	1.00 ^{c} ± 0.05	0.86 ^{a} ± 0.06	0.90 ^{a} ± 0.06	9,5	10,0	7.35 ***	32.67 ***	0,25
Hydroxycinamic acids	PCAest	mg g^{-1} CWR	14.04 ^{c} ± 1.24	11.43 ^{b} ± 0.73	10.94 ^{b} ± 0.81	8.68 ^{a} ± 0.66	22,1	24,1	33.23 ***	49.45 ***	0,19
	FAest	mg g^{-1} CWR	3.52 ^{b} ± 0.34	3.51 ^{b} ± 0.39	3.24 ^{a} ± 0.34	3.38 ^{ab} ± 0.31	8,0	3,7	0,92	8.08 ***	1,21
	Faeth	mg g^{-1} CWR	2.57 ^{b} ± 0.11	2.50 ^{a} ± 0.13	2.50 ^{a} ± 0.08	2.45 ^{a} ± 0.07	2,7	2,0	7.58 ***	6.58 ***	0,51
Structural sugars	CL.NDF	%NDF	50.38 ^{b} ± 1.62	49.87 ^{ab} ± 1.2	50.24 ^{b} ± 1.25	49.2 ^{a} ± 0.93	0,3	1,3	8.47 ***	2.41 .	1
	GLU	%CWR	39.67 ^{c} ± 1.23	38.01 ^{b} ± 1.04	37.53 ^{b} ± 0.85	36.43 ^{a} ± 0.99	5,4	4,2	19.32 ***	37.87 ***	0.86 .
	HC.NDF	%NDF	43.84 ^{a} ± 1.97	45.33 ^{b} ± 1.36	45.1 ^{b} ± 1.39	46.98 ^{c} ± 1.05	2,9	3,6	21 ***	16 ***	0,27
	ARA	%CWR	3.30 ^{a} ± 0.16	3.64 ^{b} ± 0.12	3.61 ^{b} ± 0.12	3.89 ^{c} ± 0.1	9,4	6,9	39.37 ***	34.54 ***	0,41
	GAL	%CWR	0.67 ^{a} ± 0.14	0.85 ^{b} ± 0.14	0.93 ^{b} ± 0.11	1.10 ^{c} ± 0.11	38,8	29,4	20.15 ***	42.37 ***	0,01
	XYL	%CWR	19.94 ^{b} ± 0.71	19.38 ^{a} ± 0.65	19.42 ^{ab} ± 0.79	18.99 ^{a} ± 0.97	2,6	2,0	8.42 ***	8.48 ***	0,18

[e]NDF, neutral detergent fiber; IVDMD, in vitro dry matter degradability; IVCWRD, in vitro cell wall residus degradability; ADL, acid detergent lignin; KL, Klason lignin; PCAest, esterified para-coumaric acid; FAeth, etherified ferulic acid; FAest, esterified ferulic acid; CL, cellulose; HC, hemicellulose; GLU, glucose; ARA, arabinose; GAL, galactose;

[f]When two samples show different letters after the mean, the difference between them is significant (normal letters, $P < 0.05$). [g]r^2 value for genetic, irrigation scenario and genetic-irrigation scenario interaction. * significant at $p < 0.05$, ** significant at $p < 0.01$ and *** significant at $p < 0.001$.

It is worth noting that F271 and Cm484 responded differently to the irrigation scenarios (Table 2). The agronomical traits were more impacted by the irrigation scenarios in F271 (reduction of 16.6% and 36.6% of plant height and biomass yield, respectively, in the NI scenario compared to the I scenario) than in Cm484 (reduction of 8.3% and 15.7% of plant height and biomass yield, respectively, in NI scenario compared to the I scenario). The increase in IVDMD and IVCWRD was also more pronounced in F271 (increased of 8.9% and 26.7% of IVDMD and IVCWRD in the NI scenario compared to the I scenario, respectively) than in Cm484 (increased of 1.1% and 18.4% of IVDMD and IVCWRD in the NI scenario compared to the I scenario, respectively). In contrast, the increase in NDF was more pronounced in Cm484 (9.7%) than in F271 (3.3%) under the NI scenario. Surprisingly, F271 and Cm484 showed similar responses to the irrigation scenarios for the lignin contents. These findings were in accordance to a low r^2 (0.89% and 0.44% for KL.CWR and ADL.NDF, respectively), whereas a significant interaction between the genotype and the irrigation scenarios effect was observed.

In the F271 × Cm484 RIL progeny, cell wall composition and degradability responded to the irrigation scenario

The agronomical and cell wall-related traits were then evaluated in the F271 × Cm484 RIL progeny (Table 3). The trait variation was higher in the RIL progeny than in the parental lines, illustrating the so-called transgression effect, except for IVDMD and ARA under the I condition. Moreover, a strong genotypic effect was observed for all traits. Importantly, large genotypic variability among the F271 × Cm484 RIL progeny was found in the general trend under both irrigation scenarios as shown by the minimal and maximal values (Table 3). This allowed us to obtain medium to high heritabilities for the investigated traits. The strongest heritabilities (h^2 above 0.7) were observed for plant height, biomass yield, IVCWRD, KL.CWR, ADL.NDF, PCAest, FAest, CL.NDF, HC.NDF and ARA. On the other hand, lowest heritabilities (h^2 < 0.6) were observed for traits related to lignin structure, GLU, GAL and XYL.

Principal component analysis (PCA) was performed with all the measured variables under both irrigation scenarios (Fig. 1). The first three principal components (PCs) explained 80% of the variation due to all investigated traits. The traits that contributed the most to the first principal component (PC1) were IVCWRD, KL.CWR, ADL.NDF and PCAest (Fig. 1A and supplemental Table 1). These traits were strongly correlated (*r* ranging from 0.71 to 0.95 in both irrigation scenarios; Fig. 1C) and the IVCWRD was in opposition to the KL.CWR, ADL.NDF and PCAest. It is worth noting that these traits were significantly and strongly impacted by the irrigation scenarios (Table 3). Indeed, for these traits, the percentage of the variance explained by the irrigation scenarios effect was always higher than that explained by the genotypic effect (Table 3). Hence, PC1 contributed to 59% of the irrigation scenarios effect (Fig. 1B).

Table 3. Agronomical, cell wall composition and degradability traits in the RIL progeny.

Categories	Traits[a]	Units	Irrigated			Non-Irrigated			Genetic[b]	Irrigation scenario[b]	Genetic x Irrigation scenario[b]	h^{2c}
			Mean	Min	Max	Mean	Min	Max				
Agronomic	Plant height	cm	149.18 ± 18.59	99,16	197,97	127.07 ± 13.73	91,95	185,04	49.17 ***	29.04 ***	5.14 ***	0,87
	Yield	t ha^{-1}	3.01 ± 0.92	0,92	6,50	2.18 ± 0.6	0,99	4,76	46.02 ***	19.04 ***	7.46	0,75
Cell Wall residue	NDF	%DM	53.14 ± 2.91	46,14	61,40	54.91 ± 2.52	48,40	60,74	45.48 ***	6.66 ***	15.05 ***	0,62
Degradability	IVDMD	%DM	49.44 ± 2.63	44,08	56,27	53 ± 2.56	45,42	59,40	27.11 ***	57.23 ***	3.85 *	0,65
	IVCWRD	%CWR	33.42 ± 1.95	28,39	38,23	41.31 ± 2.07	35,88	46,54	31.42 ***	55.89 ***	2.86	0,77
Lignin content	KL.CWR	%CWR	15.44 ± 0.56	13,85	17,17	13.9 ± 0.59	12,48	15,31	36.91 ***	22.59 ***	12.22 ***	0,83
	ADL.NDF	%NDF	5.16 ± 0.4	4,07	6,43	4.12 ± 0.42	3,03	5,08	15.06 ***	68.05 ***	3.26 **	0,88
Lignin structure	βO4	µmole g^{-1} KL	504.79 ± 63.72	313,91	652,76	482.36 ± 57.45	276,36	603,11	38.32 ***	2.66 ***	12.76	0,56
	βO4.H	µmole g^{-1} KL	14.97 ± 1.65	9,86	21,24	18.06 ± 1.35	14,01	20,62	24.43 ***	34.03 ***	8.51	0,56
	βO4.G	µmole g^{-1} KL	248.24 ± 34.82	132,14	329,08	254.52 ± 30.07	152,30	309,80	38.2 ***	0.15	12.29	0,57
	βO4.S	µmole g^{-1} KL	241.94 ± 32.81	132,45	334,45	217.98 ± 30.2	115,28	287,12	36.04 ***	8.46 ***	12.57	0,54
	S/G		0.96 ± 0.06	0,81	1,14	0.85 ± 0.07	0,70	1,05	29.76 ***	29.28 ***	7.49	0,66
Hydroxycinamic acids	PCAest	mg g^{-1} CWR	12.37 ± 1.09	9,51	14,91	9.39 ± 1.13	6,64	12,42	26.43 ***	55.61 ***	4.48 *	0,82
	FAest	mg g^{-1} CWR	3.3 ± 0.4	2,16	4,37	3.17 ± 0.39	2,14	4,08	49.31 ***	2.81 ***	10.92 **	0,73
	Faeth	mg g^{-1} CWR	2.54 ± 0.07	2,29	2,75	2.43 ± 0.07	2,26	2,65	27.54 ***	24.96 ***	11.54 ***	0,53
Structural sugars	CL.NDF	%NDF	50.51 ± 1.36	47,38	54,38	49.87 ± 1.44	46,44	53,92	52.38 ***	2.55 ***	9.47	0,74
	GLU	%CWR	38.35 ± 1.02	35,16	42,51	37.19 ± 0.89	34,79	40,02	30.75 ***	17.5 ***	13.49 **	0,51
	HC.NDF	%NDF	44.28 ± 1.68	39,78	48,15	46.02 ± 1.8	40,87	50,53	51.33 ***	13.43 ***	7.41	0,79
	ARA	%CWR	3.45 ± 0.13	2,97	3,77	3.73 ± 0.16	3,23	4,11	34.97 ***	38.19 ***	7.17 **	0,78
	GAL	%CWR	0.74 ± 0.1	0,38	1,01	0.96 ± 0.11	0,59	1,24	25.3 ***	37.23 ***	9.29 *	0,58
	XYL	%CWR	19.18 ± 0.47	16,92	20,56	19.04 ± 0.38	17,85	19,89	18.79 ***	1.28 ***	8.32 *	0,49

[a]NDF, neutral detergent fiber; IVDMD, *in vitro* dry matter degradability; IVCWRD, *in vitro* cell wall residus degradability; ADL, acid detergent lignin; KL, Klason lignin; PCA, *para*-coumaric acid; FA, ferulic acid; CL, cellulose; HC, hemicellulose; GLU, glucose; ARA, arabinose; GAL, galactose; XYL, xylose.

[b]r^2 value for genetic, irrigation scenario and genetic-irrigation scenario interaction. [c]Broad-sense heritability. * significant at $p < 0.05$, ** significant at $p < 0.01$ and *** significant at $p < 0.001$.

The traits that contributed the most to the second principal component (PC2) were FAest, □O4 yield, □O4.G and □O4.S (Fig.1A and supplemental Table 1). The correlation between FAest and the other traits was lower (*r* ranging from 0.32 to 0.36) than that observed between the □O4 yield and the □O4.G and □O4.S traits (*r* ranging from 0.8 to 0.96 in the I scenario; Fig. 1C). Furthermore, the percentage of variance explained by the irrigation scenarios was strikingly lower than that obtained for the genotypic effect (Table 3). Of note, the irrigation scenario had no significant impact on BO4.G in the F271 × Cm484 RIL progeny similarly to that was observed in the two parental inbred lines (Table 2). Consistently, PC2 did not allowed us to distinguish RIL cultivated under the I or the NI scenario (Fig. 1B).

The traits that contributed the most to the third principal component (PC3) were BO4H and NDF (Fig. 1A and supplemental Table 1). PC3 contributed to 16.01% of the irrigation scenarios effect and allowed us to better separate RILs cultivated under each irrigation scenario (Fig. 1B). Overall, only a few traits (NDF, KL.CWR, FAest, FAeth and GLU) showed strong (r^2>10%) and significant effects for the interaction between genotype and irrigation scenarios (Table 3). Consequently, these results suggest that there may be variation of the response to the irrigation scenario in the F271 × Cm484 RIL progeny for these traits only.

Fifteen clusters encompassed more than two third of the 213 constitutive QTLs detected

Using a mixed model, we detected constitutive QTLs, when the "m_p" term was significant (see equation (3) in materials and methods). Allelic variation present at a constitutive QTL for a given trait impacted the variation of this trait whatever the year and the irrigation scenario. For plant height, biomass yield and the 19 cell wall traits, a total of 213 constitutive QTLs were detected, spread over the 10 maize chromosomes (supplemental Table 2 and supplemental Fig. 1). Over the 213 constitutive QTLs detected, 142 (ie two-thirds) mapped in 15 clusters (Fig. 2 and supplemental Table 2). These 15 clusters contained six to 14 QTLs for the investigated traits. The 11-const cluster on chromosome 6 included 14 QTLs for 19 of the 21 investigated traits. This cluster had the highest r^2 identified among all the cluster detected in this study. At the agronomic level, 19 QTLs were detected for plant height, but only 5 colocated with the 15 identified cluster. For biomass yield, 12 QTLs were detected, but none of them were located within the 15 identified clusters. The 11 QTLs for IVCWRD, over the 14 detected, were colocated with QTLs for KL.CWR, ADL.NDF and PCAest, except three of them in clusters 7-const, 9-const and 15-const (Fig. 2 and supplemental Table 2). At the cluster 7-const, the QTL for IVCWRD colocated with QTLs for KL.CWR, ADL.NDF, FAest, CL.NDF and HC.NDF. At the cluster 9-const, the QTL for IVCWRD colocated with QTLs for KL.CWR, ADL.NDF, BO4 yield, BO4G, BO4S and PCAest.

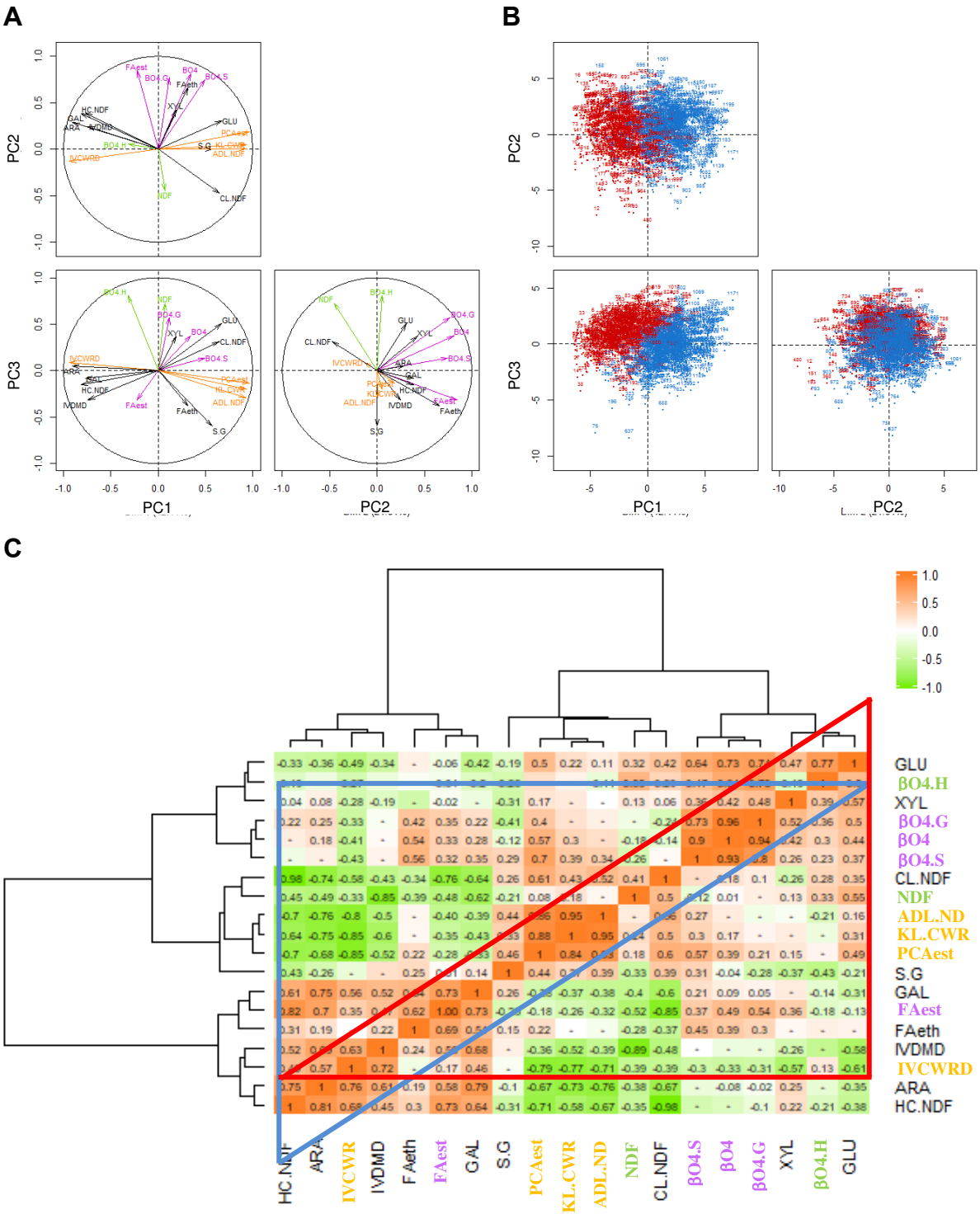


Figure 1. Principal Component Analysis (PCA) plots and correlation matrix of the investigated traits. A. Distribution of the cell wall-related traits on the first, second and third components, explaining 42.14, 21.84 and 16,01 % of the variability observed, respectively. **B**. Distribution of the F271 × Cm484 RIL progeny lines in Irrigated (blue) and Non-Irrigated (red) scenarios on the principal components PC1, PC2 and PC3. **C**. Matrix of pearson correlation in Irrigated (blue triangle, upper) and Non-Irrigated (red triangle, lower) scenarios. The positive correlations were in orange and the negative in green, the color scale were from 0 to 1 or -1.

Interestingly, 12 of the 13 detected QTLs for PC1 colocated with the 15 identified clusters (Fig. 2 and supplemental Table 2) and coincided with QTLs detected for IVCWRD, KL.CWR, ADL.NDF and PCAest. This was consistent with the fact that these traits were the major contributors to PC1 (Fig. 1A, supplemental Table 1). Seven QTLs for PC2 coincided with those for FAest, BO4yield, BO4.G and BO4.S in the 15 identified clusters (Fig. 2). This was consistent with the fact that these traits were the major contributors to PC2 (Fig. 1A and supplemental Table 1). Among the 11 identified QTLs for PC3, 7 colocated with the 15 identified clusters (Fig. 2). These QTLs coincided with those for BO4H and NDF, which were the traits that contributed the most to PC3 (Fig. 1A and supplemental Table 1). Hence, 26 QTLs for PCAest coordinates on PC1, PC2 and PC3 summarized the 15 obtained clusters.

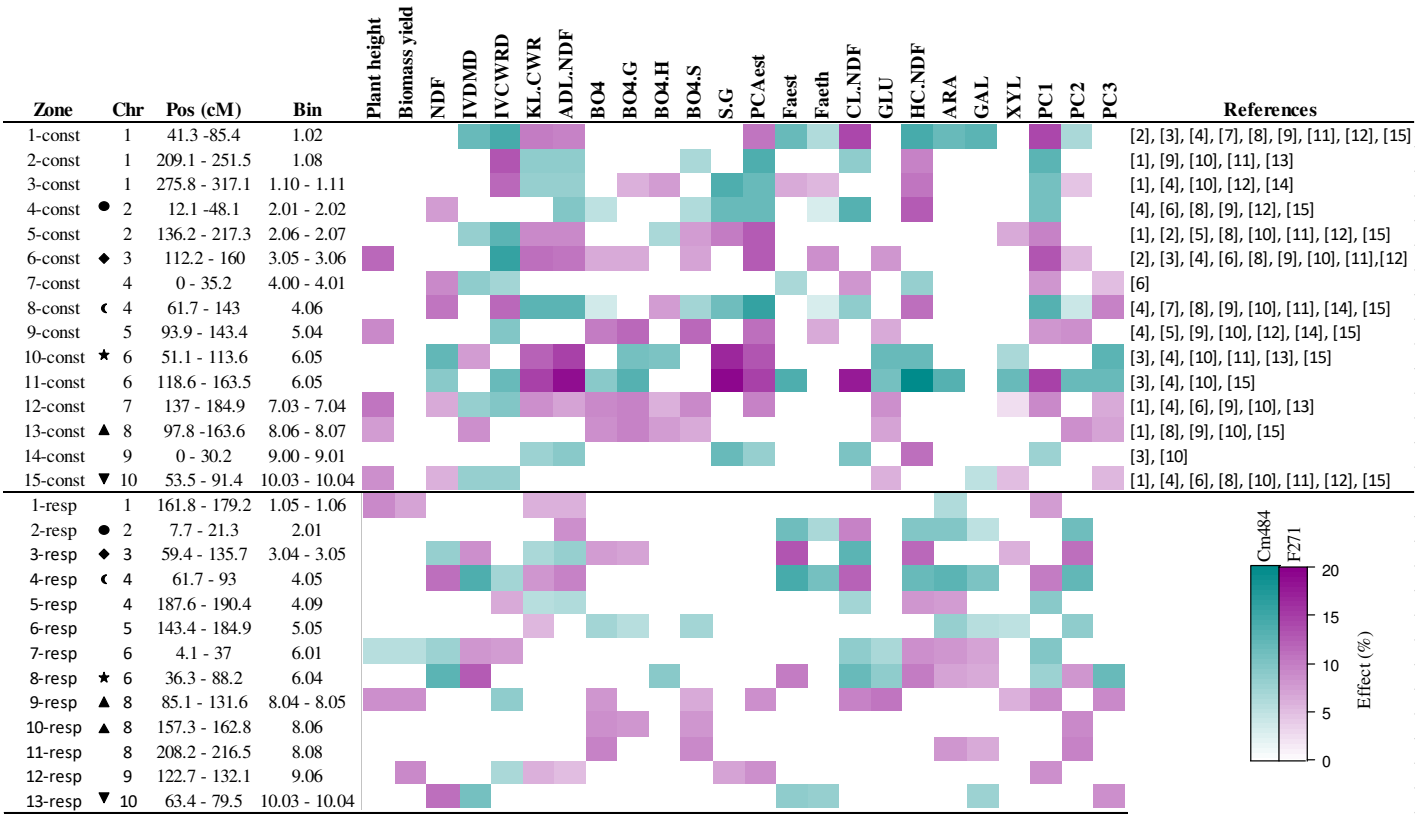
Thirteen clusters encompassed more than 60% of the 149 responsive QTL detected

Using the same mixed model, we next detected responsive QTLs, when the "m_p x e_k" term was significant (see equation (3) in materials and methods). Allelic variation at a responsive QTL explained the differences of response found for a given trait between plants carrying F271 alleles and those carrying Cm484 alleles. A total of 149 significant responsive QTLs were identified for all the individual traits (supplemental Table 2 and supplemental Fig. 1). Among them, 93 (62%) clustered on 13 loci (Fig. 2 and supplemental Table 2). At the agronomic level, 6 responsive QTLs for plant height and 8 responsive QTLs for biomass yield were detected. However, only 3 responsive QTLs for plant height and 4 responsive QTLs for biomass yield colocated with the 13 identified clusters. Interestingly, 5 of the 6 responsive QTLs for IVCWRD colocated with responsive QTLs for other traits in the 13 clusters. The two clusters 7-resp and 9-resp included responsive QTLs for plant height, biomass yield, IVCWRD, structural sugar and PCAest. In contrast, the two clusters 4-resp and 5-resp grouped responsive QTLs for IVCWRD, lignin content, HC.NDF and CL.NDF. The cluster 4-resp also included responsive QTL for FAest and FAeth.

Responsive QTLs for PCs were also mapped (supplemental Table 2 and Fig. 2). Seven of the eight responsive QTLs for PC1 colocated in seven cluster (1-resp, 4-resp, 5-resp, 7-resp, 8-resp, 9-resp and 12-resp) with responsive QTLs for traits that were the major contributors to PC1 (namely IVCWRD, KL.CWR, ADL.NDF and PCAest; Fig. 1A and supplemental Table 1). Additionally, seven of the 11 responsive QTLs for PC2 colocated with responsive QTLs for FAest (2-resp, 3-resp, 4-resp and 8-resp), □O4 yield, □O4.G or □O4.S (3-resp, 6-resp, 10-resp and 11-resp). Only three of the seven responsive QTLs for PC3 colocated with clusters of responsive QTLs. At the 8-resp locus, a responsive QTL for PC3 colocated with responsive QTLs for □O4.H and NDF which were the traits that contributed the most to PC3. However, at cluster 9-resp,

the presence of a responsive QTL for PC3 was not associated with the presence of responsive QTLs for ?O4.H nor NDF.

It is worth noting that six of the 13 clusters of responsive QTLs did not colocate with the 15 clusters of constitutive QTLs (Figure 2). Furthermore, the traits involved in 'constitutive clusters' colocating with 'responsive clusters', were not always the same. As such, the constitutive cluster 4-const which consisted of 10 QTLs and the responsive cluster 2-resp which consisted of 8 QTLs, shared only 5 QTLs for common traits.



Zone	Chr	Pos (cM)	Bin	References
1-const	1	41.3 -85.4	1.02	[2], [3], [4], [7], [8], [9], [11], [12], [15]
2-const	1	209.1 - 251.5	1.08	[1], [9], [10], [11], [13]
3-const	1	275.8 - 317.1	1.10 - 1.11	[1], [4], [10], [12], [14]
4-const	2	12.1 -48.1	2.01 - 2.02	[4], [6], [8], [9], [12], [15]
5-const	2	136.2 - 217.3	2.06 - 2.07	[1], [2], [5], [8], [10], [11], [12], [15]
6-const	3	112.2 - 160	3.05 - 3.06	[2], [3], [4], [6], [8], [9], [10], [11],[12]
7-const	4	0 - 35.2	4.00 - 4.01	[6]
8-const	4	61.7 - 143	4.06	[4], [7], [8], [9], [10], [11], [14], [15]
9-const	5	93.9 - 143.4	5.04	[4], [5], [9], [10], [12], [14], [15]
10-const	6	51.1 - 113.6	6.05	[3], [4], [10], [11], [13], [15]
11-const	6	118.6 - 163.5	6.05	[3], [4], [10], [15]
12-const	7	137 - 184.9	7.03 - 7.04	[1], [4], [6], [9], [10], [13]
13-const	8	97.8 -163.6	8.06 - 8.07	[1], [8], [9], [10], [15]
14-const	9	0 - 30.2	9.00 - 9.01	[3], [10]
15-const	10	53.5 - 91.4	10.03 - 10.04	[1], [4], [6], [8], [10], [11], [12], [15]
1-resp	1	161.8 - 179.2	1.05 - 1.06	
2-resp	2	7.7 - 21.3	2.01	
3-resp	3	59.4 - 135.7	3.04 - 3.05	
4-resp	4	61.7 - 93	4.05	
5-resp	4	187.6 - 190.4	4.09	
6-resp	5	143.4 - 184.9	5.05	
7-resp	6	4.1 - 37	6.01	
8-resp	6	36.3 - 88.2	6.04	
9-resp	8	85.1 - 131.6	8.04 - 8.05	
10-resp	8	157.3 - 162.8	8.06	
11-resp	8	208.2 - 216.5	8.08	
12-resp	9	122.7 - 132.1	9.06	
13-resp	10	63.4 - 79.5	10.03 - 10.04	

Figure 2. Summary of the clusters of constitutive and responsive QTLs identified for agronomical, cell wall composition, degradability and PCA coordinates components traits. The color corresponded to the allele increasing the traits, F271 in magenta and Cm484 in cyan. The scale of colors represented the effect at the QTL position (supplemental Table 2) over the variation of the corresponding trait on the RIL progeny lines (see materials and methods). The symbols corresponded to co-localization between constitutive and responsive QTLs. The references correspond to: [1] Méchin et al. 2001; [2] Roussel et al. 2002; [3] Cardinal et al. 2003; [4] Fontaine et al. 2003; [5] Krakowsky et al. 2005; [6] Krakowsky et al. 2006; [7] Riboulet et al. 2008; [8] Barrière et al. 2008; [9] Wei et al. 2009; [10] Truntzler et al. 2010; [11] Lorenzana et al. 2010; [12] Barrière et al. 2012; [13] Courtial et al. 2013; [14] Torres et al. 2015; [15] Leng et al. 2017.

- Discussion

Optimized and accurate NIRS equations enable the genetic analysis of a broad number of cell wall-related traits in a large set of maize stover

For maize, NIRS is routinely employed in a commercial setting for the assessment of complex forage quality traits including the analysis of cell wall digestibility properties (reviewed in Torres et al., 2015). Several published examples highlight that cell wall-related traits can be accurately predicted in maize stover. This is the case for dry matter and cell wall degradability (Jung and Phillips, 2010; Lübberstedt et al., 1997c; Riboulet et al., 2008b), as well as for the traits quantified by the Van Soest chain (Dardenne et al., 1993; Jung and Phillips, 2010; Lorenz et al., 2009). The established equations herein show also a high *r* of validation for the above mentioned traits (*r* ranging from 0.77 to 0.95).

Lignin content has been estimated following the two distinct Van Soest (ADL.NDF) and Klason (KL.CWR) methods. ADL.NDF represents the acido resistant part of the lignin polymer, whereas KL.CWR is more representative of the sum of the acido-soluble and the acido-resistant lignin part. Hames et al., 2003 (cited by Lorenz et al., 2009) reported NIRS predictive equations for both lignin contents. In the present study, the *r* of validation or cross-validation for both lignin contents was high (*r* = 0.83). It is worth noting that Barrière et al. (2010) used NIRS equations to predict both lignin contents in a RIL population and detected only 2 common QTLs for both lignin contents among the 14 detected QTLs. In the present study, 85% of the QTLs for ADL.NDF and KL.CWR colocated.

NIRS predictive equations for *p*-hydroxycinnamic acids contents have also been proposed (Jung and Phillips, 2010; Lorenzana et al., 2010; Riboulet et al., 2008b). All the proposed equations for PCAest content are satisfying with a *r* of validation ranging from 0.87 (Riboulet et al., 2008b) to 0.95 (Lorenzana et al., 2010). Our predictive equation is in the same order of magnitude (*r* of validation = 0.78). In contrast, predictive equations for FA contents are generally unreliable. Thus, the predictive equation proposed by Lorenzana et al. (2010) using stover from the studied mapping population has a r^2 of calibration of 0.04 for FA content. Jung and Philips (2010) were able to report a r^2 of 0.95 as samples used for calibration were from different plant parts harvested at different maturity stages (from immature leaf blade to mature stem samples). This r^2 of validation allows the authors to distinguish FA content between organs but does not allow to investigate the variation of FA content within the same organ harvested at the same stage. Riboulet et al., (2008) proposed NIRS predictive equation for FA contents for maize stover harvested at silage stage with a r^2 of calibration ranging from 0.64 to 0.66. In the present study, the predictive NIRS equations developed are robust, especially for FAest content (*r* of validation= 0.83, thus r2=0.69).

Thioacidolysis is a biochemical protocol to access the lignin structure (Lapierre et al., 1986). Pyrolysis has also been proposed to quantify the lignin structure (Watkins et al., 2015). Therefore, we proposed for the first time NIRS predictive equations for monolignol composition based on thioacidolyse analysis of maize stover. ?O4 yield and ?04 monolignols content in the klason lignin are robustly estimated with our established equations (r of validation ranging from 0.71 to 0.90). The prediction for the S/G ratio is slightly less robust but is nevertheless above 0.6 (r = 0.66). Pyrolysis analysis has been chosen by Jung and Philips (2010) to predict S/G ratio. However, the range of values used to establish the predictive equation for this trait was with a minimum of 0, highlighting the fact that this reference method is not accurate to estimate S/G ratio.

Overall, the NIRS predictive equations proposed herein are novel, robust and accurate to predict cell wall-related trait on maize stover harvested at silage stage. They complement existing equations recently developed by El Hage et al. (2018) using maize internodes harvested at silage stage.

A strong impact of the NI scenario on traits but an unchanged correlation structure between the traits between the two irrigation scenario

Agronomical and predicted cell wall-related traits among the RIL progeny showed a wide range of variation within each irrigation scenario. The impact of the NI scenario on agronomical and cell wall-related traits was high. Indeed, biomass yield and plant height were reduced up to 27.5% and 14.8%, respectively, on average. In sorghum, Perrier et al. (2017) noticed a reduction of plant height ranging from 17.8 to 23.4% when plants were submitted to a similar NI scenario. Furthermore, it has recently been reported that water deficit decreases lignin content in maize (El Hage et al., 2018; Emerson et al., 2014), as well as in sorghum (Perrier et al., 2017), sugarcane (dos Santos et al., 2015) and miscanthus (Emerson et al., 2014; van der Weijde et al., 2017). Consistently, in our study, the lignin and the PCAest contents were significantly reduced over the RIL progeny.

Although the irrigation scenarios were contrasted enough to provoke this agronomical and cell wall modifications, the overall structure of correlations between the traits was not affected by the NI scenario (figure 1C). Whatever the irrigation scenario, lignin and PCAest contents were tightly correlated as previously described (Hatfield et al., 1999) These two traits were strongly and negatively correlated to cell wall degradability. Zhang et al. (2011) and El Hage et al. (2018) have suggested that lignin and PCAest contents may have a distinct role on cell wall degradability. It is noteworthy that FA contents were less correlated to cell wall degradability, despite their established role in cell wall cross linking (Hatfield et al., 2017)

which was reported to be determinant for cell wall degradability (Grabber et al., 1998; Jung and Casler, 2006).

The impact of ?O4 yield on cell wall degradability has been reported by Besombes and Mazeau (2005) and Zhang et al. (2011). In the present study, the ?O4 yield was mildly correlated to cell wall degradability whatever the irrigation scenario. We observed that the NI scenario had no impact on BO4.G and BO4.S subunits, leading to the same S/G ratio in both irrigation scenario. The observed modifications on lignin and PCAest contents under the NI scenario led to a similar expected amount of S units in lignin acylated by PCAest (16.5% and 14.7% in the I and NI scenarios, respectively). However, the amount of H units in lignin was increased by the NI scenario. This is a signal observed when plants are submitted to a wide range of stress. For instance, H subunits increased when poplar plants were under ozone treatment (Cabané et al., 2004). H subunits are also terminal units of lignin polymer and their increase could contribute to the parceling out of the lignin polymer. In addition, the fact that the FAest content was not impacted under the NI scenario, while the lignin content was reduced, could reflect a lignin more fragmented under stress. Hence, the increase of cell wall degradability under the NI scenario was undoubtedly due to the decreased of lignin and PCAest contents but might also be due to the modifications of lignin structure which appeared to be more fragmented under the NI scenario.

A complex genetic architecture of cell wall composition and degradability traits over the irrigation scenarios and their responses to the NI scenario

Thus far, numerous QTL studies have been reported on traits related to cell wall composition and degradability for maize at silage stage (Barrière et al., 2001, 2008, 2012; Bohn et al., 2000; Cardinal et al., 2003; Cardinal and Lee, 2005a; Courtial et al., 2014; Fontaine et al., 2003; Krakowsky et al., 2005, 2006; Leng et al., 2018; Lorenzana et al., 2010; Lübberstedt et al., 1997a, 1997c; Méchin et al., 2001; Papst et al., 2004; Riboulet et al., 2008a; Roussel et al., 2002; Torres et al., 2015; Wei et al., 2009). These studies allowed to map over 400 QTLs all over the maize genome (Barrière et al., 2008). The present study allows the identification of 15 clusters of constitutive QTLs over the years and the irrigation scenarios for traits related to cell wall composition and degradability. All the loci detected were already mentioned in previous publications (Fig. 2). Thus, in bin 3.05 (cluster 6-const), 60% of the previous studies mapped a QTL for cell wall degradability or composition. Torres et al. (2015) already mentioned that this genomic region was often identify for these types of traits. Using the F271 x Cm484 RIL progeny, the strongest QTL region was localized on bin 6.05 (cluster 11-const). This region has already been identified as a hotspot in several studies (Courtial et al., 2013, 2014; Roussel et al., 2002) using the F271 x F288 RIL progeny, which present the common parental inbred line F271. This suggests that the alleles from F271 have a particularity, which

confers some cell wall properties relative to those from the parental inbred lines F288 and Cm484. Furthermore, the parental line F271 was found to be less degradable than the parental line Cm484, in agreement with previous studies (El Hage et al., 2018; Méchin et al., 2000). However, it is worth noting that the alleles conferring a better cell wall degradability at the constitutive detected QTLs did not always come from the better degradable inbred line Cm484. Thus, the allele from F271 conferred an increase of IVCWRD for three of the 15 detected clusters of constitutive QTLs (2-const, 3-const and 8-const).

No QTL for biomass yield was mapped among the constitutive clusters detected in the present study. Nevertheless, several QTLs for biomass yield were detected elsewhere in the genome (Supplemental Figure 1 and Supplemental Table 2). This result suggests that cell wall degradability could be increased without impacting biomass yield (Baldy et al., 2017). Additionally, numerous colocations were identified between constitutive QTLs for IVCWRD and QTLs for LK.CWR or ADL.NDF in a manner that is consistent with the strong correlation observed between the cell wall degradability and the lignin content. However, QTLs for IVCWRD were not always colocated with QTLs for lignin content in agreement with previous observations (Penning et al., 2014; Truntzler et al., 2010). We noticed that QTLs for IVCWRD and PCAest were more often colocated. For instance, the cluster 9-const involved QTLs for IVCWRD, BO4 yield, PCAest and FAest, suggesting an independent potential role of these traits in the variation of the cell wall degradability as previously described (Grabber, 2005; Zhang et al., 2011). Collectively, our results highlight again the strong complexity of the genetic determinism of traits related to the cell wall (Barrière et al., 2008; Torres et al., 2015).

In maize, QTLs for drought tolerance in grain yield have been largely studied and reported (Collins et al., 2008; Millet et al., 2016; Ribaut et al., 2010; Ribaut and Ragot, 2007). The present study identifies for the first time QTLs for traits related to cell wall degradability and composition in response to water deficit. It is noteworthy that while the interaction “genotype x irrigation scenario” among the RIL progeny did not contribute a lot to the observed trait variation, the use of a mixed linear model (Alimi et al., 2013) allowed the detection of significant responsive QTLs for all traits. Interestingly, only half of the responsive QTL clusters co-located with constitutive QTL clusters, suggesting that the genetic determinism and the molecular mechanisms involved in cell wall development are different from those involved in response to water deficit. Furthermore, our results show that the lignin content does not explain all the variation of the cell wall degradability in response to the irrigation scenario. Some responsive QTLs for IVCWRD co-located with responsive QTLs for biomass yield, and in each case, alleles that increased IVCWRD in response to the NI scenario decreased the biomass production. This shall be taken into account to select resilient lines under water stress condition.

- **Acknowledgments**
- This study was supported by the French Government Grants (LabEx Saclay Plant Sciences-SPS, Grants ANR-10-LABX- 0040-SPS and ANR-11-BTBR-0006 BIOMASS FOR THE FUTURE), managed by the French National Research Agency under an “Investments for the Future” program (Grant ANR- 11-IDEX-0003-02).
-
- **Author’s contributions**
- MR, VM and SC designed the study and supervised data collection. FEH, MPJ, AB, SL, CH, SC, VM and MR collected the samples. CB and CP conducted the field experiments. YG, MPJ and EG measured the phenotypic data. LV, FEH, MF, LM and MR conducted the genetic study. LV, SC, VM and MR wrote the manuscript.
-
- **Statement of conflict of interest**
- The authors declare no conflict of interest
- **Supplementary material**
- **Supplemental_table_1.xlsx**: Principal component analysis.
- **Supplemental_figure_1.png**: Representation of the constitutive and responsive QTLs detected for the agranomical and cell-wall related traits.

References

Alimi, N. A., Bink, M. C., Dieleman, J. A., Magán, J. J., Wubs, A. M., Palloix, A., et al. (2013). Multi-trait and multi-environment QTL analyses of yield and a set of physiological traits in pepper. *Theor. Appl. Genet.* 126, 2597–2625. doi:10.1007/s00122-013-2160-3.

Aufrère, J., and Michalet-Doreau, B. (1983). In vivo digestibility and prediction of digestibility of some by-products. in *EEC Seminar, Belgique*.

Baldy, A., Jacquemot, M.-P., Griveau, Y., Bauland, C., Reymond, M., and Mechin, V. (2017). Energy Values of Registered Corn Forage Hybrids in France over the Last 20 Years Rose in a Context of Maintained Yield Increase. *Am. J. Plant Sci.* 08, 1449–1461. doi:10.4236/ajps.2017.86099.

Barrière, Y., Gibelin, C., Argiller, O., and Méchin, V. (2001). Genetic analysis in recombinant inbred lines of early dent forage maize. I: QTL mapping for yield - earliness - starch and crude protein contents from per se value and top cross experiments. *Maydica* 47, 9–20. Available at: http://agris.fao.org/agris-search/search.do?recordID=IT2002062408 [Accessed May 17, 2018].

Barrière, Y., Méchin, V., Denoue, D., Bauland, C., and Laborde, J. (2010). QTL for Yield, Earliness, and Cell Wall Quality Traits in Topcross Experiments of the F838 × F286 Early Maize RIL Progeny. *Crop Sci.* 50. doi:10.2135/cropsci2009.11.0671.

Barrière, Y., Méchin, V., Lefevre, B., and Maltese, S. (2012). QTLs for agronomic and cell wall traits in a maize RIL progeny derived from a cross between an old Minnesota13 line and a modern Iodent line. *Theor. Appl. Genet.* 125, 531–549. doi:10.1007/s00122-012-1851-5.

Barrière, Y., Ralph, J., Méchin, V., Guillaumie, S., Grabber, J. H., Argillier, O., et al. (2004). Genetic and molecular basis of grass cell wall biosynthesis and degradability. II. Lessons from brown-midrib mutants. *C. R. Biol.* 327, 847–860. doi:10.1016/J.CRVI.2004.05.010.

Barrière, Y., Riboulet, C., Mechin, V., Maltese, S., Pichon, M., Cardinal, A., et al. (2007). Genetics and genomics of lignification in grass cell walls based on maize as model species. *Genes, Genomes and Genomics* 1, 133–156. Available at: http://203.183.32.151/JournalsSup/images/0712/GGG_1(2)133-156o.pdf%5Cnhttp://www.globalsciencebooks.info/JournalsSup/images/0712/GGG_1(2)133-156o.pdf.

Barrière, Y., Thomas, J., and Denoue, D. (2008). QTL mapping for lignin content, lignin monomeric composition, p-hydroxycinnamate content, and cell wall digestibility in the maize recombinant inbred line progeny F838 × F286. *Plant Sci.* 175, 585–595. doi:10.1016/J.PLANTSCI.2008.06.009.

Baucher, M., Bernard-vailhé, M. A., Chabbert, B., Besle, J.-M., Opsomer, C., Van Montagu, M., et al. (1999). Down-regulation of cinnamyl alcohol dehydrogenase in transgenic alfalfa (Medicago sativa L.) and the effect on lignin composition and digestibility. *Plant Mol. Biol.* 39, 437–447. doi:10.1023/A:1006182925584.

Besombes, S., and Mazeau, K. (2005). The cellulose/lignin assembly assessed by molecular modeling. Part 2: Seeking for evidence of organization of lignin molecules at the interface with cellulose. *Plant Physiol. Biochem.* 43, 277–286. doi:10.1016/j.plaphy.2005.02.004.

Bichot, A., Delgenès, J.-P., Méchin, V., Carrère, H., Bernet, N., and García-Bernet, D. (2018). *Understanding biomass recalcitrance in grasses for their efficient utilization as biorefinery feedstock*. doi:10.1007/s11157-018-9485-y.

Boerjan, W., Ralph, J., and Baucher, M. (2003). Lignin Biosynthesis. *Annu. Rev. Plant Biol.* 54,

519–546. doi:10.1146/annurev.arplant.54.031902.134938.
Bohn, M., Schulz, B., Kreps, R., Klein, D., and Melchinger, A. E. (2000). QTL mapping for resistance against the European corn borer (Ostrinia nubilalis H.) in early maturing European dent germplasm. *TAG Theor. Appl. Genet.* 101, 907–917. doi:10.1007/s001220051561.
Cabané, M., Pireaux, J.-C., Léger, E., Weber, E., Dizengremel, P., Pollet, B., et al. (2004). Condensed lignins are synthesized in poplar leaves exposed to ozone. *Plant Physiol.* 134, 586–94. doi:10.1104/pp.103.031765.
Cardinal, A. J., and Lee, M. (2005a). Genetic relationships between resistance to stalk-tunneling by the European corn borer and cell-wall components in maize population B73×B52. *Theor. Appl. Genet.* 111, 1–7. doi:10.1007/s00122-004-1831-5.
Cardinal, A. J., and Lee, M. (2005b). Genetic relationships between resistance to stalk-tunneling by the European corn borer and cell-wall components in maize population B73xB52. *Theor. Appl. Genet.* 111, 1–7. doi:10.1007/s00122-004-1831-5.
Cardinal, A. J., Lee, M., and Moore, K. J. (2003). Genetic mapping and analysis of quantitative trait loci affecting fiber and lignin content in maize. *Theor. Appl. Genet.* 106, 866–874. doi:10.1007/s00122-002-1136-5.
Casler, M. D., and Jung, H.-J. G. (1999). Selection and Evaluation of Smooth Bromegrass Clones with Divergent Lignin or Etherified Ferulic Acid Concentration. *Crop Sci.* 39, 1866–1873. doi:10.2135/cropsci1999.3961866x.
Collins, N. C., Tardieu, F., and Tuberosa, R. (2008). Quantitative trait loci and crop performance under abiotic stress: where do we stand? *Plant Physiol.* 147, 469–86. doi:10.1104/pp.108.118117.
Courtial, A., Méchin, V., Reymond, M., Grima-Pettenati, J., and Barrière, Y. (2014). Colocalizations Between Several QTLs for Cell Wall Degradability and Composition in the F288 × F271 Early Maize RIL Progeny Raise the Question of the Nature of the Possible Underlying Determinants and Breeding Targets for Biofuel Capacity. *BioEnergy Res.* 7, 142–156. doi:10.1007/s12155-013-9358-8.
Courtial, A., Thomas, J., Reymond, M., Méchin, V., Grima-Pettenati, J., and Barrière, Y. (2013). Targeted linkage map densification to improve cell wall related QTL detection and interpretation in maize. *Theor. Appl. Genet.* 126, 1151–1165. doi:10.1007/s00122-013-2043-7.
Culhaoglu, T., Zheng, D., Méchin, V., and Baumberger, S. (2011). Adaptation of the Carrez procedure for the purification of ferulic and p-coumaric acids released from lignocellulosic biomass prior to LC/MS analysis. *J. Chromatogr. B* 879, 3017–3022. doi:10.1016/J.JCHROMB.2011.08.039.
Dardenne, P., Andrieu, J., Barrière, Y., Biston, R., Demarquilly, C., Femenias, N., et al. (1993). Composition and nutritive value of whole maize plants fed fresh to sheep. II. Prediction of the in vivo organic matter digestibility. *Ann. Zootech.* 42, 251–270. doi:10.1051/animres:19930302.
Dence, C. W. (1992). “The Determination of Lignin,” in (Springer, Berlin, Heidelberg), 33–61. doi:10.1007/978-3-642-74065-7_3.
Denmead, O. T., and Shaw, R. H. (1960). The Effects of Soil Moisture Stress at Different Stages of Growth on the Development and Yield of Corn1. *Agron. J.* 52, 272. doi:10.2134/agronj1960.00021962005200050010x.
dos Santos, A. B., Bottcher, A., Kiyota, E., Mayer, J. L. S., Vicentini, R., Brito, M. dos S., et al. (2015). Water Stress Alters Lignin Content and Related Gene Expression in Two

Sugarcane Genotypes. *J. Agric. Food Chem.* 63, 4708–4720. doi:10.1021/jf5061858.

El Hage, F., Legland, D., Borrega, N., Jacquemot, M.-P., Griveau, Y., Coursol, S., et al. (2018). Tissue Lignification, Cell Wall p -Coumaroylation and Degradability of Maize Stems Depend on Water Status. *J. Agric. Food Chem.* 66, 4800–4808. doi:10.1021/acs.jafc.7b05755.

Elshire, R. J., Glaubitz, J. C., Sun, Q., Poland, J. A., Kawamoto, K., Buckler, E. S., et al. (2011). A robust, simple genotyping-by-sequencing (GBS) approach for high diversity species. *PLoS One* 6, e19379. doi:10.1371/journal.pone.0019379.

Emerson, R., Hoover, A., Ray, A., Lacey, J., Cortez, M., Payne, C., et al. (2014). Drought effects on composition and yield for corn stover, mixed grasses, and Miscanthus as bioenergy feedstocks. *Biofuels* 5, 275–291. doi:10.1080/17597269.2014.913904.

Fontaine, A.-S., Briand, M., and Barrière, Y. (2003). Genetic variation and QTL mapping of para-coumaric and ferulic acid. *Maydica* 48, 75–84.

Gabrielsen, B., Vogel, K., and Ward, J. (1990). Alkali-Labile Cell-Wall Phenolics and Forage Quality in Switchgrasses Selectedfor Differing Digestibility. *Crop Sci.* 30, 1313–1320. Available at: http://digitalcommons.unl.edu/usdaarsfacpub/1879 [Accessed October 5, 2018].

Glaubitz, J. C., Casstevens, T. M., Lu, F., Harriman, J., Elshire, R. J., Sun, Q., et al. (2014). TASSEL-GBS: A High Capacity Genotyping by Sequencing Analysis Pipeline. doi:10.1371/journal.pone.0090346.

Goering, H. K., and Van Soest, P. J. (1970). Forage fiber analyses. *Agiculture Handb.* 379, 387–598. Available at: https://naldc.nal.usda.gov/download/CAT87209099/PDF [Accessed May 17, 2018].

Goujon, T., Ferret, V., Mila, I., Pollet, B., Ruel, K., Burlat, V., et al. (2003). Down-regulation of the AtCCR1 gene in Arabidopsis thaliana: effects on phenotype, lignins and cell wall degradability. *Planta* 217, 218–228. doi:10.1007/s00425-003-0987-6.

Grabber, J. H. (2005). How Do Lignin Composition, Structure, and Cross-Linking Affect Degradability? A Review of Cell Wall Model Studies. *Crop Sci.* 45, 820. doi:10.2135/cropsci2004.0191.

Grabber, J. H., Hatfield, R. D., and Ralph, J. (1998). Diferulate Cross-Links Impede the Enzymatic Degradation of Non-Ligniüed Maize Walls. *J Sci Food Agric* 77, 193–200. Available at: https://pubag.nal.usda.gov/download/13662/PDF [Accessed May 16, 2018].

Grabber, J. H., Hatfield, R. D., and Ralph, J. (2003). Apoplastic pH and Monolignol Addition Rate Effects on Lignin Formation and Cell Wall Degradability in Maize. *J. Agric. Food Chem.* 51, 4984–4989. doi:10.1021/JF030027C.

Grabber, J. H., Quideau, S., and Ralph, J. (1996). p-coumaroylated syringyl units in maize lignin: Implications for β-ether cleavage by thioacidolysis. *Phytochemistry* 43, 1189–1194. doi:10.1016/S0031-9422(96)00431-1.

Gray, J., Caparrós-Ruiz, D., and Grotewold, E. (2012). Grass phenylpropanoids: Regulate before using! *Plant Sci.* 184, 112–120. doi:10.1016/J.PLANTSCI.2011.12.008.

Harholt, J., Jensen, J. K., Sørensen, S. O., Orfila, C., Pauly, M., and Scheller, H. V. (2006). ARABINAN DEFICIENT 1 is a putative arabinosyltransferase involved in biosynthesis of pectic arabinan in Arabidopsis. *Plant Physiol.* 140, 49–58. doi:10.1104/pp.105.072744.

Hartley, R. D. (1972). p-Coumaric and ferulic acid components of cell walls of ryegrass and their relationships with lignin and digestibility. *J. Sci. Food Agric.* 23, 1347–1354. doi:10.1002/jsfa.2740231110.

Hatfield, R. D., Grabber, J. H., Ralph, J., and Brei, K. (1999). Using the Acetyl Bromide Assay To Determine Lignin Concentrations in Herbaceous Plants: Some Cautionary Notes. *J. Agric. Food Chem.* 47, 628–632. doi:10.1021/JF9808776.

Hatfield, R. D., Rancour, D. M., and Marita, J. M. (2017). Grass Cell Walls: A Story of Cross-Linking. *Front. Plant Sci.* 7, 2056. doi:10.3389/fpls.2016.02056.

Jung, H.-J. G., and Casler, M. D. (2006). Maize Stem Tissues: Impact of Development on Cell Wall Degradability. *Crop Sci.* 46, 1801–1809. doi:10.2135/cropsci2006.02-0086.

Jung, H. G., and Phillips, R. L. (2010). Putative Seedling Ferulate Ester (sfe) Maize Mutant: Morphology, Biomass Yield, and Stover Cell Wall Composition and Rumen Degradability. *Crop Sci.* 50. doi:10.2135/cropsci2009.04.0191.

Krakowsky, M. D., Lee, M., and Coors, J. G. (2005). Quantitative trait loci for cell-wall components in recombinant inbred lines of maize (Zea mays L.) I: Stalk tissue. *Theor. Appl. Genet.* 111, 337–346. doi:10.1007/s00122-005-2026-4.

Krakowsky, M. D., Lee, M., and Coors, J. G. (2006). Quantitative trait loci for cell wall components in recombinant inbred lines of maize (Zea mays L.) II: Leaf sheath tissue. *Theor. Appl. Genet.* 112, 717–726. doi:10.1007/s00122-005-0175-0.

Lapierre, C., Monties, B., and Rolando, C. (1986). Preparative Thioacidolysis of Spruce Lignin: Isolation and Identification of Main Monomeric Products. *Holzforschung* 40, 47–50. Available at: https://www.degruyter.com/downloadpdf/j/hfsg.1986.40.issue-1/hfsg.1986.40.1.47/hfsg.1986.40.1.47.pdf [Accessed May 17, 2018].

Leng, P., Ouzunova, M., Landbeck, M., Wenzel, G., Eder, J., Darnhofer, B., et al. (2018). Quantitative trait loci mapping of forage stover quality traits in six mapping populations derived from European elite maize germplasm. *Plant Breed.* 137, 139–147. doi:10.1111/pbr.12572.

Lorenz, A. J., Coors, J. G., De Leon, N., Wolfrum, E. J., Hames, B. R., Sluiter, A. D., et al. (2009). Characterization, Genetic Variation, and Combining Ability of Maize Traits Relevant to the Production of Cellulosic Ethanol. *Crop Sci.* 49. doi:10.2135/cropsci2008.06.0306.

Lorenzana, R. E., Lewis, M. F., Jung, H.-J. G., and Bernardo, R. (2010). Quantitative Trait Loci and Trait Correlations for Maize Stover Cell Wall Composition and Glucose Release for Cellulosic Ethanol. *Crop Sci.* 50, 541–555. doi:10.2135/cropsci2009.04.0182.

Lu, F., and Ralph, J. (1999). Detection and determination of p-coumaroylated units in lignins. *J. Agric. Food Chem.* 47, 1988–92. Available at: http://www.ncbi.nlm.nih.gov/pubmed/10552483 [Accessed May 17, 2018].

Lübberstedt, T., Melchinger, A. E., Klein, D., Degenhardt, H., and Paul, C. (1997a). QTL Mapping in Testcrosses of European Flint Lines of Maize: II. Comparison of Different Testers for Forage Quality Traits. *Crop Sci.* 37, 1913–1922. Available at: https://dl.sciencesocieties.org/publications/cs/pdfs/37/6/CS0370061913 [Accessed December 8, 2017].

Lübberstedt, T., Melchinger, A. E., Schon, C. C., Utz, H. F., and Klein, D. (1997b). Cell Biology & Molecular Genetics. *Crop Sci.* 37, 921–931.

Lübberstedt, T., Melchinger, A. E., Schon, C. C., Utz, H. F., and Klein, D. (1997c). QTL Mapping in Testcrosses of European Flint Lines of Maize: I. Comparison of Different Testers for Forage Yield Traits. *Crop Sci.* 37, 921–931. Available at: https://dl.sciencesocieties.org/publications/cs/pdfs/37/3/CS0370030921 [Accessed December 8, 2017].

Méchin, V., Argillier, O., Hébert, Y., Guingo, E., Moreau, L., Charcosset, A., et al. (2001). Genetic Analysis and QTL Mapping of Cell Wall Digestibility and Lignification in Silage

Maize. *Crop Sci.* 41, 690–697. Available at: https://dl.sciencesocieties.org/publications/cs/pdfs/41/3/690 [Accessed December 11, 2017].

Méchin, V., Argillier, O., Menanteau, V., Barrière, Y., Mila, I., Pollet, B., et al. (2000). Relationship of cell wall composition toin vitro cell wall digestibility of maize inbred line stems. *J. Sci. Food Agric.* 80, 574–580. doi:10.1002/(SICI)1097-0010(200004)80:5<574::AID-JSFA575>3.0.CO;2-R.

Millet, E., Welcker, C., Kruijer, W., Negro, S., Nicolas, S., Praud, S., et al. (2016). Genome-wide analysis of yield in Europe: allelic effects as functions of drought and heat scenarios. *Plant Physiol.*, pp.00621.2016. doi:10.1104/pp.16.00621.

Papst, C., Bohn, M., Utz, H. F., Melchinger, A. E., Klein, D., and Eder, J. (2004). QTL mapping for European corn borer resistance (Ostrinia nubilalis Hb.), agronomic and forage quality traits of testcross progenies in early-maturing European maize (Zea mays L.) germplasm. *TAG Theor. Appl. Genet.* 108, 1545–1554. doi:10.1007/s00122-003-1579-3.

Penning, B. W., Sykes, R. W., Babcock, N. C., Dugard, C. K., Held, M. A., Klimek, J. F., et al. (2014). Genetic Determinants for Enzymatic Digestion of Lignocellulosic Biomass Are Independent of Those for Lignin Abundance in a Maize Recombinant Inbred Population. *Plant Physiol.* 165, 1475–1487. doi:10.1104/pp.114.242446.

Perrier, L., Rouan, L., Jaffuel, S., Clément-Vidal, A., Roques, S., Soutiras, A., et al. (2017). Plasticity of Sorghum Stem Biomass Accumulation in Response to Water Deficit: A Multiscale Analysis from Internode Tissue to Plant Level. *Front. Plant Sci.* 8, 1516. doi:10.3389/fpls.2017.01516.

Ralph, J., Hatfield, R. D., Quideau, S., Helm, R. F., Grabber, J. H., and Jung, H.-J. G. (1994). Pathway of p-Coumaric Acid Incorporation into Maize Lignin As Revealed by NMR. *J. Am. Chem. Soc.* 116, 9448–9456. doi:10.1021/ja00100a006.

Reynolds, M., and Langridge, P. (2016). Physiological breeding. *Curr. Opin. Plant Biol.* 31, 162–171. doi:10.1016/J.PBI.2016.04.005.

Ribaut, J.-M., de Vicente, M., and Delannay, X. (2010). Molecular breeding in developing countries: challenges and perspectives. *Curr. Opin. Plant Biol.* 13, 213–218. doi:10.1016/J.PBI.2009.12.011.

Ribaut, J.-M., and Ragot, M. (2007). Marker-assisted selection to improve drought adaptation in maize: the backcross approach, perspectives, limitations, and alternatives. *J. Exp. Bot.* 58, 351–360. doi:10.1093/jxb/erl214.

Riboulet, C., Fabre, Dénoue, Martinant, Lefèvre, and Barrière (2008a). QTL mapping and candidate gene research for lignin content and cell wall digestibility in a top-cross of a flint maize recombinant inbred line progeny harvested at silage stage. *Maydica* 53, 1–9. Available at: http://prodinra.inra.fr/?locale=fr#!ConsultNotice:20673 [Accessed December 11, 2017].

Riboulet, C., Guillaumie, S., Méchin, V., Bosio, M., Pichon, M., Goffner, D., et al. (2009). Kinetics of phenylpropanoid gene expression in maize growing internodes: Relationships with cell wall deposition. *Crop Sci.* 49, 211–223. doi:10.2135/cropsci2008.03.0130.

Riboulet, C., Lefèvre, B., Dénoue, D., and Barrière, Y. (2008b). Genetic variation in maize cell wall for lignin content, lignin structure, p-hydroxycinnamic acid content, and digestibility in set of 19 lines at silage harvest maturity. *Maydica* 53, 11–19.

Roussel, V., Gibelin, C., Fontaine, A.-S., and Barrière, Y. (2002). Genetic analysis in recombinant inbred lines of early dent forage maize. II-QTL mapping for cell wall

constituents and cell wall digestibility from per se value and top cross experiments. *Maydica* 47, 9–20. Available at: http://prodinra.inra.fr/?locale=fr#!ConsultNotice:66601 [Accessed December 11, 2017].

Samaniego, L., Thober, S., Kumar, R., Wanders, N., Rakovec, O., Pan, M., et al. (2018). Anthropogenic warming exacerbates European soil moisture droughts. *Nat. Clim. Chang.* 8, 421–426. doi:10.1038/s41558-018-0138-5.

Taboada, A., Novo-Uzal, E., Flores, G., Loureda, M., Ros Barceló, A., Masa, A., et al. (2010). Digestibility of silages in relation to their hydroxycinnamic acid content and lignin composition. *J. Sci. Food Agric.* 90, 1155–1162. doi:10.1002/jsfa.3933.

Tardieu, F., Simonneau, T., and Muller, B. (2018). The Physiological Basis of Drought Tolerance in Crop Plants: A Scenario-Dependent Probabilistic Approach. *Annu. Rev. Plant Biol.* 69, 733–759. doi:10.1146/annurev-arplant-042817-040218.

Torres, A. F., Noordam-Boot, C. M. M., Dolstra, O., van der Weijde, T., Combes, E., Dufour, P., et al. (2015). Cell Wall Diversity in Forage Maize: Genetic Complexity and Bioenergy Potential. *Bioenergy Res.* 8, 187–202. doi:10.1007/s12155-014-9507-8.

Truntzler, M., Barrière, Y., Sawkins, M. C., Lespinasse, D., Betran, J., Charcosset, A., et al. (2010). Meta-analysis of QTL involved in silage quality of maize and comparison with the position of candidate genes. *Theor. Appl. Genet.* 121, 1465–1482. doi:10.1007/s00122-010-1402-x.

Turc, O., and Tardieu, F. (2018). Drought affects abortion of reproductive organs by exacerbating developmentally driven processes via expansive growth and hydraulics. *J. Exp. Bot.* 69, 3245–3254. doi:10.1093/jxb/ery078.

Updegraff, D. M. (1969). Semimicro determination of cellulose inbiological materials. *Anal. Biochem.* 32, 420–424. doi:10.1016/S0003-2697(69)80009-6.

van der Weijde, T., Alvim Kamei, C. L., Torres, A. F., Vermerris, W., Dolstra, O., Visser, R. G. F., et al. (2013). The potential of C4 grasses for cellulosic biofuel production. *Front. Plant Sci.* 4, 1–18. doi:10.3389/fpls.2013.00107.

van der Weijde, T., Huxley, L. M., Hawkins, S., Sembiring, E. H., Farrar, K., Dolstra, O., et al. (2017). Impact of drought stress on growth and quality of miscanthus for biofuel production. *GCB Bioenergy* 9, 770–782. doi:10.1111/gcbb.12382.

Vanholme, R., Morreel, K., Ralph, J., and Boerjan, W. (2008). Lignin engineering. *Curr. Opin. Plant Biol.* 11, 278–285. doi:10.1016/J.PBI.2008.03.005.

Vermerris, W., and Abril, A. (2015). Enhancing cellulose utilization for fuels and chemicals by genetic modification of plant cell wall architecture. *Curr. Opin. Biotechnol.* 32, 104–112. doi:10.1016/J.COPBIO.2014.11.024.

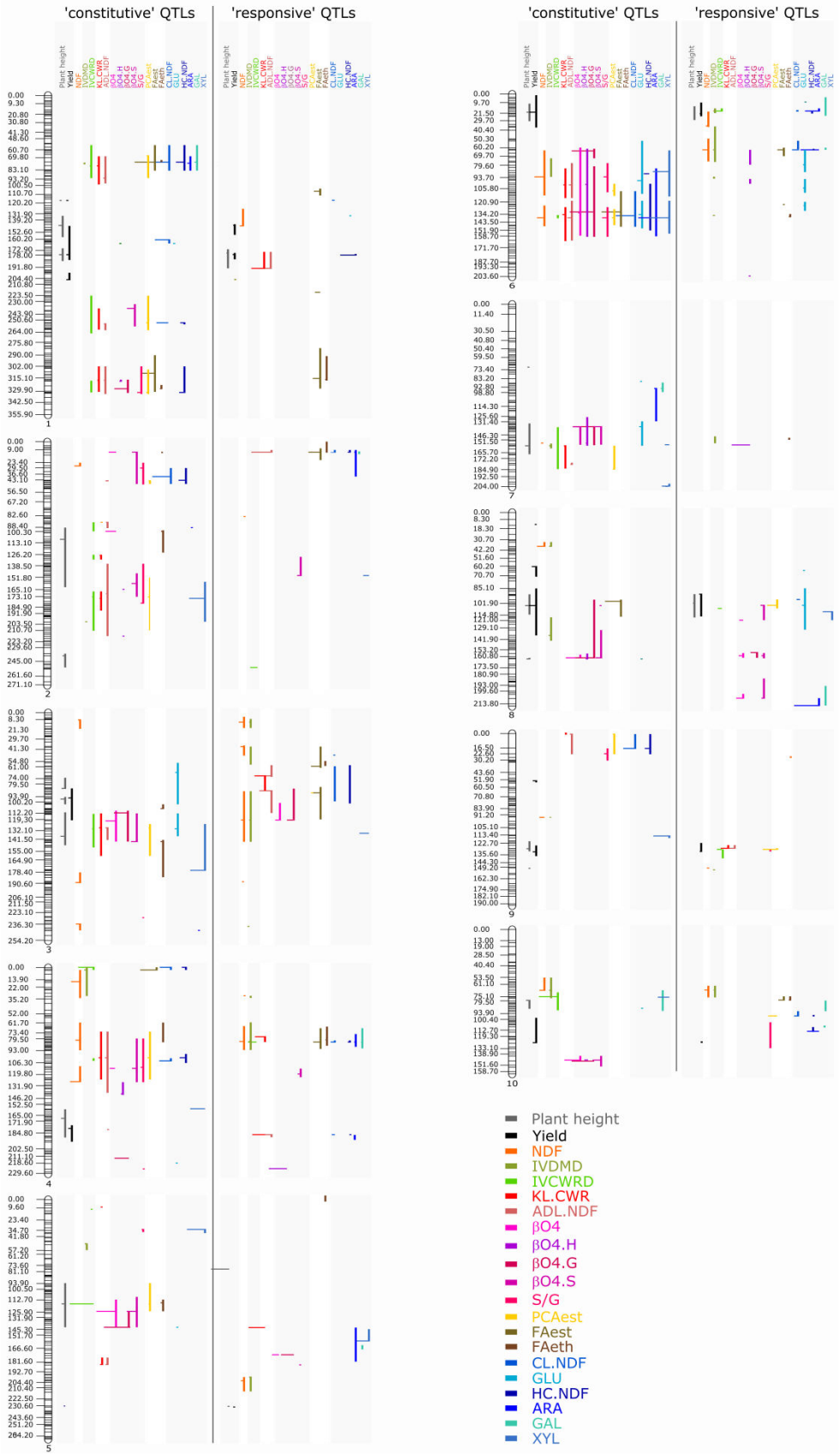
Watkins, D., Nuruddin, M., Hosur, M., Tcherbi-Narteh, A., and Jeelani, S. (2015). Extraction and characterization of lignin from different biomass resources. *J. Mater. Res. Technol.* 4, 26–32. doi:10.1016/J.JMRT.2014.10.009.

Webber, H., Ewert, F., Olesen, J. E., Müller, C., Fronzek, S., Ruane, A. C., et al. (2018). Diverging importance of drought stress for maize and winter wheat in Europe. *Nat. Commun.* 9, 4249. doi:10.1038/s41467-018-06525-2.

Wei, M., Li, X., Li, J., Fu, J., Wang, Y., and Li, Y. (2009). QTL detection for stover yield and quality traits using two connected populations in high-oil maize. *Plant Physiol. Biochem.* 47, 886–894. doi:10.1016/j.plaphy.2009.06.001.

Zhang, Y., Culhaoglu, T., Pollet, B., Melin, C., Denoue, D., Barrière, Y., et al. (2011). Impact of lignin structure and cell wall reticulation on maize cell wall degradability. *J. Agric. Food Chem.* 59, 10129–10134. doi:10.1021/jf2028279.

Supplemental Figure 1



Supplemental Table 1. Principal component analysis.

Categories	Traits[a]	Units	Component1 (42.14 %)			Component2 (21.84 %)			Component3 (16.01 %)		
			contribution (%)	r	pvalue	contribution (%)	r	pvalue	contribution (%)	r	pvalue
Cell Wall residues	NDF	%DM	0,07	0,07	1,21E-02	4,83	-0,45	5,49E-60	17,43	0,73	6,64E-198
Degradability	IVDMD	%DM	6,83	-0,74	2,58E-207	1,43	0,24	1,27E-17	3,3	-0,32	2,80E-29
	IVCWRD	%CWR	10,89	-0,93	0,00E+00	0,43	-0,13	3,72E-06	0,27	0,09	1,62E-03
Lignin content	KL.CWR	%CWR	10,83	0,93	0,00E+00	0,06	0,05	ns	1,29	-0,20	4,54E-12
	ADL.NDF	%NDF	10,70	9,30E-01	0,00E+00	4,80E-04	0,00	ns	2,74	-0,29	2,14E-24
Lignin structure	βO4	µmole g^{-1} KL	1,50	0,35	3,90E-35	15,81	0,81	5,67E-279	4,66	0,38	1,63E-41
	βO4.H	µmole g^{-1} KL	1,26	-0,32	2,43E-29	0,07	0,05	ns	21,52	0,81	8,73E-278
	βO4.G	µmole g^{-1} KL	0,19	0,12	2,02E-05	14,3	0,77	1,84E-235	10,67	0,57	7,94E-104
	βO4.S	µmole g^{-1} KL	3,03	0,49	4,69E-74	13,43	0,75	1,69E-213	0,6	0,14	2,62E-06
	S/G		4,04	5,70E-01	2,17E-103	3,50E-06	0,00	ns	11,7	-0,60	3,66E-116
Hydroxycinamic acids	PCAest	mg g^{-1} CWR	11,61	0,96	0,00E+00	0,83	0,19	8,95E-11	0,61	-0,14	2,37E-06
	FAest	mg g^{-1} CWR	0,61	-0,22	1,08E-14	17,2	0,84	0,00E+00	3,33	-0,32	1,44E-29
	Faeth	mg g^{-1} CWR	1,25	0,32	3,19E-29	10,43	0,66	4,62E-149	4,71	-0,38	4,70E-42
Structural sugars	CL.NDF	%NDF	5,18	0,64	8,04E-141	5,38	-0,47	1,60E-67	3,28	0,32	4,68E-29
	GLU	%CWR	5,65	0,67	4,21E-158	2,26	0,31	2,21E-27	8,33	0,50	9,22E-78
	HC.NDF	%NDF	8,30	-0,82	3,54E-285	3,58	0,39	1,34E-43	0,79	-0,16	6,80E-08
	ARA	%CWR	10,22	-0,9	0,00E+00	2	0,29	2,60E-24	0,07	0,05	ns
	GAL	%CWR	7,38	-0,77	9,29E-234	3,64	0,39	2,32E-44	0,23	-0,08	3,98E-03
	XYL	%CWR	0,45	0,19	2,94E-11	4,3	0,42	6,10E-53	4,45	0,37	1,24E-39

[a]NDF, neutral detergent fiber; IVDMD, *in vitro* dry matter degradability; IVCWRD, *in vitro* cell wall residus degradability; ADL, acid detergent lignin; KL, Klason lignin; PCA, *para*-coumaric acid; FA, ferulic acid; CL, cellulose; HC, hemicellulose; GLU, glucose; ARA, arabinose; GAL, galactose; XYL, xylose.

Conclusion

Despite the impossibility to calculate genotypic values overall the years and the conditions due to environmental context, the QTLs analysis performed on the histological traits and the cell wall biochemistry of the internode within the F271xCm484 RILs population was interesting at several levels. For the first time, QTLs for various histological traits were detected, and more particularly, a locus between bin 1.07 and 1.11 was identified overall the conditions for several histological traits, mainly related to the stem area, the bundle number and the rind fraction. Many noteworthy co-localizations between QTLs for cell wall biochemical traits and histological traits have also been highlighted. Either with the lignin content and the degradability or without, which let consider other potential loci to target in breeding plant for a good degradability and to impact important traits such as the esterified *p*-coumaric acid content and the Red rind without impacting cell wall lignin content. Finally, the comparison between the genetic determinism of biochemical cell wall traits at the internode level and at the whole plant level revealed several co-localizations involved in the variation of the same traits, suggesting that biochemical variation at the internode may reflect the biochemical variations at the whole plant level. Furthermore, co-localizations between the histological QTLs at bin 1.07-11 and 10.03-06 and QTLs for cell wall biochemical traits of the whole plant were also observed and suggest the possibility of genetic links between the histology and the cell wall degradability of the whole plant.

However, we may call into question the representativeness of the internode as a model and wonder if it was judicious to confront the result of the QTL detection on the internode with the QTL detection on the whole plant. This is what we will try to answer in the last chapter of this study.



Chapter 3

Chapter 3: Does histology of the internode carrying the main ear represent all the internodes of the stem and even reflect the biochemistry of whole plant without ears?

Introduction

In the previous two chapters, the studies were focused on the internode carrying the main ear, from the histological point of view as well as from the biochemical cell wall composition and degradability ones. However, one man find legitimate to interrogate the representativeness of this internode with all the other internodes of the stem and to go further by questioning the relationships between this internode and all the above ground lignocellulosic biomass from the plant.

The growth of the internode in maize stem has been previously described. At the beginning of its growth elongation began slowly and uniformly throughout its length during the first 2 or 3 days, increased in rate and shifted basipetally from the upper internode region toward the middle and later, toward the basal region of the enlarging internode. Elongation decelerated in the intercalary meristem region during the final days of internode lengthening. This pattern was observed for all internodes along the stem (Morrison et al., 1994). Which means that at any stage of development, and therefore at the silage stage, internodes of a maize stem differ in length, thickness, anatomy and consequently also in chemical composition and degradability. In forage maize, several differences between tissue types have been pointed out about their degradability (Jung and Casler 2006a) but also about the thickness of their cell walls (Boon et al., 2008; 2012), the composition of the cell wall of the rind region (Lopez et al., 1993; Chesson et al., 1997; Hatfield et al., 2017), or the impact of the tissue proportion associated with the composition (Méchin et al., 2005; Zhang et al., 2011; El Hage et al., 2018). The differences between maize tissues may also change with crop maturity (Morrison et al., 1998; Jung and Casler, 2006a & 2006b) and particularly because of the differences in the tissue lignification (Jung and Deetz, 1993). However the biochemical composition is not explaining all the observed differences of cell wall degradability and the changes in the lignification of the stem along the development (Burns, 2011), suggesting that both biochemical and histological analyses are required to understand and pinpoint the causes of these differences, as we underlined in the study presented in the chapter 1-I.

Considering all these differences among the internodes of a given stem harvested at one date, the choice of an internode that would represent all the internodes of the whole stem remains challenging. Because histological phenotyping of an internode can be time consuming, studies generally pick 1 or 2 internodes, and particularly the one carrying the

main ear of the plant. This internode has been chosen as a reference for comparison between different maize genotypes at a same developmental stage, because within a genotype the insertion of the ear is generally on the same internode from one plant to another. Thus in Mechin, the internode carrying the main ear at silage stage was chosen in 2000; Zhang et al., did the same in 2011. But this internode is not always the one chosen. In 1994 Chabbert et al., studied the biochemistry of the internodes from the bottom the middle and the top of the stem on bm2 and bm3 maize lines at grain maturity. 3 years later, they biochemically characterized sclerenchyma and parenchyma of the second internodes from the top of the plants harvested 5 days after anthesis (Chesson et al., 1997). In 2006, Jung and Casler chose to harvest the fourth internode from the bottom of the plant during the growing season which may be not far from the one carrying the main ear on hybrids. They studied both the spatial lignification and the biochemical cell wall components of the internode 4 in 3 different hybrids. In 2005, 2008 and 2012 Boon et al., studied the first internode fully elongated above the ground level. All these studies characterized certain anatomical characteristics such as the lignification within the rind or the pith (Chesson et al., 1997; Boon et al., 2008, 2012) and other studies the cell wall biochemistry of different maize internodes (Chabbert et al., 1994a, b) and at different developmental stages. When they compared genotypes, each study did it between the same internodes, however, previous studies on several internodes all along the stem already suggested that the composition was different from an internode to another, for example in switchgrass Crowe et al., (2017) showed that the lignin content increase from the bottom to the top of the plant. The same year He et al., (2017) showed the same type of variations in the maize stem. Still, we may wonder if the comparison between studies is possible and more particularly what is the representativeness of an internode compared to all the other internodes of the stem at any stage.

Therefore, in this third chapter I decided to decipher further the representativeness and features of this internode and: i) first, to compare cell wall biochemistry at this internode and at the whole plant without the ear levels; then ii) in a second part, to investigate relationships of internode histological quantifications with cell wall biochemistry of the whole plant and finally the histological variation present among all the internode of a stem. This third part was not planed when my phD started, and these interrogations came out when analyzing results presented in the chapters 1 and 2. To address these questions, all the internodes from stems of 8 genotypes were harvested at silage stage in a field experiment conducted in Versailles in 2017.

I. Variation of cell wall biochemistry of the internode carrying the main ear reflects the variations of cell wall biochemistry of the whole plant without ear

In this part, relationships between biochemical cell wall traits of the internode carrying the main ear (IN) and those of the whole plant without ears (PWE) are studied in order to investigate how representative is the biochemistry of this internode of the rest of the plant. More particularly, cell wall biochemistry of this IN of all the 11 genotypes presented in the Chapter 1-I (El Hage et al., 2018) was confronted to cell wall biochemistry of the PWE of the same genotypes cultivated in the same field experiments.

Material and Methods

Plant material.

The harvested whole plants without ears and internodes come from the field experiments performed in 2012-2013-2014 detailed in the chapter 1 Material and Methods and were harvested under the same protocol than Virlouvet et al., in prep, presented in the chapter 2-II.

Biochemical analyses.

All the biochemical traits of the cell wall of the internode were obtained with the NIRS predictive equations presented in the Material and methods of the Chapter 1. Cell wall biochemistry of the whole plant without ears of the same genotypes was obtained with NIRS predictive equations developed for the whole plant without ears and build (Virlouvet et al., in prep) in the same principle than the NIRS predictive equations of the internode to be precise and accurate for the cell wall biochemistry of the whole plant without ears of these genotypes.

Statistical analyses.

All the statistical analyses have been performed using the software R (CRAN-project).

The coefficient of determination R^2 was calculated as the squared of the Pearson correlation coefficient R.

Results and discussion

Concerning in vitro cell wall degradability, the relationship between cell wall degradability estimated from the PWE and the IN was rather good (pearson correlation factor R = 0.83, Table S-5). So 67.6 % of cell wall degradability variations of the IN represents well the variations of cell wall degradability of the PWE (Figure 44). In addition to these statistical relationships, the range of variation of each estimated degradabilities were similar at the internode and the whole plant levels (between 25 and 50 % of cell wall residue). Therefore, cell wall degradability of the IN reflects well cell wall degradability of the PWE and the ranking of cell wall degradability of the studied genotypes remained conserved when the IN and the PWE are compared. In addition, the impact of the irrigation condition on degradability is similar at the stover or at the internode level (Figure 44).

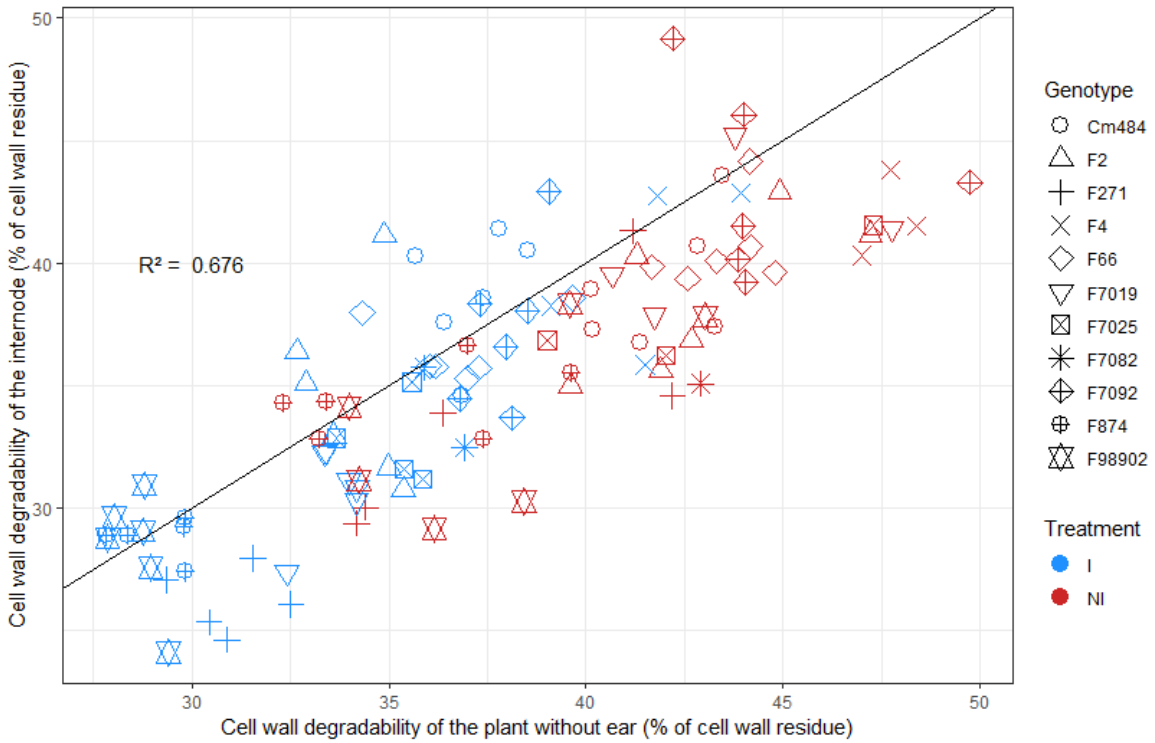


Figure 44. Relationship between *in vitro* cell wall degradability of the internode and of the whole plant without ears. The plants have been cultivated in fields during 3 years from 2012 to 2014 in 2 blocs under irrigated (in blue) and non-irrigated (in red) conditions. The black line is the function y=x.

The Klason lignin content did show the same good relationship (Pearson correlation factor R=0.84, Table S-5) between the internode and the whole PWE. The variation of Klason lignin content of the IN explained 64.8 % of the variation of Klason lignin content of the PWE (Figure 45). The lower limit of the range of the lignin content of the internode was about the same as the PWE (around 12 % of cell wall residue), whereas the upper limit of the range of the lignin content was higher in the internode of 2 points, reaching 20 % of cell wall residue

when it stood at 18 % of cell wall residue in the whole PWE. It suggests that cell walls of the internode of these genotypes may be more lignified than the other fractions of the plant such as the leaves and the other internodes. Several studies showed that the leaves were as lignified as the internode fraction. Fornalé et al. showed in 2015 on a maize hybrid at silage stage that the leaves were not less lignified than the stem. Cai et al., also showed in 2016 on maize stover that the stem fraction presented about the same lignin content as the leaf fraction. In addition, Liu and Chen, (2016) also showed the same year on maize stover that the leaf fraction and also the node fractions were as lignified as the stem fraction. Even on 3 miscanthus cultivars, da Costa et al., showed in 2018 that the leaf fraction was as lignified as the stem fraction. However the lignin content show the same variations between genotypes according to the IN as well as the PWE. Several studies showed that the lignin content was increasing in the internodes from the base where the lignin content is high to the top of the plant, in maize (Chabbert et al., 1994a, b; Crowe et al., 2017; He et al., 2017).

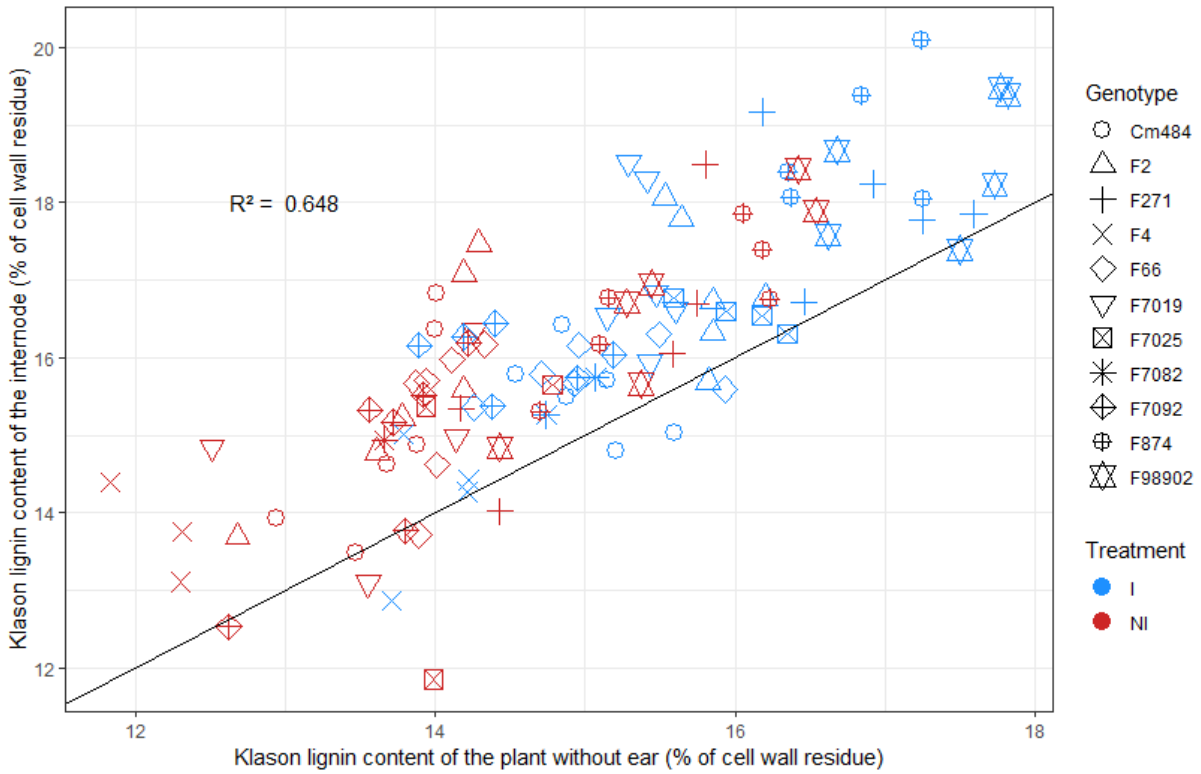


Figure 45. Relationship between the Klason lignin content of the internode and the whole plant without ears. The plants have been cultivated in fields during 3 years from 2012 to 2014 in 2 blocs under irrigated (in blue) and non-irrigated (in red) condition. The coefficient of determination R^2 = 0.648. The black line is the function y=x.

The esterified *p*-coumaric acid content also presented a good relationships between the internode and the whole plant without ears levels (Pearson correlation factor R= 0.78, Table S-5). The esterified *p*-coumaric acid content of the IN presents a rather good relationship with the *p*-coumaric acid content of the PWE (R^2=0.521, Figure 46). However, the amount of

esterified *p*-coumaric acid content in the internode was 5 to 10 mg/g of CWR more than in the whole plant without ears. Several studies quantified the *p*-coumaric acid content in several internodes all along the stem, in switchgrass (Shen et al., 2009; Crowe et al., 2017) and in maize (Chabbert et al., 1994a, b) and, depending on the stage of development the *p*-coumaroylation of the lignins all along the stem is not the same. Indeed, during stem elongation the *p*-coumaroylation is greater in the younger internodes (top of the stem) than in the older internodes (bottom of the stem) but then, at maturity stage, the internodes from the base present a greater *p*-coumaric acid content.

With the previous result on the lignin content, it is likely that the lignin content of one internode reflects well the lignin content of the PWE and we can argue that the *p*-coumaric acid content follow also the same variations between the IN and the PWE but with however a greater *p*-coumaroylation of the lignins in the IN.

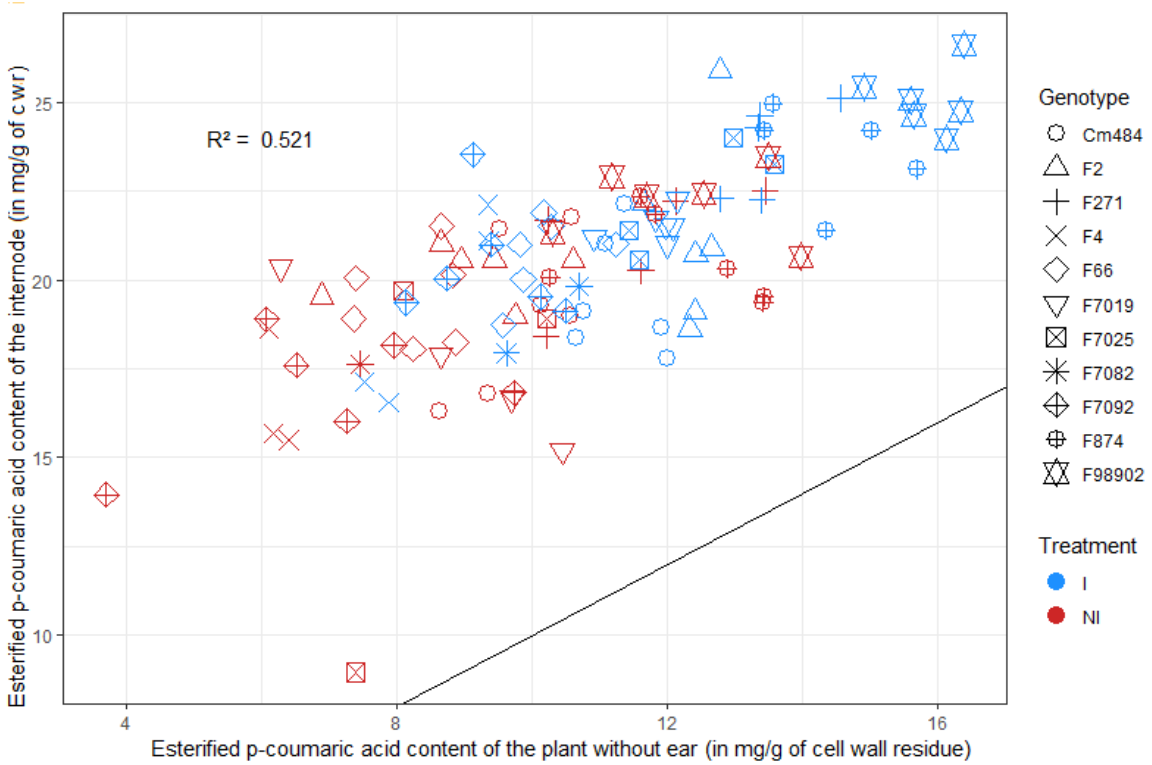


Figure 46. Relationship between the esterified *p*-coumaric acid content of the internode and the whole plant without ears. The plants have been cultivated in fields during 3 years from 2012 to 2014 in 2 blocs under irrigated (in blue) and non-irrigated (in red) condition. The coefficient of determination R^2 = 0.521. The black line is the function y=x.

All the other cell wall traits, etherified ferulic acid, BO4 linkages yield, S/G lignins subunits ratio, cellulose and hemicelluloses have respectively pearson correlation factors of 0.03, 0.31, -0.11, 0.43 and 0.38 (Table S-5). This suggests that for these cell wall biochemical traits, biochemical variation of the internode below the main ear is not reflecting the variation at the whole plant without ear level. This was also suggested by a few studies. In 2015, Fornalé

et al., showed in an (A188xB73)xB73 hybrid harvested at silage stage, S/G ratio of 1.20 was reported in the stem while it reached 0.35 in the leaf fraction. The BO4 linkages yield was also quite different with 1.8 in the stem against 1.1 in the leaf midrib. 2 others studies in 2016 showed that xylan, arabinan, and glucan, major components of the hemicelluloses and the cellulose, were more concentrated in the leaves and the nodes fraction than in the stem (Liu and Chen, 2016; Cai et al., 2016).

This study on 11 inbred lines of maize allowed us to show that for the lignin content, the *in vitro* cell wall degradability and the esterified *p*-coumaric acid content, values obtained at the internode carrying the main ear level represented quite faithfully values at the whole plant without ears level. To go further in the understanding of the cell wall composition of every fractions of the maize plant in the genotypes of our study, it would be interesting to quantify all the cell wall components of every fraction (stem, nodes, leaves, cobs) and compare them.

Finally, to evaluate cell wall biochemical traits characterizing the quality of the IN represents well the PWE for only 3 traits. Still, as previously reported in the literature, the internodes all along the stem may present different cell wall biochemistry, in particular the lignin content which increases from the bottom to the top, in maize (Chabbert et al., 1994a, b; He et al., 2017) but also in barley (Begovic et al., 2015) or in switchgrass (Sarath et al., 2007; Crowe et al., 2017); the sugars content are also reported to be higher in the internodes of the top of the stem in barley (Begovic et al., 2016). The internodes all along the stem were also reported to have different lignification patterns in maize with consistently thicker rind at the bottom of the stem and thinner at the top, in maize (Boon et al., 2005, 2008, 2012; Jung and Caster 2006), in sugarcane (Bottcher et al., 2013) and in switchgrass (Crowe et al., 2017). Knowing all this, and as we worked in the two previous chapters on the histology of the internode carrying the main ear, we may wonder now how representative is the histology of this internode for the whole plant without ears.

II. The histology of the internode carrying the main ear reflects the mean all the internodes of the stem

After comparing the cell wall biochemistry on the internode carrying the main ear of the plant with the cell wall biochemistry of the whole plant without ears, we investigated further the representativeness of its histology. And we may wonder first if it is a good estimator of the histology of all the other internodes and secondly if it can a part of the cell wall biochemistry variations of the whole plant without ears .

Material and Methods

Plant material.

In the sub-part a) of this part the presented histological analysis has been performed on 8 public maize inbred lines (Table 11) which were mostly common to the previous study presented in chapter 1 and selected from previous experiments performed at INRA Lusignan between 1997 and 2008 (Méchin et al., 2000; Méchin et al., 2005 ; Barrière et al., 2009).

Table 11. Pedigree of the studied inbred lines

Line	Pedigree
F4	Northern Flint
F7	Lacaune
F7025	Iodent x M13 Dent
F2	Lacaune Flint
F2bm3	Lacaune Flint
F271	Canadian dent
Cm484	Canada-Morden – 1989
F98902	CRANaMOF 7-2-1-2-5-4

Field experiments were carried out at Versailles (France, 78) in 2017. The seeds were sown the 10th of May, 2017. In each row they were sown every 0.2 m, the inter-row spacing was 0.80 m and the density was of 62 500 plants per hectare. From the 7th of September to the 15th of September, all the internodes of 1 plant from each genotype were harvested at silage stage. Each harvested internode was separately stored in 70 % ethanol for further histological analysis. For each plant, the internode carrying the main ear was noted “IN n”, and all the rank of the other internodes was deduced from it, with positive numbers towards the top of the stem and negative numbers towards the bottom.

In the sub-part b) of this part, the histological quantifications have been performed on the panel of 11 genotypes presented in the Chapter 1-I (El Hage et al., 2018) and they have been confronted to the biochemistry of the whole plant without ears of this same panel of 11 genotypes.

Histological analyses

Cross-sections of 150 µm thickness were cut from each internode of each harvested genotype. A total of 62 cross-sections were obtained using a sledge-microtome GSL1 (Gärtner et al., 2015) and stored in 70% ethanol. They were then stained with FASGA solution (derived from Tolivia and Tolivia, 1987). The FASGA solution, the staining protocol and the image analysis were performed according to the protocols presented in the Material and methods of the Chapter 1.

Biochemical analyses

All the biochemical traits of the cell wall of the internode were obtained with the NIRS predictive equations presented in the Material and methods of the Chapter 1. Cell wall biochemistry of the whole plant without ears of the same genotypes was obtained with NIRS predictive equations developed for the whole plant without ears and build in the same principle than the NIRS predictive equations of the internode to be precise and accurate for the cell wall biochemistry of the whole plant without ears of these genotypes.

Statistical analyses

All the statistical analyses have been performed using the software R (CRAN-project).
Each genotype had a number of internodes going from 6 to 12. The normality of the data has been tested with a shapiro-wilkinson test. Then, per histological trait and per genotype, a mean on all the internodes of the plant was calculated. For each plant and per histological trait, the statistical difference between the mean and the value of the IN n was evaluated using a two-tailed “one sample” t-test. The difference was considered significant when the p value was found under 0.05.
The multiple regressions were performed using the package FactoMineR on R. The models were calculated using a stepwise selection, by testing all the traits “backward” and “forward” to minimize the final AIC (or Akaike information criterion) of the model; which ensure the best consistency of the model for a minimum of traits selected by the model.
The coefficient of determination R^2 was calculated as the squared of the Pearson correlation coefficient R.

a) Histological pattern of the internode carrying the main ear reflects the average histological pattern of all the internodes of a maize stem

In this part, the 8 studied genotypes were cultivated in Versailles in 2017. The histological profiles of the all the internodes of one plant per genotype were characterized.

Once histological traits for all the stained cross-sections out of all the internodes of a stem per genotype were quantified, we statistically compared for every traits the mean of all the internodes with the value of the internode carrying the main ear (named “IN n”).

The first observation we did on all these genotype’s internodes cross-sections from the bottom to the top of the stem, was that the internodes below the IN n presented a higher and large amount of non-lignified fraction, stained in cyan by the Alcian Blue dye. On the other hand, the internodes above the IN n showed a histological profile with very few non-lignified fraction compared to the internodes of the bottom. It was unexpected, because the upper internodes are supposed to have a shorter time course of development than the lower ones, and that lignification is a process that is occurring during internode development. Furthermore, as demonstrated by Zhang et al., (submitted) histological profile of one internode is changing during internode elongation and maturity. This variation of histological profile is not the same than the histological variations observed between internodes along the stem at silage stage. Despite the fact that the hypothesis of spatial development is often considered as a synonym as the temporal development, this observation was made on all the 8 genotypes, and it demonstrates clearly different lignification patterns between the lowest internodes and the uppers internodes at silage stage.

In the following results, all figures are composed from left to right to all the FASGA stained cross section of the internodes from the bottom to the top of the genotype. Under each cross-section is associated its FASGA segmentation profile which highlights the different tissue types proportions. Under these images are disposed bar plots for every histological trait highlighting on the left the mean of all the internodes (All IN) with the standard error associated and on the right the value for the internode carrying the main ear (IN n). When the p-value of the one-sample t-test was under 5 %, it was mentioned on the plot.

Despite this observation, the histology of the IN n appears to reflect the histological pattern of all the internodes of the stem. As we can see for Cm484, which had 6 internodes (Figure 47), none of the histological traits showed significant difference between the average of all the internodes and the IN n.

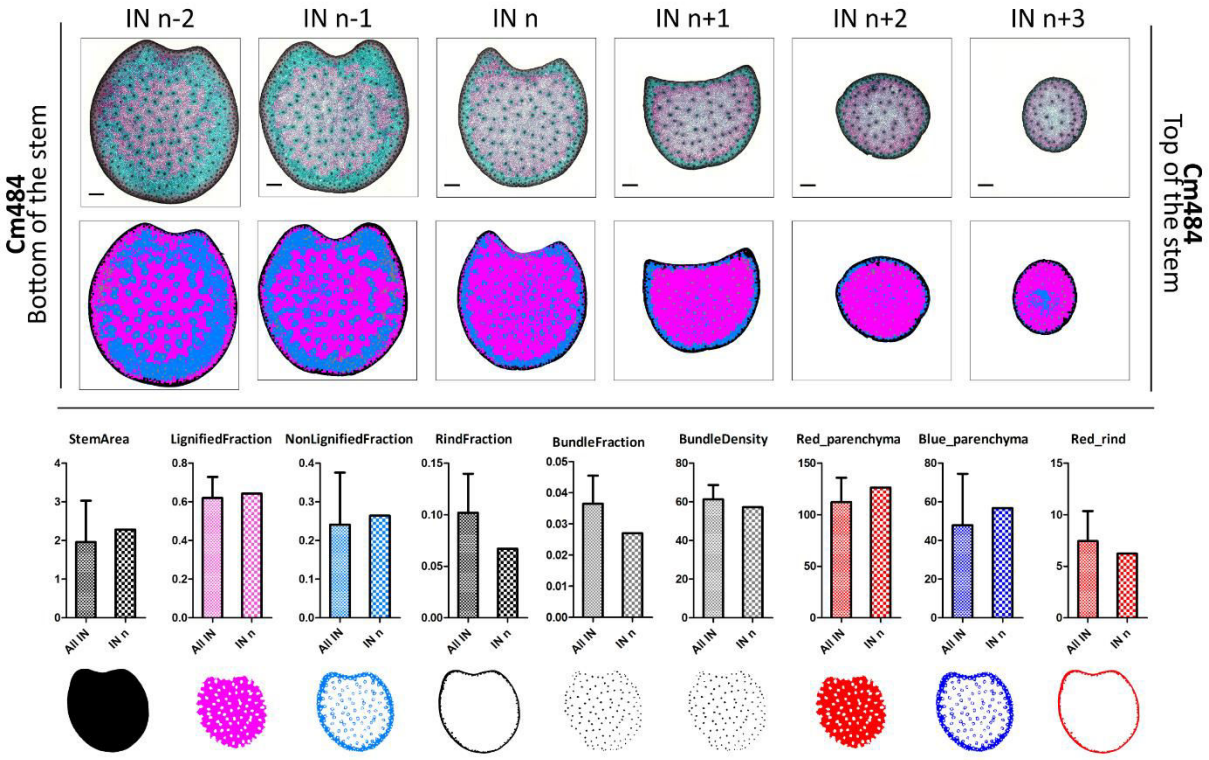


Figure 47. Histological profiles of the cross-sections of all the internodes from the bottom to the top of the stem in Cm484 and comparison with the IN n. For each histological trait, a histogram represents from left to right the mean of all the internode with the standard deviation associated and then the value of the IN n. If the one sample t-test p-value was above 0.05, the difference between the mean and the IN n value was considered non-significant.

F2 had 7 internodes and the histological variations along with the internode position in the stem follow the same trend than Cm484 (Figure 48). The lower internodes presented a larger non-lignified fraction than the upper internodes. Still, a significant difference between the mean value of all the internodes from the stem and the value of the internode bellow the main ear was found only for the bundle density. This may be explained by the fact that for the 4 upper internodes, the bundle density is quite high compared to the bigger internodes of the bottom.

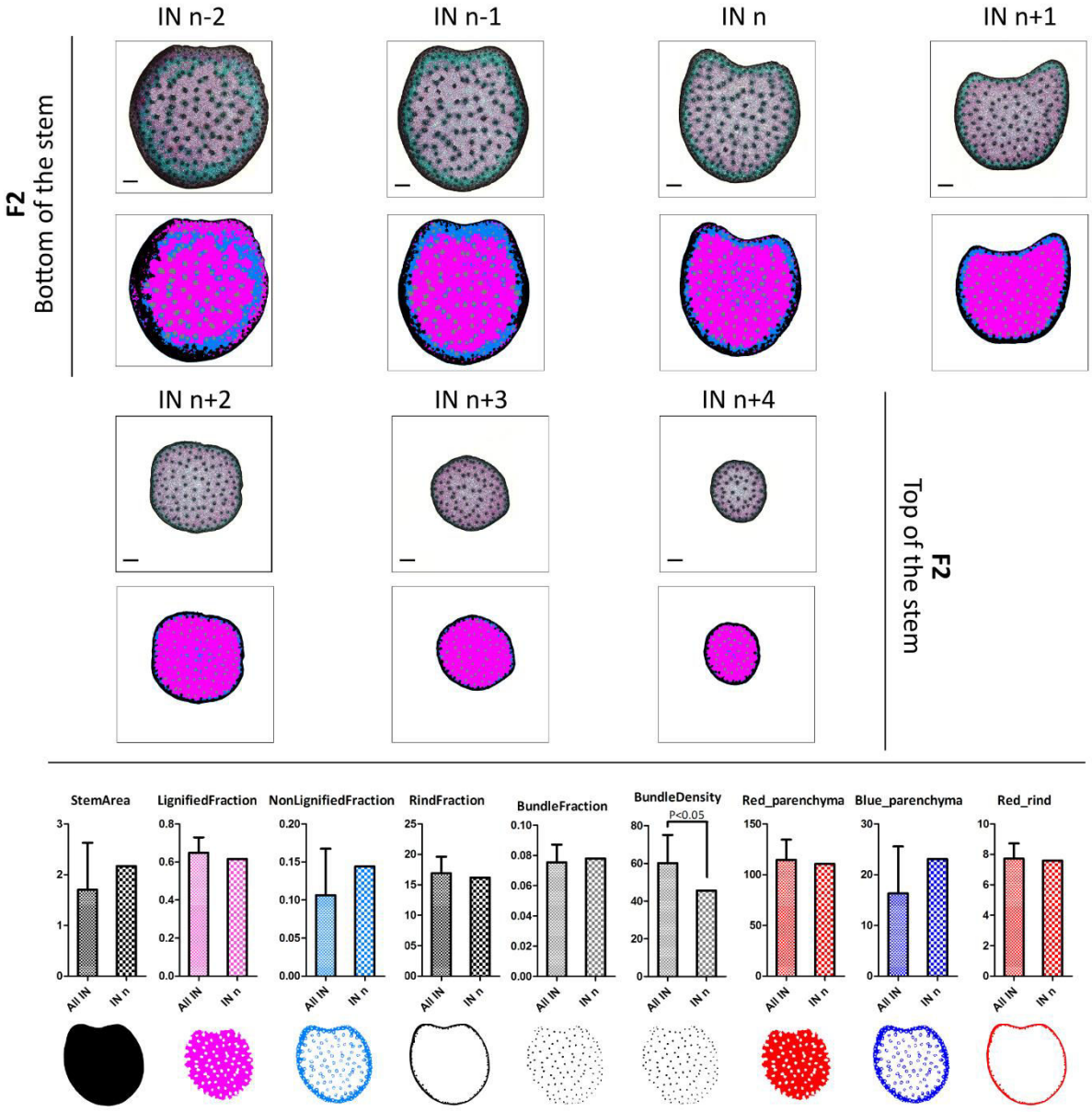


Figure 48. Histological profiles of the cross-sections of all the internodes from the bottom to the top of the stem in F2 and comparison with the IN n. For every histological trait, a histogram represents from left to right the mean of all the internode with the standard deviation associated and then the value of the IN n. If the one sample t-test p-value was above 0.05, the difference between the mean and the IN n value was considered non-significant.

F2bm3 had 7 internodes and the same histological profile tendency as Cm484 or F2 was observed from the bottom to the top of the stem (Figure 49). The lower internodes presented a larger non-lignified fraction and a much thicker rind than the upper internodes. As for F2, the bundle density was the only trait which was presenting a significant difference between the mean of all the internode and the IN n value.

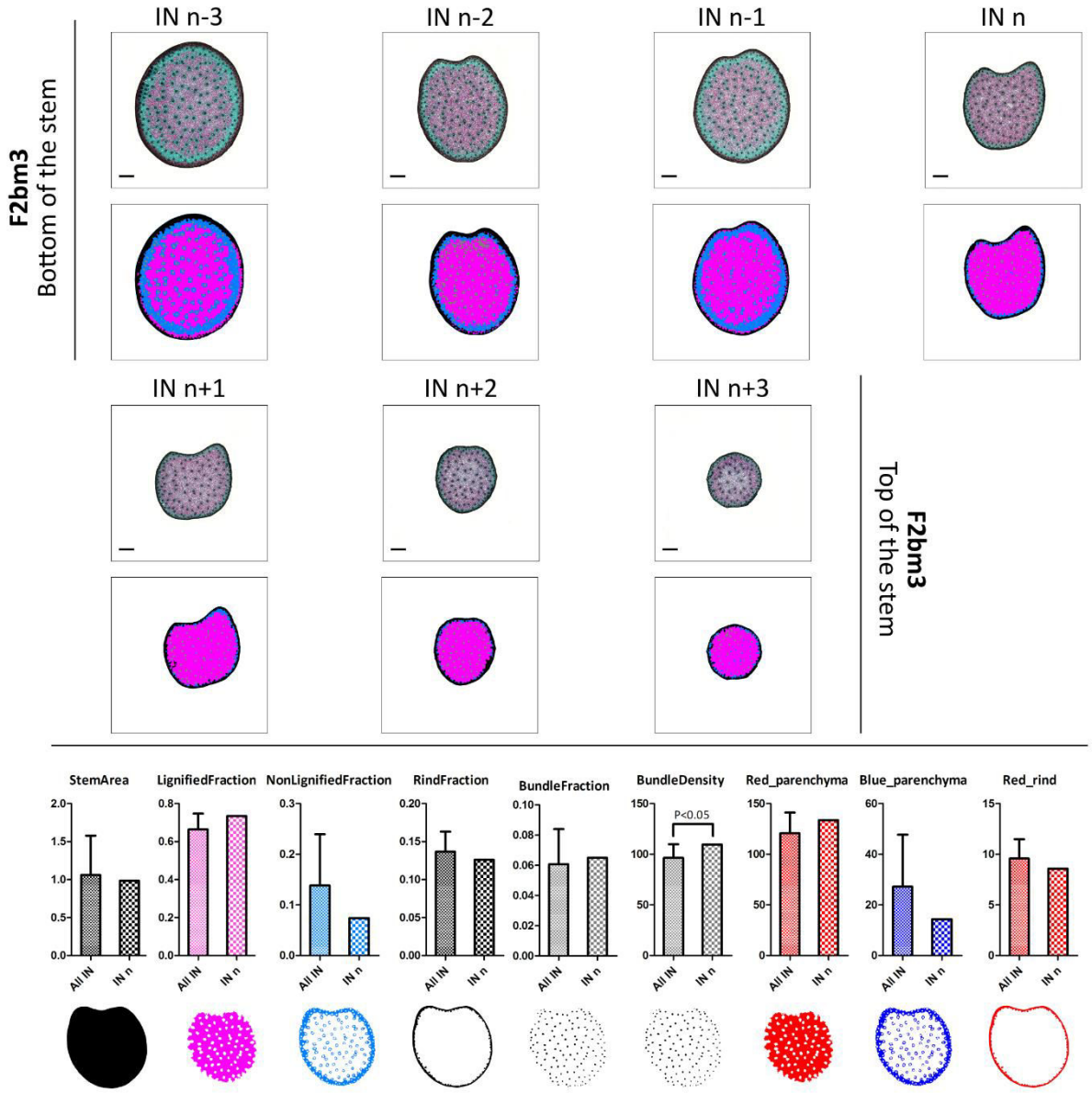


Figure 49. Histological profiles of the cross-sections of all the internodes from the bottom to the top of the stem in F2bm3 and comparison with the IN n. For every histological trait, a histogram represents from left to right the mean of all the internode with the standard deviation associated and then the value of the IN n. If the one sample t-test p-value was above 0.05, the difference between the mean and the IN n value was considered non-significant.

The genotype F7025 was the one having the highest number of internodes in its stem: 12 in total. Once again, the lowest internodes presented a larger non-lignified fraction than the upper internodes (Figure 50). Still, the 2 traits which presented significant differences between all the internodes and the IN n were the Stem area and the Rind fraction. These differences may be explicated with the same reason. 2 great types of internodes can be identified in F7025; from the IN n-4 to the IN n+1 the internodes have all a great stem area with a thick rind, while from the IN+2 to the IN+7 the Stem area is much smaller with a thinner rind.

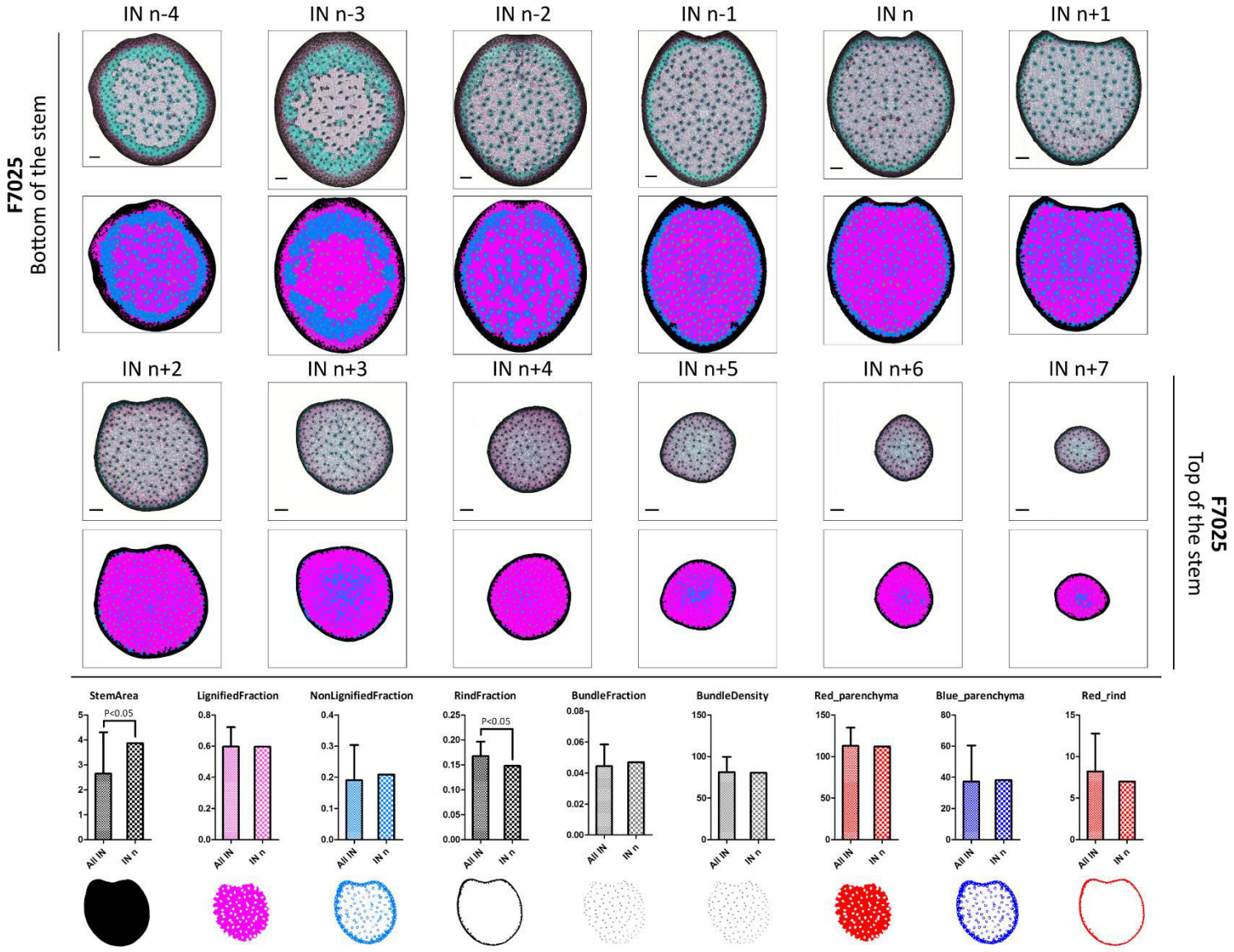


Figure 50. Histological profiles of the cross-sections of all the internodes from the bottom to the top of the stem in F7025 and comparison with the IN n. For every histological trait, a histogram represents from left to right the mean of all the internode with the standard deviation associated and then the value of the IN n. If the one sample t-test p-value was above 0.05, the difference between the mean and the IN n value was considered non-significant.

The genotype F98902 had 10 internodes. The tendency of the large amount of non-lignified fraction in the lowest internodes was the most striking with this genotype (Figure 51). Still, as the non-lignified fraction decreases progressively from the bottom to the top of the stem, the value of the IN n appeared to be not significantly different from the mean of all the internodes. The only trait which presented a significant difference between the IN n and all the internodes was the bundle fraction. The IN n here overestimates significantly the bundle fraction of all the internodes.

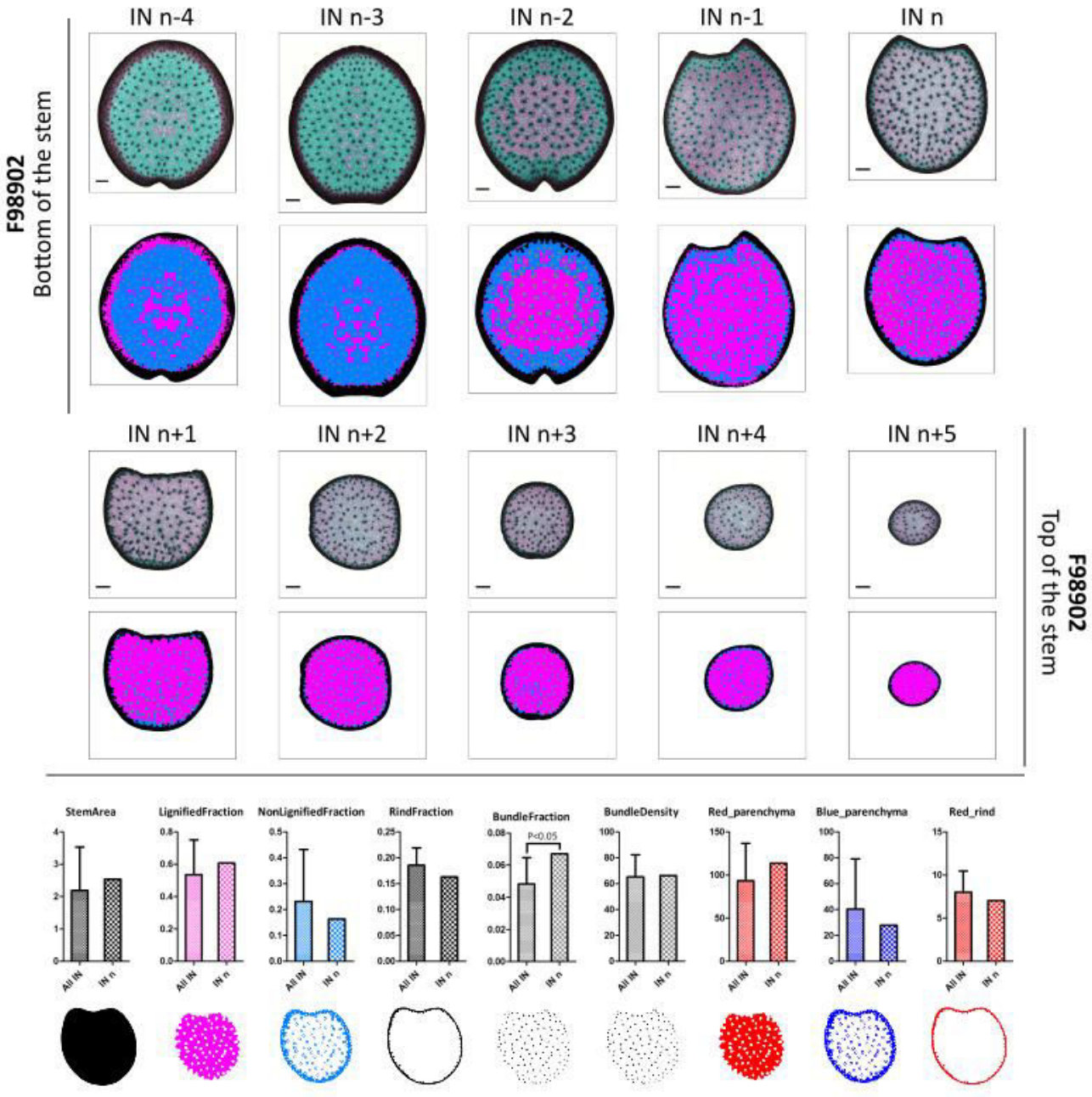


Figure 51. Histological profiles of the cross-sections of all the internodes from the bottom to the top of the stem in F98902 and comparison with the IN n. For every histological trait, a histogram represents from left to right the mean of all the internode with the standard

deviation associated and then the value of the IN n. If the one sample t-test p-value was above 0.05, the difference between the mean and the IN n value was considered non-significant.

F271 had 8 internodes. Contrary to the other genotype, F271 did not present the tendency of a large non-lignified fraction in the lower internodes decreasing to the top. The transversal section from the bottom internodes of the stem of F271 selected to perform this analysis presented stigmata of disease infection, especially in the parenchyma below the rind. This resulted in an apparent red lignin staining and thick cell walls in this region. This is particularly visible in the IN n-2 and IN n-1 (Figure 52).

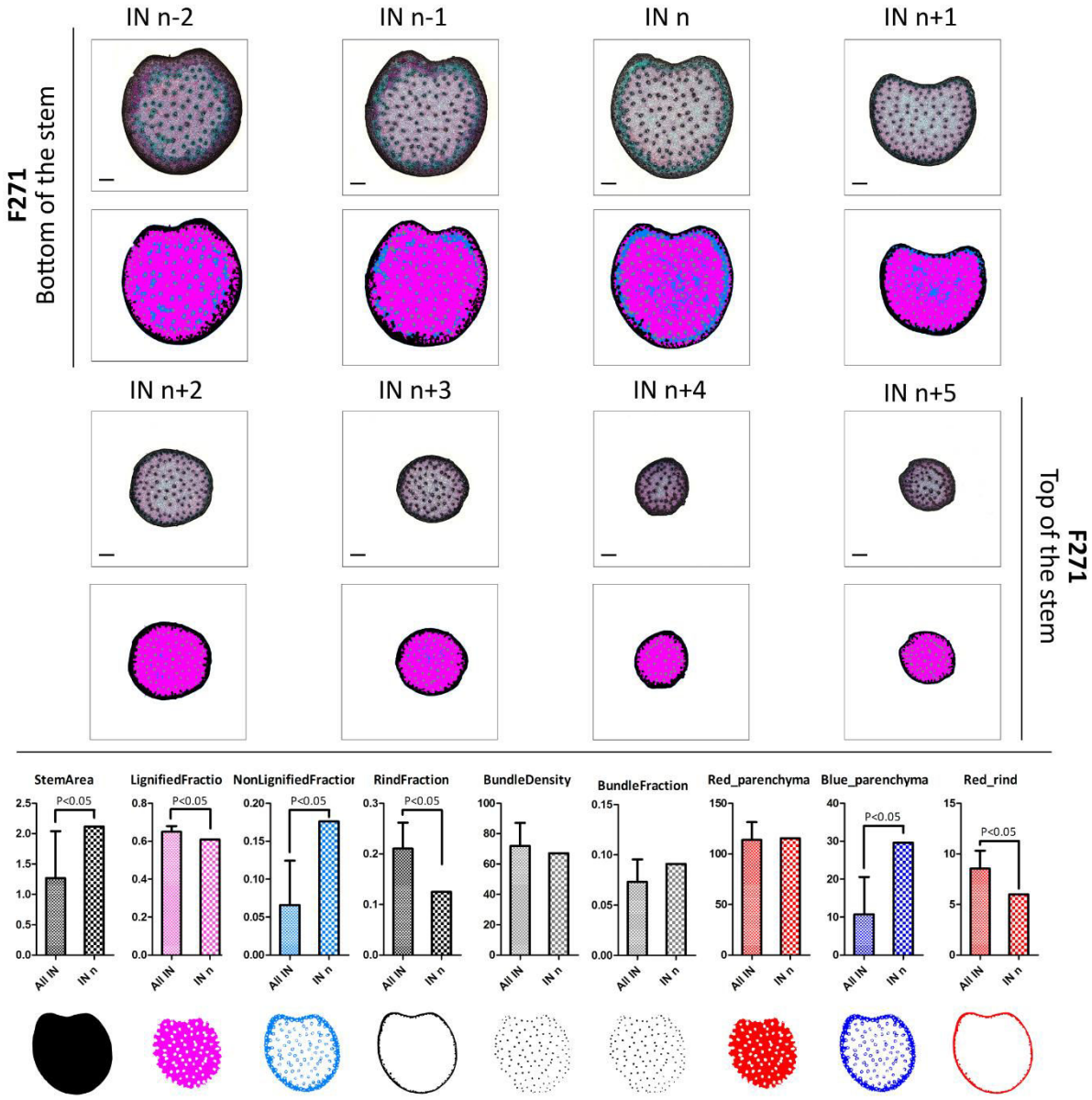


Figure 52. Histological profiles of the cross-sections of all the internodes from the bottom to the top of the stem in F271 and comparison with the IN n. For every histological trait, a histogram represents from left to right the mean of all the internode with the standard deviation associated and then the value of the IN n. If the one sample t-test p-value was above 0.05, the difference between the mean and the IN n value was considered non-significant.

Consequently the image analysis was difficult to calibrate, and many histological traits presented significant differences between the mean of all the internodes and the value of the IN n. But concerning the Stem Area, the significant difference between the IN n and the mean of all the internodes may suggest that the IN n overestimates the stem area for all the internodes. It must be due to fact that the Stem area decreases a lot after the IN n and thus, for 5 internodes. Overall the statistical differences observed here are mainly coming from the disease within the stem of F271.

Stem of F7 was composed of 6 internodes. A large non-lignified fraction was observed in the lower internodes and it decreased all along the stem until the top (Figure 53). Once again, the histological values of the IN n were not found significantly different than the mean of all the internodes of the plant, meaning that they may be considered as an estimator of the histology of all the internodes.

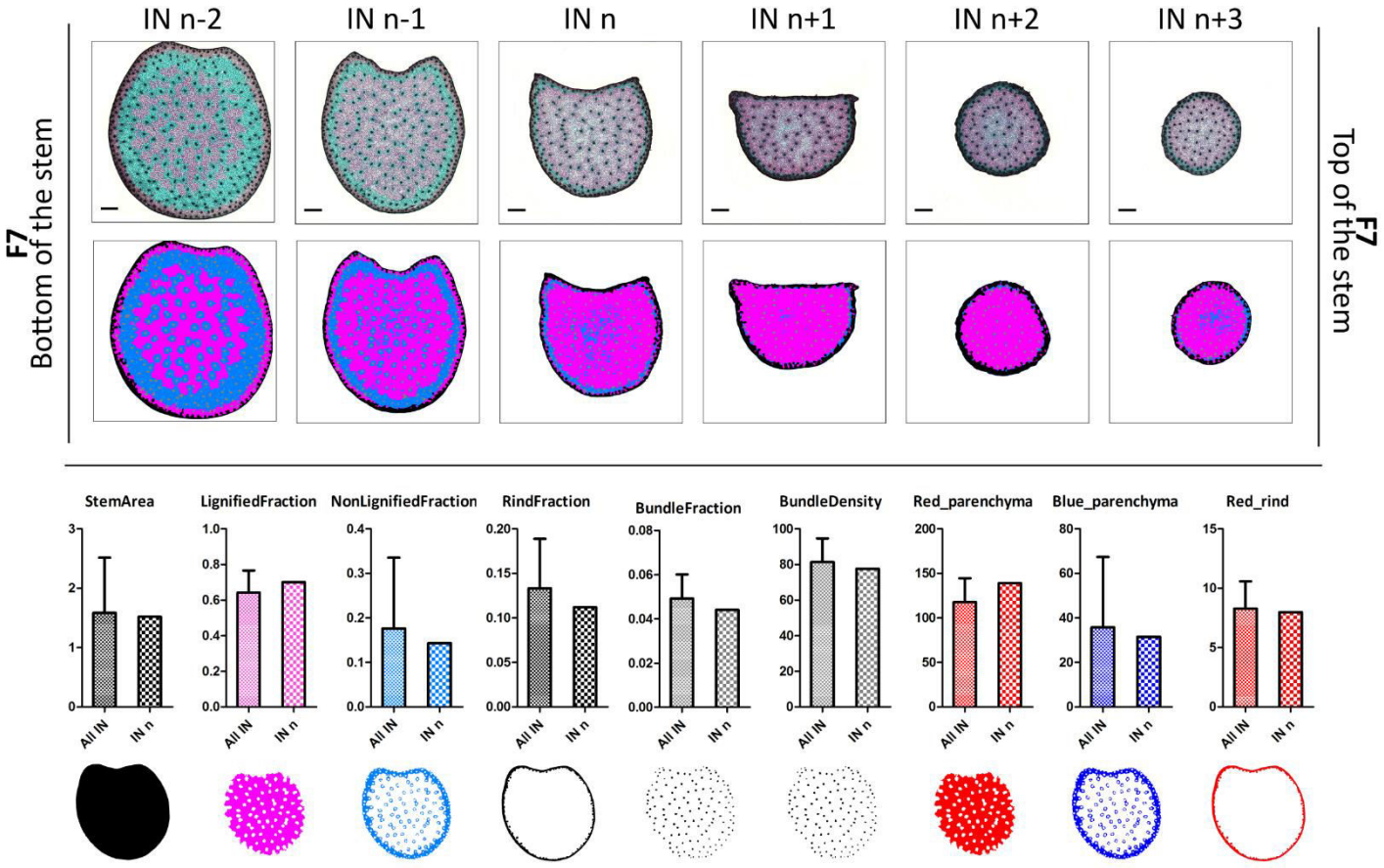


Figure 53. Histological profiles of the cross-sections of all the internodes from the bottom to the top of the stem in F7 and comparison with the IN n. For every histological trait, a histogram represents from left to right the mean of all the internode with the standard deviation associated and then the value of the IN n. If the one sample t-test p-value was above 0.05, the difference between the mean and the IN n value was considered non-significant.

F4 had also 6 internodes. F4 is known to present a histological profile with a large non-lignified parenchyma FASGA-blue stained and a thick and dark rind. Surprisingly, the upper internodes showed a lignified parenchyma (FASGA-magenta stained) which increased from the IN n+1 to the IN n+2. The lower internodes were found with a large non-lignified parenchyma and with a thick rind. The 2 histological traits which presented a significant difference between the IN n and the mean of all the internodes were the Stem area and the Bundle fraction, meaning particularly that the IN n would here overestimate these two values compared to the mean of all the internodes.

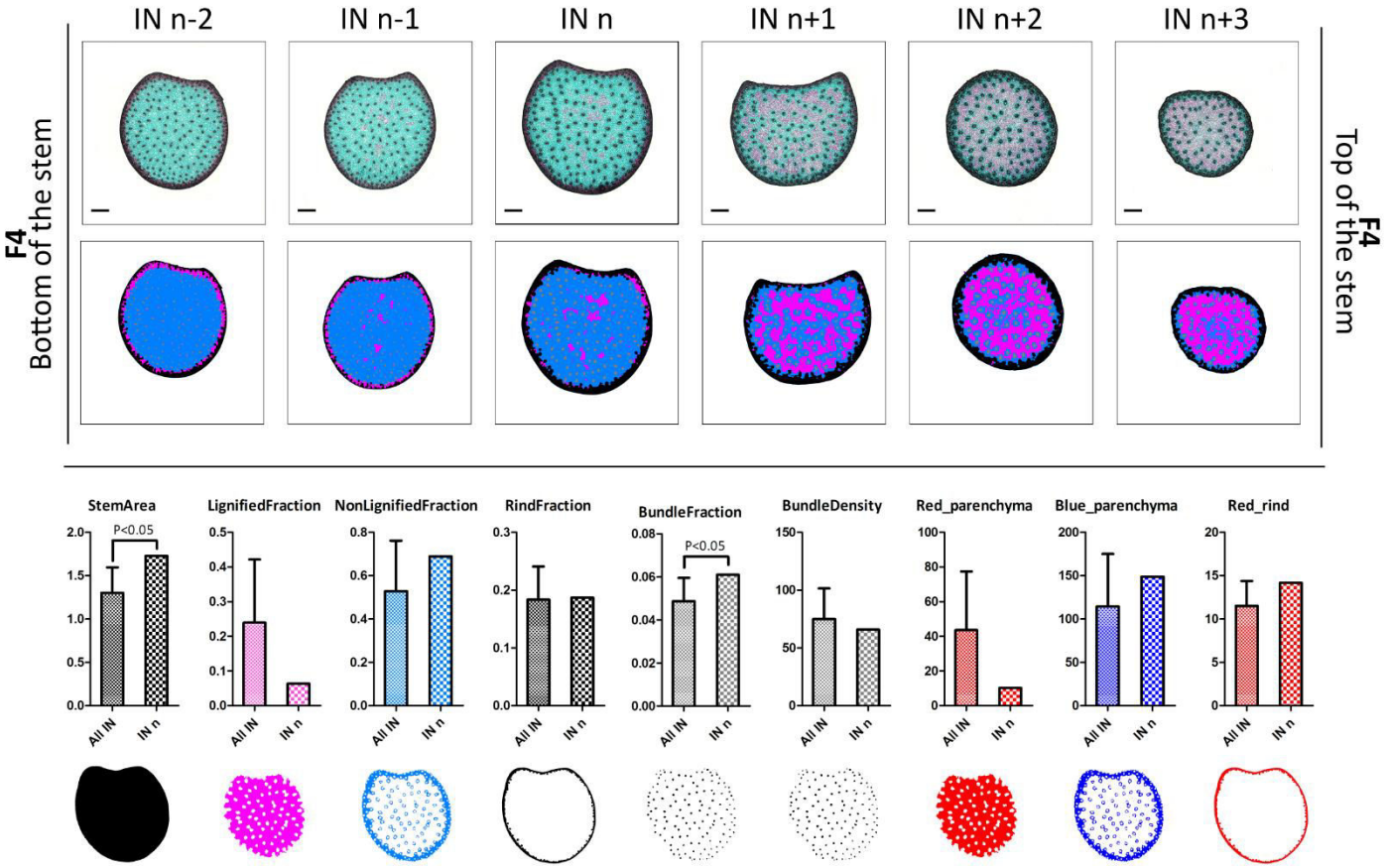


Figure 54. Histological profiles of the cross-sections of all the internodes from the bottom to the top of the stem in F4 and comparison with the IN n. For every histological trait, a histogram represents from left to right the mean of all the internode with the standard deviation associated and then the value of the IN n. If the one sample t-test p-value was above 0.05, the difference between the mean and the IN n value was considered non-significant.

Overall, these 8 genotypes harvested at silage stage showed different types of lignification patterns depending on where the internode is on the stem but despite the genetic diversity, we see the same type of patterns for a given rank. The lower internodes presented a large FASGA-blue stained non-lignified parenchyma with a thick rind while the upper internodes presented a thinner rind with a greater FASGA-magenta stained lignified parenchyma. This highlights the fact that lignin/phenolics distribution is internode dependent within a given stem of a geneotype. The light exception to this lignification pattern was F4 which kept a thick cortex until the top of the stem, but one of the reason could be that the amount of non-lignified parenchyma stays high even in the internodes of the top of the stem. F4 presented by the way in average the highest amount of Red rind (between 10 and 15) compared to all the other genotypes (globally under 10). This would suggest that a parenchyma within the pith lowly lignified would be associated to a rind more lignified.

Finally we compared if the genotypic value given by the quantification of the IN n was the same than the mean of all the internodes. This is why we plotted for each histological trait the mean of all the internode in function of the value of the IN n.

The Red rind kept globally the same differences between genotypes (Figure 55-A). The Bundle density (Figure 55-B) and the Stem Area (Figure 55-D) were overall very well represented by the value of the IN n, keeping the order between genotypes and presenting respectively a determination coefficient of 0.917 and 0.817. On the other hand, the Red parenchyma (Figure 55-C) showed that the mean of all the internodes were a bit different than the value of the IN n. The good determination coefficient is due to the particularity of F4. As the values of the other genotypes are relatively close, the differences between the mean of all the internodes and the value of the IN n show that the ranking of the genotype would be slightly different whether we consider the mean or the IN n.

To sum up, these results show, along with the study presented in the chapter 1-I (El Hage et al., 2018) that it exists differences between the stems of the genotypes, such as F4 which present a very particular Red parenchyma (Figure 55-C) or F2Bm3 which has a great bundle density (Figure 55-B) and the IN n reflects well the mean of all the internodes and therefore the stalk but also genotypic differences.

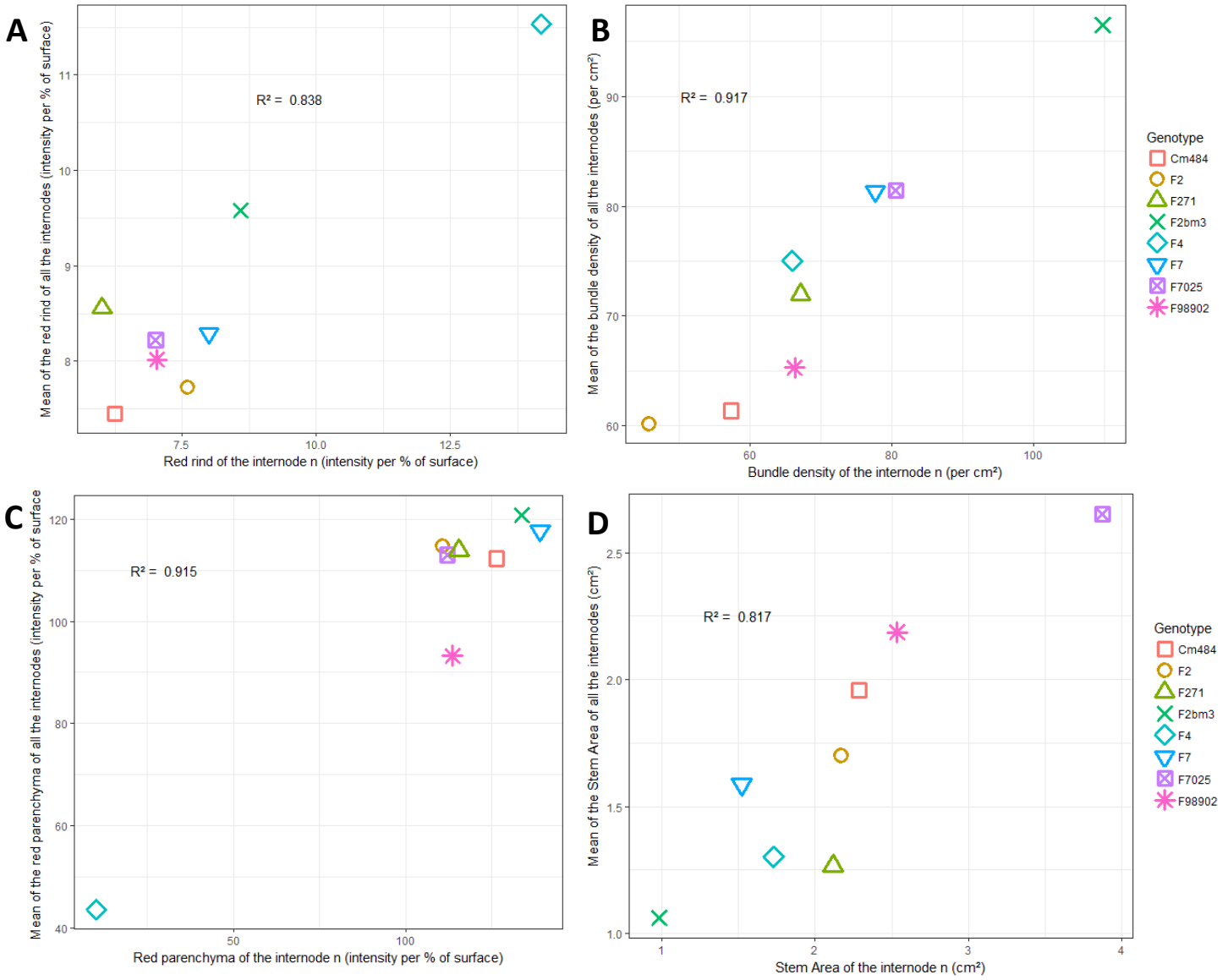


Figure 55. Mean of all the internodes per genotypes in function of the value of the IN n for 4 histological traits: A. The Red rind. B. The Bundle density. C. The Red parenchyma. D. The Stem Area.

Overall and along with all the previous chapters, these results are very positive for the consideration of the histology of the internode carrying the main ear. The internode carrying the main ear is a good histological model which reflects the average histology of the whole stem. It supports very well the choice of it when studying the relationships between the cell wall biochemistry and the spatial distribution of lignification as we did in the 2 first chapters and other studies in literature (Méchin, 2000; Mechin et al., 2005; Zhang et al., 2011). It is also raising several questions about certain studies which chose another internode to characterize the lignification distribution of the stem. Thus in the present 8 genotypes studied in this chapter, if the internode of the bottom was chosen for every genotypes, the histological quantifications would be almost all the time significantly different from the mean of all the

internode (Table 12-2). When the mean of all the internode is compared to the internode n, the differences are not significant for almost all traits and all genotypes (Table 12-1). Boon et al., (2005, 2008, 2012) chose systematically the first internode above the soil to look at a great diversity of tissues but they observed typical lignification pattern from the internode of the bottom.

Table 12. p-value of the one sample t-test between the IN n and the mean of all the internodes (1) and between the internode of the bottom of the plant and the mean of all the internodes (2). (F271 was removed because of the disease it showed).

1)

	Stem area	Lignified fraction	Non-lignified fraction	Rind fraction	Bundle fraction	Bundle number	Bundle density	Red rind	Red parenchyma	Blue parenchyma
Cm484				.	*					
F2							*			
F2bm3		.					*			
F4	*	.			*			.	.	
F7										
F7025	*			*		**				
F98902				.	**	.				

2)

	Stem area	Lignified fraction	Non-lignified fraction	Rind fraction	Bundle fraction	Bundle number	Bundle density	Red rind	Red parenchyma	Blue parenchyma
Cm484	*	*	*	.		.		*	*	*
F2	*	*	*	*	*	*	.		**	.
F2bm3	.		*	**	*		.	.		**
F4		.	.	.		*	*			.
F7	*	**	**	*	**	**	.	.	**	*
F7025	**	***	***	***	.	**	*	***	***	***
F98902	**	**	***			**	*	.	**	***

Significance: . , p ≤ 0.1; *, p ≤ 0.05; **, p ≤ 0.01; ***, p ≤ 0.001.

b) Histological variations of the internode carrying the main ear partially reflect variation of the biochemistry of the whole plant without ears.

As previously demonstrated using 8 genotypes, the internode carrying the main ear presents a histological profile which reflects well the “histological average” of all the internodes of the stem. It is therefore tempting to investigate the relationships between histological traits and the biochemical cell wall traits of the whole plant without ears. Looking at the simple relationships between histological traits and the cell wall biochemical traits of the whole plant without ear did not show strong relationships (pearson correlation factor did

not exceed -0.58 for the relationship between Red_parenchyma and the in vitro cell wall degradability or 0.56 for the relationship between Red_parenchyma and the Klason lignin content; Table S-5). We decided to investigate further these relationships by combining different histological traits to investigate the biochemical traits variations explanations. The statistical model of the multiple regressions is perfectly suitable to investigate how the combination of several traits can explain the variations of one trait in particular.

When regressing the histological traits on the in vitro cell wall residue degradability of the PWE, we found out that a combination of 3 histological traits of the internode carrying the main ear was able to explain 41 % of the cell wall degradability of the whole plant without ears, following this equation: IVCWRD ~ 59.4 – 0.06 x Red_parenchyma – 2.26 x Red_rind – 2.06 x Stem Area (Figure 56).

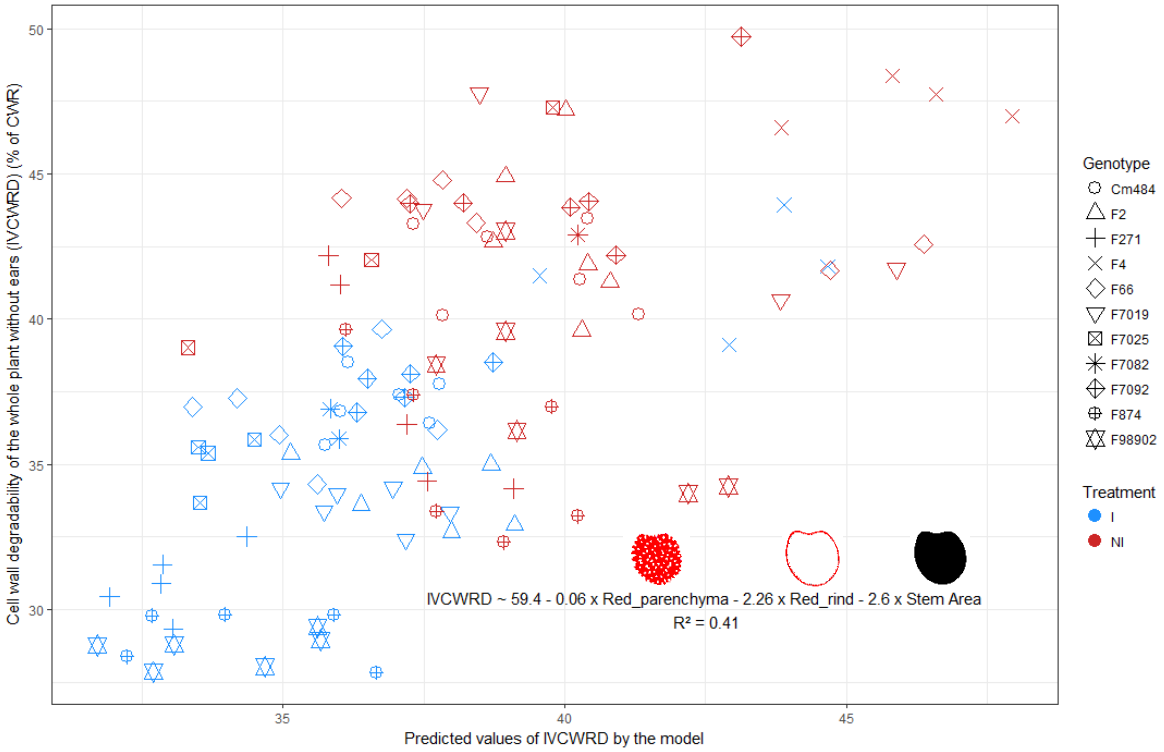


Figure 56. Relationship between the cell wall degradability of the whole plant (IVCWRD) and the model of prediction of it built with 3 histological traits according to this equation: IVCWRD ~ 59.4 – 0.06 x Red_parenchyma – 2.26 x Red_rind – 2.06 x Stem Area. $R^2 = 0.41$.

This result evokes the study carried out on chapter 1-I (El Hage et al., 2018) were the red parenchyma and the red rind were the 2 histological traits negatively related to the cell wall degradability and explaining the most its variations under both irrigated and non-irrigated conditions. The fact that their combination, along with the stem area, is the strongest to explain the variation of the cell wall degradability in the whole plant reinforces the importance of these traits among this panel of genotypic diversity. In Mechin et al. (2005), in search of a maize ideotype, they also used the same models calculation with FASGA histological profiles

and biochemistry evaluated on the plant part below to the ear (i.e. the bottom of the stem). Despite quantifying the biochemistry not on the whole plant and selecting therefore the most lignified part, they did show on 22 genotypes that an ideotype of maize with a good cell wall degradability had to have a less important “red area” corresponding here to the lignified fraction along with less PCAest and more S/G ratio. These results all together support the importance and the role of the lignification distribution in explaining the variation of the cell wall degradability.

A multiple regression on the lignin content of the whole plant without ears with histological traits gave a rather good model either. It is worth to note that under the non-irrigation condition, the variation of the genotypes seems more homogenous and fit better the relationship than under the non-irrigated treatment. However, with the 3 same histological traits, it is possible to explain until 43 % of the lignin content (Figure 57). Compared to the equation predicting the cell wall degradability, the factors of the linear combination changed: KL.CWR ~ 9.5 + 0.01 x Red_parenchyma + 0.56 x Red_rind + 0.73 x Stem Area.

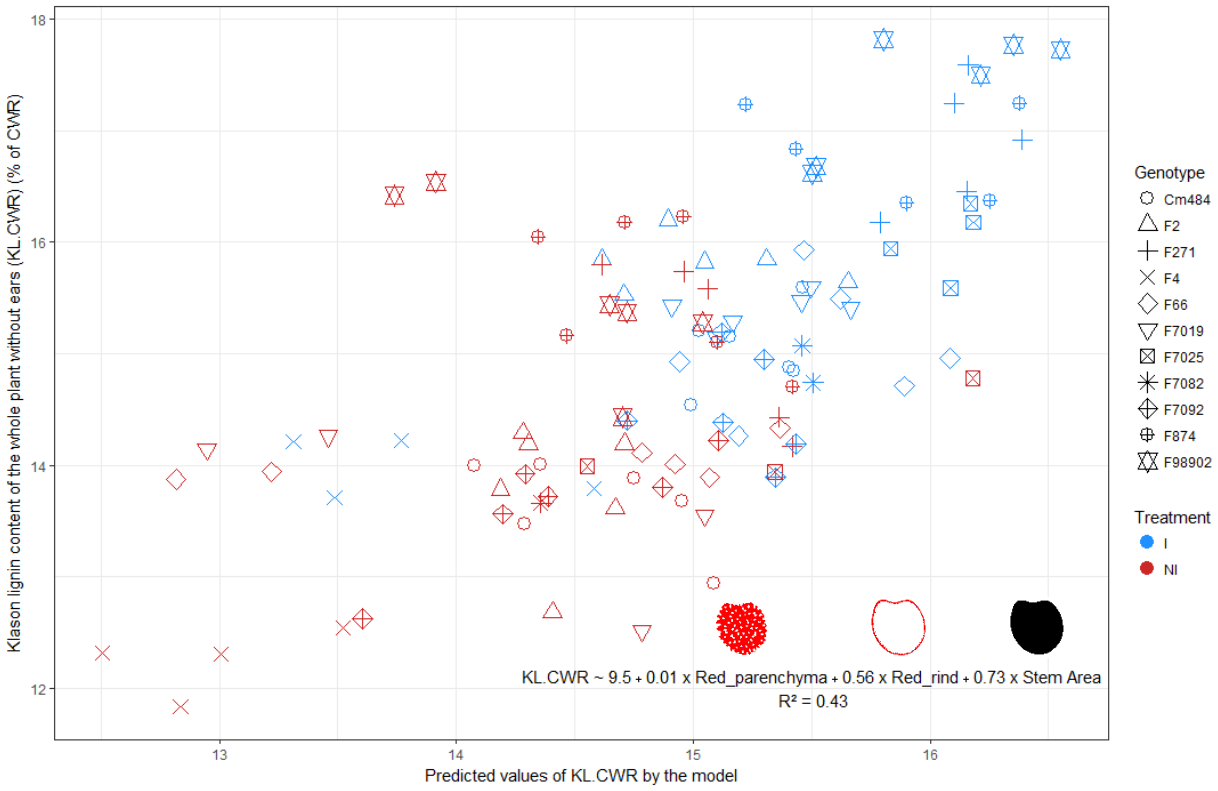


Figure 57. Relationship between the Klason lignin content of the whole plant (KL.CWR) and the model of prediction of it built with 3 histological traits according to this equation: IVCWRD ~ 9.5 + 0.01 x Red_parenchyma + 0.56 x Red_rind + 0.73 x Stem Area.

Once again, this result corroborates the hypothesis and the model proposed in El Hage et al., (2018) on the same genotypes with the red parenchyma and the red rind being the most

explicative traits positively correlated to the lignin content. Particularly in the case of the red rind, quantifying "histological lignins" in the rind, it was reported in several studies that the sclerenchyma, particularly lignified, around the vascular bundles was negatively associated to the cell wall degradability. This was shown in maize (Zhang et al., 2012; El Hage et al., 2018) but also in sugarcane (Dos Santos et al; 2015; Perrier et al., 2017) and in switchgrass (Shen et al., 2009; Crowe et al., 2017).

Finally a multiple regression gives a model where the 3 precedent histological traits allow to explain until 35 % of the variation of the esterified *p*-coumaric acid content in the whole plant without ears (Figure 58).

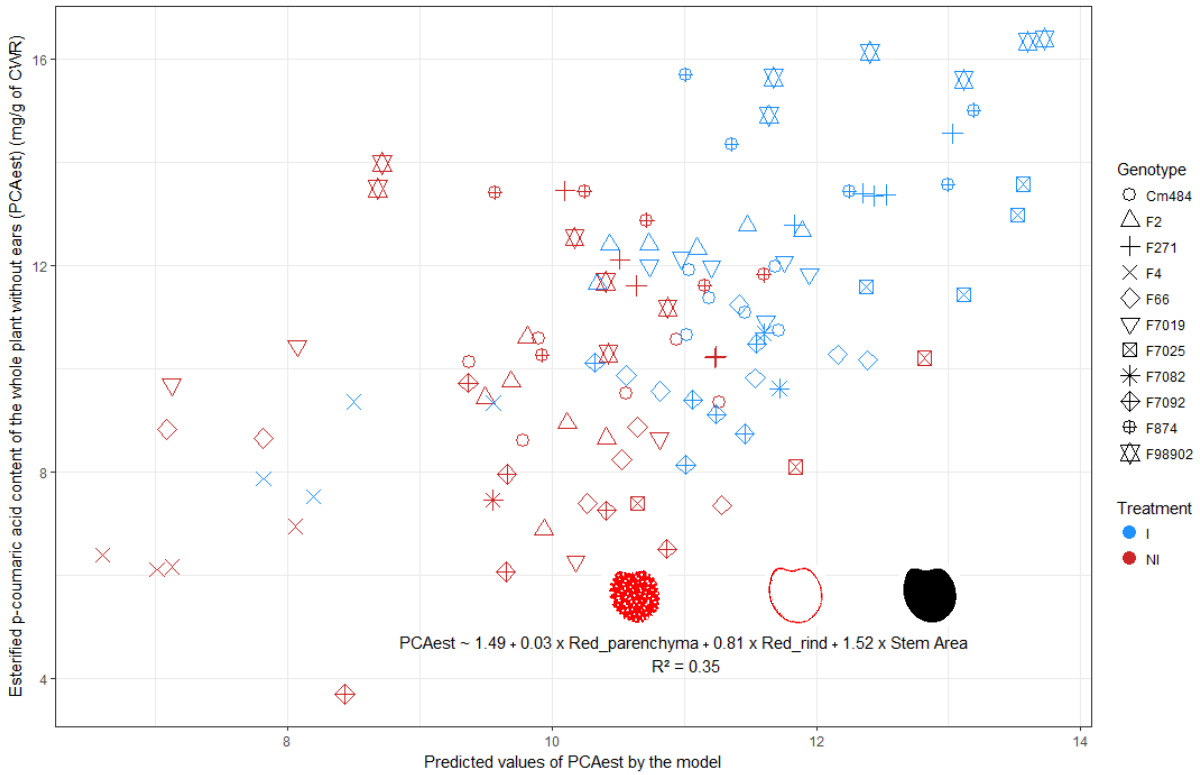


Figure 58. Relationship between the esterified *p*-coumaric acid content of the whole plant (KL.CWR) and the model of prediction of it built with 3 histological traits according to this equation: PCAest ~ 1.49 + 0.03 x Red_parenchyma + 0.81 x Red_rind + 1.52 x Stem Area.

As previously proposed in the chapter 1, the *p*-coumaroylation of the lignins in the rind and in the parenchyma is one of the major responses to the water deficit among these genotypes. Here, the fact that the red parenchyma and the red rind explain until 35 % of the PCAest of the whole plant along with the Stem Area is another argument supporting the spatial role of the *p*-coumaroylation of the lignins within the whole plant.

In every models, with only these 3 histological traits, the effect of the irrigation condition remains well predicted for every of the biochemical traits presented here. This is another argument which shows that the responses at the histological level to the irrigation

condition are probably tightly linked to the responses of the cell wall biochemistry at the whole plant level.

Overall these results support the model proposed in the first chapter but at the plant level and pinpoints the importance of the red parenchyma, the red rind, the lignin content and the *p*-coumaroylation of the lignins to explains the variations of cell wall degradability. The combination of all these traits is promising for the selection of lines with a good degradability.

Conclusion

In this third chapter we chose to investigate the representativeness of the internode carrying the main ear, as it is the internode that was always chosen in every of the experiments developed in our team either on the biochemical point of view or on the histological analyses.

Concerning the cell wall biochemistry, we found that biochemical feature of this internode was a rather good estimator of the cell wall degradability, the lignin content and the esterified *p*-coumaric acid content of the stover. However, for the other cell wall traits such as the BO4 linkages yield, the S/G ratio, the esterified ferulic acid content, the cellulose and the hemicelluloses content, the cell wall of this internode must be presenting too many differences with the other fractions of the plant such as the nodes and/or the leaves.

Comparing the histological profile of this internode with the histological profile of all the internodes of the plant we were nicely comforted to realize that for all the genotypes except F271 (studied stem of F271 showed disease symptoms), and for a large majority of the histological traits, the internode carrying the main ear did not present significant differences with the mean of all the internodes of the stem per genotype. This suggests that the internode carrying the main ear can be considered as a good estimator of the average histology of the internodes of the stem.

Finally, the histology of this internode was showed to be powerful enough to explain until 41 % of the cell wall degradability with only the 3 histological traits: the Red_parenchyma, the Red_rind and the Steam area. These same traits were able to explain 43 % and 35 % of the Klason lignin content and the esterified *p*-coumaric acid content respectively. The percentage of explanation brought by the histology is disctinct from the explanations brought by the cell wall biochemistry which put a great interest in combining them. This result corroborates with the few ones reported in the literature and highlights the importance of the histology in explaining the quality traits of the biomass.



Chapter 4

Chapter 4: General discussion

My PhD work encompassed in the objectives to better understand the relationships between the lignification distribution, the cell wall structure and composition and the cell wall degradability along with the impact of the water deficit on these traits and their relationships. This work was divided and presented in 3 main chapters in the present manuscript. After the development of high-throughput tools dedicated to the plant material studied, we first investigated the above mentioned traits variations in a maize genetic diversity panel cultivated 3 years under contrasted irrigation conditions. Secondly, the validation of the tools on this first study allowed performing histological and biochemical phenotyping at a bigger scale in a population of recombinant inbred lines to investigate the genetic determinism of these traits under contrasted irrigation conditions. Finally, as the histology quantifications were exclusively performed on the internode carrying the main ear, it rose several questions about the histological representativeness of this internode for all the others internode of the plant's stem and the legitimacy to compare the histology quantification of this specific internode with biochemical cell wall traits and cell wall degradability measured on the whole plant. All these results will be discussed here in their entirety. In a first part, an evaluation of the development and the use of the high-throughput phenotyping tools and an evaluation of what all the previous presented results bring to the understanding of cell wall degradability in maize will be done, then the impact of the water deficit on it and on both histological and biochemical traits will be presented. In a second part I will discuss the perspective of these high-throughput phenotyping tools, then about the choice of the plant material to answer to our questions, and finally about both the cell wall biochemical components distribution of the lignification both at different scale and finally the impact of the water deficit on the plant, depending on the organ and the lignification strategies that the plant might set up. In a third and final part, we will broach all the questions raised by these results and the perspectives of all what would need to be done to deal with this work in depth and improve the understanding of cell wall degradability in maize under contrasted irrigation conditions.

I. What bricks do we bring to the cell wall degradability understanding?

a) Development and probation of high-throughput tools

The development of high throughput tools was a success in many ways. One of the first originality of these tools is that they are dedicated to the studied plant material.

Concerning the NIRS predictive equations, as they were presented in each previous chapter, they were built during the time frame of my PhD to be able to predict cell wall biochemistry in contrasted irrigation conditions and for genotypes presenting a large range of variations. They were therefore dedicated to the studies in the team and the maize genetic diversity panel or the recombinant inbred lines population which were investigated. Indeed, in the work on the panel of maize genetic diversity, on the 56 internodes samples used to calibrate the equations, 45 internodes samples were belonging to the genotypes studied, to be able to predict them with the greatest accuracy. This NIRS predictive equations establishment was then enriched with 56 internodes samples coming from the recombinant inbred lines population to better predict the cell wall biochemical components of it. As the same time, NIRS predictive equations for the cell wall biochemistry of the whole plant without ears were built with the same objective. The Pearson correlation factors between the predicted values and the biochemical values of the calibration samples may vary but all above 0.65 and mainly above 0.80. All the built equations are therefore robust to predict a large spectral variability and sufficiently precise for the studied material of the maize genetic diversity panel and the RILs population. So far no NIRS predictive equations for the internode has been published. Li et al, (2017) did not give the origin and the characteristics of the NIRS equations they used to predict the stalk biochemistry of their study. In addition, the main NIRS predictive equations used to predict the cell wall biochemistry of the whole plant without ears, and often used in literature (Barrière et al., 2008; Barrière et al., 2012; Torres et al., 2016) are the ones developed in Lusignan for more than 20 years with about 700 calibrating samples (Riboulet et al., 2008b). If the great amount of calibrating sample give them a great robustness, they were not suited to predict ranges variations response to water deficit. That is why this high-throughput tool to quantify very fine cell wall biochemistry was successful to complete our needs.

On the other hand, a high-throughput tool was developed to phenotype histological profiles of FASGA stained maize stem cross-sections. As it was described in Legland et al., (2017) the FASGA staining allows a good segmentation of the different lignified tissues thanks

to the contrasts between the blue and the magenta staining from a tissue to another. Several other tools exist and have been mentioned in literature to quantify histological fractions; Guines et al., (2001; 2003) used the software Optimas on alfalfa cross-sections to quantify xylem cell wall thickness; Siqueira et al., (2011) used a scan program called APAMOS (Zeiss) to compare UV profile on small dissections of sugarcane stems; Heckwolf et al., (2015) developed a tool to quantify the bundle number and the stem area on non-stained sorghum cross-sections; and finally Perrier et al., (2017) used a series of plug-ins in ImageJ software to quantify the pith parenchyma, the rind area and the sclerenchyma area within the rind on FASGA stained stem cross-sections in sorghum. If some of these tools allow to decipher further the percentage of sclerenchyma area into the rind (Perrier et al., 2017), none of these tools quantify as much histological traits as Legland et al., (2017) and more importantly none of them allow a batch quantification analysis (great amount of cross-sections analyzed in a short time). To ensure a good repeatability, I dedicated time during my PhD in improving the protocols from the cutting, the staining to the image acquisition.

Altogether, these tools dedicated to both the histological and biochemical analyses of the maize internode were suited for the study on the maize genetic panel diversity (El Hage et al., 2018) and successfully adapted to a larger amount of samples on the RILs population. These tools pave the way of deciphering the role of tissues distribution in degradability apart of the role of biochemical contents or structure. They represent original phenotyping tools which may be used for further projects to study the cell wall biomass quality traits.

b) The understanding of cell wall degradability

In the first chapter, the selection of 11 genotypes of maize for a large range of cell wall degradability was successful to answer to our questions. The results showed a range of 19 % of cell wall degradability in the internode between the genotype the less degradable and the best one under irrigated conditions. Despite lignin content showed a strong relationship with cell wall degradability in this panel, it was however possible to highlight the importance of other biochemical factors to explain cell wall degradability variations. Indeed, along with previous studies (Mechin et al., 2005; Zhang et al., 2011), the results showed that the esterified *p*-coumaric acid was significantly relevant in the explanation of cell wall degradability and more particularly in both irrigated and non-irrigated condition.

More particularly, water deficit induced a significant increase of the cell wall degradability in both the maize genetic diversity panel and the RILs population, overall the genotypes. It also induced a great diversity of response from a genotype to another, suggesting some strategies to maintain certain biomass characteristics according to the

genotype. From a breeding point of view, it also suggests that selection for water deficit response may be considered.

QTL detection for cell wall degradability in the internode pinpointed QTL at loci known to be involved in the variation of this trait but at the whole plant level, particularly at bin 4.05 and bin 6.05. Furthermore, the combined analysis of the genetic determinism of histological traits and the genetic determinism of cell wall degradability in the whole plant without ears revealed co-localizations at bins 1.07-11 and 10.03-06. It suggests the possibility of genetic links between the histology for the internode below the main ear and the cell wall degradability of the whole plant. More particularly, at bin 10.03-06, on the whole plant without ears was detected a QTL for cell wall degradability with no other biochemical cell wall traits and on the internode QTLs for bundle density and bundle numbers. These results let consider histology as traits which may be genetically linked to regions influencing cell wall degradability variations.

Comparing further the internode biochemical characteristics with the ones of the whole plant without ears, we demonstrated for that for at least 3 biochemical traits (cell wall degradability, lignin content and *p*-coumaric acid content), the internode carrying the main ears reflected very well the variations of these traits at the whole plant without ears level. More particularly in the comparison between the internode and the whole plant, the combination of 3 histological traits (Red parenchyma, Red rind and Stem area) can explain until 41 % of the variations of cell wall degradability in the whole plant without ear in the maize genetic diversity panel and more importantly the explained variations were not the same than the one explain by cell wall biochemistry. These results underlines the results found in the QTL analysis and suggest first, that co-localization QTLs detected at different scales may not be random, and secondly, that cell wall degradability is a complex trait which may be influenced by many factors, such as histology, at different scale. It reinforces the idea that it would be possible to select plants on histological targets to improve cell wall degradability without impacting too heavily the global cell wall composition.

Altogether these results bring a greater understanding of cell wall degradability and on the cell wall traits related to it in maize both at the internode and at the whole plant scale.

c) Impact of water deficit on biomass quality

Water deficit had a strong impact both on the histological and cell wall biochemical traits, although for the RILs population, the water stress did vary between 2014 and 2015. Along with decreasing significantly the main agronomical traits such as height of plants and yield, water deficit impacted heavily the cell wall of the stem by inducing a decrease of the phenolic compounds content, particularly the lignin and esterified *p*-coumaric acid contents

and this was associated to an increase of cell wall degradability. It also reduced significantly the Red parenchyma and the bundle density within the stem. Water deficit impacted these traits itself but also their relationships. Thus, particularly in the maize genetic diversity panel the red rind, which is decreased under non-irrigated conditions, showed better relationships with the lignin content and the PCA content under non-irrigated condition whereas the red parenchyma showed good relationships with these traits mainly under irrigated condition. At the internode level, we then propose the hypothesis that the response of the plant was to lignify and to deposit more *p*-coumaric acid units preferentially in the rind, and decreasing their content between the irrigated and non-irrigated condition though.

If the 2 water deficit applied respectively in 2014 and 2015 on the RILs population did not reveal QTL specific of the non-irrigated condition, the QTL analyses were still different from one condition to another, suggesting a response of the plants at the phenotypic but also at the genetic level to these environments. However the internode was not impacted the same during these 2 years of experiment way than the whole plant during 3 years by the water deficit. This is why we did not favour a global analysis over the year for the internodes. Nevertheless, at the whole plant level, we were able to detect 149 responsive QTLs for several cell wall biochemical traits and particularly cell wall degradability, lignin content and esterified *p*-coumaric acid content.

To sum-up, we showed here that water deficit impacts strongly lignocellulosic biomass quality and induces particular responses of the lignification.

d) From the internode to the whole plant

Studying the relationships between cell wall biochemical traits from the internode and the whole plant without ears, we were able to highlight in the maize genetic diversity panel that at least 3 traits; cell wall degradability, lignin content and esterified *p*-coumaric acid content; were well reflected between these two scales. The co-localisations studies between the QTLs detections for the cell wall biochemistry of the internode with the ones of the whole plant without ears also revealed several loci in common, at bin 1.07, 4.05 and bin 6.05 for example, which were responsible of the variations of the same traits; cell wall degradability, KL.CWR, PCAest and Hemicelluloses.

The histological analyses of all the internodes for 8 genotypes also showed that the internode carrying the main ear which has been chosen so far in all our studies, was a judicious and relevant choice. It was established as a good histological average of all the internodes, despite very different lignification profiles observed from the bottom to the top of the stem at silage stage. As we also verified it, the choice of another internode, such as the one from

the bottom of the plant which has been previously studied in literature (Boon et al., 2005; 2008; 2012) would have been too far from the average of all the internodes.

Finally, we may sum up all these results by completing the diagrams of objective which was first proposed in the introduction (Figure 59).

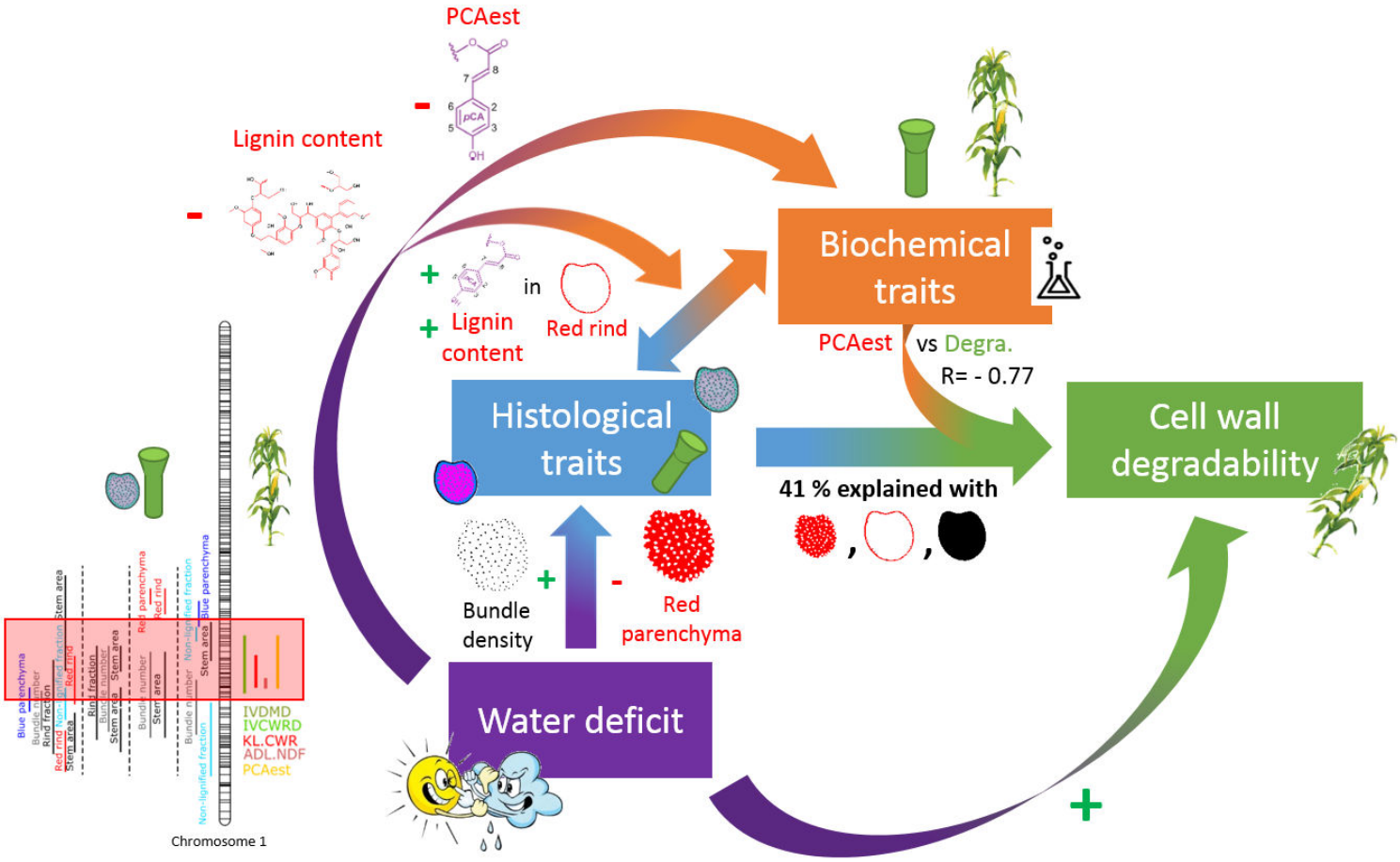


Figure 59. Answers and conclusions brought to the PhD questions.

II. All these results may be discussed further

a) Going further in the improvement of the high-throughput tools

If the several studies we presented on the internode and the whole plant without ears allowed us to decipher particular relationships between cell wall degradability and other cell wall biochemical components such as *p*-coumaric acid, it remains that the relationship of the cell wall degradability with the lignin content stays very strong within the predictions. The more the samples are diverse and enlarge the range of lignin content and cell wall degradability, the more this relationship will be present in the predictions. It means that if we want to be able to predict finer the relationships between cell wall degradability and the other cell wall components, some adjustments have to be done, like building NIRS equations with pool of genotypes selected for a narrow range of lignin content.

The histological tool to analyze a large quantity of maize stems cross-sections appeared to be very suitable to quantify histological traits for the internode carrying the main ear within a maize genetic diversity panel or a RILs population. However, when analyzing internodes as different as the internodes from the bottom and the internodes from the top, differences of profiles appeared to be so great that the analyses needed to be applied much more on a case-by-case basis. The FASGA quantification tool developed by Marc Lartaud at CIRAD quantifies the rind region, the pith region and the area of sclerenchyma within the rind. It could be used in this particular case as well as a use of our tool, image per image.

b) Choice of the plant material and monitoring the water deficit conditions to address the PhD questions

The maize genetic diversity panel was chosen on a large range of degradability and lignin content. However, a panel of genotypes selected for a large range of cell wall degradability and a narrow range of lignin content would be interesting to investigate in order to highlight other factors than lignin content (at the histological and/or biochemical levels) involved in cell wall degradability. We could consider doing the same for selecting parental inbred lines for RILs population: selecting parents with similar lignin content but showing contrasted values for all the other cell wall components. Considering the genetic determinism of histological traits, Cm484 and F271 appeared to be less contrasted once cultivated in Mauguio than when they were first characterized in Lusignan. The choice of 2 genotypes more contrasted for the histological profiles might have shown different results for the genetic determinism investigations.

The question of the water deficit in field and the repeatability is also at stake within the presented studies. The stress applied was a stop of the irrigation after the appearance of

the 5th leaf ligule on the genotype F2 and a resumption of the irrigation 14 days after the flowering. This stress may therefore be considered as intense and strong as it occurs right in the middle of the development and the elongation of the stem until the end of plant development. However we may wonder if it had been conducted at earlier or later development stages if maize plants would have presented the same responses. On the other hand, the repeatability of the water deficit in field experiment can be strongly dependent on the environmental conditions that can vary from one year to another, even when field trials are located at the same place. This was the case for the water deficit applied on the RILs population. Indeed the storm in 2015 did not allow reproducing the same water stress conditions than in 2014. Plants responded significantly differently to these two types of water deficit. A recent study on 8 sorghum genotypes investigated their response to water deficit of the biomass but also their potential recovering after a re-watering (Luquet et al.; 2018). They showed that re-watering the plants after a 25 days drought period had an effect of the plants but more particularly that the genotypes responded differently to the re-watering. The genotypes that better recovered for stem biomass growth did not necessarily better recover for cell wall residues contents. In our case, it means that the RILs may have responded differently to the storm in 2015. And despite a heavy water supply of 80 mm, the vegetative part still experienced the same temperature and humidity rate than in a water stress experiment. That is why experiments of water deficit conducted in fields can be quite tricky on the repeatability when other environmental events occur.

c) Relationships between cell wall degradability and lignification at different scales

Probably because the cell wall has a complex structure and composition, cell wall degradability is a complex trait and it has been shown that it can be improved in many ways. Thus we may consider different approaches which are currently used and presented in literature. Studies on this topic proposed generally to focus on the effect of the modification of structure and composition of the cell wall, but more and more, tissue specificity impact is being investigated.

1. Targeting the general cell wall composition within the plant

The lignin biosynthesis pathway has been investigated a lot to understand further the process but has also be one of the major levers investigated in biomass recalcitrance. As reported by Vanholme et al., (2008) many studies have presented mutants or transgenics with targeted downregulation of key biosynthetic genes in diverse plant species with results showing varying levels of reduced lignin production. However, as reported by Mottiar et al., (2016) monolignol biosynthesis is highly plastic and allows plants to substitute monolignols

when one or more of the genes is disrupted or deregulated such that lignin content and composition are both altered. This was shown on *Brachypodium* by Cass et al., (2015) where the knockdown of the PAL led to a decrease of 43% of the lignin content but a relative increase of the S and H units. In *Arabidopsis*, Marita et al., (1999) showed that a mutant presenting an almost complete loss of S units had no significant change in its total lignin content. These studies witness the plasticity and the capacity that plants have to adapt when facing a lack or major changing in the lignin biosynthesis pathway. Liu et al. (2016) showed on Arabidopsis mutant for cinnamoyl CoA reductase which led to a decrease of the lignin content that the orientation of the cellulose fibrils was also modified in all tissues of the stem. Brown-midrib mutants are natural and bright example of the plasticity of the lignins, with key enzymes knocked-down in the lignin biosynthesis pathway and associated to an increase of the cell wall degradability. *Bm3* mutants have been more particularly investigated because, compared to other maize brown-midrib mutants, the maize *bm3* mutant appeared to be especially improved in cell wall digestibility, at a greater extent than the *bm1* mutant, and because the agronomic traits are much depressed in *bm2* and *bm4* plants (reviewed by Barrière, 2017). All these studies underline the crucial place of the lignin within the plants, and if many strategies are possible for the plant to bypass major deletions, it may impact more deeply the structure of the cell wall.

Despite it is now possible to produce genetically engineered plants with levels of lignin heavily reduced to deliver plants with improved biomass degradability. But agronomically, these plants are most often less vigourous and present significant decrease in yield (Voelker et al., 2011; Bonawitz and Chapple, 2013).

That is why other cell wall biochemical components have been targeted so far. As the esterified ferulic acid may form cross-links within hemicelluloses or with lignin it has been investigated to improve biomass degradability in grasses (de Oliveira et al, 2015). It was hypothesized that these cross-links may inhibit degradability by preventing enzyme access and by tightly binding the polysaccharide substrate to non-degradable lignin. It was then supported by many works. The ferulic acid content was associated negatively with degradability in several works (Lam et al., 2003; Casler & Jung, 2006). By expressing a fungal ferulic acid esterase in *Festuca* Buanafina et al. (2008) showed an increase of biomass degradability. De Souza et al., (2018) recently investigated the suppression of BAHD gene in Sétaria viridis, a grass specie widely spread and more and more used as a plant model, and the observed decrease of cell wall feruloylation was associated to an increase of biomass degradability. These last years, the study of the feruloylation levels and the BAHD transferase family led to investigate further the role of the *p*-coumaric acid in cell wall degradability. As

reviewed by Wang et al, 2013, several works on mutant presenting higher or lower feruloylation levels have suggested that some members of the BAHD acyl-CoA transferase protein family may be responsible for catalyzing the addition of ester-linked coumarate to cell wall arabinoxylans (Fernando et al., 2009; Withers et al., 2012; Bartley et al.,2013; Molinari et al.,2013). The esterified *p*-coumaric acid has long been put aside the levers to improve cell all degradability because it is mainly known to be acylated on the S subunits of lignin and its role in cell wall degradability was always considered as redundant with the lignin one. However more and more, it is shown that its role is more complex. The studies on genes of the BAHD acyl transferase family are supporting this hypothesis. Whiters et al., (2012) identified in rice genome a member of the BAHD acyl transferase family. The analyses of the recombinant protein produced in *E. coli* showed that it had a specific coumaroyl transferase activity. This enzyme OsPMT (for *O. sativa p*-coumaric acid monolignol transferase) catalyzes the acylation of a monolignol with *p*-coumaric acid via *p*-coumaroyl CoA. Karlen et al., (2018) confirmed it in a recent study within nine families belonging to the same monophyletic group than Poaceae that lignin-linked *p*-coumarate occurs exclusively on the hydroxyl group on the γ-carbon side chains of lignin units, mostly on syringyl units and probably by BAHD acyl CoA monolignol transferases.

All these studies present possibilities to impact cell wall degradability without depleting too much lignin structure and composition by targeting *p*-hydroxicinnamates. However, their role and impact on cell wall degradability is still poorly understood and needs to be investigated further.

2. Targeting tissues specificities within the plant

The tissue specificity has been first investigated more than 20 years ago. Indeed in maize, Lopez et al, (1993) mentioned difference of cell wall composition between sclerenchyma and parenchyma. As cell wall degradability is established as a complex trait impacted by cell wall structure and composition, it is known that the latter traits may vary from one organ to another in the plant and the possibility that it may vary between tissues within an organ is more and more investigated.

Thus, Chesson et al., (1997) investigated the composition of sclerenchyma and parenchyma in maize internode and showed that the lignin structure was presenting a higher S/G ratio in sclerenchyma than in the parenchyma. A rind with bigger sclerenchyma areas was also reported as being associated to a decrease of cell wall degradability in maize (Jung and Casler, 2006; Boon et al., 2012) and in sugarcane (Bottcher et al., 2013; Guzzo de Carli Poelking et al., 2015; Dos Santos et al., 2015). The rind is therefore presented to be particularly different in its lignification than the rest of the stem in grasses. Anderson et al., (2015) showed on

mutants in *Arabidopsis* that G & S units modifications in synthesis was modifying cell wall structure, and more particularly that spatially, according to the mutant, the distribution of the lignification was different. Going even more precisely in the modifications of the structure and composition of the cell wall of particular tissues, Smith et al, 2017 demonstrated in Arabidopsis stem that the lignification was specific according to the tissue. Using cell-type-specific-promoters to knock-down or to induce monolignol synthesis genes expression, they specifically showed that xylary parenchyma and fiber cells were contributing differently to the stem lignification. Finally, Costa et al., (2016) investigated the tissue composition for other cell wall components than lignins. They looked at the tissue specific hemicellulose distribution in 6 sugarcane hybrids. They showed that xylans were predominant in vascular bundles whereas mixed linked glucan (MLG) occured mostly in parenchyma. If they also confirmed that the rind was more lignified than the pith for the 6 hybrids, they also pinpointed the cellulose was more crystalline in it. It suggests that the rind recalcitrance to cell wall degradability could be due not only from its stronger lignification but also from the structure and the deposition of other cell wall components. We suggested it with the *p*-coumaroylation of the lignins in the rind in the first chapter. It still needs to be investigated further though.

Thus, tissue-specific lignification and cell wall composition is still being investigated and, as it is not completely understood yet, the current opinion is mainly based on hypotheses. However all the recent studies bring more and more evidences that it has a key role to play in cell wall degradability understanding within the plant.

d) Impact of the water deficit on the lignification at different scales

The genetic determinism analyses we performed on the internode and on the whole plant without ears revealed that depending on the scale where we looked at, the water deficit impacted them differently. These differences of impacts could be explained by many factors. Crowe et al., (2017) showed on switchgrass that the cell wall composition of the leaf fraction was very different than the stem with less lignin content more ferulates, less *p*-coumarate and a greater proportion of polysaccharides. As the induction of lignin in plants has been correlated to stresses such as cold, drought or light as well as mechanical injuries in a number of plant species such as poplar, rice, pine, Arabidopsis and soybean (Moura et al., 2010) we may think that an organ less lignified will be more impacted by water deficit. This difference of impacts of the water stress between organs could be one reason. Ledea-Rodriguez et al., (year) characterized chemically under drought conditions new varieties of drought tolerant Cenchrus purpureus, a grass plant from Africa used as fodder, and they show that the ADF (i.e. Cellulose + Lignin content) was the most impacted trait in the stem.

It also appears that lignification could be impacted differently according to place you consider in the plant, even within a stem. Moura-Sobczak et al. (2011) reported that *Eucalyptus urograndis* subjected to drought decreased the amount of lignin in the stem apical regions and increased lignin in the basal region while *E. globulus* showed an opposite behavior in apical regions and showed no significant changes in the basal regions. A hybrid between both species (*E. uroglobulus*) showed a pattern similar to *E. urograndis* in apical regions and similar to *E. globulus* in the basal regions. This suggests possibilities to select lines that gathered the favorable responses to water stress. However, Wildhagen et al, (2018) showed on poplar that drought do not induces the same responses between 2 different genotypes of a same species. Thus a cultivar from Spain with the same lignin content than a cultivar from Italy showed a much higher saccharification than the other one under drought condition. Suggesting that, even between cultivars of the same species, the lignin content under drought condition do not explains all the variation of degradability of the plant.

Going further in the deciphering of the plant cell wall responses to water deficit, Pereira et al., (2018) mentioned that greater lignin content in the xylem could also improve resistance to embolism induced by drought. Understanding embolism resistance would be a key factor to elucidate plant responses to drought and adaptive strategies in both dry and wet environments as reported by several studies (Choat et al., 2012; Lens et al., 2013; 2016; Anderegg et al. 2016). This was recently confirmed by Rosner et al., (2018) who showed on Norway spruces that drought induced stem cracks along the trunk. It is more particularly associated to the production of extremely thin cell walls in earlywood which lead to the collapse of tracheid walls. Going into the smaller scale of the tissue allowed here to explain the effects of drought on the plant. Thus we could imagine that lignin deposition in the xylem tracheids could play the same role than lignin deposition in the rind of the stem. It would limit water evaporation and cell bursts because of the osmotic stress due to drought. From that point, being able to select plant which would lignify all the vulnerable tissues preferentially, such as the vascular bundles and the cell layers at the epidermis which suffers the drought more directly than the other cell layers, would be a key strategy to select plants resilient to water stress. The engineering tools for lignin deposition tissue-specific presented by Smith et al., (2017) could pave the way to the understanding of this. In this idea of engineering cell wall components for drought resistance, Yan et al., (2018) engineered *Arabidopsis* plants with a low degree of xylan acetylation and they show that such plants presented increased drought tolerance. They conclude that substantial changes in biomass composition can be achieved without compromising plant resilience.

To put it in a nutshell, understanding of cell wall components, structure and tissue specific lignification and particularly the deciphering of the roles and the composition of the rind and the pith parenchyma within the stem of the plant will be a crucial key to be able to select plant resilient to the climate changes incoming. Many studies need still to be done, and this is great because we are eager to dig all this up!

III. Perspectives

Several experiments are possible to consider to follow the work presented here and to answer the questions it raised.

Concerning the cell wall biochemistry, the role of the lignification and the *p*-coumaroylation within the rind has been hypothesized to be involved in response to a water deficit. Further biochemical experiment could be done to confirm it, such as mass spectrometry imaging approaches that will allow the realization of *p*-coumaroylation maps at the scale of internode cross-sections. Micro-dissection approaches followed by biochemical analyzes could also be considered. However the tries I did during my phD on micro-dissecting bundles in order to analyze lignin structure by thioacodolysis revealed a heavy and tedious work, as it was required to microdissect at least 100 to 150 bundles from 80 µm thick cross-sections to have enough material. Separating the rind from pith could be worth to consider, (as first presented by Lopez et al., 1993) and could suits more to biochemical analyses. Performing measurments of cell wall degradability directly on cross-sections could also be a way to access to a tissue-specific cell wall degradability. All of these experiments will lead to the understanding of the role of the tissue distribution of lignin and *p*-coumaroylation to better understand cell wall degradability. In terms of plant breeding and in the current context of climate change, it also opens perspectives to select plants resilient to water deficit, by considering these knew histological and biochemical targets.

The genetic determinism of histological traits could be further investigated by analyzing RILs populations from more contrasted parents for the histological profile such as F4 and F7025 presented in the chapter 1. F4 has a low yield with a very blue FASGA stained histological profile and do not respond much to water deficit while F7025 has one of the best yield of the maize genetic diversity panel, presents a great response to water deficit and present a FASGA profile more classical. But it would imply to phenotype a great amount of cross-sections, which need to be thought cautiously. Investigating further the genes under the main QTL regions responsible of the variations of many histological traits (bin 1.07/11 and 10.03/04) could also help in validating and understanding their link with cell wall degradability at the whole plant level. At the whole plant level, responsive QTLs for IVCWRD were also pinpointed to co-localize with responsive QTLs for biomass yield, and in each case, alleles that increased IVCWRD in response to the NI scenario decreased the biomass production. This shall be taken into account to select resilient lines under water stress condition.

On the histological point of view, a complementary analyze tool could be used to further analyze the intensities in the rind. This tool was presented in Zhang et al., (2013) and it measures and draws the curves of the intensities from the cortex to the center of the pith

on a straight line. Considering all the particularity of the rind, I would like to particularly investigate ways to decipher the histology of the rind. If we take the example of 2 different genotypes such as F4 and F98902 (Figure 60), as we can see, for one level of internode, either the internode of the bottom or the internode n (carrying the main ear), their rind are quite different. F98902 a very large rind at the internode from the bottom with large sclerenchyma sheath around the bundles compared to F4 but also to its own internode n. F4 does present a bigger rind at its internode from the bottom but a sclerenchyma less developed than in F98902. The rind of the internode n of F4 also presents the particularity to have cell layers FASGA stained blue parenchyma. This can be found in other genotypes but not in F98902 and not at the level of the internode of the bottom.

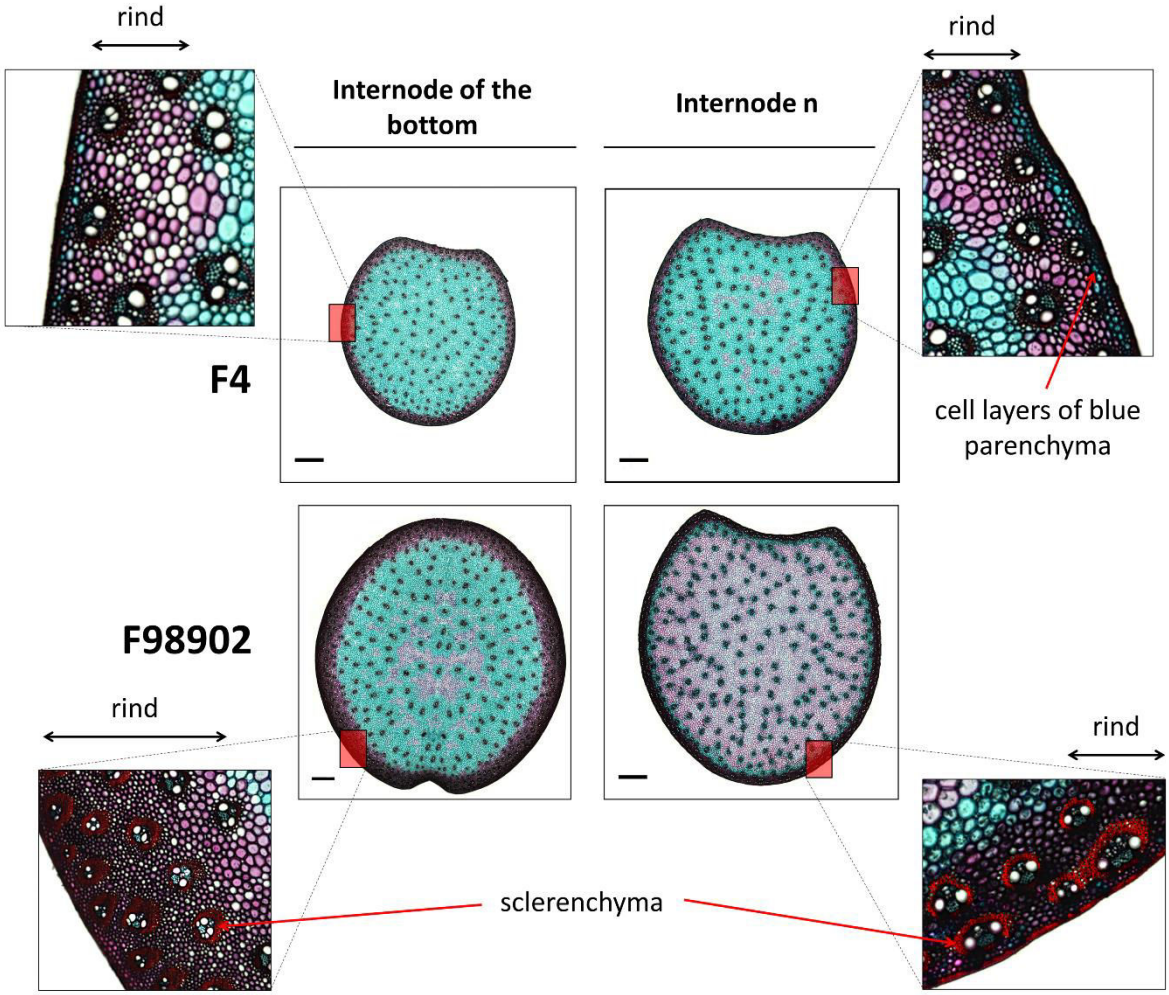


Figure 60. Comparison of the rind of the 2 genotypes F4 and F98902 at the level of the internode from the bottom and at the internode carrying the main ear. The brightness of the sclerenchyma tissues have been enhanced to allow the visibility of the red staining. Bar = 2 mm

These differences, either within the plant between its lowest internode and the internode n or between 2 genotypes at the same internode level would be worth to investigate. Moreover, they could be analyzed in response to water deficit and in association with cell wall degradability and biochemical components analyses to better understand their role within the plant. To do so, an adaptation of the tool presented in Legland et al., (2017) for the analysis of the rind tissues could be possible and needs to be looked further.

Many of these perspectives have been already initiated in several projects and collaborations within my team and I will try to continue the other ones.

References

Abraham, Y., & Elbaum, R. (2013). Quantification of microfibril angle in secondary cell walls at subcellular resolution by means of polarized light microscopy. *New Phytol., 197*, 1012-1019.

Achyuthan, K. E., Achyuthan, A. M., & Adams. (2010). Supramolecular self-assembled chaos: polyphenolic lignin's barrier to cost-effective lignocellulosic biofuels. *PD Molecules*.

Agarwal, U., & Atalla, R. (2010). Vibrational spectroscopy Lignin and lignans, Advances in Chemistry. C Heitner, D. R. Dimmel and J. A. Schmidt. *Boca Raton*, 103-136.

Albrecht, K. A., Martin, M. J., Russel, W. A., Wedin, W. F., & Buxton, D. R. (1986). Chemical and in Vitro Digestible Dry Matter Composition of Maize Stalks after Selection for Stalk Strength and Stalk-Rot Resistance1. *Crop Science, 26*, 1051.

Ali, F., Scott, P., Bakht, J., Chen, Y., & Lübberstedt, T. (2010). Identification of novel brown midrib genes in maize by tests of allelism. *Plant Breeding, 129*, 724-726.

Alimi, N. A., Bink, M. C., Dieleman, J. A., Magán, J. J., Wubs, A. M., Palloix, A., et al. (2013). Multi-trait and multi-environment QTL analyses of yield and a set of physiological traits in pepper. *TAG. Theoretical and applied genetics. Theoretische und angewandte Genetik, 126*, 2597-2625.

Allouche, F., Hanafi, M., Jamme, F., et al. (2012). Coupling hyperspectral image data having different spatial resolutions using multiple co-inertia analysis. *Chemometrics and Intelligent Laboratory Systems, 117*, 200-212.

Alvira, P., Tomas-Pejo, E., Ballesteros, M., et al. (2010). Pretreatment technologies for an efficient bioethanol production process based on enzymatic hydrolysis : A review. *Bioresour. Technol, 101*, 4851-4861.

Anderegg, W. R., Klein, T., Bartlett, M., Sack, L., Pellegrini, A. F., Choat, B., et al. (2016). Meta-analysis reveals that hydraulic traits explain cross-species patterns of drought-induced tree mortality across the globe. *Proceedings of the National Academy of Sciences of the United States of America, 113*, 5024-9.

Anderson, N., & Tobimatsu, Y. (2015). Manipulation of guaiacyl and syringyl monomer biosynthesis in an Arabidopsis cinnamyl alcohol dehydrogenase mutant results in atypical lignin biosynthesis and. *Am Soc Plant Biol*.

Andrieu, & Aufrère, J. (1996). *Prévision à partir de différentes méthodes (physique, chimique, et biologique) de la digestibilité et de la valeur énergétique de la plante de maïs à l 'état frais.* Colloque maïs ensilage.

Andrieu, J. (1995). Prediction of Digestibility and Energy Value of Corn Fodder in the Fresh State. *INRA Productions Animales, 8*, 273-274.

Argillier, O., Barrière, Y., & Hébert, Y. (1995). Genetic variation and selection criterion for digestibility traits of forage maize. *Euphytica, 82*, 175-184.

Argillier, O., Barriere, Y., Panel, A., et al. (1998). Variability of digestibility criteria in maize elite hybrids submitted for registration in the French official catalogue. *Agronomie, 18*, 639-648.

Aufrere, J. (1982). Etude de la prévision de la digestibilité des fourrages par une méthode enzymatique. *Annales de zootechnie, INRA/EDP Sciences, 31*, 111-130.

Aufrère, J., & Michalet-Doreau, B. (1983). *In vivo digestibility and prediction of digestibility of some byproducts.* Feeding value of by-products and their use by beef cattle. EEC Seminar.

Aufrère, J., Baumont, R., Delaby, L., et al. (2007). Prévision de la digestibilité des fourrages par la méthode pepsine-cellulase. Le point sur les équations proposées. *INRA Prod, 20*, 129-136.

Bai, X., Wu, B., & Xing, Y. (2012). Yield-related QTLs and Their Applications in Rice Genetic ImprovementF. *Journal of Integrative Plant Biology, 54*, 300-311.

Baldy, A., Jacquemot, M.-P., Griveau, Y., Bauland, C., Reymond, M., & Mechin, V. (2017). Energy Values of Registered Corn Forage Hybrids in France over the Last 20 Years Rose in a Context of Maintained Yield Increase. *American Journal of Plant Sciences, 08*, 1449-1461.

Barceló, A. R., Gómez Ros, L. V., Gabaldón, C., López-Serrano, M., Pomar, F., Carrión, J. S., et al. (2004, 1). Basic peroxidases: The gateway for lignin evolution? *Phytochemistry Reviews, 3*, 61-78.

Bar-On, Y. M., Phillips, R., & Milo, R. (2018). The biomass distribution on Earth. *Proceedings of the National Academy of Sciences*, 201711842.

Barrière, Y., & Argillier, O. (1993). Brown-midrib genes of maize: a review. *Agronomie, 13*, 865-876.

Barrière, Y., & Emile, J. C. (2000). Corn Fodder Evaluation and Prospects of Genetic Progression on Food Value Traits. *Fourrages, 163*, 221-238.

Barrière, Y., Alber, D., Dolstra, O., Lapierre, C., Motto, M., Ordás Pérez, A., et al. (2005). Past and prospects of forage maize breeding in Europe. I. The grass cell wall as a basis of genetic variation and future improvements in feeding value.

Barrière, Y., Chavigneau, H., Delaunay, S., & A. C. (2008). Different mutations in the ZmCAD2 gene underlie the maize brown-midrib1 (bm1) phenotype with similar effects on lignin characteristics and have potential. *Maydica*.

Barrière, Y., Gallais, A., & Berthet, H. (1988). Utilisation du gène brown-midrib-3 pour l'amélioration du maïs fourrage. II. Sélection récurrente de populations. *Agronomie, 8*, 625-631.

Barriere, Y., Gibelin, C., Argiller, O., & Mechin, V. (2001). Genetic analysis in recombinant inbred lines of early dent forage maize. 1: QTL mapping for yield-earliness-starch and crude protein contents from per se value and top cross experiments [Zea mays L.]. *Maydica*

Barrière, Y., Gibelin, C., Argiller, O., & Méchin, V. (2001). Genetic analysis in recombinant inbred lines of early dent forage maize. I: QTL mapping for yield - earliness - starch and crude protein contents from per se value and top cross experiments. *Maydica, 47*, 9-20.

Barrière, Y., Guillaumie, S., Denoue, D., Pichon, M., Goffner, D., & Martinant, J.-P. (2018). Investigating the unusually high cell wall digestibility of the old INRA early flint F4 maize inbred line. *Maydica, 62*, 21.

Barrière, Y., Méchin, V., Denoue, D., Bauland, C., & Laborde, J. (2010). QTL for Yield, Earliness, and Cell Wall Quality Traits in Topcross Experiments of the F838 × F286 Early Maize RIL Progeny. *Crop science, 50*.

Barrière, Y., Méchin, V., Lefevre, B., & Maltese, S. (2012). QTLs for agronomic and cell wall traits in a maize RIL progeny derived from a cross between an old Minnesota13 line and a modern Iodent line. *Theoretical and Applied Genetics, 125*, 531-549.

Barrière, Y., Ralph, J., Méchin, V., & S Guillaumie (2004). Genetic and molecular basis of grass cell wall biosynthesis and degradability. II. Lessons from brown-midrib mutants. *Comptes-rendus*.

Barrière, Y., Ralph, J., Méchin, V., Guillaumie, S., Grabber, J. H., Argillier, O., et al. (2004, 9). Genetic and molecular basis of grass cell wall biosynthesis and degradability. II. Lessons from brown-midrib mutants. *Comptes Rendus Biologies, 327*, 847-860.

Barrière, Y., Riboulet, C., Mechin, V., Maltese, S., Pichon, M., Cardinal, A. (2007). Genetics and genomics of lignification in grass cell walls based on maize as model species. *Genes, Genomes and Genomics, 1*, 133-156.

Barrière, Y., Thomas, J., & Denoue, D. (2008). QTL mapping for lignin content, lignin monomeric composition, p-hydroxycinnamate content, and cell wall digestibility in the maize recombinant inbred line progeny F838 × F286. *Plant Science, 175*, 585-595.

Barrière, Y., Traineau, R., Emile, J. C., & Hébert, Y. (1991). Variation and covariation of silage maize digestibility estimated from digestion trials with sheep. *Euphytica, 59*, 61-72.

Barros-Ríos, J., Malvar, R. A., & Santiago, R. (2011). Función de la pared celular del maíz (Zea mays L.) como mecanismo de defensa frente a la plaga del taladro (Ostrinia nubilalis Hüb. y Sesamia nonagrioides Lef.). *Revista de Educación Bioquímica, 30*, 132-142.

Barros-Rios, J., Malvar, R. A., Jung, H.-J. G., Bunzel, M., & Santiago, R. (2012). Divergent selection for ester-linked diferulates in maize pith stalk tissues. Effects on cell wall composition and degradability. *Phytochemistry, 83*, 43-50.

Barros-Rios, J., Romaní, A., Garrote, G., & Ordas, B. (2015). Biomass, sugar, and bioethanol potential of sweet corn. *GCB Bioenergy, 7*, 153-160.

Barros-Rios, J., Santiago, R., Jung, H.-J. G., & Malvar, R. A. (2015). Covalent Cross-Linking of Cell-Wall Polysaccharides through Esterified Diferulates as a Maize Resistance Mechanism against Corn Borers. *Journal of Agricultural and Food Chemistry, 63*, 2206-2214.

Barros-Rios, J., Santiago, R., Malvar, R. A., & Jung, H.-J. G. (2012). Chemical composition and cell wall polysaccharide degradability of pith and rind tissues from mature maize internodes. *Animal Feed Science and Technology, 172*, 226-236.

Bartley, L. E., Peck, M. L., Kim, S. R., & B Ebert (2013). Overexpression of a BAHD acyltransferase, OsAt10, alters rice cell wall hydroxycinnamic acid content and saccharification. *Am Soc Plant Biol*.

Battegay, S. (2016). *Eléments d'introduction : Maïs fourrage et bovins : nouvelles approches de la valeur alimentaire et de sa valorisation.*

Baucher, M., Bernard-Vailhé, M. A., & B Chabbert, et al. (1999). Down-regulation of cinnamyl alcohol dehydrogenase in transgenic alfalfa (Medicago sativa L.) and the effect on lignin composition and digestibility. *Plant Molecular Biology*.

Baucher, M., Bernard-vailhé, M. A., Chabbert, B., Besle, J.-M., Opsomer, C., Van Montagu, M., et al. (1999). Down-regulation of cinnamyl alcohol dehydrogenase in transgenic alfalfa (Medicago sativa L.) and the effect on lignin composition and digestibility. *Plant Molecular Biology, 39*, 437-447.

Baucher, M., Monties, B., Montagu, M. V., & Boerjan, W. (1998). Biosynthesis and Genetic Engineering of Lignin. *Critical Reviews in Plant Sciences, 17*, 125-197.

Baumont, R., Delmas, B., Violleau, S., Zapata, J., Chabalier, C., Picard, F., et al. (2009). The utilisation of grasses functional types and of the cumulated sum of temperatures to evaluate permanent grassland digestibility in PDO cheese farms of the Massif Central in France. *Proceeding of the 15 th Meeting of the FAO CIHEAM Mountain Pastures Network*, (p. 111).

Bell, K., Mitchell, S., Paultre, D., et al. (2013). Correlative imaging of fluorescent proteins in resin-embedded plant material. *Plant Physiol, 161*, 1595-1603.

Benjamin, Y., Görgens, J. F., & Joshi, S. V. (2014). Comparison of chemical composition and calculated ethanol yields of sugarcane varieties harvested for two growing seasons. *Industrial Crops and Products, 58*, 133-141.

Bernard-Vailhé, M.-A., Cornu, A., Robert, D., Maillot, M.-P., & Besle, J.-M. (1996). Cell Wall Degradability of Transgenic Tobacco Stems in Relation to Their Chemical Extraction and Lignin Quality. *Journal of Agricultural and Food Chemistry, 44*, 1164-1169.

Bhalla, A., Bansal, N., Kumar, S., Bischoff, K. M., & Sani, R. K. (2013). Improved lignocellulose conversion to biofuels with thermophilic bacteria and thermostable enzymes. *Bioresource technology, 128*, 751-759.

Bhawana, M. J., & Cahoon, A. B. (2014). 3D plant cell architecture of Arabidopsis thaliana (Brassicaceae) using focused ion beam-scanning electron microscopy. *Appl Plant Sci, 2*.

Bichot, A., Delgenès, J.-P., Méchin, V., Carrère, H., Bernet, N., & García-Bernet, D. (2018). *Understanding biomass recalcitrance in grasses for their efficient utilization as biorefinery feedstock* (Vol. 0123456789).

Boerjan, W., Ralph, J., & Baucher, M. (2003). Lignin Biosynthesis. *Annual Review of Plant Biology, 54*, 519-546.

Bohn, M., Schulz, B., Kreps, R., Klein, D., & Melchinger, A. E. (2000). QTL mapping for resistance against the European corn borer (Ostrinia nubilalis H.) in early maturing European dent germplasm. *TAG Theoretical and Applied Genetics, 101*, 907-917.

Bonawitz, N. D., & Chapple, C. (2010). The Genetics of Lignin Biosynthesis: Connecting Genotype to Phenotype. *Annual Review of Genetics, 44*, 337-363.

Boon, E. J., Engels, F. M., Struik, P. C., & Cone, J. W. (2005). Stem characteristics of two forage maize (Zea mays L.) cultivars varying in whole plant digestibility. I. Relevant morphological parameters. *NJAS - Wageningen Journal of Life Sciences, 53*, 71-85.

Boon, E. J., Engels, F. M., Struik, P. C., & Cone, J. W. (2005). Stem characteristics of two forage maize (Zea mays L.) cultivars varying in whole plant digestibility. II. Relation between in vitro rumen fermentation characteristics and anatomical and chemical features within a single internode. *NJAS - Wageningen Journal of Life Sciences, 53*, 87-109.

Boon, E. J., Struik, P. C., Engels, F. M., & Cone, J. W. (2012). Stem characteristics of two forage maize (Zea mays L.) cultivars varying in whole plant digestibility. IV. Changes during the growing season in anatomy and chemical composition in relation to fermentation characteristics of a lower internode. *NJAS - Wageningen Journal of Life Sciences, 59*, 13-23.

Boon, E. J., Struik, P. C., Tamminga, S., Engels, F. M., & Cone, J. W. (2008). Stem characteristics of two forage maize (Zea mays L.) cultivars varying in whole plant digestibility. III. Intra-stem variability in anatomy, chemical composition and in vitro rumen fermentation. *NJAS - Wageningen Journal of Life Sciences, 56*, 101-122.

Boughton, B. A., Thinagaran, D., Sarabia, D., et al. (2016). Mass spectrometry imaging for plant biology : a review. *Phytochem Rev, 15*, 445-488.

Bout, S., & Vermerris, W. (2003). A candidate-gene approach to clone the sorghum Brown midrib gene encoding caffeic acid O-methyltransferase. *Molecular Genetics and Genomics, 269*, 205-214. Bowes, B. G., & Mauseth, J. D. (2012). Structure des plantes.

Broman, K. W., & Sen, S. (2009). *A Guide to QTL Mapping with R/qtl.* New, York, NY: Springer New York.

Brown, R. M., & Saxena, I. M. (2007). *Cellulose : molecular and structural biology : selected articles on the synthesis, structure, and applications of cellulose.* Springer.

Brunow, G., Kilpelainen, I., Sipila, J., & Syrjanen, K. (1998). Oxidative coupling of phenols and the biosynthesis of lignin.

Buanafina, M. M., Langdon, T., Hauck, B., Dalton, S., & Morris, P. (2008). Expression of a fungal ferulic acid esterase increases cell wall digestibility of tall fescue (Festuca arundinacea). *Plant Biotechnology Journal, 6*, 264-280.

Burnham, C. R. (1947). Maize genetics. *Cooperation Newsletter, 21*, 36.

Burnham, C. R., & Journal, R. A. (1932). Linkage Relations of a Second Brown Midrib Gene (bm2) in Maize 1. *Agronomy Journal*.

Cabané, M., Pireaux, J.-C., Léger, E., Weber, E., Dizengremel, P., Pollet, B., et al. (2004). Condensed lignins are synthesized in poplar leaves exposed to ozone. *Plant physiology, 134*, 586-94.

Campbell, M. M., & Sederoff, R. R. (1996). Variation in Lignin Content and Composition (Mechanisms of Control and Implications for the Genetic Improvement of Plants). *Plant physiology, 110*, 3-13.

Cardinal, A. J., & Lee, M. (2005). Genetic relationships between resistance to stalk-tunneling by the European corn borer and cell-wall components in maize population B73×B52. *Theoretical and Applied Genetics, 111*, 1-7.

Cardinal, A. J., & Lee, M. (2005). Genetic relationships between resistance to stalk-tunneling by the European corn borer and cell-wall components in maize population B73xB52. *Theoretical and Applied Genetics, 111*, 1-7.

Cardinal, A. J., Lee, M., & Moore, K. J. (2003). Genetic mapping and analysis of quantitative trait loci affecting fiber and lignin content in maize. *Theoretical and Applied Genetics, 106*, 866-874.

Carpita, N. C. (1996). STRUCTURE AND BIOGENESIS OF THE CELL WALLS OF GRASSES. *Annual Review of Plant Physiology and Plant Molecular Biology, 47*, 445-476.

Carpita, N. C., & Gibeaut, D. M. (1993). Structural models of primary cell walls in flowering plants: consistency of molecular structure with the physical properties of the walls during growth. *The Plant Journal, 3*, 1-30.

Carroll, A., & Specht, C. D. (2011). Understanding Plant Cellulose Synthases through a Comprehensive Investigation of the Cellulose Synthase Family Sequences. *Frontiers in Plant Science, 2*, 5.

Casler, M. D., & Jung, H.-J. G. (1999). Selection and evaluation of smooth bromegrass clones with divergent lignin or etherified Ferulic acid concentration. *Crop Science, 39*, 1866-1873.

Chabbert, B., Habrant, A., Herbaut, M., et al. (2017). Action of lytic polysaccharide monooxygenase on plant tissue is governed by cellular type. *Sci Rep, : 17792, 7*.

Chabbert, B., Tollier, M. T., & Monties, B. (1993). Lignin variability among different brown midrib sorghum lines. *Proceedings of the 7th International Symposium on Wood and Pulping Chemistry*, *1*, pp. 462-468.

Cherney, D. J., & JA Patterson, et al. (1990). Digestibility and feeding value of pearl millet as influenced by the brown-midrib, low-lignin trait. *Journal of animal science*.

Chesson, A., Provan, G. J., Russell, W., Scobbie, L., Chabbert, B., & Monties, B. (1997). Characterisation of Lignin from Parenchyma and Sclerenchyma Cell Walls of the Maize Internode. *Journal of the Science of Food and Agriculture, 73*, 10-16.

Choat, B., Jansen, S., Brodribb, T. J., Cochard, H., Delzon, S., Bhaskar, R., et al. (2012). Global convergence in the vulnerability of forests to drought. *Nature, 491*, 752-755.

Cloetens, P., Mache, R., Schlenker, M., et al. (2006). Quantitative phase tomography of Arabidopsis seeds reveals intercellular void networkx. Proc. Natl. *Acad, 103*.

Coaker, G. L., Meulia, T., Kabelka, E. A., Jones, A. K., & Francis, D. M. (2002). A QTL controlling stem morphology and vascular development in Lycopersicon esculentumxLycopersicon hirsutum (Solanaceae) crosses is located on chromosome 2. *American Journal of Botany, 89*, 1859-1866.

Collazo, P., Montoliu, L., Puigdom_nech, P., & Rigau, J. (1992). Structure and expression of the lignin O-methyltransferase gene from Zea mays L. *Plant Molecular Biology, 20*, 857-867.

Collins, N. C., Tardieu, F., & Tuberosa, R. (2008). Quantitative trait loci and crop performance under abiotic stress: where do we stand? *Plant physiology, 147*, 469-486.

Corcel, M., Devaux, M. F., Guillon, F., et al. (2017). Comparison of UV and visible autofluorescence of wheat grain tissues in macroscopic images of cross-sections and particles. *Computers and Electronics in Agriculture, 127*, 281-288.

Corcel, M., Devaux, M. F., Guillon, F., et al. (2017). Identification of tissular origin of particles based on autofluorescence multispectral image analysis at the macroscopic scale. *Powders and Grains_ 8th International Conference on Micromechanics on Granular Media.* 140.

Cosgrove, D. J. (2005). Growth of the plant cell wall. *Nature Reviews Molecular Cell Biology, 6*, 850-861.

Costa, T. H., Vega-Sánchez, M. E., Milagres, A. M., Scheller, H. V., & Ferraz, A. (2016). Tissue-specific distribution of hemicelluloses in six different sugarcane hybrids as related to cell wall recalcitrance. *Biotechnology for Biofuels, 9*, 99.

Courtial, A., Méchin, V., Reymond, M., Grima-Pettenati, J., & Barrière, Y. (2014). Colocalizations Between Several QTLs for Cell Wall Degradability and Composition in the F288 × F271 Early Maize RIL Progeny Raise the Question of the Nature of the Possible Underlying Determinants and Breeding Targets for Biofuel Capacity. *BioEnergy Research, 7*, 142-156.

Courtial, A., Thomas, J., Reymond, M., Méchin, V., Grima-Pettenati, J., & Barrière, Y. (2013). Targeted linkage map densification to improve cell wall related QTL detection and interpretation in maize. *Theoretical and Applied Genetics, 126*, 1151-1165.

Credou, J., & T Berthelot, B. (2014). Cellulose: from biocompatible to bioactive material. *Journal of Materials Chemistry*.

Cui, K., Peng, S., Xing, Y., Yu, S., Xu, C., & Zhang, Q. (2003). Molecular dissection of the genetic relationships of source, sink and transport tissue with yield traits in rice. *Theoretical and Applied Genetics, 106*, 649-658.

Culhaoglu, T., Zheng, D., Méchin, V., & Baumberger, S. (2011). Adaptation of the Carrez procedure for the purification of ferulic and p-coumaric acids released from lignocellulosic biomass prior to LC/MS analysis. *Journal of Chromatography B, 879*, 3017-3022.

De Boever, J. L., Cottyn, B. G., Andries, J. I., et al. (1988). The use of a cellulase technique to predict digestibility, metabolizable and net energy of forages. *Anim. Feed Sci. Technol, 19*, 247-260.

Deinum, B., & Struik, P. C. (1989). Genetic variation in digestibility of forage maize (Zea mays L.) and its estimation by near infrared reflectance spectroscopy (NIRS). An analysis. *Euphytica, 42*, 89-98.

Denmead, O. T., & Shaw, R. H. (1960). The Effects of Soil Moisture Stress at Different Stages of Growth on the Development and Yield of Corn1. *Agronomy Journal, 52*, 272.

Devaux, M. F., & Legland, D. (2014). Grey level granulometry for histological image analysis of plant tissues. *Microscopy : advances in scientific research and education*, 681-688.

Devaux, M. F., Jamme, F., Andre, W., et al. (2018). Synchrotron Time-Lapse Imaging of Lignocellulosic Biomass Hydrolysis : Tracking Enzyme Localization by Protein Autofluorescence and Biochemical Modification of Cell Walls by Microfluidic Infrared Microspectroscopy. *Front Plant Sci, 9*, 200.

Devaux, M. F., Sire, A., & Legland, D. (2009). Macrovision et analyse granulométrique en niveaux de gris pour l'analyse histologique de tissus végétaux Cahier technique de l'INRA. *n° spécial Des développement méthodologiques en imagerie à l'INRA*, 93-100.

Dhondt, S., Vanhaeren, H., Loo, D. V., et al. (2010). Plant structure visualization by high-resolution X-ray computed tomography. *Trends Plant Sci, 15*, 419-422.

Doebley, J., Stec, A., & Hubbard, L. (1997). The evolution of apical dominance in maize. *Nature, 386*, 485-488.

Domozych, D. S. (2012). The quest for four-dimensional imaging in plant cell biology : it's just a matter of time. *Annals of Botany, 110*, 461-474.

Donaldson, L. A. (2013). Softwood and hardwood lignin fluorescence spectra of wood cell walls in different mounting media. *IAWA Journal, 34*, 3-19.

Dong, Y., Li, B., & Aharoni, A. (2016). More than Pictures : When MS Imaging Meets Histology. *Trends Plant Sci, 21*, 686-698.

Dos Santos, A. B., Bottcher, A., Kiyota, E., et al. (2015). Water stress alters lignin content and related gene expression in two sugarcane genotypes. *J. Agric. Food Chem, 63*, 4708-4720.

Dreisewerd, K., & Yew, J. Y. (2017). Mass spectrometry imaging goes three dimensional. *Nat Methods, 14*, 1139-1140.

Ebringerová, A., Hromádková, Z., & Heinze, T. (2005). Structural diversity and application potential of Hemicelluloses. *Polysaccharides I* (pp. 1-67).

El Hage, F., Legland, D., Borrega, N., Jacquemot, M.-P., Griveau, Y., Coursol, S., Méchin V., and Reymond M. (2018). Tissue Lignification, Cell Wall *p*-Coumaroylation and Degradability of Maize Stems Depend on Water Status. *Journal of Agricultural and Food Chemistry, 66*, 4800-4808.

Elmore, R. W. (2012). Stress , Anthesis — Silk Interval and Corn Yield Potential. 12-15.

Elshire, R. J., Glaubitz, J. C., Sun, Q., Poland, J. A., Kawamoto, K., Buckler, E. S. (2011). A robust, simple genotyping-by-sequencing (GBS) approach for high diversity species. *PloS one, 6*, e19379.

Emerson, R. A., Beadle, G. W., & Fraser, A. C. (1935). Cornell Univ. *Agric. Exp. Stn. Memoir, 180*.

Emerson, R., Hoover, A., Ray, A., et al. (2014). Drought effects on composition and yield for corn stover, mixed grasses, and Miscanthus as bioenergy feedstocks Biofuels. *5*, 272-291.

Emerson, R., Hoover, A., Ray, A., Lacey, J., Cortez, M., Payne, C., et al. (2014). Drought effects on composition and yield for corn stover, mixed grasses, and *Miscanthus* as bioenergy feedstocks. *Biofuels, 5*, 275-291.

Eyster, W. H. (1926). Chromosome VIII in maize. American Association for the Advancement of Science

Fackler, K., & Thygesen, L. G. (2013). Microspectroscopy as applied to study of wood molecular structure. *Wood Science Technology, 47*, 203-222.

Faulds, C. B., & Williamson, G. (1999). The role of hydroxycinnamates in the plant cell wall. *Journal of the Science of Food and Agriculture, 79*, 393-395.

FAZARY, A. E., & Yi-Hsu, J. U. (2007). Feruloyl Esterases as Biotechnological Tools: Current and Future Perspectives. *Acta Biochimica et Biophysica Sinica, 39*, 811-828.

Fontaine, A.-S., Briand, M., & Barrière, Y. (2003). Genetic variation and QTL mapping of para-coumaric and ferulic acid. *Maydica, 48*, 75-84.

Gabrielsen, B., Vogel, K., & Ward, J. (1990). Alkali-Labile Cell-Wall Phenolics and Forage Quality in Switchgrasses Selectedfor Differing Digestibility. *Crop Science, 30*, 1313-1320.

Garcia-Plazaola, J. G., Fernandez-Marin, B., Duke, S. O., et al. (2015). Autofluorescence : biologicalfunctions and technical applications. *Plant Science, 236*, 136-145.

Gay, J. P. (1984). Fabuleux mais: histoire et avenir d'une plante. Pau (France) AGPM.

Gierlinger, N. (2014). Revealing changes in molecular composition of plant cell walls on the micron-level by Raman mapping and vertex component analysis (VCA). *Front Plant Sci, 5*.

Gierlinger, N., Keplinger, T., & Harrington, M. (2012). Imaging of plant cell walls by confocal Raman microscopy. *Nat Protoc, 7*, 1694-1708.

Gierlinger, N., Luss, S., Konig, C., et al. (2010). Cellulose microfibril orientation of Picea abies and its variability at the micron-level determined by Raman imaging. *J. Exp. Bot, 61*, 587-595.

Glaubitz, J. C., Casstevens, T. M., Lu, F., Harriman, J., Elshire, R. J., Sun, Q., et al. (2014). TASSEL-GBS: A High Capacity Genotyping by Sequencing Analysis Pipeline.

Goering, H. K., & Van Soest, P. J. (1970). Forage fiber analyses. *Agiculture Handbook, 379*, 387-598.

Gondos, G., Constantinescu, O., Gheorghiu, A., Lupan, L., Gondos, M., Petrescu, C.(1960). Milk production by cows fed on maize silage compared to those given clover silage. *Lucrarile stiintifice ale Institutul de cercetari zootehnice, 18*, 59-71.

Goujon, T., Ferret, V., Mila, I., Pollet, B., Ruel, K., & V. B. (2003). Down-regulation of the AtCCR1 gene in Arabidopsis thaliana: effects on phenotype, lignins and cell wall degradability. *Planta*.

Grabber, J. H. (2005). How Do Lignin Composition, Structure, and Cross-Linking Affect Degradability? A Review of Cell Wall Model Studies. *Crop Science, 45*, 820.

Grabber, J. H., Hatfield, R. D., & Ralph, J. (1998). Diferulate Cross-Links Impede the Enzymatic Degradation of Non-Ligniüed Maize Walls. *J Sci Food Agric, 77*, 193-200.

Grabber, J. H., Jung, G. A., Abrams, S. M., & Howard, D. B. (1992). Digestion Kinetics of Parenchyma and Sclerenchyma Cell Walls Isolated from Orchardgrass and Switchgrass. *Crop Science, 32*, 806.

Grabber, J. H., Quideau, S., & Ralph, J. (1996). p-coumaroylated syringyl units in maize lignin: Implications for β-ether cleavage by thioacidolysis. *Phytochemistry, 43*, 1189-1194.

Grabber, J. H., Ralph, J., & Hatfield, R. D. (1998). Severe inhibition of maize wall degradation by synthetic lignins formed with coniferaldehyde. *Journal of the Science of Food and Agriculture, 78*, 81-87.

Grabber, J. H., Ralph, J., Lapierre, C., & Barrière, Y. (2004). Genetic and molecular basis of grass cell-wall degradability. I. Lignin–cell wall matrix interactions. *Comptes Rendus Biologies, 327*, 455-465.

Gray, J., Caparrós-Ruiz, D., & Grotewold, E. (2012). Grass phenylpropanoids: Regulate before using! *Plant Science, 184*, 112-120.

Grimault, V., Vian, B., Perino, C., et al. (1997). Degradation patterns of pecti substrate related to the localization of bacterial pectate-lyase in the model Erwinia chrysanthemi. *Physiological and Molecular Plant Pathology, 51*, 45-62.

Grobman, A. (1961). *Races of Maize in Peru: Their Origins, Evolution and Classification - (Vol. 915). National Academies.*

Guillemin, F., Devaux, M. F., & Guillon, F. (2004). Evaluation of plant histology by automatic clustering based on individual cell morphological features. *Image Analysis and Stereology, 23*, 13-22.

Guines, F., Julier, B., Ecalle, C., & Huyghe, C. (2003). Among and within-cultivar variability for histological traits of lucerne (Medicago sativa L.) stem. *Euphytica, 130*, 293-301.

Guines, F., Julier, B., Poussot, P., & Huyghe, C. (2001). Investigating variation for histological characters in alfalfa stems. Quality in lucerne and medics for animal production, 47-51.

Guo, L., Wang, X., Zhao, M., Huang, C., Li, C., Li, D., et al. (2018). Stepwise cis-Regulatory Changes in ZCN8 Contribute to Maize Flowering-Time Adaptation. *Current Biology, 28*, 3005--3015.e4.

Guzzo de Carli Poelking, V., Giordano, A., Ricci-Silva, M. E., Rhys Williams, T. C., Alves Peçanha, D., Contin Ventrella, M., et al. (2015). Analysis of a Modern Hybrid and an Ancient Sugarcane Implicates a Complex Interplay of Factors in Affecting Recalcitrance to Cellulosic Ethanol Production. (S. Yang, Éd.) *PLOS ONE, 10*, e0134964.

Haney, L. J., Hake, S., & Cooperative, M. P. (2008). Allelism testing of Maize Coop Stock Center lines containing unknown brown midrib alleles. *Maize Genetics*.

Hartley, R. D. (1972). p-Coumaric and ferulic acid components of cell walls of ryegrass and their relationships with lignin and digestibility. *Journal of the Science of Food and Agriculture, 23*, 1347-1354.

Hartley, R. D. (1978). The lignin fraction of plant cell walls. *The American Journal of Clinical Nutrition, 31*, S90--S93.

Hatfield, R. D., & Chaptman, A. K. (2009). Comparing Corn Types for Differences in Cell Wall Characteristics and *p*-Coumaroylation of Lignin. *Journal of Agricultural and Food Chemistry, 57*, 4243-4249.

Hatfield, R. D., Grabber, J. H., Ralph, J., & Brei, K. (1999). Using the Acetyl Bromide Assay To Determine Lignin Concentrations in Herbaceous Plants: Some Cautionary Notes. *Journal of agricultural and food chemistry, 47*, 628-632.

Hatfield, R. D., Jung, H.-J. G., Ralph, J., Buxton, D. R., & Weimer, P. J. (1994). A comparison of the insoluble residues produced by the Klason lignin and acid detergent lignin procedures. *Journal of the Science of Food and Agriculture, 65*, 51-58.

Hatfield, R. D., Marita, J. M., Hatfield, R. D., & Marita, J. M. (2017). Maize development: cell wall changes in leaves and sheaths. *American Journal of Plant Sciences, 8*, 1248-1263.

Hatfield, R. D., Rancour, D. M., & Marita, J. M. (2017). Grass cell walls: a story of cross-linking. *Frontiers in Plant Science, 7*, 2056.

Hatfield, R. D., Wilson, J. R., & Mertens, D. R. (1999). Composition of cell walls isolated from cell types of grain sorghum stems. *Journal of the Science of Food and Agriculture, 79*, 891-899.

Hatfield, R., Ralph, J., & Grabber, J. H. (2008, 11). A potential role for sinapyl p-coumarate as a radical transfer mechanism in grass lignin formation. *Planta, 228*, 919-928.

Heckwolf, S., Heckwolf, M., Kaeppler, S. M., Leon, N., & Spalding, E. P. (2015). Image analysis of anatomical traits in stalk transections of maize and other grasses. *Plant Methods, 11*, 26.

Higuchi, T., Ito, Y., & Kawamura, I. (1967). p-hydroxyphenylpropane component of grass lignin and role of tyrosine-ammonia lyase in its formation. *Phytochemistry, 6*, 875-881.

Huang, C., Chen, Q., Xu, G., Xu, D., Tian, J., & Tian, F. (2016). Identification and fine mapping of quantitative trait loci for the number of vascular bundle in maize stem. *Journal of Integrative Plant Biology, 58*, 81-90.

Inoue, N., & Kasuga, S. (1989). Agronomic traits and nutritive value of stover in brown midrib-3 maize hybrids. *Journal of Japanese Society of Grassland Science (Japan)*.

Ishii, T. (1997). Structure and functions of feruloylated polysaccharides. *Plant Science, 127*, 111-127.

Ishii, T., & Matsunaga, T. (2001). Pectic polysaccharide rhamnogalacturonan II is covalently linked to homogalacturonan. *Phytochemistry*.

Jacquet, G. (1997). Structure et réactivité des lignines de graminées et des acides phénoliques associés: développement des méthodologies d'investigation.

Jane M. Marita., Wilfred Vermerris, John Ralph & Hatfield, R. D. (2003). Variations in the Cell Wall Composition of Maize brown midrib Mutants.

Jarvis, M. C., & McCann, M. C. (2000). Macromolecular biophysics of the plant cell wall; concepts and methodology Plant Physiology and Biochmistry. *38*, 1-13.

Ji, Z., Ding, D. Y., Ling, Z., et al. (2014). In situ microscopic investigation of plant cell walls deconstruction in biorefinrey. *Microscopy : advances in scientific research and education*, 426-433.

Jorgenson, L. R. (1931). Brown Midrib in Maize and its Linkage Relations1. *Agronomy Journal, 23*, 549.

Jung, H. G., & Casler, M. D. (2006). Maize Stem Tissues. *Crop Science, 46*, 1793.

Jung, H. G., & Deetz, D. A. (1993). Cell wall lignification and degradability. Forage Cell Wall Structure and Digestibility. H. G. *Jung, D. R. Buxton, R. D. Hatfield and J. Ralph*, 315-346.

Jung, H. G., & Engels, F. M. (2002). Alfalfa stem tissues. *Crop science*.

Jung, H. G., Morrison, T. A., & Buxton, D. R. (1998). Degradability of Cell-Wall Polysaccharides in Maize Internodes during Stalk Development. *Crop Science, 38*, 1047.

Jung, H. J. (2003). Maize stem tissues: Ferulate deposition in developing internode cell walls. *Phytochemistry, 63*, 543-549.

Jung, H.-J. G., & Buxtono, D. R. (1994). Forage quality variation among maize inbreds: Relationships of cell-wall composition and in-vitro degradability for stem internodes. *Journal of the Science of Food and Agriculture, 66*, 313-322.

Jung, H.-J. G., & Casler, M. D. (2006). Maize Stem Tissues: Impact of Development on Cell Wall Degradability. *Crop Science, 46*, 1801-1809.

Jung, H.-J. G., Samac, D. A., & Sarath, G. (2012). Modifying crops to increase cell wall digestibility. *Plant Science, 185-186*, 65-77.

Jurasek, L. (1998). Experimenting with virtual lignins. *Lignin and lignan biosynthesis*.

Karlen, S. D., Free, H. C., Padmakshan, D., & BG Smith, (2018). Commelinid Monocotyledon Lignins Are Acylated by p-Coumarate. *Plant Science*.

Kasten, F. H., Burton, V., & Glover, P. (1959). Fluorescent schiff-type reagents for histochemical detection of polyaldehyde moities in sections and smears. *Nature (London), 184*, 1797-1798.

Kiesselbach, T. A. (1922). Corn investigations.

Kjd, L., Marcus, S. E., & Knox, P. (2011). Cell wall biology : perspectives from cell wall imaging. *Molecular plant, 4*, 212-219.

Koch, G. W., Sillett, S. C., Jennings, G. M., & Davis, S. D. (2004). The limits to tree height. *Nature, 428*, 851-854.

KONDO, T. S., MIZUNO, K. A., & TADASHI, K. A. (1990). Cell-wall bound *p*-coumaric acid and ferulic acid in italian Raygrass. *Canadian Journal of Plant Science, 70*, 495-499.

Kondo, T., Watanabe, T., Ohshita, T., & T. K. (1998). Physico-chemical characteristics of soluble lignin fractions released from forage grasses by ruminant digestion. *JARQ*.

Krakowsky, M. D., Lee, M., & Coors, J. G. (2005). Quantitative trait loci for cell-wall components in recombinant inbred lines of maize (Zea mays L.) I: stalk tissue. *Theoretical and Applied Genetics, 111*, 337-346.

Krakowsky, M. D., Lee, M., & Coors, J. G. (2006). Quantitative trait loci for cell wall components in recombinant inbred lines of maize (Zea mays L.) II: leaf sheath tissue. *Theoretical and Applied Genetics, 112*, 717-726.

Kumar, A. K., Parikh, B. S., & Pravakar, M. (2016). Natural deep eutectic solvent mediated pretreatment of rice straw: bioanalytical characterization of lignin extract and enzymatic hydrolysis of pretreated biomass residue. *Environmental Science and Pollution Research, 23*, 9265-9275.

Lam, T. B., & Iiyama, K. (1992). Cinnamic acid bridges between cell wall polymers in wheat and phalaris internodes. *Phytochemistry*.

Lapierre, C., Monties, B., & Rolando, C. (1986). Preparative Thioacidolysis of Spruce Lignin: Isolation and Identification of Main Monomeric Products. *Holzforschung, 40*, 47-50.

Lapierre, C., Pollet, B., & Rolando, C. (1995). New insights into the molecular architecture of hardwood lignins by chemical degradative methods. *Research on Chemical Intermediates, 21*, 397-412.

Largo-Gosens, A., Hernandez-Altamirano, M., Garcia-Calvo, L., et al. (2014). Fourier transform mid infrared spectroscopy applications for monitoring the structural plasticity of plant cell walls. *Front Plant Sci, 5*, 303.

Ledea-Rodríguez, J. L., Verdecia-Acosta, D., La-O-León, O., Ray-Ramírez, J. V., Reyes-Pérez, J. J., & Murillo-Amador, B. (2018). Caracterización química de nuevas variedades de Cenchrus purpureus tolerantes a la sequía. *Agronomía Mesoamericana, 29*, 655.

Lee, M. H., & Brewbaker, J. L. (1984). Effects of Brown Midrib-3 on Yields and Yield Components of Maize1. *Crop Science, 24*, 105.

Legland, D., Devaux, M. F., & Guillon, F. (2014). Statistical mapping of maize bundle intensity at the stem scale using spatial normalisation of replicated images. *PLoS One, 9*.

Legland, D., Devaux, M. F., Bouchet, B., et al. (2012). Cartography of cell morphology in tomato pericarp at the fruit scale. *Journal of Miscroscopy, 247*, 78-93.

Legland, D., El Hage, F., Mechin, V., et al. (2017). Histological quantification of maize stem sections from FASGA stained images. *Plant methods, 13*, 84.

Leng, P., Ouzunova, M., Landbeck, M., Wenzel, G., Eder, J., Darnhofer, B., et al. (2018). Quantitative trait loci mapping of forage stover quality traits in six mapping populations derived from European elite maize germplasm. (J. Leon, Éd.) *Plant Breeding, 137*, 139-147.

Lens, F., Picon-Cochard, C., Delmas, C. E., Signarbieux, C., Buttler, A., Cochard, H., et al. (2016, 10). Herbaceous Angiosperms Are Not More Vulnerable to Drought-Induced Embolism Than Angiosperm Trees. *Plant physiology, 172*, 661-667.

Lens, F., Tixier, A., Cochard, H., Sperry, J. S., Jansen, S., & Herbette, S. (2013). Embolism resistance as a key mechanism to understand adaptive plant strategies. *Current Opinion in Plant Biology, 16*, 287-292.

Li, G., Jones, K. C., Eudes, A., Pidatala, V. R., Sun, J., Xu, F., et al. (2018). Overexpression of a rice BAHD acyltransferase gene in switchgrass (Panicum virgatum L.) enhances saccharification. *BMC Biotechnology, 18*, 54.

Li, K., Wang, H., Hu, X., Ma, F., Wu, Y., Wang, Q., et al. (2017). Genetic and Quantitative Trait Locus Analysis of Cell Wall Components and Forage Digestibility in the Zheng58 × HD568 Maize RIL Population at Anthesis Stage. *Frontiers in Plant Science, 8*, 1472.

Li, M.-F., Fan, Y.-M., Xu, F., & Sun, R.-C. (2010). Characterization of extracted lignin of Bamboo (Neosinocalamus affinis) pretreated with sodium hydroxide/urea solution at low temperature *BioResources, 5*, 1762-1778.

Liesche, J., Ziomkiewicz, I., & Schilz, A. (2013). Super resolution imaging with Pontamine Fast Scarlet 4BS enable direct visualization of cellulose orientation and cell connection architecture in onion epidermis cells. *BMC Plant Biol, 13*.

Lila, M., Barrière, Y., & Traineau, R. (1986). Mise au point et étude d?un test enzymatique de la digestibilité des fourrages pauvres ou riches en amidon. *Agronomie, 6*, 285-291.

Lion, C., Simon, C., Huss, B., et al. (2017). BLISS : A Bioorthogonal Dual-Labeling Strategy to Unravel Lignification Dynamics in Plants. *Cell Chem Biol, 24*, 326-338.

Liu, J., Kim, J. I., Cusumano, J. C., Chapple, C., Venugopalan, N., Fischetti, R. F., et al. (2016). The impact of alterations in lignin deposition on cellulose organization of the plant cell wall. *Biotechnology for Biofuels, 9*, 1-17.

Locquin, M., & Langeron, M. (1978). *Manuel de Microscopie.* Paris: Editions Masson.

Lopez, S., Murison, S. D., Travis, A. J., & Chesson, A. (1993). Degradability of parenchyma and sclerenchyma cell walls isolated at different developmental stages from a newly extended maize internode. *Acta botanica neerlandica, 42*, 165-174.

Loqué, D., Scheller, H. V., & Pauly, M. (2015). Engineering of plant cell walls for enhanced biofuel production. *Current Opinion in Plant Biology, 25*, 151-161.

Lorenz, A. J., Coors, J. G., De Leon, N., Wolfrum, E. J., Hames, B. R., Sluiter, A. D., et al. (2009). Characterization, Genetic Variation, and Combining Ability of Maize Traits Relevant to the Production of Cellulosic Ethanol. *CROP SCIENCE, 49*.

Lu, F., & Ralph, J. (1999). Detection and determination of *p*-coumaroylated units in lignins. *Journal of agricultural and food chemistry, 47*, 1988-92.

Lübberstedt, T., Melchinger, A. E., Klein, D., Degenhardt, H., & Paul, C. (1997). QTL Mapping in Testcrosses of European Flint Lines of Maize: II. Comparison of Different Testers for Forage Quality Traits. *Crop Science, 37*, 1913-1922.

Lübberstedt, T., Melchinger, A. E., Schön, C. C., Utz, H. F., & Klein, D. (1997). QTL Mapping in Testcrosses of European Flint Lines of Maize: I. Comparison of Different Testers for Forage Yield Traits. *Crop Science, 37*, 921.

MacAdam, J., & Grabber, J. (2002). Relationship of growth cessation with the formation of diferulate cross-links and p -coumaroylated lignins in tall fescue leaf blades. *Planta, 215*, 785-793.

Machinet, G. E., Bertrand, I., & Chabbert, B. (2011). Assessment of Lignin-Related Compounds in Soils and Maize Roots by Alkaline Oxidations and Thioacidolysis. *Soil Science Society of America Journal, 75*, 542.

Manley, M. (2014). Near-infrared spectroscopy and hyperspectral imaging: non-destructive analysis of biological materials. *Chem. Soc. Rev., 43*, 8200-8214.

Matsunaga, T., Ishii, T., Matsumoto, S., & M Higuchi (2004). Occurrence of the primary cell wall polysaccharide rhamnogalacturonan II in pteridophytes, lycophytes, and bryophytes. Implications for the evolution of vascular. *Am Soc Plant Biol*.

McFarlane, H. E., Döring, A., & Persson, S. (2014). The Cell Biology of Cellulose Synthesis. *Annual Review of Plant Biology, 65*, 69-94.

McNeil, M., Darvill, A. G., Fry, S. C., & Albersheim, P. (1984). Structure and Function of the Primary Cell Walls of Plants. *Annual Review of Biochemistry, 53*, 625-663.

Mechin, V., Argillier, O., & V Menanteau (2000). Relationship of cell wall composition to in vitro cell wall digestibility of maize inbred line stems. *Journal of the Science of Food and Agriculture*.

Mechin, V., Argillier, O., Barrière, Y., & Menanteau, V. (1998). Genetic variation in stems of normal and brown-midrib 3 maize inbred lines. Towards similarity for in vitro digestibility and cell wall composition. *Maydica, 43*, 205-210.

Méchin, V., Argillier, O., Hébert, Y., Guingo, E., Moreau, L., Charcosset, A., et al. (2001). Genetic Analysis and QTL Mapping of Cell Wall Digestibility and Lignification in Silage Maize. *Crop Science, 41*, 690.

Méchin, V., Argillier, O., Menanteau, V., et al. (2000). Relationship of cell wall composition to in vitro cell wall digestibility of maize inbred line stems. *J. Sci. Food Agric, 80*, 574-580.

Méchin, V., Argillier, O., Rocher, F., et al. (2005). In search of a maize ideotype for cell wall enzymatic degradability using histological and biochemical lignin characterization. *J. Agric. Food Chem, 53*, 5872-5881.

Méchin, V., Baumberger, S., Pollet, B., & Lapierre, C. (2007). Peroxidase activity can dictate the in vitro lignin dehydrogenative polymer structure. *Phytochemistry*.

Méchin, V., Laluc, A., Legee, F. et al. (2014). Impact of the brown-midrib bm mutation on maize lignins. *J. Agric. Food Chem, 5*, 5102-5107.

Meshitsuka, G., & Nakano, J. (1979). Studies on the mechanism of lignin color reaction (XIII). *Mäule color reaction , 9*, 588-594.

Metcalfe, C. R. (1960). Anatomy of the Monocotyledons. I. Gramineae. *Anatomy of the Monocotyledons. I. Gramineae.*

Meyer, K., Kohler, A., & Letters, H. K. (1991). Biosynthesis of ferulic acid esters of plant cell wall polysaccharides in endomembranes from parsley cells. *FEBS*.

Miedes, E., Vanholme, R., Boerjan, W., & Molina, A. (2014). The role of the secondary cell wall in plant resistance to pathogens. *Frontiers in Plant Science, 5*, 358.

Millet, E., Welcker, C., Kruijer, W., Negro, S., Nicolas, S., Praud, S., et al. (2016). Genome-wide analysis of yield in Europe: allelic effects as functions of drought and heat scenarios. *Plant Physiology*, pp.00621.2016.

Mitchell, R. A., Dupree, P., & Shewry, P. R. (2007). A Novel Bioinformatics Approach Identifies Candidate Genes for the Synthesis and Feruloylation of Arabinoxylan. *Plant Physiology, 144*, 43-53.

Mohnen, D. (2008). Pectin structure and biosynthesis. *Current Opinion in Plant Biology, 11*, 266-277.

Molinari, H. B., Pellny, T. K., Freeman, J., Shewry, P. R., & Mitchell, R. A. (2013). Grass cell wall feruloylation: distribution of bound ferulate and candidate gene expression in Brachypodium distachyon. *Frontiers in Plant Science, 4*.

Morgan, J. L., Strumillo, J., & Zimmer, J. (2012). Crystallographic snapshot of cellulose synthesis and membrane translocation. *Nature, 493*, 181-186.

Morrison, T. A., Jung, H. G., Buxton, D. R., & Hatfield, R. D. (1998). Cell-Wall Composition of Maize Internodes of Varying Maturity. *Crop Science, 38*, 455.

Morrison, T. A., Kessler, J. R., Hatfield, R. D., & Buxton, D. R. (1994). Activity of two lignin biosynthesis enzymes during development of a maize internode. *Journal of the Science of Food and Agriculture, 65*, 133-139.

Moura, J. C., Bonine, C. A., Oliveira Fernandes Viana, J., Dornelas, M. C., & Mazzafera, P. (2010). Abiotic and biotic stresses and changes in the lignin content and composition in plants. *Journal of integrative plant biology, 52*, 360-76.

Moura-Sobczak, J., Souza, U., & Mazzafera, P. (2011). Drought stress and changes in the lignin content and composition in Eucalyptus. *BMC Proceedings, 5*, P103.

Myton, K., & Fry, S. (1994). Intraprotoplasmic feruloylation of arabinoxylans in Festuca arundinacea cell cultures. *Planta, 193*.

Nakamura, A., Furuta, H., Maeda, H., Takao, T., & Nagamatsu, Y. (2002). Structural Studies by Stepwise Enzymatic Degradation of the Main Backbone of Soybean Soluble Polysaccharides Consisting of Galacturonan and Rhamnogalacturonan. *Bioscience, Biotechnology, and Biochemistry, 66*, 1301-1313.

Nakano, J., & Meshitsuka, G. (1992). *The detection of lignin Methods in lignin chemistry.* Berlin: C. Dence and S. Lin.

Naz, A. A., Reinert, S., Bostanci, C., Seperi, B., Leon, J., Böttger, C., et al. (2017). Mining the global diversity for bioenergy traits of barley straw: genomewide association study under varying plant water status. *GCB Bioenergy, 9*, 1356-1369.

Nordfeldt, S. (1959). Silage of green fodder maize. Digestibility and feeding trials. *Vaxtodling*, 65-76.

Obel, N., Porchia, A., & Scheller, H. (2003). Intracellular feruloylation of arabinoxylan in wheat: evidence for feruloyl-glucose as precursor. *Planta*.

Oehme, D. P., Downton, M. T., Doblin, M. S., Wagner, J., Gidley, M. J., & Bacic, A. (2015). Unique Aspects of the Structure and Dynamics of Elementary I β Cellulose Microfibrils Revealed by Computational Simulations. *Plant Physiology, 168*, 3-17.

Oliveira, D. M., Finger-Teixeira, A., Rodrigues Mota, T., Salvador, V. H., Moreira-Vilar, F. C., Correa Molinari, H. B., et al. (2015). Ferulic acid: a key component in grass lignocellulose recalcitrance to hydrolysis. *Plant Biotechnology Journal, 13*, 1224-1232.

O'Neill, M. A., & Wall, W. S. (2003). The composition and structure of plant primary cell walls. *The plant cell*.

O'NEILL, M., ALBERSHEIM, P., & Biochemistry, A. D. (1990). The pectic polysaccharides of primary cell walls. *Methods in plant*.

Önnerud, H., Zhang, L., & Cell, G. G. (2002). Polymerization of monolignols by redox shuttle–mediated enzymatic oxidation: a new model in lignin biosynthesis I. *Am Soc Plant Biol*.

Palmer, A., Trede, D., & Alexandrov, T. (2016). *Where imaging mass spectrometry stands here are the numbers.*

Papst, C., Bohn, M., Utz, H. F., Melchinger, A. E., Klein, D., & Eder, J. (2004). QTL mapping for European corn borer resistance (Ostrinia nubilalis Hb.), agronomic and forage quality traits of testcross progenies in early-maturing European maize (Zea mays L.) germplasm. *TAG Theoretical and Applied Genetics, 108*, 1545-1554.

Papst, C., Eder, J., Melchinger, A. E., Klein, D., Bohn, M., & Schulz, B. (2001). QTL mapping for resistance to European corn borer (Ostrinia nubilalis Hb.) in early maturing European dent maize (Zea mays L.) germplasm and comparison of genomic regions for resistance across two population of F3 families. *Maydica (Italy)*.

Pawley, J. B. (2006). *Handbook of biological confocal microscopy.* New York: Springer.

Perrier, L., Rouan, L., Jaffuel, S., et al. (2017). Plasticity of Sorghum Stem Biomass Accumulation in Response to Water Deficit : A Multiscale Analysis from Internode Tissue to Plant Level. *Front Plant Sci, 8*.

Perrier, L., Rouan, L., Jaffuel, S., Clément-Vidal, A., Roques, S., Soutiras, A., et al. (2017). Plasticity of Sorghum Stem Biomass Accumulation in Response to Water Deficit: A Multiscale Analysis from Internode Tissue to Plant Level. *Frontiers in Plant Science, 8*, 1516.

Perrier, L., Rouan, L., Jaffuel, S., Clément-Vidal, A., Roques, S., Soutiras, A., et al. (2017). Plasticity of Sorghum Stem Biomass Accumulation in Response to Water Deficit: A Multiscale Analysis from Internode Tissue to Plant Level. *Frontiers in plant science, 8*, 1516.

Peyrat, J. (2016). *Prediction of the Energy of the Whole Plant, Cell Wall and Starch.* Colloque Maïs fourrage et bovins: Nouvelles approches de la valeur alimentaire et de sa valorisation.

Piston, F., Uauy, C., Fu, L., Langston, J., Labavitch, J., & Dubcovsky, J. (2010). Down-regulation of four putative arabinoxylan feruloyl transferase genes from family PF02458 reduces ester-linked ferulate content in rice cell walls. *Planta, 231*, 677-691.

Porter, K. S., Axtell, J. D., & VL Lechtenberg, et al. (1978). Phenotype, Fiber Composition, and in vitro Dry Matter Disappearance of Chemically Induced Brown Midrib (bmr) Mutants of Sorghum 1. *Crop Science*.

Pouzet, D. (2011). *Production durable de biomasse : la lignocellulose des poacées.* Quae.

Puri, V. P. (1984). Effect of crystallinity and degree of polymerization of cellulose on enzymatic saccharification. *Biotechnology and Bioengineering, 26*, 1219-1222.

Qi, B., Chen, X., Shen, F., et al. (2016). Optimization of enzymatic hydrolysis of wheat straw pretreated by alkaline peroxide using response surface methodology. *Ind Eng Chem Res, 48*, 7346-7353.

Ralph, J. (2010). Hydroxycinnamates in lignification. *Phytochemistry Reviews, 9*, 65-83.

Ralph, J., & Helm, R. F. (1993). Lignin/hydroxycinnamic acid/polysaccharide complexes: Synthetic models for regiochemical characterization. *dl.sciencesocieties.org, Forage cel*.

Ralph, J., Grabber, J. H., & R. D. (1995). Lignin-ferulate cross-links in grasses: active incorporation of ferulate polysaccharide esters into ryegrass lignins. *Carbohydrate Research*.

Ralph, J., Hatfield, R. D., J Piquemal Proceedings, et al. (1998). NMR characterization of altered lignins extracted from tobacco plants down-regulated for lignification enzymes cinnamylalcohol dehydrogenase and cinnamoyl-CoA. *National Acad Sciences*.

Ralph, J., Hatfield, R. D., Quideau, S., & RF Helm, et al. (1994). Pathway of p-coumaric acid incorporation into maize lignin as revealed by NMR. *ACS Publications*.

Ralph, J., Hatfield, R. D., Quideau, S., Helm, R. F., Grabber, J. H., & Jung, H.-J. G. (1994). Pathway of p-Coumaric Acid Incorporation into Maize Lignin As Revealed by NMR. *Journal of the American Chemical Society, 116*, 9448-9456.

Reddy, M. S., Chen, F., Shadle, G., Jackson, L., Aljoe, H., & Dixon, R. A. (2005). Targeted down-regulation of cytochrome P450 enzymes for forage quality improvement in alfalfa (Medicago sativa L.). *Proceedings of the National Academy of Sciences of the United States of America, 102*, 16573-8.

Reymond, M., Muller, B., & Tardieu, F. (2004). Dealing with the genotypexenvironment interaction via a modelling approach: a comparison of QTLs of maize leaf length or width with QTLs of model parameters. *Journal of Experimental Botany, 55*, 2461-2472.

Reynolds, M., & Langridge, P. (2016). Physiological breeding. *Current Opinion in Plant Biology, 31*, 162-171.

Ribaut, J.-M., & Ragot, M. (2007). Marker-assisted selection to improve drought adaptation in maize: the backcross approach, perspectives, limitations, and alternatives. *Journal of Experimental Botany, 58*, 351-360.

Ribaut, J.-M., Fracheboud, Y., Monneveux, P., Banziger, M., Vargas, M., & Jiang, C. (2007). Quantitative trait loci for yield and correlated traits under high and low soil nitrogen conditions in tropical maize. *Molecular Breeding, 20*, 15-29.

Ribaut, J.-M., Vicente, M. C., & Delannay, X. (2010). Molecular breeding in developing countries: challenges and perspectives. *Current Opinion in Plant Biology, 13*, 213-218.

Riboulet, C., Fabre, Dénoue, Martinant, Lefèvre, & Barrière. (2008). QTL mapping and candidate gene research for lignin content and cell wall digestibility in a top-cross of a flint maize recombinant inbred line progeny harvested at silage stage. *Maydica, 53*, 1-9.

Riboulet, C., Guillaumie, S., Méchin, V., Bosio, M., Pichon, M., Goffner, D., et al. (2009). Kinetics of phenylpropanoid gene expression in maize growing internodes: Relationships with cell wall deposition. *Crop Science, 49*, 211-223.

Ride, J. P. (1975). Lignification in wounded wheat leaves in response to fungi and its possible rôle in resistance. *Physiological Plant Pathology, 5*, 125-134.

Ridley, B. L., O'Neill, M. A., & Mohnen, D. (2001). Pectins: structure, biosynthesis, and oligogalacturonide-related signaling. *Phytochemistry*.

Ronsin, T. (1990). Use of NIR prediction of digestibility in a breeding program for silage maize. *Proceeding of the 15th congress of maize and sorghum section of Eucarpia. Baden*, (pp. 277-288).

Rose, J. K. (2003). *The plant cell wall.* Blackwell.

Rosner, S., Gierlinger, N., Klepsch, M., B Karlsson Forest Ecology, (2018.). Hydraulic and mechanical dysfunction of Norway spruce sapwood due to extreme summer drought in Scandinavia. *Elsevier*.

Rousseau, D., Chéné, Y., Belin, E., . (2015). Multiscale imaging of plants : current approaches and challenges. *11*.

Roussel, V., Gibelin, C., Fontaine, A. S., & Barriere, Y. (2002). Genetic analysis in recombinant inbred lines of early dent forage maize. 2: QTL mapping for cell wall constituents and cell wall digestibility from per se value and top cross experiments [Zea mays L.-France]. *Maydica*

Roussel, V., Gibelin, C., Fontaine, A.-S., & Barrière, Y. (2002). Genetic analysis in recombinant inbred lines of early dent forage maize. II-QTL mapping for cell wall constituents and cell wall digestibility from per se value and top cross experiments. *Maydica, 47*, 9-20.

Ruprecht, C., Bartetzko, M. P., Senf, D., et al. (2017). A Synthetic Glycan Microarray Enables Epitope Mapping of Plant Cell Wall Glycan-Directed Antibodies. *Plant Physiol, 175*, 1094-1104.

Samaniego, L., Thober, S., Kumar, R., Wanders, N., Rakovec, O., Pan, M., et al. (2018). Anthropogenic warming exacerbates European soil moisture droughts. *Nature Climate Change, 8*, 421-426.

Samaniego, L., Thober, S., Kumar, R., Wanders, N., Rakovec, O., Pan, M., et al. (2018). Elucidating the impact of global warming levels to agricultural droughts in Europe. *20th EGU General Assembly, EGU2018, Proceedings from the conference held 4-13 April, 2018 in Vienna, Austria, p.5518, 20*, 5518.

Sanaullah, M., Chabbi, A., Girardin, C., Durand, J.-L., Poirier, M., & Rumpel, C. (2014). Effects of drought and elevated temperature on biochemical composition of forage plants and their impact on carbon storage in grassland soil. *Plant and Soil, 374*, 767-778.

Sang, Y., Deng, Z. Y., Zhao, L., Zhang, K. P., Tian, J. C., & Ye, B. X. (2010, 12). QTLs for the vascular bundle system of the uppermost internode using a doubled haploid population of two elite Chinese wheat cultivars. *Plant Breeding, 129*, 605-610.

Santiago, R., Barros-Rios, J., & Malvar, R. A. (2013). Impact of cell wall composition on maize resistance to pests and diseases. *International Journal of Molecular Sciences, 14*, 6960-6980.

Santos, A. B., Bottcher, A., Kiyota, E., Mayer, J. L., Vicentini, R., Brito, M. d., et al. (2015). Water Stress Alters Lignin Content and Related Gene Expression in Two Sugarcane Genotypes. *Journal of Agricultural and Food Chemistry, 63*, 4708-4720.

Santos, M. B., Nader, G. A., Robinson, P. H., & D Kiran, et al. (2010). Impact of simulated field drying on in vitro gas production and voluntary dry matter intake of rice straw. *Animal Feed Science and Technology*.

Santos, R. B., Capanema, E. A., Balakshin, M. Y., Chang, H.-m., & Jameel, H. (2012). Lignin Structural Variation in Hardwood Species. *Journal of Agricultural and Food Chemistry, 60*, 4923-4930.

Sasahara, H., Fukuta, Y., & Fukuyama, T. (1999). Mapping of QTLs for vascular bundle system and spike morphology in rice, Oryza sativa L. *Breeding science, 49*, 75-81.

Satiat-Jeunemaitre, B., & Hawes, C. (2001). *Immunocytochemistry for ligth microscopy.* Oxford: Plant Cell Biology- A Pratical Approach.

Satiat-Jeunemaitre and C. Hawes. Sattler, S. E., Funnell-Harris, D. L., & Pedersen, J. F. (2010). Brown midrib mutations and their importance to the utilization of maize, sorghum, and pearl millet lignocellulosic tissues. *Plant Science, 178*, 229-238.

Scheller, H. V., & Ulvskov, P. (2010). Hemicelluloses. *Annual Review of Plant Biology, 61*, 263-289.

Scheller, H. V., Jensen, J. K., Sørensen, S. O., Harholt, J., & Geshi, N. (2006). Biosynthesis of pectin. *Physiologia Plantarum, 129*, 283-295.

Schubiger, F. X., Lehmann, J., Daccord, R., Arrigo, Y., Jeangros, B., & Scehovic, J. (2001). Nutritive value of grassland plants. 5. Digestibility of organic matter. *Revue Suisse Agric, 33*, 275-279. Scobbie, L., Russell, W., Provan, G. J., & Chesson, A. (1993). The newly extended maize internode: A model for the study of secondary cell wall formation and consequences for digestibility. *Journal of the Science of Food and Agriculture, 61*, 217-225.

Scott, J. E. (1985). Proteoglycan histochemistry. *A valuable tool for connective tissue biochemists Collagen and Related Research, 5*, 541-575.

Seeley, E. H., & Caprioli, R. M. (2012). 3D imaging by mass spectrometry : a new frontier. *Anal. Chem, 84*, 2105-2110.

Simmons, T. J., Mortimer, J. C., & OD Bernardinelli, et al. (2016). Folding of xylan onto cellulose fibrils in plant cell walls revealed by solid-state NMR. *Nature*.

Siqueira, G., Milagres, A. M., Carvalho, W., Koch, G., & Ferraz, A. (2011). Topochemical distribution of lignin and hydroxycinnamic acids in sugar-cane cell walls and its correlation with the enzymatic hydrolysis of polysaccharides. *Biotechnology for Biofuels, 4*, 7.

Skirycz, A., & Inzé, D. (2010). More from less: plant growth under limited water. *Current Opinion in Biotechnology, 21*, 197-203.

Smith, R. A., Schuetz, M., Karlen, S. D., Bird, D., Tokunaga, N., Sato, Y., et al. (2017). Defining the Diverse Cell Populations Contributing to Lignification in Arabidopsis Stems. *Plant physiology, 174*, 1028-1036.

Somerville, C., Youngs, H., Taylor, C., Davis, S. C., & Long, S. P. (2010). Feedstocks for lignocellulosic biofuels. *Science (New York, N.Y.), 329*, 790-2.

Souza, W. R., Martins, P. K., Freeman, J., Pellny, T. K., Michaelson, L. V., Sampaio, B. L., et al. (2018). Suppression of a single BAHD gene in *Setaria viridis* causes large, stable decreases in cell wall feruloylation and increases biomass digestibility. *New Phytologist, 218*, 81-93.

Spence, J. (2001). Plant histology Plant Cell Biology- A Pratical Approach. C. *Hawes and B. Satiat-Jeunemaitre. Oxford*, 189-206.

Spengler, B. (2015). Mass spectrometry imaging of biomolecular information. *Anal. Chem, 87*, 64-82.

Srebotnik, E., & Messner, K. (1994). A Simple Method That Uses Differential Staining and Light Microscopy To Assess the Selectivity of Wood Delignification by White Rot Fungi. *Appl. Environ, 60*, 1383-1386.

Steeves, V., Förster, H., & Pommer, U. (2001). Coniferyl alcohol metabolism in conifers—I. Glucosidic turnover of cinnamyl aldehydes by UDPG: coniferyl alcohol glucosyltransferase from pine cambium. *Phytochemistry*.

Stevenson, J. C., & Goodman, M. M. (1972). Ecology of Exotic Races of Maize. I. Leaf Number and Tillering of 16 Races Under Four Temperatures and Two Photoperiods1. *Crop Science, 12*, 864.

Stuppy, W. H., Maisano, J. A., Colbert, M. W., et al. (2003). Three-dimensional analysis of plant structure using high-resolution X-ray computed tomography. *Trends Plant Sci, 8*, 2-6.

Sun, L., Singh, S., Joo, M., et al. (2016). Non-invasive imaging of cellulose microfibril orientation within plant cell walls by polarized Raman microspectroscopy. *Biotechnol. Bioeng., 113*, 82-90.

Surault, F., Emile, J. C., Briand, M., et al. (2005). Genetic Variability of Corn Hybrids in Vivo Digestibility : A Review of years of Measures. *Fourrages, 34*, 459-474.

Syrjänen, K., & Brunow, G. (2000). Regioselectivity in lignin biosynthesis. The influence of dimerization and cross-coupling. *Journal of the Chemical Society, Perkin Transactions 1, 0*, 183-187.

Taboada, A., Novo-Uzal, E., Flores, G., Loureda, M., Ros Barceló, A., Masa, A., et al. (2010). Digestibility of silages in relation to their hydroxycinnamic acid content and lignin composition. *Journal of the Science of Food and Agriculture, 90*, 1155-1162.

Tardieu, F., & Tuberosa, R. (2010). Dissection and modelling of abiotic stress tolerance in plants. *Current Opinion in Plant Biology, 13*, 206-212.

Tardieu, F., Simonneau, T., & Muller, B. (2018, 4). The Physiological Basis of Drought Tolerance in Crop Plants: A Scenario-Dependent Probabilistic Approach. *Annual Review of Plant Biology, 69*, 733-759.

Tenaillon, M. I., & Charcosset, A. (2011). A European perspective on maize history. *Comptes Rendus - Biologies, 334*, 221-228.

Thomas, L. H., Forsyth, V. T., Sturcova, A., Kennedy, C. J., May, R. P., Altaner, C. M., et al. (2013). Structure of Cellulose Microfibrils in Primary Cell Walls from Collenchyma. *PLANT PHYSIOLOGY, 161*, 465-476.

Tobimatsu, Y. (2014). Van de Wouwer D, Allen E et al. (2014). A click chemistry strategy for visualization of plant cell wall lignification. *Chemical communications, 50*, 12262-12265.

Tobimatsu, Y., Wagner, A., Donaldson, L., et al. (2013). Visualization of plant cell wall lignification using fluorescence-tagged monolignols. *The Plant journal : for cell and molecular biology, 76*, 357-366.

Tolivia, D., & Tolivia, J. (1987). Fasga: A new polychromatic method for simultaneous and differential staining of plant tissues. *Journal of Microscopy, 148*, 113-117.

Torres, A. F., Noordam-Boot, C. M., Dolstra, O., Vlaswinkel, L., Visser, R. G., & Trindade, L. M. (2015). Extent of genotypic variation for maize cell wall bioconversion traits across environments and among hybrid combinations. *Euphytica, 206*, 501-511.

Torres, A. F., Noordam-Boot, C. M., Dolstra, O., Weijde, T., Combes, E., Dufour, P., et al. (2015). Cell Wall Diversity in Forage Maize: Genetic Complexity and Bioenergy Potential. *Bioenergy Research, 8*, 187-202.

Trachsel, S., Sun, D., SanVicente, F. M., Zheng, H., Atlin, G. N., Suarez, E. A., et al. (2016). Identification of QTL for Early Vigor and Stay-Green Conferring Tolerance to Drought in Two Connected Advanced Backcross Populations in Tropical Maize (Zea mays L.). (M. Li, Éd.) *PLOS ONE, 11*, e0149636.

Truntzler, M., Barrière, Y., Sawkins, M. C., Lespinasse, D., Betran, J., Charcosset, A., et al. (2010). Meta-analysis of QTL involved in silage quality of maize and comparison with the position of candidate genes. *Theoretical and Applied Genetics, 121*, 1465-1482.

Turc, O., & Tardieu, F. (2018). Drought affects abortion of reproductive organs by exacerbating developmentally driven processes via expansive growth and hydraulics. *Journal of Experimental Botany, 69*, 3245-3254.

Türker, S., & Huck, C. W. (2017). A review of mid-infrared and near-infrared imaging : principles. *conceptes and application in Plant tissue analysis Molecules, 22*.

Turner, S. R., & Somerville, C. R. (1997). Collapsed Xylem Phenotype of Arabidopsis Identifies Mutants Deficient in Cellulose Deposition in the Secondary Cell Wall. *THE PLANT CELL ONLINE, 9*, 689-701.

Unknown, A.; Doe, J. (2020). From the plant cell wall to the infinty of the Dragon Ball universe. *Journal of the non-related and ununderstood things, 13, 13-113.*

Updegraff, D. M. (1969). Semimicro Determination of Cellulose in Biological Materials. *Analytical Biochemistry, 32*, 420-424.

Updegraff, D. M. (1969). Semimicro determination of cellulose inbiological materials. *Analytical Biochemistry, 32*, 420-424.

Vallet, C., Chabbert, B., Czaninski, Y., et al. (1996). Histochemistry of lignin deposition during sclerenchyma differentiation in alfalfa stems. *Annals of Botany, 78*, 625-632.

Vanholme, R., Demedts, B., Morreel, K., & J. R. (2010). Lignin biosynthesis and structure. *Am Soc Plant Biol*.

Vanholme, R., Morreel, K., Darrah, C., Oyarce, P., Grabber, J. H., Ralph, J., et al. (2012). Metabolic engineering of novel lignin in biomass crops. *New Phytologist, 196*, 978-1000.

Vanholme, R., Morreel, K., Ralph, J., & Boerjan, W. (2008). Lignin engineering. *Current Opinion in Plant Biology, 11*, 278-285.

Velickovic, D., Ropartz, D., Guillon, F., et al. (2014). New insights into the structural and spatial variability of cell-wall polysaccharides during wheat grain development, as revealed through MALDI mass spectrometry imaging. *J. Exp. Bot, 65*, 2079-2091.

Velickovic, D., Saulnier, L., Lhomme, M., et al. (2016). Mass Spectrometric Imaging of Wheat (Triticum spp.) and Barley (Hordeum vulgare L.) Cultivars : Distribution of Major Cell Wall Polysaccharides According to Their Main Structural Features. *J. Agric. Food Chem, 64*, 6249-6256.

Vermerris, W., & Abril, A. (2015). Enhancing cellulose utilization for fuels and chemicals by genetic modification of plant cell wall architecture. *Current Opinion in Biotechnology, 32*, 104-112.

Vignau-Loustau, L., Huyghe, C., & Mame), I. (2008). *Stratégies fourragères.* Éd. France agricole.

Vignols, F., Rigau, J., Torres, M. A., Capellades, M., & Puigdomènech, P. (1995). The brown midrib3 (bm3) mutation in maize occurs in the gene encoding caffeic acid O-methyltransferase. *The Plant cell, 7*, 407-16.

Vogel, J. (2008, 6). Unique aspects of the grass cell wall. *Current Opinion in Plant Biology, 11*, 301-307.

Waduwara, C. I., Walcott, S. E., & Peterson, C. A. (2008). Suberin lamellae of the onion root endodermis : their pattern of development and continuity. *Botany, 86*, 623-632.

Wang, H., Nussbaum-Wagler, T., Li, B., Zhao, Q., Vigouroux, Y., Faller, M., et al. (2005). The origin of the naked grains of maize. *Nature, 436*, 714-719.

Wang, Y., Chantreau, M., Sibout, R., & Hawkins, S. (2013). Plant cell wall lignification and monolignol metabolism. *Frontiers in Plant Science, 4*.

Watkins, D., Nuruddin, M., Hosur, M., Tcherbi-Narteh, A., & Jeelani, S. (2015). Extraction and characterization of lignin from different biomass resources. *Journal of Materials Research and Technology, 4*, 26-32.

Webber, H., Ewert, F., Olesen, J. E., Müller, C., Fronzek, S., Ruane, A. C., et al. (2018). Diverging importance of drought stress for maize and winter wheat in Europe. *Nature Communications, 9*, 4249.

Wei, M., Li, X., Li, J., Fu, J., Wang, Y., & Li, Y. (2009). QTL detection for stover yield and quality traits using two connected populations in high-oil maize. *Plant Physiology and Biochemistry, 47*, 886-894.

Weijde, T., Alvim Kamei, C. L., Torres, A. F., Vermerris, W., Dolstra, O., Visser, R. G., et al. (2013). The potential of C4 grasses for cellulosic biofuel production. *Frontiers in Plant Science, 4*, 1-18.

Wellhausen, E. J., Roberts, L. M., Hernandez, X., E., & Mangelsdorf, P. C. (1952). Races of maize in Mexico. Their origin, characteristics and distribution. *Races of maize in Mexico. Their origin, characteristics and distribution.*

Wells, C. I., McCall, J. L., & Plank, L. D. (2018). Relationship between total body protein and cross-sectional skeletal muscle area in liver cirrhosis is influenced by overhydration. *Liver Transplantation*, 436-450.

Wende, G., & Fry, S. C. (1997, 3). 2-O-β-d-xylopyranosyl-(5-O-feruloyl)-l-arabinose, a widespread component of grass cell walls. *Phytochemistry, 44*, 1019-1030.

Whetten, R., & Sederoff, R. (1991, 10). Genetic engineering of wood. *Forest Ecology and Management, 43*, 301-316.

Wildhagen, H., Paul, S., Allwright, M., Smith, H. K., Malinowska, M., Schnabel, S. K., et al. (2018). Genes and gene clusters related to genotype and drought-induced variation in saccharification potential, lignin content and wood anatomical traits in Populus nigra†. *Tree Physiology, 38*, 320-339.

Willats, W. G., McCartney, L., Mackie, W., & Knox, J. P. (2001). Pectin: cell biology and prospects for functional analysis. *Plant Molecular Biology, 47*, 9-27.

Wilson, J. R., & Hatfield, R. D. (1997). Structural and chemical changes of cell wall types during stem development: consequences for fibre degradation by rumen microflora. *Australian Journal of Agricultural Research, 48*, 165.

Wilson, J. R., & Research, R. D. (1997). Structural and chemical changes of cell wall types during stem development: consequences for fibre degradation by rumen microflora. *Australian Journal of Agricultural*.

Withers, S., Lu, F., Kim, H., Zhu, Y., Ralph, J., & Wilkerson, C. G. (2012). Identification of grass-specific enzyme that acylates monolignols with p-coumarate. *The Journal of biological chemistry, 287*, 8347-55.

Wolf, D. P., Coors, J. G., Albrecht, K. A., Undersander, D. J., & Carter, P. R. (1993). Forage Quality of Maize Genotypes Selected for Extreme Fiber Concentrations. *Crop Science, 33*, 1353.

Wood, P. J., Fulcher, R. G., & Stone, B. A. (1983). Studies on the specificity of interactions of cereal cell-wall components with congo red and calcofluor-speficic detection and hystochemistry of (1-3)(1-4) beta D glucan. *Journal of Cereal Science, 1*, 95-110.

Xie, M., Zhang, J., Tschaplinski, T. J., Tuskan, G. A., Chen, J.-G., & Muchero, W. (2018). Regulation of Lignin Biosynthesis and Its Role in Growth-Defense Tradeoffs. *Frontiers in Plant Science, 9*, 1427.

Yan, J., Aznar, A., Chalvin, C., Birdseye, D. S., Baidoo, E. E., Eudes, A., et al. (2018). Increased drought tolerance in plants engineered for low lignin and low xylan content. *Biotechnology for Biofuels, 11*, 195.

Zablackis, E., Huang, J., Muller, B., Darvill, A. G., & Albersheim, P. (1995). Characterization of the Cell-Wall Polysaccharides of Arabidopsis thaliana Leaves. *Plant Physiology, 107*, 1129-1138.

Zandbergen, N. (2006). Brown mid-rib corn showcased. *AgriNews Interactive, 30*.

Zhang, Y., Culhaoglu, T., Pollet, B., Melin, C., Denoue, D., Barrière, Y., et al. (2011). Impact of lignin structure and cell wall reticulation on maize cell wall degradability. *Journal of Agricultural and Food Chemistry, 59*, 10129-10134.

Zhang, Y., Culhaoglu, T., Pollet, B., Melin, C., Denoue, D., Barrière, Y., et al. (2011). Impact of Lignin Structure and Cell Wall Reticulation on Maize Cell Wall Degradability. *Journal of Agricultural and Food Chemistry, 59*, 10129-10135.

Zhang, Y., Legay, S., Barriere, Y., et al. (2013). Color quantification of stained maize stem section describes lignin spatial distribution within the whole stem. *J. Agric. Food Chem, 61*, 3186-3192.

Zhang, Z.-H., Li, P., Wang, L.-X., Tan, C.-J., Hu, Z.-L., Zhu, Y.-G., et al. (2002). Identification of quantitative trait loci (QTLs) for the characters of vascular bundles in peduncle related to indica-japonica differentiation in rice (Oryza sativa L.). *Euphytica, 128*, 279-284.

Zykwinska, A. W., Ralet, M. C., & CD Garnier, et al. (2005). Evidence for in vitro binding of pectin side chains to cellulose. *Am Soc Plant Biol*.

French abstract

Ce projet de thèse s'inscrit dans un contexte de changement climatique et de remplacement des énergies fossiles, où la réduction des apports en eau et l'optimisation de la valorisation de la biomasse sont deux enjeux majeurs des systèmes de productions durables. La dégradabilité de la biomasse est principalement limitée par la dégradabilité des parois et afin de l'améliorer, il est nécessaire de comprendre quels facteurs sont impliqués dans cette limitation de dégradabilité. Plusieurs études ont montré que la dégradabilité pariétale est impactée par la composition biochimique et la structure de la paroi mais aussi par la distribution des tissus lignifiés au sein des organes. Pour faire la part entre l'impact de la biochimie et celui de l'histologie sur la dégradabilité dans différentes conditions d'irrigation, des outils haut-débit de quantifications biochimiques et histologiques ont été développés et dédiés à l'étude d'entrenoeuds portant l'épi principal. Les études ont porté sur un panel de diversité génétique de maïs et d'une population de lignées recombinantes, cultivés durant plusieurs années dans des conditions d'irrigation contrastées dans le sud de la France.

Après développement et publication d'un pipeline de coloration, d'acquisition, d'analyse d'image et de quantification des caractères histologiques chez l'entrenoeud sous-épi chez le maïs, nous avons tout d'abord phénotypé et analysé le panel de diversité génétique de maïs. Ce dernier a été cultivé durant 3 ans dans des conditions d'irrigation contrastées afin de pouvoir évaluer l'impact d'un déficit hydrique sur la dégradabilité, la composition et structure biochimique de la paroi ainsi que les caractères histologiques chez des lignées de maïs principalement adaptées au climat Nord européen et sélectionnées pour une large gamme de dégradabilité. La variabilité génétique observée pour les caractères biochimiques et histologiques ainsi que leur réponse à la condition d'irrigation suggèrent des cibles possibles pour la sélection variétale. Plus particulièrement, nos résultats mettent en évidence que le déficit hydrique induit une augmentation de la dégradabilité pariétale, accompagnée par une diminution de la teneur en lignines pariétales et par une induction préférentielle d'une lignification corticale, plus *p*-coumaroylée. Ces observations ouvrent, elles aussi, la voie vers une meilleure compréhension de la réponse au déficit hydrique à la fois en termes de

dégradadabilité de paroi, structure, composition biochimique et distribution de la lignification chez le maïs.

Ensuite un phénotypage histologique haut-débit de 1387 échantillons a été réalisé au sein de la population de 183 lignées recombinantes issues des deux parents F271 et Cm484 cultivées pendant 2 ans dans des conditions d'irrigation contrastées. De façon originale nous avons ainsi cartographié 90 QTLs de caractères histologiques dans les différentes conditions d'irrigation sur le génome du maïs. Plus particulièrement, une large région entre le bin 1.07 et le bin 1.11 est impliquée dans les variations observées du nombre de faisceaux vasculaires et de la surface de section des entrenoeuds. De façon globale, de nombreux QTLs de composition pariétale de l'entrenoeud co-localisent avec ceux obtenus au niveau de la plante entière sans épis chez la même population.

Enfin après une étude sur les relations l'entrenoeud portant l'épi principal et la plante entière sans l'épi a été faîte. Ainsi une analyse de la biochimie de l'entrenoeud portant l'épi principal et de la biochimie plante entière sans l'épi puis une analyse de l'histologie de l'entrenoeud portant l'épi principal et de l'histologie de tous les autres entrenoeuds nous a permis de mieux comprendre la représentativité de cet entrenoeud vise à vis de la plante entière sans épi. Nous avons pu démontrer que le choix de l'entrenoeud portant l'épi principal est judicieux pour représenter à la fois les caractéristiques histologiques des tiges entières et biochimiques de la biomasse lignocellulosique des plantes entières.

Ainsi, ce travail de thèse propose les caractéristiques histologiques et biochimiques des entrenoeuds de maïs comme des cibles de choix pour sélectionner des lignées de maïs résilientes au déficit hydrique.

ANNEXES

Supplemental Table S1-1. Variations of the histological and biochemical traits within the RILs population in the 4 conditions: 2014-I, 2014-NI, 2015-I, 2015-NI. Each year, a one sample t-test has been calculated to evaluate the significance of the condition on the means.

RILs population																	
	2014								2015								
	I			NI			t-test between the 2 conditions		I			NI			t-test between the 2 conditions	
	Mean	Min	Max	**Mean**	Min	Max	p-value[a]	Significance[b]	**Mean**	Min	Max	**Mean**	Min	Max	p-value[a]	Significance[b]
IVCWRD	30,62	22,07	40,02	33,36	23,86	44,20	9,2E-10	***	29,52	22,84	39,45	33,43	23,43	41,51	9,7E-19	***
IVDMD	53,48	36,79	69,29	55,99	37,59	74,20	2,2E-03	**	52,17	37,94	66,97	56,52	35,78	36,27	1,4E-07	***
Stem area	1,63	0,77	3,07	1,25	0,62	2,30	2,1E-19	***	1,75	1,07	2,91	1,89	0,84	3,08	2,5E-03	**
Lignified fraction	0,63	0,34	0,77	0,61	0,26	0,75	1,7E-01		0,64	0,33	0,78	0,62	0,39	0,75	6,0E-02	.
Non-lignified fraction	0,16	0,05	0,45	0,20	0,05	0,59	4,8E-04	***	0,16	0,04	0,46	0,17	0,04	0,40	2,1E-01	
Rind fraction	0,16	0,08	0,28	0,14	0,08	0,26	1,8E-04	***	0,14	0,08	0,24	0,15	0,07	0,28	2,1E-01	
Bundle fraction	0,054	0,031	0,107	0,049	0,024	0,096	3,2E-04	***	0,055	0,022	0,081	0,056	0,025	0,120	4,4E-01	
Bundle number	126	58	237	120	61	251	1,0E-01		139	66	228	140	57	234	7,0E-01	
Bundle density	78,04	52,71	110,60	98,69	56,53	152,43	7,1E-28	***	81,02	32,94	115,24	74,99	45,60	115,97	1,7E-04	***
Red rind	9,93	5,71	16,80	9,07	6,03	13,36	7,7E-07	***	8,52	5,51	14,04	8,61	4,60	13,32	6,0E-01	
Red parenchyma	113,59	60,34	150,78	107,93	44,53	144,34	8,6E-03	**	117,13	60,26	155,32	116,31	69,83	147,13	6,8E-01	
Blue parenchyma	34,10	6,83	107,78	41,93	7,96	132,18	7,5E-04	***	32,90	6,56	97,80	33,72	8,09	85,21	6,7E-01	
CWR	57,25	38,81	76,81	55,84	35,42	77,60	1,3E-01		57,24	44,18	73,54	55,65	39,33	76,62	9,1E-02	.
KL.CWR	16,24	13,77	19,55	15,68	12,03	18,78	2,5E-05	***	16,39	14,00	18,54	15,53	12,86	18,41	9,7E-12	***
PCAest	21,37	15,96	25,49	18,48	11,41	24,57	1,9E-23	***	19,84	15,47	25,77	18,13	12,89	25,90	1,0E-11	***
FAest	3,97	2,80	4,79	4,30	2,97	5,11	1,1E-11	***	3,97	2,91	5,04	3,69	2,27	4,57	4,6E-07	***
FAeth	4,28	3,09	5,74	4,23	2,88	5,92	4,8E-01		4,70	3,75	5,98	4,15	3,07	5,75	1,0E-13	***
BO4 yield	799,09	721,61	931,80	816,66	680,06	929,91	7,8E-05	***	813,84	675,61	954,96	742,18	660,83	845,28	1,2E-40	***
BO4.H	27,79	7,71	40,76	24,92	7,72	37,43	1,5E-06	***	30,07	9,19	45,15	25,53	15,83	39,44	3,9E-16	***
S.G	1,10	0,95	1,29	0,96	0,70	1,16	3,2E-44	***	1,10	0,91	1,35	1,12	0,84	1,50	6,5E-02	.
Cellulose	38,96	34,34	43,84	37,70	30,72	42,99	3,1E-06	***	39,24	33,46	43,47	37,54	31,50	42,29	5,3E-12	***
Hemi-celluloses	28,38	20,58	33,97	30,84	25,35	35,92	2,3E-24	***	29,60	25,33	34,17	30,93	25,07	36,27	7,6E-10	***
Yield	2,93	0,90	6,78	1,52	0,35	3,79	6,0E-38	***	3,18	1,53	6,35	2,46	0,86	4,73	2,1E-10	***
Plant height	126,73	100,11	169,90	89,01	59,24	119,24	5,1E-74	***	159,02	117,26	213,70	144,92	108,31	180,85	2,7E-11	***

[a] : t-test performed between the average of every traits in the two watering conditions.

[b]: Significance : . , $p \leq 0.1$; *, $p \leq 0.05$; **, $p \leq 0.01$; ***, $p \leq 0.001$.

Supplemental Table S1-2. Variations of the histological and biochemical traits for the parent Cm484 n the 4 conditions : 2014-I, 2014-NI, 2015-I, 2015-NI. Each year, a one sample t-test has been calculated to evaluate the significance of the condition.

	Cm484															
	2014								2015							
	I			NI			t-test between the 2 conditions		I			NI			t-test between the 2 conditions	
	Mean	Min	Max	**Mean**	Min	Max	p-value[a]	Significancy[b]	**Mean**	Min	Max	**Mean**	Min	Max	p-value[a]	Significance[b]
IVCWRD	35,28	34,14	37,01	37,75	35,31	40,42	3,9E-03	**	33,97	32,63	35,61	37,72	35,06	39,72	6,1E-04	***
IVDMD	63,16	58,81	65,63	66,80	61,22	72,15	3,9E-02	*	60,06	56,62	62,90	64,94	61,69	67,01	2,9E-04	***
Stem area	1,79	1,26	2,10	1,49	1,09	1,80	2,2E-02	*	1,79	1,21	2,05	1,81	1,60	2,22	9,1E-01	
Lignified fraction	0,63	0,58	0,68	0,63	0,51	0,69	9,2E-01		0,63	0,60	0,67	0,64	0,55	0,69	6,9E-01	
Non-lignified fraction	0,18	0,12	0,24	0,20	0,15	0,30	4,7E-01		0,19	0,11	0,24	0,16	0,10	0,27	4,2E-01	
Rind fraction	0,14	0,11	0,17	0,13	0,11	0,15	3,7E-01		0,13	0,11	0,17	0,15	0,12	0,17	1,7E-01	
Bundle fraction	0,05	0,04	0,06	0,04	0,03	0,04	3,6E-02	*	0,05	0,04	0,06	0,05	0,04	0,05	7,2E-01	
Bundle number	114	75	135	115	93	129	9,2E-01		123	77	143	113	91	140	2,8E-01	
Bundle density	64,03	56,76	69,83	78,39	63,93	89,60	9,9E-04	***	68,70	63,42	74,83	62,68	50,32	70,04	6,4E-02	.
Red rind	9,59	7,17	11,53	8,90	8,13	9,76	2,6E-01		7,73	6,24	9,70	8,52	6,98	9,48	1,7E-01	
Red parenchyma	122,39	110,64	132,18	116,74	92,59	130,81	2,7E-01		114,59	108,63	119,94	119,62	102,09	127,99	1,9E-01	
Blue parenchyma	37,24	24,27	48,58	41,39	27,31	64,97	4,8E-01		36,37	21,10	49,13	31,73	19,31	54,05	4,1E-01	
CWR	45,84	42,71	52,52	43,30	37,71	49,84	2,1E-01		49,10	45,64	52,52	47,05	45,23	48,67	4,4E-02	*
KL.CWR	15,39	14,70	16,12	15,12	14,44	15,69	2,6E-01		15,70	15,32	16,03	15,06	14,36	15,72	2,3E-02	*
PCAest	20,43	19,18	21,94	18,45	16,31	21,20	1,1E-02	*	19,66	18,89	20,70	17,19	15,18	18,95	2,1E-03	**
FAest	3,87	3,68	4,07	4,36	4,18	4,75	9,1E-05	***	3,89	3,56	4,07	3,72	3,07	3,97	2,4E-01	
FAeth	3,55	3,39	3,94	3,32	3,04	3,69	4,1E-02	*	4,25	3,97	4,87	3,56	3,17	3,77	2,7E-04	***
BO4 yield	792,48	782,37	815,93	830,29	792,90	878,85	1,4E-02	*	804,84	784,14	872,93	735,92	717,67	749,60	1,1E-04	***
BO4 H	26,66	23,39	31,10	22,81	19,49	27,12	3,3E-03	**	26,14	23,72	29,35	23,88	21,15	26,42	3,7E-02	*
S/G	1,10	1,07	1,15	0,92	0,83	1,05	1,9E-04	***	1,12	1,01	1,17	1,14	1,08	1,22	5,4E-01	
Cellulose	37,44	35,07	38,79	35,71	33,44	37,94	4,7E-02	*	37,76	34,30	39,76	36,87	35,25	38,83	3,1E-01	
Hemi-celluloses	28,37	26,69	29,76	29,44	28,50	30,38	4,5E-02	*	29,38	28,40	30,05	30,41	29,14	31,55	1,6E-02	*
Yield	2,74	2,23	3,09	1,53	1,06	1,80	1,6E-07	***	2,68	2,31	2,94	2,47	2,11	3,00	2,2E-01	
Plant height	123,12	115,11	136,84	91,25	82,95	98,35	1,0E-07	***	143,69	138,71	149,02	144,58	132,86	162,63	8,2E-01	

Supplemental Table S1-3. Variations of the histological and biochemical traits for the parent F271 in the 4 conditions : 2014-I, 2014-NI, 2015-I, 2015-NI. Each year, a one sample t-test has been calculated to evaluate the significance of the condition.

F271	2014								2015							
	I			NI			t-test between the 2 conditions		I			NI			t-test between the 2 conditions	
	Mean	Min	Max	Mean	Min	Max	p-value[a]	Significance[b]	Mean	Min	Max	Mean	Min	Max	p-value[a]	Significance[b]
IVCWRD	27,20	23,38	30,90	28,97	27,03	31,50	1,1E-01		24,95	23,75	26,76	32,27	28,96	33,81	4,9E-04	***
IVDMD	51,93	45,80	59,20	51,78	47,59	59,48	9,5E-01		48,89	45,93	51,80	58,01	45,82	63,06	4,4E-02	*
Stem area	1,42	1,27	1,52	1,05	0,85	1,30	1,8E-04	***	1,73	1,31	1,96	1,72	1,63	1,88	8,9E-01	
Lignified fraction	0,70	0,67	0,72	0,69	0,63	0,74	4,6E-01		0,70	0,65	0,75	0,68	0,63	0,71	3,2E-01	
Non-lignified fraction	0,10	0,07	0,14	0,09	0,06	0,14	4,8E-01		0,07	0,04	0,09	0,11	0,08	0,17	4,6E-02	*
Rind fraction	0,16	0,15	0,18	0,16	0,14	0,20	6,9E-01		0,17	0,14	0,23	0,15	0,13	0,18	8,3E-02	.
Bundle fraction	0,04	0,03	0,06	0,05	0,04	0,07	1,2E-03	**	0,06	0,05	0,08	0,06	0,05	0,07	9,9E-01	
Bundle number	115	102	128	113	89	135	8,0E-01		128	91	167	147	125	190	2,1E-01	
Bundle density	81,54	71,02	91,78	109,56	99,11	134,16	1,3E-04	***	74,06	64,45	86,99	85,65	76,81	102,14	7,1E-02	.
Red rind	8,85	5,58	13,18	10,31	8,30	12,80	1,8E-01		9,85	7,35	13,34	7,54	5,32	10,76	1,0E-01	
Red parenchyma	140,85	134,45	153,22	135,00	116,55	155,02	3,1E-01		135,73	125,68	153,41	130,10	120,48	141,94	2,8E-01	
Blue parenchyma	14,98	8,84	24,80	16,54	11,62	22,63	4,9E-01		11,63	8,00	18,12	18,62	10,95	37,75	2,3E-01	
CWR	57,14	49,29	63,01	58,72	50,15	63,92	5,2E-01		58,55	54,17	61,92	52,88	46,05	68,74	2,5E-01	
KL.CWR	17,29	16,73	18,41	16,70	15,76	17,18	5,2E-02	.	17,32	16,95	17,73	16,27	15,92	16,73	2,2E-04	***
PCAest	22,96	22,22	23,86	20,04	19,27	21,06	1,8E-07	***	21,73	20,98	22,31	19,27	18,05	22,40	3,6E-02	*
FAest	4,17	3,86	4,64	4,30	3,94	4,47	3,3E-01		4,22	3,92	4,44	3,59	3,03	3,87	9,7E-03	**
FAeth	4,22	3,66	4,70	4,40	3,69	4,90	3,9E-01		4,71	4,45	5,03	3,90	3,43	5,34	8,9E-02	.
BO4 yield	802,66	765,85	821,47	831,66	784,36	900,14	9,0E-02	.	831,91	778,60	867,01	728,94	696,70	820,51	8,2E-03	**
BO4 H	28,94	23,93	32,78	28,35	25,02	33,59	7,1E-01		32,07	28,36	36,58	25,77	21,88	29,60	4,5E-03	**
S/G	1,12	1,09	1,18	0,97	0,89	1,09	1,1E-04	***	1,12	1,08	1,17	1,16	1,01	1,23	4,1E-01	
Cellulose	38,08	35,80	40,73	36,73	35,11	38,31	8,9E-02	.	38,76	36,98	40,89	36,57	36,08	37,29	6,6E-04	***
Hemi-celluloses	29,60	27,70	31,83	29,53	28,56	31,65	8,9E-01		28,59	27,79	29,64	29,79	27,40	31,67	1,7E-01	
Yield	3,63	3,33	3,90	1,47	1,15	2,15	1,7E-09	***	3,95	3,26	4,43	2,41	1,81	3,44	3,1E-03	**
Plant height	141,87	131,84	147,59	95,50	86,09	109,24	1,3E-08	***	178,12	170,10	189,19	161,58	152,63	170,55	3,3E-03	**

Supplemental table S2. Pearson correlation table between histological and biochemical cell wall traits within the RILs population in 2014 and 2015 under irrigated condition (blue) and non-irrigated condition (pink). Significance : . , p ≤ 0.1; *, p ≤ 0.05; **, p ≤ 0.01; ***, p ≤ 0.001.

Year 2014	Irrigated condition / Non irrigated condition									
	IVCWRD	Stem area	Lignified fraction	Non-lignified fraction	Rind fraction	Bundle fraction	Bundle number	Bundle density	Red rind	Red parenchyma	Blue parenchyma
IVCWRD		0,08	-0,09	0,04	0,05	0,12	0,00	-0,14 .	-0,07	-0,10	0,02
Stem area	0,09		-0,03	0,25 **	-0,43 ***	0,00	0,77 ***	-0,30 ***	-0,31 ***	0,06	0,26 **
Lignified fraction	-0,14 ,	0,09		-0,82 ***	-0,29 ***	-0,22 **	-0,02	0,03	-0,23 **	0,89 ***	-0,75 ***
Non-lignified fraction	0,02	0,04	-0,91 ***		-0,29 ***	-0,18 *	0,34 ***	0,13 .	-0,10	-0,57 ***	0,99 ***
Rind fraction	0,23 **	-0,40 ***	-0,16 *	-0,26 **		0,49 ***	-0,62 ***	-0,31 ***	0,54 ***	-0,51 ***	-0,38 ***
Bundle fraction	0,24 **	0,10	-0,06	-0,21 *	0,39 ***		0,00	-0,03	0,35 ***	-0,38 ***	-0,24 **
Bundle number	-0,04	0,76 ***	0,01	0,19 *	-0,61 ***	0,14 ,		0,36 ***	-0,30 ***	0,09	0,37 ***
Bundle density	-0,21 *	-0,47 ***	-0,12	0,21 **	-0,25 **	0,01	0,20 *		-0,02	0,07	0,16 *
Red rind	-0,06	-0,42 ***	-0,02	-0,23 **	0,60 ***	0,31 ***	-0,40 ***	0,09		-0,26 **	-0,12
Red parenchyma	-0,21 **	0,19 *	0,91 ***	-0,76 ***	-0,27 ***	-0,20 **	0,06	-0,20 *	-0,09		-0,48 ***
Blue _parenchyma	-0,01	0,06	-0,87 ***	0,99 ***	-0,33 ***	-0,27 **	0,22 **	0,22 **	-0,26 ***	-0,70 ***	
CWR	-0,64 ***	-0,17 *	0,09	0,04	-0,25 **	-0,30 ***	0,01	0,28 ***	-0,08	0,07	0,08
KL.CWR	-0,84 ***	0,00	0,15 ,	-0,08	-0,13	-0,17 *	0,09	0,12	0,10	0,26 **	-0,06
PCAest	-0,48 ***	0,25 **	0,13	-0,02	-0,26 ***	-0,04	0,26 **	-0,02	-0,03	0,19 *	0,00
FAest	0,28 ***	0,01	-0,02	-0,10	0,22 **	0,30 ***	0,02	0,02	0,13	-0,11	-0,12
FAeth	-0,61 ***	-0,15 .	0,06	0,09	-0,29 ***	-0,34 ***	0,02	0,27 ***	-0,11	0,06	0,13
IVDMD	0,80 ***	0,16 .	-0,09	-0,05	0,28 ***	0,31 ***	-0,02	-0,28 ***	0,05	-0,11	-0,09
BO4 yield	-0,42 ***	0,05	0,15 .	-0,09	-0,13	-0,10	-0,03	-0,09	0,03	0,18 *	-0,07
BO4 H	-0,54 ***	-0,14 .	0,01	0,08	-0,20 *	-0,15 .	-0,04	0,19 *	0,02	0,02	0,11
S/G	0,55 ***	0,01	-0,14 .	0,04	0,19 *	0,22 **	0,01	-0,02	0,05	-0,21 **	0,01
Cellulose	-0,70 ***	0,04	0,14 .	0,03	-0,35 ***	-0,29 ***	0,17 *	0,18 *	-0,10	0,15 .	0,07
Hemicelluloses	0,24 **	-0,28 ***	-0,06	-0,02	0,19 *	0,09	-0,19 *	0,16 *	0,03	-0,20 *	-0,04

Year 2014	Irrigated condition / Non irrigated condition									
	CWR	KL.CWR	PCAest	FAest	FAeth	IVDMD	BO4 yield	BO4 H	S/G	Cellulose	Hemicelluloses
IVCWRD	-0,63 ***	-0,85 ***	-0,52 ***	0,16 .	-0,63 ***	0,80 ***	-0,34 ***	-0,24 **	0,54 ***	-0,63 ***	0,29 ***
Stem area	-0,27 ***	0,02	0,24 **	-0,12	-0,17 *	0,21 **	0,02	-0,20 *	-0,01	-0,11	-0,31 ***
Lignified fraction	0,11	0,10	-0,14 .	-0,17 *	0,08	-0,08	-0,04	0,12	-0,13	0,18 *	0,02
Non-lignified fraction	-0,02	-0,09	0,18 *	-0,07	0,04	0,00	0,10	0,08	0,02	-0,04	-0,18 *
Rind fraction	-0,10	0,01	-0,10	0,36 ***	-0,17 *	0,10	-0,10	-0,29 ***	0,18 *	-0,20 *	0,27 ***
Bundle fraction	-0,20 *	-0,07	0,10	0,37 ***	-0,23 **	0,21 *	-0,03	-0,34 ***	0,15 ,	-0,24 **	0,12
Bundle number	-0,10	0,03	0,24 **	-0,11	-0,02	0,07	0,06	-0,06	-0,08	-0,02	-0,30 ***
Bundle density	0,27 ***	0,03	-0,01	-0,02	0,26 **	-0,24 **	0,05	0,23 **	-0,12	0,17 *	0,01
Red rind	0,00	0,13	-0,02	0,15 .	-0,06	-0,03	-0,14 .	-0,13	0,10	0,08	0,19 *
Red parenchyma	0,11	0,10	-0,06	-0,29 ***	0,12	-0,10	-0,02	0,21 *	-0,17 *	0,21 **	-0,09
Blue _parenchyma	0,02	-0,09	0,18 *	-0,11	0,09	-0,04	0,11	0,12	0,00	0,00	-0,21 *
CWR		0,28 ***	0,03	-0,11	0,95 ***	-0,96 ***	0,18 *	0,42 ***	-0,31 ***	0,62 ***	0,13
KL.CWR	0,32 ***		0,53 ***	-0,23 **	0,29 ***	-0,47 ***	0,05	-0,05	-0,41 ***	0,52 ***	-0,37 ***
PCAest	0,02	0,44 ***		0,13	0,04	-0,17 *	0,43 ***	-0,18 *	-0,34 ***	0,09	-0,47 ***
FAest	-0,24 **	-0,35 ***	0,17 *		-0,29 ***	0,15 .	0,17 *	-0,38 ***	0,11	-0,26 **	0,45 ***
FAeth	0,97 ***	0,29 ***	-0,02	-0,34 ***		-0,93 ***	0,16 *	0,37 ***	-0,32 ***	0,57 ***	-0,05
IVDMD	-0,96 ***	-0,48 ***	-0,16 *	0,31 ***	-0,95 ***		-0,27 ***	-0,41 ***	0,44 ***	-0,67 ***	0,02
BO4 yield	0,10	0,19 *	0,53 ***	0,15 ,	0,08	-0,22 **		0,31 ***	-0,71 ***	0,02	-0,35 ***
BO4 H	0,43 ***	0,21 *	0,22 **	-0,29 ***	0,41 ***	-0,53 ***	0,43 ***		-0,30 ***	0,38 ***	0,12
S/G	-0,29 ***	-0,50 ***	-0,16 *	0,39 ***	-0,31 ***	0,41 ***	-0,59 ***	-0,33 ***		-0,34 ***	0,35 ***
Cellulose	0,75 ***	0,53 ***	0,28 ***	-0,40 ***	0,73 ***	-0,80 ***	0,07	0,45 ***	-0,28 ***		0,11
Hemicelluloses	0,27 ***	-0,43 ***	-0,45 ***	0,25 **	0,24 **	-0,12	-0,34 ***	0,04	0,37 ***	-0,01	

Year 2015	Irrigated condition / Non irrigated condition																					
	IVCWRD		Stem area		Lignified fraction		Non-lignified fraction		Rind fraction		Bundle fraction		Bundle number		Bundle density		Red rind		Red parenchyma		Blue parenchyma	
IVCWRD			0,07		-0,15	,	0,13		0,05		-0,02		-0,02		-0,09		-0,20	*	-0,22	**	0,10	
Stem area	0,02				0,01		0,08		-0,26	***	0,10		0,64	***	-0,39	***	-0,25	**	0,03		0,07	
Lignified fraction	-0,25	**	-0,13	,			-0,89	***	-0,25	**	-0,05		0,05		0,06		-0,05		0,88	***	-0,85	***
Non-lignified fraction	0,14		0,31	***	-0,83	***			-0,20	**	-0,26	***	0,14		0,06		-0,19	**	-0,70	***	0,99	***
Rind fraction	0,23	**	-0,40	***	-0,34	***	-0,21	*			0,41	***	-0,54	***	-0,30	***	0,49	***	-0,35	***	-0,27	***
Bundle fraction	0,08		0,22	**	-0,27	***	-0,03		0,29	***			0,09		-0,02		0,28	***	-0,23	*	-0,30	***
Bundle number	-0,06		0,71	***	-0,02		0,36	***	-0,70	***	0,18	*			0,42	***	-0,09		0,10		0,17	.
Bundle density	-0,10		-0,21	*	0,13		0,13		-0,51	***	-0,03		0,52	***			0,20	*	0,09		0,11	
Red rind	0,00		-0,17	*	-0,13		-0,13		0,38	***	0,42	***	-0,13		0,07				0,00		-0,18	**
Red parenchyma	-0,32	***	0,03		0,90	***	-0,63	***	-0,49	***	-0,33	***	0,14		0,17	.	-0,13				-0,64	***
Blue _parenchyma	0,07		0,32	***	-0,72	***	0,97	***	-0,36	***	-0,11		0,45	***	0,24	**	-0,11		-0,49	***		
CWR	-0,71	***	-0,22	**	0,36	***	-0,17	.	-0,29	***	-0,34	***	-0,04		0,19	*	-0,08		0,38	***	-0,06	
KL.CWR	-0,77	***	0,06		0,08		-0,04		-0,10		0,09		0,09		0,06		0,05		0,16	.	-0,02	
PCAest	-0,44	***	0,40	***	0,00		0,10		-0,24	**	0,16	.	0,38	***	0,03		0,07		0,15	.	0,14	
FAest	0,47	***	0,02		-0,15	.	-0,04		0,29	***	0,26	**	-0,08		-0,13		0,11		-0,26	**	-0,08	
FAeth	-0,71	***	-0,13		0,34	***	-0,12		-0,34	***	-0,32	***	0,03		0,19	*	-0,11		0,38	***	-0,02	
IVDMD	0,84	***	0,19	*	-0,34	***	0,16	.	0,28	**	0,30	***	0,04		-0,16	.	0,07		-0,37	***	0,07	
BO4 yield	-0,45	***	0,09		0,04		-0,02		-0,05		0,03		0,06		-0,04		-0,07		0,09		-0,01	
BO4 H	-0,37	***	-0,16	.	0,05		0,05		-0,15	.	-0,13		0,00		0,17	*	0,05		0,14	.	0,09	
S/G	0,57	***	0,07		-0,01		-0,02		0,04		0,07		0,07		0,02		0,12		-0,06		0,01	
Cellulose	-0,55	***	-0,03		0,19	*	-0,04		-0,25	**	-0,13		0,09		0,16	.	0,00		0,19	*	0,04	
Hemicelluloses	0,46	***	-0,26	**	-0,06		-0,03		0,18	*	0,00		-0,22	*	0,00		0,08		-0,20	*	-0,05	

2015	Irrigated condition / Non irrigated condition																					
	CWR		KL.CWR		PCAest		FAest		FAeth		IVDMD		BO4 yield		BO4 H		S/G		Cellulose		Hemicelluloses	
IVCWRD	-0,38	***	-0,85	***	-0,44	***	0,18	*	-0,23	**	0,60	***	-0,26	***	-0,32	***	0,41	***	-0,54	***	0,40	***
Stem area	-0,07		-0,03		0,16	*	-0,13	.	0,00		0,07		-0,04		-0,08		0,07		-0,05		-0,16	*
Lignified fraction	0,11		0,19	*	-0,01		-0,14	.	0,08		-0,13		-0,10		0,07		0,00		0,16	*	-0,04	
Non-lignified fraction	-0,01		-0,19	*	0,02		0,04		0,03		0,03		0,13	.	0,03		-0,02		-0,11		-0,01	
Rind fraction	-0,21	**	-0,02		-0,06		0,20	*	-0,23	**	0,20	*	-0,05		-0,20	*	0,03		-0,10		0,11	
Bundle fraction	-0,15	.	0,07		0,10		0,14	.	-0,16	*	0,11		-0,06		-0,14	.	0,05		-0,10		0,05	
Bundle number	0,10		0,03		0,22	**	-0,14	.	0,15	.	-0,09		-0,01		0,08		0,05		-0,02		-0,14	,
Bundle density	0,21	**	0,08		0,04		-0,04		0,19	*	-0,20	*	0,00		0,18	*	-0,02		0,03		0,04	
Red rind	-0,09		0,21	**	0,13	.	-0,01		-0,12		0,01		-0,01		0,07		-0,04		0,04		-0,06	
Red parenchyma	0,09		0,26	***	0,06		-0,22	**	0,06		-0,13		-0,11		0,11		0,02		0,20	*	-0,14	,
Blue _parenchyma	0,03		-0,17	*	0,03		0,00		0,07		-0,01		0,16	*	0,09		-0,05		-0,09		-0,04	
CWR			0,09		-0,23	**	-0,22	**	0,88	***	-0,95	***	0,25	**	0,66	***	-0,37	***	0,41	***	-0,01	
KL.CWR	0,26	**			0,48	***	-0,30	***	-0,01		-0,29	***	0,00		0,09		-0,33	***	0,47	***	-0,33	***
PCAest	0,12		0,49	***			0,12		-0,27	***	0,08		0,18	*	-0,18	*	-0,10		-0,06		-0,46	***
FAest	-0,44	***	-0,41	***	-0,13				-0,33	***	0,27	***	0,20	*	-0,51	***	0,18	*	-0,41	***	0,24	**
FAeth	0,96	***	0,29	***	0,14	.	-0,56	***			-0,85	***	0,39	***	0,64	***	-0,52	***	0,23	**	-0,07	
IVDMD	-0,97	***	-0,42	***	-0,20	*	0,52	***	-0,95	***			-0,38	***	-0,72	***	0,51	***	-0,46	***	0,15	*
BO4 yield	0,28	***	0,22	**	0,34	***	-0,15	.	0,36	***	-0,38	***			0,34	***	-0,78	***	-0,24	**	-0,44	***
BO4 H	0,41	***	0,10		-0,02		-0,59	***	0,44	***	-0,47	***	0,36	***			-0,49	***	0,31	***	-0,07	
S/G	-0,30	***	-0,55	***	-0,13		0,57	***	-0,40	***	0,45	***	-0,62	***	-0,35	***			0,04		0,36	***
Cellulose	0,52	***	0,43	***	0,10		-0,29	***	0,51	***	-0,53	***	0,10		0,26	**	-0,09				0,04	
Hemicelluloses	-0,18	*	-0,48	***	-0,47	***	0,58	***	-0,30	***	0,30	***	-0,49	***	-0,19	*	0,60	***	0,04			

Supplemental table S3. List of QTLs detected for the histological traits.

QTL	Year.Condition	Trait	Chromosome	Position (cM)	Position (Bin)	Interval (cM)	LOD	Pvalue	R^2	Effect
1@256.6	2014.I	Blue parenchyma	1	256.600118	1.09	251.5-269.4	4,5	0,0102	4,883	7,013
2@44.6	2014.I	Blue parenchyma	2	44.600015	2.03	36.6-67.2	3,3	0,3489	0,634	2,490
10@85.8	2014.I	Bundle density	10	85.80003	10.04	61.1-100.4	5,8	0,0079	5,258	-6,289
3@254.2	2014.I	Bundle density	3	254.200122	3.09	202.5-256	3,2	0,8596	0,023	0,049
5@135.1	2014.I	Bundle density	5	135.100059	5.05	131.9-138.6	3,6	0,6904	0,115	-0,860
4@205.3	2014.I	Bundle fraction	4	205.300095	4.09	195-218.6	3,3	0,0527	2,792	0,004
1@280.7	2014.I	Bundle number	1	280.70013	1.09	253.5-282.6	5,6	0,0091	4,649	15,106
2@44.6	2014.I	Bundle number	2	44.600015	2.02	39.1-60	3,3	0,0035	5,867	16,851
6@15.1	2014.I	Bundle number	6	15.100008	6.01	9.7-19.6	4,7	0,1037	1,782	9,364
1@254.7	2014.I	Non-lignified fraction	1	254.700117	1.08	251.5-275.8	3,8	0,0221	3,848	0,029
2@67.2	2014.I	Non-lignified fraction	2	67.200027	2.03	36.6-73.6	3,9	0,1770	1,321	0,017
3@169.4	2014.I	Red parenchyma	3	169.400083	3.06	163.4-171.8	3,0	0,4182	0,477	2,422
5@57.2	2014.I	Red parenchyma	5	57.200019	5.03	34.7-73.6	3,3	0,0935	2,066	-5,160
6@7.2	2014.I	Red parenchyma	6	7.200003	6.01	0-11.1	4,4	0,0763	2,310	-5,352
1@239.7	2014.I	Red rind	1	239.700109	1.08	228-264	3,3	0,3710	0,591	0,240
1@290.0	2014.I	Red rind	1	290.000133	1.1	282.6-313.1	4,2	0,0633	2,573	-0,503
10@15.4	2014.I	Red rind	10	15.400002	10.01	0-19	3,4	0,6141	0,187	-0,122
7@83.2	2014.I	Red rind	7	83.200025	7.02	73.4-96.6	3,2	0,0827	2,242	-0,479
1@294.3	2014.I	Rind fraction	1	294.300135	1.1	231.2-300.2	6,7	0,0074	5,152	-0,017
2@56.5	2014.I	Rind fraction	2	56.500023	2.03	50-59.5	4,5	0,0452	2,845	-0,013
1@198.8	2014.I	Stem area	1	198.800092	1.06	169.4-239.7	8,9	0,0003	9,104	0,265
1@282.6	2014.I	Stem area	1	282.600131	1.09	269.4-298.7	5,4	0,4684	0,354	0,051
2@130.0	2014.I	Stem area	2	130.000058	2.05	123.8-131.8	4,4	0,7786	0,053	-0,016
2@197.1	2014.I	Stem area	2	197.100096	2.07	184.9-203.5	3,4	0,0322	3,141	0,149
5@135.1	2014.I	Stem area	5	135.100059	5.05	127.1-146.9	9,8	0,3613	0,562	-0,063
6@11.1	2014.I	Stem area	6	11.100005	6.01	7.2-14.2	15,0	0,3048	0,710	0,069
8@157.3	2014.I	Stem area	8	157.30006	8.06	151.1-163.6	3,1	0,2492	0,897	-0,079
9@130.0	2014.I	Stem area	9	130.000048	9.06	66-138.7	4,8	0,2010	1,106	-0,088
10@47.2	2014.NI	Bundle density	10	47.200011	10.03	43.6-100.4	7,4	0,0649	2,342	-4,227
2@144.7	2014.NI	Bundle density	2	144.700068	2.05	110.9-162.8	3,6	0,3600	0,570	2,046
3@33.2	2014.NI	Bundle density	3	33.200016	3.02	25.7-41.3	3,6	0,6636	0,128	0,954
6@15.1	2014.NI	Bundle density	6	15.100008	6.01	11.1-34.4	3,1	0,0378	2,975	4,691
7@184.9	2014.NI	Bundle density	7	184.900072	7.05	116.5-187.3	3,5	0,0013	7,314	-7,590
10@84.1	2014.NI	Bundle fraction	10	84.100029	10.04	15.4-90.6	4,3	0,0010	7,843	-0,007
1@290.0	2014.NI	Bundle number	1	290.000133	1.1	231.2-294.3	3,2	0,0075	5,113	16,100
6@19.6	2014.NI	Bundle number	6	19.600011	6.01	7.2-12.6	3,5	0,0453	2,837	11,690
6@203.6	2014.NI	Non-lignified fraction	6	203.600083	6.07	189.2-203.6	3,1	0,0969	2,058	0,021
1@190.0	2014.NI	Red parenchyma	1	190.000086	1.06	185-197.2	3,2	0,5078	0,329	-2,035
10@59.4	2014.NI	Red parenchyma	10	59.400016	10.03	53.5-68.2	3,4	0,3845	0,568	2,713
4@85.5	2014.NI	Red parenchyma	4	85.500035	4.05	78.2-93	5,0	0,6285	0,175	1,486
5@131.9	2014.NI	Red parenchyma	5	131.900056	5.05	125.9-136.8	4,8	0,6009	0,205	-1,464
6@196.3	2014.NI	Red parenchyma	6	196.300081	6.07	190.4-203.6	3,7	0,0678	2,530	-5,859
1@198.8	2014.NI	Red rind	1	198.800092	1.06	185-204.4	3,4	0,4234	0,481	-0,203
2@271.1	2014.NI	Red rind	2	271.100121	2.09	261.6-271.1	4,4	0,4061	0,518	-0,213
7@158.9	2014.NI	Red rind	7	158.900063	7.04	153-172.2	3,7	0,1715	1,410	0,352



QTL	Year.Condition	Trait	Chromosome	Position (cM)	Position (Bin)	Interval (cM)	LOD	Pvalue	R^2	Effect
1@290.0	2014.NI	Stem area	1	290.000133	1.1	231.2-294.3	6,9	0,0629	2,488	0,131
5@189.4	2014.NI	Stem area	5	189.40008	5.06	127.1-194.2	5,0	0,0499	2,770	-0,139
6@21.5	2014.NI	Stem area	6	21.500012	6.01	7.2-25.8	12,9	0,1684	1,357	0,095
10@70.4	2015.I	Bundle density	10	70.400021	10.03	56.3-98.9	6,2	0,0449	2,846	-4,616
2@194.8	2015.I	Bundle density	2	194.800094	2.07	187.4-198.8	3,0	0,0416	2,938	-4,748
3@248.6	2015.I	Bundle density	3	248.600121	3.09	216.3-256	7,6	0,4147	0,465	-1,764
3@39.1	2015.I	Bundle density	3	39.100018	3.02	26.9-79.5	5,2	0,5675	0,228	-1,296
9@102.4	2015.I	Bundle density	9	102.400037	9.04	98.3-106.3	3,0	0,0194	3,886	5,476
10@93.9	2015.I	Bundle fraction	10	93.900035	10.05	15.4-114.5	4,0	0,0002	10,105	-0,008
3@95.3	2015.I	Bundle fraction	3	95.300045	3.04	88.4-101.7	5,6	0,5289	0,269	-0,001
1@279.5	2015.I	Bundle number	1	279.500129	1.09	231.2-294.3	5,9	0,0037	6,131	17,215
9@75.7	2015.I	Bundle number	9	75.700024	9.03	63.2-80.3	4,4	0,1709	1,330	-8,164
2@158.2	2015.I	Lignified fraction	2	158.200075	2.06	147-174.8	3,3	0,6800	0,122	0,005
8@189.6	2015.I	Lignified fraction	8	189.600072	8.08	185.8-194.4	4,4	0,0046	5,935	-0,038
1@30.8	2015.I	Red parenchyma	1	30.800014	1.01	21.4-38.3	3,5	0,8033	0,045	0,465
5@57.2	2015.I	Red parenchyma	5	57.200019	5.03	50.6-65.8	3,1	0,0643	2,530	-5,718
7@131.4	2015.I	Red parenchyma	7	131.400046	7.03	125.6-142.9	3,6	0,8093	0,042	-0,101
9@16.5	2015.I	Red parenchyma	9	16.500001	9.01	0-22.6	3,2	0,0440	3,007	6,293
8@65.1	2015.I	Red rind	8	65.10002	8.03	51.6-72.4	3,5	0,5823	0,228	-0,136
1@259.9	2015.I	Rind fraction	1	259.90012	1.08	231.2-300.2	3,0	0,0037	6,152	-0,018
1@239.7	2015.I	Stem area	1	239.700109	1.08	231.2-250.6	3,2	0,0852	1,980	0,138
1@264.0	2015.I	Stem area	1	264.000123	1.09	261.2-275.8	3,3	0,0406	2,815	0,195
1@280.7	2015.I	Stem area	1	280.70013	1.09	276.6-308.8	3,6	0,8480	0,024	0,015
3@248.6	2015.I	Stem area	3	248.600121	3.09	242-254.2	4,4	0,0776	2,083	0,121
1@204.4	2015.NI	Blue parenchyma	1	204.400093	1.06	195.8-214.8	4,1	0,0002	8,409	9,284
6@170.2	2015.NI	Blue parenchyma	6	170.20007	6.07	163.5-205	5,1	0,0000	10,435	10,295
1@45.1	2015.NI	Bundle density	1	45.100021	1.02	31.7-54.2	3,7	0,0002	10,225	-8,657
10@98.9	2015.NI	Bundle fraction	10	98.900037	10.05	87.9-127.1	3,4	0,0001	10,333	-0,008
1@129.7	2015.NI	Bundle number	1	129.700054	1.04	125.6-133.8	6,0	0,0077	3,849	13,959
1@290.0	2015.NI	Bundle number	1	290.000133	1.1	253.5-294.3	7,3	0,0007	6,318	17,976
1@48.6	2015.NI	Bundle number	1	48.600023	1.02	19.3-64.6	6,7	0,0000	11,457	-23,993
10@84.1	2015.NI	Bundle number	10	84.100029	10.04	82.6-108.7	3,4	0,0005	6,795	-18,271
6@167.7	2015.NI	Bundle number	6	167.700069	6.07	158.7-171.7	4,1	0,0187	2,977	12,158
4@131.0	2015.NI	Lignified fraction	4	131.000059	4.07	125.6-135.6	3,7	0,0011	7,030	-0,043
8@201.1	2015.NI	Lignified fraction	8	201.100076	8.08	194.4-208.2	4,4	0,0009	7,371	-0,043
1@139.2	2015.NI	Non-lignified fraction	1	139.20006	1.04	131.9-142	3,2	0,0141	3,576	0,029
1@220.6	2015.NI	Non-lignified fraction	1	220.600101	1.07	214.8-225.8	3,4	0,0019	5,783	0,037
1@303.9	2015.NI	Non-lignified fraction	1	303.900142	1.1	270-324	3,6	0,0160	3,442	0,027
8@189.6	2015.NI	Non-lignified fraction	8	189.600072	8.08	188.3-194.4	3,6	0,0000	10,220	0,046
8@201.1	2015.NI	Red parenchyma	8	201.100076	8.08	194.4-213.8	3,1	0,0004	9,016	-10,656
1@220.6	2015.NI	Stem area	1	220.600101	1.07	211.2-239.7	4,2	0,0001	8,920	0,246
2@194.8	2015.NI	Stem area	2	194.800094	2.07	182.8-210.7	3,4	0,0081	4,085	0,169
2@33.5	2015.NI	Stem area	2	33.50001	2.02	14.9-60	4,2	0,0003	7,844	0,231
7@195.1	2015.NI	Stem area	7	195.100075	7.05	187.3-200.5	3,2	0,0076	4,159	0,167
8@24.9	2015.NI	Stem area	8	24.900004	8.01	14.3-30.7	3,3	0,0008	6,614	0,217

Supplemental table S4. List of QTLs detected for thebiochemical cell wall traits

QTL	Year.Condition	Trait	Chromosome	Position (cM)	Position (bin)	Interval (cM)	LOD	Pvalue	R^2	Effect
1@170.6	2014.I	BO4 H	1	170.600077	1.05	149.8-172.4	4,34	0,048	2,902	1,544
2@130.0	2014.I	BO4 yield	2	130.000058	2.05	126.2-135.2	3,25	0,621	0,182	-2,900
3@138.0	2014.I	BO4 yield	3	138.000067	3.06	124-145.1	3,24	0,070	2,466	-11,251
6@115.8	2014.I	BO4 yield	6	115.80005	6.05	110.9-131.2	4,64	0,672	0,133	2,244
6@135.5	2014.I	BO4 yield	6	135.500059	6.05	114-158.7	4,28	0,344	0,666	-7,405
5@135.1	2014.I	CWR	5	135.100059	5.05	127.1-140.2	3,94	0,515	0,320	1,015
5@135.1	2014.I	FAeth	5	135.100059	5.05	127.1-138.6	3,78	0,478	0,379	0,083
1@224.7	2014.I	Hemicelluloses	1	224.700103	1.07	170.6-239.7	4,53	0,107	1,583	-0,464
2@219.8	2014.I	Hemicelluloses	2	219.800105	2.08	213.2-229.6	3,24	0,132	1,378	0,449
5@109.5	2014.I	Hemicelluloses	5	109.500045	5.04	86.7-112.7	5,17	0,117	1,497	0,449
6@118.6	2014.I	Hemicelluloses	6	118.600051	6.05	113.6-122.8	4,61	0,131	1,388	0,645
6@131.2	2014.I	Hemicelluloses	6	131.200057	6.05	125.5-137.8	5,64	0,020	3,321	1,105
2@189.7	2014.I	KL.CWR	2	189.70009	2.07	184.9-201.3	4,31	0,118	1,724	-0,297
3@124.0	2014.I	KL.CWR	3	124.000062	3.05	110.5-128.8	3,63	0,002	7,048	-0,595
1@225.8	2014.I	PCAest	1	225.800104	1.07	220.6-230	10,26	0,001	7,102	1,157
2@44.6	2014.I	PCAest	2	44.600015	2.02	36.6-50	4,13	0,001	7,419	1,158
3@231.6	2014.I	PCAest	3	231.600114	3.09	228.7-239.7	3,34	0,049	2,312	0,647
4@93.0	2014.I	PCAest	4	93.000042	4.05	81.9-107.2	5,12	0,111	1,500	0,523
5@109.5	2014.I	PCAest	5	109.500045	5.04	50.6-114.7	3,83	0,012	3,804	-0,828
7@89.3	2014.I	PCAest	7	89.300027	7.02	40.8-109.9	3,10	0,014	3,618	-0,858
1@169.4	2014.I	Plant height	1	169.400076	1.05	156.3-172.9	3,47	0,046	2,805	-5,271
1@218.4	2014.I	Plant height	1	218.4001	1.07	206.1-210.8	4,65	0,015	4,222	6,522
4@184.8	2014.I	Plant height	4	184.800087	4.09	169.2-189.2	8,49	0,023	3,646	5,630
5@131.9	2014.I	Plant height	5	131.900056	5.05	119.5-138.6	7,94	0,112	1,758	-4,005
8@108.2	2014.I	Plant height	8	108.200037	8.05	103.1-169.6	4,74	0,685	0,114	-0,952
8@40.3	2014.I	Plant height	8	40.300009	8.02	38.4-45.9	3,01	0,110	1,782	4,040
9@125.1	2014.I	Plant height	9	125.100046	9.05	120.3-130	8,35	0,052	2,650	-4,832
1@230.0	2014.I	S/G	1	230.000106	1.07	218.4-239.7	4,70	0,778	0,056	0,005
2@130.0	2014.I	S/G	2	130.000058	2.05	128.2-136.2	3,99	0,020	3,859	0,043
5@145.3	2014.I	S/G	5	145.300064	5.05	112.7-202.8	3,39	0,205	1,134	-0,023
6@125.4	2014.I	S/G	6	125.400055	6.05	120.9-137.8	3,90	0,014	4,310	0,046
6@15.1	2014.I	Yield	6	15.100008	6.01	9.7-19.6	4,68	0,729	0,099	0,048
1@175.0	2014.NI	BO4 H	1	175.000079	1.05	165.6-177	3,71	0,065	2,432	1,409
5@46.5	2014.NI	BO4 H	5	46.500016	5.03	27.7-50.6	3,63	0,012	4,565	-1,881
6@29.7	2014.NI	BO4 H	6	29.700016	6.02	21.5-34.4	3,55	0,268	0,868	-0,821
8@146.0	2014.NI	BO4 H	8	146.000054	8.06	108.2-149.2	3,54	0,309	0,729	0,847
8@180.9	2014.NI	BO4 H	8	180.900067	8.08	138-188.3	3,70	0,075	2,254	-1,475
1@245.9	2014.NI	BO4 yield	1	245.900112	1.08	241.1-245.9	5,78	0,737	0,084	-1,878
10@56.3	2014.NI	BO4 yield	10	56.300014	10.03	49.1-61.1	5,17	0,053	2,835	11,673
7@11.4	2014.NI	BO4 yield	7	11.400003	7.01	4.9-83.2	4,24	0,823	0,037	-1,013
8@70.7	2014.NI	BO4 yield	8	70.700022	8.03	65.1-85.1	3,91	0,658	0,146	2,495
3@15.5	2014.NI	FAest	3	15.500007	3.01	12-26.9	3,11	0,554	0,243	-0,044
4@80.6	2014.NI	FAest	4	80.600031	4.05	73.4-85.5	4,73	0,007	5,117	-0,231
6@131.2	2014.NI	FAest	6	131.200057	6.05	122.8-137.8	4,14	0,013	4,377	0,220
1@190.0	2014.NI	Hemicelluloses	1	190.000086	1.06	170.6-239.7	5,84	0,252	0,764	-0,329
10@161.3	2014.NI	Hemicelluloses	10	161.300061	10.06	138.9-163	4,02	0,003	5,383	0,866
2@23.4	2014.NI	Hemicelluloses	2	23.400007	2.02	7.7-136.2	4,05	0,025	2,973	-0,638
5@100.5	2014.NI	Hemicelluloses	5	100.500038	5.04	86.7-102.5	4,67	0,033	2,667	0,608
6@149.7	2014.NI	Hemicelluloses	6	149.700064	6.06	125.4-155.8	3,38	0,000	14,741	1,443
7@52.8	2014.NI	Hemicelluloses	7	52.80001	7.02	40.8-59.5	4,04	0,438	0,350	-0,206
1@165.6	2014.NI	IVCWRD	1	165.600075	1.05	147.4-185.7	3,79	0,230	1,082	-0,845
1@190.0	2014.NI	KL.CWR	1	190.000086	1.06	189.8-230	3,32	0,286	0,753	0,195
4@89.4	2014.NI	KL.CWR	4	89.400039	4.05	73.4-93	6,78	0,000	11,401	0,758
1@243.9	2014.NI	PCAest	1	243.900111	1.08	241.1-245.9	7,17	0,001	7,226	1,133
4@91.3	2014.NI	PCAest	4	91.30004	4.05	84.2-116.6	3,31	0,059	2,485	0,661
1@209.1	2014.NI	Plant height	1	209.100096	1.07	198.8-275.8	3,50	0,055	2,630	4,717
4@170.7	2014.NI	Plant height	4	170.700079	4.08	165-181.8	3,80	0,298	0,768	2,576
5@131.9	2014.NI	Plant height	5	131.900056	5.05	95.3-143.4	3,57	0,233	1,011	-3,012
3@45.5	2014.NI	S/G	3	45.50002	3.02	41.3-61	3,44	0,510	0,293	0,011
4@75.1	2014.NI	S/G	4	75.100027	4.04	68.5-81.9	6,15	0,000	9,590	-0,068
5@267.0	2014.NI	S/G	5	267.000113	5.08	253.1-268.2	4,20	0,564	0,225	0,010
6@85.8	2014.NI	S/G	6	85.800034	6.05	76.3-120.9	5,10	0,039	2,919	0,038
5@15.1	2015.I	BO4 H	3	8.300005	3.01	0-23.4	3,51	0,078	2,319	1,335
7@156.1	2015.I	BO4 yield	7	156.100061	7.04	149.3-167.5	3,23	0,536	0,288	-3,593
4@110.5	2015.I	CWR	4	110.50005	4.06	104.7-116.6	3,15	0,252	0,987	-1,785
6@131.2	2015.I	FAest	6	131.200057	6.05	127.9-137.8	4,28	0,013	4,570	0,224
4@110.5	2015.I	FAeth	4	110.50005	4.06	101.7-116.6	3,26	0,538	0,286	-0,071
5@109.5	2015.I	Hemicelluloses	5	109.500045	5.04	86.7-111.5	3,31	0,124	1,421	0,436
6@120.9	2015.I	Hemicelluloses	6	120.900052	6.05	82.3-143.5	5,14	0,000	19,839	1,675

QTL	Year.Condition	Trait	Chromosome	Position (cM)	Position (bin)	Interval (cM)	LOD	Pvalue	R^2	Effect
4@104.7	2015.I	KL.CWR	4	104.700047	4.06	92-110.5	4,13	0,000	12,393	0,783
10@75.1	2015.I	PCAest	10	75.100023	10.03	63.4-84.1	3,33	0,026	3,278	-0,780
2@44.6	2015.I	PCAest	2	44.600015	2.02	33.5-47.6	3,48	0,003	6,107	1,047
4@104.7	2015.I	PCAest	4	104.700047	4.06	85.5-116.6	3,72	0,036	2,907	0,730
1@164.2	2015.I	Plant height	1	164.200074	1.05	160.2-175	10,38	0,165	0,882	-2,970
2@139.8	2015.I	Plant height	2	139.800065	2.05	130-147	8,16	0,004	3,853	-6,062
2@223.2	2015.I	Plant height	2	223.200107	2.08	207.2-249	4,43	0,399	0,323	1,745
2@67.2	2015.I	Plant height	2	67.200027	2.03	51.7-85.2	4,12	0,009	3,228	5,572
3@141.5	2015.I	Plant height	3	141.500068	3.06	140-163.4	9,21	0,001	5,175	-7,505
3@39.1	2015.I	Plant height	3	39.100018	3.02	33.2-45.5	3,78	0,179	0,825	-2,816
4@104.7	2015.I	Plant height	4	104.700047	4.06	96.7-123.3	6,55	0,001	4,881	6,625
4@176.6	2015.I	Plant height	4	176.600082	4.09	140-178.4	4,13	0,326	0,439	2,065
5@145.3	2015.I	Plant height	5	145.300064	5.05	140.2-154.2	6,14	0,237	0,639	-2,692
5@231.4	2015.I	Plant height	5	231.400096	5.08	173.8-243.6	8,97	0,141	0,989	3,053
5@90.6	2015.I	Plant height	5	90.600033	5.04	89.9-100.5	7,01	0,032	2,122	-4,746
6@29.7	2015.I	Plant height	6	29.700016	6.02	23.9-40.4	5,40	0,712	0,062	0,501
7@158.9	2015.I	Plant height	7	158.900063	7.04	149.3-192.5	12,50	0,000	10,162	-10,554
8@108.2	2015.I	Plant height	8	108.200037	8.05	47.4-173.5	3,17	0,773	0,038	0,516
9@105.1	2015.I	Plant height	9	105.100038	9.04	104.1-157.7	4,28	0,711	0,062	-0,415
9@125.1	2015.I	Plant height	9	125.100046	9.05	120.3-132.1	3,26	0,080	1,412	-4,885
9@156.2	2015.I	Plant height	9	156.200058	9.06	147.1-167.8	3,20	0,372	0,363	2,080
1@139.2	2015.NI	BO4 H	1	139.20006	1.04	127.1-151	5,00	0,001	7,671	2,457
8@97.8	2015.NI	BO4 H	8	97.800032	8.04	51.6-189.6	3,38	0,009	4,547	1,910
2@203.5	2015.NI	BO4 yield	2	203.500098	2.07	194.2-213.2	4,28	0,007	5,000	-16,054
2@95.9	2015.NI	BO4 yield	2	95.90004	2.04	92.4-110.9	3,84	0,059	2,375	-10,738
8@121.0	2015.NI	BO4 yield	8	121.000044	8.05	116.4-124.8	6,20	0,002	6,763	18,304
4@170.7	2015.NI	CWR	4	170.700079	4.08	161.2-225.3	4,53	0,004	4,464	-3,844
6@25.2	2015.NI	CWR	6	25.200015	6.01	7.2-34.4	4,19	0,001	5,904	-4,364
8@137.5	2015.NI	CWR	8	137.500049	8.06	129.1-137.5	4,57	0,000	8,644	5,392
8@208.2	2015.NI	CWR	8	208.200078	8.08	199.6-216.5	3,30	0,003	4,757	-3,955
9@83.9	2015.NI	CWR	9	83.900029	9.03	77.8-87.9	3,12	0,001	5,802	-4,479
6@62.7	2015.NI	FAest	6	62.700026	6.04	52.7-69.7	4,78	0,000	9,162	0,317
8@208.2	2015.NI	FAest	8	208.200078	8.08	194.4-216.5	3,59	0,001	7,580	0,281
6@25.2	2015.NI	FAeth	6	25.200015	6.01	21.5-29.7	3,55	0,002	6,147	-0,332
8@114.8	2015.NI	FAeth	8	114.80004	8.05	108.2-118.4	3,96	0,001	7,008	0,364
9@85.9	2015.NI	FAeth	9	85.90003	9.03	77.8-93.6	3,10	0,002	6,145	-0,344
2@9.0	2015.NI	Hemicelluloses	2	9.000004	2.01	6.5-14.9	3,18	0,000	8,844	-1,093
4@110.5	2015.NI	Hemicelluloses	4	110.50005	4.06	106.3-113.4	3,25	0,004	4,083	-0,780
4@35.2	2015.NI	Hemicelluloses	4	35.200012	4.02	24.3-40	3,07	0,045	1,967	-0,536
6@120.9	2015.NI	Hemicelluloses	6	120.900052	6.05	112.3-155.8	5,70	0,000	15,121	1,477
1@190.0	2015.NI	IVCWRD	1	190.000086	1.06	162-197.2	3,30	0,045	2,102	-1,170
1@60.7	2015.NI	IVCWRD	1	60.700027	1.02	54.2-64.6	4,93	0,006	4,072	1,592
2@253.5	2015.NI	IVCWRD	2	253.500118	2.09	219.8-255.5	3,58	0,083	1,563	1,007
2@95.9	2015.NI	IVCWRD	2	95.90004	2.04	51.7-105.7	4,15	0,001	5,669	1,874
3@109.5	2015.NI	IVCWRD	3	109.500054	3.05	109.4-163.4	3,85	0,058	1,874	1,148
4@110.5	2015.NI	IVCWRD	4	110.50005	4.06	107.2-116.6	7,70	0,003	4,802	-1,800
4@173.9	2015.NI	IVCWRD	4	173.900081	4.08	170.3-207.5	4,87	0,004	4,445	1,750
5@138.6	2015.NI	IVCWRD	5	138.600061	5.05	106-140.2	4,59	0,006	4,006	-1,690
6@25.2	2015.NI	IVCWRD	6	25.200015	6.01	21.5-36.3	8,64	0,000	8,719	2,315
8@131.6	2015.NI	IVCWRD	8	131.600048	8.05	131.6-144.6	5,86	0,002	5,380	-1,898
2@201.3	2015.NI	IVDMD	2	201.300097	2.07	187.4-207.2	4,45	0,004	4,247	3,393
4@173.9	2015.NI	IVDMD	4	173.900081	4.08	169.2-181.8	3,02	0,025	2,483	2,517
6@25.2	2015.NI	IVDMD	6	25.200015	6.01	7.2-34.4	5,06	0,001	5,982	3,855
8@116.4	2015.NI	IVDMD	8	116.400041	8.05	108.2-121	5,26	0,000	10,201	-5,124
8@208.2	2015.NI	IVDMD	8	208.200078	8.08	147.5-209.1	4,76	0,001	5,463	3,712
9@83.9	2015.NI	IVDMD	9	83.900029	9.03	63.2-98.3	4,73	0,001	5,503	3,840
2@203.5	2015.NI	KL.CWR	2	203.500098	2.07	180.4-210.7	3,29	0,001	6,463	-0,569
3@141.5	2015.NI	KL.CWR	3	141.500068	3.06	132.1-145.1	4,14	0,000	7,858	-0,629
4@110.5	2015.NI	KL.CWR	4	110.50005	4.06	101.7-113.4	5,51	0,000	10,529	0,724
2@60.0	2015.NI	PCAest	2	60.000024	2.03	51.7-63.9	3,01	0,000	9,988	1,348
5@95.3	2015.NI	PCAest	5	95.300035	5.04	9.6-95.9	3,61	0,000	13,206	-1,536
1@209.1	2015.NI	Plant height	1	209.100096	1.07	198.8-239.7	7,81	0,000	7,689	8,382
2@135.2	2015.NI	Plant height	2	135.20006	2.05	128.2-141.5	4,35	0,053	1,630	-4,711
2@156.5	2015.NI	Plant height	2	156.500074	2.06	151.8-165.1	4,10	0,092	1,236	-4,288
3@203.4	2015.NI	Plant height	3	203.400103	3.08	189-239.7	3,78	0,000	6,691	7,620
3@95.3	2015.NI	Plant height	3	95.300045	3.04	91.9-96.4	5,76	0,000	9,999	-9,283
7@146.3	2015.NI	Plant height	7	146.300056	7.04	138.6-156.1	3,69	0,000	6,307	-7,531
7@71.1	2015.NI	Plant height	7	71.10002	7.02	67.4-74.6	8,12	0,000	10,950	-10,618
2@203.5	2015.NI	S/G	2	203.500098	2.07	197.1-208.8	3,29	0,001	6,243	0,056
2@89.9	2015.NI	S/G	2	89.900037	2.04	85.7-92.4	3,32	0,003	4,621	0,047
4@85.5	2015.NI	S/G	4	85.500035	4.05	68.5-87.6	4,72	0,000	10,746	-0,071
6@155.8	2015.NI	S/G	6	155.800066	6.06	143.5-167.7	4,00	0,000	9,278	0,067

Supplemental table S5. Pearson correlation between all the histological traits (yellow), all the cell wall traits of the internode (ocre) and all the cell wall traits of the whole plant without ears (orange) quantified in the panel of 11 genotypes cultivated 3 years under contrasted irrigation condition

	CWR_PWE	LK.CWR_PWE	PCAest_PWE	FAest_PWE	FAeth_PWE	IVDMD_PWE	IVCWRD_PWE	BO4.yield_PWE	S.G_PWE	Cellulose_PWE	HCELL_PWE
Stem area	-0,13	0,29	0,33	0,45	0,30	-0,22	-0,25	0,35	0,30	0,04	0,18
Lignifed fraction	0,06	0,52	0,48	0,23	0,44	-0,45	-0,46	0,31	0,14	0,30	-0,12
Non lignified fraction	-0,10	-0,51	-0,45	-0,31	-0,46	0,47	0,44	-0,25	-0,14	-0,25	0,02
Rind fraction	0,18	0,21	0,09	0,25	0,21	-0,25	-0,17	-0,15	0,12	-0,02	0,20
Bundle fraction	0,00	-0,28	-0,36	0,35	-0,11	0,18	0,36	-0,24	-0,18	-0,26	0,55
Bundle number	-0,07	0,14	0,19	0,28	0,17	-0,14	-0,05	0,27	0,10	0,00	0,17
Bundle density	0,15	-0,19	-0,19	-0,32	-0,21	0,06	0,24	-0,13	-0,32	0,01	-0,04
Red parenchyma	0,05	0,56	0,54	0,15	0,43	-0,46	-0,52	0,36	0,19	0,34	-0,20
Blue parenchyma	-0,07	-0,48	-0,41	-0,34	-0,44	0,42	0,40	-0,23	-0,13	-0,23	-0,03
Red rind	0,12	0,52	0,42	-0,09	0,27	-0,41	-0,50	0,04	0,27	0,37	-0,26
Bundle density	0,15	-0,19	-0,19	-0,32	-0,21	0,06	0,24	-0,13	-0,32	0,01	-0,04
CWR_IN	0,36	0,56	0,52	0,10	0,30	-0,63	-0,63	0,19	0,14	0,28	-0,02
KL.CWR_IN	0,21	0,84	0,79	0,12	0,52	-0,72	-0,86	0,37	0,42	0,47	-0,20
BO4.yield_IN	0,22	0,40	0,47	0,10	0,26	-0,41	-0,53	0,31	0,31	0,24	0,01
S.G_IN	-0,22	-0,56	-0,58	-0,06	-0,29	0,55	0,65	-0,46	-0,11	-0,42	0,23
FAest_IN	0,07	0,13	0,17	0,42	0,30	-0,19	-0,18	0,16	0,18	-0,03	0,38
FAeth_IN	0,43	0,50	0,41	-0,19	0,03	-0,56	-0,57	0,02	0,08	0,25	-0,21
PCAest_IN	-0,09	0,72	0,78	0,13	0,59	-0,50	-0,75	0,54	0,42	0,53	-0,27
IVDMD_IN	-0,36	-0,67	-0,61	-0,04	-0,31	0,68	0,74	-0,23	-0,22	-0,36	0,13
IVCWRD_IN	-0,20	-0,77	-0,77	-0,13	-0,53	0,70	0,83	-0,42	-0,37	-0,48	0,13
Cellulose_IN	-0,21	0,45	0,52	0,06	0,44	-0,25	-0,47	0,52	0,07	0,43	-0,33
Hemicelluloses_IN	-0,30	-0,13	-0,08	0,38	0,33	0,21	0,17	0,00	0,07	-0,16	0,38
CWR_PWE	1,00	0,23	-0,03	-0,30	-0,32	-0,67	-0,21	-0,45	-0,13	-0,10	-0,25
LK.CWR_PWE	0,23	1,00	0,91	0,04	0,54	-0,85	-0,94	0,38	0,48	0,57	-0,45
PCAest_PWE	-0,03	0,91	1,00	0,09	0,69	-0,69	-0,92	0,66	0,60	0,67	-0,35
FAest_PWE	-0,30	0,04	0,09	1,00	0,53	0,06	-0,03	0,37	0,03	-0,17	0,68
FAeth_PWE	-0,32	0,54	0,69	0,53	1,00	-0,31	-0,57	0,63	0,46	0,31	0,07
IVDMD_PWE	-0,67	-0,85	-0,69	0,06	-0,31	1,00	0,80	-0,13	-0,31	-0,38	0,40
IVCWRD_PWE	-0,21	-0,94	-0,92	-0,03	-0,57	0,80	1,00	-0,48	-0,44	-0,59	0,41
BO4.yield_PWE	-0,45	0,38	0,66	0,37	0,63	-0,13	-0,48	1,00	0,20	0,66	0,04
S.G_PWE	-0,13	0,48	0,60	0,03	0,46	-0,31	-0,44	0,20	1,00	0,22	-0,10
Cellulose_PWE	-0,10	0,57	0,67	-0,17	0,31	-0,38	-0,59	0,66	0,22	1,00	-0,36
HCELL_PWE	-0,25	-0,45	-0,35	0,68	0,07	0,40	0,41	0,04	-0,10	-0,36	1,00

	Stem area	Lignifed fraction	Non lignified fraction	Rind fraction	Bundle fraction	Bundle number	Bundle density	Red parenchyma	Blue parenchyma	Red rind	Bundle density
Stem area	1,00	0,11	-0,09	-0,14	0,04	0,70	-0,54	0,14	-0,08	-0,21	-0,54
Lignifed fraction	0,11	1,00	-0,97	0,13	-0,21	0,02	-0,08	0,97	-0,95	0,26	-0,08
Non lignified fraction	-0,09	-0,97	1,00	-0,37	0,01	0,05	0,11	-0,90	1,00	-0,39	0,11
Rind fraction	-0,14	0,13	-0,37	1,00	0,46	-0,40	-0,20	0,00	-0,38	0,69	-0,20
Bundle fraction	0,04	-0,21	0,01	0,46	1,00	0,08	0,05	-0,35	-0,03	0,03	0,05
Bundle number	0,70	0,02	0,05	-0,40	0,08	1,00	0,18	0,04	0,06	-0,35	0,18
Bundle density	-0,54	-0,08	0,11	-0,20	0,05	0,18	1,00	-0,12	0,11	-0,05	1,00
Red parenchyma	0,14	0,97	-0,90	0,00	-0,35	0,04	-0,12	1,00	-0,88	0,22	-0,12
Blue parenchyma	-0,08	-0,95	1,00	-0,38	-0,03	0,06	0,11	-0,88	1,00	-0,37	0,11
Red rind	-0,21	0,26	-0,39	0,69	0,03	-0,35	-0,05	0,22	-0,37	1,00	-0,05
Bundle density	-0,54	-0,08	0,11	-0,20	0,05	0,18	1,00	-0,12	0,11	-0,05	1,00
CWR_IN	0,08	0,32	-0,37	0,31	-0,02	0,10	0,05	0,30	-0,35	0,36	0,05
KL.CWR_IN	0,18	0,42	-0,44	0,27	-0,20	0,06	-0,16	0,47	-0,41	0,54	-0,16
BO4.yield_IN	0,17	0,03	-0,03	0,07	-0,12	0,14	-0,07	0,08	-0,02	0,17	-0,07
S.G_IN	-0,21	-0,25	0,21	0,01	0,29	-0,19	0,02	-0,30	0,19	-0,23	0,02
FAest_IN	0,22	0,06	-0,13	0,29	0,19	0,15	-0,14	0,00	-0,14	0,09	-0,14
FAeth_IN	-0,05	0,18	-0,18	0,09	-0,18	0,03	0,14	0,24	-0,16	0,28	0,14
PCAest_IN	0,19	0,33	-0,33	0,19	-0,30	0,05	-0,17	0,37	-0,29	0,53	-0,17
IVDMD_IN	-0,10	-0,32	0,35	-0,27	0,12	-0,09	-0,01	-0,33	0,32	-0,41	-0,01
IVCWRD_IN	-0,20	-0,37	0,40	-0,29	0,12	-0,16	0,06	-0,39	0,37	-0,51	0,06
Cellulose_IN	0,10	0,30	-0,24	-0,02	-0,40	0,07	-0,02	0,32	-0,21	0,36	-0,02
Hemicelluloses_IN	0,03	0,11	-0,19	0,30	0,25	-0,08	-0,13	0,02	-0,20	0,09	-0,13
CWR_PWE	-0,13	0,06	-0,10	0,18	0,00	-0,07	0,15	0,05	-0,07	0,12	0,15
LK.CWR_PWE	0,29	0,52	-0,51	0,21	-0,28	0,14	-0,19	0,56	-0,48	0,52	-0,19
PCAest_PWE	0,33	0,48	-0,45	0,09	-0,36	0,19	-0,19	0,54	-0,41	0,42	-0,19
FAest_PWE	0,45	0,23	-0,31	0,25	0,35	0,28	-0,32	0,15	-0,34	-0,09	-0,32
FAeth_PWE	0,30	0,44	-0,46	0,21	-0,11	0,17	-0,21	0,43	-0,44	0,27	-0,21
IVDMD_PWE	-0,22	-0,45	0,47	-0,25	0,18	-0,14	0,06	-0,46	0,42	-0,41	0,06
IVCWRD_PWE	-0,25	-0,46	0,44	-0,17	0,36	-0,05	0,24	-0,52	0,40	-0,50	0,24
BO4.yield_PWE	0,35	0,31	-0,25	-0,15	-0,24	0,27	-0,13	0,36	-0,23	0,04	-0,13
S.G_PWE	0,30	0,14	-0,14	0,12	-0,18	0,10	-0,32	0,19	-0,13	0,27	-0,32
Cellulose_PWE	0,04	0,30	-0,25	-0,02	-0,26	0,00	0,01	0,34	-0,23	0,37	0,01
HCELL_PWE	0,18	-0,12	0,02	0,20	0,55	0,17	-0,04	-0,20	-0,03	-0,26	-0,04

	CWR_IN	KL.CWR_IN	BO4.yield_IN	S.G_IN	FAest_IN	FAeth_IN	PCAest_IN	IVDMD_IN	IVCWRD_IN	Cellulose_IN	Hemicelluloses_IN
Stem area	0,08	0,18	0,17	-0,21	0,22	-0,05	0,19	-0,10	-0,20	0,10	0,03
Lignifed fraction	0,32	0,42	0,03	-0,25	0,06	0,18	0,33	-0,32	-0,37	0,30	0,11
Non lignified fraction	-0,37	-0,44	-0,03	0,21	-0,13	-0,18	-0,33	0,35	0,40	-0,24	-0,19
Rind fraction	0,31	0,27	0,07	0,01	0,29	0,09	0,19	-0,27	-0,29	-0,02	0,30
Bundle fraction	-0,02	-0,20	-0,12	0,29	0,19	-0,18	-0,30	0,12	0,12	-0,40	0,25
Bundle number	0,10	0,06	0,14	-0,19	0,15	0,03	0,05	-0,09	-0,16	0,07	-0,08
Bundle density	0,05	-0,16	-0,07	0,02	-0,14	0,14	-0,17	-0,01	0,06	-0,02	-0,13
Red parenchyma	0,30	0,47	0,08	-0,30	0,00	0,24	0,37	-0,33	-0,39	0,32	0,02
Blue parenchyma	-0,35	-0,41	-0,02	0,19	-0,14	-0,16	-0,29	0,32	0,37	-0,21	-0,20
Red rind	0,36	0,54	0,17	-0,23	0,09	0,28	0,53	-0,41	-0,51	0,36	0,09
Bundle density	0,05	-0,16	-0,07	0,02	-0,14	0,14	-0,17	-0,01	0,06	-0,02	-0,13
CWR_IN	1,00	0,62	0,57	-0,56	0,37	0,77	0,38	-0,96	-0,85	0,17	-0,10
KL.CWR_IN	0,62	1,00	0,47	-0,53	0,22	0,57	0,83	-0,71	-0,84	0,47	0,00
BO4.yield_IN	0,57	0,47	1,00	-0,67	0,48	0,44	0,38	-0,65	-0,68	0,01	-0,36
S.G_IN	-0,56	-0,53	-0,67	1,00	-0,37	-0,55	-0,50	0,64	0,66	-0,43	0,57
FAest_IN	0,37	0,22	0,48	-0,37	1,00	0,13	0,25	-0,34	-0,41	-0,21	-0,03
FAeth_IN	0,77	0,57	0,44	-0,55	0,13	1,00	0,27	-0,85	-0,64	0,16	-0,41
PCAest_IN	0,38	0,83	0,38	-0,50	0,25	0,27	1,00	-0,48	-0,72	0,66	0,04
IVDMD_IN	-0,96	-0,71	-0,65	0,64	-0,34	-0,85	-0,48	1,00	0,90	-0,22	0,23
IVCWRD_IN	-0,85	-0,84	-0,68	0,66	-0,41	-0,64	-0,72	0,90	1,00	-0,36	0,09
Cellulose_IN	0,17	0,47	0,01	-0,43	-0,21	0,16	0,66	-0,22	-0,36	1,00	0,16
Hemicelluloses_IN	-0,10	0,00	-0,36	0,57	-0,03	-0,41	0,04	0,23	0,09	0,16	1,00
CWR_PWE	0,36	0,21	0,22	-0,22	0,07	0,43	-0,09	-0,36	-0,20	-0,21	-0,30
LK.CWR_PWE	0,56	0,84	0,40	-0,56	0,13	0,50	0,72	-0,67	-0,77	0,45	-0,13
PCAest_PWE	0,52	0,79	0,47	-0,58	0,17	0,41	0,78	-0,61	-0,77	0,52	-0,08
FAest_PWE	0,10	0,12	0,10	-0,06	0,42	-0,19	0,13	-0,04	-0,13	0,06	0,38
FAeth_PWE	0,30	0,52	0,26	-0,29	0,30	0,03	0,59	-0,31	-0,53	0,44	0,33
IVDMD_PWE	-0,63	-0,72	-0,41	0,55	-0,19	-0,56	-0,50	0,68	0,70	-0,25	0,21
IVCWRD_PWE	-0,63	-0,86	-0,53	0,65	-0,18	-0,57	-0,75	0,74	0,83	-0,47	0,17
BO4.yield_PWE	0,19	0,37	0,31	-0,46	0,16	0,02	0,54	-0,23	-0,42	0,52	0,00
S.G_PWE	0,14	0,42	0,31	-0,11	0,18	0,08	0,42	-0,22	-0,37	0,07	0,07
Cellulose_PWE	0,28	0,47	0,24	-0,42	-0,03	0,25	0,53	-0,36	-0,48	0,43	-0,16
HCELL_PWE	-0,02	-0,20	0,01	0,23	0,38	-0,21	-0,27	0,13	0,13	-0,33	0,38

Cell wall lignification and *p*-coumaroylation evolved differently in pith and rind of maize internodes

Running title: Pith and rind lignification and *p*-coumaroylation

Y. Zhang[ab], D. Legland[c], F. El Hage[ad], M.F. Devaux[c], F. Guillon[c], M. Reymond[a], V. Méchin[a]*

[a] *UMR 1318, Institut Jean-Pierre Bourgin, INRA, AgroParisTech, CNRS, Université Paris-Saclay, 78000, Versailles, France*
[b] *current address: Weed Research Laboratory, Nanjing Agricultural University, Nanjing 210095, China*
[c] *UR1268, Biopolymères, Interactions et Assemblages, INRA, 44000, Nantes, France*
[d] *Ecole Doctorale 567 Sciences du Vegetal, University Paris-Sud, University of Paris-Saclay, bat 360, 91400, Orsay, France*

*Corresponding author. Dr. Valérie Méchin valerie.mechin@inra.fr

Abstract
Plant cell wall development is an integrated process during which several components are deposited successively. In grass cell wall accessibility to structural polysaccharides is limited by cell wall structure and composition and mainly by phenolic compounds. We study here the patterns of cell wall establishment in the internode supporting the ear of three distinct maize genotypes. Developmental patterns for internode cell wall composition are reported with an emphasis on lignification, *p*-coumaroylation and feruloylation. We combined biochemical and histological approaches and highlighted than maize internode cell wall development was characterized before flowering by a fast deposition of secondary cell wall with strong lignification of both pith and rind. After flowering and until silage maturity a slow deposition of secondary wall occurs in the cortical region and the deposited lignins are then rich in β-O-4 bonds and highly *p*-coumaroylated. We conclude the paper by proposing a revised spatiotemporal model of that proposed by Terashima et al. (1993) for grass cell wall development.

Keywords:
Internode development, lignification, maize, *p*-coumaric acid, rind, pith.

Abbreviations:
G: guaiacyl lignin unit
H: *p*-hydroxyphenyl lignin
unit S: syringyl lignin unit
V8 stage: eight expanded leaves
stage V10 stage: ten expanded
leaves stage

1. Introduction

Grasses plays a crucial role in agriculture for animal nutrition, both as fresh forage or silage. Their valorization via the production of bioethanol is also current. In both cases, structural cell wall polysaccharides (cellulose and hemicelluloses) must be valorized at best. Their accessibility is greatly limited by cell wall structure and composition and mainly by phenolic compounds, namely lignins and *p*-hydroxycinnamic acids (ferulic and *p*-coumaric acids). Glucuronoarabinoxylan are the main hemicelluloses encounter in grass cell wall. Non-xylan and non-cellulosic polysaccharides only represent 10 to 15% of the cell wall [1]. An important specificity of grass xylan compared to dicots lies in the fact that ferulic and *p*-coumaric acids are added to the arabinofuranosyl backbone. As recalled in Hatfield et al. [1] ferulic acid content varies between grasses. Genetic variability has also been frequently highlighted in maize [2-5]. Hatfield and Chaptman [6] demonstrated the important variability for ferulic acid content according to organs and tissues. The ferulic acid content was found higher in roots compared to stem. In stem, pith and rind present quite equivalent amounts of esterified ferulic acids. However the esterified ferulic monomers were a bit more abundant in pith than in rind. For a long time, the role of crosslinking agent of ferulic acid has been studied [7-11]. Ferulic acid is effectively able to covalently linked hemicelluloses and lignins. Ferulic esters are thus presented as nucleation sites for lignification [11, 12] and one can intuit the potential impact of ferulic esters availability in cell wall on lignification process. The level of *p*-coumaric acid linked to arabinoxylans is much more lower and varies from undetectable fractions to 1:15 that to say 10 to 15 times less than for ferulic acid. Cross-linking between hemicelluloses or between hemicelluloses and lignins through p-coumaric acid has never been highlighted. In fact, *p*-coumaric acid is very predominantly associated with lignins. Despite the very high levels of esterified *p*-coumaric acid (2 to 3 times more than esterified + etherified ferulic acids) its role in grass cell wall is not very clear. *p*-coumaric acid is implicated in the radical coupling of S units into the lignin polymer and is known to be ester- linked to the γ-position of the side chains of S lignin units [13]. A few works have demonstrated that S units were enzymatically preacylated by *p*-coumaric acid in the cytosol [14]. These acylated monolignols are then incorporated into the lignin polymer by polymerization and co-polymerization with the traditional monolignols, resulting in acylated lignin [15]. Lignin is formed via the oxidative coupling of three main monolignols: *p*- coumaryl alcohol, coniferyl alcohol, and sinapyl alcohol, which give rise to p-hydroxyphenyl (H), guaiacyl (G), and syringyl (S) units interconnected by aryl ether bonds (β-O-4 linkages) and/or carbon-carbon bonds. The deposition of lignin in cell walls has far-reaching consequences for the mechanical stability, apoplastic solute conductance and pathogen resistance of forage crops [16, 17]. In parallel, the enzymatic degradability of forage declines during maturation because of accumulation and progressive lignification of primary and secondary cell walls [18]. Until now, many studies

related to genetics, genomics and biochemistry of lignin have been performed on grass and have revealed that lignin content is the first factor negatively correlated with cell wall degradability. However, simple reduction in lignin content may risk losing the forage agricultural fitness traits [19, 20]. So studies related to the quest for explanatory factors for cell wall degradability variations have focused on the influence of other cell wall parameters such as lignin composition, structure and distribution and *p*-hydroxycinnamic acids content [3-5, 21-26]. In spite of many data in the literature on cell wall biochemical factors and their impact on degradability, the role of these factors remains uncertain and conclusions are often opposite. Several studies suggested that cross-linking between lignin and polysaccharides through ferulic acid may be a major determinant of cell wall degradability, nevertheless, consistent relationship have not always been observed for this parameter [3, 5, 27, 28]. Concerning lignin structure, it has been proposed that lignin rich in carbon-carbon bonds are more inhibitory for cell wall degradability [18].

However, in a previous published study, we demonstrated that β-O-4 rich lignin have a more extended shape likely to adsorb all along the cellulose fibers, thus resulting in a lower accessibility of hydrolytic enzymes to polysaccharides [3].

In stem, if several cell wall components influence cell wall degradability, proportions of the different cell types could also strongly impact degradability [29, 30]. In 1991, Grabber et al.

[31] showed how the sclerenchyma and the parenchyma were degraded with rumen fluid after several hours on stem cross-sections of switchgrass and orchardgrass. Jung and Casler [32] did a similar study on maize stem cross-sections and showed that degradability differed between cell types. Méchin et al. [26] investigated the link between lignin distribution in maize stem, cell wall biochemical traits and cell wall degradability. For these authors a highly digestible maize silage may be poorly lignified with lignin richer in S than in G units and preferentially localized in the cortical region than in the pith. In alfalfa, degradability variation was partly relied to the different cell types proportions [33, 34]. An anatomical comparison of switchgrass stems selected for contrasted degradability showed striking differences in the lignified cell types distribution [35]. Overall, these works clearly indicate that differences between tissues lignification influence the cell wall degradability at the organ level [36, 37]. Plant cell wall development is an integrated process during which several components are deposited successively. Some studies describe this sequential process in a biochemical point of view in detail [8, 38, 39]. Contrariwise, to our knowledge, there is no data concerning the genetic variability for cell wall establishment in maize excepted a comparison between two hybrids performed by Boon et al. [39-41] for cell wall thickness and VanSoest measurements. In Jung [42] or in Jung and Casler [32] three maize hybrids were studied two years all along

internode development but quite surprisingly presented data were averaged across the three genotypes and two years.

We present here a study conducted to describe the patterns of cell wall establishment in three distinct genotypes selected for their quite similar lignin content and their contrasted cell wall degradability at silage stage. Study was conducted using the maize internode supporting the ear. Developmental patterns for internode cell wall composition are reported with an emphasis on the pattern of lignification, *p*-coumaroylation and feruloylation. The objective was to identify if genotypes with quite similar mature lignin content but with contrasted cell wall degradability presented equivalent cell wall structure, reticulation and tissue lignification. The ultimate goal was to propose developmental scheme for cell wall establishment.

2. Materials and Methods

2.1. Plant material

Three maize inbred lines F324, F66 and F7037 were cropped at INRA Lusignan (86, France) for three successive years (2009, 2010 and 2011). The trials were randomized block designs with three replicates. Plots consisted of one 5.2m long row and the density was 90 000 plants per hectare. Irrigation was applied from mid-June to end of August to prevent water stress.

In 2009 and 2010, for biochemical analysis, principal ear's internode was sampled at 6 stages of development beginning when the plants had reached V8 stage (eight expanded leaves). The next five stages were V10 (ten expanded leaves), tasselling, silking, 14 days after silking and silage stage. For each inbred line, 50 internodes were sampled at V8 and V10, 15 internodes were sampled at the four other stages. The internodes were chopped, oven dried (70°C) and ground with a hammer mill to pass through a 1 mm screen for biochemical analyses.

During the summer 2011, five ear internodes were sampled per developmental stage and were immediately placed in 70% ethanol:water (v/v) for subsequent histological analysis. The length and diameter (in the middle of the internode, across the short axes) of the internodes were measured with a ruler.

2.2. Biochemical analyses

Cell wall residue was obtained after a two-stage extraction of the dry matter by ethanol and water [43]. Lignin content was estimated according to the Klason procedure [44] and expressed as the weight percentage of Klason lignin in cell wall residue.

Para-hydroxycinnamic acid content was measured after treating cell wall residue fractions with NaOH according to a previously described procedure [5] which involves two alkaline treatments with different levels of severity. Esterified *p*-hydroxycinnamic acids were released by subjecting cell wall residue samples (50 mg) to a mild alkaline hydrolysis (NaOH 2N, 5 ml, 20h at room temperature). Other cell wall residue samples (50 mg) were treated with 5 ml of 4 M NaOH for 2h at 170°C to release both esterified and etherified hydroxycinnamates. Samples recovered from mild and severe alkaline hydrolysis were subjected to the same precipitation procedure [45] prior to HPLC-MS analysis. The concentration of esterified *p*- coumaric and ferulic acids correspond to the amount of *p*-coumaric and ferulic acids released by mild alkaline hydrolysis whereas etherified ferulic acid was calculated as the difference between ferulic acid amounts released by the severe and mild alkaline treatments.

Lignin monomeric composition was studied by thioacidolysis performed on 15 mg of cell wall residue placed in a screw-cap glass tube together with 1ml of internal standard (C19, C21, C22 0.5mg/ml each) and 10 mL of dioxane/ethanethiol mixture (9:1, v/v) containing 0.2 M boron trifluoride etherate, for 4h in an oil bath at 100°C [46]. After extraction of the lignin-derived monomers, the analysis of their trimethylsilyl derivatives was run by GC/MS. The molar yield in H, G and S lignin-derived monomers was calculated on the basis of the Klason lignin content of the sample.

We also estimated the percentage of S lignin units acylated by p-coumaric acid (S-PC) assuming that all the *p*-coumaric acid was esterified to S lignin units and extrapolating the percentage of S units in the uncondensed to the whole lignin. Thus S-PC was calculated as mentioned above:

S-PC = (100 × esterified *p*-coumaric acid content) / (LK × %S) All the biochemical analyses were performed in duplicate.

2.3. Anatomical analyses

A 1-cm-long segment was sampled in the middle part of each of the five internodes and soaked in water for one night. For each segment, 15 serial stem cross-sections, 150-µm thick, were prepared with a vibratome (Leica VT1000 S).

Slices were imaged using the “BlueBox” macro-imaging system developed at INRA Nantes [47]. An optical fiber ring (SCHOTT DCRIV Light Source, Mainz, Germany) provides a controlled darkfield illumination. Mosaic images were acquired of size approximately 4500x4500 pixels, with a pixel size of 3.6 µm x 3.6 µm. Grey values were coded between 0 (black) and 255 (white). As the diameter of most parenchyma cells ranged between 50 and

150, the resolution of macroscopy images made it possible to observe together the cellular morphology and the whole slices.

Images were analyzed by using grey level granulometry, which consists in applying image transformations with increasing sizes of the structuring element [48, 49]. The method can be compared to a sieving of the images and the structuring elements to the mesh of the sieve. By applying morphological closings of increasing sizes and a square as structuring element, cells progressively disappear from the tissue images. A granulometric curve is built by measuring the variations of the sum of grey levels after each closing step. Granulometric curves can be compared to usual granulometric distributions except that they are calculated taking grey level variations into consideration. The geometrical mean of the distribution was used as a summary parameter describing the average size of the cells in a given image [49].

2.4. Histological analyses

Stem cross-sections were stained overnight using a Fasga solution diluted in distilled water (1:8, v/v). The Fasga solution was composed of 0.05% safranin O, 0.2% Alcian blue, 1.5% acetic acid and 46% glycerin in distilled water. Safranin is a red, basic, cationic dye, and Alcian blue is an acidic anionic dye. Fasga stained lignified tissues in red, whereas non- lignified or poorly lignified tissues appeared as blue. After staining, sections were rinsed twice for 5 min with distilled water. Sections were examined under a magnifying glass (×1, Nikon SMZ 1000) and were digitalized as color images with a resolution of 10µm per pixel. Images acquired for the six development stages are presented in Fig. 1.

Each image was numerically automatically analyzed on the ImageJ software with the plugin presented in Zhang et al. [50] to segment and evaluate the red/blue intensity ratio relative to the distance to the outer epidermis for the six stages of development. On each image, morphological image filtering was applied to keep the local color of the tissue. The region corresponding to the stem section was identified and divided into a fixed number of concentric regions of interest. The average color within each region of interest was measured; resulting in curves describing the variations of tissue color with the distance to the epidermis. Afterward, the evolution of the lignification rate for each region (pith, rind and blue ring) of the stem sections during internode development was assessed. After all, we measured the average intensity of the red, the blue and the green on the whole cross-section for each genotype and each stage in order to establish the average profile of each RGB channel during development for the three genotypes.

2.5. Statistical analysis

Any block effect nor interaction with any other factor with block was detected thus to compare the relative influence of genotype, year and stage, variance analysis was carried out using R according to the following model:

$$Vijkl = \mu + Yi + Gj + Sk + YGij + YSik + GSjk + Rijkl$$

where Vijkl is the value of genotype j, in year i, for stage k and for block l; μ is the overall mean; Yi denotes the main effect of year i; Gj denotes the effect of genotype j; Sk denotes the main effect of stage k; YGij denotes the interaction effect between genotype j and year i; YSik denotes the main effect of stage k nested in year i; GSjk denotes the main effect of genotype j nested in stage k; and Rijk is the random residual term.

Data were combined over year, field and analysis replicates before determination of correlation coefficients using R.

3. Results and discussion

Three public early/medium-early maize inbred lines were selected on the bases of results obtained from experiments performed in 2006 and 2008 at INRA Lusignan [51]. F324, F66 and F7037 lines were chosen to display fairly comparable lignin contents (5.2, 4.8 and 5.1 % of ADL in the cell wall respectively) for very different cell wall degradability (38.8, 34.8 and 27.6 % of the cell wall respectively) at silage stage. Cell wall deposition was studied all along plant development for these three inbred lines to decipher on the existence of one or more cell wall developmental models both biochemically and in terms of lignin distribution within the different stem tissues. Most of the scientists currently working on lignification rely on the models of cell wall polymers deposition presented in Terashima et al. [8]. Briefly, in this model, the authors presented the successive formation of cell layers in the order of middle lamella, primary wall, outer, middle and inner layers of secondary wall. They described both the deposition of carbohydrates and phenolic compounds. Concerning lignification they argued that monolignols were provided in the order of H, G and S lignin subunits and that lignins formed at an early stage were always more condensed than those formed at a late stage. They also stated that ferulic acids were incorporated earlier than p-coumaric acids in cell wall. The results obtained in this study will be discussed with regard to this model.

3.1. Genetic variation for internode elongation, cross section surface and cell size within the three genotypes throughout internode development

The length of the principal ear's internode was measured at each developmental stage for each genotype. The three inbred lines presented different elongation patterns along development (Figure 1a). F66 and F324 were two early genotypes and presented a rapid growth compared to F7037 which was medium-early and displayed a slower elongation. The 10cm length was reached in about 10 days for F66 and F324 against more than 20 days for F7037. However, it should be noted that the 3 genotypes completed their elongation at or just before silking, regardless the silking date. This physiological stage marked the end of the

internode elongation whatever the considered genotype. At silage maturity, the length of F7037 internode was greater than the two others. Scobbie et al. [52] showed that, when elongation ceased in maize internodes cells near the upper part of the internode had already shifted to extensive secondary wall deposition, whereas at the bottom of the internode cell walls appeared to still be more primary in nature. Similarly, Jung [42] indicated that cell wall development shifted from a mixture of primary and secondary wall deposition to only secondary wall development after the end of elongation of the internode. Thus, in our three inbred lines the shift in the developmental pattern for internode elongation should be associated with different process of cell wall development/deposition over time. These differences should be visible in our in depth biochemical and histological characterizations.

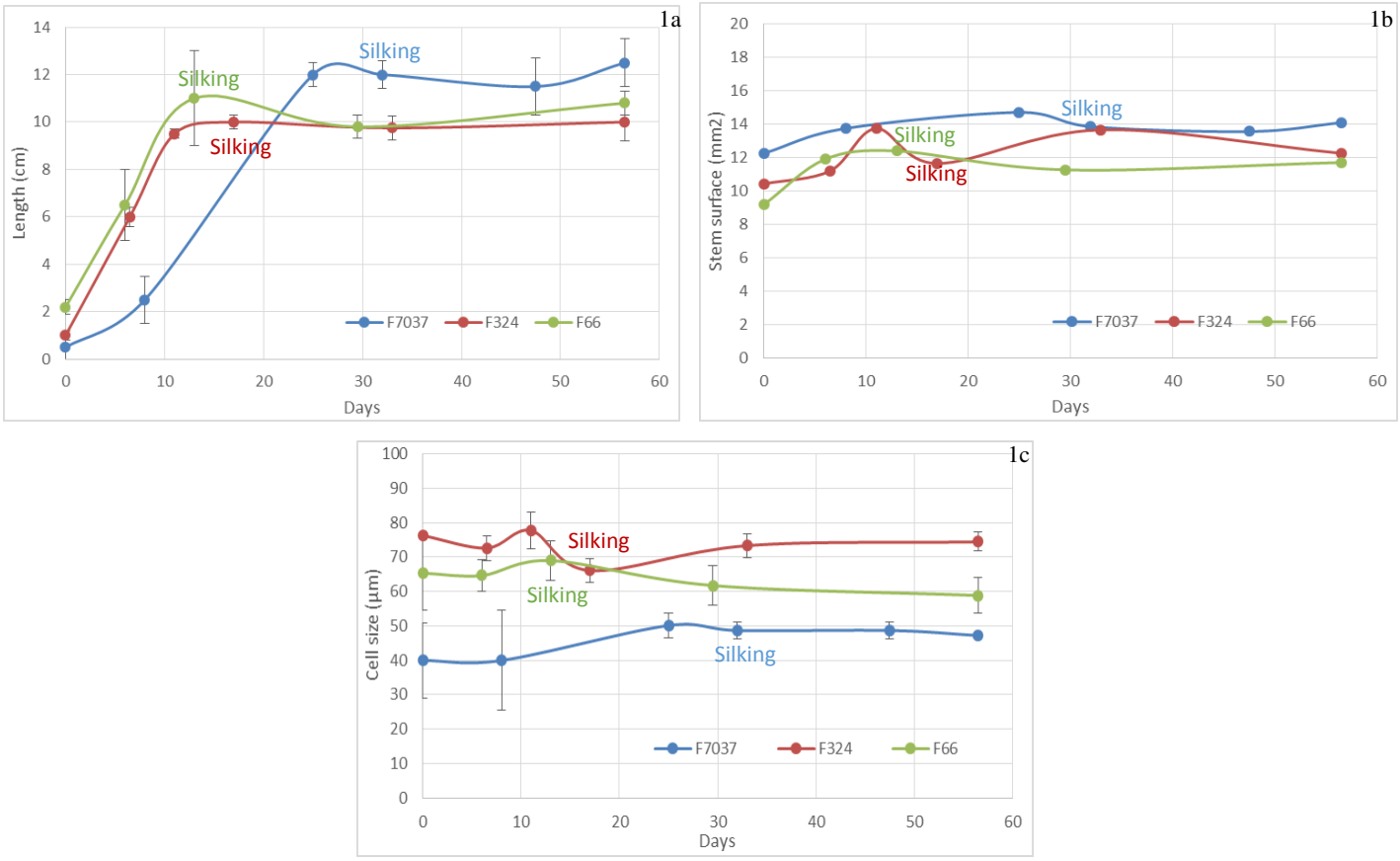


Figure 1. Evolution of morphological parameters during internode development for the three genotypes. 1a: length of the principal ear's internode, 1b: cross section surface and 1c: cell size of the parenchyma cells. Data were averaged across the three blocks collected in 2011. «Silking » indicated the time of female flowering for each genotype. Smooth curves were used only for graphical purposes.

Evolution of internode diameter was less important than length and was also complete when elongation ended for the three inbred lines. At silage stage, F7037 showed a larger internode diameter (1.33 ± 0.01 cm) than F324 (1.20 ± 0.05 cm) and F66 (1.13 ± 0.02 cm). The stem cross section surface did not evolve considerably after the second stage (V10, Figure 1b). The cell size (Figure 1c) was stable within each line over time but was contrasted between lines. Indeed, a twofold variation was observed between lines with F7037 which displayed 45µm cell size and F324 which presented 75µm cell size. Thus F7037 while it has the largest internode diameter displayed the smallest cell size which implied an increased cell wall density compared to the two others genotypes and potentially associated with its lower degradability.

3.2. The main differences for internode elongation and cell wall phenolic composition were positioned at young stages, before silking

The variance analysis for cell wall biochemical composition indicated that throughout internode development, the three inbred lines differed for most biochemical parameters. Indeed, the genotype effect was very significant ($P < 0.001$) for Klason lignin content, G, β- O-4 yield, *p*-coumarate esters and ferulate esters (Table 1). In previous studies, no differences in pattern of development have been pointed out according to species [32, 42, 53]. The inbred lines used in our study have been chosen to limit the variation in lignin content in the cell wall at silage stage. They showed significant difference in phenolic composition during internode development suggesting that the cell wall pattern of lignification differed. This is the first time that genetic variation for cell wall phenolic composition during internode development is reported.

As observed in previous studies [32, 42], the stage effect was very significant ($P < 0.001$) for all cell wall phenolic parameters. To further investigate the stage effect variance analyses was applied to two distinct periods, from V8 to silking and from silking to silage (Table1). The variance analysis carried out for each period indicated no significant genotype*stage interaction over the late stages (Table 1). Thus at late stages, accumulation of cell wall components among the three inbred lines followed similar pattern. The main differences for all phenolic parameters were thus concentrated at young stages, before silking.

Table 1. ANOVA results for fixed effects for cell wall biochemical composition of the principal ear's internode for the three maize lines (F324, F66, and F7037) grown in 2009 and 2010 and sampled at 6 developmental stages.

		Variance effects					
		Y_i	G_j	S_k	YG_{ij}	YS_{ik}	GS_{jk}
All stages	L Internode	ns	*	***	ns	ns	**
	KL	***	***	***	ns	***	***
	G	***	***	***	**	***	ns
	S	***	**	***	ns	***	***
	β-O-4 yield	***	***	***	ns	***	**
	S/G	ns	ns	***	***	ns	***
	PC est	***	***	***	ns	***	***
	SPC	ns	**	***	ns	*	***
	FA est	***	***	***	*	***	***
	FA eth	***	ns	***	ns	*	***
V8 to silking stages	L Internode	ns	ns	***	ns	ns	**
	KL	***	***	***	ns	**	***
	G	***	***	***	ns	***	ns
	S	***	*	***	ns	***	**
	β-O-4 yield	***	***	***	ns	***	*
	S/G	ns	ns	***	*	*	***
	PC est	***	***	***	**	***	***
	SPC	ns	ns	***	ns	*	**
	FA est	***	***	***	ns	***	***
	FA eth	ns	**	***	ns	ns	***
Silking to silage stages	L Internode	ns	***	ns	ns	ns	ns
	KL	*	***	*	*	ns	ns
	G	***	**	**	**	ns	ns
	S	***	***	***	ns	ns	ns
	β-O-4 yield	***	***	***	*	ns	ns
	S/G	ns	ns	***	**	ns	ns
	PC est	ns	***	***	ns	ns	ns
	SPC	ns	***	**	ns	*	*
	FA est	***	***	***	ns	ns	**
	FA eth	***	ns	*	ns	ns	ns

*: $P < 0.05$; **: $P < 0.01$; ***: $P < 0.001$; ns: $P > 0.05$.

L internode: length of the internode supporting the ear, KL: klason lignin content in the cell wall, G and S: molar yield in β-O-4 linked G and S lignin-derived monomers calculated on the basis of the Klason lignin content in the cell wall, β-O-4 yield: sum of the H, G and S β-O- 4 linked lignin-derived monomers, S/G: S/G ratio, PC est: esterified *p*-coumaric acid content in the cell wall, SPC: percentage of S lignin units acylated by p-coumaric acid, FA est: esterified ferulic acid content in the cell wall, FA eth: etherified ferulic acid content in the cell wall.

3.3. Different developmental patterns were observed for lignin content, composition, structure and distribution

3.3.1. Evolution of lignin content all along the internode development

The three genotypes were initially retained to display quite similar lignin content on the basis of their ADL lignin content at silage stage (from 4.8 to 5.2%). The Klason lignin content for these three genotypes at silage stage were ultimately quite comparable (from 14% for F66 and F324 to 16% for F7037, Figure 2a). As exposed in Hatfield and Fukushima [54] when applied to grasses, the acid detergent solution used in the Van Soest procedure dissolves more than 50% of the lignin, which explains the drastically lower values encountered for the ADL lignin content compared to the values obtained with the Klason procedure. As detailed in Zhang et al. [3] lignin content estimated by the Van Soest (ADL) or the Klason methods do not represent the same lignin part. The Klason lignin is a better estimation of the whole lignin content in the cell wall whereas the ADL lignin content represents mainly the condensed (C-C linkages) lignin part.

Among the three genotypes, quite similar low lignin contents were observed at first stages of development (4.5 ± 0.5 %, 5.6 ± 1.0% and 5.2 ± 1.0% for F324, F66 and F7037 respectively, Figure 2a). A rapid increase in Klason lignin content was observed for the three genotypes in a first developmental period between V8 and Silking stages (Figure 2a). At silking stage all the three genotypes nearly reached their final Klason lignin content (Figure 2a). F66 and F324 thus accumulated about 10% of lignin in their cell walls in only 2 weeks while F7037 accumulated about 10% of lignin in more than 4 weeks (Figure 2a). After silking, in a comparable way for the three genotypes, lignin content increased negligibly (Table 1 and Figure 2a).

3.3.2. Evolution of lignin structure and composition all along development

The proportion of H, G and S lignin subunits was evaluated by thioacidolysis and thus reflects the lignin units only involved in β-O-4 bonds. The total β-O-4 yield provides an estimate of the proportion of lignin units only involved in β-O-4 bonds (β-O-4 yield), the so-called “uncondensed” part of the lignin polymer. An important effect of stage ($P < 0.001$, Table 1) was observed for β-O-4 yield which corresponded to a consistent increase of the uncondensed part of the lignin polymer in the principal ear’s internode during internode development (Figure 2b).

At earlier stages, the three studied genotypes presented poor β-O-4 linkages in their lignins. In accordance with Terashima et al. [8], lignin formed at an early stage were always more condensed than those formed at a late stage. The three genotypes did not differ drastically in their developmental pattern for β-O-4 yield accumulation, but differed for their

developmental pattern for Klason lignin content. Between Silking and Silage stages about 150 µmol.g-1 Klason lignin of β-O-4 lignin units were deposited while the total lignin content only increased in a very few extent. Therefore, β-O-4 was probably the main linkage formed during this late and slow lignification period. Rapid polymerization favors C-C coupling of monolignols; in contrast, gradual polymerization favors β-O-4 coupling between monolignols into lignin polymer [55]. This is in accordance with our results which showed that rapid lignin accumulation was certainly the place for mixed bonding pattern within the lignin polymer, with an important place for C-C bonds whereas the slow and late lignin accumulation period was the place of β-O-4 bonding pattern within the lignin polymer. We can wonder if the establishment of β-O-4 bonds is only constrained by chemical features (oxidative coupling, reactivity, quinone stability and so one) or if genetic determinism involved in spatio-temporal regulation of this pattern also occurred, but the objective of this paper is not to debate this point.

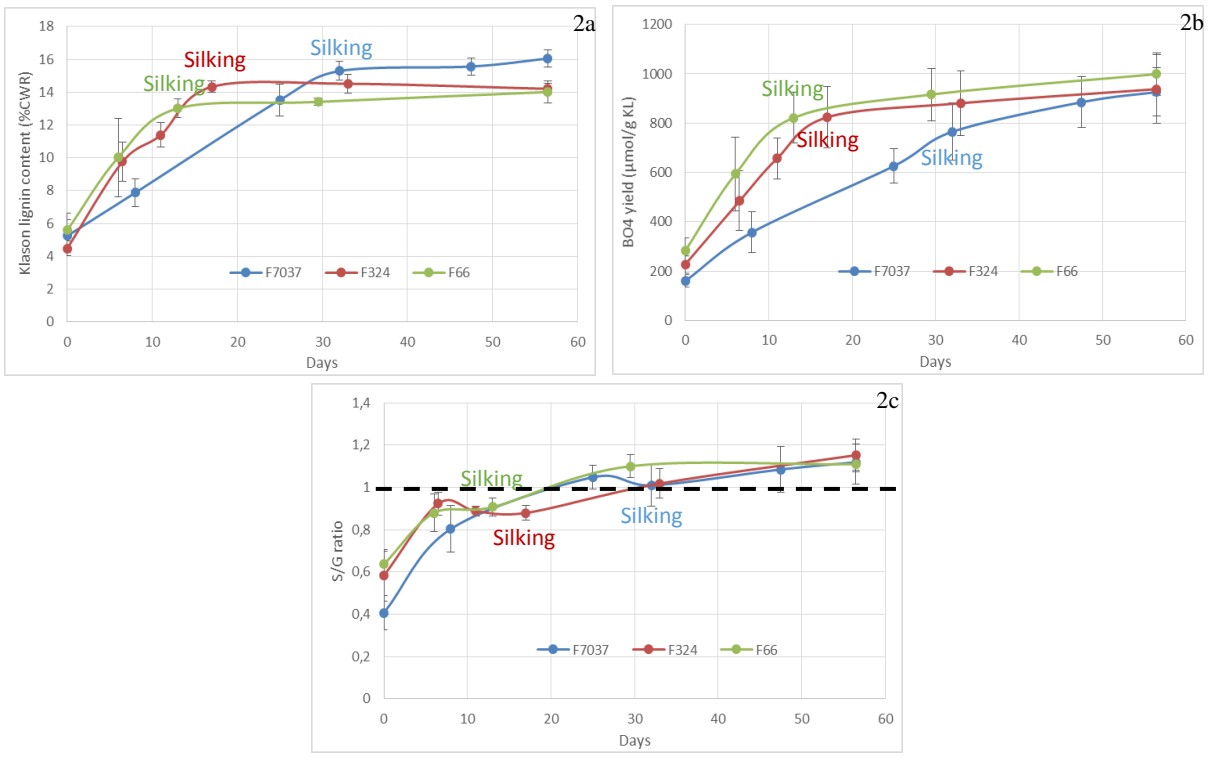


Figure 2. Evolution of lignin content, composition and structure during internode development for the three genotypes. 2a: Klason lignin content, 2b: lignin units only involved in β-O-4 bonds (uncondensed lignin part) and 2c: S/G thioacidolysis ratio. Data were averaged across the blocks collected in 2009 and 2010. «Silking » indicated the time of female flowering for each genotype. Smooth curves were used only for graphical purposes.

At the first stage of development, the relatively low syringyl to guaiacyl ratio (S/G ratio) was consistent with the well-known shift in H, G and S lignin subunit deposition during lignification as highlighted by Terashima et al. [8]. We actually observed that G accumulation ceased before S accumulation which continued until the last stage (S/G > 1, Figure 2c). Surprisingly, the S/G ratio evolution for F7037 was quite synchronous with that of F66 and F324 despite the important delay in their lignin deposition. Thus, during more than half of the accumulation phase of its lignins F7037 accumulated more S than G units contrary to the other two genotypes (Figure 2c). Therefore, in addition to the Gramineae lignification model proposed by Terashima et al. [8] we believed that many lignification models are possible. A strong genetic variability is present in maize (and more generally in grass) in the timing of lignin composition evolution even if indeed the S/G ratio increases all along development. Jung and Casler [32] stated that the shift from guaiacyl rich lignin to syringyl rich lignin is a general phenomenon of secondary cell wall development in grass tissues and Terashima et al. [8] proposed that when lignification reached the secondary cell wall, syringyl rich lignin content and S/G ratio increased. That would mean that for F7037 either the deposition of the secondary wall started earlier, or the primary wall was richer in S units.

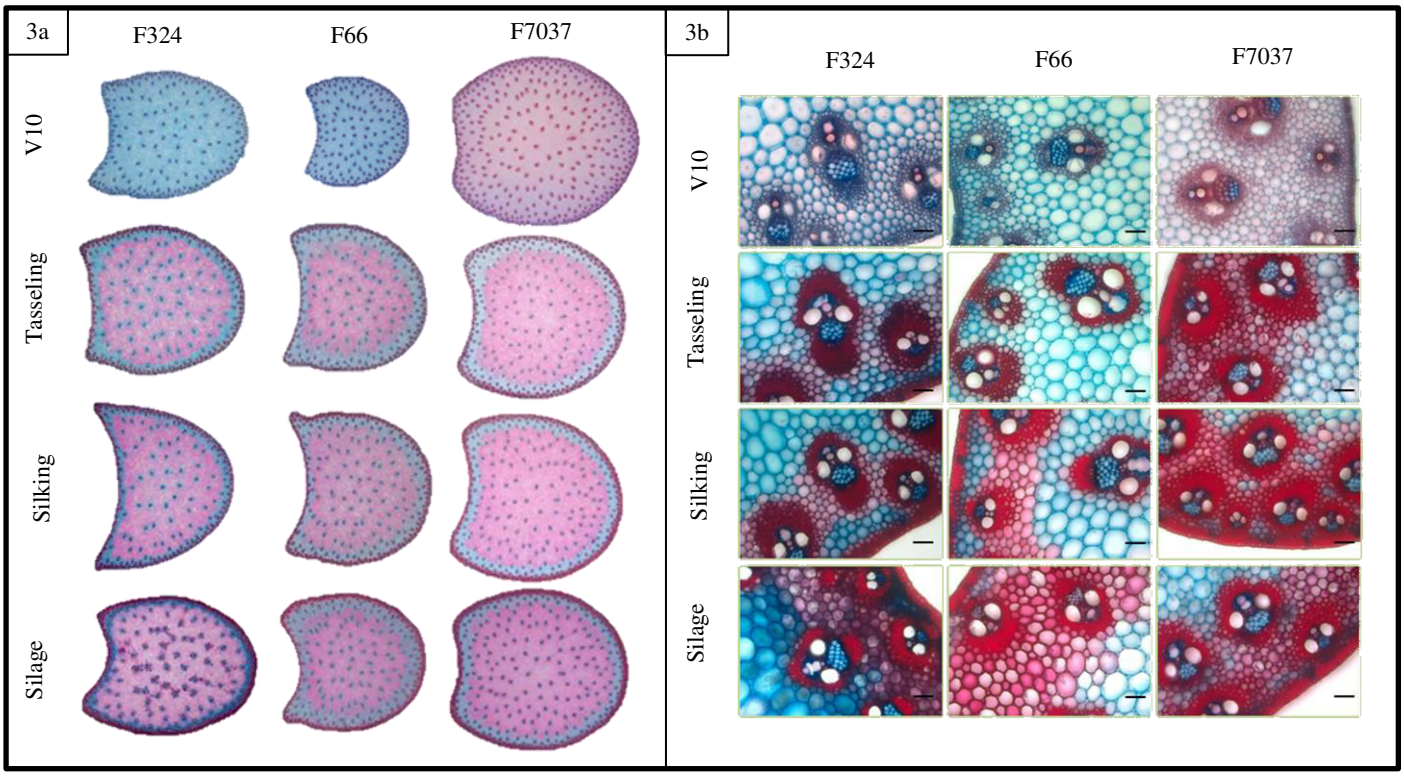
3.3.3. Evolution of lignin distribution at tissue level all along the internode development

Tissue lignification on internode development was followed by fasga staining. Lignified tissues are stained in red, whereas non lignified or poorly lignified tissues are colored in cyan/blue. For each fasga stained cross section of the three genotypes at the 6 developmental stages (Figure 3a) we evaluated the red/blue intensity ratio relative to the distance to the outer epidermis using the plugin developed and presented in Zhang et al. [50]. We defined three main regions from the color profiles: pith, blue layer in the pith and rind. We assessed the evolution of the lignification rate for each region, at each stage for each genotype (Figure 3c). The blue ring appeared at the third stage (tasseling) for the 3 genotypes. The lignification of this poorly-lignified parenchyma region was low and did not change along internode development after tasseling stage.

As presented in details for F324 in Zhang et al. [50] a great increase in the red/blue intensity ratio of the rind and pith regions for the 3 genotypes between V10 (stage 2) and tasseling (stage 3) was related to the lignification of these two regions. In the rind region, relatively high values of the red/blue intensity ratio indicated that cells from this region were much more lignified than those of other regions. After tasseling the red/blue intensity ratio in the pith remained steady whereas in the rind this ratio continued to increase (Figure 3c). Thus both blue ring and pith regions stopped their lignification after tasseling. Therefore the lignins which accumulated after this stage were deposited predominantly in the rind region. This was perfectly illustrated by figure 3a and even more by figure 3b on which we could observe the intense lignification of the rind region for all the 3 genotypes after tasseling.

If we compared the 3 genotypes, the three main points to keep in mind are i) the highest blue intensity of the F324 blue ring, ii) the highest red/blue rind ratio for F7037 compared to F66 and F324 and at least iii) the quite comparable profiles of pith region lignification for the 3 genotypes. F7037 was thus globally a more intensely lignified genotype with in particular a highly lignified rind.

In conclusion, lignification takes place largely before flowering stage both in the pith and in the rind. After flowering and until maturity, the deposited lignins are very rich in BO4 bonds and mainly localized in the rind.



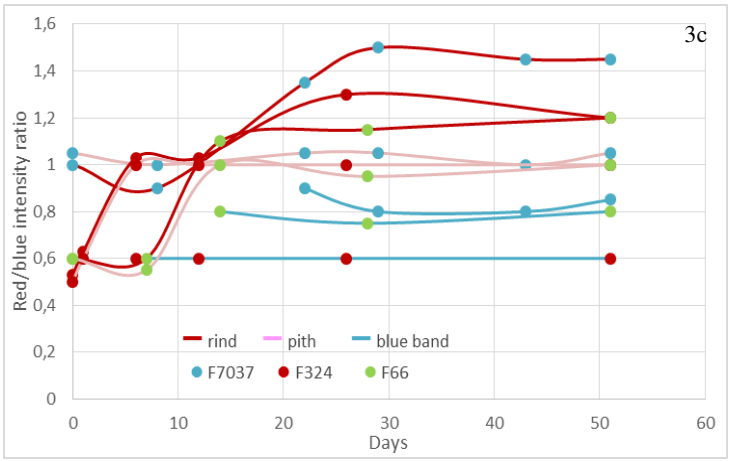


Figure 3. Evolution of tissues lignification during internode development for the three genotypes.3a: whole internode FASGA stained cross section, 3b: rind region of the FASGA stained cross section (bar = 100µm) and 3c: Red/blue intensity ratio. Smooth curves were used only for graphical purposes.

3.4. Throughout internode growth different developmental patterns were observed for p-hydroxycinnamic acids accumulation

Evolution of esterified p-coumaric acid content all along internode development

Deposition of *p*-coumaric acid followed the same pattern as observed for the Klason lignin content (Figure 4a). Strong correlation was observed between esterified *p*-coumaric acid content and Klason lignin content over both the earlier and maturity stage intervals (Data not show).

The %S-PC increased amazingly over earlier stages nearly reaching its maximum at V10 (stage 2) for F66 and F324 by going from 12-15% to 25% in just a few days. However, for F7037 the %S-PC increased from 7% to 30% in 3 weeks. Analysis of variance showed a significant genotype effect for *p*-coumaric acid content and %S-PC over the maturity stages. At the silage stage, large genotypic variations were observed for *p*-coumaric acid content and

%S-PC. F7037 which had the highest Klason lignin content had also the highest *p*-coumaric acid content and %S-PC. F324 and F66 had similar Klason lignin content and also presented similar *p*-coumaric acid content and %S-PC.

In grass, *p*-coumaric acid is mainly esterified to the γ-position of the side chains of S lignin units, making *p*-coumaric acid accumulation an indicator of lignin deposition [56]. Several studies have shown a positive relationship between *p*-coumaric acid content in the cell wall and level of lignin [6, 52, 57]. The current study reinforces this observation. During maize cell wall development esterified *p*-coumaric acid content increased following the same trajectory as Klason lignin content.

It is well established that *p*-coumaric acid content in the cell wall dramatically increased during maize secondary cell wall deposition and that *p*-coumaric acid is mainly associated to the syringyl-rich lignin [32]. Recent work has demonstrated that S units were enzymatically preacylated by *p*-coumaric acid in the cytosol [14], these acylated monolignols are then incorporated into the lignin polymer by polymerization and co-polymerization with the traditional monolignols, resulting in acylated lignin [15]. The role of lignin acylated by *p*-coumaric acid is not yet very clear. It is pretty sure that *p*-coumaroylated S unit is crucial for radical transfer mechanisms in order to improve S unit incorporation into lignin polymer. From stage three, the %S-PC leveled off. This plateau was higher for F7037 compared to F324 and F66. Thus, about 31% of the S units appeared to be acylated by *p*-coumaric acid in F7037 to about 25% in the two other genotypes. We have shown that at late stages, mainly uncondensed β-O-4 lignin was formed; these lignins are thus also strongly p-coumaroylated. The enzymatic step of S unit acylation by *p*-coumaric acid could thus be a key step to control

lignin final structure and composition. Especially when considering the results obtained by Zhang et al. [3] which demonstrated that *p*-coumaroylated S lignin units were a major limiting factor for cell wall degradability when lignin content variations were small. Works presented by Withers et al. [58] on an acyltransferase that catalyzes the acylation of monolignols in grass open up the possibility to modify gene expression and thus to modulate and regulate acylation in plants. In a recent study, Sibout et al. [59] introduced such a brachypodium *p*- coumaroyl-coenzyme A monolignol transferase in arabidopsis and succeeded in altering both the arabidopsis lignin content/structure/composition and consequently in impacting cell wall degradability.

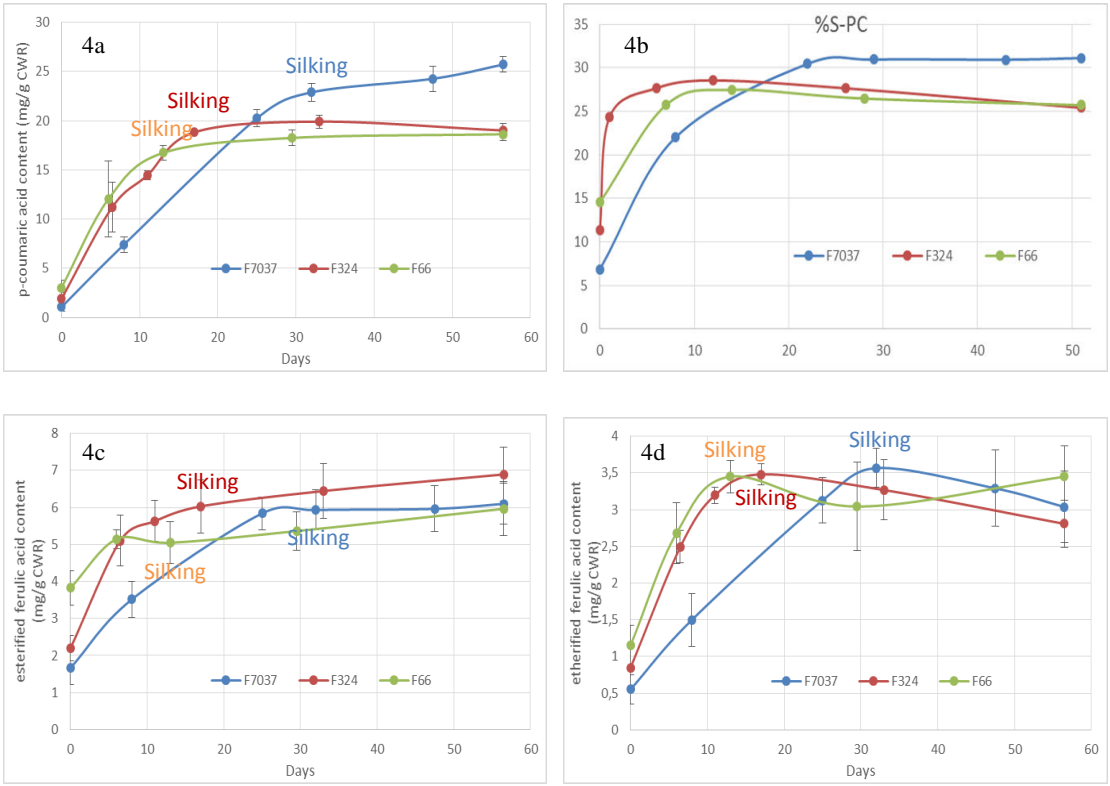


Figure 4. Evolution of *p*-coumaroylation and feruloylation during internode development for the three genotypes. 4a: esterified *p*-coumaric acid content, 4b: percentage of S lignin subunit acylated by *p*- coumaric acid, 4c: esterified ferulic acid content and 4d: etherified ferulic acid content. Data were averaged across the blocks collected in 2009 and 2010. «Silking » indicated the time of female flowering for each genotype. Smooth curves were used only for graphical purposes.

3.4.1. Esterified ferulic acids were deposed all along plant development but used to anchor lignification only at early stages

Variance analysis indicated that the three genotypes differed for esterified ferulic acid content (FAest) over developmental stages ($P < 0.01$) (Table 1). In grass ferulic acid firstly ester linked to arabinoxylans are deposited in the primary cell wall [60]. Once incorporated into the wall peroxidases oxidize the ferulic acid to form several possible ferulic acid dimers [61] but also couple ferulic acid to monolignols [62]. Ralph et al. [11] suggested that esterified ferulic acid probably serve as initialization site for lignification. In the present study, esterified ferulic acid was relatively high from the first stage, especially for F66 (Figure 4c). This early deposition of esterified ferulic acid should play a crucial role for the development of lignification in primary wall. Esterified ferulic acid accumulation was high during the three first stages and slowed down once secondary wall deposition begun. Esterified ferulic acid accumulation continued during the late stages for F66 and F324 but surprisingly not for F7037 (Figure 4c). Our results are consistent with those presented by Jung (2003) indicating that esterified ferulic acid deposition is not limited to primary walls but that approximately 60% of esterified ferulic acid are presents when the secondary wall formation begins in maize. In 2008, Hatfield et al. [63] reported the constant level of ester linked ferulic acid across internodes tissues of developing maize stems thus demonstrating that ferulic acid was continually incorporated in secondary cell walls as well as primary walls. The highest amount of etherified ferulic acid was quantified at the third stage. Etherified ferulic acids are supposed to bridge together hemicelluloses and lignins. Beyond stage three, the etherified ferulic acid content did not further increased suggesting that no supplementary bridge between these two polymers were thus set up (Figure 4d). The possibility remained that feruloyl arabinoxylan polymers continued to be laid down in the secondary wall, but no more ferulic acid radically couple to monolignol. This is extremely consistent with the fact that lignin synthesized during the last stages were mainly constituted of β-O-4 bond subunits. This predominance of β-O-4 bonds was the sign of an endwise mechanism as debate in Demont-Caulet et al. [64]. Thus, at the end of the plant development few lignins were synthesized but the new ones were not fixed to new ferulic acid primers but were an elongation via β-O-4 bonding of the existent lignins. Ferulic acid primers were thus recruited before stage 4 to install lignification.

3.5. Combination of the biochemical and histological findings to propose a model of spatiotemporal cell wall development

In the present study, we combined biochemical and histological approaches to characterize cell wall deposition and lignification during maize stem development. Maize internode cell wall development followed three different steps (1) a fast deposition of primary

cell wall in the whole cross section; (2) a fast deposition of secondary wall and (3) a slow deposition of secondary wall in the cortical region (Figure 5). Spatial and temporal deposition of cell wall components and development of cell wall structure varied among these three cell wall developmental steps and was also clearly genotype dependent. In primary cell wall, esterified ferulic acid was predominantly deposed, and the large genetic variation for esterified ferulic acid content was likely to be critical for the variation of lignification in the primary cell wall. In the second step, deposition of both fast C-C and β-O-4 bonds lignins lead to the fast deposition and lignification of secondary cell wall. Once the fast C-C bonds lignin deposition ended, β-O-4 bonds lignins were likely the major ones formed during the late lignification and were predominantly deposited in the cortical region. This cortical region thus appeared to be very specific regarding its composition. Our results suggested that cortical region was in fact highly lignified with lignin rich in β-O-4 bonds and highly p-coumaroylated. Barros-Rios et al. [29] compared cell wall composition in separated maize pith and rind tissues. They demonstrated that rind tissues were less degradable than pith tissues and richer in etherified ferulic acids, in esterified p-coumaric acids and also more lignified. In the same way, Hatfield and Chapman [6] have demonstrated that pith tissues had lower levels of lignin and *p*- coumaric acid. As established in Zhang et al. [3] lignin rich in bO4 bonds and highly *p*-coumaroylated were the more inhibitory ones for cell wall degradability. Thus the spatial and temporal developmental scheme for cortical region made it a highly undegradable and resistant tissue. This reinforced our recent results suggesting that in drought context rind region was preferentially lignified and *p*-coumaroylated [65] in order to assure plant posture and resistance with a decreased global lignification at internode level. In agreement with Hatfield and Chapman [6] in particular, we think that *p*-coumaric acid have an active role in the formation of lignin in grass cell walls and results presented in this publication underline also the fact that its distribution at the tissue level is important to take into account to better understand genetic variation of overall cell wall composition and degradability of internode. In our opinion, the impact of lignified tissue distribution on cell wall degradability is preponderant and has long been underestimated.

Selection of lines with improvement of cell wall degradability should include these considerations of lignin and *p*-hydroxycinnamic acids tissue distribution both in quantity and composition.

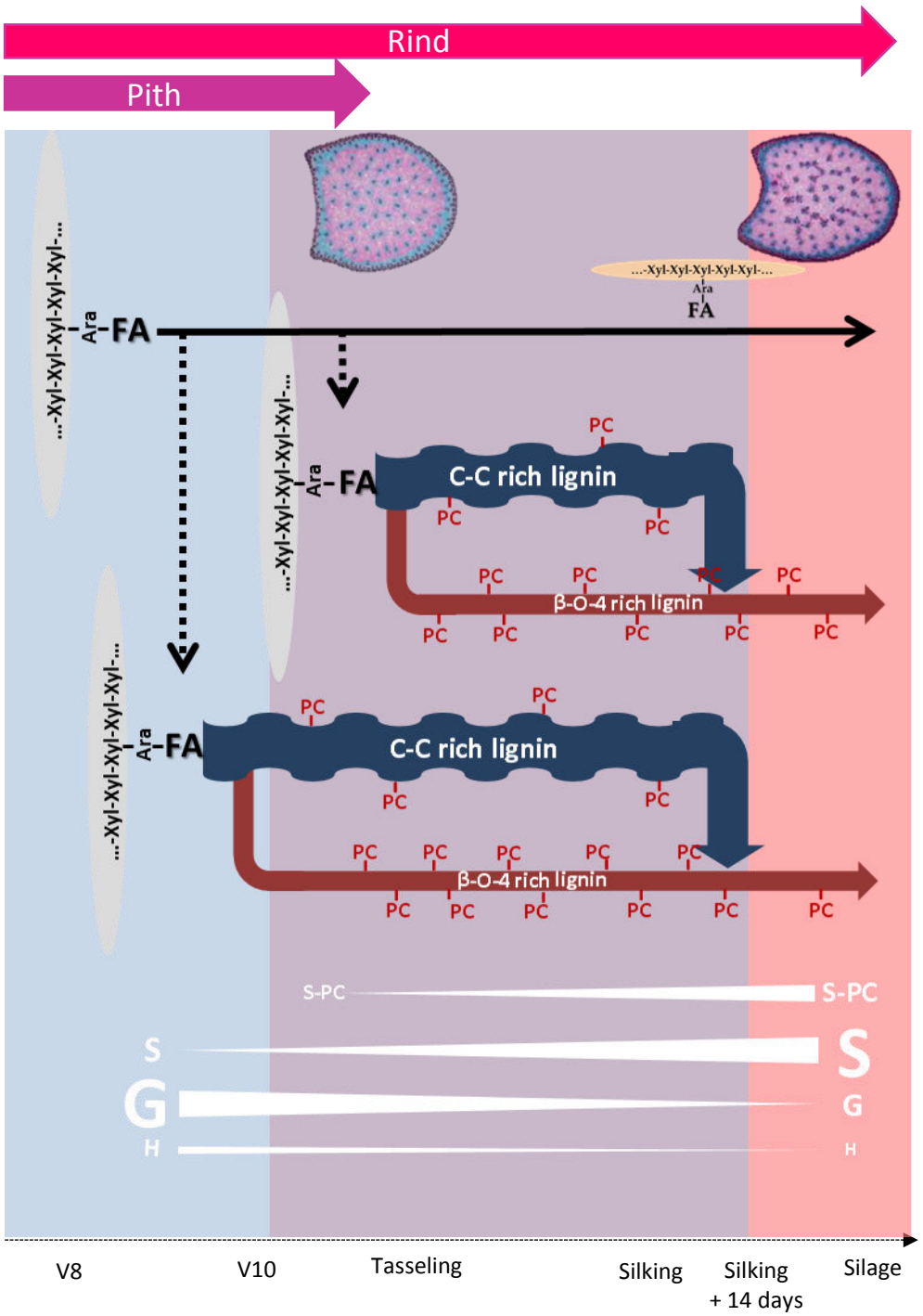


Figure 5. Schematic illustration of the spatio-temporal evolution of the maize internode cell wall.

Acknowledgments

The authors sincerely acknowledge L. Cézard and F. Legée for their participation in lignin analysis, C. Minault, P. Vernoux, and D. Denoue for their precious contribution in field experiments.

Funding sources

This work has benefited from French Government Grants (LabEx Saclay Plant Sciences-SPS, ref. ANR-10-LABX-0040-SPS, and ANR-11-BTBR-0006 BIOMASS FOR THE FUTURE), managed by the French National Research Agency under an "Investments for the Future" program (ref. ANR-11-IDEX-0003-02). This work has also benefited from CEPIA INRA Division grants (AIC HistoChem and Intégrale). The école doctorale Sciences du Végétal provided funding for Fadi El Hage's salary.This work was also supported by the French Research National Agency (ANR) in the context of the MAGIC program (ANR-08-BLAN- 0307-01) and Y. Zhang was supported by a grant from INRA CEPIA and INRA BV. Many results presented in this paper come from unpublished results presented in Yu Zhang's thesis [66].

Author contributions statement

VM designed the research and supervised experiments and YZ PhD work. YZ performed the biochemical and histological experiments. DL developed the image analysis methodology and implemented the software. FG, DL and MFD developed and performed anatomical analyses. VM, YZ, FEH and MR analyzed the data. VM and YZ wrote the manuscript. All authors read and approved the final manuscript.

References

[1] R.D. Hatfield, D.M. Rancour, J.M. Marita, Grass Cell Walls: A Story of Cross-Linking, Front Plant Sci, 7 (2017) 2056.

[2] H.J.G. Jung, M.A. Jorgensen, J.G. Linn, F.M. Engels, Impact of accessibility and chemical composition on cell wall polysaccharide degradability of maize and lucerne stems, J. Sci. Food Agric., 80 (2000) 419-427.

[3] Y. Zhang, T. Culhaoglu, B. Pollet, C. Melin, D. Denoue, Y. Barriere, S. Baumberger, V. Méchin, Impact of Lignin Structure and Cell Wall Reticulation on Maize Cell Wall Degradability, J. Agric. Food Chem., 59 (2011) 10129-10135.

[4] F. El Hage, D. Legland, N. Borrega, M.-P. Jacquemot, Y. Griveau, S. Coursol, V. Méchin, M. Reymond, Tissues lignification, cell wall p-coumaroylation and degradability of maize stems depend on water status, J. Agric. Food Chem., (Submitted).

[5] V. Méchin, O. Argillier, V. Menanteau, Y. Barriere, I. Mila, B. Pollet, C. Lapierre, Relationship of cell wall composition to in vitro cell wall digestibility of maize inbred line stems, J. Sci. Food Agric., 80 (2000) 574-580.

[6] R.D. Hatfield, A.K. Chaptman, Comparing corn types for differences in cell wall characteristics and p-coumaroylation of lignin, J. Agric. Food Chem., 57 (2009) 4243-4249.

[7] T. Ishii, T. Hiroi, Isolation and characterization of feruloylated arabinoxylan oligosaccharides from bamboo shoot cell-walls, Carbohydr. Res., 196 (1990) 175-183.

[8] N. Terashima, K. Fukushima, L.F. He, K. Takabe, Comprehensive model of the lignified plant cell wall., in: H.G. Jung, D.R. Buxton, R.D. Hatfield, J. Ralph (Eds.) Forage Cell Wall Structure and Digestibility, ASA-CSSA-SSSA, Madison, WI, 1993, pp. 247-270.

[9] J.H. Grabber, J. Ralph, R.D. Hatfield, Model studies of ferulate-coniferyl alcohol cross-product formation in primary maize walls: implications for lignification in grasses, J. Agric. Food Chem., 50 (2002) 6008-6016.

[10] M. Bunzel, J. Ralph, H. Steinhart, Association of non-starch polysaccharides and ferulic acid in grain amaranth (Amaranthus caudatus L.) dietary fiber, Mol Nutr Food Res, 49 (2005) 551-559.

[11] J. Ralph, J.H. Grabber, R.D. Hatfield, Lignin-Ferulate Cross-Links in Grasses - Active Incorporation of Ferulate Polysaccharide Esters into Ryegrass Lignins, Carbohydr. Res., 275 (1995) 167-178.

[12] J.H. Grabber, J. Ralph, R.D. Hatfield, Ferulate cross-links limit the enzymatic degradation of synthetically lignified primary walls of maize, J. Agric. Food Chem., 46 (1998) 2609-2614.

[13] J.H. Grabber, S. Quideau, J. Ralph, p-coumaroylated syringyl units in maize lignin: Implications for beta-ether cleavage by thioacidolysis, Phytochemistry, 43 (1996) 1189-1194.

[14] R.D. Hatfield, J.M. Marita, K. Frost, J. Grabber, J. Ralph, F. Lu, H. Kim, Grass lignin acylation: p-coumaroyl transferase activity and cell wall characteristics of C3 and C4 grasses, Planta, 229 (2009) 1253-1267.

[15] J. Ralph, Hydroxycinnamates in lignification, Phytochemistry Reviews, 9 (2010) 65-83.

[16] N.G. Lewis, E. Yamamoto, Lignin: occurrence, biogenesis and biodegradation, Annual Review of Plant Physiology and Plant Molecular Biology, 41 (1990) 455-496.

[17] G. Wallace, S.C. Fry, Phenolic components of the primary cell wall, International

Review of Cytology - a Survey of Cell Biology, Vol 151, 151 (1994) 229-267.

[18] H.G. Jung, D.A. Deetz, Cell Wall Lignification and Degradability, Forage Cell Wall Structure and Digestibility, acsesspublicati (1993) 315-346.

[19] M.D. Casler, D.R. Buxton, K.P. Vogel, Genetic modification of lignin concentration affects fitness of perennial herbaceous plants, Theor. Appl. Genet., 104 (2002) 127-131.

[20] J.F. Pedersen, K.P. Vogel, D.L. Funnell, Impact of reduced lignin on plant fitness, Crop Sci., 45 (2005) 812-819.

[21] H.J.G. Jung, W.T. Ni, C.C.S. Chapple, K. Meyer, Impact of lignin composition on cell-wall degradability in an Arabidopsis mutant, Journal of the Science of Food and Agriculture, 79 (1999) 922-928.

[22] J.H. Grabber, D.R. Mertens, H. Kim, C. Funk, F. Lu, J. Ralph, Cell wall fermentation kinetics are impacted more by lignin content and ferulate cross-linking than by lignin composition, Journal of the Science of Food and Agriculture, 89 (2009) 122-129.

[23] J.H. Grabber, How do lignin composition, structure, and cross-linking affect degradability? A review of cell wall model studies, Crop Science, 45 (2005) 820-831.

[24] M.A. Bernard-Vailhe, A. Cornu, D. Robert, M.P. Maillot, J.M. Besle, Cell wall degradability of transgenic tobacco stems in relation to their chemical extraction and lignin quality, J. Agric. Food Chem., 44 (1996) 1164-1169.

[25] M. Baucher, M.A. Bernard-Vailhe, B. Chabbert, J.M. Besle, C. Opsomer, M. Van Montagu, J. Botterman, Down-regulation of cinnamyl alcohol dehydrogenase in transgenic alfalfa (Medicago sativa L.) and the effect on lignin composition and digestibility, Plant Mol. Biol., 39 (1999) 437-447.

[26] V. Méchin, O. Argillier, F. Rocher, Y. Hebert, I. Mila, B. Pollet, Y. Barriere, C. Lapierre, In search of a maize ideotype for cell wall enzymatic degradability using histological and biochemical lignin characterization, J. Agric. Food Chem., 53 (2005) 5872-5881.

[27] H.J.G. Jung, D.R. Buxton, Forage quality variation among maize inbreds: Relationships of cell-wall composition and in-vitro degradability for stem internodes, Journal of the Science of Food and Agriculture, 66 (1994) 313-322.

[28] T.B. Lam, K. Iiyama, B.A. Stone, Hot alkali-labile linkages in the walls of the forage grass Phalaris aquatica and Lolium perenne and their relation to in vitro wall digestibility, Phytochemistry, 64 (2003) 603-607.

[29] J. Barros-Rios, R.A. Malvar, H.J. Jung, M. Bunzel, R. Santiago, Divergent selection for ester-linked diferulates in maize pith stalk tissues. Effects on cell wall composition and degradability, Phytochemistry, 83 (2012) 43-50.

[30] R.D. Hatfield, J.R. Wilson, D.R. Mertens, Composition of cell walls isolated from cell types of grain sorghum stems, J. Sci. Food Agric., 79 (1999) 891-899.

[31] J. Grabber, H. Jung, R.R. Hill, Chemical composition of parenchyma and sclerenchyma cell walls isolated from orchardgrass and switchgrass, Crop Sci., 31 (1991) 1058-1065.

[32] H.G. Jung, M.D. Casler, Maize stem tissues : cell wall concentration and composition during development, Crop Sci, 46 (2006) 1793-1800.

[33] H.G. Jung, F.M. Engels, Alfalfa stem tissues: cell wall deposition, composition, and degradability, Crop Sci, 42 (2002) 524-534.

[34] F. Guines, B. Julier, C. Ecalle, C. Huyghe, Among and within-cultivar variability for histological traits of lucerne (Medicago sativa L.) stem, Euphytica, 130 (2003) 293-301.

[35] G. Sarath, L.M. Baird, K.P. Vogel, R.B. Mitchell, Internode structure and cell wall

composition in maturing tillers of switchgrass (Panicum virgatum. L), Bioresour. Technol., 98 (2007) 2985-2992.

[36] G. Sarath, D.E. Akin, R.B. Mitchell, K.P. Vogel, Cell-wall composition and accessibility to hydrolytic enzymes is differentially altered in divergently bred switchgrass (Panicum virgatum L.) genotypes, Appl. Biochem. Biotechnol., 150 (2008) 1-14.

[37] S. Lopez, S.D. Murison, A.J. Travis, A. Chesson, Degradability of parenchyma and sclerenchyma cell walls isolated at different developmental stages from a newly extended maize internode, Acta Bot. Neerl., 42 165-174.

[38] R.D. Hatfield, Cell Wall Polysaccharide Interactions and Degradability, Forage Cell Wall Structure and Digestibility, acsesspublicati (1993) 285-313.

[39] E.J.M.C. Boon, P.C. Struik, F.M. Engels, J.W. Cone, Stem characteristics of two forage maize (Zea mays L.) cultivars varying in whole plant digestibility. IV. Changes during the growing season in anatomy and chemical composition in relation to fermentation characteristics of a lower internode, Njas-Wageningen Journal of Life Sciences, 59 (2012) 13- 23.

[40] E. Boon, F.M. Engels, P.C. Struik, J.W. Cone, Stem characteristics of two forage maize (Zea mays L.) cultivars varying in whole plant digestibility. II. Relation between in vitro rumen fermentation characteristics and anatomical and chemical features within a single internode, Njas-Wageningen Journal of Life Sciences, 53 (2005) 87-109.

[41] E.J.M.C. Boon, P.C. Struik, S. Tamminga, F.M. Engels, J.W. Cone, Stem characteristics of two forage maize (Zea mays L.) cultivars varying in whole plant digestibility. III. Intra-stern variability in anatomy, chemical composition and in vitro rumen fermentation, Njas-Wageningen Journal of Life Sciences, 56 (2008) 101-122.

[42] H.J.G. Jung, Maize stem tissues: ferulate deposition in developing internode cell walls, Phytochemistry, 63 (2003) 543-549.

[43] M.J. Effland, Modified procedure to determine acid-insoluble lignin in wood and pulp., Tappi, 60 (1977) 143-144.

[44] C. Dence, S.Y. Lin, The Determination of Lignin. In Methods in Lignin Chemistry, Springer: Berlin, (1992) 33-61.

[45] T. Culhaoglu, D. Zheng, V. Mechin, S. Baumberger, Adaptation of the Carrez procedure for the purification of ferulic and p-coumaric acids released from lignocellulosic biomass prior to LC/MS analysis, Journal of Chromatography B-Analytical Technologies in the Biomedical and Life Sciences, 879 (2011) 3017-3022.

[46] C. Lapierre, B. Monties, C. Rolando, Preparative Thioacidolysis of Spruce Lignin: Isolation and Identification of Main Monomeric Products, Holzforschung, 40 (1986) 47-50.

[47] M.F. Devaux, A. Sire, P. Papineau, Macrovision et analyse granulométrique en niveaux de gris pour l'analyse histologique de tissus végétaux, Cahiers Techniques de l'INRA, Numéro spécial imagerie (2009) 93-100.

[48] M.F. Devaux, B. Bouchet, D. Legland, F. Guillon, M. Lahaye, Macro-vision and grey level granulometry for quantification of tomato pericarp structure, Postharvest Biol Technol, 47 (2008) 199-209.

[49] M.F. Devaux, D. Legland, Grey level granulometry for histological image analysis of plant tissues in: A. Mendez-Vilas (Ed.) Microscopy: advances in scientific research and education, 2014, pp. 681-688.

[50] Y. Zhang, S. Legay, Y. Barriere, V. Mechin, D. Legland, Color quantification of stained maize stem section describes lignin spatial distribution within the whole stem, J. Agric. Food Chem., 61 (2013) 3186-3192.

[51] Y. Barrière, V. Méchin, F. Lafarguette, D. Manicacci, F. Guillon, H. Wang, D. Lauressergues, M. Pichon, M. Bosio, C. Tatout, Toward the discovery of maize cell wall genes involved in silage quality and capacity to biofuel production, Maydica, 54 (2009) 161-198.

[52] L. Scobbie, W. Russell, G.J. Provan, A. Chesson, The Newly Extended Maize Internode: A. Model for the Study of Secondary Cell Wall. Formation and Consequences for Digestibility, Journal of the Science of Food and Agriculture, 61 (1993) 217-225.

[53] F.M. Engels, H.G. Jung, Alfalfa stem tissues: Cell-wall development and lignification, Annals of Botany, 82 (1998) 561-568.

[54] R. Hatfield, R.S. Fukushima, Can lignin be accurately measured?, Crop Sci., 45 (2005) 832-839.

[55] V. Méchin, S. Baumberger, B. Pollet, C. Lapierre, Peroxidase activity can dictate the in vitro lignin dehydrogenative polymer structure, Phytochemistry, 68 (2007) 571-579.

[56] F.C. Lu, J. Ralph, Detection and determination of p-coumaroylated units in lignins, J. Agric. Food Chem., 47 (1999) 1988-1992.

[57] T.A. Morrison, H.G. Jung, D.R. Buxton, R.D. Hatfield, Cell-wall composition of maize internodes of varying maturity, Crop Sci., 38 (1998) 455-460.

[58] S. Withers, F. Lu, H. Kim, Y. Zhu, J. Ralph, C.G. Wilkerson, Identification of grass-specific enzyme that acylates monolignols with p-coumarate, The Journal of biological chemistry, 287 (2012) 8347-8355.

[59] R. Sibout, P. Le Bris, F. Legee, L. Cezard, H. Renault, C. Lapierre, Structural Redesigning Arabidopsis Lignins into Alkali-Soluble Lignins through the Expression of p-Coumaroyl-CoA:Monolignol Transferase PMT, Plant Physiol., 170 (2016) 1358-1366.

[60] R.D. Hatfield, J. Ralph, J.H. Grabber, Cell wall cross-linking by ferulates and diferulates in grasses, Journal of the Science of Food and Agriculture, 79 (1999) 403-407.

[61] J. Ralph, S. Quideau, J.H. Grabber, R.D. Hatfield, Identification and synthesis of new ferulic acid dehydrodimers present in grass cell walls, Journal of the Chemical Society-Perkin Transactions 1, 23 (1994) 3485-3498.

[62] S. Quideau, J. Ralph, Lignin-ferulate cross-links in grasses .4. Incorporation of 5-5-coupled dehydrodiferulate into synthetic lignin, Journal of the Chemical Society-Perkin Transactions 1, (1997) 2351-2358.

[63] R.D. Hatfield, J.M. Marita, K. Frost, Characterization of p‐coumarate accumulation, p‐coumaroyl transferase, and cell wall changes during the development of corn stems, J. Sci. Food. Agric., 88 (2008) 2529-2537.

[64] N. Demont-Caulet, C. Lapierre, L. Jouanin, S. Baumberger, V. Mechin, Arabidopsis peroxidase-catalyzed copolymerization of coniferyl and sinapyl alcohols: Kinetics of an endwise process, Phytochemistry, 71 (2010) 1673-1683.

[65] F. El Hage, D. Legland, N. Borrega, M.-P. Jacquemot, Y. Griveau, S. Coursol, V. Mechin, M. Reymond, Tissue Lignification, Cell Wall p-Coumaroylation and Degradability of Maize Stems Depend on Water Status, J. Agric. Food Chem., 66 (2018) 4800-4808.

[66] Y. Zhang, Mise en place de la réticulation des parois de maïs au cours du développement et impact sur la variabilité de la dégradabilité des polysaccharides pariétaux, in: Sciences agricoles, AgroParisTech, Paris, 2012, pp. 206.

Titre: Impact du déficit hydrique sur la dégradabilité, la biochimie pariétale et la répartition des tissus lignifiés chez l'entrenœud de maïs et déterminisme génétique de ces caractères.

Mots clés: Maïs, stress hydrique, dégradabilité, histologie, lignification, déterminisme génétique.

Résumé:

Ce projet de thèse s'inscrit dans un contexte de changement climatique et de remplacement des énergies fossiles, où la réduction des apports en eau et l'optimisation de la valorisation de la biomasse sont deux enjeux majeurs des systèmes de productions durables. La dégradabilité de la biomasse est principalement limitée par la dégradabilité des parois et afin de l'améliorer, il est nécessaire de comprendre quels facteurs sont impliqués dans cette limitation de dégradabilité. Plusieurs études ont montré que la dégradabilité pariétale est impactée par la composition et la structure de la paroi mais aussi par la distribution des tissus lignifiés au sein des organes. Pour faire la part entre l'impact de la biochimie et celui de l'histologie sur la dégradabilité dans différentes conditions d'irrigation, des outils haut-débit de quantifications biochimiques et histologiques ont été développés et dédiés à l'étude d'entrenœuds portant l'épi principal. Les études ont porté sur un panel de diversité génétique de maïs et d'une population de lignées recombinantes, cultivés durant plusieurs années dans des conditions d'irrigation contrastées dans le sud de la France. Nos résultats mettent en évidence que le déficit hydrique induit une augmentation de la dégradabilité pariétale, accompagnée par une diminution de la teneur en lignines pariétales et par une induction préférentielle d'une lignification corticale, plus *p*-coumaroylée. De façon originale, nous avons aussi cartographié 90 QTLs de caractères histologiques dans les différentes conditions d'irrigation sur le génome du maïs. Plus particulièrement, une large région entre le bin 1.07 et le bin 1.11 est impliquée dans les variations observées du nombre de faisceaux vasculaires et de la surface de section des entrenoeuds. De façon globale, de nombreux QTLs de composition pariétale de l'entrenoeud co-localisent avec ceux obtenus au niveau de la plante entière sans épis chez la même population. Enfin nous avons pu démontrer que le choix de l'entrenœud portant l'épi principal est judicieux pour représenter à la fois les caractéristiques histologiques des tiges entières et biochimiques de la biomasse lignocellulosique des plantes entières. Ainsi, les caractéristiques histologiques et biochimiques des entrenoeuds de maïs sont proposées comme des cibles de choix pour sélectionner des lignées de maïs résilientes au déficit hydrique.

Title: Impact of water deficit on degradability, cell wall biochemistry and lignified tissue distribution in the maize internode and genetic determinism of these traits.

Keywords: Maize, water stress, degradability, histology, lignification, genetic determinism.

Abstract:

This PhD project encompass in a context of global warming and replacement of fossil resources, where both water supply decrease and biomass valorisation optimisation are two major issues for providing sustainable systems of production. Biomass degradability is mainly limited by cell wall degradability and in order to improve it, it is necessary to understand what are the factors involved in the limitation of the degradability. Several studies have shown that cell wall degradability is impacted by the structure and the composition of the cell wall but also by the distribution of the lignified tissues within the organs. To decipher the impact of the biochemistry and from the one of the histology on degradability under different watering conditions, high-throughput quantifications tools for histology and biochemistry have been developed and dedicated to the study of the internode carrying the main ear. The studies were conducted on a maize genetic diversity panel and a recombinant inbred lines population, cultivated during several years under contrasted irrigation conditions in South of France. Our results highlight that water deficit induce an increase of the cell wall degradability, associated to a decrease of the cell wall lignin content and a preferential induction of a cortical lignification, more *p*-coumaroylated. In original ways, we also detected 90 QTLs for histological traits under the different irrigations scenarios on the maize genome. More particularly, a large region between bin 1.07 and bin 1.11 is involved in the observed variations of the bundle number and the stem section area of the internodes. More generally, numerous QTLs of cell wall composition of the internode co-localised with the ones detected for the whole plant without ear level in the same population. Finally we were able to demonstrate that the choice of the internode carrying the main ear is judicious to represent both histological characteristics from the whole stem and biochemical characteristics from the lignocellulosic biomass of the whole plant. Thus, histological and biochemical traits in maize internode are proposed as particular targets to select lines resilient to water deficit.

Université Paris-Saclay
Espace Technologique / Immeuble Discovery
Route de l'Orme aux Merisiers RD 128 / 91190 Saint-Aubin, France